ATMOSPHERIC SCIENCES SECTION
ILLINOIS STATE WATER SURVEY

FINAL REPORT

ILLINOIS PRECIPITATION ENHANCEMENT PROGRAM

(PHASE I)

AND

DESIGN AND EVALUATION TECHNIQUES

FOR

HIGH PLAINS COOPERATIVE PROGRAM

for

1 September 1971 -- 30 September 1977

to

Division of Atmospheric Water Resources Management
Bureau of Reclamation
U. S. Department of Interior

Prepared by:

Gary L. Achtemeier, Peter H. Hildebrand, Paul T. Schickedanz,
Bernice Ackerman, Stanley A. Changnon, Jr., Richard G. Semonin

Stanley A. Changnon, Jr.
Principal Investigator

Contract 14-06-D-7197

TABLE OF CONTENTS

Page

Page

LIST OF FIGURES

Page

Page

ABSTRACT

This report covers six years of research dealing with weather modification. The first 3 1/2 years were devoted to a series of ten background studies aimed at designing a precipitation modification experiment (PEP) in Illinois. A reduction in federal funding ended that program prematurely with some of the studies done, some partially accomplished and two uninitiated. Essentially, the social and environmental impact studies indicated the desirability of precipitation modification, whereas the atmospheric potential studies were ended too soon to provide desired information.

The research in the last 2 1/2 years of this project was focused on the High Plains Cooperative Program (HIPLEX). An extensive design for HIPLEX was developed initially. Ensuing research has dealt with various statistical and physical aspects for use in the evaluation of future HIPLEX experimentation.

KEY WORDS

Weather modification, precipitation enhancement, rainfall, snowfall, economics, social attitudes, environmental impacts, weather and law, experimental design, experimental evaluation, monitoring, Midwest weather and climate, game animals, water resources, atmosphere, moisture, cloud physics, atmospheric chemistry, and ecology.

INTRODUCTION

This serves as the final report for a 6-year research effort under a contract between the Illinois State Water Survey and the Division of Atmospheric Water Resourees Management (DAWRM) of the Bureau of Reclamation, U. S. Department of the Interior. This contract was identified as U. S. Department of Interior 14-06-D-7197. The project began on 1 September 1971 and ended on 30 September 1977.

This research contract had two distinctly different efforts, both with a central focus on the design of experiments to modify convective clouds and precipitation in a controlled manner.

The first of these efforts was the Precipitation Enhancement Program (PEP) which lasted for approximately 3 1/2 years. It was originally planned as a 5-year effort to design an experiment to modify warm or cold season precipitation in Illinois. In that sense, it was considered Phase 1 of a two-phase effort. The second phase of PEP was to have been an actual field experiment to be launched in 1976, given that the Phase 1 design efforts indicated the physical and social desirability of such an experiment. As originally planned, the Phase 1, 5-year effort, was to cost approximately $1.25 million with $950,000 to be furnished by the DAWRM and $300,000 by the State of Illinois.

A major reduction in funding available to the Bureau of Reclamation, which occurred in 1973; led to the near termination of PEP and the launching of a second and distinctly different research effort. This second research effort was initiated in February 1975 and continued through 30 September 1977. This new effort focused on the design of the High Plains Cooperative Program (HIPLEX), a 3-area experiment of the DAWRM for the ultimate modification of convective rainfall in the Great Plains. Funding for this second effort approximated $380,337 from the Bureau of Reclamation and approximately $100,000 from the State of Illinois.

The Precipitation Enhancement Program for Illinois was focused on the development of a design of a future Illinois-centered field experiment concerning the modification of warm and/or cold season precipitation. This 5-year design effort had ten specific study areas aimed collectively at answering two questions. First "What is the feasibility for modification of precipitation in Illinois (which has a climate representative of the Midwest)?" and second "Is precipitation modification in Illinois desirable?" Actually PEP lasted about 3 1/2 years and had two different periods of activity. The first of these, which lasted from 1 September 1971 through 30 June 1973, might be best labeled as the "active" period. This period was one of total funding, as planned, from DAWRM and the

State of Illinois. The second period, which would be best labeled as the "low effort period," lasted from 1 July 1973 through 31 January 1975. This period of minimal effort resulted because of a major reduction in funding available to DAWRM which occurred on 1 July 1973. This sizeable reduction produced a comparable reduction in the level of state support of PEP.

The HIPLEX phase of this 6-year research contract, which followed the termination of PEP, was focused on the design of HIPLEX. This second major activity extended from 1 February 1975 through the termination of the contract on 30 September 1977. The Illinois State Water Survey became involved in the HIPLEX design activities because the prior work on PEP had provided many essential results and staff experience related to the development of an integrated experimental design. It was believed that the HIPLEX design effort would be useful experience in the subsequent design of an Illinois precipitation modification experiment.

The 2 1/2-year HIPLEX design effort consisted of two phases. The first phase concerned the development of a design document for HIPLEX. Its primary focus was on the second phase of HIPLEX which is devoted to single cloud experimentation. The design document was completed in the summer of 1976. The second phase of the HIPLEX design effort, which extended from the summer of 1976 through the termination of the project, involved a) work with the areal design, including redesign efforts for the single cloud experiment, and b) evaluation of the capabilities of the HIPLEX radar.

The major accomplishments of this 6-year research project include the completion of all or parts of seven of the ten study areas of PEP. These completed or partially completed studies (modeling, water resource economic impacts, legal-legislative-institutional arrangements, ecological impacts, downwind assessment, potential precipitation modification in clouds, and atmospheric chemistry studies) together provide extensive background information essential for a well-designed midwestern experiment. A second major accomplishment of this research contract was the preparation of the design for HIPLEX. Many reports and scientific papers were prepared as part of this project (these are enumerated in the appendix). Included are five interim reports, seven technical reports, five annual reports, the HIPLEX design document, a report on the climatography of the Great Plains, and twenty-four published scientific papers. The major disappointment of the 6-year project related to the inability to complete the atmospheric sampling project, the seeding technology study, and the integrative, program design effort for PEP.

This 6-year project has involved many of the senior scientists of the Illinois State Water Survey. Stanley A. Changnon, Jr. has

served as the Principal Investigator on this contract throughout its duration, with the addition of Bernice Ackerman as Co-Principal Investigator during 1975-1976, and Paul T. Schickedanz as Co-Principal Investigator during 1977. In the initial 2 1/2 years of PEP, Richard G. Semonin and Floyd A. Huff played key roles in the PEP activities. Other senior staff members played significant roles including Griffith M. Morgan, Peter H. Hildebrand, Herbert Appleman, and Gary L. Achtemeier.

This report has two major sections; one dealing with the Precipitation Enhancement Program of the 1971-1975 period, and the other the HIPLEX design effort of the 1975-1977 period. The section on PEP includes an introduction describing the effort, a summary of the social, economic, environmental, and legal research, a summary of the atmospheric research studies, and a summary of the results of the limited but useful 1973 atmospheric and cloud sampling effort. The section focusing on the HIPLEX design effort contains two parts. The first of these deals with the development of the design, and the second part describes the subsequent research dealing with the re-design and evaluation of HIPLEX.

PRECIPITATION ENHANCEMENT PROGRAM

Introduction

The Precipitation Enhancement Program (PEP) in Illinois was conceived and conducted for 3 1/2 years as part of a program planned to last 5 years and aimed at establishing whether it would be a) socially and environmentally desirable, and b) scientifically feasible to enhance precipitation in Illinois. The PEP consisted of ten study areas, as shown in Figure 1. As a consequence of the major reduction in support during mid-1973, all of the study efforts, other than the atmospheric sampling project, were terminated on 30 June 1973. The work and findings from six of the study areas that were either completed or partially completed are described in seven technical reports (see appendix for project publications).

The research plan and associated field and data collection efforts were all focused on the goal of defining the feasibility and desirability of precipitation modification in Illinois which has a climate representative of conditions throughout the Midwest.

The rationale for PEP being initiated by the. Illinois State Water Survey begins with the fact that purposeful precipitation modification had been scientifically established in certain areas and for certain precipitation types and under specific weather conditions. With this recognition there developed first a host of questions for Illinois regarding weather modification and its potential economic benefits (and disbenefits), public concerns and institutional arrangements for weather modification, legal problems, and uncertainties about environmental effects. Thus, one of the two primary program objectives of PEP was to provide answers as to the question of "desirability of precipitation enhancement in Illinois." Four of the ten individual program efforts in PEP were aimed at answering the desirability questions. These four specific study areas, shown on Figure 1, included 1) study of the potential benefits of precipitation augmentation to agriculture and water supplies (both studies were completed); 2) studies of possible environmental effects (a portion of the study was completed); 3) the legislative and legal aspects of weather modification (the study was completed); and 4) the societal aspects of weather modification. This last study was completed but under a subsequent NSF grant to the Illinois State Water Survey involving the design of an experiment on hail suppression (Changnon and Morgan, 1976).

The other major goals of PEP were aimed at discerning whether and how meaningful increases in precipitation could be obtained from the various cloud-rain systems found in Illinois during each season. The lack of prior concerted research in the Midwest dealing with the

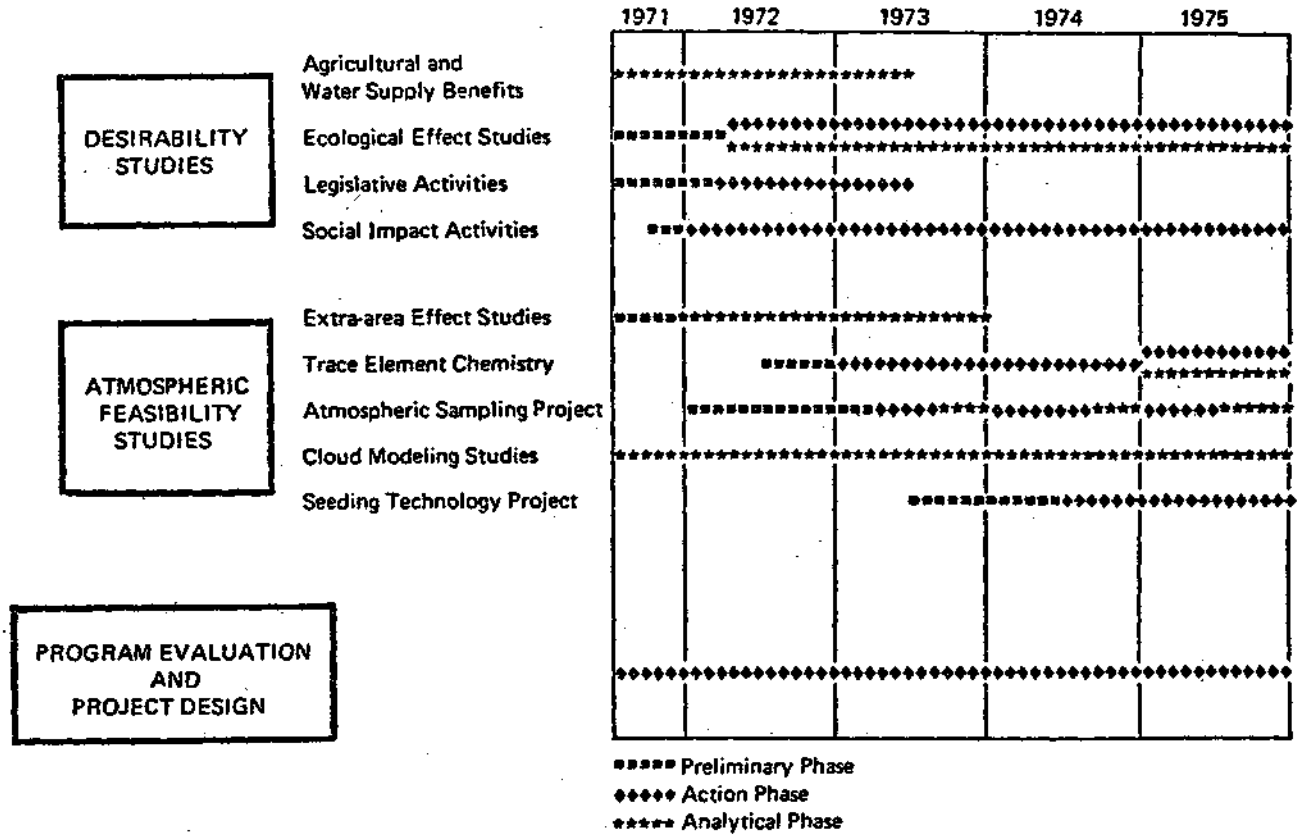

Figure 1. The original program schedule for the Illinois Precipitation Enhancement Program

feasibility question meant that several study areas were needed to answer this question. The five study areas (Figure 1) of PEP included 1) an atmospheric (aircraft-radar) sampling project (partially completed for only one summer); 2) seedability and modeling (cloud and mesoscale) studies which were partially completed; 3) a study of extra-area rainfall effects that might result from seeding (partially completed); 4) a trace element chemistry project relating to study of seeding materials (completed); and 5) a seeding technology project (no results obtained).

The tenth major activity area of PEP was the project integrative and design effort. The results of the nine specific study areas shown in Figure 1 were constantly reviewed as part of this effort. When major support for PEP ended in the summer of 1973, too little research had been completed to develop the design of a precipitation modification program for any season. In particular, the lack of cloud and rainfall studies using meteorological aircraft and radar in each of the various seasons precluded a meaningful design of a followup experiment. The inability to complete PEP, plus the need for the Survey staff to gain experience in performing an integrative design effort, were all factors leading to the Water Survey's decision in the late fall of 1974 to undertake the design of HIPLEX. In retrospect, this was a wise decision because it enabled Survey scientists to address all of the complex issues relating to the design of an experiment. This experience has served the Water Survey and the State of Illinois well as it develops the design of a future Illinois experiment.

Summary of the Desirability Studies of PEP

Study of Potential Effects of Weather Modification on Water Supply. An investigation was made of the potential benefits of enhanced precipitation and resulting increases in runoff on the alleviation of surface water shortages in Illinois (Huff, 1973). Runoff and weather data for 14 basins of various sizes of locations, and with records of 30 years or longer, were used to develop basin equations relating runoff to antecedent runoff indices, various precipitation parameters, and mean temperature. Hypothetical seeding-induced increases in precipitation were then used with the appropriate basin equation to obtain an estimate of average runoff increases in the cold season (October-March), the warm season (April-September), and two subseasons, December-March and July-August. This was done for all seasons combined, seasons having near-normal to below-normal runoff, and seasons with below-normal streamflow.

Results indicated that successful modification could result in substantial increases in runoff during near-normal to slightly below-normal years. However, substantial runoff would be difficult to achieve in drought years unless exceptional rainfall increases could be achieved. Previous hydrologic studies at the Water Survey

indicated that major benefits to water supply in Illinois would only result if substantial gains could be made in moderate to severe drought conditions. Consequently, it appears that the major beneficiary of weather modification in Illinois would be agriculture, and that future effects should be concentrated on weather modification applications in the growing season (Huff and Changnon, 1972).

A second investigation pursued concerned the potential of precipitation modification during moderate to severe droughts in Illinois to alleviate water shortages. This study involved time and space analyses of the natural precipitation distribution and consisted of two phases. The first involved analyses of monthly precipitation characteristics in major 12-month and 24-month droughts in the 50-year period, 1906-1955. The second phase was a detailed study of storm characteristics in the severe 1953-1954 drought. In the monthly analyses, emphasis was placed upon the areal extent and duration of temporary disruptions of the 12-month and 24-month droughts by natural precipitation occurrences. In the 1953-1954 drought, analyses were made of the frequency and areal extent of natural rainstorms of varying intensity, the distribution of rainstorms by synoptic weather types, and the diurnal properties of rainfall in the drought-associated rainstorms. All of these factors are of importance in evaluating both the potential for successful weather modification and the planning of any cloud seeding operations during droughts. Results indicated that conditions occasionally prevail in some moderate to severe droughts during which successful cloud seeding might provide temporary relief over portions of an extensive drought region, especially with respect to providing agricultural benefits. Successful modification of frontal storms, and both day and night success, would be essential in extensive drought situations.

Environmental Impact Study. The purpose of this PEP project was to determine the effect, if any, of several weather factors, and rainfall in particular, on six species of game animals in Illinois. This research effort was conducted by staff members of the Illinois Natural History Survey under a subcontract with the Water Survey. The research of the first game animal, the Eastern Cottontail Rabbit, was essentially completed, but the research on the other species was concluded with the general termination of most PEP research on 30 June 1973.

The completed research studied the relationships between Illinois weather and cottontail populations from 1955 through 1971 (Havera, 1973). The basic tasks undertaken were 1) the determination of relationships of monthly weather parameters to indices of cottontail abundance and harvest, 2) determination of relationships of weather parameters during critical periods of the rabbit's life cycle to rabbit harvest, 3) determination of the effect of total

precipitation on cottontail harvest, 4) determination of the relationships of crop acreages to cottontail harvest, and 5) the modeling of weather, crop, and cottontail data. A contiguous 68-county area within Illinois was examined. This area consisted of four "game regions."

Statistical analyses of monthly weather data with cottontail harvest and census data revealed several weather parameters were associated with fluctuations in cottontail abundance. The cottontail populations were apparently influenced by several weather factors during the same year, and the same weather factor affected the rabbit populations differently at various times of the same year. Generally, during the months of December, February, and March, snowfall was unfavorable to cottontail populations. Warm temperatures in January along with precipitation were weakly favorable to Illinois rabbits. During the spring, cottontails were unfavorably related to the percentage of possibel sunshine in March, and to warm temperatures and total precipitation in April. Cottontails reacted favorably to added precipitation and reduced sunshine in July. Minimum temperature in August was favorable. The number of days with precipitation ≥0.10 inch during September and October were negatively correlated with the rabbit data.

The weather parameter that had the greatest effect on cottontail harvest was total snowfall from December through March. Years of heavy snowfall, especially in February and March, tended to be related to a decrease in cottontails measured in the next fall. Heavy snowfall during the late winter months may decrease the breeding stock of cottontails, reduce their physical condition, and delay the onset of the breeding season, which may result in lessened reproduction.

Generally the magnitudes of the linear correlation coefficients between weather and cottontail parameters were well below the 5% level of significance.

The effects of monthly precipitation on the cottontail populations vary throughout the year. Positive correlations of population parameters with precipitation occurred in February, May-June-July, and November. Negative correlations of cottontail abundance indices with total precipitation occurred in January, April, and September-October. The most critical months for precipitation appeared to have been April and July. Precipitation in April was negatively related to the cottontail populations and precipitation in July was positively correlated.

Total precipitation during the period May through August was positively correlated with cottontail harvest and appeared more important than seasonal precipitation during any other period of the rabbit's life. Precipitation in the summer months has a

favorable effect on vegetation which is vital to cottontail nutrition, protection, and reproduction.

Based on data from 1956 through 1971, increased total precipitation in July and August that does not exceed normal limits would be expected to have little direct effect on the cottontail harvest. The number of days with precipitation ≥0.10 inch generally had higher correlation coefficients than total precipitation with cottontail populations in the summer months and during other times of the year.

Cottontail populations are strongly tied to the kinds of crops grown in Illinois. Corn and soybeans are significantly and negatively correlated with cottontail populations. Precipitation enhancement along with the recent high prices offered for cash-grain crops, would very probably influence farmers to increase corn and soybean acreage. This increase would result in a reduction of favorable habitat not only for cottontails, but for other wildlife species as well.

Legislative and Legal Activities. A systematic, well-planned activity primarily involving two staff members of the Illinois State Water Survey and Professor Ray J. Davis of the University of Arizona, as a consultant, led from the recognized need for a weather modification statute in 1971 through to its completion and enactment as state law in 1973 (Changnon, 1973). This 24-month activity to secure proper weather modification control legislation for Illinois is considered to be one of the primary achievements of PEP and the entire effort was state funded.

The activity began with an intensive literature review to determine the status of other state legislation and the legal aspects of weather modification; then a well executed development of a statute document using a national expert to write the basic document; concurrently informing the public and interest groups who in turn reviewed and altered it; and finally the implementation of the statute which was handled through the considerable interest of the Illinois Agricultural Association and then through the skillful handling of it in the legislature by the sponsors of the bill.

The termination of this activity has resulted in a weather modification permissive-control law that is considered to be a "model law" for state weather modification legislation (Ackerman et al., 1974). It is deemed to be the optimum type of document to secure the proper control leading to protection and benefit to the citizens of Illinois from weather modification in the future.

Social Aspects of Weather Modification. The general purposes of the Social Aspects Study were 1) to study public attitudes toward weather modification; 2) to educate and inform the people of Illinois about weather modification and PEP; 3) to consider various institutional needs and arrangements for weather modification in Illinois; and

4) to establish public relations channels which could be utilized before, during, and after a precipitation enhancement experiment is conducted. Extensive activities in this activity area initially were not envisioned to begin until 1973, pending results from other PEP tasks. However, several opportunities to describe PEP at meetings of civic, school, and agricultural groups occurred. Eighteen presentations were made on radio and TV shows in Illinois. Talks describing PEP were given at four scientific meetings. Over 15,000 copies of a special information pamphlet describing both weather modification and PEP have been distributed in Illinois since 1972.

Discussions were begun in 1973 with sociologists to perform a study of public attitudes. However, when the financial support for the PEP activities was essentially terminated, the social attitudes research could not be pursued. However, a Weather Attitude Sampling Project (WASP) was initiated in 1974 under NSF sponsorship to sample Central Illinois citizens so as to gain information 1) on the impact of weather on their lives, 2) on their attitudes towards hail suppression specifically and weather modification in general, and 3) their beliefs about institutional roles and control of projects (Changnon and Morgan, 1976). Such information was considered an essential part of 1) the design of any future weather modification experiment and 2) the advice given the State on the desirability and management of such a project. WASP was conducted jointly with the Human Ecology Research Services, a Colorado group experienced in sampling of public attitudes about weather modification. Sampling occurred in April 1974 using some 275 randomly chosen citizens from a potential project area of 5,000 km^2 in Central Illinois.

Basically, attitudes about weather and nature in Illinois are similar to those found in Colorado and South Dakota. Results for 6 of the 108 questions appear in Table 1. The majority, 54%, favored an experimental program, whereas only 33% favored an operational program. Answers to questions about successful weather modification indicated that 54% believed that moisture could be increased, but only 20% thought hail could be decreased. With regard to decision-making about weather modification, half, thought local residents should decide, but only 20% believed locals would decide. There also was a strong indication that the state, rather than the federal government, should and will decide on weather modification in Illinois.

Summary of Atmospheric Research of PEP

One-Dimensional Cloud Model Studies. The PEP required the use of a computationally simple and efficient one-dimensional cloud model for two aspects of the program. First, it was important for the development of a long-period climatology of seeding opportunities for the Midwest, as exemplified by Illinois. For this development, the selected cloud model was run on a large number of atmospheric

Table 1. Attitudes of Illinois citizens in 1974 towards weather modification issues, with frequency expressed as percent of the total in each column.

Position toward types of weather modification program			Can weather modification			Decision-making about experimental hail or rain program in Ill.		
	Experimental	Operational		Increase moisture?	Decrease hail?		Who should decide?	Who will decide?
Strongly Oppose	5	9	No	11	14	Don't Know	7	13
Oppose	16	19	Perhaps, doubt it	4	4	Local Residents	49	20
Neutral	25	39	Don't Know	31	62	Federal Alone	1	4
Favor	48	30	Think so	15	7	State Alone	28	44
Strongly Favor	6	3	Yes	39	13	State + Federal	6	8
						Scientists & Others	9	8

soundings, and the results were summarized to indicate the frequency and characteristics of large-scale environmental conditions that reflect positive seeding potential. Secondly, it was desirable to provide a forecast model for summer cloud-sampling flights and related field operations. This in-the-field model, by necessity, was designed to use minimal computation time so that the results would be available to the project forecaster for decision-making on a daily bases. A second requirement of this operational model was that it must be inexpensive to operate since the model calculations would be carried out at least once each day during a field program.

The cloud model selected to meet the above stated needs was a variation of that developed by Hirsch at the South Dakota School of Mines. It is basically a variation of the Weinstein-Davis model and incorporates the microphysical parameterizations proposed by Kessler. The model is steady-state and includes entrainment with options to specify sodium chloride or silver iodide seeding affects during cloud computations. The parameters required to initiate integration in the vertical include: updraft speed, updraft radius, cloud base, a vertical sounding of temperature and relative humidity, and wind speed.

The only available data for the climatological study included the vertical sounding of temperature, relative humidity, and wind speed which necessitated the arbitrary selection of the remaining parameters including updraft speed, updraft radius, and cloud base. The updraft velocity was fixed at a constant of 1 m s^{-1} for all calculations. The cloud base height was computed from the sounding by assuming that the moisture in the lower 100 millibars was thoroughly mixed and then raised conservatively along the mixing ratio line until it intersected the temperature sounding. Essentially, this determination of the cloud base height was equivalent to the convective condensation level. The calculation resulted in occasional extremely high bases when the lower atmosphere was dry.

Separate computations were made for updraft radii of 2,5 km and 5.0 km. This choice of radii was based on a preliminary experiment obtained with a similar model during the course of field work involving the release of tracer chemicals into convective clouds. It was found, after operating the model each day during a summer period, that the best correlation between predicted cloud tops and observed radar tops was the 5.0 km radius. Hence, the 5 km updraft radius was used in this study, but it was felt that since it was derived from data with a great many squall lines a smaller radius would be more appropriate for scattered storms.

For each input sounding, 6 separate cloud computations were made. These 6 computations included unseeded, salt seeded, and AgL seeded clouds for each of the 2 prescribed radii. These multiple computations for each sounding were intended to cover a reasonably broad range of physical processes and seeding potential under a wide variety of weather conditions.

The climatological study of seeding opportunities was initiated by obtaining radiosonde data for 4 midwestern stations covering the period 1953 through 1962. Data more recent then 1962 were not obtained because of the reported error in relative humidity observations which might negate any conclusions from their use. The period chosen for the study included the drought years of 1953-55 in Illinois as well as the subsequent wet years of 1957-58. Fundamental differences of large-scale environmental conditions between dry and wet years were expected to be depicted by the cloud model computations.

The radiosonde data were available in 2 separate forms, standard level data (each 50 mb in the vertical) and significant level data (points were the vertical gradient of temperature or humidity changed dramatically). The model computations required the merger of these 2 sets of data when ever significant level data were available. The central Illinois station was located at Rantoul and operated by the U. S. Air Force Air Weather Service early in the period, and was subsequently moved to Peoria with operations carried out by National Weather Service personnel. The Air Weather Service radiosonde stations were not required to record significant level data for archival purposes and, consequently, input data for the cloud model consisted of a minimum vertical resolution of 50 mb.

The one-dimensional cloud model applied to 10 years of soundings for Peoria produced a printout for immediate use and a tape for permanent recording of the following data: precipitation, duration of precipitation, cloud base height, cloud top, base temperature, top temperature, maximum vertical speed, height of the maximum vertical speed, freezing level, depth and windshear between cloud base and -20°c, and between cloud base and cloud top, and several other parameters.

The primary results from the climatological study were reported by Huff and Semonin (1975) with a direct application to the problem of seeding potential during moderate to severe droughts in Illinois. On average, during the agricultural year between May and October there are a fairly large number of opportunities which present themselves for seeding operations. During the intense part of the growing season between June and August, approximately 30% of the days are predicted to produce clouds of sufficient depth and top height for application of current seeding technologies. During moderate to severe drought periods, as shown by Huff and Semonin (1975) , the frequency of the predicted cloud occurrences is somewhat below the expected 10 year value. However, seeding each opportunity during such dry periods is a possible means of lessening the impact of drought on water resources for agriculture,

Two-Dimensional Cloud-Scale Model. A complex two-dimensional, time-dependent, cloud-scale numerical model that depicts atmospheric convection and cumulus development in a vertical cross-section of the atmosphere is necessary to fulfill certain requirements of PEP. This work was pursued by Dr. Harry T. Ochs and Dr. Ben Ceselski.

The specific area of interest to Phase I of PEP was the application of this model to the determination of the extent and magnitude of the possible extra-area (downwind) effects of planned weather modification. The development of a sophisticated cloud model was initiated to meet this requirement. The model included a sufficiently large domain to allow the inclusion of more than a single convective element. Thus, seeding in one cloud could be simulated and the resulting effect on an unseeded neighboring cloud could be studied. The results of these model experiments could then be parameterized in a three-dimensional meso-scale model to determine the extent and duration of any broader scale extra-area effect.

The two-dimensional cumulus cloud model was also conceived to be used in other important ways. Seeding in various portions of a cloud could be simulated and a determination of the most effective seeding locations could be made. Similar investigations could be accomplished with respect to the optimum stage of cloud development that should be seeded. The effects of over- or under-seeding on the life cycle of clouds and their efficiency in producing precipitation could also be studied.

Significant headway was made towards the development of a two-dimensional model that meets the requirements of PEP. However, the cessation of the PEP program necessitated termination of the work before all aspects were included in the model.

The accomplished research centered on the extensive testing and evaluation of current mathematical techniques. A new and accurate time and space differencing formulation was incorporated in the model. The calculations which were completed depicted realistic moist convection in the atmosphere. The only area in this effort to date that may require future study is the incorporation of a non-linear eddy viscosity. There are schemes available which appear to be directly applicable to two-dimensional cumulus cloud models.

The greatest possible gain in future efforts would be achieved if a suitable microphysical description of in-cloud processes were incorporated. At the point at which work on the two-dimensional cloud scale model was terminated this inclusion was underway.

An ambitious and potentially extremely fruitful choice of microphysical schemes was made. Instead of breaking the liquid water into just cloud and hydrometeor water, a complete spectrum was envisioned. As a part of the description of the warm rain process condensation nuclei and water drops, as well as calculatipns of stochastic collection was included. If this general approach was extended to the ice phase of a cloud, the complete description of cloud processes would follow and quite realistic seeding experiments could be conducted numerically. The value of the achievements at the termination stage of the modeling effort was primarily recognition of its future potential.

Three-Dimensional Modeling. It was anticipated that one of the desired goals to pursue in PEP was the development of a three-dimensional cloud model that was sufficiently large to include more than one cloud. This type of model would have a grid spacing of about 100 m and would represent an extension of the two-dimensional model described in the previous section. A large-scale three-dimensional model that had been used previously in tropical studies was available as a research tool. The model, integrated with grid intervals of Ax~170 km, had demonstrated skill in simulating subsynoptic-scale bands and regions of convection in tropical disturbances.

Although it was not obvious what the optimum grid interval to use in studying convection over the continental United States would be, the potential benefits of such a study were clear. If the model was capable of predicting the occurrence of convection in time and space, it could be useful both prognostically and diagnostically. If successful, the model could eventually be used in conjunction with field operations. The efficiency of a field operation could be significantly improved by using a forecast of the type and intensity of convection during a particular day. The forecast would have advantages over a one-dimensional forecast because the model is time-dependent and includes effects of the large-scale three-dimensional dynamics.

The model-generated data can be studied diagnostically to examine energy exchanges between the meso-scale and large-scale flows. Such mechanisms as convective energy 'feedback' to the large-scale should be reasonably well understood before any attempts are made to alter the meso-scale disturbances (squall lines, etc.) by seeding.

This modeling effort would also interact with the two-dimensional modeling task in terms of the method of parameterizing convection. Simulated seeding experiments in the two-dimensional model would help define the parameterization of a seeded-cloud in the three-dimensional model. In this manner, seeding and its effects in time could be simulated. An extra-area seeding effects study is an example of the type of work that could be pursued. Based upon two-dimensional cloud model computations, a squall-line previously predicted in a large-scale forecast, could be seeded at a particular point in time in a second large-scale forecast. The effects of simulated squall-line seeding in the large-scale prediction could be examined with respect to line intensification or dissipation. The first integration with no seeding would serve as a basis for comparison.

One preliminary connective case study and integration was made before the termination of this PEP task. Based upon considerations cited in the previous paragraph, the grid interval used was ~170 km which insured that the full grid covered an adequate total area. The object was to examine model-capabilities of simulating organized convection over the United States, Dr. Ceselski pursued this research.

Results of this preliminary primitive equation forecast were encouraging. Qualitative agreement between model-computed and radar-observed convection was found. This agreement is believed to be due to the following analysis and predictive procedures: (1) the careful subjective analyses of weak systems defined in the initial wind data; (2) the use of an initialization scheme that retained those systems; (3) the use of an advective scheme that maintained the energy of the weak systems in time; and (4) the incorporation of a cumulus parameterization scheme that simulated the first order effects of cumulus energy feedback to the large-scale. These procedures allowed the evolution of weak fields of large-scale low-level ascent that produced convection in the model.

Although somewhat speculative after a single forecast, there appeared to be a correlation between the location of maximum predicted convective heating and observed severe convection (tornadoes, hail, heavy rain, etc.). More case studies were planned at the termination of this activity.

The results from the first attempt to use a three-dimensional model to eventually diagnose extra-area effects from seeding were sufficiently successful that additional effort should be directed to this task. Admittedly, the use of such a model for operational forecasts is remote, but its use to address the questions associated with the seeding of meso-scale systems justifies further model development.

Extra-Area Effects on Precipitation. Two climatic investigations concerning detection of precipitation shifts beyond a target (modified) area were pursued. In the first investigation, monthly and seasonal precipitation data were used to study the natural distribution of highs and lows in the precipitation patterns over a 325,000 mi^2 area centered in southern Illinois during the period 1950-69. The highs were studied in regard to their location, spacing, frequency, and persistence. Overall, the most frequent distance between highs is in the range of 40-60 miles. However, on 1-yr and 5-yr patterns the mean distance is in the range 75-95 miles and when the mean distance is determined in a directional sense (downwind) the mean distance is 100-117 miles. The mean distance between persistence areas and preferred locations of highs is approximately 60 miles. The implication of the natural distribution study is two-fold: 1) the mean and median distances between natural occurring precipitation highs in the Midwest are in the range of downwind highs reported caused by seeding; 2) the broadness of the correlation patterns between points in a pattern indicates that one must be very cautious when postulating extra-area effects out to distances as great as 300 miles from the target in weather modification experiments.

The second investigation concerned the monthly and seasonal precipitation patterns (1950-69) in and downwind of large cities having urban-induced increases in precipitation. Overall the results indicated that the urban effect is limited to 50 miles of the city, and that no downwind effect occurs beyond 50 miles. There was also some indication that rainfall deficits tend to occur in the

neighborhood of excesses. In addition, the individual storm patterns in and downwind of St, Louis were investigated in most detail using 1972 METROMEX data. The analysis indicated that the major effect occurs within 0-25 miles with a smaller increase in the area 25-50 miles of the city. However, the storm analysis was based on a 1-yr sample only, and additional data and analyses are required to confirm the storm results. Both studies are described in technical report published in 1973 (Schickedanz).

Trace Element Chemistry Project. The purpose of this work was to measure "background" concentrations of silver (Ag) in the proposed seeding area, Jefferson and Marion Counties in southern Illinois. Such an assessment of current conditions was needed 1) as a baseline for comparison against Ag concentrations in precipitation during future cloud-seeding operations, and 2) to evaluate the feasibility of using the Ag content of precipitation to identify precipitation treated by seeding material.

Sampling was carried out from December 1972 to May 1973 at 5 sites in southern Illinois, Volunteers collected precipitation at 4 of these sites and water from the Big Muddy River at the other.

Because Ag in water solutions tends to deposit on container walls, a special chemical method was developed to insure stability of the water samples. The analysis method was reported by Rattonetti (1974) and has been adopted toy other laboratories for silver analysis.

The results of Ag analyses on the samples are summarized in Table 2 and were presented by Gatz (1975). The rainfall-weighted mean concentration of 73 ng/liter in precipitation is somewhat higher than the 20-50 ng/liter mean concentrations observed in non-seeded precipitation in the western United States. However, comparison of Ca/Ag ratios expected in precipitation and upwind soils suggests that wind-blown soil dust could account for the higher concentrations.

The observed concentrations are probably not sufficient to interfere with the identification of precipitation from seeded convective clouds. Even if difficulty was found in using the absolute Ag concentration as such an indicator, another more sensitive method using element ratios is available.

Study of the Feasibility of Precipitation Enhancement, An integral part of PEP was the Atmospheric Sampling Project which had, as its primary objective, the assessment of the physical potential for the modification of rainfall in Illinois, To achieve this objective, a multi-season research program was developed which had as its focus the establishment of population statistics of the cloud variables important in the precipitation process. The key

Table 2. Summary of results —- Ag in precipiation and river samples, Jefferson and Marion Counties, Illinois.

Station	Sample Type	Number of Samples Collected	Number of Samples Analyzed	Mean Ag Concentration, ng/liter	
				Arithmetic	Rainfall-Weighted
Centralia	Precipitation	7	4	37	14
Forbes	Precipitation	35	31	103	98
Ina	Precipitation	32	28	99	71
Mt. Vernon	Precipitation	34	19	80	69
Total	Precipitation	108	82	93	73
Walton-ville	River	24	24	70	--

element in the program was a field experiment in which a number of cloud and environmental parameters were to be measured by aircraft, radiosondes, and radar. Data collection was originally planned for periods in each season of the year, but the loss of funding resulted in only one field season, the months of June and July in 1973. The reduction of support in 1973 also required that the experiment be carried out in southwestern Illinois and eastern Missouri (rather than south-central Illinois as originally planned), so that the existing ISWS facilities of METROMEX could be utilized as support. These facilities included two radars, a dense recording raingage and hailpad network, and radiosonde and pibal networks.

The data acquisition in 1973 focused on the cloud dynamical and bulk microphysical characteristics by aircraft. Data were collected during eighty-nine flight hours on 36 flights, between 5 June and 31 July 1973, Cloud penetrations were made on 24 of these flights. On eight days with suppressed cloud conditions, flights were devoted to the measurement of ice and cloud condensation nuclei near cloud base.

A wide variety of clouds were studied during the flight program, ranging from families of towering cumuli to thunderstorm feeder clouds. The operations involved a mix of multiple penetrations for cloud cycle documentation and single-pass sampling for a census study. Most of the cloud penetrations were made near the freezing level; the high incidence of static charge buildup on the airplane at higher altitudes resulting in shorting of a key electronic component in the data system did not permit cloud penetration at colder temperatures. Cloud condensation nuclei measurements were made just below cloud base level. On most flights airplane soundings were made in the vicinity of the cloud area being worked.

The analyses that have been carried out emphasized the study of the water substance near the freezing level, and its partition between vapor, cloud particles (drop diameters less than about 70 μ) and incipient or existing precipitation particles. The significance of these analyses is twofold. Firstly, since the cloud penetrations were made between +2 and -5°C, the total liquid condensate specifies the maximum amount of latent heat (and therefore additional buoyant energy) that can be realized by inducing freezing or initiating the Bergeron process through seeding. Secondly, the relative fractions of the condensate in cloud (small drop) water and precipitation (large drop) water, along with the calculated "adiabatic" water provide a measure of the natural efficiency of the coalescence process.

The clouds penetrated, all visually classified as vigorous, had bases near 1200 m MSL (18 to 20°C) and tops estimated between 5200 and 7500 m at the time of entry. Approximately 75% to 85% of the condensation expected from a unit volume in ascending from cloud base to observed cloud top would have occurred by the time the volume reached the measurement level of 600 mb (4450 m).

As a group, the total water contents (as measured by the Naval Research Laboratory total water meter) were significantly higher than that cited for most previous measurement programs. This could be a reflection of the limitations of most other liquid water content meters, which have upper limits of 5 to 10 gm/m^3. The NRL total water meter which was used in this program first evaporates all the condensate and then senses the vapor of the air sample. Thus, the limitations are only those of the evaporator — roughly 16 to 18 gms/m3 at the air speeds used. An overall accuracy of about ±20% is cited by the developer Dr. R. Ruskin, of the Naval Research Laboratory. However, there are two possible sources of error stemming from a) the identification of zero-base for clear air (all vapor, no condensate), and b) the sampling volume. The former is done for each flight altitude and is based on the clear air reading of the dew-point hygrometer. A recent review of the data suggests that the hygrometer calibration used in the data reduction may have been slightly in error. However this would represent a relatively small bias in the condensate calculated and would not significantly change the indications concerning the partition of the condensate. The sampling volume presents a more difficult problem (Smith, 1976; Kyle, 1976), Because of the small sampling volume there could possibly be an overestimation of water content due to the bias introduced by infrequent large drops. When averaging across the whole cloud this error is probably small, if only one or two large drops are encountered. When there are many such large drops in the cloud volumes, sampling may *underestimate* because of the small sampling cross-section.

Individual cloud penetrations *invariably revealed a complex structure,* so often documented by aircraft measurements, but so difficult to deal with numerically. Most visual cloud masses were composed of two or more well-defined cloud units. The approach has been to consider the cloud "unit" rather than the visual cloud as

the entity of interest. However, categorization of cloud types was based on the *visual cloud mass.* Five types have been defined. Two categories are predominately "isolated" entities: a) towering cumulus and cumulus congestus, b) cumulus congestus showers and small cumulonimbus calvus. There are two types associated with large thunderstorms, c) nearby cumulus congestus, and d) "back feeders," i.e., towering cumulus to cumulus congestus nestled close to the rear side of the trunks of a large thunderstorm. The fifth cloud type e) covers towering cumuli and cumulus congestus imbedded in extensive, supercooled, alto cumulus layers.

Analyses have dealt primarily with the population statistics for the condensate near the freezing level, stratified by cloud type and activity (i.e., draft velocity). The results of analyses of nearly half the flights indicate the following:

1. The total condensate (when compared to adiabatic) tended to be greater in cumulus congestus clouds and small cumulonimbus than in other cloud types, including thunderstorm feeder clouds.

   As a corrolary, the fraction of cloud units in which the measured condensate was in excess of the adiabatic water content was large for air mass showers than for thunderstorm feeders. As might be expected, when the average total liquid water content in the cloud unit was greater than the adiabatic value, the cloud water fraction tended to be smaller, than when it was less than the adiabatic water,

2. On the average, around three quarters of the condensate in isolated cumulus congestus showers and small cumulonimbus was in precipitation particles, whereas in "back feeders" well over half of the condensate was in cloud particles, In general, in the system-associated convective clouds the condensate was more evenly divided between cloud and precipitation particles than was true in the isolated "single" cloud systems,

3. In general, both the average cloud and precipitation water contents were higher in updraft areas than in the cloud as a whole, but the partition of the total condensate was about the same. In most cases peak updrafts, as determined from airplane rate of climb, were between 2 and 10 mps, although updraft speeds up to 25 mps were encountered.

4. The *cloud water* content, normalized by the adiabatic value, tended to be similar in magnitude to that reported by other researchers for other areas. However, as indicated above, the total liquid water content, similarly normalized, tended to be considerably higher than previously reported.

A number of other exploratory or preliminary studies have been carried out. A single case study of a cloud system in which new cells continuously developed on the "back" side i.e., on the side opposite to that in which the cloud cells were moving, indicates that the development of vigorous new cells may also cause a short pause in the decay of older cells. A preliminary review of a few multi-penetration cases which provide documentation of the spread of the rain shaft through the cloud, the depletion of the cloud water, and the destruction of the updraft, suggests an evolution similar to the Midwest thunderstorm cell model. Preparatory work has been done for other studies also; e.g., techniques have been developed for correcting the locations of cloud penetrations for analyses relating internal cloud parameters to radar echo characteristics.

HIGH PLAINS EXPERIMENT PROJECTS

The Design Framework for a Comprehensive Program

The Water Survey took a broad approach in developing a design for HIPLEX. We considered both the socio-economic and meteorological aspects of the program. The essential features of a design for the overall program, which was submitted to DAWRM in July 1976, (Ackerman et al», 1976) are briefly summarized here.

At the time that the Water Survey (ISWS) undertook the design task in 1975, DAWRM had identified the convective rains of the growing season as the target for the modification effort. In the course of some two years of DAWRM planning, organization of field activities, in-house research, and selection of research sites and equipment types, the following critical decisions had been made:

1. A single cloud seeding experiment which included evaluation of surface rainfall should precede an areal experiment, in order to increase our understanding of the physical changes in cloud and precipitation brought about by the seeding.

2. The whole of the High Plains, from Texas to Montana, was identified as the experimental region, with field research to take place in areas centered in western Texas, northwestern Kansas and eastern Montana.

3. 5-cm radars had been procurred as a key tool for evaluation of seeding effects on rainfall as well as for research.

These, as well as other prior decisions, were re-examined by the ISWS as to their appropriateness for the program as it was understood by the design group.

There is little disagreement that the physical processes affected by seeding can be studied more effectively in (relatively) simple systems such as a semi-isolated convective cloud. However, the need for a full scale seeding experiment on such clouds is sometimes questioned because the rain they produce represents a very small fraction of the seasonal areal precipitation. Although the overall economic impact of the augmented rainfall has not been determined, a scientifically-oriented single cloud experiment will contribute to the development of a more efficient area-wide experiment by shedding light on the mechanisms by which the precipitation may be modified. Thus, the single cloud experiment

was judged a viable approach for meeting the ultimate goals of HIPLEX and was the focus of the initial effort by ISWS in HIPLEX.

The extensive regional commitment presents a tremendous task and an overwhelmingly expensive one. Although the precipitation climatology of all of the High Plains is similar, it is not at all clear from the information readily available that the rain-bearing weather systems are the same throughout the region. There is also a good likelihood that significant differences exist in cloud characteristics as well as in agricultural and economic interests. In order to attain the goals of HIPLEX, the program should be comprehensive, and universal in the sense that it is applicable to any part of the High Plains. It becomes site specific as a detailed design and work plan are developed, based on local meteorological, economic and sociological conditions. If resources are not sufficient to carry out the comprehensive program at all three sites, it should be implemented at one, primary experimental site, in lieu of diffusing the resources and mounting subcritical efforts at two or three locations. If funds are insufficient to carry out the full program well at other than the primary location(s), the efforts at the other site(s) should be directed toward the collection of the critical measurements needed for establishing transferability. The primary site should be carefully selected, with local meteorological and cloud conditions and representativeness for the High Plains given priority consideration.

The evaluation of seeding effects on surface rainfall in the single cloud experiment puts great demands on the precipitation measurement system. A combined system of radar and raingages holds the potential for providing adequate coverage and accuracy. Two main problems have to be addressed with regard to radar: 1) an assessment of the effect of attenuation of 5-cm radar waves on the radar's ability to measure rainfall, and 2) an assessment of numerical techniques by which a radar-raingage mix can provide the necessary rainfall measurements for HIPLEX. Studies addressing these points have been carried out at ISWS and are discussed in the sections starting on pages 182 and 239.

The ISWS design incorporates a sequential scientific approach to define the capability 1) to enhance the precipitation from individual clouds, and then 2) to enhance the precipitation over an area as a consequence of the augmentation of all convective precipitation. The recommended program consists of two components: an atmospheric effort and a socio-economic and environmental effort. The experimental components are divided into phases consistent with the sequential approach. The parallel efforts are essential for the full realization of the scientific and socio-economic potential of the program.

The key aspect of the atmospheric component is the sequential experimental approach based on sound scientific research. A shift from background and field studies of clouds and precipitation to a

series of proof of concept experiments (POCE) *should occur only when critical unknowns are removed, allowing physically sound hypotheses appropriate to the High Plains to be developed and tested.*

The atmospheric effort (Fig. 2) has three overlapping phases. Phase 1 covers exploratory and background studies. These studies are of two types. One is problem-oriented and addresses the major components of rain modification experiments, namely, the formulation and selection of modification hypotheses, selection of modification techniques, prediction of the consequences of treatment, identification of conditions suitable for manipulation of the precipitation process, and measurement and evaluation of alterations. At the outset, it was found that most of the cloud, precipitation, and weather system climatologies and the information on cloud characteristics needed for development of a specific design for a seeding experiment were not available. Immediate undertaking of such background studies was strongly recommended to DAWRM.

The second type of background studies is concerned with basic research which is needed to increase our knowledge of the natural and modified physical processes. These should include both empirical and modeling research and should continue throughout the duration of HIPLEX.

Phase 2 is concerned with the establishment of an acceptable level of scientific certainty of the consequences of modification efforts on relatively simple, semi-isolated cloud entities. These entities may be single or multi-cellular, of limited horizontal extent and separated from other such entities by significant distances, e.g., one or more cloud diameters. *Provision must be made for monitoring physical characteristics of cloud as well as precipitation and there must be continuous evaluation using both physical and statistical principles.* Moreover interactions between seeded and unseeded cloud entities and effects on other cloud groups should be monitored in preparation for Phase 3, the area experiment. Additional details of the design of the single cloud experiment are given in the next section.

The area rain modification experiment (Phase 3) is concerned with developing an overall level of confidence in producing a net benefit over an area from efforts to modify cumuliform clouds, semi-isolated or embedded in systems. Progression from Phase 2 to Phase 3 depends on attainment of the goal of Phase 2, i.e., reaching an acceptable level of certainty that the outcome of the deliberate modification was as expected. Ultimately the decision as to what is an acceptable level must rest with those who will be running the risk of being wrong, namely DAWRM. It is the recommendation of the design group that HIPLEX advance to Phase 3 only when the most sensitive of the statistical tests that can be devised show significant results and these results are supported by physical theory.

COMPONENTS OF HIPLEX - RAINFALL ENHANCEMENT

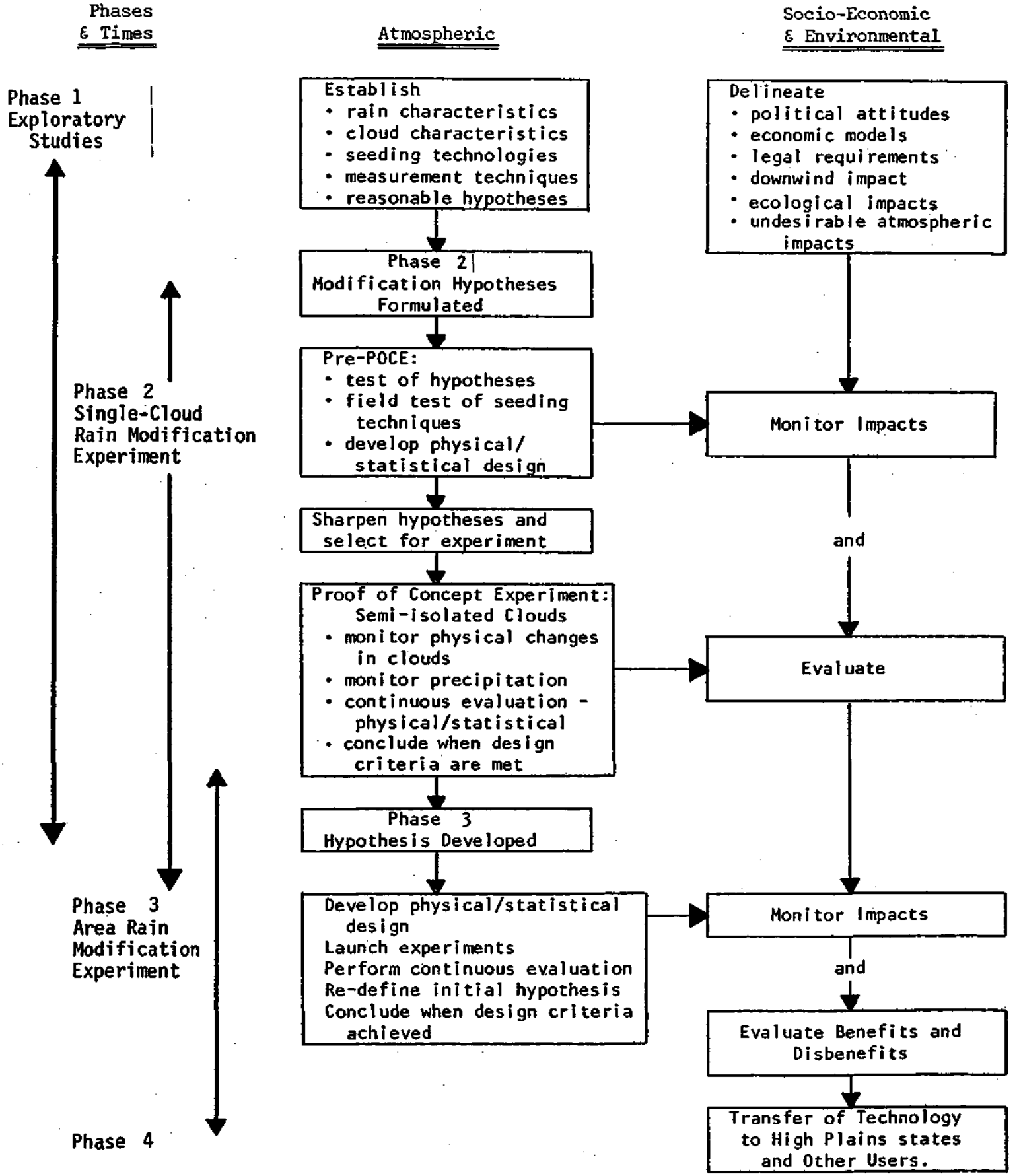

Figure 2. Flow of experimental effort in HIPLEX.

Phase 3 should include monitoring of physical characteristics of cloud *systems* as well as a precipitation, with monitoring of changes in individual clouds at a much reduced level. Monitoring for seeding effects should be extended to areas around and downwind of the target area, in order to detect extra-area effects, if any. Exploratory studies leading to Phase 3 should be initiated as soon as feasible, and well before the end of Phase 2.

A fourth phase involves the transfer of the developed technology to all areas in the High Plains where meteorological studies indicate it is applicable and socio-economic studies indicate a net benefit.

Concurrent with all four phases of the meteorological effort, there should be an integrated series of activities 1) to assess the various impacts of the weather modified by HIPLEX, 2) to inform all interested parties of the activities and consequences of the experiment, and 3) to conduct the experiments within a proper social, legal, and environmental framework. Proper integration of local and regional individuals and groups in the experiments, including certain operational decisions, will sustain public and scientific acceptance and will ultimately lead to much more effective technology transfers.

It is important that the planning for the atmospheric research, and in particular field operations and data collection, be done in conjunction with the planning for the data collection for the Social, Economic and Environmental Studies (SEES). The environmental studies include such factors as the measurement of silver in water supplies and in ecosystems, and ecosystem response to increased rainfall. The social studies include studies of social attitudes as well as administrative and legal factors ranging from liason with other modification projects in the area to developing mechanisms for dealing with potential alligations of liability. The economic studies deal with all aspects of the regional economy. SEES should be phased also and include both background studies involving existing information, model simulations, and field studies.

An overview of the meteorological activities and SEES and how they should interrelate in time is shown in the flow diagram in figure 3. The interactions of the meteorological experimentation with users and public are shown on the left, whereas the interactions of the SEES with the users is shown to the right.

Frequent - and open - communication with potential users and other interested parties should be practiced. It is important to inform the local people about the project and to involve them in key decisions to the extent possible. Past sociological studies generally point to a favorable public attitude towards weather modification prior to experimentation. They have revealed that the majority of the public tends to depend on key local (township, city, and county) decision makers for opinion development. In the

early stages of the project at any one site, these key people must be identified, and then systematically informed about all aspects of the experiment.

There are also non-local interests among the potential users of the project results. These include affected businesses (the weather modification industry among them), scientist, agricultural interests and various government entities. Channels for distribution of pertinent information to these groups must be found and kept open during and subsequent to the projects.

The SEES may be divided into four task areas. The *environmental task* area is concerned with the impacts on both the target and extra regional area of the seeding material, of the altered rainfall and of possible second order effects on the weather. *Administrative-legal tasks* relate to keeping the project within a proper jurisdictional-legal framework. *Social tasks* largely involve monitoring of public attitudes. *Economic tasks* are the most extensive of the four topical areas. They involve modeling of benefits and losses from altered weather, cost assessments, and site and regional studies of responses.

A final activity of the SEES effort area (Fig. 3), in Phase 4, will involve designing the best possible measurement systems, the drafting of suitable regulations, and summarizing the economic aspects, all as input into the total design of an operational project.

HIPLEX: The Single-Cloud Experiment. A design framework for a single cloud experiment has been provided to DAWRM, for use in developing the final, detailed operation plan. The basic background data needed for the design was, in many cases, not available so that in some instances the design may have to be changed as more information becomes available.

Key elements in a seeding experiment are 1) the modification hypothesis, 2) the seeding technique, 3) the statistical (randomization) design, 4) monitoring and evaluation of effects, 5) operations needed for implementation. The goal of the experiment is, of course, to increase the productivity of the clouds. The productivity of a cloud (the amount of surface rainfall) can be increased by increasing the amount of vapor transported into the cloud system or by increasing the efficiency with which the cloud converts vapor to precipitation. It is important to realize that an increase in efficiency does not necessarily increase productivity. For example, if increased efficiency brought about by treatment is accompanied by a decrease in the active lifetime of the treated cloud so that, overall, less water vapor is processed, the productivity could conceivably be decreased. Conversely, if an increase in productivity is due to an increase in the amount of vapor drawn into the cloud, there may be no change, or even a decrease, in cloud efficiency.

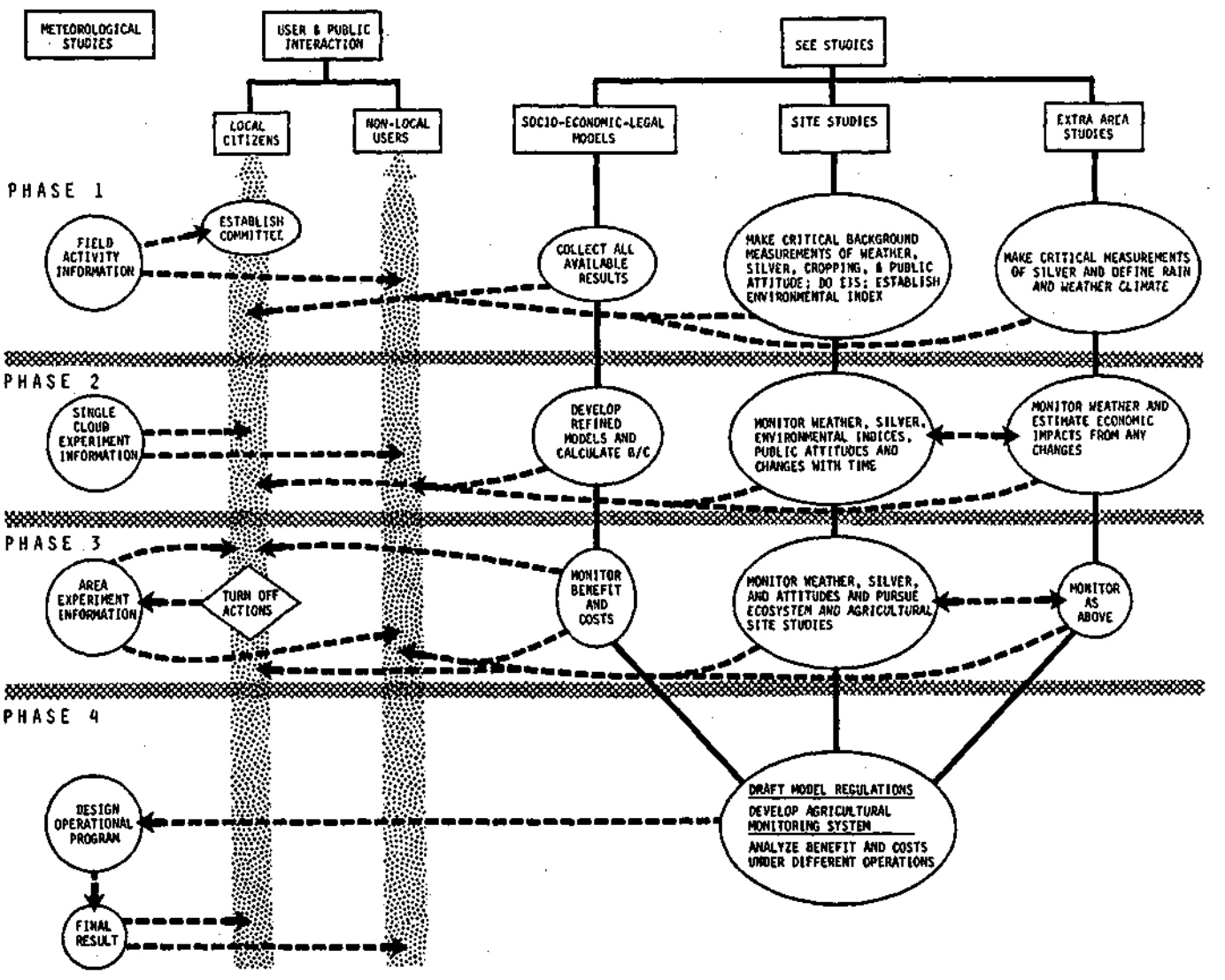

Figure 3. Flow diagram providing an overview of the impact and information activities and their interaction.

Most seeding hypotheses are based on the assumption that the production of precipitation from a suitable cloud (system) can be increased either by adding large condensation nuclei (CCN) to speed up the warm-rain (coalescence) process, or adding artificial ice nuclei (IN) at an appropriate temperature level to start the cold-rain process. The sequence of events following the development of the large drops due to treatment with either large CCN or IN may take a number of paths, most of which are poorly understood. As a consequence, any number of physical hypotheses can be developed covering the chain between the introduction of additional nuclei into a cloud and subsequent precipitation at the ground.

It is obvious that the number of hypotheses must be limited if the experiment is to be of reasonable length. Thus, a hierarchy of hypotheses were screened for the following factors: 1) suitability for the cloud populations in the area, 2) accumulated body of knowledge regarding techniques, 3) accumulated body of knowledge regarding the outcome of modification attempts, both operational and experimental, and 4) logistic requirements.

Background information on the characteristics of the growing-season clouds in the High Plains is very limited. A conceptual model based on cloud features distilled from somewhat fragmentary information available from early 1975 field analyses and from other projects in the Plains States was used for screening modification hypotheses. Modification of the cold rain process was found to be favored over modification of the warm rain process on all four factors listed above. As a consequence the design recommends that the seeding experiment be based on the manipulation of the ice process by increasing the number of available ice nuclei active at lower (warmer) levels in the cloud.

There are two modes by which the ice process can be modified. In one, light to moderate seeding rates (static seeding)leads to the production of a relatively small number of ice particles (e.g., 1 to 10 crystals/liter at -10°C) which can grow rapidly by sublimation into 100-μ precipitation "embryos" which then collect smaller particles lying in their fall paths. The second method uses massive seeding to produce over 100 crystals/liter throughout the supercooled cloud, thus releasing large amounts of latent heat. This leads to increased buoyancy, an acceleration of the updraft, greater cloud growth, increased inflow of water vapor, and greater precipitation. This is known as dynamic seeding.

A modification hypothesis based on static seeding has been recommended as the primary one for testing in the single cloud experiment. The efficacy of dynamic seeding in the High Plains has been questioned because the limited frequency of environmental conditions favorable for significant artifically-stimulated cloud growth or because of the probability of overseeding and loss of condensate to the cirrus outflow. Nevertheless in the absence of

key pieces of information about cloud structure, the concepts of dynamic seeding have not been rejected since it may prove to be the more productive method for rainfall enhancement. Thus, a second *hypothesis based upon massive seeding for major dynamic enhancement has also been tentatively proposed for testing, to be included in the seeding experiment if environmental thermodynamic data and cloud measurements in the pre-POCE period indicate that it may be a fruitful approach.*

The artificial transformation of cloud particles from water to ice at relatively low (but subfreezing) levels of the cloud can be effected 1) by injecting artificial nuclei or 2) by lowering the cloud temperature to the point where natural nuclei will be activated or homogeneous nucleation will occur. The latter, which has been tried in a few exploratory and experimental programs, has some advantages, e.g., problems of "contamination" of other clouds, surface waters or the ecosystem due to artificial nucleation agents are removed. But, there are disadvantages also and it is not clear that cooling will be an economically-feasible operational technique. From consideration of the same factors by which the hypotheses were screened, the cooling technique was rejected in favor of injection of artificial nuclei, specifically silver-iodide. Of course many uncertainties still remain about the use and efficacy of silver iodide, ranging from the technology of generation to the subsequent diffusion and true activity in the atmosphere. However, these problems have been identified and the attack for their solution has begun.

For massive seeding leading to rapid glaciation, injection of the seeding material directly into the turret near its summit is probably the most effective since conversion can be initiated through a deeper layer in a shorter period of time. For static seeding, injection into the inflow areas or updrafts just below cloud base is favored because it provides more time for natural diffusive processes to disperse the material. However, if identification of the cloud inflow or updraft proves too difficult, the material should be injected just below actively growing summits.

Exploratory studies which should shed some light on some of the uncertainties surrounding silver iodide seeding have been recommended and final decision on technique should await the findings of these studies.

The modification hypotheses which have been formulated for both static and dynamic seeding trace the effects of seeding with artificial nuclei through the modifications expected in microphysical and dynamical characteristics of the cloud which would lead to increases in surface rainfalls At many critical points, the hypothesized sequence of events is based more on speculation than scientific deduction either because of lack of information or because available evidence is contradictory. Nevertheless these

hypotheses, and some qualitative predictions they imply, present strawmen to be pretested, corrected and refined on the basis of observations of naturally occurring phenomena and computer simulations using appropriate numerical cloud models and environmental and cloud conditions common to the High Plains. Refinement of these hypotheses must continue throughout the single cloud experiment in order that the hypotheses formulated for the area experiment have the firmest scientific foundation possible.

The hypothesized effects in the physical characteristics of the cloud must be evaluated as well as the rainfall if the goal of reduction in scientific uncertainties is to be achieved. Since the predictions of the magnitude of these effects, by whatever method, are of low or uncertain accuracy, statistical comparison of seeded and unseeded samples is an absolute necessity. Thus, the statistical design for the experiment is very important. The preliminary statistical design, developed at the ISWS on the basis of Illinois data is summarized later in this report.

Many parameters have been identified which may be useful in trying to judge the effects of seeding on cloud and precipitation processes and on rainfall. All are capable of measurement with available technology, albeit with varying degrees of accuracy and coverage. Some of the parameters are diagnostic, indicative of cloud structure and cloud processes. Most of these were selected to permit evaluation of the hypothesized changes and/or to shed light on some critical uncertainties. Other parameters were included either because there have been indications of modification in other seeding projects or because there is a likelihood that they might be modified. Variables considered critical and measurable by ISWS have been identified. Others will no doubt quickly fall out early in the experiment either due to obvious lack of sensitivity or to crudeness of measurement.

The evaluation of the effect of seeding in surface rainfall is critical for determining the economic benefit. The measurement of rainfall by a combination radar-raingage system has been studied by ISWS and is discussed on pages 182-207 of this report.

Independent variables which appear to have some relationship to cloud behavior and the production of rain have been used in one way or another in the evaluation of seeding projects for many years. The use of these "covariates" can greatly increase the sensitivity of the statistical tests by providing more homogeneous samples.

Covariates can be of three types. *Environmental covariates* are parameters which reflect the control of large-scale processes on local convection and precipitation processes. Candidate environmental covariates for HIPLEX have been studied extensively at ISWS, These studies are summarized elsewhere in this report. *Storm or cloud group covariates* (e.g., duration, propogation) reflect the influence of meso-scale processes on cloud and

precipitation history and the interactions between the meso- and cloud-scale. *Cloud covariates* reflect the local or small scale control of the precipitation. Cloud base and top heights, updraft velocity and extent, amount and characteristics of condensate, etc., prior to treatment may serve as good estimators of subsequent natural behavior and rain production. Numerical-model predictions such as seedability of sample cloud, maximum cloud top height, etc. are also potential covariates.

The cloud and storm covariates should be screened in tests similar to those used in screening the environmental covariates. A general data base for such a test does not now exist but data from the HIPLEX field efforts should be carefully studied to determine which of these parameters have true potential as estimators of single cloud rainfall. Some of the cloud and cloud group covariates may be response variables as well as estimators. In these cases values prior to seeding may be used as predictors of future behavior.

An operations plan which covers personnel and facilities needed to carry out the exploratory and seeding experiments, identification of operational days and suitable clouds, forecasting requirements, etc. has been drawn up as part of the design. Since many parts of this plan are not location or experiment specific, this plan is quite detailed. Some developmental research, e.g., in forecasting operational conditions, is needed to refine those aspects which are dependent on specific location and on the modification hypotheses and techniques.

Design Studies for the Single Cloud and Area Experiments

Introduction. In an earlier report by Ackerman et al. (1976), the design for HIPLEX was developed. There were two general areas identified that needed further work before the overall objectives of the design could be obtained. These included 1) work with the areal design, including redesign efforts for the Single Cloud Experiment, and 2) evaluation of the capabilities of the HIPLEX radar. Work on these two areas was performed during the period July 1, 1976 through September 30, 1977. The first area of work (design and evaluation) is reported on in this section, and the second area is described in a subsequent section.

Since the initial statistical design of the Single Cloud Experiment was completed and reported on in the HIPLEX design document, the major emphasis during FY-77 was to be on predictor variables and the Area Experiment. However, certain efforts had been envisioned for the Single Cloud Experiment. These included 1) the specific application of the predictor variables to the Single Cloud Experiment, 2) redesign efforts for the Single Cloud Experiments as more data and information become

available, and 3) the modification (if necessary) of sampling requirements as the radar, rain and other cloud data from the 1976 field operations were amassed and analyzed.

The third item was included because some of the recommendations in the design document concerning the statistical design of the Single Cloud Experiment were derived from METROMEX rain data due to the unavailability of a climatological data base of surface raincells and radar cells determined by the 5-cra radar system. However, the crucial characteristics (i.e., frequency, size, duration, intensity, etc.) of radar cells and surface raincells typical of the High Plains were not available during the research period.

Therefore no work was performed on the third item. Also, very little work was done on the second item because of the lack of data and information. Thus, this section deals mostly with predictor variables, the area experiment, and some special climatological studies.

Predictor Variables. *(1) General Background*, The importance of using the most efficient design and statistical test in weather modification has often been stressed by various authors (Neyman and Scott, 1967; Schickedanz and Krause, 1970; Simpson et al., 1973; Olsen, 1974; Mielke, 1972; Brier, 1974), However, even in the most efficient statistical test, the sample size required to detect seeding effects is often too large to permit an evaluation program to be effective. Certainly, one way to reduce the sample sizes required would be to use a more lenient significance level (0,10 rather than 0.05), However, this increases the probability of erroneously asserting that an effect is present when, in fact, it is not. A more promising method or reducing sample sizes is to incorporate covariates (predictor variables) into the design and evaluation (Neyman and Scott, 1967; Schickedanz and Changnon, 1970; Changnon and Morgan, 1976; Brier, 1974; Ackerman et al., 1976; Simpson and Woodley, 1974; Biondini et al, , 1977).

The predictor variables which are customarily used in weather modification experiments are the precipitation or hailfall amounts in control areas adjacent to, but not connected to, the target area. However, there is always the danger of contamination of control areas by seeding in the target areas. If the two areas are located far enough apart to avoid any possible contamination, the correlation between the areas is often reduced to a point beyond usefulness.

Neyman and Scott (1967) have suggested that comparison areas are not the only source of predictor variables. They point to the ingenuity of Spar (1957) who used three meteorological predictor variables in Project Scud, Subsequent calculations by Neyman and Scott indicate that the use of the three predictor variables in

Project Scud was equivalent to multipling the number of observations by a factor of 4.6. However, predictor variables that work well in one experiment may not work well in another experiment. Thus, it was concluded that a search for meteorological variables which could be used as covariates would be a very important part of the HIPLEX design effort.

The predictor variables used in this study are derived from four basic sources of data. These sources include: 1) the meteorological upper air soundings (including variables derived from one-dimensional parameterized cloud models); 2) objective fields of surface meteorological observations; 3) National Weather Service radar summary charts; and 4) rainfall prior to the operational period as well as rainfall from surrounding areas during the operational period. Predictor variables derived from these sources can be described as either environmental or storm predictors.

However, many of the potential storm predictors such as those suggested by Ackerman et al. (1976) were not investigated in this study because of the unavailability of storm data from the HIPLEX field data. These include potential predictors such as 1) areal extent of storm, 2) cloud cover within storm, 3) duration of storm, 4) general movement (speed, direction) of clouds within storm, 5) movement of storm as whole, 6) general cloud characteristics at time storm declared an experimental unit (e.g., maximum cloud (echo) height, cloud-size spectrum), 7) thermodynamic stratification in storm area, and 8) convergence in storm area. These can be used as stratification parameters for single cloud data or as estimators of the (unseeded) storm rainfall. However, since these can also be response variables*, they should generally be measured before the treatment begins. As an estimation of the storm rainfall, they are more appropriate to the area experiment than the single cloud experiment.

In addition, empirical and theoretical studies have shown that precipitation produced by individual clouds is also a function of certain cloud characteristics, some of which can be considered as candidate predictors (Ackerman et al., 1976). However, predictors derived from this latter source of data are generally obtained from data collected during the pre-experimental or experimental period, and these data were not readily available in the sense of a climatological data base. Thus, for the present study, the effort was concentrated on the four basic data sources mentioned above,

* Response variables are parameters that may change in response to the treatment, either as a direct or indirect consequence of the treatment.

The inclusion of predictor variables or covariates into the design of weather modification experiments has resulted in much confusion concerning the statistical and meteorological concepts of predictors and the appropriate terminology. Therefore, for purposes of HIPLEX evaluation, we have defined all predictors and/or covariates to be SPECs (Statistical-Physical Estimator Covariates).

SPECs can be used in the design and evaluation for both *ad hoc* analyses (analyses organized for a specific purpose, or extended here to mean analysis determined for analytical purposes prior to the experiment) and for *post hoc* analyses (analyses determined after the experiment), The *ad hoc* analyses can be generalized without further testing and can be used in *a priori* testing of hypotheses. However, the *post hoc* analysis cannot be generalized without further testing and can only be used for testing a *posteriori* hypotheses. Statistical validation of results is always more acceptable if the results have been derived from a *priori* hypotheses (as opposed to those derived from a *posteriori* hypotheses). This does not mean that *post hoc* analyses should not be performed during the experiment, which can lead to a *posteriori* hypotheses, but simply that the results need further testing in the a *priori* framework.

Whether the SPECs are determined in a *priori* or a *posteriori* framework, they can be used to decrease the natural variability, thereby increasing the precision and making it easier to detect seeding effects. The SPECs can also be used in a meteorological prediction sense. That is, SPECs which are based on information prior to the seeding period on a given day can also be used for experimental day declaration. On the other hand, those SPECs which are determined from data during the daily seeding period cannot be used in the meteorological prediction sense. Thus, we define 1) SYNSPEC (SYNoptic Statistical-Physical Estimator Covariate) and 2) PROGSPEC (PROGnosic Statistical-Physical Estimator Covariate) as the two general types of SPECs, The SYNSPECs are determined from soundings, rainfall, radar, surface predictors, etc., during or after the seeding period. The PROGSPECs are determined from soundings, rainfall, radar, surface predictors, etc, prior to the daily seeding period. Both SYNSPECs and PROGSPECs can be used in *ad hoc* or *post hoc* analyses depending upon whether they were declared before or after the initiation of the experiment. Furthermore, if the *post hoc* analysis of data from the first year of the experiment indicates that additional variables are required, the determination of these variables prior to the second year of the experiment would permit them to be used in *ad hoc* analyses of data from future years.

The initial selection of SPECs should be based on sound meteorological and physical concepts. The physical and meteorological concepts underlying the initial selection of SPECs are now described.

(2) Criteria for Selection and Development of SPECs. SPEC development for the HIPLEX relies in part on an extensive literature review directed toward the identification and evaluation of meteorological variables that are correlated with convective rainfall. Many SPECs have been identified for other parts of the country and/or for other convective phenomena (hailstorms, tornado-producing thunderstorms). These and other SPECs deduced from High Plains synoptic climatology and from the recommendations of persons with operational experience in the High Plains have been assessed for applicability in HIPLEX.

The following set of criteria have been developed so as to insure that the candidate SPECs would be sufficiently diverse to capture the broad spectrum of possible physical processes that lead to High Plains convective rainfall.

1. The SPECs should draw from data taken from diverse sources. Meteorological upper air soundings and surface observations provide measurements of standard meteorological quantities; satellites and surface observations provide cloud information; radar and precipitation records provide cloud structure and rainfall data. With the exception of the satellite data, these data sources exist historically and are useful for HIPLEX climatological studies. Radar information can be extracted from the National Weather Service radar summary charts.

2. The SPECs should include as many of the observed variables as possible - either alone or in combinations. Measurements of wind conditions, air temperature, moisture, pressure (height), cloud types, cloud cover, precipitation patterns, intensities, etc. all relate to convective rainfall in some manner. Spatial and temporal combinations of observed variables should also be considered.

3. The SPECs should be developed with varying complexity. SPECs used for HIPLEX range in complexity from simple numbers such as dewpoint at a particular level to the results from a one dimensional parameterized numerical cloud model (Kreitzburg and Perkey, 1976) that simulates complex nonlinear processes that lead to convection.

4. The SPECs should address the relative importance of environmental controls such as airmass stability, moisture and the dynamic "trigger" that can initiate deep convection. The background studies that included moisture found that rainfall was critically dependent upon an abundant moisture supply. A strong relationship

between convective rainfall and stability was found for Florida (Estoque and Partagas, 1974) where nearly homogeneous convectively unstable airmasses are often present both spatially and temporally. These airmasses are not as prevalent over the central and northern High Plains where stability was found to be poorly correlated with convective rainfall (Madigan, 1959; Dennis et al., 1967). SPECs indicative of triggering mechanisms relate to a wide range of surface and upper air phenomena. Quantities derived from field analyses such as upslope flow, convergence, vorticity, and the Laplacian of pressure or height, help identify areas where airmasses undergo vertical displacements. Other SPECs indicative of systems producing vertical motion include frontal positions, 500-mb height, 500-mb height gradients, vorticity advection, positions of low- and mid-level jet streams, and net vertical displacements of selected air parcels estimated from numerical trajectory-prediction models. Various combinations of these and others with parameters from the stability and moisture categories increase the number and complexity of SPECs.

5. The SPECs should be tailored to the High Plains convective precipitation types. Airmass showers form when conditions within convectively unstable airmasses are such that surface heating can initiate deep convection. System showers require an additional destabilization mechanism such as a front, squall line, disturbance aloft, etc. Mountain drift showers form over the mountains during the heated daytime hours and drift eastward over the plains as they dissipate. These clouds differ from system initiated showers in that they are relatively independent of the low level stability and moisture over the plains.

6. The SPECs must have a physical connection with High Plains precipitation. Our studies have concentrated on SPECs derived from observations taken within the general area of the proposed experiment and within 24 hours of the observation of the dependent variables.

For ease of presentation, the candidate SPECs for HIPLEX will be treated in the following order: upper air SPECs derived directly from radiosonde observations, surface field SPECs taken from the Airways surface observations, SPECs derived from a one-dimensional parameterized cloud model, and SPECs deduced from National Weather Service Radar Summary Charts.

The SPECs will be tested against the hourly and daily rainfall for Kansas and parts of Colorado. Figure 4 shows the grid for the surface objective analysis (large grid) and the rainfall grid (smaller grid) that contains six sampling areas. Each sampling area is 175 km on a side and is equal in area to a circle of radius 100 km - typical of an operations area as viewed from a radar scope.

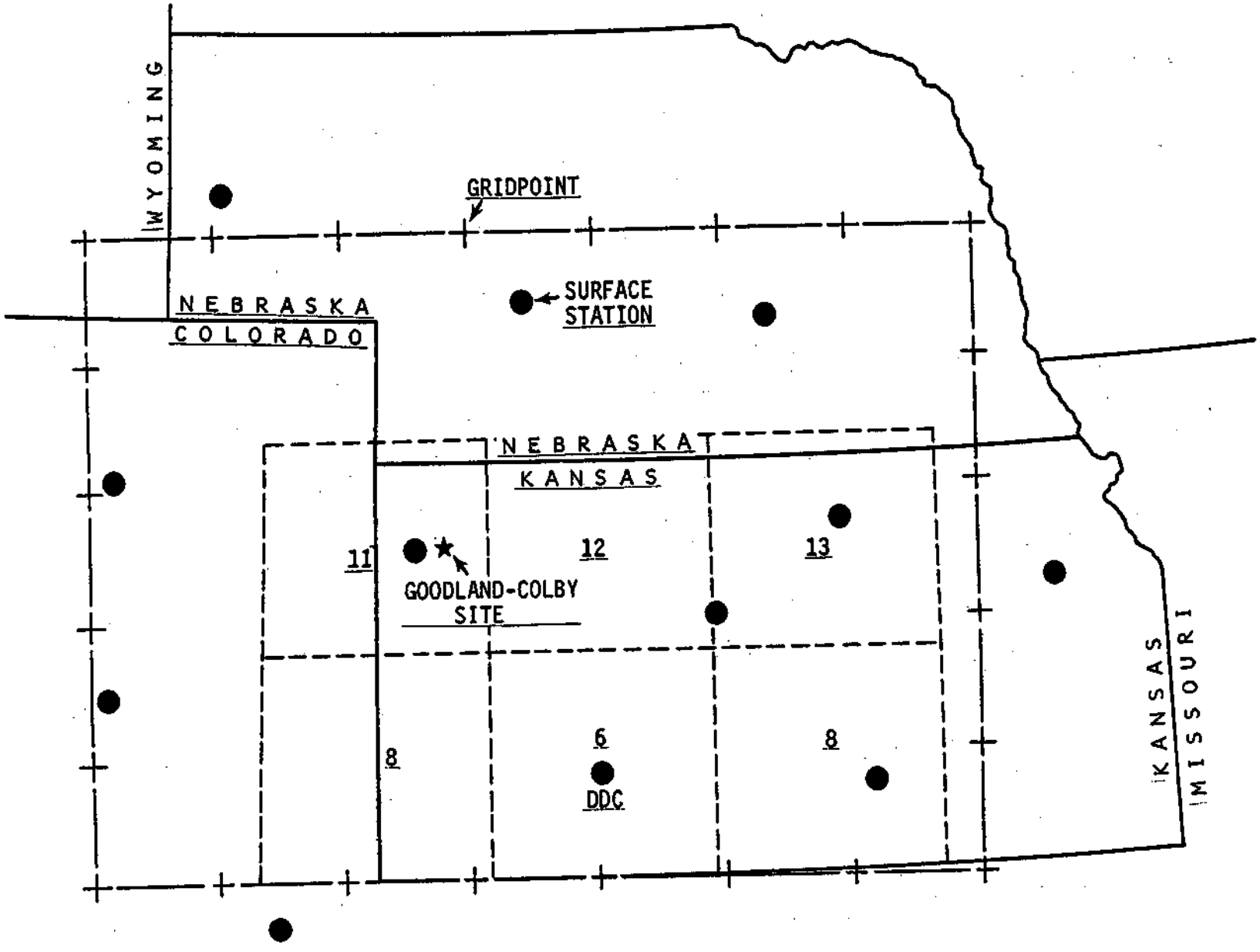

Figure 4. Map showing locations of surface SPEC grid, the rawinsonde site (DDC), the locations of surface observation sites, and the 6 average rainfall sampling areas.

The rainfalls for the hourly and daily precipitation reporting stations within each square were averaged. The number of hourly rainfall stations available within each sampling area is given at the center of each square.

The proposed Goodland-Colby experimental area in northwestern Kansas is shown by the star. The surface meteorological stations (black circles) provided spatial estimates for the objective interpolation to the large grid. Upper air SPECs were derived from rawinsonde data taken at Dodge City (DDC), about 200 km southeast of the Goodland-Colby site.

(3) Literature Review-Survey of Candidate SPECs. About 200 "candidate" SPECs have been found thus far. Many of these can be determined at several levels in the atmosphere so that potentially the number may increase to much beyond 200. Other possible SPECs could be synthesized but it is doubtful they would improve upon these already identified. Most of the candidates have been screened out as poorly correlated with convective phenomena; however, all SPECs are reviewed in this section in order to avoid duplication of effort by others.

Listed in Table 3 are authors and publication dates of papers which dealt with this problem (complete citations are given in the list of references). When SPECs were correlated with convective phenomena other than rainfall, the phenomenon is also listed.

The SPECs were found to fall within one of four categories:

1. Point SPECs that are available from single soundings or single surface observations.

2. Line SPECs that require two soundings or two surface observations in either a spatial or temporal setting.

3. Field SPECs based on observed spatial distributions of meteorological parameters. (Various derivative quantities fall into this category.)

4. Field SPECs derived from the output from numerical weather prediction models. These comprise an almost limitless number of possibilities and have the advantage that the predicted variable can be valid at the time operations are conducted and yet not be contaminated by side effects. The disadvantage of these variables is that they contain the inaccuracies and poor resolution (particularly along the vertical coordinate) typical of today's numerical forecast models.

The candidate SPECs are listed by category in Tables 4-7. (The numbers in parentheses in these tables refer to the references listed in Table 3). Some variables are ambiguous (no. 45 in

Table 4, for example) and some are nearly redundant. These are given in order to provide a complete list of quantities which have in the past been investigated.

Most of the field SPECs were derived for tornado conditions (Endlich and Mancusso, 1967; Charba, 1975). However, this does not lessen their potential importance to the general convective rain study, and in particular to the heavier rains. Environmental conditions favorable for thunderstorms tend to maximize just prior to and during severe weather outbreaks. These same conditions are present in general thunderstorm outbreaks but are perhaps less intense and not in the same order of importance as in severe thunderstorm outbreaks.

The results of the various studies in the literature varied, depending on the geographical location and the predictand. All of the studies that included moisture found that rainfall was critically dependent upon an abundant moisture supply. Convective rainfall over Florida was inversely correlated with stability (Estoque and Partagas, 1974) but convective rainfall over the central and northern High Plains showed little or no correlation with stability (Madigan, 1959; Dennis et al., 1967). The precipitation regime in Florida differs from the precipitation regime in the High Plains. A goodly fraction of summer precipitation in Florida is due to airmass shower activity which results when solar insolation heats the surface layers and releases latent convective instability. A convectively unstable environment above 850 mb often extends over large areas of the Florida Peninsula and the southeastern United States and tends to persist from the early morning time of the sounding throughout the day. Thus, the early morning sounding yields information pertaining to the midafternoon stability.

The High Plains is characterized by three diverse precipitation regimes. These are the airmass shower type, the frequent system type (frontal, squall line, mesosystem), and the mountain drift type. A possible explanation for the poor correlation between stability and precipitation draws upon the transience of the system type. Rapid destabilization can occur within mesoscale upward vertical velocity zones along and ahead of cold fronts and squall lines. Low level inversions have been destroyed over a period of time from 1-3 hours in advance of squall lines (Long, 1963). The temperature and moisture lapse rates within these convergent zones can be expected to differ considerably from the lapse rates obtained from the morning soundings unless these are located within the convergent zones. Thus, the stability SPECs derived from morning soundings could have little or no correlation with events that occur later in the day.

The mountain drift type precipitation events may also have little or no correlation with stability indices. Afternoon thunderstorms form over the mountains and tend to drift eastward

over the High Plains as they dissipate. These clouds originate within local mountain induced circulations and are transient systems that have little or no dependence upon the low level stability over the plains.

A number of excellent SPECs that address the triggering mechanisms have been developed. Mid-level vorticity advection (Dennis et al., 1967; Dennis and Koscielski, 1969), surface convergence (Bermowitz, 1971; Charba, 1975; Endlich and Mancusso, 1967; Renne and Sinclair, 1969; Reap and Alaka, 1969; Reap and Foster, 1975; Reap, 1976) boundary layer vertical velocity (Achtemeier and Morgan, 1975; Whitehead, 1971; Reap, 1975; Bonner, Reap and Kemper, 1971) and vertical displacements of air trajectories (Bonner, Reap and Kemper, 1971; Hammond and Clark, 1975; Clark, 1973; Reap and Foster, 1975; Reap, 1976; Reap and Alaka, 1969) have been found to be highly correlated with convective precipitation and severe weather occurrences. A less sophisticated SPEC based upon the location of nearby fronts (Dirks, 1969) was not well correlated with convective precipitation.

The candidate SPECs extracted from the literature (Tables 5-8) have been reduced to a manageable number for study in the High Plains. The SPECs derived from the output of numerical weather prediction models (Table 7) have been dropped from consideration because of the short lengths of the primitive equation (PE), limited fine mesh (LFM) and trajectory models archives. (The archives begin on 3 July 1969 (PE), 1 October 1972 (LFM) and 3 July 1969 (Trajectory)).

In soliciting variables for study, redundancy has to be eliminated and SPECs that best address the physical processes that govern the meteorology of the High Plains must be chosen. The selected set should contain SPECs derived from as many of the fundamental meteorological variables (wind components, temperature, dewpoint temperature, pressure) as possible. Further, the set should contain SPECs that address the three physical categories: moisture, stability, and trigger mechanism.

The relatively poor correlation between rainfall and the stability indices for the High Plains (Madigan, 1959; Dennis et al., 1967) should not lead to the total elimination of stability-related SPECs from the test set. Rather, stability indices and other SPECs that address thermodynamic structures should be extensively tested and poor candidates should be screened out.

SPECs that address triggering mechanisms should be sensitive to the presence of transient precipitation-producing systems. Therefore, high priority is placed upon covariates that are derived from the hourly surface observations.

Most of the SPECs discussed on the pages to follow are taken directly from Tables 4 through 7. Some have been modified slightly

Table 3. References included in the candidate SPEC review.

Reference

1. Achtemeier and Morgan (1975)
2. Bermowitz (1971)
3. Bonner, Reap, Kemper (1971) (Tornado)
4. Boyden (1963)
5. Cahir (1971)
6. Charba (1975) (Tornado)
7. Clark (1973)
8. Darkow (1968)
9. David (1974) (Tornado)
10. David and Smith (1971)
11. Dennis, Koscielski (1969)
12. Dennis, Schock, Koscielski, Mielke (1967)
13. Dirks (1969)
14. Endlich and Mancusso (1967) (Tornado)
15. Estoque and Partages (1974)
16. Foster (1964) (Tornado)
17. Fujita and Bradbury (1966)
18. Galway (1956)
19. George (1960)
20. Glahn, Lowry, Hollenbaugh (1969)
21. Hammond and Clark (1975) (Tornado)
22. Harley (1971)
23. Jefferson (1963)
24. Maddox (1973) (Tornado)
25. Madigan (1959)
26. Miller (1967) (Tornado)
27. Miller, Bidner, Maddox (1971) (Tornado)
28. Miller, Dennis, Boyd, Smith, Cain (1974)
29. Rackliff (1962)
30. Reap (1976)
31. Reap and Foster (1975); also Reap (1975)
32. Reap and Alaka (1969) (Tornado)
33. Renne and Sinclair (1969) (Hailstorm)
34. Schaefer (1975)
35. Schleusener and Auer (1964)
36. Showalter (1953)
37. Sly (1966)
38. Whitehead (1971) (Tornado)
39. Williams (1968)

Table 4. List of point SPECs that can be taken from single soundings or single surface observations.

(Numbers in parentheses are the references given in Table 3)

1. Temperature (6, 9, 33)
2. Dewpoint temperature (9, 33)
3. Sea level pressure (6, 9)
4. Wind speed (9, 33)
5. Wind direction (9)
6. Cloudiness (9)
7. Visibility (9)
8. Cloud base height (9)
9. Moisture at 850 mb (13)
10. 500 mb dryness (13)
11. 700-900 mb relative humidity (RH) or humidity in general (13)
12. RH 1000-600 mb (15)
13. Dewpoint at Goodland, Kansas 06Z (35)
14. Dewpoint at Cheyenne, Wyoming 06Z (35)
15. 500 mb temp over Denver, Colorado (DEN) 00Z (35)
16. 500 mb height over DEN 00Z (35)
17. Surface mixing ratio (6)
18. Surface wet bulb potential temperature (6, 39)
19. Surface isobaric equivalent potential temperature (6)
20. Maximum mean wet bulb potential temperature (θw) for a 100 mb column within a 160 mb column (39)
21. Maximum mean 6w for a 160 mb column within a 240 mb column (39)
22. Station pressure (39)
23. Previous day's maximum temperature in Colorado (35)
24. Previous day's maximum temperature in Wyoming (35)
25. Previous day's maximum precipitation in Wyoming (35)
26. Previous day's maximum precipitation in Kansas (35)
27. Previous day's $\log_{10} E_{max}$ (maximum hail impact energy ft-lb/ft^2) in Colorado or Nebraska (35)
28. Precipitable water >.75 inches (28)
29. Precipitable water to 500 mb >.70 (11)
30. 1000-850 mb thickness (39)
31. 1000-500 mb thickness (39)
32. Saturation thickness (20)
33. 700-500 mb saturation thickness defined as the 700-500 mb thickness minus the thickness of the 700-500 mb layer given the temperatures along the ascent of a 160 mb deep air column that originates near the surface (39)
34. Severe storm positive area. The saturation thickness from the level of free convection to 500 mb (see 33) using a 100 mb deep moist column (39)
35. Pressure at the lifted condensation level (LCL) (39)
36. Pressure at the level of free convection (LFC) (39)
37. Pressure at the base of the 100 mb moist layer (see 20) (39)

Table 4. (Continued)

38. Pressure at the convective condensation level (CCL) (39)
39. Convective temperature (39)
40. Height of the CCL (25,33)
41. Height of the LCL (25)
42. Height of the freezing level (25)
43. Height of the wet bulb zero (25)
44. Depths of layers where the mixing ratio was greater than 3, 5, 8 g/kg (25)
45. Stability indices (no detail) (13, 25)
46. Showalter index (12, 15, 33, 36, 39)
47. Lifted index (12, 18, 33, 38)
48. K-Index (19, 39)
49. Total energy index (8, 33)
50. Convective index positive area. The same as severe storm positive area (34) except use a 160 mb deep moist column. (39)
51. Severe storm index. The severe storm positive area plus the negative area between the LCL and LFC (39)
52. Convective index. The same as severe storm index except use a 160 mb deep moist column (39)
53. Summer index (5)
54. Vertical Totals index (temperature at 500 mb minus temperature at 850 mb) (26)
55. Cross Totals index (500 mb temperature minus 850 mb dewpoint temperature) (26)
56. Total Totals index (sum of the Vertical Totals with the Cross Totals (26)
57. Sly index (37)
58. Best lifted index (17)
59. Potential wet bulb index (10)
60. Surface potential index (24)
61. Boyden index (4)
62. Rackliff index (29)
63. Latent and potential instability index (22)
64. 500 mb temperature minus the temperature at 500 mb of the wet bulb curve passing through the sea level wet bulb temperature (16)
65. Jefferson index (23)
66. SWEAT index (27, 38)
67. Low level jet on 12Z sounding (13)
68. Direction of averaged prevailing winds 1000-600 mb (15)
69. 850 mb wind speed > 15. kt (11, 28)
70. 850 mb wind direction 270-120 clockwise (11, 28)
71. 500 mb wind speed (33)
72. Positive vertical wind shear (13)
73. 850-200 mb vertical wind shear (15)
74. Sine day of year (30, 31)
75. Cosine day of year (30, 31)
76. Sine latitude (30, 31)
77. Cosine latitude (30, 31)
78. Solar altitude (30, 31)

Table 5. List of line SPECs that require two soundings or two surface observations in either a spatial or temporal setting for their calculation.

(Numbers in parentheses are the references given in Table 3)

1. 24 hr change in difference of reduced sea level pressure between Cheyenne, Wyoming and Trinidad, Colorado, 06Z (35)
2. 24 hr change in difference of reduced sea level pressure between Kansas City, Missouri and Amarillo, Texas, 06Z (35)
3. 24 hr change in dewpoint at Goodland, Kansas 06Z (35)
4. 24 hr change in dewpoint at Oklahoma City, Oklahoma, 06Z (35)
5. 24 hr change in dewpoint at Cheyenne, Wyoming, 06Z (35)
6. 24 hr change in 500 mb temp over Denver, Colorado 00Z (35)
7. 24 hr change in 500 mb height over Denver, Colorado, 00Z (35)
8. 24 hr change in maximum temp observed the previous day in Wyoming (35)
9. Difference in reduced sea level pressure between Cheyenne, Wyoming and Trinidad, Colorado (35)
10. Difference in reduced sea level pressure between Kansas City, Missouri and Amarillo, Texas (35)
11. Surface temperature tendency (6)
12. Tendency of the mean sea level pressure (6)
13. Surface mixing ratio tendency (6)
14. Surface wet bulb potential temperature tendency (6)
15. Isobaric equivalent potential temperature tendency (6)
16. Spokane and Tatoosh, Washington 700 mb temperature (35)
17. Dodge City, Kansas minus North Platte, Nebraska, 700 mb height (35)

according to the meteorology and topography of the High Plains. For example, some stability indicies will be computed using the temperature and moisture at 900 mb instead of at the non-existent 1000 mb pressure level. Other SPECs have been added, some on the recommendation of participants in the 1975 HIPLEX field program.

(4) The upper Air SPECs. Table 8 lists 38 candidate SPECs that can be computed from single soundings. When the number of levels and some computational expansions are included, the actual number is increased to 136. These were selected for two studies for western Kansas; correlations with daily rainfall for 13 Junes from 1958-1970 and correlations with 3-hourly rainfall for 7 Junes from 1965-1971. The SPECs were correlated with the occurrence or non-occurrence of rain and with the rainfall depth. Those that correlated poorly are screened out.

Table 6. List of field SPECs (not predicted) that rely upon spatial distributions of variables.

(Numbers in parentheses are the references given in Table 3)

1. Upper level trough (13)
2. Strength 500 mb flow (13)
3. Curvature 500 mb flow (13)
4. 700 mb dewpoint gradient (14)
5. 500 mb cold advection (13)
6. Temperature gradient near tropopause (14)
7. Maximum 500 mb wind over Utah or Colorado 00Z (35)
8. Maximum 500 mb wind over Arizona or New Mexico 00Z (35)
9. Wind speed at 200 mb (14)
10. Positive vorticity advection at 500 mb (11)
11. Position of surface fronts (13)
12. 24 hr change in maximum 500 mb wind over Arizona and New Mexico 00Z (35)
13. Temperature advection (sfc) (2)
14. Magnitude of the horizontal gradient of mixing ratio (6)
15. Product of the mixing ratio with the magnitude of its horizontal gradient (6)
16. Magnitude of the horizontal gradient of the wet bulb potential temperature, 6e (6)
17. Product of 6e with the magnitude of its horizontal gradient (6)
18. Biconstituent diffusion (34)
19. Horizontal Laplacian of the MSL pressure (6)
20. The tendency of the horizontal Laplacian of the mean sea level pressure (6)
21. Pressure trough analysis (curvature of pressure field normal to trough axis) (1)
22. Divergence (sfc) (2, 6, 33)
23. Vorticity (sfc) (2, 6)
24. Surface moisture divergence (6, 14)
25. Surface moisture divergence tendency (6)
26. Equivalent potential temperature divergence (6)
27. Equivalent potential temperature divergence tendency (6)
28. Divergence of the temperature flux (14)
29. Horizontal divergence in the upper troposphere (14)
30. Frontogenesis of temperature (sfc) (2, 14)
31. Frontogenesis of moisture (14)
32. Terrain induced vertical velocity (6, 33)
33. Product of the equivalent potential temperature with the terrain induced vertical velocity (6)
34. The qw index (w is vertical velocity at top of 300 m layer (38)
35. Cumulative lift (5 hr net surface layer vertical displacement (1)
36. Thunderstorm forecast algorithm (cumulative lift is restricted to where the dewpoint temperature exceeds 50°F and to where the vector wind has a southerly component (1)
37. Vertical velocity at 850 mb (14)
38. Area between low level temperature and moisture axes (14)

Table 6. (Continued)

39. Destabilizing temperature advection between low and mid-troposphere (14)
40. Destabilizing distribution of the divergence of the temperature flux between low and mid-troposphere (14)
41. Intersection of 850-500 mb 4260 thickness line and the thickness ridge (14)
42. Vorticity of the wind shear vector between 500 mb and the boundary layer (14)
43. Vorticity acceleration (16)
44. Thunderstorm relative frequency distribution (30, 31)

Table 7. List of SPECs derived from the output from numerical weather prediction models.

(Numbers in parentheses are the references given in Table 3)

1. Mean relative humidity from lowest 3 layers in 6 layer PE model (9)
2. Mean boundary layer potential temperature (9, 3.0)
3. Mean boundary layer sea level pressure (9)
4. Temperature (sfc, 850, 700, 500 mb 24 hour forecast (24F)) (3, 30, 31)
5. Dewpoint (sfc, 850, 700 mb (24F)) (3, 30, 31)
6. Relative humidity (sfc, 850, 700 mb (24F)) (3, 30, 31)
7. Mean relative humidity (sfc to 700 mb (24F)) (30, 31)
8. Surface pressure (24F) (3, 30, 31)
9. Height of constant pressure surface (1000, 850, 500 mb (24F)) (3, 30, 31)
10. 1000-500 mb thickness (9)
11. Thickness (850 to 500 mb (24F)) (30, 31)
12. Air parcel stability. The temperature difference between a parcel lifted from the surface to 500 mb and the forecast 500 mb temperature (6)
13. Air parcel stability tendency (6)
14. Convective instability (sfc to 700 mb 24F) (defined as 700 mb θe) average 1000-850 mb θe (30, 31)
15. Horizontal temperature advection (850 mb (24F)) (30, 31)
16. Dewpoint advection (700 mb (24F)) (30, 31)
17. Temperature lapse rate (850 to 500 mb (24F)) (30, 31)
18. Wet bulb potential temperature lapse rate (surface to 700 mb (24F)) (30)
19. Height of wet bulb zero (24F) (30)
20. Convective instability (surface to 500 mb (24F)) (3, 32)
21. Magnitude of the horizontal dewpoint gradient (1000 mb (24F)) (32)

Table 7. (Continued)

22. Total Totals index (24F) (30, 31)
23. K-Index (24F) (30, 31)
24. Showalter index (24F) (7, 30, 31)
25. Modified Showalter index plus 12 hour net vertical displacement at 700 mb (30)
26. SWEAT index (24F) (30)
27. Lifted parcel temperature advection at 500 mb (30)
28. 18-24 hour height change (30)
29. U component horizontal wind (boundary layer, 850, 700, 500 mb (24F)) (3, 30, 31)
30. V component horizontal wind (boundary layer, 850, 700, 500 mb (24F)) (3, 30, 31)
31. Wind direction (boundary layer, 500 mb (24F)) (30, 31)
32. Wind speed (boundary layer, 500 mb (24F)) (30, 31)
33. U wind component (500 mb) plus V component (boundary layer) (24F) (30)
34. U gradient (500 mb) plus V gradient (boundary layer (24F) (30)
35. Vector wind shear (24F) (30, 31)
36. U, V, components of mean boundary layer wind (9)
37. Moisture divergence (24F) (30, 31)
38. Wind divergence (boundary layer (24F)) (30, 31, 32)
39. Relative vorticity (boundary layer (24F)) (30, 31)
40. Geostrophic vorticity (1000, 500 mb (24F)) (30, 31)
41. Thermal vorticity (1000 to 500 mb (24F)) (30, 31)
42. Vorticity advection (500 mb (24F)) (30, 31)
43. 850 mb wind divergence (24F) (32)
44. 1000 mb temperature flux (24F) (32)
45. 1000 mb dewpoint flux (24F) (32)
46. Convergence (boundary layer, 850 mb 12F) (3)
47. 700 mb vertical velocity (9)
48. Vertical velocity (1000, 850, 650 mb (24F)) (3, 30, 31)
49. Terrain-induced vertical velocity (24F) (30, 31)
50. 12 hour net vertical displacement (sfc, 850, 700 mb) (3, 30, 31)
51. 24 hour net vertical displacement (sfc, 850, 700 mb) (3, 30, 31)
52. 48 hour vertical displacement from 500 mb (7)
53. Gradient of 12-hour net vertical displacement (30)
54. Trajectory convergence (sfc, 850 mb) (30, 31)
55. Convective instability times 12 hour 700 mb net vertical displacement (30, 31)
56. Modified Showalter index plus 12 hour net vertical displacement from 700 mb (30)
57. Convective instability times net vertical displacement of parcels ending at 500 mb during the last 6 hours of the forecast period (32)
58. Severe weather forecast trajectory and thermodynamics signature (21)
59. 6 hourly quantitative precipitation forecast (9)
60. Precipitation amount (24F) (3)

Dodge City, Kansas, is the radiosonde station used for the Kansas study (see fig. 4). The SPECs are computed for the 1200 GMT (morning) soundings. It is possible that the SPECs computed from the 0000 GMT (evening) soundings would be more highly correlated with precipitation than those computed from the 1200 GMT soundings because late afternoon and early evening is the climatological time of maximum precipitation frequency for the High Plains, and much of this precipitation is initiated by spatially and temporally transient weather disturbances. However, the morning soundings were chosen because 1) the SPECs can be useful for operational forecasts (PROGSPECs), and 2) there will be no possibility of the SPECs being contaminated by modification of thermodynamic structures brought on by the seeding experiment.

The derivation and interpretation of the sounding derived SPECs is as follows.

1) Layer Precipitable Water

Derivation: The layer precipitable water is given by the product of the mean mixing ratio with the depth of the layer in mb and divided by the acceleration of gravity. The mixing ratio is calculated from the Clausius-Clapeyron equation (Berry et al., 1945).

Interpretation: Moisture is often found in layers near the surface and in the lower half of the troposphere. These layers may yield measurable precipitation and may be correlated with certain plains precipitation systems.

2) Total Precipitable Water

Derivation: The depth of precipitable water from the surface to a specified pressure level is found by the summation of the individual layer precipitable waters.

Interpretation: Deep moisture layers are often associated with substantial rainfall. They are good indicators of the maximum available moisture in an airmass.

3) Saturation Deficit

Derivation: The saturation deficit is given by the difference between the temperature and the dewpoint temperature.

Interpretation: It is a measure of the relative moistness of an airmass. An airmass can be moist but very warm and consequently relatively dry. Clouds are more likely in relatively moist airmasses.

4) Height of the Convective Condensation Level

Derivation: The height of the convective condensation level is given by the point of intersection of the sounding temperature curve with the saturation mixing ratio line that corresponds to the average mixing ratio in the "surface" layer below 820 mb. Following

Table 8. SPECs taken from soundings.

1. Layer precipitable water (sfc-900, 900-850, 850-800, 800-700, 700-600, 600-500, 500-400, 400-200 mb).
2. Total precipitable water (sfc-900, 850, 800, 700, 600, 500, 400, 200 mb).
3. Saturation deficit computed at the following levels: surface, 900, 850, 800, 700, 600, 500, 400, 200 mb.
4. Height of the convective condensation level.
5. Convective temperature.
6. Difference between the convective temperature and the 850 mb temperature.
7. Height where T = 0°C, T = -5°C, T = -10°C, T = -15°C, T = -20°C.
8. Warm convective depth - the difference between the height where T = 0°C and the height of the convective condensation level.
9. The mean mixing ratio between the surface and the convective condensation level.
10. Height of wet bulb zero.
11. K-Index.
12. D-Index.
13. Showalter index.
14. Boyden index.
15. Cross Totals index.
16. Vertical Totals index.
17. Total Totals index.
18. Potential Wet Bulb index.
19. Energy index.
20. Severe Storm index.
21. Equivalent potential temperature index.
22. SWEAT index.
23. Wind speed at the levels given in (3).
24. Wind direction at the levels given in (3).
25. U-component of the wind speed at 850 and 500 mb.
26. V-component of the wind speed at 850 and 500 mb.
27. U-component wind shear 500-850 mb.
28. V-component wind shear 500-850 mb.
29. Wind speed shear 500-850 mb.
30. Wind direction shear 500-850 mb.
31. Difference in wind direction between 300 and 700 mb.
32. The wind speed shear between 300 and 500 mb.
33. Temperature at mandatory levels.
34. Height at mandatory levels.
35. Dewpoint at mandatory levels.
36. Equivalent potential temperature at mandatory levels.
37. Mean equivalent potential temperature in the lowest 100 mb.
38. Surface pressure.

the development of Berry et al., (1945), page 703, we add 2 gm/kg to the layer average mixing ratio for the surface layer as defined above to approximate the increase in moisture expected from daytime evaporation from the ground. At each significant or standard pressure level, Tetan's formula (Berry et al., 1945, p. 343) is solved for the temperature a parcel would have if it were saturated with a mixing ratio equal to the adjusted average surface-layer mixing ratio. The saturation mixing ratio line intersects the sounding temperature curve within a pressure layer if the sounding temperature at the top (bottom) of the layer is less (greater) than the computed temperature. Then the height is found by linear interpolation.

Interpretation: The convective condensation level is the height that convective clouds will have their bases assuming that the surface air has been carried aloft without mixing. It is expected that lower cloud bases are linked to greater boundary layer moisture and hence greater precipitation potential of convective systems.

5) Convective Temperature

Derivation: Compute the potential temperature at the height and temperature of the convective condensation level, then find the surface temperature.

Interpretation: The convective temperature is the surface temperature to which air must be heated before a parcel can rise dry adiabatically to its convective condensation level without ever being colder than its environment. It is the temperature at which convective clouds should start to form if no mixing in ascent takes place.

6) Difference Between the Convective Temperature and the 850 mb Temperature

Derivation: Subtract the 850 mb temperature from the convective temperature.

Interpretation: The surface layers must be warmer relative to the layers aloft for stable dry conditions than for moist unstable conditions for deep convection to commence. This SPEC removes the temperature dependency upon season and airmass carried by the convective temperature.

7) Height Where T = 0°, T = -5°, T = -10°, T = -15°, T = -20°C

Derivation: SPECS obtained directly from sounding upon linear interpolation in pressure.

Interpretation: These are critical heights where the AgI agent is active within clouds. They will aid in assessing seeding hypotheses and in establishing opportunity climatologies.

8) Warm Convective Depth

Derivation: The difference between the height where T = 0°C and the convective condensation level.

Interpretation: The depth of warm cloud through which a seeding agent must pass if introduced at cloud base should be useful in assessing seeding hypotheses.

9) Mean Surface to Convective Condensation Level Mixing Ratio

Derivation: It is a layer depth weighted average of the mixing ratios at all standard and significant levels below the convective condensation level.

Interpretation: The mixing ratio of the convective layer rather than the surface layer mixing ratio determines the cloud base height if the convective layer is well mixed. It also gives a measure of the available low level moisture.

10) Wet Bulb Zero Height

Derivation: For each level, compute the temperature a parcel of air would have if lifted to its condensation level (LCL). Then find the wet bulb temperature. We interpolate from tables of temperature, pressure, and wet bulb temperature. Proceed upward level by level to where the wet bulb temperature is less than 0°C. Then interpolate linearly in height from the surrounding levels.

Interpretation: The height of the wet bulb zero (WBZ) has been shown to be a good indicator of tornado or hail producing conditions. Tornadoes and large hail most often occur when the WBZ is 2-3 km AGL. The occurrence of these weather situations diminishes rapidly as the WBZ height goes above or below this layer.

11) K-Index

Derivation: The K-index is given by the difference between the 850 mb and 500 mb temperatures minus the difference between the 700 mb temperature and dewpoint plus the 850 mb dewpoint.

Interpretation: The K-index (George, 1960) combines a measure of the 850-500 mb stability with the 850 mb moisture and the depth of the moist layer given by the 700 mb dewpoint depression. Larger values of the K-index indicate greater thunderstorm potential. If the index is less than 20 expect no thunderstorms, expect isolated activity if between 20-25, widely scattered activity if between 25-30, scattered activity if between 30-35, and numerous showers if greater than 35.

12) D-Index

Definition: The thickness of the 900-700 mb layer minus the thickness of the 700-500 mb layer.

Interpretation: The D-index gives atmospheric stability through the thickness difference between two layers. Larger D-values are found when a warm layer is overlain by a cold layer, a condition most favorable for deep convection.

13) Showalter Index

Definition: Use Tetan's formula to compute the LCL of a parcel of air initially at 850 mb. Then use the wet bulb temperature tables to interpolate the temperature the parcel would have upon moist adiabatic ascent to 500 mb. Subtract this temperature from the 500 mb sounding temperature.

Interpretation: The Showalter index (Showalter, 1953) gives a measure of the convective potential of parcel ascent. Values greater than zero generally indicate stable conditions. Negative values indicate unstable thunderstorm-likely conditions.

14) Boyden Index

Definition: The Boyden index (Boyden, 1963) has been modified for the High Plains. It is given by the 900-700 mb thickness minus the mean temperature of the 700-200 mb layer.

Interpretation: Like the D-index, the Boyden index gives a measure of stability by the difference in layer thicknesses.

15) Cross Totals Index

Definition: The 850 mb dewpoint minus the 500 mb temperature.

Interpretation: See 17).

16) Vertical Totals Index

Definition: The 850 mb temperature minus the 500 mb temperature.

Interpretation: See 17).

17) Total Totals Index

Definition: The sum of the cross totals and the vertical totals indices.

Interpretation: The total totals and its components were developed for forecasting severe storm conditions (Miller, 1967). The greater the value of the total totals, the greater the chance of severe weather. A value of 44 is a lower threshold for light to moderate thundershowers. Values in excess of 52 are considered an indication of severe weather with hail and possible tornadoes.

18) The Potential Wet Bulb Index

Derivation: The difference in the wet bulb potential temperatures at 500 and 850 mb gives this index.

Interpretation: The wet bulb temperature is defined as the temperature to which air may be cooled by evaporating water into it at constant pressure until it is saturated. The wet bulb potential temperature is the temperature the air would have if brought moist adiabatically to 1000 mb. Decreasing values of this index indicate increasing severe thunderstorm potential. Evaporation into very dry air at mid levels is a factor in producing strong thunderstorm downdrafts. Very moist air at lower levels is essential for thunderstorm formation. Both combine to yield low values of the potential wet bulb index (David and Smith, 1971).

19) The Total Energy Index

Derivation: The total energy of an air parcel is given by the sum of its internal, potential, latent and kinetic energies. The total energy index (Darkow, 1968) is given by the difference between the total energies at 500 and 850 mb.

Interpretation: Low values of the total energy are associated with cold and dry airmasses. The greatest severe thunderstorm potential exists when low energy air at 500 mb overlies high energy (warm and moist) air at 850 mb. Thus, decreasing values of the total energy index is indicative of increasing severe storm potential.

20) The Severe Storm Index

Derivation: The severe storm index (Williams, 1968) is the sum of the saturation thicknesses from the level of free convection (LFC) to 500 mb and from the lifted condensation level (LCL) to the LFC, where the saturation thickness is the difference between the thickness of the layer calculated from the parcel temperature and that calculated from the sounding temperature.

Interpretation: Physically, the severe storm index combines a measure of the potential buoyant energy of an ascending air parcel above its LFC and the work required to bring the parcel to its LFC from its LCL. Williams found a good correlation between the index and convective precipitation at stations in the western United States.

21) The Equivalent Potential Temperature Index

Derivation: Predict or compute from the sounding the maximum daytime surface temperature. Predict the dewpoint at the time of maximum surface temperature. Then compute the equivalent potential temperature for all significant and standard levels from the surface to 400 mb. The equivalent potential temperature index is given by the maximum equivalent potential temperature in the sfc-850 mb layer minus the minimum equivalent potential temperature.

Interpretation: Severe thunderstorm potential increases with increasing equivalent potential temperature index. When cold and dry layers aloft overlie warm moist surface layers, a convectively unstable condition exists. Strong cold downdrafts can also be produced under these conditions.

22) The SWEAT Index

Derivation: The SWEAT index (Miller et al., 1971) is an empirical relationship that includes the 850 mb moisture, the total totals index, and the wind speeds and directions at 850 and 500 mb. The index is given by

$$SWEAT = 12\ TD_{850} + 20\ (TOT - 49) + 4\ WS_{850} + .2\ WS_{500} + 125\ [.2 + SIN\ (WD_{500} - WD_{850})]$$

Interpretation: Increasing severe weather potential can be associated with high 850 mb dewpoint, strong convective instability as measured through the total totals index, strong wind speeds at 850 and 500 mb, and significant wind direction shear between 850 and 500 mb. These individual factors have all been determined as important indicators of severe weather conditions.

23) The Wind Speed

Derivation: The wind speeds at the levels given in 3) are taken directly from the sounding.

Interpretation: Wind speeds aloft determine the speed of movement of showers. A correlation between radar echo - shower movement and rainfall has been documented in other seeding experiments (Biondini, 1976).

24) The Wind Direction

Derivation: The wind directions at the levels given in 3) are taken directly from the sounding. Then the unit wind vectors are projected onto four straight line segments which are oriented progressively at 45 degree intervals. This has been done to eliminate bi-polar distributions introduced as a consequence of the transition of northerly winds from 359 to 00 degrees.

Interpretation: Wind directions indicate the position of the experimental site with respect to synoptic weather disturbances, hence the signs of the vertical motion, and of the moisture transport.

25) The U-Component of the Wind at 850 mb and 500 mb

Derivation: Taken from the sounding.

Interpretation: See 26) below.

26) The V-Component of the Wind at 850 mb and 500 mb

Derivation: Taken from the sounding.

Interpretation: The magnitude of the wind blowing from moist regions is an indicator of moisture advection.

27) The U-Component of the 500-850 mb Wind Shear

Derivation: The u-component of the 500 mb wind minus the u-component of the 850 mb wind.

Interpretation: See 29) below.

28) The V-Component of the 500-850 mb Wind Shear

Derivation: The v-component of the 500 mb wind minus the v-component of the 850 mb wind.

Interpretation: See 29) below.

29) The 850-500 mb Wind Speed Shear

Derivation: The wind shear is found by the vector combination of the u and v component shears.

Interpretation: The magnitude of the speed shear has been found to be an important factor in the intensity of deep convection. Weak clouds tend to be destroyed in strong shear but strong convection is often intensified and severe weather sometimes occurs.

30) The 850-500 mb Wind Direction Shear

Derivation: The wind direction shear is found by subtracting the 850 mb wind direction from the 500 mb wind direction.

Interpretation: Strong positive wind direction shear as the wind goes from southerly to westerly has been found to be associated with severe thunderstorm activity. This shear configuration is often found with the conjunction of low and mid-level jet streams, an area of strong moisture advection and rapid destabilization.

31) The 300-700 mb Wind Direction Shear

Derivation: Subtract the 700 mb wind direction from the 300 mb wind direction.

Interpretation: The 300-700 mb wind shear gives an indication of the sign of the mid and upper level stability tendency as deduced from the thermal wind equation.

32) The 300-500 mb Wind Speed Shear

Derivation: The wind speed shear is the difference between the 300 and 500 mb wind speeds taken directly from the sounding.

Interpretation: This SPEC is designed to indicate the strength of the upper level jet stream, often associated with thunderstorm activity.

33) The Temperature at Mandatory Levels

Derivation: Temperatures are taken directly from the sounding.

Interpretation: Temperatures aloft often are indicative of the type of airmass present.

34) The Height at Mandatory Levels

Derivation: Heights are taken directly from the sounding.

Interpretation: The heights are indicative of the strength of synoptic scale disturbances which are often accompanied by convective activity.

35) The Dewpoint at Mandatory Levels

Derivation: Dewpoints are taken directly from the soundings.

Interpretation: The dewpoints are a measure of available moisture for precipitation systems.

36) The Equivalent Potential Temperature

Derivation: Equivalent potential temperatures are calculated from sounding temperatures and mixing ratios. Find the temperatures and pressures of the lifted condensation levels. Then compute the equivalent potential temperatures with standard formulas.

Interpretation: The equivalent potential temperature gives a measure of heat and moisture within airmasses.

37) The Mean Equivalent Potential Temperature in the Lowest 100 mb

Derivation: Determine the mean temperature and moisture of the lowest 100 mb layer. Then use the procedure described in 36) above to derive the equivalent potential temperature.

Interpretation: The equivalent potential temperature is a measure of the heat and moisture in an airmass. Then, taken within the surface layer, higher equivalent potential temperatures indicate the presence of warm moist convectively unstable airmasses.

38) The Surface Pressure

Derivation: The surface pressure is the first reported pressure on the sounding.

Interpretation: Low surface pressures are often indicative of precipitation producing cyclone and frontal disturbances.

Most of the SPECs in Table 6 address stability (items 4, 5, 6, 10-22, 32). The moisture category includes variables 1-3, 9, 24-26, 35-37. Variables 23 and 27-31 use wind speed, wind direction, and variations of the wind with height to detect the presence and/or the approach of trigger mechanisms. Variables 7 and 8 are aids for the refinement of the seeding effort. They give climatological information on the heights critical to seeding agent activation and on an estimate of the depth of warm cloud through which the seeding agent must pass if released at cloud base. Note that the warm convective depth may differ from the actual warm depth of the cloud, but short of using observed cloud bases (which are seldom available), there is no means of computing the latter.

(a) Statistical Summary of Upper Air SPECs. The 1200 GMT Dodge City, Kansas soundings for 13 Junes from 1958-1970 were used to develop 136 candidate SPECs (expanded from Table 8) and their linear correlations with the dependent variable, the 7 AM - 7 AM daily rainfall averaged over a square 170 km on a side centered on Dodge City. In general, the correlations confirm the findings of past studies that rainfall is poorly correlated with environmental SPECs. Table 9 shows that no one variable explained more than 10% of the rain variance.

The number of candidate SPECs was reduced from 136 to 42 by discarding those with correlation coefficient magnitudes less than 0.15. Those retained are identified with a number to the right of the correlation values in Table 9. The 42 variables retained break down into 4 categories: moisture category (32), stability category (5), trigger mechanism category (4), and special aids category (1). The moisture variables are highly intercorrelated. Many are taken from tables of dewpoint, saturation deficit, and precipitable water.

The intercorrelation between rainfall and the 42 variables are shown in Table 10. The candidate SPECs were found to be more highly correlated with each other than with rainfall. The identifying numbers for the rows and columns of Table 10 are the numbers of the 42 retained variables listed in Table 9.

A new set of 136 SPECs were determined by computing the 24 hr tendencies of the variables listed in Table 9. These were found to be more poorly correlated with daily rainfall than with the former SPEC set. One possible explanation for this is that changes in the environmental structure that lead to a brief shower takes place over a period of several days. No further consideration was given to the tendency variables.

(5) The Problem of Transience. The vertical motion fields of the meteorological systems (front, squall line, jet streak, dry line, convergence zone, etc.) that often trigger High Plains convective showers frequently occur on space scales no larger than 100 km and on time scales of a few hours. Rapid destabilization can occur within mesoscale upward vertical velocity zones along and ahead of cold fronts and squall lines. Low level inversions have been destroyed over a period of time from 1-3 hours in advance of squall lines (Long, 1963). The temperature and moisture lapse rates within these convergent zones can be expect to differ considerably from the lapse rates obtained from the morning soundings unless these are located within the convergent zones. In the latter instances, the sounding may pass through extensive cloud layers or be taken through environmental layers that have experienced cloud scale subsidence. These soundings would be representative only of the column of air through which the balloon ascended,

PROGSPECs derived from the early morning soundings are likely to have little or no correlation with events that occur later in the day when precipitation is initiated by a dynamic trigger.

Table 9. List of candidate sounding derived SPECs and their linear correlations with rainfall.

		Variable ID	Linear Correlation		Number of Variable as it Appears in Table 10
			Variable	24 Hour Tendency	
1	PIN(1)	Pressure (mb) sfc	.00	.04	
2	TIN(1)	Temp (°C) sfc	.08	.02	
3	TD(1)	Dewpoint (°C) sfc	.17	.06	1
4	θ(1)	Potential Temp sfc	.14	.05	
5	HIN(1)	Height sfc	.01	.00	
6	PIN(2)		.00	.00	
7	TIN(2)		-.04	-.02	
8	TD(2)	at 900 mb	.18	.08	2
9	θ(2)	level	.12	.06	
10	HIN(2)		-.01	.04	
11	PIN(3)		.00	.00	
12	TIN(3)		-.07	-.02	
13	TD(3)	850 mb	.21	.08	3
14	θ(3)		.14	.06	
15	HIN(3)		-.03	-.01	
16	PIN(4)		.00	.00	
17	TIN(4)		-.05	-.03	
18	TD(4)	800 mb	.23	.10	4
19	θ(4)		.16	.08	5
20	HIN(4)		.02	.01	
21	PIN(5)		.00	.00	
22	TIN(5)		-.07	-.07	
23	TD(5)	700 mb	.19	.11	6
24	θ(5)		.11	.07	
25	HIN(5)		.06	.00	
26	PIN(6)		.00	.00	
27	TIN(6)		-.09	-.02	
28	TD(6)	600 mb	.25	.10	7
29	θ(6)		.15	.08	
30	HIN(6)		.05	-.00	
31	PIN(7)		.00	.00	
32	TIN(7)		-.02	-.03	
33	TD(7)	500 mb	.27	.09	8
34	θ(7)		.12	.04	
35	HIN(7)		.02	.01	
36	PIN(8)		.00	.00	
37	TIN(8)		.02	-.02	
38	TD(8)		.17	.09	9
39	θ(8)	400 mb	.07	.02	
40	HIN(8)		.01	-.03	
41	PIN(9)		.00	.00	
42	TIN(9)		-.17	-.12	10

		Variable ID	Linear Correlation Variable	Linear Correlation 24 Hour Tendency	Number of Variable as it Appears in Table 10
43	TD(9)		.15	-.11	11
44	θ(9)	200 mb	-.17	-.12	12
45	HIN(9)		.08	-.10	
46	SATDF(1)	sfc	.07	-.05	
47	SATDF(2)	900 mb	-.20	-.08	13
48	SATDF(3)	Saturation deficit 850 mb	-.19	-.05	14
49	SATDF(4)	800 mb	-.18	-.08	15
50	SATDF(5)	700 mb	-.19	-.14	16
51	SATDF(6)	600 mb	-.24	-.12	17
52	SATDF(7)	500 mb	-.24	-.10	18
53	SATDF(8)	400 mb	.10	-.11	
54	SATDF(9)	200 mb	.14	-.13	
55	HCCL	Height of CCL	-.18	-.09	19
56	TCC	Convective temperature	.11	-.07	
57	TC850	TCC - T_{850}	.08	-.05	
58	HTEM(1)	Height of 0°C	.02	-.03	
59	HTEM(2)	Height of -5°C	.01	-.02	
60	HTEM(3)	Height of -10°C	.01	-.02	
61	HTEM(4)	Height of -15°C	.02	-.06	
62	HTEM(5)	Height of -20°C	.05	-.04	
63	WCDEP	Warm convective depth	.18	.08	20
64	WSFCCL	Mean mixing ratio sfc to HCCL	.24	.15	21
65	KINDX	K - index	.24	.13	22
66	DINDX	D - index	.07	-.00	
67	SINDX	Showalter index	-.16	-.07	23
68	BINDX	Boyden index	.07	.00	
69	CROST	Cross total	-.23	-.09	24
70	VERT	Vertical total	.05	-.01	
71	TTT	Total total	.14	-.07	
72	WETB	WETBULB Potential temperature index	.07	-.04	
73	EINDX	Energy index	.04	.02	
74	THESFC	Mean equivalent potential temperature in lowest 100 mb	.14	.05	
75	WD(1)	Wind direction	-.19	-.05	25
76	WS(1)	Wind speed at sfc level	-.05	-.01	
77	WQ(1)	Wind direction category	-.19	-.05	26
78	WD(2)		-.17	-.09	27
79	WS(2)	Wind information at 900 mb	-.10	-.02	
80	WQ(2)		-.17	-.09	28
81	WD(3)		-.06	-.09	
82	WS(3)	Wind information at 850 mb	-.04	-.04	
83	WQ(3)		-.05	-.09	
84	WD(4)		-.04	-.06	
85	WS(4)	Wind information at 800 mb	-.00	-.05	
86	WQ(4)		-.04	-.07	
87	WD(5)		-.04	-.02	
88	WS(5)	Wind information at 700 mb	-.00	-.09	
89	WQ(5)		-.04	-.02	

	Variable ID		Linear Correlation Variable	Linear Correlation 24 Hour Tendency	Number of Variable as it Appears in Table 10
90	WD(6)		-.01	.01	
91	WS(6)	Wind information at 600 mb	-.04	-.08	
92	WQ(6)		.01	-.00	
93	WD(7)		-.03	.01	
94	WS(7)	Wind information at 500 mb	-.02	-.02	
95	WQ(7)		-.03	.02	
96	WD(8)		-.04	-.02	
97	WS(8)	Wind information at 400 mb	-.01	-.01	
98	WQ(8)		-.06	-.02	
99	WD(9)		-.04	-.04	
100	WS(9)	Wind information at 200 mb	.05	-.00	
101	WQ(9)		-.03	-.04	
102	WD850	Wind direction at 850 mb	-.06	-.09	
103	WS850	Wind speed at 850 mb	-.04	-.04	
104	WD500	Wind direction at 500 mb	-.03	.01	
105	WS500	Wind speed at 500 mb	-.02	-.02	
106	WD300	Wind direction at 300 mb	-.07	-.05	
107	WS300	Wind speed at 300 mb	.05	.05	
108	WD700	Wind direction at 700 mb	-.04	-.02	
109	WS700	Wind speed at 700 mb	-.00	-.09	
110	U(1)	Wind U-component of WS850	-.14	-.14	
111	V(1)	Wind V-component of WS850	.05	.05	
112	U(2)	Wind U-component of WS500	-.02	-.01	
113	V(2)	Wind V-component of WS500	.13	-.00	
114	SU	U(2) - U(1)	.07	.10	
115	SV	V(2) - V(1)	.05	-.04	
116	MV	Wind shear speed	-.10	-.02	
117	ANG	Wind shear direction	.10	.08	
118	DELD	WD300 - WD700	-.03	-.03	
119	DELS	WS300 - WS500	.08	.04	
120	PRECP(1)	Precipitable water sfc - 900 mb	.16	.09	29
121	PRECP(2)	900 - 850 mb	.20	.07	30
122	PRECP(3)	850 - 800 mb	.23	.09	31
123	PRECP(4)	800 - 700 mb	.24	.13	32
124	PRECP(5)	700 - 600 mb	.26	.13	33
125	PRECP(6)	600 - 500 mb	.30	.11	34
126	PRECP(7)	500 - 400 mb	.26	.10	35
127	PRECP(8)	400 - 200 mb	.00	.00	
128	PRECPT(1)	sfc - 900 mb	.16	.09	36
129	PRECPT(2)	Precipitable water sfc - 850 mb	.21	.09	37
130	PRECPT(3)	sfc - 800 mb	.23	.09	38
131	PRECPT(4)	sfc - 700 mb	.25	.12	39
132	PRECPT(5)	sfc - 600 mb	.28	.13	40
133	PRECPT(6)	sfc - 500 mb	.29	.13	41
134	PRECPT(7)	sfc - 400 mb	.30	.14	42
135	PRECPT(8)	sfc - 200 mb	.00	.00	
136	SSI	Severe storm index	-.10	-.11	

Table 10. Correlation matrix for 42 sounding derived predictor variables and rainfall.

	1	2	3	4	5	6	7	8	9	10	11	12	13	14
1	1.00													
2	.88	1.00												
3	.61	.77	1.00											
4	.45	.53	.81	1.00										
5	.62	.66	.73	.78	1.00									
6	.32	.30	.47	.66	.51	1.00								
7	.31	.25	.32	.42	.37	.72	1.00							
8	.31	.24	.26	.33	.30	.48	.73	1.00						
9	.22	.16	.22	.27	.15	.35	.48	.62	1.00					
10	.01	.04	.04	.03	.09	-.06	-.06	-.08	-.02	1.00				
11	-.01	.03	.04	.04	.07	-.04	-.05	-.06	.02	.98	1.00			
12	.00	.04	.04	.03	.09	-.06	-.06	-.08	-.02	1.00	.98	1.00		
13	-.17	-.34	-.43	-.35	-.00	-.22	-.13	-.13	-.15	.10	.07	.10	1.00	
14	.03	-.12	-.49	-.43	.06	-.24	-.11	-.07	-.19	.07	.04	.07	.76	1.00
15	.16	.08	-.26	-.50	.11	-.33	-.12	-.07	-.23	.07	.04	.07	.57	.81
16	.16	.17	-.05	-.28	.23	-.57	-.32	-.19	-.27	.11	.06	.11	.41	.55
17	.08	.12	-.03	-.16	.19	-.43	-.66	-.45	-.38	.13	.10	.13	.30	.38
18	.07	.13	.06	-.02	.21	-.18	-.36	-.64	-.36	.16	.12	.16	.23	.22
19	-.26	-.36	-.48	-.44	-.06	-.24	-.10	-.07	-.23	.05	.03	.05	.57	.62
20	.49	.60	.67	.58	.36	.29	.14	.12	.23	.02	.03	.02	-.48	-.49
21	.61	.72	.82	.70	.56	.44	.31	.29	.29	.02	.01	.02	-.50	-.51
22	.47	.51	.68	.74	.58	.82	.55	.40	.29	-.03	-.02	-.03	-.25	-.26
23	-.60	-.68	-.72	-.52	-.68	-.23	-.16	-.17	-.03	-.03	-.02	-.03	.06	-.01
24	-.41	-.58	-.85	-.67	-.44	-.33	-.20	-.18	-.14	.01	.01	.01	.53	.62
25	-.16	-.19	-.28	-.27	-.22	-.24	-.21	-.21	-.15	.15	.14	.15	.23	.20
26	-.16	-.19	-.29	-.28	-.23	-.25	-.21	-.21	-.14	.15	.14	.15	.23	.19
27	-.05	-.10	-.18	-.17	-.05	-.14	-.16	-.14	-.15	.14	.12	.14	.27	.24
28	-.05	-.10	-.18	-.17	-.05	-.15	-.17	-.14	-.16	.14	.11	.14	.27	.24
29	.64	.62	.55	.49	.39	.35	.23	.21	.26	-.07	-.06	-.07	-.30	-.30
30	.78	.92	.90	.65	.73	.35	.27	.25	.18	.05	.04	.05	-.39	-.29
31	.54	.67	.92	.88	.76	.50	.32	.26	.23	.03	.03	.03	-.42	-.49
32	.41	.44	.68	.88	.66	.78	.50	.38	.34	-.01	.00	-.01	-.33	-.41
33	.34	.28	.40	.56	.41	.85	.80	.61	.49	-.06	-.03	-.06	-.22	-.24
34	.30	.21	.28	.37	.28	.59	.84	.83	.61	-.08	-.05	-.08	-.17	-.15
35	.25	.16	.23	.31	.20	.44	.61	.85	.81	-.06	-.02	-.06	-.18	-.18
36	.64	.62	.55	.49	.39	.35	.23	.21	.26	-.06	-.06	-.07	-.30	-.30
37	.81	.90	.86	.66	.68	.39	.28	.26	.23	.01	.00	.01	-.39	-.32
38	.73	.84	.93	.79	.75	.45	.31	.28	.24	.02	.01	.02	-.42	-.41
39	.64	.73	.89	.88	.76	.63	.42	.34	.30	.01	.01	.01	-.41	-.44
40	.61	.67	.83	.87	.73	.74	.55	.44	.37	-.01	-.00	-.01	-.39	-.42
41	.60	.64	.79	.83	.70	.76	.63	.54	.44	-.02	-.01	-.02	-.38	-.40
42	.60	.62	.77	.82	.69	.76	.66	.59	.49	-.02	-.01	-.03	-.37	-.39
Rainfall	.17	.18	.22	.24	.17	.22	.26	.27	.18	-.17	-.16	-.17	-.20	-.19

Table 10. (Continued)

15	16	17	18	19	20	21	22	23	24	25	26	27	28	29
1.00														
.77	1.00													
.49	.73	1.00												
.28	.44	.64	1.00											
.61	-.48	.34	.18	1.00										
-.42	-.23	-.08	.03	-.89	1.00									
-.36	-.20	-.13	-.02	-.61	.74	1.00								
-.31	-.50	-.42	-.28	-.42	.46	.60	1.00							
-.15	-.18	-.06	.12	.23	-.39	-.55	-.66	1.00						
.41	.24	.23	.28	.57	-.60	-.71	-.70	.75	1.00					
.15	.12	.14	.11	.16	-.23	-.26	-.24	.18	.25	1.00				
.16	.12	.13	.11	.15	-.23	-.27	-.26	.19	.25	.99	1.00			
.19	.11	.13	.07	.15	-.18	-.20	-.09	.02	.15	.65	.65	1.00		
.19	-.12	.14	.07	.14	-.17	-.20	-.09	.01	.15	.65	.65	.99	1.00	
-.25	-.18	-.06	.03	-.40	.54	.61	.44	-.33	-.43	-.24	-.25	-.12	-.12	1.00
-.03	-.13	.10	.12	-.40	.64	.80	.57	-.74	-.71	-.26	-.26	-.15	-.14	.60
-.37	-.11	-.04	.05	-.46	.64	.79	.66	-.63	-.77	-.32	-.33	-.21	-.21	.52
-.51	-.43	-.26	-.07	-.40	.51	.63	.75	-.38	-.54	-.32	-.33	-.21	-.21	.50
-.32	-.53	-.56	-.30	-.23	.28	.40	.69	-.17	-.28	-.28	-.28	-.18	-.20	.38
-.17	-.34	-.62	-.52	-.14	.16	.29	.47	-.11	-.19	-.23	-.23	-.16	-.17	.24
-.21	-.31	-.49	-.61	-.19	.18	.27	.37	-.08	-.18	-.20	-.20	-.14	-.15	.22
-.25	-.18	-.06	.03	-.40	.54	.61	.44	-.33	-.43	-.24	-.25	-.12	-.12	1.00
-.12	.03	.05	.09	-.44	.67	.81	.58	-.66	-.68	-.28	-.28	-.15	-.15	.82
-.23	-.03	.01	.08	-.47	.69	.84	.64	-.68	-.75	-.31	-.32	-.18	-.18	.73
-.37	-.21	-.11	.02	-.48	.66	.81	.74	-.60	-.71	-.34	-.35	-.21	-.21	.68
-.38	-.31	-.24	-.06	-.45	.61	.76	.78	-.53	-.65	-.35	-.36	-.22	-.22	.65
-.36	-.32	-.31	-.14	-.41	.56	.73	.79	-.50	-.62	-.34	-.35	-.21	-.21	.67
-.36	-.33	-.33	-.19	-.41	.55	.71	.78	-.48	-.61	-.34	-.34	-.21	-.22	.61
-.18	-.19	-.24	-.24	-.18	.18	.24	.25	-.16	-.23	-.21	-.20	-.19	-.18	.15

Table 10. (Continued)

30	31	32	33	34	35	36	37	38	39	40	41	42	Rainfall
1.00													
.85	1.00												
.56	.83	1.00											
.32	.47	.79	1.00										
.24	.30	.49	.82	1.00									
.19	.24	.39	.62	.86	1.00								
.60	.52	.50	.38	.24	.22	1.00							
.95	.82	.60	.38	.26	.22	.82	1.00						
.95	.94	.73	.43	.29	.24	.73	.97	1.00					
.85	.96	.90	.62	.40	.32	.68	.88	.95	1.00				
.78	.90	.94	.77	.55	.43	.65	.81	.89	.98	1.00			
.74	.85	.92	.82	.66	.53	.62	.77	.84	.94	.98	1.00		
.72	.83	.91	.84	.71	.59	.61	.75	.82	.92	.97	1.00	1.00	
.21	.24	.25	.27	.31	.27	.15	.21	.23	.26	.28	.29	.30	1.00

Stability indicies are particularly sensitive to local variations in moisture and temperature stratifications. Moisture variables are subject to changes as dry airmasses advance or retreat locally. PROGSPECs derived from wind observations cannot carry those events where circulations associated with dynamic triggers are small in scale.

Should the transience of the dynamic trigger be a significant contributor to poor correlations with convective rain, there should be a time decay of the magnitudes of the correlations between the early morning sounding SPECs and the hourly rainfall. The hourly rainfall was grouped into 3-hourly periods and linear correlations computed between each period and the 136 sounding SPECs are listed in Table 9. Since the sounding ascent time is between 05-06 LST, the SPECs are not predictive for the first two periods.

The correlations exceeded 0.15 in magnitude for only 84 SPECs. These are listed in Table 11. The variable ID is cross referenced with the variable listing in Table 11. Part of the explanation for the low correlations rests with the paucity of hourly rainfall data - one station per 6500 km^2 on the average. However, the trends should enlighten the transience problem. A summary of the number of SPECs retained is presented at the bottom of Table 11. About 40 variables were retained for the two periods (0100-0300, 0400-6000) of rainfall that occurred prior to the sounding ascent time. After that, the number of SPECs retained drops rapidly. This decline is shown graphically in Figure 5. Subjective best fit straight lines have been constructed to reveal the daily trends. The time decay is dramatic for all but the stability category for which there were too few SPECs to define a trend. After 1500 LST, none of the trigger SPECs exceeded the cutoff magnitude. The total number of SPECs decreased from near 40 for the non-predictive periods to just a few by the end of the day. Physically, the figure reveals that ambient meteorological conditions at sounding time are not representative of meteorological conditions a few hours later.

The purpose of the SPEC analysis was to find SPECs that related well with the afternoon convective period (1100-2200 LST) rainfall. Table 11 shows that only 36 of the 84 variables retained had correlation magnitudes exceeding 0.15 for at least one of the four convective period rainfall intervals. These retained variables show virtually no time continuity between rainfall periods. No variables were retained for the 1600-1800 LST period. We find the low correlations and the poor continuity to be firm indicators that the 1200 GMT upper air derived variables are virtually useless as PROGSPECs for convective period rainfall. However, PROGSPECs derived from soundings taken at mid-morning just prior to the convective period may be more productive than those discussed herein.

(6) Surface Fields and their Application to the SPEC Analysis. The lists of SPECs derived from the spatial distributions of meteorological variables are given in Tables 6 and 7. Field

Table 11. Linear correlation coefficients for 84 SPECs with correlation coefficient magnitudes exceeding 0.15 for at least one rainfall period.

Variable ID	Var. No.	Rainfall Period (LST) 01-03	04-06	07-09	10-12	13-15	16-18	19-21	22-24
T (sfc)	2	-.16							
T (900 mb)	7	-.26	-.18						
TD (900 mb)	8							.15	
T (850 mb)	12	-.22	-.19	-.15					
TD (850 mb)	13							.15	
T (800 mb)	17	-.22	-.21	-.17					
TD (800 mb)	18	.15				.16			
T (700 mb)	22	-.19	-.20	-.17					
TD (700 mb)	23	.20	.17	.16					
T (600 mb)	27				.16				
TD (600 mb)	28	.23	.19	.16					.15
TD (500 mb)	33	.22	.23	.16	.15	.19			
TD (400 mb)	38	.18	.21			.19			
T (200 mb)	42		-.16	-.15					
θ (200 mb)	44		-.16	-.15					
SATDF (sfc)	46	-.24	-.17						
SATDF (900 mb)	47	-.26	-.19	-.15		-.16			
SATDF (850 mb)	48	-.22	-.20	-.16		-.16			
SATDF (800 mb)	49	-.25	-.24	-.20		-.17			
SATDF (700 mb)	50	-.27	-.25	-.24					
SATDF (600 mb)	51	-.30	-.27	-.24					
SATDF (500 mb)	52	-.22	-.20		-.16	-.18		-.15	
HCCL	55		-.19	-.20	.17				
TCC	56		-.17	-.18	.24				
TCC-T (850)	57				.34	.19			
Hgt 0°C	58		-.16	-.15					
Hgt -5°C	59		-.15	-.17					
Hgt -10°C	60			-.16					
WCDEP	63			.15	-.20				
WSFCCL	64	.15				.17		.18	
KINDEX	65	.16	.15			.15			
SINDEX	67							-.20	
CROST	69					-.15		-.19	
VERT	70	.22	.20						
TOT	71							-.20	
WETB	72							-.15	
SSI	136							-.15	
WD (sfc)	75	-.18				-.21			
WD (900 mb)	78	-.24	-.25	-.21					
WD (850 mb)	81	-.19	-.16						
WS (600 mb)	91	.22	.18						
WS (500 mb)	94	.18							

Table 11. (Continued)

Variable ID	Var. No.	01-03	04-06	07-09	10-12	13-15	16-18	19-21	22-24
WS (700 mb)	109		.15						
U at 850 mb	110	-.23	-.20	-.21		-.15			
V at 850 mb	111	-.15	-.16						
U at 500 mb	112	.18							
U(500)-U(850)	114	.30	.15						
V(500)-V(850)	115	.17	.24	.16					
WS(500)-WS(850)	116	.17							
WD(500)-WD(850)	117	.17							
PCP(900-850)	121							.17	
PCP(850-800)	122					.15		.16	
PCP(800-700)	123	.20	.21	.16		.16			
PCP(700-600)	124	.27	.26	.21		.16			.16
PCP(600-500)	125	.28	.27	.18		.19			
PCP(500-400)	126	.25	.29	.22		.23			
PCP(sfc-850)	129							.16	
PCP(sfc-800)	130							.17	
PCP(sfc-700)	131					.16			
PCP(sfc-600)	132	.17	.18	.16		.17			
PCP(sfc-500)	133	.21	.20			.19			
PCP(sfc-400)	134	.22	.22			.20			
Total PROGSPEC	136	39	38	23	12	22	0	13	2
Total Moisture	37	20	20	14	7	17	0	8	2
Total Stability	11	2	2	0	1	3	0	5	0
Total Trigger	36	17	14	8	1	2	0	0	0
Days with rain		90	51	39	28	34	53	74	86

analyses are especially useful for SPECs because derivative quantities such as gradients, advections, deformations, vorticity, and divergence are physically related to processes that lead to destabilization and vertical displacements.

Field SPECs can be obtained for any level. Above the surface the data density is such that subsynoptic and mesoscale disturbances can go undetected. While recognizing that some of the parameters important for precipitation cannot be evaluated from surface observations only, we proceed with the supposition that the vertically integrated effects of subsynoptic and mesoscale phenomena are detectable in the surface observations both in space and time. This is not to say that these systems can be accurately described by the surface observations, but just that their presence can be detected in them. From an analysis standpoint, the surface observations are denser in space and time than are the upper air observations and are the only climatological large scale network that can resolve subsynoptic scale phenomena.

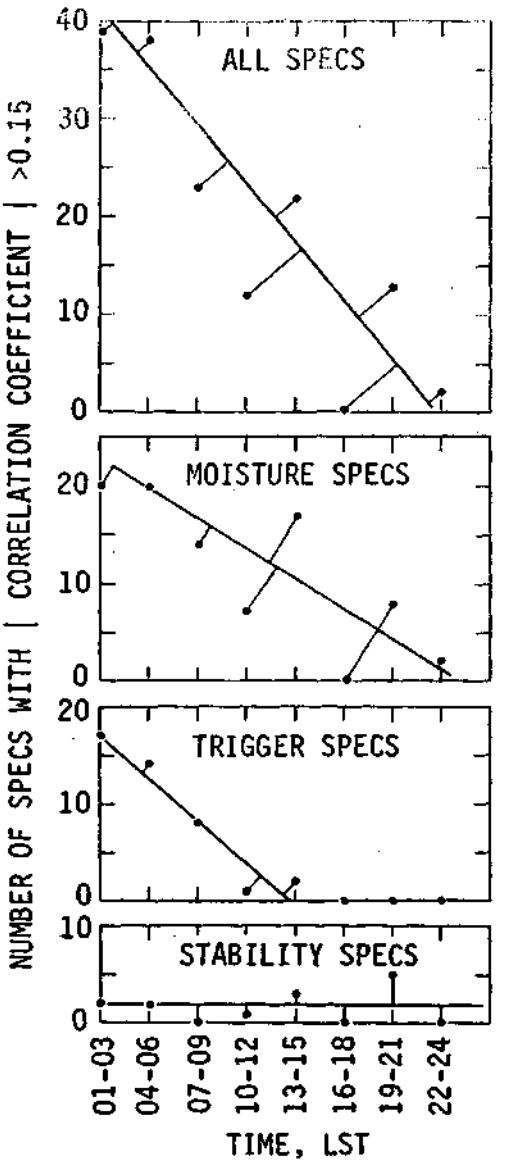

Figure 5. Time decay of the number of SPECs correlated with 3-hourly rainfall correlation coefficients greater than 0.15 in. magnitude.

The lifetimes of mesoscale and subsynoptical scale precipitation producing systems is often on the order of 6-10 hours or longer. The transience problem discussed in the previous section arises because the residence time for these systems at any given location may be less than one hour. Utilization of the surface observations allows the transformation of a very difficult trigger mechanism timing problem into a relatively simple field presentation wherein the trigger can be located within a spatial setting. Given a regime where the precipitation frequency shows a pronounced maximum during a small portion of a day such as occurs over the Kansas high plains, (see section on diurnal rainfall variability), the problem reduces to one of finding the preferred spatial location of triggers that contribute most to rainfall over the target area.

Surface observations of pressure, temperature, dewpoint temperature, wind speed and wind direction were interpolated to a regular mesh to allow the calculation of derivative quantities. The necessary interpolation of the five basic variables for the historical period of 10 years (1965-74) requires in excess of 36,000 objectively analyzed fields. Part of our effort to develop the surface PROGSPECs was directed toward finding a fast and economical objective interpolation method to produce the initial fields. An objective interpolation scheme was developed based upon the method of successive corrections (Bergthorssen and Doos, 1955; Cressman, 1959) that uses a variation of the exponential (Gaussian) weight presented by Barnes (1964). The technique is described in the Appendix on an objective analysis scheme for surface analysis.

(7) Physical Constraints Upon Surface PROGSPECs. There are many possible candidate PROGSPECs that can be derived from the surface observations. The number can be limited by the need to avoid redundancy, the requirement that the PROGSPECs be physically related to the dependent variable, and the limitations imposed by the distribution of surface observations. In regard to the latter, the smallest resolvable disturbance is determined by twice the average station separation (the Nyquist frequency). Figure 4 shows the distribution of surface stations surrounding the Goodland site. The station separation is on the order of 250 km and would imply that systems with dimensions smaller than 500 km could not be resolved. Fortunately, many triggering mechanisms are often located at a sharp interface between two synoptic scale airmasses. These air masses can be easily described with the surface network and the interface located with an error of less than half the station separation by some candidate PROGSPECs. Some quantities such as the sign of the velocity divergence can be determined but the actual magnitudes of the small scale disturbances will remain obscure.

The surface network should surround the proposed site and should extend far enough outward from the site to contain important triggering disturbances at the analysis time. Our grid extends westward to Denver where the mountains disrupt the natural movement

of surface systems. The movement of moist airmasses is captured by observations located east and southeast of the site.

Examples of the resolution of the objective analysis of surface pressure, temperature, dewpoint, and wind field (streamlines and divergence) are shown in Figure 6.

In the synoptic setting, a cold front stretches across the upper left one fifth of the grid. Cooler temperatures occupy this area. The dewpoint analysis shows a west to east increase in dewpoint; the increase is not associated with the cold frontal system. Gradients in both temperature and dewpoint are established in part by the data distribution and in part by the intensity of airmass contrasts. The pressure analysis shows an inverted trough extending northeastward from the southwest corner of the grid. The trough position corresponds well with the implied frontal position in the temperature field and with the streamlines of the wind field. A zone of weak convergence is implied along the front.

The site should be far removed from the boundaries of the grid where fields often contain values extrapolated from the interior. In this aspect we failed, as our evaluation of the surface PROGSPECs was made in relation to the rainfall for an area surrounding Dodge City, located near the lower boundary of the grid. Since the closest surface station south of Dodge City, Oklahoma City, was located 350 km away, movement of the grid southward would have barely alleviated the problem. Thus we could not correlate the Dodge City rainfall with systems moving from the southwest or to the south of Dodge City.

An important physical constraint is imposed by the orographic characteristics of the site. In the Colby-Goodland, Kansas area, the general relief slopes downward from west to east. There is very little roughness in the sense of deep river valleys or basins in the area. The general slope is about 330 m per 100 km, a ratio of 0.0033. A 10 m sec^{-1} wind component slowing normal to the relief would generate a surface vertical velocity of 3.3 cm sec^{-1}. These vertical velocities are similar in magnitude to vertical velocities calculated for subsynoptic scale precipitation producing disturbances. Thus we conclude that upslope flow may be a significant destabilization mechanism operative in the Kansas high plains.

Elevations above sea level or the Kansas site analysis grid were obtained by objective interpolation from estimates of the elevation given at one degree latitude-longitude intersections by Berkofsky and Bertoni (1960). The weighting scheme was chosen so that the scale of orographic features would be comparable with the minimum wavelength of meteorological patterns resolvable with the surface observation network. The resulting elevation pattern is shown in Figure 7. The observation site elevations are included for comparison. The steep slopes along the front ranges of the Rocky Mountains have been smoothed with the result that higher elevations have been extrapolated eastward approximately 100 km.

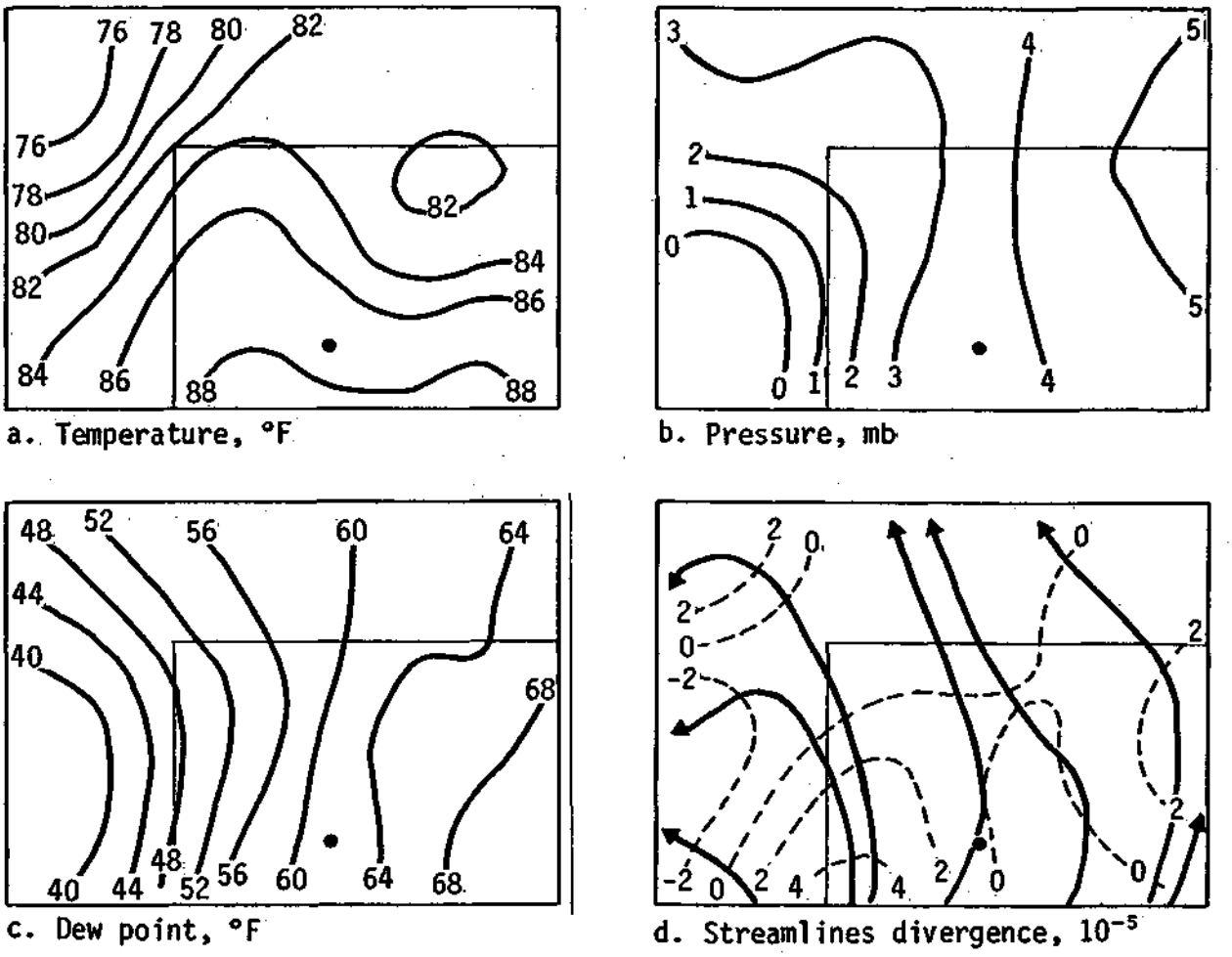

Figure 6. Examples of objectively analyzed meteorological fields of temperature, dewpoint, streamlines, divergence and pressure for 1 June 1965, 1500 LST using the station array and grid shown in figure 4.

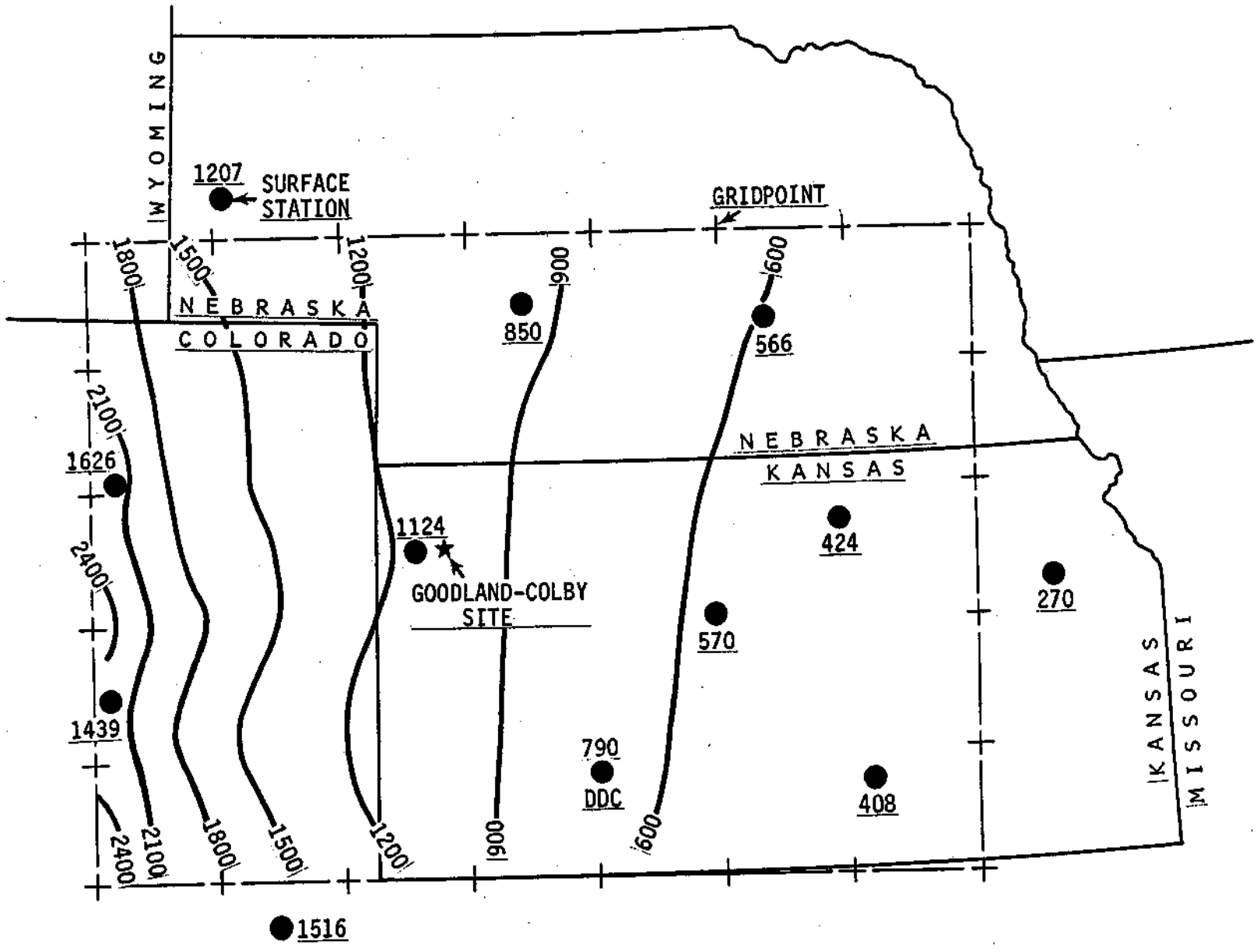

Figure 7. Elevations (meters) for the surface stations and for the analysis grid as determined by objective analysis.

Still, the Arkansas and South Platte river basins near Pueblo and Denver, Colorado are apparent as indentations in the overall pattern. Elsewhere the interpolated elevation field largely conforms to the point elevations taken at the observation sites.

(8) Use of Orography in Surface PROGSPEC Design. An important aspect of the PROGSPEC development is that the candidate independent variables have some physical relationship with the dependent variable. The convergence of the horizontal wind is an ideal PROGSPEC because the sign and magnitude of the vertical velocity, hence the extent of vertical displacement of airmasses, has been quantitatively tied to the vertical integral of the horizontal convergence. However, studies by Shaeffer (1973) have shown that when the divergence is computed over a non-horizontal surface, additional terms appear in the defining equations. The magnitudes of these terms over sloping terrain similar to the terrain of the High Plains are 10^{-5} sec^{-1} - within the range of magnitudes for the horizontal convergence.

The effects of strong boundary layer vertical wind shear above a non-horizontal surface upon the net horizontal convergence have not been fully investigated. Studies by Leichter (1974) suggest that the shear terms can significantly change the vertical displacements implied by the convergence taken alone. We have examined the convergence-shear relationship to develop PROGSPECs that may be more suitable for airmass vertical displacements than the convergence alone.

Let the surface coordinate system be designated by x, y, z. This coordinate system is to be rotated into a new coordinate system x", y", z" where the x", y" plane is horizontal and the z" axis points to the vertical. Let the surface coordinate system be first rotated through on arbitrary angle θ in the x, z plane. From Hess (1959) the transformation equations are

$$\begin{aligned} x' &= x \cos\theta - z \sin\theta \\ y' &= y \\ z' &= x \sin\theta + z \cos\theta \end{aligned} \qquad (1)$$

This new coordinate system is then rotated through an arbitrary angle a in the y", z" frame to form the horizontal coordinate system x", y", z". Thus

$$\begin{aligned} x'' &= x' \\ y'' &= y' \cos\alpha - z' \sin\alpha, \\ z'' &= y' \sin\alpha + z' \cos\alpha. \end{aligned} \qquad (2)$$

Combining (2) with (1) gives

$$\begin{aligned} x'' &= x \cos\theta - z \sin\theta \\ y'' &= y \cos\alpha - x \sin\alpha \sin\theta - z \sin\alpha \cos\theta, \\ z'' &= y \sin\alpha + x \cos\alpha \sin\theta + z \cos\alpha \cos\theta. \end{aligned} \tag{3}$$

It follows that the velocities can be obtained by differentiating (3) with respect to time. However, this step carries with it the assumption that the velocity components are measured along the respective axes of the surface coordinate system. This is not true in practice. Wind measuring instruments are placed with respect to the horizontal coordinate system and the velocity components measured are taken along the respective axes of the horizontal coordinate system. Thus

$$\begin{aligned} u'' &= u, \\ v'' &= v, \\ w'' &= w. \end{aligned} \tag{4}$$

Following through the necessary matrix inversions, the space derivatives of the wind components are found by

$$\begin{aligned} \frac{du}{dx''} &= \cos\theta \frac{du}{dx} - \sin\theta \frac{du}{dz}, \\ \frac{dv}{dy''} &= -\sin\theta \sin\alpha \frac{dv}{dx} + \cos\alpha \frac{dv}{dy} - \cos\theta \sin\alpha \frac{dv}{dz}, \\ \frac{dw}{dz''} &= \sin\theta \cos\alpha \frac{dw}{dx} + \sin\alpha \frac{dw}{dy} + \cos\theta \cos\alpha \frac{dw}{dz}. \end{aligned} \tag{5}$$

These equations give the relationship between the wind component derivatives in the horizontal coordinate system and the wind component derivatives in a surface coordinate system. The slope angles, given by the 0.0033 High Plains (Kansas) orographic slope, are small and the trigonometric quantities in (5) may be approximated by

$$\begin{aligned} &\cos\theta \sim \cos\alpha \sim 1.0, \\ &\sin\theta \simeq \tan\theta = \frac{\Delta E}{\Delta x} \\ &\sin\alpha \simeq \tan\alpha = \frac{\Delta E}{\Delta y} \end{aligned} \tag{6}$$

where E is the surface elevation above sea level. Formulating the horizontal divergence from (5) gives

$$\frac{du}{dx''} + \frac{dv}{dy''} = \frac{du}{dx} + \frac{dv}{dy} - \frac{\Delta E}{\Delta x}\frac{du}{dz} - \frac{\Delta E}{\Delta y}\frac{dv}{dz} - \frac{\Delta E}{\Delta x}\frac{\Delta E}{\Delta y}\frac{dv}{dx} \tag{7}$$

and

$$\frac{dw}{dz''} = \frac{dw}{dz} + \frac{\Delta E}{\Delta x}\frac{dw}{dx} + \frac{\Delta E}{\Delta y}\frac{dw}{dy} \tag{8}$$

The orders of magnitude for the quantities that make up the terms of (7) and (8) are as follows:

$$u \sim v \sim 10 \text{ m sec}^{-1},$$

$$w \sim 10 \text{ cm sec}^{-1} = 10^{-1} \text{ m sec}^{-1},$$

$$\Delta x \sim \Delta y \sim 100 \text{ km} = 10^{5}\text{m},$$

$$\Delta z \sim 10 \text{ km} = 10^{4}\text{m},$$

$$\frac{\Delta E}{\Delta x} \sim \frac{\Delta E}{\Delta y} \sim 10^{-3}$$

The vertical wind shear, $\frac{du}{dz}$, is ~ 10^{-2} sec^{-1} for the 1 km above the surface. Also,

$$\frac{du}{dx} \sim \frac{dv}{dy} \sim 10^{-4} \text{ sec}^{-1},$$

$$\frac{dw}{dz} \sim 10^{-5} \text{ sec}^{-1},$$

$$\frac{dw}{dx} \sim \frac{dw}{dy} \sim 10^{-6} \text{ sec}^{-1}.$$

The following orders of magnitude are deduced for the terms of (7) and (8):

$$\frac{du}{dx} + \frac{dv}{dy} \sim 10^{-5} \text{ sec}^{-1},$$

$$\frac{\Delta E}{\Delta x}\frac{du}{dz} \sim \frac{\Delta E}{\Delta y}\frac{dy}{dz} \sim 10^{-5} \text{ sec}^{-1},$$

$$\frac{\Delta E}{\Delta x}\frac{\Delta E}{\Delta y}\frac{dv}{dx} \sim 10^{-10}\ \text{sec}^{-1},$$

$$\frac{dw}{dz} \sim 10^{-5}\ \text{sec}^{-1},$$

$$\frac{\Delta E}{\Delta x}\frac{dw}{dx} \sim \frac{\Delta E}{\Delta y}\frac{dw}{dy} \sim 10^{-9}\ \text{sec}^{-1}.$$

Dropping the higher order terms, (7) and (8) simplify to

$$\frac{du}{dx''} + \frac{dv}{dy''} = \frac{du}{dx} + \frac{dv}{dy} - \frac{\Delta E}{\Delta x}\frac{du}{dz} - \frac{\Delta E}{\Delta y}\frac{dv}{dz} \tag{9}$$

and

$$\frac{dw}{dz''} = \frac{du}{dz}. \tag{10}$$

Equation (9) gives the transformations between the horizontal convergence and the surface convergence as presented by Schaeffer (1973). Had the surface wind measurements been actually taken along the surface plane, additional terms, some including the spatial variation of the slope, would have been included in both (9) and (10).

Upslope flow has been found to produce vertical velocities of magnitude similar to vertical velocities produced by subsynoptic scale triggering mechanisms. The net contribution of the two displacement systems can be found by integrating (9) with respect to height to find the vertical velocity at the top of a layer of depth z. Defining

$$DIV_e \equiv \frac{du}{dx} + \frac{dv}{dy},$$

substituting the vertical velocity term for the left hand side of (9), and integrating through a layer of depth z gives

$$-\int_0^z \frac{dw}{dz}\,dz = \int_0^z DIV_e\,dz - \frac{\Delta E}{\Delta x}\int_0^z \frac{du}{dz}\,dz - \frac{\Delta E}{\Delta y}\int_0^z \frac{dv}{dz}\,dz. \tag{11}$$

Evaluation of the integral yields

$$w_z = w_0 - \int_0^z DIV_e \, dz + \frac{\Delta E}{\Delta x}(u_z - u_0) + \frac{\Delta E}{\Delta y}(v_z - v_0) \quad (12)$$

However,

$$w_0 = \vec{V}_0 \cdot \nabla E \simeq u_0 \frac{\Delta E}{\Delta x} + v_0 \frac{\Delta E}{\Delta y} \quad (13)$$

The vertical velocity at z is then

$$w_z = - \int_0^z DIV_e \, dz + \vec{V}_z \cdot \nabla E \quad (14)$$

Equation (14) shows that the vertical velocity at the top of a layer z is given by the integral sum of the divergences taken parallel to the slope of the surface and the scalar product of the vector velocity at the top of the layer with the gradient of the surface elevation. If z is divided into n layers of uniform thickness Δz, (14) can be approximated by

$$w_z = -\Delta z \sum_1^n DIV_e + \vec{V}_z \cdot \nabla E \quad (15)$$

When the surface observations are the only available data, the vertical distribution of divergence must be approximated as a function of the surface divergence DIV_E. If it is assumed that the divergence is constant through z and equal to DIV_E, the vertical velocity at z is approximated by

$$w_z' = -n\Delta z \, DIV_E + \vec{V}_0 \cdot \nabla E \quad (16)$$

The error, ε, that arises when (16) is used in place of (15) to estimate the vertical velocity at z is expressed by

$$\varepsilon = w_z - w'_z = -\Delta z \sum_{1}^{n} (DIV_e - DIV_E) + (\vec{V} - \vec{V}_0)\cdot \nabla E \qquad (17)$$

The last term of (17) can be traced to the vertical shear terms that arise from the transformation from the surface plane to the horizontal plane. It would be tempting to estimate the vertical shear terms as Schaeffer has done, however, there must also be estimates for the first term on the right hand side of (17). It has not yet been determined to what extent compensation between these two terms occurs. Indeed, compensation must occur with those events where the wind field streamlines do not blow parallel to the ground.

Several PROGSPECs that draw upon (16) can be synthesized. These are described in detail in the following section. These PROGSPECs are physically valid to the extent that the assumptions made in deriving (16) are valid.

(9) The Surface PROGSPECs. The surface PROGSPECs were derived from surface meteorological data presented at points of a regular mesh so that derivative quantities could be calculated. It is the derivative quantities such as divergence, vorticity, advection, and gradients that are physically related to airmass contrasts and vertical displacements that trigger convective rainfall. These are all first derivative quantities. Noise due to poor instrument exposure, poor instrument calibration, errors in observation and transmission, channeling by local topography, and effects of subscale phenomena contaminates surface observations. Therefore, we did not attempt to calculate PROGSPECs that involve higher order derivatives or products of first order derivatives because physical relationships with rainfall might be obscured by noise.

Table 12 lists 20 candidate surface PROGSPECs that can be computed from the surface fields. The wind directions are computed by projecting the unit wind vectors onto four straight line segments which are oriented progressively at 45 degree intervals. This was done to eliminate bi-polar distributions introduced as a consequence of the transition of northerly winds from 359 to 00 degrees. Each line segment becomes a covariate so the total number of candidate PROGSPECs being tested is increased to 26.

The surface PROGSPECs relate to moisture distributions and triggering mechanisms. The surface variables alone cannot describe stability. The derivation and interpretation of the surface PROGSPECs is as follows.

Table 12. List of surface PROGSPECs.

1. Surface mixing ratio.
2. Wet bulb potential temperature.
3. Height of the lifted condensation level (LCL) for surface air.
4. Temperature of the LCL.
5. Moisture advection by geostrophic wind.
6. Moisture advection by the observed wind.
7. Advection of the virtual potential temperature by observed wind.
8. The geostrophic wind direction (four line projections).
9. The direction of the observed wind (four line projections).
10. Convergence of the observed wind.
11. Moisture convergence.
12. Cumulative lift.
13. Vorticity of the observed wind.
14. Vertical velocity induced by the geostrophic wind flow over terrain.
15. Vertical velocity induced by the observed wind flow over terrain.
16. The 3 hr ($t-t_{-3}$) tendency of the surface wind speed.
17. Surface pressure.
18. The 3 hr ($t-t_3$) tendency of the surface pressure.
19. Pressure trough analysis.
20. Magnitude of the gradient of the surface mixing ratio.

1) Surface Mixing Ratio

Derivation: The vapor pressure is determined from the dewpoint temperature through the Clausius-Clapeyron equation. Then the mixing ratio is found as a function of the surface pressure and the vapor pressure. An alternative formulation can be made through Tetan's formula (Berry et al., 1945).

Interpretation: The mixing ratio is a height independent measure of the water present in an airmass. As the water content of the surface layers increases, the rainfalls can become more frequent and/or intense.

2) Wet Bulb Potential Temperature

Derivation: Compute the temperature a parcel of air would have if lifted from the surface to its condensation level (LCL). Then interpolate from tables of temperature and pressure to find the wet bulb potential temperature.

Interpretation: The wet bulb potential temperature gives a measure of the sensible and latent energy contained within a surface airmass. The greater the moisture content and/or temperature of a surface airmass, the greater the probability for deep convective overturning.

3) Height of the Lifted Condensation Level (LCL) for Surface Air

Derivation: A rather complicated computer program is used to determine the height of the LCL. In principle, the LCL height is the height on a psuedo-adiabatic diagram where the mixing ratio curve intersects the dry adiabat that passes throuqh the surface temperature.

Interpretation: See 4) below.

4) Temperature at the LCL

Derivation: From 3) above, the temperature at the LCL is the temperature at the intersection of the mixing ratio line that passes through the surface dewpoint with the dry adiabat that passes through the surface temperature.

Interpretation: Both the temperature and height at the LCL are most useful as PROGSPECs when calculated from data taken during the heated mid-afternoon hours. Low cloud bases and warm cloud base temperatures accompany warm humid airmasses that can produce copious amounts of rainfall.

5) Moisture Advection by the Geostrophic Wind

Derivation: The moisture advection is given by the scalar product of the geostrophic wind vector with the gradient of the mixing ratio.

Interpretation: The rapid transfer of moisture into the High Plains is often accompanied by conditions of destabilization and upslope and system caused vertical displacements. The geostrophic wind, derived from the pressure field, has continuity with the pressure field just above the friction layer. Thus the surface pressure field can be used to estimate the moisture advection within the low level free flowing 'frictionless' airmasses.

6) Moisture Advection by the Observed Wind

Derivation: The moisture advection by the observed wind is given by the scalar product of the observed surface wind vector with the gradient of the mixing ratio.

Interpretation: The interpretation is the same as in 5) above with the exception that the moisture advection within the friction layer is calculated.

7) Advection of the Virtual Potential Temperature by the Observed Wind

Derivation: Calculate the virtual temperature as a function of the surface temperature and mixing ratio. Then calculate the virtual potential temperature from Poisson's equation. The virtual potential temperature advection is given by the scalar product of the observed wind vector with the gradient of the virtual potential temperature.

Interpretation: The virtual potential temperature gives a measure of the relative densities of adjacent moist and dry airmasses and hence an estimate of whether one airmass may undercut and lift the other airmass. These vertical displacements are often associated with deep convection.

8) The Geostrophic Wind Direction

Derivation: Four coordinate axes, oriented along 270°-90°, 3150-135°, 1800-359°, and 225°-45° have been defined. The unit wind vector is projected onto each of the four coordinate axes. This method eliminates bi-pblar distributions introduced as a consequence of the transition of northerly winds from 359 to 00 degrees.

Interpretation: The geostrophic wind direction is oriented parallel to the isobars of pressure. It gives a measure of the wind flow above the friction layer. Winds blowing from the southwest, west or northwest are associated with dry, stable conditions. Winds from the northeast are relatively moist and winds from the east and southeast bring copious amounts of moisture to the High Plains.

9) The Observed Wind Direction

Derivation: See 8) above.

Interpretation: Same as in 8) above with the exception that the surface winds are taken within the friction layer.

10) Convergence of the Observed Wind

Derivation: The convergence is given by the scalar product of the Del operator with the surface wind vector.

Interpretation: Convergence within the boundary must be compensated by upward motion which increases the depth of the moist layer and destabilizes the airmass. Both conditions render the airmass more favorable for deep convection and precipitation.

11) Moisture Convergence

Derivation: The moisture convergence is given by the scalar product of the Del operator with the product of the mixing ratio , and the surface wind vector.

Interpretation: The potential for deep convection with copious precipitation increases with the moisture content of a converging airmass. The inclusion of moisture is intended to help stratify out those events with strong convergence within dry airmasses. Obviously, if no moisture is present in an airmass, no amount of convergence will lead to precipitation.

12) The Cumulative Lift

Derivation: Calculate the vertical velocity at the top of a 1 km deep layer by assuming that the layer average convergence is equal to the surface convergence. Then add to this the vertical velocity induced by flow over unlevel terrain. Find the average vertical velocity over a period of 5-6 hr by averaging with previously calculated vertical velocities. The 5-6 hr time span period was

chosen as representative of the residence time of a typical mesosystem between observation sites with average separation similar to that of the current United States surface network. Multiply the average vertical velocities by the time period to convert to net vertical displacements.

Interpretation: Weak vertical motion fields associated with subsynoptic disturbances must often act for several hours before the troposphere is sufficiently destabilized to initiate deep convection. Low-level inversions have been destroyed over a period of time from 1-3 hrs in advance of squall lines (Long, 1963). Anderson and Uccellini (1974) found identifiable zones of convergence preceeding convective rainfall by up to 5 hrs for several northeast Colorado thunderdays. The cumulative lift estimates the net vertical displacement over a specified time period. The method of averaging helps to eliminate some of the noise inherent in the convergence calculations and thus isolates the important meteorological disturbances.

13) The Vorticity of the Observed Wind

Derivation: The vorticity is given by the curl of the horizontal wind vector.

Interpretation: The vorticity of the surface wind field can identify low pressure centers, frontal shear zones and other circulation systems that often are accompanied by convective precipitation. Conversely, circulation systems that give negative vorticity are often associated with stable lower atmospheric conditions.

14) Vertical Velocity Induced by the Geostrophic Wind Flow Over Terrain

Derivation: The terrain induced vertical velocity is found by the scalar product of the geostrophic wind with the horizontal gradient of the surface elevation.

Interpretation: Upward vertical displacements caused by flow over uneven terrain tend to destabilize airmasses and increase the possibility for convection. Downslope flow tends to increase the stability of airmasses and inhibit convection.

15) Vertical Velocity Induced by the Observed Wind Flow over Terrain

Derivation: Same as 14) above.

Interpretation: Same as 14) above.

16) The 3 hr ($t-t_{-3}$) Tendency of the Surface Wind Speed

Derivation: Subtract the wind speed observed at time t_{-3} from the currently observed wind speed.

Interpretation: The breakup of the boundary layer during the late morning is often accompanied by a marked change in the surface wind speed as air with different momentum is mixed downward from aloft. The rapid increase in the depth of the mixed layer is often associated with the initiation of deep convection.

17) Surface Pressure

Derivation: The surface pressure is taken directly from the objectively interpolated fields of pressure.

Interpretation: Low pressure centers and pressure troughs in the pressure field identify triggering mechanisms that destabilize the troposphere. High pressure centers and ridges are associated with stable conditions.

18) The 3 hr (t-t_3) Tendency of the Surface Pressure

Derivation: Subtract from the current pressure the pressure observed observed 3 hrs prior.

Interpretation: The pressure tendency gives the temporal change in surface pressure that precede advancing triggering mechanisms. Pressure falls precedes lows, fronts, squall lines, and other convergence zones. The strength of the pressure falls indicates the rapidity of movement and/or the intensity of the trigger. Thus pressure falls are most often indicators of coming inclement weather. Pressure rises indicate clearing stable weather conditions.

19) The Pressure Trough Analysis

Derivation; The locations of pressure troughs are found empirically by a computer program and the trough intensities are determined by calculating the curvature of the pressure field normal to the trough axis. Convergences are computed upon the assumption that the atmosphere is initially at rest and the trough is stationary for 3 hrs. The convergences are converted to vertical displacements at the top of a 1 km deep layer upon the assumption that the layer convergence is equal to the surface convergence.

Interpretation: The pressure trough analysis is a scheme to assess vertical displacements independently of the observed winds. It is assumed that an airmass, initially at rest with respect to the pressure field, is accelerated into frictionless motion by the pressure field which is held constant for a specified time interval. Flow into trough axes or pressure centers would necessarily have to be compensated by a vertical component of motion. The upward vertical displacements are related to destabilization and precipitation. The pressure trough analysis is much less noisy than the Laplacian of the pressure field.

20) The Magnitude of the Gradient of the Surface Mixing Ratio

Derivation: Compute the modulus of the mixing ratio gradient.

Interpretation: Strong moisture gradients often identify the presence of a dry line, an abrupt boundary between moist and dry airmasses. The dry line is often a trigger of intense convective activity.

(10) Evaluation of the Surface PROGSPECs. The surface data was interpolated to a regular 8x6 =48 point mesh so that derivatives could be calculated using finite differences. These spatial representations greatly increased the number of independent points to be correlated with the dependent variable (rainfall). The 26 surface PROGSPECs times 48 grid points gives a total of 1248 independent and highly intercorrelated variables to be correlated with only 180 rainfall days (June 1965-1970). Obviously, there would be no degrees of freedom if standard multiple correlation methods were used.

Schickedanz (1976) applied a multivariate statistical method called Factor Analysis to spatial distributions of rainfall data. The matrix formed by the number of analyses and the 48 grid points is transformed into a matrix of factors which are orthogonal (uncorrelated) functions of space. These spatial functions are linear combinations of the various grid points. Only a few of the 48 resulting factors will be correlated significantly with rainfall. These few patterns are retained and the rest is discarded. Thus, the number of independent variables per PROGSPEC is reduced from 48 to just a few. The significant factors for a surface PROGSPEC are mutually uncorrelated but can be highly correlated with the factors of other PROGSPECs. A multiple correlation analysis is performed on the factors to yield the total rainfall variance explained by the surface PROGSPECs.

Schickedanz and Sun (1977) have presented the theoretical development of the applications of factor analysis to HIPLEX and a more complete development is given in the section on statistical techniques for the incorporation of covariates into the design and evaluation. Here we present the correlations of the surface PROGSPECs and a physical description (when possible) of the contributing factors.

The correlations of the 0600 CST surface PROGSPECs with the daily rainfall (0700-0700 CST) for June 1965-1970 using an eigenvalue cutoff limit of greater than or equal to 1.0 (absolute value) are shown in Table 13. The variables are listed in decreasing order according to the explained rainfall variance. Table 13 gives the number of factors that exceeded the cutoff, the total field pattern variance contained in those factors, the rainfall variance explained by the factors, and the total correlation with rainfall.

Table 13 shows that the top 4 PROGSPECs were related to the observed wind. Moisture flow onto the plains with southeast winds contrasted with dry flow from the northwest with frontal passages would explain the importance of the observed wind direction along an axis oriented from 315 to 135 degrees in the meteorological framework. The upslope vertical velocity is tied closely to the observed wind direction when a significant component of the wind blows normal to slope. This is the case for both PROSPECs 1 and 6. Moisture convergence and cumulative lift carry wind field initiated triggering mechanisms.

Table 13, Correlation of 0600 CST surface PROGSPECs with daily rainfall (0700-0700 CST) for June 1965-70 using an eigenvalue limit of ≥1.0 and a correlation limit of ≥|0.10|.

Number	Variable	No. of Factors ≥|0.10|	Total Factor Variance %	Rain Variance Explained by Factor %	Total Correlation
1	Obs. Wind Dir. (135-315)	5	59.8	10.4	0.32
2	Upslope Vertical Velocity (observed wind)	4	70.9	10.4	0.32
3	Moisture Convergence	4	28.6	10.0	0.32
4	Cumulative Lift	2	36.4	8.9	0.30
5	Geo. Wind Dir. (135-315)	1	38.2	7.3	0.27
6	Obs. Wind Dir. (90-270)	4	56.6	7.4	0.27
7	Vorticity Obs. Wind	3	40.3	7.4	0.27
8	Pressure Tendency	3	70.9	7.4	0.27
9	Upslope Vertical Velocity (geostrophic wind)	3	22.8	6.9	0.26
10	Divergence	3	35.2	6.5	0.26
11	Geo. Wind Dir. (180-359)	3	71.2	6.4	0.25
12	Surface Wind Speed Tendency (3 hr)	4	33.3	6.2	0.25
13	Geo. Wind Dir. (90-270)	2	53.8	6.0	0.24
14	Mixing Ratio Advection (observed wind)	4	49.9	5.9	0.24
15	Surface Pressure	1	2.1	5.8	0.24
16	Geo. Wind Dir. (45-225)	1	2.9	5.3	0.23
17	Mixing Ratio	2	65.5	5.0	0.22
18	LCL Temperature	1	59.3	4.4	0.21
19	Wet Bulb Pot. Temp.	2	71.6	4.2	0.21
20	Virtual Pot. Temp. Adv.	2	39.0	4.2	0.21
21	LCL Height	2	65.6	4.0	0.20
22	Obs. Wind Dir. (180-359)	2	9.6	3.9	0.20
23	Obs. Wind Dir. (45-225)	2	47.7	3.1	0.18
24	Mixing Ratio Advection (geostrophic wind)	1	24.7	2.6	0.16
25	Pressure Trough Analysis	1	10.4	2.6	0,16

The best PROGSPECs were able to explain only about 10% of the rainfall variance. The reason for this may be partly physical, (the surface flow is not coupled with rainfall-producing mechanisms), the paucity of the daily rainfall data, or the paucity of the surface data. When surface data are sparse, noise in just one or two observations can greatly distort derivative fields. For example, four moisture convergence factors explained 10% of the rainfall variance. Yet those four factors accounted for only 28.6% of the total variance of the moisture convergence fields. This means that 71.4% of the moisture convergence was not significantly related to the rainfall.

The poorer (relatively speaking) showing of pressure field-related PROGSPECs lends more confusion to the interpretation of the factors since well-defined troughs are usually found with strong early summer frontal systems. Only one factor which accounted for only 2.1% of the variance of the pressure fields was related to rainfall. This factor explained only 5.8% of the rainfall variance. The pressure trough analysis, designed to detect the intensity of pressure troughs, could explain only 2.6% of the rainfall variance.

Other PROGSPECs have high factor variance related to rainfall. For example, 71.6% of the wet bulb potential temperature field variance was related to rainfall but could explain only 4.2% of the rainfall variance.

Table 14, gives the correlations of 0600 CST surface PROGSPECs with daily rainfall (0700-0700 CST) for July 1965-1970 using an eigenvalue limit of greater than 1.0. In contrast with Table 13, the pressure field-related PROGSPECs were most highly correlated with July rainfall. The top seven PROGSPECs were in some manner related to the pressure field. The pressure trough analysis, the poorest PROGSPEC for June, was found to correlate most highly with July rainfall. Four pressure trough analysis factors explained 23.0% of the rainfall variance and gave a total correlation with rainfall of 0.48. These are followed by the pressure tendency with a correlation of 0.37. Wind directions derived from the pressure field strongly weight the next 5 PROGSPECs.

Wind field derivative quantities frequently associated with convective rainfall-convergence, moisture convergence, cumulative lift, and vorticity-are found at positions 15, 11, 14, and 9, respectively. Light, variable July winds could have increased the noise and decreased the signal magnitudes to decrease the correlations for these PROGSPECs.

Four PROGSPECs were eliminated for having no factors that exceeded the eigenvalue cutoff. These were the mixing ratio, the observed wind direction (90-270), the wet bulb potential temperature, and the lifted condensation level temperature. We did not expect the LCL temperature to perform well as an 0600 CST PROGSPEC because the surface air is nocturnally cooled and would poorly estimate LCL conditions during the convective period. That the wet bulb potential temperature would change little in pattern or magnitude would suggest

Table 14. Correlation of 0600 CST surface PROGSPECs with daily rainfall (0700-0700 CST) for July 1965-70 using an eigenvalue limit of ≥1.0 and a correlation limit of ≥|0.10|.

Number	Variable	No. of Factors ≥|0.10|	Total Factor Variance %	Rain Variance Explained by Factor %	Total Correlation
1	Pressure Trough Analysis	4	44.7	23.0	0.48
2	Pressure Tendency	3	54.1	13.4	0.37
3	Geo. Wind Dir. (180-359)	4	52.6	13.0	0.36
4	Upslope Vertical Velocity (geostrophic wind)	3	68.5	12.0	0.35
5	Mixing Ratio Advection (geostrophic wind)	3	40.0	11.4	0.34
6	Geo. Wind Dir. (90-270)	4	63.0	11.2	0.33
7	Geo. Wind Dir. (45-225)	4	82.9	11.1	0.33
8	Obs. Wind Dir. (180-359)	4	69.9	11.0	0.33
9	Vorticity	4	66.3	10.1	0.32
10	Obs. Wind Dir. (45-225)	3	60.0	9.7	0.31
11	Moisture Convergence	5	41.2	8.9	0.30
12	Geo. Wind Dir. (135-315)	4	26.3	8.5	0.29
13	Virtual Pot. Temp. Adv.	5	58.9	8.7	0.29
14	Cumulative Lift	3	42.0	8.4	0.29
15	Divergence	2	19.1	7.7	0.28
16	LCL Height	4	35.1	7.7	0.28
17	Wind Speed Tendency (3 hr)	4	42.8	6.6	0.26
18	Surface Pressure	1	8.4	6.3	0.25
19	Obs. Wind Dir. (135-315)	3	50.8	4.7	0.22
20	Upslope Vertical Velocity (observed wind)	2	12.7	3.9	0.20
21	Mixing Ratio Advection (observed wind)	1	2.7	1.2	0.11
22	Mixing Ratio	0	0	0	0
23	Obs. Wind Dir. (90-270)	0	0	0	0
24	Wet Bulb Pot. Temp.	0	0	0	0
25	LCL Temperature	0	0	0	0

that essentially the same airmass occupies the Dodge City area during July. Such could also be the case with the mixing ratio.

The 180-359 degree axis leads both the geostrophic and observed wind direction PROGSPEC categories. This would suggest a greater prevalence of southerly and/or northerly flow over the High Plains in July as contrasted with southeasterly and easterly flow in June. The poor showing for easterly flow in July may occur because easterly flow is not frequent in July and therefore accounts for little July rainfall variance. It follows then that the upslope vertical velocity of the observed wind should also be very poorly correlated with rainfall. Table 14 shows that this PROGSPEC explained only 3.9% of the rainfall variance. The gradient of the mixing ratio is predominantly an east-west gradient. With few instances of easterly or westerly flow, the mixing ratio gradient would never be large and would be expected to be poorly correlated with rainfall. This PROGSPEC was found to explain only 1.2% of the rainfall variance.

The correlations of 0600 CST surface PROGSPECs with daily rainfall (0700-0700 CST) for August 1965-1970 using an eigenvalue limit of 0.10 are shown in Table 15. The most powerful PROGSPECs are found to be related to the observed wind field. The cumulative lift explained 18.7% of the rainfall variance. The upslope vertical velocity and the mixing ratio correlated at 0.39. The mixing ratio advection for the observed and geostrophic wind both accounted for about 14% of the rainfall variance.

Pressure field related PROGSPECs generally were more poorly correlated with rainfall than were the wind field PROGSPECs. Thus the August covariate analysis shows some similarity to the June covariate analysis. The pressure trough analysis, powerful in July, explained only 5.6% of the August rainfall variance. The pressure field failed to place any factors above the cutoff limit.

A comparison of the performance of the surface PROGSPECs with the performance of the sounding SPECs (Table 9) shows that the surface PROGSPECs generally explained twice as much rainfall variance. Surface PROGSPEC correlations ranged between 0.0-0.48, however, individual factor correlations ranged from 0.1-0.2, a suggestion that no particular surface pattern is the dominant High Plains precipitation producer.

In a second study, the surface PROGSPECs were correlated with 6 hr surface rainfall for the Dodge City sampling area. The hourly rainfall for six reporting stations was averaged and then summed over the period 1200-1800 CST . This very sparse data set gives an average of one hourly rainfall station per 6500 km^2. The 6 hr period was chosen to be representative of rainfall during the convective period. Our climatological studies show that it is not the period of maximum rainfall frequency. More rain falls during the period 1800-midnight. However, the 1200-1800 period is the period of rapid increases in convective activity.

Table 15. Correlation of 0600 CST surface PROGSPECs with daily rainfall (0700-0700 CST) for August 1965-70 using an eigenvalue limit of ≥1.0 and a correlation limit of ≥|0.10|.

Number	Variable	No. of Factors ≥|0.10|	Total Factor Variance %	Rain Variance Explained by Factor %	Total Correlation
1	Cumulative Lift	3	41.9	18.7	0.43
2	Upslope Vertical Velocity (observed wind)	5	61.1	15.5	0.39
3	Mixing Ratio	3	86.6	15.2	0.39
4	Obs. Wind Dir. (45-225)	5	77.3	15.1	0.39
5	Divergence	4	54.8	14.9	0.39
6	Mixing Ratio Advection (geostrophic wind)	7	71.2	14.4	0.38
7	Obs. Wind Dir. (90-270)	4	59.8	14.2	0.38
8	Mixing Ratio Advection (observed wind)	5	32.2	14.0	0.37
9	Upslope Vertical Velocity (geostrophic wind)	4	61.7	13.5	0.37
10	Wet Bulb Pot. Temp.	4	90.5	13.2	0.36
11	Vorticity	3	28.9	12.9	0.36
12	Virtual Pot. Temp. Adv.	4	13.5	12.9	0.36
13	LCL Temperature	2	81.8	12.8	0.36
14	Obs. Wind Dir. (180-359)	4	29.5	11.7	0.34
15	Moisture Convergence	3	43.3	10.9	0.33
16	Geo. Wind Dir. (135-315)	3	46.7	10.3	0.32
17	Geo. Wind Dir. (90-270)	3	53.0	9.0	0.30
18	LCL Height	3	76.6	7.4	0.27
19	Obs. Wind Dir. (135-315)	2	43.5	6.5	0.26
20	Wind Speed Tendency (3 hr)	4	10.4	6.2	0.25
21	Pressure Trough Analysis	3	51.6	5.6	0.24
22	Pressure Tendency	2	77.3	4.4	0.21
23	Geo. Wind Dir. (45-225)	2	10.4	3.2	0.18
24	Geo. Wind Dir. (180-359)	1	4.7	2.9	0.17
25	Surface Pressure	0	0	0	0

Table 16 gives the correlations of the 0600 CST surface PROGSPECs with the 1200-1800 CST rainfall. An eigenvalue cutoff of 1.0 was used. Correlation magnitudes for the 6 hr period are similar to the magnitudes found with the daily rainfall. Upslope vertical velocity (observed wind), wind speed tendency, and pressure tendency all correlated at greater than 0,30. The moisture convergence and cumulative lift, which did well in the daily rainfall correlations (Table 13), fared poorly in the 6 hr correlations. The moisture convergence ranked 6th and explained only 7.6% of the rainfall variance. The cumulative lift failed to place any factors above the cutoff.

The correlations between the 0600 CST PROGSPECs and 1200-1800 CST rainfall for July are given in Table 17. The 6 hr correlations were generally lower than the daily rainfall correlations. The pressure trough analysis, which explained 23.0% of the daily rainfall variance (Table 14) accounted for less than 3% of the afternoon rainfall variance. The pressure tendency was dropped from 13.4% to 2.4% of the variance. The rankings of the PROGSPECs in Table 14 were found to be nearly randomly related to the PROGSPEC rankings in Table 17. No variables consistently correlated well with rainfall in both rankings although some consistently correlated poorly. Since the afternoon rainfall began the diurnal rainfall frequency peak for Dodge City, it was expected that those variables that correlated well with the daily rainfall should correlate better with the 6 hr rainfall. Such was not the case. The lack of PROGSPEC correlation consistency between the two periods is reflective of the generally low correlations.

The PROGSPEC correlations for August (Table 18) are more consistent with the August daily correlations in Table 15. Eight of the first nine PROGSPECs ranked in the daily correlations appear in the first nine positions ranked in the 6 hr correlations, although the 6-hr correlations are somewhat lower. The cumulative lift and the upslope vertical velocity (observed wind) ranked near the top on both lists, although the 6 hr correlations were lower. The pressure related quantities performed poorly in both rankings.

A second study was conducted to see if higher correlations with the 6 hr rainfall could be obtained if the 1200 CST PROGSPECs were used in place of the 0600 CST PROGSPECs. These correlations are summarized in Table 19. There was little change in correlation magnitudes and minor changes in PROGSPEC ranking. The upslope vertical velocity (observed wind) and the pressure tendency correlated above 0.30 for both runs. The lack of improvement in the 1200 CST PROGSPECs suggests that the transient trigger mechanisms are stable in time and so can be equally well detected in the 0600 CST surface analyses. The low correlations may arise due to the paucity of the rainfall and/or surface data, or may simply signal that there is little consistent physical coupling between these PROGSPECs and the areal mean rainfall.

Table 16. Correlation of 0600 CST surface PROGSPECs with 6 hr rainfall (1200-1800 CST) for June 1965-70 using an eigenvalue limit of ≥1.0 and a correlation limit of ≥|0.10|.

Number	Variable	No. of Factors ≥|0.10|	Total Factor Variance %	Rain Variance Explained by Factor %	Total Correlation
1	Upslope Vertical Velocity (observed wind)	3	15.9	14.2	0.38
2	Wind Speed Tendency (3 hr)	5	46.1	10.6	0.32
3	Pressure Tendency	4	65.2	9.9	0.31
4	Geo. Wind Dir. (135-315)	3	52.9	8.7	0.29
5	Obs. Wind Dir. (135-315)	3	13.1	7.7	0.28
6	Moisture Convergence	3	35.9	7.6	0.27
7	Obs. Wind Dir. (90-270)	4	32.7	7.3	0.27
8	Divergence	3	18.1	7.3	0.27
9	Geo. Wind. Dir. (150-359)	3	17.4	6.0	0.25
10	Vorticity	3	17.3	5.7	0.24
11	Geo. Wind Dir. (90-270)	3	24.9	5.6	0.24
12	Geo. Wind Dir. (45-225)	2	9.6	5.2	0.23
13	Obs. Wind Dir. (150-359)	2	9.2	5.4	0.23
14	Pressure Trough Analysis	2	9.6	5.3	0.23
15	Upslope Vertical Velocity (geostrophic wind)	2	8.9	3.7	0.19
16	LCL Temperature	1	59.3	2.6	0.16
17	Mixing Ratio	1	59.8	2.3	0.15
18	LCL Height	1	14.6	1.7	0.13
19	Wet Bulb Pt. Temp.	1	67.1	1.7	0.13
20	Mixing Ratio Advection (geotrophic wind)	1	2.5	1.2	0.11
21	Mixing Ratio Advection (observed wind)	1	21.6	1.2	0.11
22	Virtual Pot. Temp. Adv.	1	7.0	1.0	0.10
23	Obs. Wind Dir. (45-225)	0	0	0	0
24	Cumulative Lift	0	0	0	0

Table 17. Correlation of 0600 CST surface PROGSPECs with 6 hr rainfall (1200-1800 CST) for July 1965-70 using an eigenvalue limit of ≥1.0 and a correlation limit of ≥|0.10|.

Number	Variable	No. of Factors ≥|0.10|	Total Factor Variance %	Rain Variance Explained by Factor %	Total Correlation
1	Geo. Wind Dir. (90-270)	5	71.8	9.8	0.31
2	Geo. Wind Dir. (45-225)	1	5.9	6.3	0.25
3	Virtual Pot. Temp. Adv.	4	26.2	6.1	0.25
4	Obs. Wind Dir. (45-225)	1	15.2	6.0	0.24
5	Cumulative Lift	1	6.5	5.3	0.23
6	Obs. Wind Dir. (180-359)	2	21.4	5.1	0.22
7	Geo. Wind Dir. (135-315)	2	11.9	4.9	0.22
8	Divergence	2	7.8	4.3	0.21
9	Upslope Vertical Velocity (geostrophic wind)	2	57.2	4.1	0.20
10	Obs. Wind Dir. (135-315)	2	7.2	3.9	0.20
11	Wet Bulb Pot. Temp.	2	9.1	3.7	0.19
12	Obs. Wind Dir. (90-270)	2	8.3	3.3	0.18
13	Geo. Wind Dir. (180-359)	1	5.7	3.2	0.18
14	Vorticity	2	12.0	2.9	0.17
15	Pressure Trough Analysis	2	12.9	2.9	0.17
16	Mixing Ratio Advection (geostrophic wind)	2	21.8	2.7	0.16
17	Moisture Convergence	1	6.7	2.6	0.16
18	Pressure Tendency	2	15.8	2.4	0.16
19	Mixing Ratio	1	2.8	7.3	0.15
20	LCL Temperature	2	24.2	2.0	0.14
21	Mixing Ratio Advection (observed wind)	1	5.6	1.7	0.13
22	LCL Height	1	13.6	1.2	0.11
23	Upslope Vertical Velocity (observed wind)	1	4.4	1.0	0.10
24	Wind Speed Tendency (3 hr)	0	0	0	0
25	Surface Pressure	0	0	0	0

In summary, it was found that the correlations of the surface pattern PROGSPECs with the 6 hourly rainfall for the Dodge City area, though much improved over the sounding SPECs, were disappointingly low. Correlation coefficients ranged from 0.0-0.40. No one PROGSPEC was outstanding and thus no one physical process could be isolated as especially productive for High Plains rainfall. Individual factor correlations were small, a suggestion that no single field pattern was outstanding for any PROGSPEC. No one PROGSPEC consistently ranked well throughout the 3 month period. The upslope vertical velocity (observed wind) ranked high in June and August but did poorly in July. Further, the daily vs. 6 hr rainfall relative rankings were highly variable; the relative rankings in July were nearly random. There was also found considerable noise in many meteorological patterns; only a small percentage of the total factor variance was related to rainfall.

(11) Physical Analysis of Selected PROGSPEC Factors, The total factor correlations shown in Tables 13-19 are composed of the correlations of several pattern types. These pattern types can indicate the locations, signs, and, to an extent, the intensities of meteorological disturbances that are related to the Dodge City area rainfall. The factor analysis as applied here cannot discriminate between cold fronts, occluded fronts, squall lines, and instability lines according to the traditional methods of synoptic typing (Morgan et al., 1975). Synoptic typing should be unnecessary unless there are preconvective-release atmospheric structures, unique to the synoptic type, which control the convection. It would be difficult to demonstrate the existence of such structures given the climatological data base. Further, Bark (1975) has shown that synoptic typing was of little value in his classification of west Kansas radar echoes from 1972-1974.

Our development of the candidate PROGSPECs was constrained by the requirement that the variables be related to the rainfall through known physical processes. This requirement offers a method independent of statistical verification on independent data by which the variable-rainfall relationship may be evaluated critically. A physically consistent interpretation strengthens a variable as a candidate PROGSPEC.

A factor pattern consists of an array of numbers, either positive and/or negative in sign, that constitutes all or parts of meteorological patterns recurrent in the fields of particular variables. Then, each factor has a coefficient of correlation with the areal mean rainfall, the sign of which determines whether the factor pattern is associated with increasing rainfall or with decreasing rainfall. Since several synoptic systems can produce similar patterns, it was expected that multiple physical explanations for some factor patterns could be found. However, these explanations should be unique with respect to the sign of the correlation coefficient. For example, given a factor pattern that correlates positively with rainfall (the pattern tends to be associated with rainfall situations), all physical explanations for

Table 18. Correlation of 0600 CST surface PROGSPECs with 6 hr rainfall (1200-1800 CST) for August 1965-70 using an eigenvalue limit of ≥1.0 and a correlation limit of ≥|0.10|.

Number	Variable	No. of Factors ≥|0.10|	Total Factor Variance %	Rain Variance Explained by Factor %	Total Correlation
1	Mixing Ratio Advection (geostrophic wind)	5	51.3	16.3	0.40
2	Upslope Vertical Velocity (geostrophic wind)	3	56.1	9.9	0.31
3	Upslope Vertical Velocity (observed wind)	4	54.2	9.3	0.31
4	Cumulative Lift	3	41.9	8.5	0.29
5	Mixing Ratio Advection (observed wind)	4	28.1	8.3	0.29
6	Pressure Trough Analysis	2	10.3	6.8	0.26
7	Obs. Wind Dir. (45-225)	4	64.7	6.1	0.25
8	Obs. Wind Dir. (90-270)	2	42.7	6.1	0.25
9	Divergence	2	24.7	5.4	0.23
10	Vorticity	3	25.9	5.4	0.23
11	Geo. Wind Dir. (90-270)	2	42.5	4.8	0.22
12	Moisture Convergence	2	21.1	4.6	0.21
13	Mixing Ratio	3	89.9	3.4	0.19
14	Geo. Wind Dir. (180-359)	2	11.0	3.8	0.19
15	Wind Speed Tendency (3 hr)	2	14.8	3.0	0.17
16	Geo. Wind Dir. (135-315)	2	50.5	2.9	0.17
17	LCL Temperature	2	81.8	2.9	0.17
18	Virtual Pot. Temp. Adv.	1	28.4	2.9	0.17
19	Geo. Wind Dir. (45-225)	1	2.3	2.6	0.16
20	LCL Height	1	12.9	2.6	0.16
21	Wet Bulb Pot. Temp.	2	74.5	2.4	0.16
22	Obs. Wind Dir. (135-315)	0	0	0	0
23	Obs. Wind Dir. (180-359)	0	0	0	0
24	Pressure Tendency	0	0	0	0
25	Surface Pressure	0	0	0	0

Table 19. Correlation of 1200 CST surface PROGSPECs with 6 hr rainfall (1200-1800 CST) for June 1965-70 using an eigenvalue limit of ≥1.0 and a correlation limit of ≥|0.10|.

Number	Variable	No. of Factors ≥|0.10|	Total Factor Variance %	Rain Variance Explained by Factor %	Total Correlation
1	Obs. Wind Dir. (90-270)	3	50.5	10.4	0.32
2	Upslope Vertical Velocity (observed wind)	4	48.1	9.8	0.31
3	Divergence	4	77.9	9.4	0.31
4	Pressure Tendency	2	12.9	9.0	0.30
5	Geo. Wind Dir. (135-315)	4	57.2	8.8	0.30
6	Vorticity	4	30.7	7.8	0.28
7	Obs. Wind Dir. (135-315)	4	63.0	7.0	0.26
8	Mixing Ratio Advection (observed wind)	4	43.1	6.9	0.26
9	Obs. Wind Dir. (180-359)	3	14.4	6.8	0.26
10	Moisture Convergence	4	48.2	6.6	0.26
11	Geo. Wind Dir. (180-359)	2	8.0	6.5	0.25
12	Upslope Vertical Velocity (geostrophic wind)	3	52.9	5.5	0.23
13	LCL Temperature	2	64.5	5.0	0.22
14	Wind Speed Tendency (3 hr)	3	20.7	4.8	0.22
15	Virtual Pot. Temp. Adv.	2	6.2	4.7	0.22
16	Pressure Trough Analysis	3	19.4	4.6	0.21
17	Mixing Ratio	2	64.3	4.2	0.21
18	LCL Height	1	67.6	3.6	0.19
19	Obs. Wind Dir. (45-225)	2	12.9	3.1	0.18
20	Cumulative Lift	1	20.0	1.7	0.13
21	Mixing Ratio Advection (geostrophic wind)	1	2.4	1.4	0.12
22	Geo. Wind Dir. (90-270)	1	3.5	1.2	0.11
23	Geo. Wind Dir. (45-225)	1	4.1	1.2	0.11
24	Wet Bulb Pot. Temp.	0	0	0	0
25	Surface Pressure	0	0	0	0

the pattern should relate to systems that increase rainfall. It is acceptable to reverse the signs for both the correlation coefficient and the factor pattern elements. Then, following the above example, the rainfall correlates negatively with the factor pattern and all physical interpretations should suggest little or no rainfall when meteorological patterns are similar to this factor pattern. The physical interpretation of some of the factor patterns can be difficult for the following reasons:

1) The factor, correlations with rainfall are low. No single factor explained more than 3% of the rainfall variance. At such low correlations, the factors are likely to contain spurious (non-physical) elements.

2) Some higher order factors were correlated significantly with rainfall. The factor loadings are such that the first few factors give smooth subsynoptic-scale patterns consistent with the data spacing. The spatial variability of the factor patterns increases with increasing order. The highest order factors generally contain noise and little if any pattern is discernible. Factors of order greater than 3 contain considerable spatial variation. When these factors were retained, the physical interpretations were limited to those features most highly correlated with rainfall. Low correlation features near the grid boundaries were de-emphasized.

3) The physical interpretations were non-unique. It was possible to assign rainfall probable or dry probable physical explanations to a factor pattern regardless of the sign of its correlation with rainfall.

4) The factor patterns defied physical interpretation. Schickedanz (1976) notes that some factor structures are more meaningful than others and it is often desirable to rotate the factors to a terminal solution that satisfies both the practical and theoretical needs of the research problem. It is to be expected, therefore, that some of the initial facture factor structures used here may not be revealing.

Selected factor patterns for the upslope vertical velocity (observed wind), the observed wind direction projected onto a 135-315 degree axis, the vorticity, and the moisture convergence are presented in figure 8. These are taken from the correlations between the 0600 CST PROGSPECs and the 1200-1800 CST Dodge City sampling area average rainfall for June 1965-1971. These factors were selected for their widely varying physical interpretations, the consistency between patterns, and to demonstrate the difficulties of interpretation. The physical interpretations must take into consideration the 6-12 hr lag between independent and dependent variables.. Our climatological studies show that Dodge City rainfall is more frequent toward the end of period (1800 CST); many correlations may be weighted toward this time. If a trigger

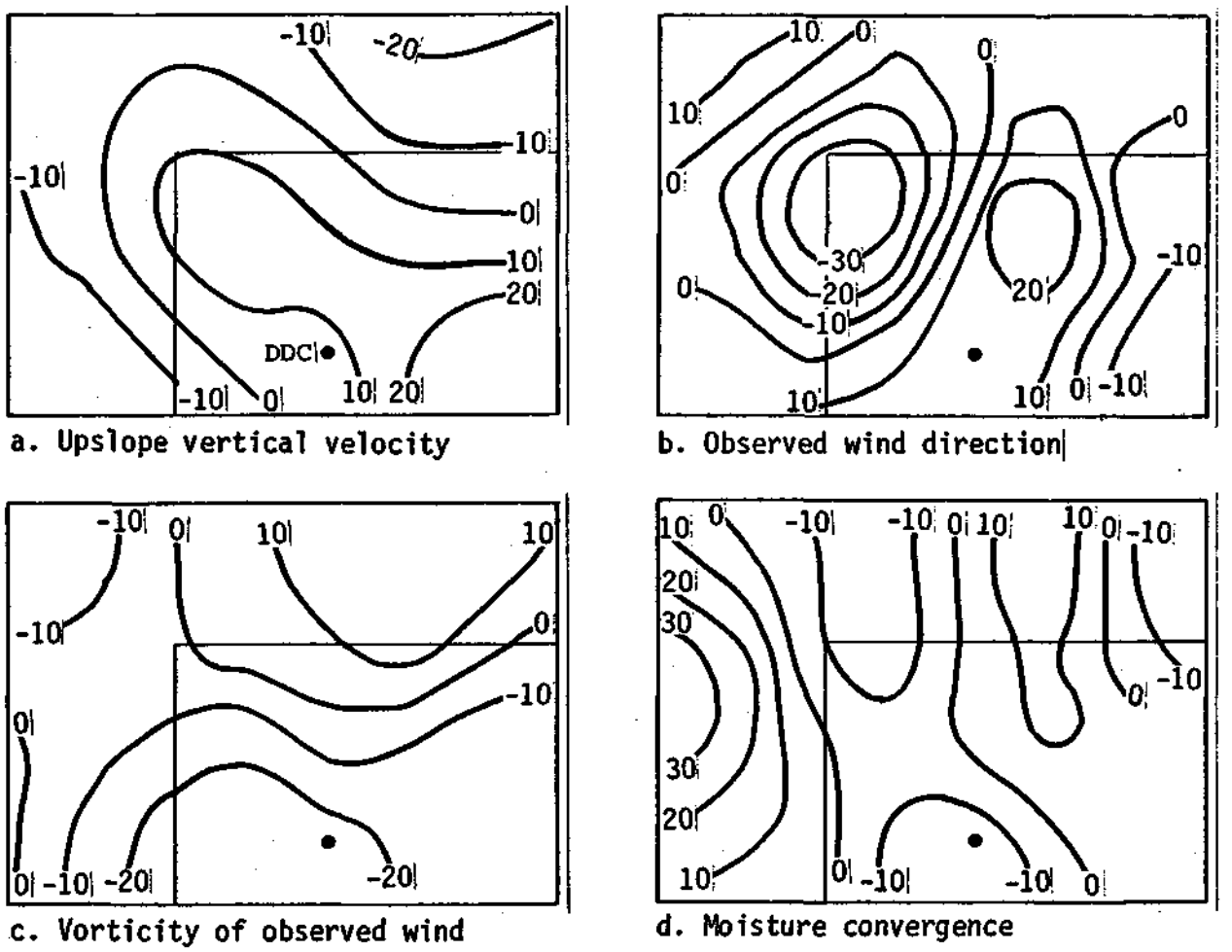

Figure 8. Factor patterns for selected surface PROGSPECs correlated with Dodge City area average rainfall for June 1965-1971.

mechanism that was located over the Dodge City area at 1800 CST had an average eastward translation speed of 10 m sec^{-1}, it would have been found over the extreme western or northwestern part of the grid at 0600 CST. If the same system had an average translation speed of 15 m sec^{-1}, it would have been located to the west off the grid at 0600 CST. If the trigger moved slower or the rainfall occurred closer to 1200 CST, the trigger would have been found over eastern Colorado at 0600 CST.

Factor 5 of the upslope vertical velocity, figure 8, shows a broad tongue of positive correlations that extends from eastern Kansas northwestward. Negative coefficients are found over southern Nebraska at the top of the grid and over eastern Colorado near the lower left boundary of the grid. The pattern correlation coefficient is 0.27; factor 5 is correlated positively with the rainfall. Positive upward vertical velocities are associated with destabilization and an increased potential for precipitation. The probability of rainfall at Dodge City increases as the amplitude of the wave-like pattern giving upslope. flow over most of Kansas increases. The negative correlations over southeast Colorado are associated with downslope flow which would occur if the winds switch from southeasterly over Kansas to southerly and southwesterly over southeast Colorado. A convergence zone, such as the dry line located over eastern Colorado, would be implied by this flow pattern. A similar vertical velocity pattern could be developed around a surface high pressure center located near the Kansas-Colorado border.

Another physical interpretation can be obtained by reversing the signs of the factor coefficient pattern and the correlation with the rainfall. It follows that rainfall over the Dodge City sampling area decreases as the amplitude of the wave-like pattern giving downslope flow over Kansas increases. The downslope flow would be associated with westerly or northwesterly dry post-cold frontal flow. Further, the Dodge City rainfall decreases with an increasing tendency for upslope flow over Nebraska. The pattern of westerly flow over Kansas and easterly flow over Nebraska would be consistent with the circulation around a surface low pressure center located near the Kansas-Nebraska border and possibly trailing a cold front southward through central Kansas.

Figure 8b gives factor 7 of the observed wind direction projected onto an axis oriented from 135-315 degrees. Northwesterly flow is given by the negative coefficients and southeasterly flow is given by the positive coefficients. This higher order factor shows considerable spatial variability. The correlation coefficient with rainfall is negative (C = -.20). The rainfall in the Dodge City area tends to decrease as northwesterly flow over northwestern Kansas increases and southeasterly flow over central Kansas increases. This pattern could be associated with a triggering mechanism located across northwest Kansas at 0600 CST approximately 100-200 km from Dodge City. It would be expected to push through before 1200 CST and leave Dodge City within stable post-frontal northwesterly flow during the 1200-1800 CST period.

By reversing the signs, we find that the rainfall in the Dodge City area tends to increase with increasing southeasterly flow over northwest Kansas. This pattern could be associated with a high pressure ridge located over central Kansas at 0600 CST and moving eastward. The increasing southeasterly flow would accelerate air toward a triggering mechanism moving through northeast Colorado (given by the change in sign of the factor coefficients there). A triggering mechanism located along the zero line over northeast Colorado at 0600 CST would, if moving at 10 m sec^{-1}, be found in the Dodge City area 10-12 hours later.

Factor 3 of the vorticity of the observed wind (Fig. 8c) is correlated negatively (C = -.16) with the Dodge City rainfall. Negative vorticities (negative coefficients) are associated with anticyclonic conditions and positive vorticities (positive coefficients) are associated with cyclonic conditions. Rainfall in the Dodge City area tends to decrease with an increasing tendency for anticyclonic flow over southwest Kansas. Cyclonic flow is shown over Nebraska. This pattern is suggestive of a low pressure center over Nebraska with a trailing cold front over central Kansas at 0600 CST; the Dodge City area would be in post frontal flow 6 to 12 hours later.

Another likely meteorological setting can be obtained by reversing the coefficient signs. It follows that rainfall increases as the tendency for cyclonic circulation over southwest Kansas increases. This pattern would favor low pressure centers located over southeast Colorado, southeast Kansas or over Oklahoma south of Kansas. Should the lows move eastward, the Dodge City area would be found to the north of the center and in an area favorable for widespread system type precipitation brought on by moist airmasses overrunning cooler airmasses north of the low center.

Factor 8 of the moisture convergence (Fig. 8d) is included as an example of a pattern with non-unique physical interpretations. The negative coefficients are associated with convergence, upward motion, destabilization, and an increased tendency for convective rainfall. Positive coefficients are associated with divergence and subsidence. The factor is correlated positively with the rainfall (C = .16). The 1200-1800 CST rainfall increases as the moisture convergence along a north-south axis located west of Dodge City increases. This pattern may be associated with a stationary front, a dry line, or with return southerly flow behind a retreating anticyclone. If the moisture convergence zone forms along the confluence of southeasterly winds over Kansas with southwesterly winds over southeast Colorado, the implied flow pattern would be consistent with the flow pattern implied by the upslope vertical velocity factor 5 (Fig. 8a).

Now, if the signs of the pattern coefficients and the correlation coefficient are reversed, a non-unique physical interpretation can be obtained. The rainfall over Dodge City is seen to increase as the moisture convergence to the lee of the Rocky Mountains over Colorado increases. A triggering mechanism

located at the west edge of the grid at 0600 CST would, upon moving at moderate speeds, pass through the Dodge City area by 1800 CST. The zone of now weak divergence over Kansas west of Dodge City would develop as the air accelerates into the approaching system. This interpretation fits well with the pattern implied by pressure tendency factor 4 (not shown) which correlated pressure falls over the west edge of the grid and pressure rises over central Kansas with a tendency for increased rainfall at Dodge City. Thus,for factor 8, reasonable physical interpretations that lead to increasing rainfall can be obtained regardless of the sign of the correlation coefficient.

Some of the factor patterns found to be correlated with rainfall at Dodge City can be interpreted while others cannot. Those for which physically consistent interpretations were obtained were correlated more highly with rainfall than those that were not. In all cases, the correlations were low; no one factor explained more than 3% of the rainfall variance. We have found non-unique factor interpretations for the moisture convergence factor 8. Both interpretations find support in the interpretations of other factor patterns. It is possible that the time of the initial analysis, 0600 CST, is too far removed from the rainfall event to allow adequate interpretation when there is large spatial variability within the pattern. Correlations using the moisture convergence PROGSPEC should be calculated from observations taken at a later time (0900 or 1200 CST).

(12) Cloud Model PROGSPECs. Numerical cloud models are an attractive source for PROGSPECs for several reasons. The cloud model combines all or nearly all of the observed environmental characteristics to simulate the complicated nonlinear processes of cloud growth. The depth and moistness of the "fuel" air, the depth and dryness of mid level entrained air, the vertical wind shear, the vertical stability structure, and the microphysics can be melded by physical quantitative relationships. The optimum covariate should be the one where the physical relationships between the independent variables and the dependent variables are known exactly.

Cloud models have been found to be useful in other seeding experiments. Positive relationships between expected natural and observed seeded cloud tops have been found through seedability studies in Florida (Simpson and Wiggert, 1971), in North Dakota (Dennis et al., 1975), and in Texas (Smith et al., 1974).

Table 20 lists 33 SPECs deduced from the MESOCU cloud model developed by Kreitzberg and Perkey (1976). This model was selected because it is a quasi-time dependent model which can simulate a history of cloud populations, and because preliminary evaluations for selected High Plains case days were available (Matthews and Henz, 1975). Generally, the SPECs address the properties of the first cloud, the cloud with maximum properties, and the average cloud property for the cloud ensemble.

Table 20. Correlations between 33 SPECs derived from the MESOCU numerical cloud model and 6 hr and daily areal average rainfall and daily areal maximum rainfall for the Dodge City sampling area for June 1965-70.

		Areal Average Rainfall		Areal Max. Rainfall
	Variable List	12-18	Daily	Daily
1	Duration 1	-0.06	0.13	0.18
2	Average Duration	-0.07	0.14	0.20
3	Total Duration	-0.06	0.13	0.16
4	Base Height 1	-0.04	0.15	0.17
5	Lowest Base Height	-0.04	0.15	0.16
6	Average Base Height	-0.04	0.15	0.16
7	Top Height 1	-0.06	0.13	0.18
8	Maximum Top Height	-0.06	0.13	0.18
9	Average Top Height	-0.06	0.14	0.19
10	Top Height with Max. Precip.	-0.06	0.13	0.18
11	Temp. at Maximum w 1	0.07	-0.09	-0.15
12	Coldest Temp. at Max. w	0.07	-0.10	-0.13
13	Temp. at Max. w with Max. Precip.	0.07	-0.10	-0.11
14	Mass Flux at Base 1	-0.05	0.12	0.15
15	Total Mass Flux at Base	-0.06	0.10	0.09
16	Precip. 1	-0.04	0.14	0.12
17	Total Precip.	-0.05	0.14	0.15
18	Areal Coverage 1	-0.05	0.15	0.19
19	Average Areal Coverage	-0.04	0.16	0.19
20	Total Areal Coverage	-0.05	0.13	0.13
21	Areal Coverage with Max. Precip.	-0.04	0.14	0.17
22	Average Areal RF 1	-0.04	0.18	0.17
23	Total Average Areal RF	-0.04	0.16	0.19
24	Maximum Updraft 1	-0.06	0.14	0.19
25	Maximum Updraft	-0.06	0.13	0.19
26	Average Maximum Updraft	-0.07	0.14	0.21
27	Cloud Efficiency 1	-0.05	0.19	0.17
28	Maximum Cloud Efficiency	-0.06	0.20	0.17
29	Height of Maximum Updraft 1	-0.06	0.10	0.15
30	Average Height of Max. Updraft	-0.06	0.11	0.15
31	Total Number of Clouds	-0.06	0.10	0.10
32	Depth of Cloud 1	-0.06	0.12	0.17
33	Depth of Cloud with Max. Precip.	-0.06	0.12	0.17

The MESOCU model is a fast one-dimensional quasi-time dependent model which may be used to operationally forecast convective development and to aid in decision making in weather modification programs. It incorporates the interactive phenomena of subsidence mixing, meso/synoptic lifting and subcloud evaporation of precipitation. The model simulates the formation of the cloud from the level where there is realized maximum energy produced by buoyancy forces as a parcel rises dry or saturated adiabatically. The initial impulse velocity and cloud radius are specified. The updraft calculations include the effects of entrainment, thermodynamics, parameterized microphysics, mass continuity on updraft and radius, and upper boundary conditions. The effects of horizontal subsidence are evaluated and more clouds are developed if the potential exists.

Since the cloud model SPECs are derived from a more complete physical description of the cloud development processes than are the simple sounding parameters and indices, it is expected that the cloud model SPECs should be superior to the sounding SPECs, However, it was found that initialization is crucial to the model's predictions. The model was initialized with the 0600 CST (1200 GMT) Dodge City soundings with a modified boundary layer. It has already been demonstrated that the morning sounding can have little relevance to afternoon and evening precipitation conditions when atmospheric structures are significantly modified by transient triggering mechanisms.

An attempt has been made to treat the boundary layer in a realistic way rather than to "tune" the model to an unmodified sounding. Following a method presented by Achtemeier and Morgan (1976), the maximum daytime temperature was selected from either the 1200 or 1500 LST WABAN surface observations. The dewpoint at the hour of maximum temperature was also retained. These temperatures were then reduced slightly according to the percentage and time of day of cloudiness. This adjustment was necessary because the observations are taken within the 10 m deep near-surface layer often characterized by super-adiabatic lapse rates. Temperatures taken within this layer often overestimate the heat actually available for deep convection. The modified temperature and the dewpoint were used to construct an adiabatic mixed layer; the depth of the layer was determined by the intersection of the mixed layer adiabat with the sounding temperature curve or the 800 mb level, whichever came first. Clouds are possible within this layer if it is sufficiently moist. If the mixed layer is terminated at 800 mb, the lapse rate from the mixed layer temperature to the sounding temperature is super-adiabatic. The truncation at 800 mb is made because the moist adiabatic ascent carried upward will produce a deep saturated layer, A saturated sounding gives no net parcel buoyancy and MESOCU, so initialized, will not develop a cloud. No adjustments for airmass vertical displacements have been made.

The linear correlations between the cloud model SPECs and the 1200-1800 CST and daily area average rainfall and the daily area maximum rainfall are shown in Table 20. A comparison of the sounding SPECs (Table 9) with the areal average daily rainfall correlations shown here shows no substantial improvement over the sounding SPECs. Correlations are disappointingly low. Less than 4% of the rainfall variance was explained by any one SPEC. Further, Table 21, which gives part of the cloud model SPEC correlation matrix, shows that the SPECs are highly intercorrelated. Most correlation coefficients range above 0.70 (greater than 50% of the variance is intercorrelated) and many are found above 0.90 (80% or more of the variance is intercorrelated).

The cloud model SPEC correlations improved when the areal maximum rainfall was used as the dependent variable (Table 20). The explained variance was nearly doubled for many SPECs but remained generally below about 4%.

Very poor results were obtained when the cloud model SPECs were correlated against the 1200-1800 CST area average rainfall. These correlations, also shown in Table 20, were so low as to be meaningless. Table 22 has been included to contrast the 6 hr, daily, and cloud model rainfalls. There were 31 rain events (6 hr) and the model with the above-described initialization predicted 51 rain events - an overforecast of 65%. The table also shows that most of the model-predicted precipitation days do not correspond with the days precipitation was reported.

We do not consider that our version of the MESOCU cloud model is incapable of simulating High Plains convective precipitation. Rather, the fault lies in the paucity of hourly climatological rainfall data and the problems inherent in providing the model with a representative initial state. (An attempt has been made to improve on the initial state through a combination of the surface and the sounding data into a diagnostic four-dimensional analysis of atmospheric structure. Various aspects of this approach have been tested with Illinois mid-summer data and have yielded mixed results. Problems with the spatial analysis and with temporal and spacial paucity of climatological surface data for the High Plains dictated that a low priority be placed on this approach for SPEC development. The four-dimensional method is reported in more detail in the Appendix.) However, model studies should be continued with the data collected during the HIPLEX program.

(13) Radar Summary SPECs, Radar is useful for the development of SPECs for both the area and single cloud efforts. Quantities that can be evaluated for the single cloud experiment are given by Ackerman (1976). Our climatological studies have centered on the use of radar data in correlations with the 1200-1800 CST 6 hr rainfall and for use as a source of dependent

Table 21. Correlation matrix for 33 cloud model variables (Table 20) with rainfall. Variable 34 is the 6 hr 1200-1800 CST rainfall.*

	1	2	3	4	5	6
1	1.0000					
2	0.9788	1.0000				
3	0.7684	0.7658	1.0000			
4	0.7345	0.7249	0.5983	1.0000		
5	0.7200	0.7000	0.5044	0.9838	1.0000	
6	0.7350	0.7060	0.5649	0.9902	0.9914	1.0000
7	0.9689	0.9463	0.7382	0.8547	0.8449	0.8542
8	0.9691	0.9473	0.7647	0.8541	0.8383	0.8508
9	0.9625	0.9631	0.7385	0.8566	0.8417	0.8462
10	0.9691	0.9473	0.7605	0.8538	0.8393	0.8512
11	-0.9116	-0.9037	-0.6575	-0.8573	-0.8554	-0.8544
12	-0.9147	-0.9100	-0.7323	-0.8516	-0.8372	-0.8462
13	-0.9019	-0.8931	-0.6572	-0.8400	-0.8450	-0.8444
14	0.8026	0.7771	0.5820	0.8786	0.8847	0.8830
15	0.6384	0.5812	0.7897	0.6943	0.6399	0.6953
16	0.7207	0.6712	0.4866	0.4922	0.5081	0.5170
17	0.6863	0.6564	0.8574	0.4564	0.4094	0.4534
18	0.6860	0.6802	0.6039	0.8556	0.8381	0.8487
19	0.6688	0.6592	0.5309	0.8701	0.8615	0.8663
20	0.5240	0.4903	0.7090	0.6745	0.6076	0.6673
21	0.6120	0.6048	0.4335	0.8398	0.8404	0.8389
22	0.7855	0.7396	0.6151	0.5284	0.5341	0.5518
23	0.6780	0.6568	0.8831	0.4678	0.4039	0.4548
24	0.9373	0.9240	0.7699	0.8323	0.8131	0.8281
25	0.9374	0.9251	0.7766	0.8345	0.8121	0.8286
26	0.9315	0.9381	0.7308	0.8313	0.8089	0.8169
27	0.7853	0.7481	0.5901	0.6830	0.6915	0.7008
28	0.8200	0.7930	0.7414	0.6880	0.6719	0.6944
29	0.9263	0.9169	0.6779	0.8568	0.8526	0.8539
30	0.9234	0.9230	0.6736	0.8600	0.8541	0.8553
31	0.6410	0.5829	0.7978	0.7114	0.6546	0.7133
32	0.9848	0.9597	0.7396	0.7709	0.7634	0.7730
33	0.9842	0.9622	0.7828	0.7759	0.7563	0.7719
34	-0.0551	-0.0650	-0.0572	-0.0435	-0.0397	-0.0352

* Only the first 6 columns of the 34 column matrix are shown.

Table 22. Reported 6 hr, daily and cloud model predicted (SPEC 17, Table 20) rainfall for the Dodge City sampling area for June 1965-70. Rainfall amounts in mm.

	1965			1966			1967	
Day	12-18	Daily	Cloud Model	12-18	Daily	Cloud Model	12-18	Daily	Cloud Model
1	00	00	00	00	15.2	24.3	00	0.3	00
2	00	00	00	00	00	00	00	00	00
3	00	20.1	22.9	00	0.3	11.3	00	00	0.8
4	22.4	25.9	00	00	00	00	3.6	3.6	00
5	00	2.0	3.7	00	0.3	00	00	00	00
6	00	00	00	00	4.6	00	4.1	9.1	4.7
7	00	5.1	28.3	00	3.3	45.2	00	0.5	5.4
8	00	0.3	00	00	00	00	00	00	0.1
9	11.2	24.1	00	00	00	00	00	2.3	00
10	1.0	7.6	00	00	00	00	0.3	15.2	5.3
11	2.0	0.8	00	00	00	10.6	2.5	1.8	00
12	2.3	17.0	3.5	00	4.6	00	00	00	00
13	00	0.3	00	00	00	00	00	00	00
14	00	00	00	00	0.5	7.4	00	0.3	00
15	00	00	12.7	0.8	00	1.7	1.8	26.4	1.1
16	3.0	7.1	00	00	0.3	00	00	15.2	00
17	00	0.5	00	0.5	1.5	00	00	16.5	00
18	00	0.3	17.4	00	0.3	00	00	1.3	00
19	00	00	36.1	00	00	00	1.0	10.7	00
20	00	00	00	00	00	00	00	9.7	00
21	00	3.6	3.7	3.0	2.3	0.7	00	00	00
22	00	1.3	21.2	00	00	0.4	00	5.8	00
23	00	2.0	23.2	00	1.0	00	00	16.5	2.1
24	2.8	3.8	23.8	00	00	5.8	00	00	00
25	00	4.3	00	00	3.8	00	00	00	00
26	00	0.5	18.4	4.6	9.7	00	00	5.3	00
27	0.5	1.3	1.8	5.3	2.0	00	00	1.5	00
28	00	00	43.3	00	0.3	00	00	23.6	00
29	00	1.5	00	00	00	00	00	00	00
30	00	00	6.4	00	00	00	00	00	00

Table 22 (continued)

	1968			1969			1970		
Day	12-18	Daily	Cloud Model	12-18	Daily	Cloud Model	12-18	Daily	Cloud Model
1	00	00	00	00	00	00	0.3	3.0	2.4
2	00	00	00	00	2.0	00	00	0.3	1.4
3	00	00	00	00	00	00	00	1.0	00
4	00	00	00	00	00	1.7	00	0.3	00
5	00	00	00	00	00	6.3	00	00	00
6	00	2.0	00	00	1.0	1.0	00	00	00
7	00	2.0	00	00	11.7	00	00	00	00
8	0.3	6.9	6.7	00	2.0	00	00	00	00
9	5.1	20.1	00	00	00	00	0.3	0.3	00
10	1.5	0.5	00	00	4.8	6.5	00	0.3	00
11	00	00	00	00	1.3	00	1.5	11.7	00
12	00	00	00	00	1.0	00	00	1.3	1.8
13	00	3.3	1.9	00	9.7	6.6	0.5	24.1	34.2
14	00	5.1	00	00	0.8	7.3	0.8	10.7	00
15	00	17.0	0.9	00	2.3	00	00	00	00
16	0.5	7.6	00	00	30.5	13.5	00	00	00
17	00	00	00	0.8	1.5	00	00	00	00
18	00	3.8	3.3	00	00	00	00	16.0	00
19	00	00	5.6	00	00	00	00	00	00
20	00	00	10.2	00	00	00	0.5	00	00
21	00	00	00	00	00	2.4	00	00	00
22	00	00	1.8	00	0.3	00	00	00	00
23	00	2.0	00	2.8	5.3	00	00	0.5	00
24	00	7.6	00	00	0.3	31.0	00	00	00
25	00	00	00	00	00	00	00	00	00
26	00	00	00	00	00	00	00	00	00
27	00	00	00	00	00	00	00	00	00
28	00	00	00	00	00	1.3	00	00	0.6
29	00	00	00	00	00	00	00	00	00
30	00	00	00	00	00	00	00	00	00

variables for correlations with the surface and cloud model PROGSPECs. The Weather Service Radar Summary (RADU) Charts provide a rough summary of the radar echo character in a spatial setting. RADU microfilms containing summaries at 3 hr intervals for June 1960-1970 were scanned to retain gross echo characteristics for comparison with the area averaged rainfall for the Dodge City and neighboring sampling squares.

The RADU SPECs are as follows:

1. Percent Coverage of Sampling Square

The area of a sampling square covered by some concentration of radar echoes (designated by a scalloped line) in proportion to the total sampling area is converted into one of five coverage categories. These are coverages for 1) no coverage, 2) 0-25%, 3) 25-50%, 4) 50-75%, and 5) greater than 75% coverage.

2. Echo Density

The echo density is an estimate of the percent echo coverage within the areas designated as containing radar echoes. The echo density is given by one of five density categories: 1) no echoes, 2) isolated echoes, 3) scattered echoes, 4) closely spaced echoes (broken), and 5) 100% coverage (solid).

3. Echo Organization

Precipitation elements are found in random, disorganized, irregular patterns or in organized lines or bands. When echo patterns are disorganized, precipitation can be spotty with some areas receiving heavy rainfall and other areas receiving little or no rainfall. When the elements are organized into lines, precipitation tends to be more widespread and storms more intense with higher cloud tops. The echo organization was coded for either areal or linear patterns. When both types were present simultaneously the linear designation was used.

4. Echo Type

Echo pattern shapes, reflectivity gradients, reflectivity intensities, and echo depths are often used to subjectively categorize the precipitation elements into 1) general stratiform rain, 2) showers, 3) thundershowers. Prior to 1963, radar echoes were designated as weak, moderate, or strong. These were redesignated into either the shower or the thundershower category depending upon whether the maximum top was above or below 25,000 ft (7 km).

5. Echo Intensity

Echo pattern characteristics listed in 4. above are also used to subjectively estimate the intensity of the precipitation elements. These were categorized into weak, moderate, and strong.

6. Maximum Echo Height

The maximum echo height is reported generally for just a few tall echoes within the range of the radar. There are few times that a maximum echo will be reported within a specified sampling area. We have developed the following scheme to estimate the missing top heights. If echo tops are reported within the sampling area the tallest is taken as the maximum echo top. If average echo tops are given for the immediate vicinity of the sampling area, the average echo tops are used for the maximum echo top. If neither the average nor the maximum echo top is given, use the following averaging scheme. Search forward in time not to exceed 6 hrs to find the reported echo top at specified and surrounding sampling areas. Do the same by searching backward in time not to exceed 6 hrs. There can be a maximum of 4 echo tops retained by this method; specified area forward in time, specified area backward in time, surrounding area forward in time and surrounding area backward in time. Then find the average echo top. Only the echo tops for the same echo organization (area, line) may be used. If there are no reported echo tops with the spatial or temporal limits, maximum tops of 19,900 ft (6 km) are imposed for areal organization and maximum tops of 29,900 ft (9 km) are imposed for lines.

7. and 8. Echo Direction of Motion and Echo Speed

The echo speeds and directions of motion were found in the same manner described for the maximum echo top. The exceptions were that there were no imposed directions. Also, when area or line directions and speeds were given in absence of cell movements, it was assumed that the cells moved in the same manner as the areas.

9. Surrounding Echo Data

Since the RADU data were summarized for all six Kansas sampling areas, the data from the surrounding sampling areas can also be used for SPECs for a specified sampling area.

The codings for the first six SPECs were designed so that the numbers increased with increasing coverage, intensity, density, organization, and echo height. We combined the 1200, 1500, and 1800 CST radar summaries to produce a single 6 hr 1200-1800 CST summary for comparisons with the rainfall for the same period. The final coding was the maximum of the three codings for each SPEC. The results of the RADU-rainfall correlations are shown in Table 23. The percent sampling area designated as covered with echoes (SPEC 1) explained 25% of the rainfall variance. The remaining RADU SPECs explained less than 15% of the rainfall variance. These correlations were unexpectedly low and may reflect the coarseness of the radar summary methods, the paucity of hourly rainfall data measurements, or both. The RADU SPECs were also highly inter-correlated as is shown by the maximum intercorrelation coefficients. No less than 75% of the variance of one SPEC could be explained by another SPEC.

Table 23. Linear correlation between the radar summary (RADU) SPECS and 6 hr (1200-1800 CST) rainfall.

SPEC		Correlation	Maximum Intercorrelation
1.	Percent of sampling area covered with echoes.	0.51	0.87
2.	Echo density (isolated, scattered, broken, solid).	0.37	0.96
3.	Echo organization (area, line).	0.36	0.95
4.	Echo type (rain, shower, thundershower).	0.34	0.97
5.	Echo intensity.	0.40	0.93
6.	Maximum echo height.	0.36	0.94
7.	Echo direction of motion.	0.30	0.97
8.	Echo speed of motion.	0.32	0.90

(14) Surface PROGSPEC and Cloud Model SPEC Correlations with the RADU SPECs as Dependent Variables. The covariate study has been plagued throughout by an uncertainty brought on by the paucity of the hourly rainfall data (one station per 6500 km2). Many convective rains could escape detection by this network. These rain days, possibly highly correlated with the SPECs, would be treated as dry days. The overall SPEC-rainfall correlations could thus be greatly reduced.

The radar summary data provide an independent means of assessing whether rain producing clouds were over the sampling areas during a specified period of time. The surface and cloud model SPECs were correlated against the RADU SPECs, Only the results for the maximum percent sampling area coverage (RADU SPEC 1) are presented since the RADU SPECs were highly intercorrelated (Table 23) and there were only minor differences when the correlations were taken with the other RADU dependent variables. Table 24 summarizes the correlations between the 0600 CST surface PROGSPECs and the five categories of maximum percent sampling area coverage. The observed wind direction (90-270 deg, axis), moisture convergence, upslope vertical velocity (observed wind), and geostrophic wind direction (135-315 deg, axis) each explained more than 20% of the RADU SPEC 1 variance. A comparison with the PROGSPEC correlations with June areal average rainfall (Table 16) shows that the PROGSPECs are somewhat more correlated with radar echo coverage. The correlation with area rain ranged from 0.0-0.38, and the correlation with RADU ranged from 0.14-0.47.

Table 24. Correlation of 0600 CST surface PROGSPECs with the maximum percent sampling area coverage with radar echoes (RADU SPEC No. 1) for the period 1200-1800 CST for June 1965-70 using an eigenvalue limit ≥1.0 and factor correlation limit ≥|0.10|.

	Variable	No. of Factors ≥|0.10|	RADU SPEC Variance Explained by Factor %	Total Correlation
1	Obs. Wind Dir. (90-270)	4	21.9	0.47
2	Moisture Convergence	4	20.9	0.46
3	Upslope Vertical Velocity (observed wind)	4	20.3	0.45
4	Geo. Wind Dir. (135-315)	1	20.3	0.45
5	Surface Pressure	1	19.0	0.44
6	Upslope Vertical Velocity (geostrophic wind)	3	18.0	0.42
7	Obs. Wind Dir. (45-225)	2	16.8	0.41
8	Geo. Wind Dir. (90-270)	2	16.6	0.41
9	Obs. Wind Dir. (135-315)	5	16.7	0.41
10	Vorticity	3	17.0	0.41
11	Cumulative Lift	2	15.1	0.39
12	Geo. Wind Dir. (180-359)	3	14.8	0.38
13	LCL Height	2	10.2	0.32
14	Virtual Pot. Temp. Adv.	2	9.7	0.31
15	Geo. Wind Dir. (45-225)	1	8.7	0.30
16	Obs. Wind Dir. (180-359)	2	8.2	0.29
17	Mixing Ratio Advection (observed wind)	4	7.5	0.27
18	Mixing Ratio	2	7.0	0.26
19	Divergence	3	6.8	0.26
20	Pressure Tendency	3	6.8	0.26
21	Wet Bulb Pot. Temp.	2	6.6	0.26
22	LCL Temperature	1	6.3	0.25
23	Mixing Ratio Advection (geostrophic wind)	1	4.6	0.21
24	Pressure Trough Analysis	1	4.0	0.20
25	Wind Speed Tendency (3 hr)	4	2.1	0.14

Now the areal average rainfall does not necessarily increase with increased radar echo coverage. However, if any precipitation systems of duration greater than 3 hr were present over the sampling area, the coverage accorded was a number greater than zero. The removal of precipitation days from the no rain category and the placement of them into another category that confirmed the presence of rain was a contributing factor to the increase in the PROGSPEC correlations.

The cloud model SPECs were also correlated with the RADU SPEC 1. Table 25 shows that the correlations are greater than the correlations with the areal average rainfall (Table 20) but were much less than the correlations obtained with the surface PROGSPECs (Table 24). The first three SPECs shown related to model cloud precipitation and explained about 4% or less of the RADU SPEC 1 variance.

Table 25. Correlation of 0600 CST boundary layer modified cloud model SPECs With the maximum percent sampling area radar echo coverage (RADU SPEC No. 1) for the period 1200-1800 CST for June 1965-70 using a correlation limit ≥0.10.

Variable	RADU SPEC Variance Explained by Cloud Model SPECs %	Correlation
Maximum Cloud Efficiency	4.2	0.18
First Cloud Area Average Rainfall	3.7	0.14
Total Cloud Precipitation	3.5	0.12
Average Cloud Base Height	3.5	0.12
First Cloud Percent Areal Coverage	3.3	0.11

(15) Summary of Physical Environmental Covariate Search for HIPLEX. The previous sections have described the methods of selection, the description, and the simple correlation analyses for candidate SPECs derived from four sources: sounding only, surface data only, cloud model (sounding and surface data combined), and radar summary. The correlation analyses for these SPEC sets are summarized below.

(a) The Sounding SPECs. Out of a possible 200 candidate variables, 38 variables were selected to be tested. These included 17 stability, 10 moisture, and 6 trigger mechanism

related variables. The list was expanded to 136 variables when the variables were computed at various atmospheric levels. This number was increased by an additional 136 to 272 variables by formulating the 24 hr tendencies. The linear correlations with the June 1958-70 daily (7 AM - 7 AM) rainfall for the Dodge City sampling area showed that no one variable explained more than 10% of the rainfall variance. Only 42 sounding SPECs had correlation coefficients greater than 0.15 in magnitude.

The sounding SPECs were also correlated with the 3 hourly rainfall for the Dodge City sampling area. The following results were obtained:

1) Only 84 variables had correlation coefficient magnitudes exceeding 0.15 for at least one 3 hr period.

2) There was found a rapid decline in the number of variables correlated with rainfall from about 40 early in the morning to just a few by late in the day. Thus the SPECs had little or no predictive power for mid-afternoon to late evening convective conditions.

3) The SPECs had no temporal continuity between successive 3 hourly periods. Thus there was no consistent predictive power among those SPECs retained for the convective period.

These findings showed that the sounding SPECs were poorly correlated with rainfall and were especially poor predictors of convective period rainfall in the High Plains precipitation regime dominated by transient weather systems (Bark, 1975), Additional work in the next section involving SPEC equations also indicated the poor relationship with soundings. Thus the sounding SPECs were dropped from further consideration as candidate covariates for HIPLEX.

(b) The Surface PROGSPECs. The surface PROGSPECs specifically addressed triggering mechanisms. Twenty candidate covariates were selected; the number expanded to 26 when the multiple wind direction categories were included. The PROGSPECs were presented as fields on a 8 x 6 regular mesh covering most of Kansas and parts of Nebraska and Colorado. The fields were transformed into pattern types by factor analysis. Correlations with the daily and 6 hr (1200-1800 CST) rainfall revealed the following:

1) The correlations with rainfall, though much improved over the sounding SPECs, were still disappointingly low. No single variable explained more than 23% of the rainfall variance.

2) No one pattern and no one variable was isolated as especially indicative of High Plains rainfall.

3) There was no consistent month to month ranking of the PROGSPECs. This result was anticipated because the rainfall-producing regimes vary throughout the June-August summer season.

4) Interpretations of factors indicated that some factor-rainfall correlation patterns were consistent with known physical processes that lead to convectiye rainfall. However, other factor-rainfall patterns were physically inconsistent and still others were not revealing.

These results, though generally discouraging, were encouraging enough to warrant further investigation.

(c) The cloud Model SPECs. Conceptually, the cloud model SPECs should have been highly correlated with convective rainfall since the model simulates physical processes of cloud development. One drawback of the cloud models is that they are sensitive to errors in the initial state. The Kreitzberg-Perkey MESOCU cloud model was initialized with the morning soundings modified in the lower levels for maximum reported daytime temperatures and moisture. Thirty-three SPECs were developed from MESOCU and correlated with the daily and 6 hourly rainfall. The following results were obtained:

1) The cloud model SPECs were correlated poorly with the daily rainfall. Less than 4% of the rainfall variance was explained by any one variable. The variables were also highly intercorrelated.

2) The correlation with the 6 hourly rainfall was extremely low. The maximum correlation was 0.07.

Thus, the cloud model SPECs were eliminated from further consideration as candidate covariates for HIPLEX,

(d) The Radar Summary SPECs. Nine SPECs were derived from the National Weather Service radar summary RADU charts. These SPECs could be used either as independent or dependent variables. Correlation of the RADU SPECs with the 6 hourly rainfall averaged over the Dodge City sampling area indicated the following:

1) The RADU SPECs were highly intercorrelated.

2) Almost 25% of the rainfall variance was explained by the percent sampling area areal coverage SPEC. This SPEC was included in further statistical analysis.

(16) Statistical Techniques for the Incorporation of Covariates into the Design and Evaluation. In the last section, the physical and meteorological concepts underlying the initial

selection of SPECs, list of "candidates," and some initial screening of "candidates" were presented. However, even after this initial selection is made, a large number of variables remains to be manipulated. These variables are usually intercorrelated so that classical multiple regression techniques are extremely questionable, if not totally inappropriate. Furthermore, a method is needed whereby the pattern types of the surface predictor fields can be described and then analytically entered into a SPEC equation.

For example, the objective surface fields used as SPECs in the Kansas-Nebraska-Colorado area are composed of 25 different meteorological fields. Each field is composed of 48 grid points. In order to describe these fields, 1200 (25 x 48) variables are needed for the surface SPECs alone. In addition, there are 128 candidate variables from the meteorological soundings. Thus, there is a total of 1328 candidate variables in addition to those derived from radar, rain, and cloud models.

Thus, statistical techniques developed for the incorporation of SPECs into the HIPLEX design and evaluation were designed to 1) handle the highly intercorrelated variables, 2) effectively reduce the number of variables, and 3) effectively identify and describe the pattern types from the meteorological surface fields that are instrumental in producing rainfall in and surrounding the target area.

In order to describe the variability of meteorological surface fields over time and space, a multivariate statistical technique known as factor analysis is proposed. This approach, when extended to multiple regression of the temporal components derived from the factor analysis, provides a method of incorporating the pattern information into the SPEC equation.

The factor analysis is applied to the meteorological field of interest during a particular month (May, June, July, August, or September) over each of the 104 km x 104 km sampling areas shown on figure 4. First, the meteorological field values from the 48 grid points (variables) are determined for each day (observation) and for each of the months for the period 1965-1970.

The field values from the 48 grid points are used to form a m x n (m = 172 days x n = 48 grid points) matrix X for a given month. The matrix is then subjected to a R-type factor analysis. This analysis was performed by first standardizing each of the columns (grid points of the X matrix) by their respective means and variances so that a m x n matrix Z of standardized variates was obtained. The correlation matrix R, which is a matrix of correlation coefficients between the columns (grid points) of Z, was then determined. From the R matrix, a set of new variables was constructed such that the new variables are exact mathematical transformations of the original data. This transformation is accomplished by determining the characteristic scalar roots (eigenvalues) and the non-zero vectors (eigenvectors) of R which simultaneously satisfy the equation;

$$RE = \lambda E \tag{18}$$

where E is the n x n matrix consisting of a set of orthonormal eigenvectors of R as the columns and λ represents the eigenvalues (characteristic scalar roots) of R. Equation 18 can be rewritten in the form:

$$(R - \lambda I_n)\, E = 0 \tag{19}$$

where I_n is the identity matrix of order n x n. The solution of the scalars λ and the eigenvectors E is the classical Characteristic Value Problem of matrix theory (Hohn, 1960).

The magnitude of the eigenvalues represents the variance of the observations in the Z matrix explained by each eigenvector. The eigenvectors are then ordered so that the first diagonal element of λI_n represents the largest eigenvalue, and the second the next largest, etc. The eigenvectors are also scaled by multiplying each orthonormal eigenvector by the square root of its eigenvalue to obtain the "principal components loading matrix":

$$A = ED^{1/2} \tag{20}$$

where $D = \lambda I_n$, the n x n diagonal matrix of the eigenvalues of R. The columns of the A matrix are called factors and are independent of each other. This extraction of factors results in a principal component solution (i.e., an exact mathematical transformation without assumptions), and the factors are designated as defined factors (Kim, 1975). If the diagonal elements of the R matrix are replaced with initial estimates of communalities (i.e., the squared multiple correlation between each variable and all others in the set) prior to factoring, the result is the principal factor solution (Kim, 1975). In this case, the matrix is defined to be the "principal factors loading matrix," and the factors are called inferred factors (i.e., assumptions about the variance in common have been imposed), Whether the factors be defined or inferred, the first factor explains the largest amount of the combined variance of the observations in the Z matrix; the second factor explains the second largest amount of variance, and so on.

The exact configuration of the factor (eigenvector) structure is not unique; one factor solution can be transformed into another without violating the assumptions or mathematical properties of a given solution (Kim, 1975). Since some factor structures are more meaningful than others (i.e., some are more simple, some are more informative, some are more revealing), it is often desirable to rotate the factors to a terminal solution that satisfies both the

practical and theoretical needs of the research problem. Occasionally, the initial factor structure satisfies these needs and can be used for the terminal solution.

The A matrix consists of factors (scaled eigenvectors) which are orthogonal (uncorrelated) functions of space. These spatial functions are linear combinations of the various grid points. Each grid point possesses a certain amount of variance contained within a particular eigenvector (Fig. 9). For example, the negative areas enclosed by the -.10 isoline contain a high amount of variance (large negative values of the fourth factor). The area enclosed within the -.15 isoline contains an even higher amount of variance. Similarly, the area enclosed by the .15 isoline contains a high amount of variance (large positive values).

Furthermore, the highs and lows in the factor patterns are representative of spatial highs and lows in the original pressure tendency fields, and hence, representative of pattern types. However, in order to determine on which day a certain pattern type prevails, and to relate these pattern types to the SPEC equations, it is necessary to derive the matrix of principal components (principal factors).

The matrix A is a transformation matrix which can be used to transform the matrix into a set of principal components (or principal factors).

$$F = Z(A^T)^{-1} \qquad (21)$$

where F is the principal components (or principal factors) matrix of order m x n. The scaled eigenvectors (factors) of the A matrix are orthogonal (uncorrelated) functions of space and the principal components of the F matrix are orthogonal (uncorrelated) functions of time.

There are m = 172 elements in the column vectors of the matrix. Each element is associated with one of the m days. If the element of a certain day is a large positive value, then there are highs (pressure rises) in the positive regions and lows (pressure falls) in the negative regions on that day in the pressure tendency field (Fig. 9). Conversely, if the element is a large negative value, then there are highs (pressure rises) in the negative regions and lows (pressure falls) in the positive regions.

The application of the factor analysis to a particular meteorological field (pressure tendency, for example) results in a set of principal components for that field. If the intention of the analysis is to relate only the pressure tendency field to the rainfall, then the rainfall should be multiply regressed on the principal components of the pressure tendency field. However,

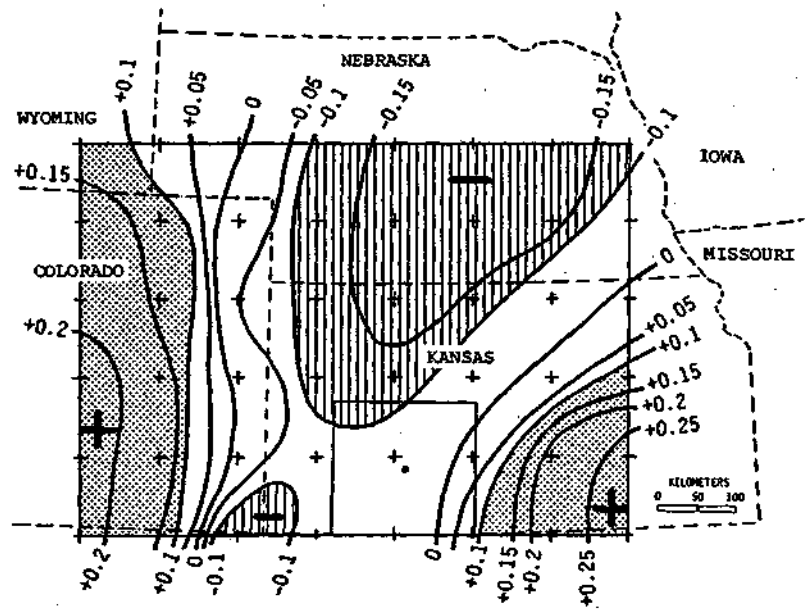

Figure 9. Spatial representation of Factor 4 (pattern type) of the 0600 pressure tendency field for June 1965-1970.

there are many other fields (in this case, 25) as well as meteorological sounding variables, radar variables, rainfall variables, etc., and all must be related to the rainfall by a SPEC equation.

The proposed procedure to handle all the variables is to retain only those components from each set of variables (i.e., fields, soundings, radar, etc.) which have associated eigenvalues ≥ C1 (the cutoff value) and correlation coefficients with the rainfall ≥ C2 (the cutoff value). In this manner, a huge reduction in the independent variable space is obtained and only the portion of each variable (fields, soundings, radar, etc.) that contributes to the rainfall variance is retained. A multiple regression of the rainfall on the principal components is then performed and the resulting regression equation becomes the final SPEC equation.

This procedure 1) extracts only the portion of each variable that is important in predicting rainfall, 2) reduces the dimensionality of the independent variable space (thereby increasing the degrees of freedom and making the manipulation of variables manageable), 3) effectively combines the information from all variables, and 4) permits a quantitative-physical interpretation of the influence of the meteorological variables (particularly, various pattern types associated with the meteorological fields) on precipitation.

It is duly noted that some correlation will remain between the sets of variables (fields, sounding, radar, etc.), but that within each set of variables for which the factor analysis is performed, the derived principal components (new variables) are uncorrelated with each other. If a significant amount of correlation remains, then a standard principal components regression (Massey, 1965) can be performed on this new set of variables. This final step is seldom necessary.

In addition, the components can be used to determine rain or no rain over the area of interest. This is accomplished by classifying the m days into rain and no rain days, and then performing a stepwise discriminant analysis (Klecka, 1970) on the two classes using the various components. The resulting discriminant relationships can then be used for the purpose of declaring rain or no rain.

(17) Results of the SPEC Equation Determinations. (a) Daily Rainfall. The aforementioned techniques were used to obtain SPEC equations for the mean areal rainfall during the period 0700-0700 LST (dependent variables) in the 29,300 km^2 area surrounding Dodge City (depicted by the square area surrounding Dodge City on Fig. 4) for June, July, and August 1965-1970. For June, the 25 surface fields, the 128 sounding variables, and the mean areal rainfall (0700-0700) in the 29,300 km^2 area surrounding Dodge City (Fig. 4) were considered as potential SPECs for the daily rainfall.

First, the sounding variables were correlated with the daily rainfall, and only those sounding variables with correlations ≥.15 were retained for further analysis. (This resulted in the retention of 48 sounding variables for June.) The R mode factor analysis was then performed individually on each of the 25 fields (48 variables each), the set of 48 sounding variables, and the five surrounding areas of precipitation.

For the PROGSPEC variables (0600 sounding variables and 0600 surface fields), there were 67 factors with eigenvalues = C1≥1.0 and with correlation coefficient = C2≥.10. The retention of only those factors permits a first reduction of the various patterns of each surface field to a limited number of pattern types representative of the overall variability of the field. The associated principal components can then be used to identify the day on which these pattern types occurred and the relative magnitude of each pattern type. (In the case of the sounding variables, the magnitude of the linear combination is still being portrayed, but the spatial pattern is not being portrayed.)

The areal mean rainfall during the daily period 0700-0700 (dependent variable) in the 29,300 km2 area surrounding Dodge City was then regressed on the 67 PROGSPEC factors. This resulted in a multiple correlation coefficient of 0.68, with 46.5% of the rain variance explained by the multiple regression.

There was only one SYNSPEC factor, and it was obtained from the daily rainfall of the five surrounding areas. This factor is correlated 0.69 with the daily rainfall and explains 48% of the rain variance. Thus, the one SYNSPEC variable explains as much variance as the totality of the PROGSPEC variables.

The areal mean rainfall was then regressed on a combination of the SYNSPEC and PROGSPEC variables. The multiple correlation for the SYNSPEC-PROGSPEC combination was 0.81 with 66% of the variance explained. Overall, more of the rain variance was explained by the surface fields than by the sounding variables. Also, as discussed previously, the sounding variables are limited since they cannot adequately measure atmospheric conditions when precipitation is produced by transient mechanisms. Thus, the multiple correlation was re-done for the PROGSPEC variables, excluding the sounding variables. This resulted in a multiple correlation of 0.65 with 43% of the variance explained. Thus, there is only a slight improvement in the amount of variance explained when the sounding variables are included. Since 1) the soundings are questionable because of the transient problem, 2) there is only a slight increase in variance when the soundings are included, and 3) a great amount of additional computer effort was needed to derive the sounding variables, the sounding variables were not determined for July and August. Overall results for all three months are given in Table 26.

Table 26. Results concerning the relationship of PROGSPECs (0600) and SYNSPECs (0700-0700) with the daily rainfall (0700-0700) during June, July, and August 1965-1970 using an eigenvalue limit of ≥1.0 and a correlation limit of ≥.10.

PROGSPEC			SYNSPEC			PROGSPEC - SYNSPEC Combination		
Number of factors	% Rain variance explained by factors	Total corr. (abs.)	Number of factors	% Rain variance explained by factors	Total corr. (abs.)	Number of factors	% Rain variance explained by factors	Total corr. (abs.)
				June (N = 172)*				
67	46.5	.68	1	48.0	.69	68	66.0	.81
				July (N = 186)				
70	63.4	.80	2	32.8	.57	72	68.9	.83
				August (N = 186)				
83	65.6	.81	2	49.9	.71	85	77.4	.88

* June analysis includes sounding variables

When only PROGSPEC variables are used, 46.5% of the daily rain variance can be explained during June, 64.4% can be explained during July, and 65.6% can be explained during August. A combination of PROGSPECs and SYNSPECs increases these percentages to 66%, 68.9%, and 77.4%, respectively. Clearly, these percentages are large enough to be useful in the design and evaluation.

The results for the SYNSPEC variables indicate that less variance is explained in July than in August. Since this set of variables is comprised of rain from surrounding areas, this indicates that less areal correlation of rain occurs in July than in August. For both July and August, more variance is explained by the totality of the PROGSPEC variables than by the SYNSPEC variables.

To determine the usefulness of the SYNSPEC and PROGSPEC variables for the purpose of predicting rain or no rain during the day, a stepwise multiple discriminant analysis was performed for the rain and no rain classes using the factors as the discriminants. The results are shown in Table 27. The skill in determining that rain will fall during a particular day from the 0600 PROGSPECs varies from 74.5% to 78.7% depending on the month. The prediction skill is only slightly improved by inclusion of the SYNSPEC variables. Overall, there is less prediction skill during July than during June or

August, a reflection of the more variable and isolated rainfall characteristics during July.

Table 27. Results concerning the jackknifed classification of rain and non-rain days using a stepwise discriminant analysis of the rain and non-rain cases. (Prior classification probability is based on the number of rain and non-rain cases in the sample.)

PROGSPEC				PROGSPEC-SYNSPEC Combination			
Number of factors selected	Percent correct			Number of factors selected	Percent correct		
	rain	non-rain	overall		rain	non-rain	overall
			June (N = 172)*				
14	78.7	71.8	75.6	14	83.0	85.9	84.3
			July (N = 186)				
7	77.6	58.2	69.4	15	78.5	74.7	76.9
			August (N = 186)				
21	74.5	81.5	78.0	12	77.7	84.8	81.2

* June analysis includes sounding variables

Since the jackknifed classification of rain and non-rain was used (i.e., the discriminant function was developed without the case being classified), it is unnecessary to perform an additional test for an independent period.

(b) 6-Hourly Rainfall. As mentioned earlier, the mean areal rainfall was computed for 3-hr periods during the day in the six areas shown on figure 4. The 3-hr areal rainfalls were then summed to obtain the mean areal rainfall for the six areas during the 6-hr period 1200-1800 CST, the major convective period of the day. The 6-hr rainfall for the Dodge City area was then correlated with the 0600 PROGSPECs and the SYNSPECs obtained from the 6-hourly rainfall of the surrounding five areas shown on figure 4.

In addition, the rainfall amounts during the period 0900-1200 in the six areas were designated as pre-wetness variables. Factor analysis was performed on the pre-wetness variables, and the resulting factors were correlated with the 6-hr rainfall in the Dodge

City area. Only those factors with eigenvalues ≥1.0 and correlation coefficients ≥.10 were retained for further analysis. The 6-hr rainfall was then regressed on several combinations of surface, pre-wetness, and area rain SPECs, and the results are presented in Table 28.

Table 28. The relationship of PROGSPEC and SYNSPEC combinations of surface, pre-wetness, and area rain SPECs with the 6-hour rainfall during June, July, and August 1965-1970.

	PROGSPEC				PROGSPEC-SYNSPEC Combination			
	Surface		Surface & pre-wetness		Surface & area rain		Surface, pre-wetness & area rain	
Month	No. of factors	R^2* (%)	No. of factors	R^2 (%)	No. of factors	R^2 (%)	No. of factors	R^2 (%)
June	52	47.0	54	50.3	53	51.6	55	53.8
July	42	31.6	45	39.0	43	40.8	46	42.2
August	52	41.5	55	64.5	54	45.0	57	65.6

* R^2 = Amount of rain variance explained by factors

For all combinations, the variance explained is smallest in July. Because of the more isolated nature of rain showers in July, this was to be expected. Although the inclusion of pre-wetness increased the amount of variance explained in all months, the increase is the greatest during August. Also, with the exception of August, the amount of variance explained for the PROGSPEC combination of surface (meteorological fields) and pre-wetness is similar to the PROGSPEC-SYNSPEC combination of surface fields and areal rain. The greater contribution of the pre-wetness during August appears to be related to the fact that, according to the diurnal studies, twice as many rains occur during 0900-1500 in August than during the same period in June and July. Also, less rain fell in the late afternoon in August than in June and July. Thus, a greater possibility of carry-over of morning precipitation into the afternoon exists in August than in June and July.

For the overall combination of PROGSPEC and SYNSPEC variables, 53.8% of the variance is explained in June, 42.2% in July, and 65.6% in August. Certainly, insofar as evaluation is concerned, the overall PROGSPEC-SYNSPEC combination should be used. However, the

results of Table 28 indicate that the PROGSPECs with pre-wetness included also explain a considerable amount of the variance.

An additional run that included the June RADU SPEC of percent of areal coverage was made. One factor representing this areal RADU SPEC from all surrounding areas was used as the independent variable. This factor was included in the SPEC equation along with the other 55 factors of the PROGSPEC-SYNSPEC combination of surface, pre-wetness, and area rain. The inclusion of this factor increased the variance explained to 58.2% from 53.8%. Therefore, it increased the variance explained a greater amount than did the pre-wetness variable. The factor by itself explains 19.1% of the rainfall variance.

To determine the usefulness of the SYNSPEC and PROGSPEC variables for the purpose of predicting rain and no-rain during the 6-hr period, the stepwise multiple discriminant analysis was performed on the rain and no-rain classes using the factors as the discriminants. The results for the PROGSPEC combination of surface and pre-wetness, and the PROGSPEC-SYNSPEC combination of surface fields, area rain, and pre-wetness are listed in Table 29.

The skill in determining that rain will fall during a particular 6-hr period from the PROGSPECs varies from 33.3% to 35.5% for prior probabilities based on sample size. Obviously, there is no skill in the rain prediction when the prior probability of size is used. However, if an equal probability is used for the prior probability, then the skill for rain prediction varies from 63.3% to 71.0%. The effect of using an equal probability is to decrease the skill in predicting the non-rain cases. This, occurs because the probability of rain is considerably less that the probability of non-rain during 6-hr periods in June, July, and August. (For example, during June, 18% of the 6-hr periods are rain periods, and 82% of the 6-hr periods are non-rain periods.)

Generally, the choice of the prior probability should be based on size. However, as indicated by the table, it is possible to improve the rain predictions at the expense of the non-rain predictions. Thus, if it is more important to predict rain than non-rain, one can "hedge" the outcome by using equal probabilities and predict rain with a degree of skill greater than chance.

(c) independent Data Test. To determine the adequacy of the SPEC equations, they should be tested on a period of record other than that on which the equations were determined. Thus, a set of principal components must be obtained for the independent period using the SPEC equations determined from the historical period 1965-1970. This is accomplished by using the X matrices involving surface fields and area rain variables for the period 1971-1973, and the factors from the A matrices involving surface fields and rain variables from the period 1965-1970. (Since the sounding variables contributed slightly to the areal SPEC equations, they were not used in the independent data test.)

Table 29. Results concerning the jackknifed classification of rain and non-rain during 6-hr periods using a stepwise discriminant analysis of the rain and non-rain cases.

	PROGSPEC Only				PROGSPEC-SYNSPEC Combination			
	Number of factors	Percent correct rain	Percent correct non-rain	Percent correct overall	Number of factors	Percent correct rain	Percent correct non-rain	Percent correct overall
				Prior prob (size)				
June	17	35.5	94.3	83.7	12	41.9	93.6	84.3
July	11	33.3	98.7	89.2	4	37.0	99.4	90.3
August	13	33.3	94.1	83.3	22	42.4	94.8	85.5
				Prior prob (equal)				
June	10	71.0	77.3	76.2	9	58.1	80.9	76.7
July	7	66.7	87.4	84.4	16	66.7	89.3	86.0
August	16	63.3	87.6	83.3	11	60.6	88.2	83.3

Each of the X matrices was standardized to form the Z matrices of standard variates. A new A' matrix was formed for each field and the set of area rain variables that contained only the factors with associated eigenvalues ≥1.0 and correlation coefficients ≥.10 during the historical period of 1965-1970. Each A' matrix was then transposed and used to compute the principal components for each of the fields and for the set of area rain variables through the use of Equation 21.

The principal components are then used as the independent variables in the SPEC equations determined from the historical period to estimate precipitation values for the test period. This procedure was used to estimate daily precipitation values for June 1971-1973 from the SPEC equation determined for June 1965-1970. (This SPEC equation had only 63 factors since the June sounding factors have been eliminated.) The variances of the actual values, the predicted values, and residuals between predicted and actual were determined for both the historical period of 1965-1970 and the test period of 1971-1973.

The fractional amount of variance explained was then determined by Equation 22.

$$\text{Variance explained} = 1.0 - \text{(variance of residuals/variance of actual values)} \quad (22)$$

The results are shown in Table 30.

Table 30. Independent data test for PROGSPEC-SYNSPEC relationship with June daily rain.

Correlation limit	Variance 1965-1970 actual	residual	explained (%)	1971-1973 actual	residual	explained (%)
≥.10	.06593	.04186	36.5	.03851	.04070	----
≥.15	.06593	.03512	47.0	.03851	.03081	20.0
≥.20	.06593	.03297	50.0	.03851	.02455	36.3

It was found that the use of all 63 factors in the SPEC equation produced a residual variance larger than the actual variance during the 1970-1973 test period. This indicated that the SPEC equations could not be used to reduce the explained variance. However, if only those factors with correlation coefficients ≥.15 and eigenvalues ≥1.0 were used in the SPEC equation, 20% of the variance during the independent data period could be explained. If only those factors with correlation coefficients ≥.20 were used, 36.3% of the variance could be explained. This compares to 50% of the variance explained for the historical period when a correlation limit of ≥.20 is used.

Since better results were obtained for the independent period when only those factors ≥.20 were being used in the SPEC equations, the SPEC equations were re-done for the PROGSPEC-SYNSPEC combinations involving the daily and 6-hr rainfall. Only those factors with correlation coefficients ≥.20 and eigenvalues ≥1.0 were used and the results for daily rainfall are shown in Table 31 along with the corresponding results for SPEC equations based on correlation coefficients ≥.10.

The number of factors retained varies from 7 to 26, while the amount of variance explained ranges from 44.9% to 57.8% during the three months. For a correlation limit of ≥.20, the number of factors retained varies from 63 to 85, while the amount of variance explained varies from 62.4% to 77.4%.

Table 31. Relationships of PROGSPECs and SYNSPECs with daily rain based on a correlation limit of ≥.10 as compared to a correlation limit of ≥.20.

Correlation limit	Number of factors	Amount of variance explained (%)	Total corr. (abs.)
		PROGSPEC-SYNSPEC Combination	
		June	
≥.10	63	62.4	.79
≥.20	7	50.4	.71
		July	
≥.10	72	68.9	.83
≥.20	15	44.9	.67
		August	
≥.10	85	77.4	.88
≥.20	26	57.8	.76

Therefore, the results indicate that less variance is explained when a correlation limit of ≥.20 is used than when a correlation limit of ≥.10 is used. However, it would appear that the results based on correlation coefficients ≥.20 are more comparable to results obtained from an independent data test.

The independent data test for June indicated that the variance explained in the independent period was about 27% less than the variance explained for historical SPEC equations with correlation limits ≥.20. Since a large amount of computer and analytical time was needed to test the July and August SPEC equations, the independent data test was performed only for the June daily rainfall. If one assumes that the 27% reduction is typical of the other months, then 32.8% of the variance in July and 44.5% of the variance in August will be explained with the independent data test.

The 6-hr results are shown in Table 32. For the correlation limit of ≥.20, 5-7 factors are retained and the amount of variance explained varies from 26.0% to 46.2%. For a correlation limit of ≥.10, 46-57 factors are retained and the amount of variance explained varies from 42.2% to 65.6%.

Table 32. Relationships of PROGSPECs with 6-hourly rain based on a correlation limit of £.10 as compared to a correlation limit of ≥.20.

PROGSPEC-SYNSPEC Combination			
Correlation limit	Number of factors	Amount of variance explained (%)	Total corr. (abs.)
		June	
≥.10	55	53.8	.73
≥.20	5	26.0	.51
		July	
≥.10	46	42.2	.65
≥.20	6	27.0	.52
		August	
≥.10	57	65.6	.81
≥.20	7	46.2	.68

Thus, as with the daily data, less variance is explained with the correlation limit ≥.20 than with the correlation limit ≥.10. It is also noted that the variance explained is somewhat less than that obtained for corresponding correlation limits with the daily rainfall. Since the independent data test was not performed for the 6-hr data, it is uncertain whether the variance explained with the correlation limit ≥.20 would be reduced further. However, it is believed that the results with the ≥.20 correlation limits are more representative of the independent period than those results with the £.10 correlation limit.

The overall results indicate that the amount of variance explained by the SPEC equation varies from 44.9% to 57.8% for daily data, and from 26.2% to 46.2% for precipitation during the period 1200-1800. The independent data test for the daily data in June indicated that the variance for the daily data might be as low as 32.8% to 44.5%. However, it is noted that the independent data test was based only on SPEC equations from the period 1965-1970. In an actual experiment, the equations could be updated each year with the inclusion of the previous year into the SPEC equation. (That is, 1965-1971 would be used to predict 1972, 1965-1972 would be used to predict 1973, and so on.)

Also, the non-seeded days from the experiment could be used to 1) adjust equations, if necessary, or 2) develop the SPEC equations without historical data. Thus, it is believed that the 44.9% to 57.8% values for daily data and the 26.2% to 46.2% for 6-hr precipitation are possible and that the 32.8% to 44.5% figures represent a lower limit to the amount of variance it is possible to explain. Although there was insufficient time on this project to perform independent data tests for the daily rain in July and August, and for the 6-hourly rain in June, July, and August, such tests would be desirable to firm up the percentage estimates shown above. Also, the development of SPEC equations for other areas on figure 4 would be desirable, particularly for the Goodland-Colby area.

Can the percentage estimates be improved? It is believed that some improvement in the variance explained might be obtained if a more dense network of precipitation gages was used. However, it is doubtful whether the variance explained can be increased by decreasing the area of rain measurement without increasing the density of the surface field observational network. If the density of the surface observational network were to be increased to allow for the decrease in rain measurement area, it would have to be increased sufficiently to allow for resolution of systems of the same scale as the rain measurement area. This assumes that the areal size of the spatial surface network remains sufficiently large so that transient systems moving into the area during the forecast period will not go undetected.

(18) Sample Size Requirements for the Areal Experiment. The determination of sample size requirements for the areal experiment should be done using data collected during the Single Cloud experiment. During the Single Cloud experiment, decisions will be made concerning the location and size of the areal experiment. However, in order to obtain some preliminary estimates of sample size required, the mean areal rainfall in the 29,300 km^2 area surrounding Dodge City (Fig. 4) was used.

Since the contemplated design for the Single Cloud experiment involves randomization between experimental units (either storms or days), the random-experimental design was chosen as a realistic design to obtain preliminary estimates of the sample size for the area experiment. This design involves the randomization of the experimental unit (usually days or some subset of day) over a single target area into seeded and non-seeded units. This design does not incorporate historical data, and the evaluation is based strictly on data collected during the experimental period.

The total number of units needed to obtain significance for a specified difference and level of precision is given by Schickedanz and Changnon (1970) as

$$N = [(\mu_\alpha + \mu_\beta)^2 \sigma^2]/[D^2 \pi(1 - \pi)] \quad (23)$$

where: μ_α = the normal deviate for α probability level

μ_β = the normal deviate for β probability level

D = the difference in means it is desired to detect

σ^2 = the variance of the non-seeded sample (assumed to be equal to the seeded variance)

π = the randomization factor (equal to 0.5 for a 50-50 randomization)

also, δ = the reduction of the non-transformed mean.

If the data are log-normally distributed, σ^2 is the log-transformed variance. If sample size requirements are desired for a reduction in the non-transformed mean, then D is equal to the logarithm of (1 - 6). In order to apply the equation, an estimate of a^2 must be obtained prior to experimentation and these estimates are obtained from the historical climatological data. The estimates from equation 23 then provide information on the expected duration level for a specific level of precision under the assumption that the future experiment will be performed in the same conditions as those reflected in the historical data. Thus, one limitation is that the weather conditions of the historical period will not necessarily be duplicated during the period of the experiment; hence, the required sample size will not be exactly as estimated. But, projection of past experience into the future is still the best estimate available. It is emphasized, however, that in the actual evaluation of the experiment, only data from the experimental period are used.

Predictor variables (covariates) can be included in the design to increase the sensitivity of the test. The number of units required for the random-experimental design can be obtained by multiplying equation 23 by $(1 - R^2)$

$$N = [(\mu_\alpha + \mu_\beta)^2 \sigma^2 (1 - R^2)]/[D^2 \pi(1 - \pi)] \quad (24)$$

where R is the multiple correlation between the rainfall and the predictor variables.

The above equations are for a log-normal test of the null hypothesis that seeding does not affect the conditional distribution of rain, given that rain occurs.

The log-normal distribution was fitted to the mean daily areal rainfall in the Dodge City area (non-zero values only) during the period 1949-1973. Separate parameter estimates were made for

June, July, August, and Summer rainfall. Under the assumption that seeding has a multiplicative effect on rainfall, estimated sampling requirements were obtained for a significance level of a = .05 and for power levels (percent chance of detection) of .5 and .7. The results for the log-normal test of hypothesis are listed in Table 33.

Table 33. Sampling requirements for the log-normal test of hypothesis (α = .05, 1-tail test).

Log-normal standard deviation	Power	Sample Size Required for Differences of: 10% Days	10% Years	20% Days	20% Years	40% Days	40% Years	60% Days	60% Years
				June					
1.433	.5	2448	49.8	669	13.6	197	4.0	101	2.1
	.7	4256	86.5	1163	23.6	342	7.0	175	3.6
				July					
1.351	.5	2174	44.2	595	12.1	175	3.6	90	1.8
	.7	3780	76.8	1033	21.0	304	6.2	156	3.2
				August					
1.390	.5	2303	46.8	630	12.8	185	3.8	95	1.9
	.7	4003	81.4	1094	22.2	322	6.5	165	3.4
				Summer					
1.393	.5	2314	47.0	633	12.9	186	3.8	96	2.0
2.169	.7	4024	81.8	1100	22.4	323	6.6	166	3.4

The number of days required to obtain significance is nearly the same for all months. Therefore, there is no need to estimate the parameters or sampling requirements individually for various months unless the seeding experiment is to be performed only during a one month period. Therefore, it is assumed that any month is typical of the summer conditions insofar as sampling requirements are concerned. Accordingly, in the conversion to years, the average number of rainfalls per summer (49.9) during the 1949-1973 period were used to convert the number of days to the number of years.

Inspection of the 40% increase values indicates that the number of years needed to obtain significance is nearly the same

regardless of the month from which the sampling requirements were derived. For a 50% chance of detection in the summer data, 3.8 years are required to detect a 40% increase and 2.0 years are required to detect a 60% increase. For a 70% chance of detection, a period of 6.5 years is required to detect a 40% increase and a period of 3.8 years is required to detect a 60% increase. If the experiment was conducted only during a one month period, it would take approximately 3 times as long to detect the same increases for the same probability of detection levels. Clearly, the detection times would be too long for a one month period, so the experiment must be conducted for the entire summer period.

Thus, there is a 50% chance of detecting a 40% increase within 5 years using the log-normal test. However, the test will not permit a detection of a 20% increase within a reasonable amount of time. For example, one has only a 50% chance to detect a 20% increase in the summer data in 12.9 years. In order to have a 70% chance of detection, 22.4 years are required.

In order to obtain the sample size requirements for the areal design when covariates are incorporated into the design, an estimate of σ^2 is needed for the log-normal model. The SPEC equations were derived for both rain and non-rain days whereas the log-normal model was derived for the rain only cases. Hence, to get an accurate estimate of the sample size required, the SPECs would be derived again for the rain only cases. Furthermore, the SPEC equations were derived for the period 1965-1970, whereas the distribution models were derived for the longer period 1949-1973.

Since much of the work has just recently been completed, there was not sufficient time to develop new SPEC equations for rain days only. Therefore, estimates of sample size were obtained by assuming that the amount of log-normal variance explained by the SPECs on rain days only would be comparable to the amount of non-transformed variance explained by SPECs on rain and non-rain days combined.

The numbers in Table 33 were multipled by $1-R^2$ for the appropriate month to obtain sample size requirements when SPECs are included in the design. Since the results using a correlation limit of $\geq .2$ were closer to those of the independent data test, the R^2 values corresponding to the correlation limit of $\geq .2$ from Table 31 were used. The results are listed in Table 34 (for the Summer case, the average R^2 for June, July, and August was used).

When one compares the Summer sample sizes to those of Table 34, it is clear that the sample sizes have been reduced approximately 50% by the inclusion of the SPECs. For a 50% chance to detect a 20% increase in the Summer data, 6.3 years are required; for a 40% increase, 1.9 years are required; for a 60% increase, <1 year is required. For a 70% chance to detect a 20% increase, 11.0 years are required; for a 40% increase, 3.2 years are required; and for

a 60% increase, 1.7 years are required. Thus, for a 20% increase, more than 5 years are still required. Again, if the experiment was conducted only during a one month period, it would take approximately 3 times as long to detect for the same probability of detection levels.

Table 34. Sampling requirements for the log-normal test (a = .05, one-tail test) when SPECs are included in the design.

	Sample size (years) required for differences of:			
Power	10%	20%	40%	60%
		June		
.5	24.7	6.7	2.0	1.0
.7	42.9	11.7	3.5	1.8
		July		
.5	24.3	6.7	2.0	<1
.7	42.3	11.6	3.4	1.8
		August		
.5	19.7	5.4	1.6	<1
.7	34.3	9.4	2.7	1.4
		Summer		
.5	23.0	6.3	1.9	<1
.7	40.1	11.0	3.2	1.7

Another estimate fo the sample size in June can be obtained by using the amount of variance explained from the independent data test of the SPEC equations. The amount of variance explained in the independent data test was 36.3%. Sample sizes for June in Table 34 would then be 36.3% less than those in Table 33. However, the estimate in the independent data period can probably be improved by updating the SPEC equation each year, or by using the non-seeded data during the seeded period. Therefore, the true estimate of sample size should be less than that indicated by the independent data test.

The overall sample sizes are reduced on the order of 36% to 50% by the inclusion of the SPECs into the design. However, the estimates of sample size are only approximate since the true amount of log variance on rain days was unknown. Thus, any future research on SPECs should include the development of SPEC equations for rain days only in addition to SPEC equations for rain and non-rain days combined.

Climatological Studies in Support of the Overall Design Effort. During the course of the covariate analysis, several climatological studies designed to provide background information useful in the physical interpretation of SPECs and for the experimental design were undertaken. The studies centered on diurnal rainfall distributions, cloud climatologies, seeding opportunities, and severe weather operations.

(1) The Diurnal Rainfall Variability for Kansas. Detailed diurnal rainfall frequencies for Kansas are necessary for determining the optimum time span for seeding opportunities, precipitation intensities for seeding opportunities, and for assessing the transferability of covariate analysis results from Dodge City to the Goodland-Colby site. The hour of maximum summertime thunderstorm frequency for the Plains has been given by Rasmusson (1971). Other summer thunderstorm frequencies have been presented by Wallace (1975).

In our studies into the rainfall climatology in the area of the proposed Kansas site, the hourly rainfall data have been grouped by 3 hr periods for each of the six sampling areas shown in figure 4. The data base was for the period 1965-1973 and included the summer months (June, July, and August). The total number of hourly rainfall stations for each sampling area was as follows: Area 1 (11), Area 2 (12), Area 3 (13), Area 4 (8), Area 5 (6), Area 6 (8). On the average, there were 63% more hourly rainfall observing sites over the northern half of the network than over the southern half. We found that the northern half of the network had 44% more days in which there was measurable areal-average rainfall. This increase was primarily in light amounts and was attributed to the greater station density there.

The rainfall amounts were stratified into three categories. These are 0.01-0.09, 0.10-0.24, and 0.24+ inches. The highest frequencies occurred in the light category; 67% in June, 78% in July, and 70% in August.

Figure 10 presents the diurnal distributions of 3-hr rainfall frequencies for June, July, and August. We have averaged the area frequencies by columns to eliminate the bias brought on by the spatial variation in station density. All three sets of curves show that the rainfall frequency minimizes near local noon. Precipitation frequency maximizes in the westernmost areas during the 18-21 LST

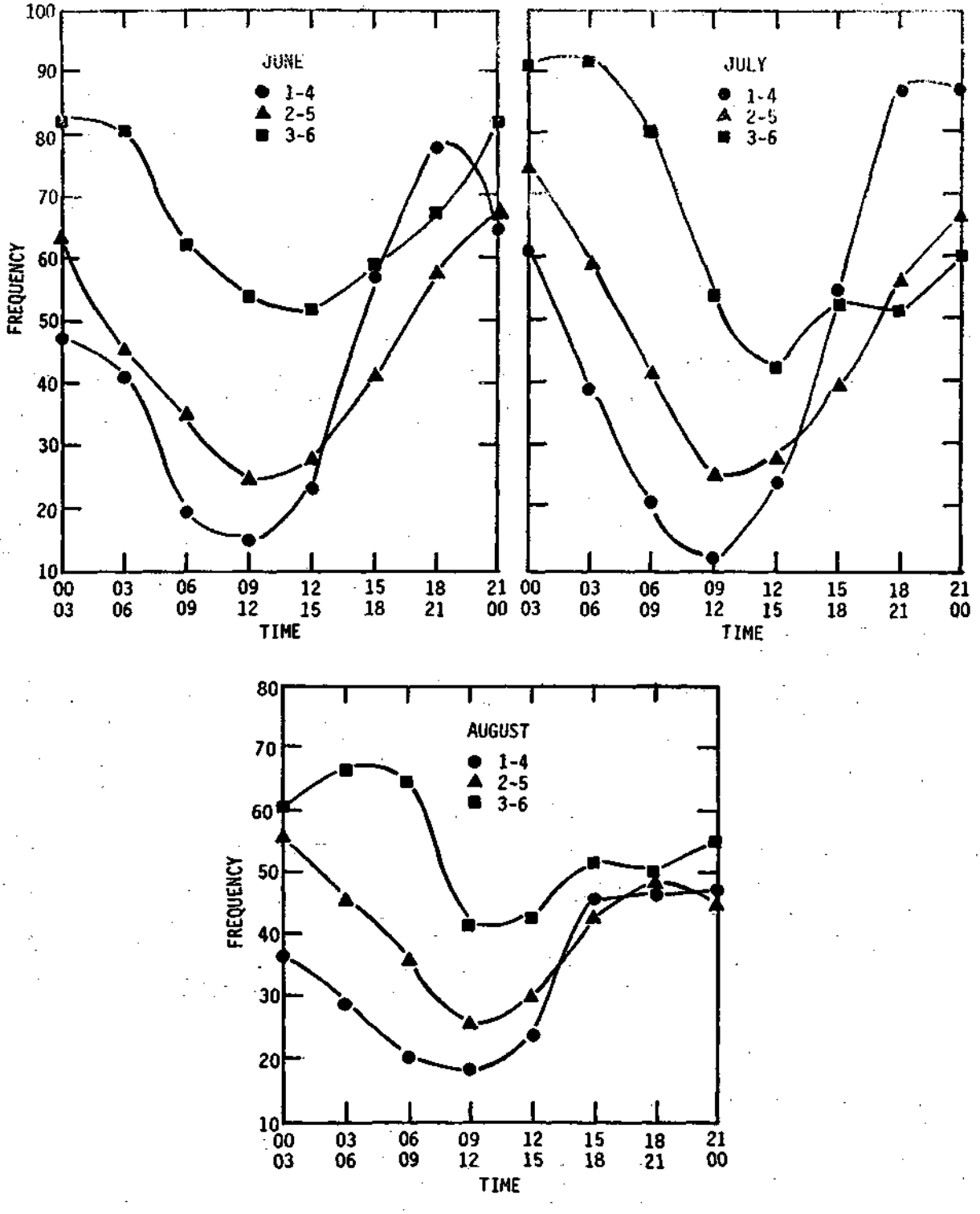

Figure 10. 1965-73 total two sampling area averaged diurnal rainfall frequency distribution for June, July, and August.

period. This maximum displaces eastward and reaches areas 3-6 at about 00-03 LST. These results are in accord with the frequencies presented by Rasmusson (1971). The trend is also seen in the July and August curves with the exception that the eastern area maxima shift toward the early morning (03-09 LST) . The nocturnal low level jet-related precipitation systems in the eastern areas may be more frequent in July and August or the summertime convective systems may drift eastward more slowly than they do in the late spring.

The maximum rainfall frequency in the Goodland-Colby area is from 1800-midnight LST. Single cloud seeding opportunities should exist before this period because there should be present towering cumulus clouds which will develop into showers that intensify and merge. After 21 LST, the precipitation frequencies generally decline. However, Bark (1975) notes that 35% of the echoes forming over western Kansas did so at night and that the percentage of treatable size clouds is the same in darkness and in daylight. Thus, a seeding experiment should be prepared to extend beyond 21 LST.

Figure 10 also shows that rainfall frequencies increase eastward. This was expected since the low level moisture is more abundant over the eastern areas. In all three months, the frequency maxima are greater for the eastern areas than for the central areas (Areas 2-5). This means that many precipitation systems form in the eastern area, particularly during the early morning hours.

Woodley et al. (1977) have shown that the inclusion of precipitation as a PROGSPEC (pre-wetness) may substantially increase the sensitivity of the statistical model. The following combinations of PROGSPECs and SYNSPECs were used to estimate the rainfall for the Dodge City area: 0600 CST surface PROGSPECs only, 0600 CST surface PROGSPECs + 0900-1200 CST 3-hourly rainfall (pre-wetness), 0600 CST surface PROGSPECs + 1200-1800 CST rainfall in surrounding areas (SYNSPECs), and 0600 CST surface PROGSPECs + pre-wetness PROGSPEC + SYNSPECs. The above combinations are listed under the respective categories A, B, C, D in Table 35.

Comparing B with A, pre-wetness increased the explained variance 3% in June, 7% in July, and 23% in August. The SYNSPECs increased the explained variance 4% in June, 9% in July, and 3% in August. The combination (D) explained the most rainfall variance.

The large August pre-wetness contribution to rainfall variance needs closer scrutiny. Figure 11 shows the rainfall frequency distributions for the Dodge City sampling area for the three summer months. The broad features of the curves are generally similar with minima around local noon and maxima around midnight.

We found that the amplitude of the August curve was much less than the amplitudes for the June and July curves. There were almost twice as many rains during the period 0900-1500 CST in August than

during the same period in June or July. The diurnal rainfall distribution for Dodge City area (Fig. 12) shows that more than twice as much rain fell during the late morning in August than in June or July. Note also that the late afternoon amplitudes of frequency and amount for August are less than those for June or July. Thus, there is more continuity between morning and afternoon precipitation in August than in June or July.

Table 35. Rainfall variance explained by the PROGSPEC-SYNSPEC combinations A, B, C, D, for the months of June, July, and August.

Month	A	B	C	D
June	47.0%	50.3	51.6	53.8
July	31.6	39.0	40.8	42.7
August	41.5	64.5	45.0	64.9

How representative is the Dodge City area of the Goodland experiments area? Figure 10 shows that, for the area 2-5, curves generally lie between the curves for the western and eastern areas. The western areas have the greatest temporal variation in rainfall frequency. Since pre-wetness was a much less powerful PROGSPEC in June or July than in August for area 5, we can expect that pre-wetness will be less powerful in western areas for all three months. Thus, our findings for pre-wetness for Dodge City must be viewed with caution if our results are to be transferred westward into the Goodland-Colby area.

Figure 13 presents the frequencies of rainfalls greater than 0.10 inches for the Dodge City area. Heavier rains are most frequent during the late afternoon and evening convective period and in June and August.

(2) Summary of Convective Rain Events for Five High Plains Stations. The objective of this study was to determine a climatology of rain events subject to conditions most favorable for precipitation management activities. These conditions fulfill the criteria that the rain event be convective (TRW, A, RW) and that cumulus (Cu) or cumulonimbus (Cb) be present one hour prior to the rain event. It does not include stratifications of Cu

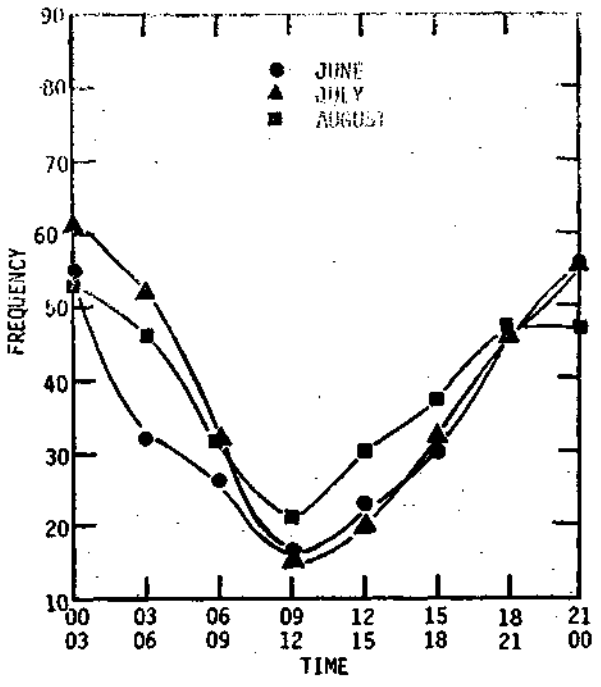

Figure 11. 1965-73 total diurnal rainfall frequencies for sampling area 5 - Dodge City.

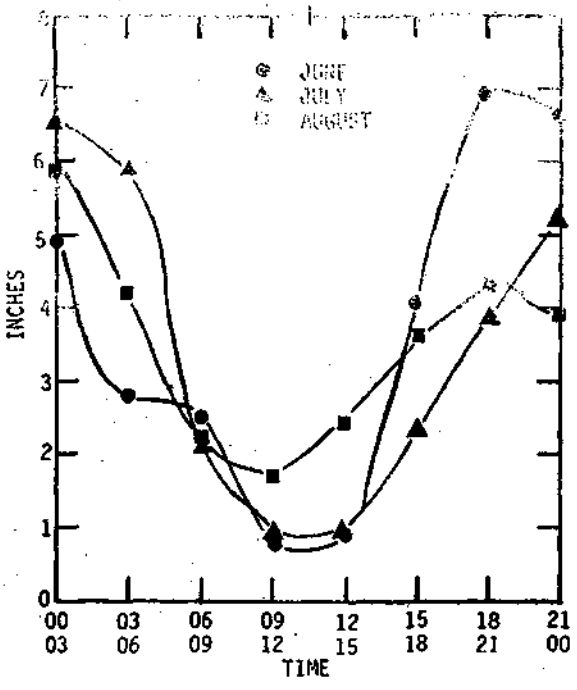

Figure 12. 1965-73 total rainfall diurnal distribution for sampling area 5 - Dodge City.

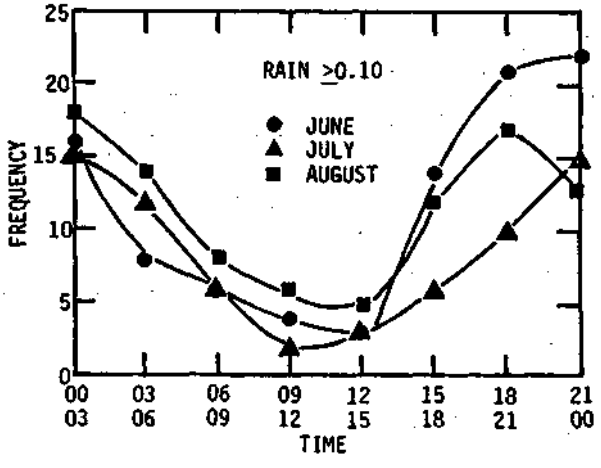

Figure 13. 1965-73 total diurnal rainfall frequencies R ≥ 0.10 in. for sampling area 5 - Dodge City.

or Cb in the presence of middle or higher clouds because these clouds often develop rapidly in association with precipitating convective clouds and the presence of these clouds one hour prior to the initiation of precipitation at a station does not preclude the possibility that these clouds were not present at an earlier time.

(a) The Data. Tables 01-05 of the Bureau of Reclamation Cloud Study prepared by the National Climatic Center presents frequencies of rain events and a multitude of stratifications therefrom. The rain event is defined by the consecutive hours of precipitation in the WABAN current weather records. The rain events are categorized as follows:

1. deep convective - thundershower (TRW) and/or hail shower (A),
2. moderately deep convective - rainshower (RW),
3. stratiform - general rain (R) and/or drizzle (L), and
4. stratiform with convective elements - general rain with thunder (TR).

The category of the weather event is determined by the current weather category at the FIRST hour of the rain event. To clarify these definitions, consider the following example of hourly rainfall and current weather data.

Hour	01	02	03	04	05	06	07	08	09	10	11	12	13	14	15	16	17	18	19	20	21
Rain		.01	.15	1.3	.06	.19		.07	.03		T			.03		.26	.01	.18	.02		
Cur Wea		R-	RW	TRW+	RW-			TRW-			RW-					RW+A		R			

Traces should be considered as precipitation. By our definition, the rain event is given by the consecutive hours of precipitation; there were 5 rain events when defined from the hourly precipitation records and 5 (not entirely coincidental) rain events based on the WABAN record. (If traces have not been considered as precipitation, then in the available tabulations there were 4 rain events shown for precipitation records and 5 from WABAN records.) The first rain event began before 02 and continued after 05 but ended before 06. The second rain event began before 08 and ended before 09. The third event was centered at 11 AM. The fourth event began and ended sometime between 13 and 14. The fifth rain event began before 16 and ended after 18, but there was obviously a break in the rain since no weather was reported at 1700. Since no current weather was reported at hour 17, the rain event (defined from the hourly precipitation) from hours 16-19 becomes two rain events when the rain event is defined by the weather category. But note that no

weather is reported on the WABAN at hour 14 though measurable precipitation fell during the previous hour. Thus, the total number of rain events are the same (for trace amounts considered rain). This may not always be the case, however. For instance, if the only precipitation had been between 1600 and 1900, there would have been 1 rain event based on precipitation records but 2 rain events if based on WABAN.

When the rain events are identified from the WABAN and stratified by weather category, there are 2 in the R class (R- at 02, R at 18), 2 in the TRW class (TRW- at 08, RW+A at 16), and 1 in the RW class (RW- at 11). There would be no contribution to the RW class from the RW+A at 16 since the classes are mutually exclusive and the TRW/A group takes precedent. Other current weather categories should not be included in either the rain event count or in the weather category stratifications.

The months are classified according to dry, moderate, or wet types as the preciptiation amounts fell into the respective thirds of the 30-year (1931-1960) cumulative precipitation frequency curves for each station. See Tables 36-41 for the year-month classifications. The rain events were further stratified according to whether cumulus (Cu)or cumulonimbus (Cb) were present one hour prior to the rain event. Other stratifications within these categories were made as follows:

1. Cu - all occurrences
2. Cu only
3. Cu with less that 4/10 middle cloud
4. Cu with less than 4/10 middle cloud and 4/10 high cloud.

These stratifications were repeated for Cb's.

The rain events are classed by month (April-September) and frequencies cumulated for a period of record of approximately 14 years. Breakdowns per station are as follows:

1. BIL 4/51 - 9/64
2. GGW 4/1/55 - 8/25/57 (00-23 LST); 8/26/57 - 5/5/59 (03-21 LST); 5/6/59 - 9/30/64 (04-23 LST)
3. GLD 6/51 - 9/64
4. ABI 6/51 - 9/64
5. MAF 6/51 - 9/64

A set of tables containing raw frequencies and percentages for all rain events for June, July, and August, is presented for each station. Frequencies are normalized to a 10 year base. These tables are identified by the station call letters. Then comparisons of convective period (11-22 LST), convective category (TRW, A, RW) - with Cu or Cb present one hour prior to rain events are shown in a second set of tables.

Table 36. Monthly precipitation April-September for 1951-64 stratified by light, moderate, heavy amounts as determined from 30 year (1931-60) cumulative precipitation curves for the Billings, Montana water plant.

	April		May		June		July		August		September	
	Year	Amount	Year	Amount	Year	Amount	Year	Amount	Year	Amount	Year	Amount
	0 - 0.60		0 - 1.35		0 - 2.00		0 - 0.55		0 - 0.65		0 - 0.75	
LIGHT	1952	0.52	1958	0.92	1951	1.94	1953	0.13	1954	0.54	1952	0.28
	1954	0.48	1959	1.21	1952	1.06	1954	0.11	1955	0.14	1954	0.59
	1962	0.04	1960	0.94	1954	1.76	1957	0.38	1958	0.28	1955	0.69
					1955	1.95	1959	0.30	1961	0.15	1957	0.73
					1956	0.73	1960	0.34	1963	0.10	1958	0.44
					1959	0.93	1964	0.02			1960	0.12
					1960	1.12					1964	0.06
					1961	0.32						
	0.61 - 1.45		1.36 - 2.60		2.01 - 3.10		0.56 - 1.10		0.66 - 1.25		0.76 - 1.50	
					1953	2.20	1951	0.68	1952	0.86	1951	1.20
MODERATE	1953	0.93	1953	1.92	1962	2.06	1952	1.03	1959	0.73	1953	1.12
	1956	1.14	1954	1.72	1963	2.73	1956	0.75			1956	0.76
	1958	1.19	1956	1.66			1961	0.84			1959	1.28
	1960	0.90	1961	1.63			1963	0.79			1962	1.03
			1963	2.29								
	>1.45		>2.60		>3.10		>1.10		>1.25		>1.50	
	1955	2.83	1952	3.73			1955	1.14	1951	1.99	1961	4.30
	1957	4.21	1955	4.15	1957	4.94	1958	2.34	1953	2.97	1963	1.87
HEAVY	1959	2.00	1957	4.24	1958	3.35	1962	1.56	1956	1.38		
	1961	2.08	1962	3.70	1964	5.54			1957	1.89		
	1963	2.36	1964	4.56					1960	1.26		
	1964	4.36							1962	1.29		
									1964	3.08		
Normal (30 Yr)		1.53		2.37		2.99		0.82		1.05		1.42

Table 37. Monthly precipitation April-September for 1951-64 stratified by light, moderate, heavy amounts as determined from 30 year (1931-60) cumulative precipitation curves for the Glasgow, Montana water plant.

	April		May		June		July		August		September	
	Year	Amount	Year	Amount	Year	Amount	Year	Amount	Year	Amount	Year	Amount
	0 - 0.45		0 - 1.05		0 - 2.10		0 - 0.71		0 - 0.65		0 - 0.40	
LIGHT	1956	0.07	1957	1.00	1955	0.69	1959	0.57	1955	0.09	1956	0.10
	1959	0.42	1958	0.03	1956	1.68	1960	0.55	1958	0.52	1958	0.31
	1962	0.21	1961	1.04	1958	2.06			1959	0.59	1960	0.04
	1964	0.41			1960	1.61			1961	0.38	1963	0.32
					1961	1.17						
	0.46 - 1.19		1.06 - 1.59		2.11 - 3.29		0.72 - 1.59		0.66 - 1.55		0.41 - 0.94	
MODERATE	1958	0.58	1959	1.18	1957	2.86	1957	0.98	1960	0.95	1955	0.42
	1960	0.72	1960	1.43	1959	2.79	1958	1.15	1964	0.85	1957	0.51
	1961	0.55	1963	1.13	1964	2.78	1964	1.20			1962	0.48
											1964	0.52
	>1.19		>1.59		>3.29		>1.59		>1.55		>0.94	
HEAVY	1955	2.62	1955	3.11	1962	4.43	1955	2.60	1956	2.03	1959	1.26
	1957	1.33	1956	2.29	1963	5.36	1956	1.62	1957	2.01	1961	2.04
	1963	1.22	1962	2.50			1961	1.66	1962	1.87		
			1964	2.52			1962	5.17	1963	3.30		
							1963	1.65				
Normal (30 Yr)		1.01		1.49		2.98		1.33		1.49		0.96

Table 38. Monthly precipitation April-September for 1951-64 stratified by light, monderate, heavy amounts as determined from 30 year (1931-60) cumulative precipitation curves for the Goodland, Kansas water plant.

	April		May		June		July		August		September	
	Year	Amount	Year	Amount	Year	Amount	Year	Amount	Year	Amount	Year	Amount
	0 - 0.85		0 - 1.65		0 - 1.64		0 - 1.75		0 - 1.59		0 - 0.50	
LIGHT	1954	0.36	1955	1.22	1952	0.67	1953	1.41	1955	0.54	1952	0.31
	1956	0.67	1956	0.98	1956	0.59	1954	1.00	1956	1.35	1953	0.03
	1959	0.62	1959	1.36	1958	1.64	1955	1.03	1960	1.29	1956	0.05
	1960	0.83			1959	1.14	1957	1.69	1962	1.46	1957	0.31
	1962	0.33			1963	1.36	1960	1.21	1964	0.13		
	1963	T			1964	1.50						
	0.86 - 1.74		1.66 - 2.64		1.65 - 3.00		1.76 - 2.74		1.60 - 2.54		0.51 - 1.29	
MODERATE	1955	1.01	1952	2.56	1953	1.82	1952	2.48	1951	1.81	1954	0.79
	1958	1.73	1953	2.39	1954	1.78	1956	1.93	1952	2.25	1960	0.65
	1961	1.26	1954	2.53	1955	2.59	1959	2.54	1954	1.77	1962	0.79
	1964	1.36	1958	1.91	1957	2.99	1962	2.29	1957	1.81		
			1960	1.72	1960	2.78	1964	1.97	1958	2.01		
			1963	1.72	1961	2.88			1959	2.45		
									1961	2.33		
									1963	1.76		
	>1.74		>2.64		>3.00		>2.74		>2.54		>1.29	
HEAVY	1952	1.98	1957	6.00	1951	7.14	1951	4.58	1953	4.48	1951	1.46
	1953	1.83	1961	3.69	1962	7.62	1958	3.62			1955	1.69
	1957	2.15	1962	4.25			1961	3.91			1958	1.39
			1964	2.68			1963	3.22			1959	2.97
											1961	1.64
											1963	4.84
											1964	1.56
Normal (30 Yr)		1.59		2.41		2.66		2.67		2.28		1.24

Table 39. Monthly precipitation April-September for 1951-64 stratified by light, moderate, heavy amounts as determined from 30 year (1931-60) cumulative precipitation curves for the Abilene, Texas water plant.

	April		May		June		July		August		September	
	Year	Amount	Year	Amount	Year	Amount	Year	Amount	Year	Amount	Year	Amount
	0 - 1.55		0 - 3.00		0 - 1.64		0 - 0.87		0 - 0.45		0 - 0.85	
LIGHT	1961	T	1952	2.43	1952	0.04	1952	0.70	1951	0.22	1951	0.83
	1962	1.37	1956	0.15	1954	0.03	1954	0.08	1952	0.02	1954	0.77
	1963	1.53	1959	2.34	1956	0.12	1956	0.87			1956	T
			1960	1.93	1963	1.63	1957	0.62			1959	0.77
			1961	1.29	1964	1.55	1963	0.28			1963	0.67
			1962	1.55								
			1964	1.53								
	1.56 - 2.49		3.01 - 5.24		1.65 - 3.44		0.88 - 3.05		0.46 - 1.80		0.86 - 1.95	
MODERATE	1952	2.04	1953	3.70	1951	3.03	1951	1.47	1953	0.76	1953	1.24
	1953	1.89	1954	4.61	1953	2.41	1955	1.36	1954	0.85	1960	1.43
	1955	1.82	1958	3.45	1957	2.30	1964	2.58	1955	1.56		
	1956	2.32			1958	2.08			1956	0.55		
	1959	1.88			1960	1.95			1957	0.47		
	1960	2.42							1959	0.72		
									1961	1.41		
									1962	1.48		
	>2.49		>5.24		>3.44		>3.05		>1.80		>1.95	
HEAVY	1954	4.28	1955	5.94	1955	4.71	1953	3.98	1958	2.06	1952	2.34
	1957	6.52	1957	13.19	1959	7.22	1958	3.12	1960	2.68	1955	3.85
	1958	3.50	1963	6.21	1961	9.60	1959	4.93	1963	3.56	1957	2.92
	1964	2.76			1962	7.65	1960	4.51	1964	5.87	1958	4.23
							1961	4.35			1961	7.86
							1962	4.52			1962	5.12
											1964	2.07
Normal (30 Yr)		2.27		4.33		2.67		2.28		1.47		2.07

Table 40. Monthly precipitation April-September for 1951-64 stratified by light, moderate, heavy amounts as determined from 30 year (1931-60) cumulative precipitation curves for the Midland, Texas water plant

	April		May		June		July		August		September	
	Year	Amount	Year	Amount	Year	Amount	Year	Amount	Year	Amount	Year	Amount
	0 - 0.30		0 - 1.00		0 - 1.00		0 - 0.43		0 - 0.85		0 - 0.85	
LIGHT	1955	T	1953	0.08	1951	0.05	1951	0.05	1953	0.18	1951	0.34
	1960	0.28	1962	T	1952	0.37	1953	0.09	1955	0.46	1953	0.68
	1961	0.02			1953	0.06	1954	T	1961	0.21	1954	0.15
	1964	T			1958	0.50	1957	0.40	1964	0.58	1955	0.35
					1960	0.42	1964	0.24			1956	0.17
					1964	0.40					1960	0.14
											1963	0.39
	0.31 - 0.94		1.01 - 2.69		1.01 - 1.99		0.44 - 2.12		0.86 - 2.00		0.86 - 2.00	
MODERATE	1953	0.87	1952	1.15	1954	1.97	1956	1.71	1951	1.26	1957	1.56
	1957	0.44	1955	2.06	1955	1.88	1958	0.89	1952	1.07		
	1958	0.78	1956	1.41	1956	1.40	1962	2.12	1954	1.26		
	1959	0.39	1960	1.55	1959	1.89	1963	1.17	1956	1.73		
	1962	0.79	1961	2.63	1962	1.83			1957	1.19		
			1963	2.62					1959	0.90		
			1964	2.14					1963	1.24		
	>0.94		>2.69		>1.99		>2.12		>2.00		>2.00	
HEAVY	1952	0.95	1954	4.11	1957	2.55	1952	2.34	1958	3.84	1952	2.34
	1954	1.39	1957	4.30	1961	2.96	1955	2.95	1960	2.59	1958	3.42
	1956	1.15	1958	3.24	1963	2.61	1959	4.46	1962	2.66	1959	2.48
	1963	0.95	1959	4.99			1960	3.33			1961	3.12
							1961	6.73			1962	4.06
											1964	2.19
Normal (30 Yr)		0.83		2.08		1.63		1.88		1.48		1.79

(b) Rain Event Summaries for Each Site. Billings is representative of meteorological conditions of the local mountainous areas of south central Montana. The orographic contribution to convective cloud development particularly to the west of Billings is expected to exceed that for the other stations presented in this study.

The rain events for Billings for the June period are summarized in Tables 41-43. Table 41 shows that 236 rain events occurred and that only 22 were not included within a convective category. Rain and drizzle events were found mainly during the early morning hours while thundershowers showed a pronounced afternoon maximum. Rain showers, reported throughout the day, maximized during the afternoon.

The rain events for each two-hour category expressed as a percentage of the total number of rain events is shown in Table 42. About 91% of all rain events were convective and about 75% of these were showers. Additional stratifications were made according to the cloud type reported one hour prior to the rain event (Table 43). Rain events which are preceded by cumulus or cumulonimbus clouds constitute approximately one half (56%) of the total number of rain events and these occurred mostly during the convective period (11-22 LST). One explanation for the low percentages for the dark hours rests with the difficulty of observing cloud types at night. However, low percentages are found in the daylight hours (7-8 LST). These rain events may have been remnants of system type rains that occurred during the night.

The number of rain events at Billings for the July period (Table 44) was 139 which were proportioned between the weather types in a way similar to the June rain events. Thundershowers occurred almost exclusively during the convective period. Showers were spread throughout the day and accounted for 73% of the total rain events (Table 45). About 95% of the total rain events fell into the convective category (Table 46) and Cu or Cb were reported one hour prior to 66% of these (63% of the total).

The August summary Table 47-49 is similar to the July summary. There were 151 rain events and 94% of these were in the convective category. Showers occurred throughout the day and both showers and thundershowers maximized during the afternoon. Sixty-two percent of the rain events were in the convective category with Cu or Cb reported one hour earlier.

The Glasgow site is typical of the northern plains of Montana. The ten year normalized frequencies (Table 50) show 198 June rain events of which 161 are classified as convective. Rain events for both showers and thundershowers maximize during the afternoon. There were 36 stratified rain or drizzle events distributed fairly uniformly throughout the day. These rain events were probably associated with stable synoptic weather systems. Table 52 gives

the bi-hourly weather type breakdowns expressed as percentages of the total. The convective category accounted for 81% of the rain events and 56% of the total were showers. When the rain events where Cu or Cb were not reported one hour prior to the event were dropped from the sample, less than one half (49%) of the rain events remained and these were scattered throughout the day with a moderate peak during the afternoon hours.

In July (Tables 53-55), 138 of 147 rain events were classified as convective. These events could occur at almost any time during the day with a greater chance of these being showers during the morning and late evening and thundershowers during the afternoon. Only 68% of the rain events could be confirmed as having convective clouds present one hour prior to the event.

The August rain event frequencies (Tables 56-58) show a moderate maximum for showers in the early morning and a maximum for thundershowers in the late evening. The relative minimum from 23-04 should be discounted because the record was not continuous for these hours. It would appear that the summer season rain events at Glasgow shift from an afternoon convective regime in June to a nocturnal regime in August. Layer clouds such as altocumulus or stratocumulus are likely to obscure convective clouds in the nocturnal regime. The number of rain events with Cu or Cb reported (Table 58) decreased to only 47% of the total.

The Goodland site is typical of the high plains of western Kansas. The terrain is characterized by a flat relief with a gradual (2 m/km) incline towards the west. The June rain event frequencies (Tables 59-61) show that thundershowers outnumber showers and account for 89 of the 214 rain events. Thundershowers show a pronounced maximum centered in the late afternoon (17-18 LST). Showers occur throughout the day and show a moderate maximum within the convective period. Rain and drizzle events are numerous at Goodland (26% of total) and can occur anytime during the day. These stratiform events minimize during the convective period. Only 74% of the total number of rain events at Goodland were classified as convective. Sixty-three percent of these (47% of total) were accompanied by convective clouds reported one hour prior to the event.

The rain event frequencies for July and August almost mirror the June tables (see Tables 62-67). The non-convective rain and drizzle account for just over 20% of the total events. Of the remaining convective events, 56% and 52%, respectively, fall into the Cu or Cb classification. Showers are scattered fairly uniformly throughout the day and thundershowers maximize late in the afternoon (about 17-18 LST).

Tables 68-70 show there were 112 rain events for Abilene, Texas, for June. Of these, 18, or 16% of the total, were classified as stratiform. Showers maximized in the early morning and late

evening hours and thundershowers tended to occur primarily during the convective period. Those rain events that were within the convective category and with Cu or Cb reported one hour prior accounted for 53% of the total. Showers outnumbered thundershowers 46% to 38%.

The frequencies for July (Tables 71-73) show that both showers and thundershowers tend to occur throughout the day. There were only 86 rain events and 11% of these were classified as stratiform. Fifty-five percent of the total satisfied both convective criteria in Table 75b. Maxima in shower occurrence occurred at 07-08 and 15-16 LST.

In August (Tables 74-76), there were only 72 reported rain events. Thundershowers were concentrated mainly during the convective period and showers were scattered throughout the day. Sixty percent of the rain events satisfied both convective criteria.

Twenty-five percent of the 87 rain events for June at Midland, Texas, (Tables 77-79) were classified as stratiform. The remaining 75% of the total was almost equally divided between showers and thundershowers. Thundershowers occurred late in the convective period and into the nighttime hours. Showers were most predominant during the day time. Fifty-three percent of the rain events satisfied both convective criteria.

The number of rain events increased to 107 for July and 91 of these were classified as convective (Tables 80-82). These were divided equally between showers and thundershowers. Thundershowers tended to maximize during the convective period and showers tended to occur throughout the day with no apparent preferred occurrence time. Fifty-six percent of the rain events satisfied both convective criteria.

In August, the number of rain events decreased to 80 (Tables 83-85). Both the showers and thundershowers maximized during the convective period. There were more showers than thundershowers (38 vs. 28) during August and this may indicate suppression of deep convection by stable airmasses aloft as reported by investigators in the Big Springs area. Sixty percent of the rain events were convective with Cu or Cb reported one hour prior to the event.

(c) Rain Event Comparisons Between Sites. The convective period between 11-22 LST includes the period of greatest cumuliform cloud response to local heating and is considered the prime time for operational weather modification activities. The convective category rain events for the convective period at the five sites are compared in Table 86. Aside from the high number at Billings in June and the low number at Glasgow in August, there was found virtually no difference in the number of convective rain events for the first three stations. Abilene and Midland group together and have approximately one half of the convective rain events of the sites to the north.

Table 87 give the total number of convective category rain events with Cu or Cb reported one hour prior to the rain event for the convective period. When compared with Table 86, it is evident that the additional convective constraint has decreased the number of rain events by about 50% or greater. Billings, with 269 total convective rain events, is followed by Goodland with 240. Midland, with 114 rain events, has 12 more rain events than Abilene, which is located further east within a more moist climate. The data provide no obvious explanation for the small number of rain events (34) at Glasgow in August. The 10 year Glasgow record is evenly stratified between light and heavy precipitation years (4) for August (Table 37). Two years fall into the moderate precipitation category.

The convective category rain events that satisfy the convective cloud criteria were further stratified into the convective type; shower or thundershower. Tables 88 and 89 present these stratifications. The number of total summer shower events decreases southward. Billings and Glasgow reported 171 and 88 showers, respectively. This was followed by Goodland with 87 showers and by the Texas stations with about 45 showers. Table 89 shows that Goodland was the leader in thundershowers with 153. The two Montana stations followed with just over 100 thundershowers and then came the Texas sites with 58 and 69 thundershowers at Abilene and Midland, respectively.

The ratios of thundershowers to showers presented in Table 90 reveals some of the differing meteorological characteristics of the five sites. Billings is within a shower dominated regime. Some possible explanations for this are: 1) Billings is within a developmental area and clouds do not have time to develop fully into thundershowers before they drift eastward over the plains; 2) the mountains to the west are such formidable triggers that clouds develop and shade the land surfaces long before the time of maximum daytime heating. Thus, low level instability necessary for deep convection is not realized; and 3) The tropospheric stratification is such to prevent deep convection.

Goodland is within a thundershower dominated regime. There are twice as many thundershowers as showers in June. Some possible explanations for this are 1) mature thunderstorms that develop in eastern Colorado drift through the Goodland area late in the convective period, and 2) the tropospheric stratification is such that once convective clouds develop, they deepen rapidly reaching heights near or above the tropopause within a short period of time. This latter explanation finds support in reports of a tendency for "all or nothing" cumulus cloud development given by the Goodland forecasters.

Table 90 shows a transition from a thundershower to a shower dominated regime at Midland. This finding is in accordance with observations that the subtropical high aloft tends to suppress deep convection in the late summer (Girdzus, 1976) . Note that Abilene

Table 41. Two hourly rain event frequencies by weather type as reported on the WABAN 10 forms.

JUNE BILLINGS

	Hour											
	1-2	3-4	5-6	7-8	9-10	11-12	13-14	15-16	17-18	19-20	21-22	23-00	Total
TRW, A	1	0	0	0	2	5	15	12	7	4	4	2	52
RW	7	12	13	12	10	10	18	23	15	18	12	12	162
R, L	2	3	4	4	1	1	0	1	1	1	1	3	22
TR	0	0	0	0	0	0	0	0	0	0	0	0	0
Total	10	15	17	16	13	16	33	36	23	23	17	17	236

Table 42. Rain events for each two hour category by weather type expressed as percent of total. June, Billings

	Hour											
	1-2	3-4	5-6	7-8	9-10	11-12	13-14	15-16	17-18	19-20	21-22	23-00	Total
TRW, A	10	0	0	0	15	31	45	33	30	17	24	12	22
RW	70	80	76	75	77	63	55	64	65	78	71	71	69
R, L	20	20	24	25	8	6	0	3	5	5	5	17	9
TR	0	0	0	0	0	0	0	0	0	0	0	0	0

Table 43. a) all convective category (TRW, A, RW) and b) convective category with Cu, Cb reported 1 hour prior to rain event, expressed as percent of total rain events. June, Billings

	Hour											
	1-2	3-4	5-6	7-8	9-10	11-12	13-14	15-16	17-18	19-20	21-22	23-00	Total
a	80	80	76	75	92	94	100	97	95	95	95	83	91
b	10	7	12	6	38	63	82	94	74	83	71	24	56

Table 44. Two hourly rain event frequencies by weather type as reported on the WABAN 10 forms.

JULY BILLINGS

	Hour											
	1-2	3-4	5-6	7-8	9-10	11-12	13-14	15-16	17-18	19-20	21-22	23-00	Total
TRW, A	0	1	0	0	0	2	7	7	6	3	4	1	31
RW	7	4	7	4	4	10	11	16	13	11	9	6	102
R, L	1	0	0	1	0	2	1	0	0	0	1	0	6
TR	0	0	0	0	0	0	0	0	0	0	0	0	0
Total	8	5	7	5	4	14	19	23	19	14	14	7	139

Table 45. Rain events for each two hour category by weather type expressed as percent of total. July, Billings

	Hour											
	1-2	3-4	5-6	7-8	9-10	11-12	13-14	15-16	17-18	19-20	21-22	23-00	Total
TRW, A	0	20	0	0	0	14	37	30	32	21	29	14	22
RW	88	80	100	80	100	72	58	70	68	79	64	86	73
R, L	12	0	0	20	0	14	5	0	0	0	7	0	4
TR	0	0	0	0	0	0	0	0	0	0	0	0	0

Table 46. a) all convective category (TRW, A, RW) and b) convective category with Cu, Cb reported 1 hour prior to rain event, expressed as percent of total rain events. July, Billings

	Hour											
	1-2	3-4	5-6	7-8	9-10	11-12	13-14	15-16	17-18	19-20	21-22	23-00	Total
a	88	100	100	80	100	85	95	100	100	100	93	100	95
b	0	0	14	40	25	50	68	96	95	71	79	43	63

Table 47. Two hourly rain event frequencies by weather type as reported on the WABAN 10 forms.

AUGUST BILLINGS

	Hour											
	1-2	3-4	5-6	7-8	9-10	11-12	13-14	15-16	17-18	19-20	21-22	23-00	Total
TRW, A	1	1	2	1	1	3	9	11	6	6	2	1	44
RW	6	5	8	5	5	6	16	12	11	9	8	7	98
R, L	1	1	1	1	0	1	1	0	0	1	1	1	9
TR	0	0	0	0	0	0	0	0	0	0	0	0	0
Total	8	7	11	7	6	10	26	23	17	16	11	9	151

Table 48. Rain events for each two hour category by weather type expressed as percent of total. August, Billings

	Hour											
	1-2	3-4	5-6	7-8	9-10	11-12	13-14	15-16	17-18	19-20	21-22	23-00	Total
TRW, A	13	14	18	14	17	30	35	48	35	38	18	11	29
RW	74	72	73	72	83	60	61	52	65	56	73	78	65
R, L	13	14	9	14	0	10	4	0	0	6	9	11	6
TR	0	0	0	0	0	0	0	0	0	0	0	0	0

Table 49. a) all convective category (TRW, A, RW) and b) convective category with Cu, Cb reported 1 hour prior to rain event, expressed as percent of total rain events. August, Billings

	Hour											
	1-2	3-4	5-6	7-8	9-10	11-12	13-14	15-16	17-18	19-20	21-22	23-00	Total
a	88	85	91	85	100	90	97	100	100	94	91	89	94
b	25	29	27	29	50	50	81	83	88	81	55	22	62

Table 50. Two hourly rain event frequencies by weather type as reported on the WABAN 10 forms.

JUNE GLASGOW

	Hour											
	1-2	3-4	5-6	7-8	9-10	11-12	13-14	15-16	17-18	19-20	21-22	23-00	Total
TRW, A	0	3	1	3	0	2	5	8	10	8	6	3	49
RW	2	8	7	7	7	11	14	16	15	10	8	7	112
R, L	2	2	5	5	2	2	1	4	2	5	5	1	36
TR	1	0	0	0	0	0	0	0	0	0	0	0	1
Total	5	13	13	15	9	15	20	28	27	23	19	11	198

Table 51. Rain events for each two hour category by weather type expressed as percent of total. June, Glasgow

	Hour											
	1-2	3-4	5-6	7-8	9-10	11-12	13-14	15-16	17-18	19-20	21-22	23-00	Total
TRW, A	0	23	8	20	0	13	25	29	37	35	32	27	25
RW	40	62	54	47	78	74	70	57	56	43	42	64	56
R, L	40	15	38	33	22	13	5	14	7	22	26	9	18
TR	20	0	0	0	0	0	0	0	0	0	0	0	1

Table 52. a) all convective category (TRW, A, RW) and b) convective category with Cu, Cb reported 1 hour prior to rain event, expressed as percent of total rain events. June, Glasgow

	Hour											
	1-2	3-4	5-6	7-8	9-10	11-12	13-14	15-16	17-18	19-20	21-22	23-00	Total
a	40	85	62	67	78	87	95	86	93	78	74	91	81
b	40	31	15	20	22	60	60	54	78	61	47	36	49

Table 53. Two hourly rain event frequencies by weather type as reported on the WABAN 10 forms.

JULY GLASGOW

	Hour											
	1-2	3-4	5-6	7-8	9-10	11-12	13-14	15-16	17-18	19-20	21-22	23-00	Total
TRW, A	2	1	1	2	1	4	2	11	13	8	10	2	57
RW	2	8	9	8	8	6	8	6	2	7	13	4	81
R, L	0	2	1	4	1	0	0	1	0	0	0	0	9
TR	0	0	0	0	0	0	0	0	0	0	0	0	0
Total	4	11	11	14	10	10	10	18	15	15	23	6	147

Table 54. Rain events for each two hour category by weather type expressed as percent of total. July, Glasgow

	Hour											
	1-2	3-4	5-6	7-8	9-10	11-12	13-14	15-16	17-18	19-20	21-22	23-00	Total
TRW, A	50	9	9	14	10	40	20	61	87	53	43	33	39
RW	50	73	82	57	80	60	80	33	13	47	57	67	55
R, L	0	18	9	29	10	0	0	6	0	0	0	0	6
TR	0	0	0	0	0	0	0	0	0	0	0	0	0

Table 55. a) all convective category (TRW, A, RW) and b) convective category with Cu, Cb reported 1 hour prior to rain event, expressed as percent of total rain events. July, Glasgow

	Hour											
	1-2	3-4	5-6	7-8	9-10	11-12	13-14	15-16	17-18	19-20	21-22	23-00	Total
a	100	82	91	81	90	100	100	94	100	100	100	100	94
b	25	64	55	29	20	80	90	78	93	93	78	50	68

Table 56. Two hourly rain event frequencies by weather type as reported on the WABAN 10 forms.

AUGUST GLASGOW

	Hour											
	1-2	3-4	5-6	7-8	9-10	11-12	13-14	15-16	17-18	19-20	21-22	23-00	Total
TRW, A	2	2	2	0	1	0	1	1	2	9	7	5	32
RW	2	6	7	12	3	5	6	5	7	5	8	3	69
R, L	0	1	4	3	4	2	2	0	0	1	1	2	20
TR	0	0	0	0	0	0	0	0	0	0	0	0	0
Total	4	9	13	15	8	7	9	6	9	15	16	10	121

Table 57. Rain events for each two hour category by weather type expressed as percent of total. August, Glasgow

	Hour											
	1-2	3-4	5-6	7-8	9-10	11-12	13-14	15-16	17-18	19-20	21-22	23-00	Total
TRW, A	50	22	15	0	13	0	11	17	22	60	44	50	26
RW	50	67	54	80	37	71	67	83	78	33	50	30	57
R, L	0	11	31	20	50	29	22	0	0	7	6	20	17
TR	0	0	0	0	0	0	0	0	0	0	0	0	0

Table 58. a) all convective category (TRW, A, RW) and b) convective category with Cu, Cb reported 1 hour prior to rain event, expressed as percent of total rain events. August, Glasgow

	Hour											
	1-2	3-4	5-6	7-8	9-10	11-12	13-14	15-16	17-18	19-20	21-22	23-00	Total
a	100	89	69	80	50	71	78	100	100	93	94	80	83
b	25	33	31	40	13	14	44	100	55	67	50	80	47

Table 59. Two hourly rain event frequencies by weather type as reported on the WARAN 10 forms.

JUNE GOODLAND

	Hour											
	1-2	3-4	5-6	7-8	9-10	11-12	13-14	15-16	17-18	19-20	21-22	23-00	Total
TRW, A	2	3	1	2	2	4	4	13	20	18	11	9	89
RW	4	5	3	4	2	4	8	9	8	11	7	4	69
R, L	8	4	6	6	3	3	3	1	2	6	4	9	55
TR	0	0	0	0	0	0	0	0	0	0	1	0	1
Total	14	12	10	12	7	11	15	23	30	35	23	22	214

Table 60. Rain events for each two hour category by weather type expressed as percent of total. June, Goodland

	Hour											
	1-2	3-4	5-6	7-8	9-10	11-12	13-14	15-16	17-18	19-20	21-22	23-00	Total
TRW, A	14	25	10	17	29	36	27	57	67	51	48	41	42
RW	29	42	30	33	29	36	53	39	27	31	30	18	32
R, L	57	33	60	50	43	27	20	4	7	17	17	41	26
TR	0	0	0	0	0	0	0	0	0	0	4	0	0

Table 61. a) all convective category (TRW, A, RW) and b) convective category with Cu, Cb reported 1 hour prior to rain event, expressed as percent of total rain events. June, Goodland

	Hour											
	1-2	3-4	5-6	7-8	9-10	11-12	13-14	15-16	17-18	19-20	21-22	23-00	Total
a	43	67	40	50	58	72	80	96	94	82	78	59	74
b	21	25	10	8	29	55	60	74	73	60	39	32	47

Table 62. Two hourly rain event frequencies by weather type as reported on the WABAN 10 forms.

JULY GOODLAND

	Hour											
	1-2	3-4	5-6	7-8	9-10	11-12	13-14	15-16	17-18	19-20	21-22	23-00	Total
TRW, A	4	2	0	1	1	2	8	12	16	7	9	8	70
RW	2	2	6	3	2	9	9	5	7	9	8	9	65
R, L	7	6	8	3	0	2	1	1	0	3	1	4	36
TR	0	1	0	0	0	0	0	0	0	0	0	0	1
Total	13	11	14	7	3	7	18	18	23	19	18	21	172

Table 63. Rain events for each two hour category by weather type expressed as percent of total. July, Gbodland

	Hour											
	1-2	3-4	5-6	7-8	9-10	11-12	13-14	15-16	17-18	19-20	21-22	23-00	Total
TRW, A	31	18	0	14	33	29	44	67	70	37	50	38	41
RW	15	18	43	43	67	43	50	28	30	47	44	43	38
R, L	54	55	57	43	0	29	6	6	0	16	6	19	21
TR	0	9	0	0	0	0	0	0	0	0	0	0	0

Table 64. a) all convective category (TRW, A, RW) and b) convective category with Cu, Cb reported 1 hour prior to rain event, expressed as percent of total rain events. July, Goodland

	Hour											
	1-2	3-4	5-6	7-8	9-10	11-12	13-14	15-16	17-18	19-20	21-22	23-00	Total
a	46	36	43	57	100	72	94	95	100	84	94	81	79
b	23	9	14	14	0	71	89	83	87	63	67	43	56

Table 65. Two hourly rain event frequencies by weather type as reported on the WABAN 10 forms.

AUGUST GOODLAND

	Hour											
	1-2	3-4	5-6	7-8	9-10	11-12	13-14	15-16	17-18	19-20	21-22	23-00	Total
TRW, A	3	1	0	0	2	3	8	12	9	15	6	6	65
RW	7	5	5	6	6	3	4	5	8	8	14	11	82
R, L	2	8	9	6	2	1	1	1	0	3	3	5	41
TR	0	0	0	0	0	0	0	0	1	0	0	0	1
Total	12	14	14	12	10	7	13	18	18	26	23	22	189

Table 66. Rain events for each two hour category by weather type expressed as percent of total. August, Goodland

	Hour											
	1-2	3-4	5-6	7-8	9-10	11-12	13-14	15-16	17-18	19-20	21-22	23-00	Total
TRW, A	25	7	0	0	20	43	62	67	50	58	26	27	34
RW	58	36	36	50	60	43	31	28	44	31	61	50	43
R, L	17	57	64	50	20	14	8	6	0	12	13	23	22
TR	0	0	0	0	0	0	0	0	6	0	0	0	1

Table 67. a) all convective category (TRW, A, RW) and b) convective category with Cu, Cb reported 1 hour prior to rain event, expressed as percent of total rain events. August, Goodland

	Hour											
	1-2	3-4	5-6	7-8	9-10	11-12	13-14	15-16	17-18	19-20	21-22	23-00	Total
a	83	43	36	50	80	86	93	95	94	89	87	77	77
b	33	14	0	17	30	43	85	83	78	77	57	50	52

Table 68, Two hourly rain event frequencies by weather type as reported on the WABAN 10 forms.

JUNE ABILENE

	Hour											
	1-2	3-4	5-6	7-8	9-10	11-12	13-14	15-16	17-18	19-20	21-22	23-00	Total
TRW, A	4	2	0	1	3	3	5	4	5	10	1	5	43
RW	5	4	5	7	4	2	0	4	4	6	7	3	51
R, L	1	2	2	1	3	2	0	2	0	1	1	3	18
TR	0	0	0	0	0	0	0	0	0	0	0	0	0
Total	10	8	7	9	10	7	5	10	9	17	9	11	112

Table 69. Bain events for each two hour category by weather type expressed as percent of total. June, Abilene

	Hour											
	1-2	3-4	5-6	7-8	9-10	11-12	13-14	15-16	17-18	19-20	21-22	23-00	Total
TRW, A	40	25	0	11	30	43	100	40	56	59	11	45	38
RW	50	50	71	78	40	29	0	40	44	35	78	27	46
R, L	10	25	29	11	30	29	0	20	0	6	11	27	16
TR	0	0	0	0	0	0	0	0	0	0	0	0	0

Table 70. a) all convective category (TRW, A. RW) and b) convective category with Cu, Cb reported' 1 hour prior to rain event, expressed as percent of total rain events, June, Abilene

	Hour											
	1-2	3-4	5-6	7-8	9-10	11-12	13-14	15-16	17-18	19-20	21-22	23-00	Total
a	90	75	71	89	70	72	100	80	100	94	89	72	84
b	50	25	29	33	30	29	80	50	89	82	44	64	53

Table 71. Two hourly rain event frequencies by weather type as reported on the WABAN 10 forms.

JULY ABILENE

	Hour											
	1-2	3-4	5-6	7-8	9-10	11-12	13-14	15-16	17-18	19-20	21-22	23-00	Total
TRW, A	2	1	4	2	2	3	3	6	4	2	2	0	31
RW	4	4	2	10	3	3	2	9	3	1	2	3	46
R, L	1	0	2	1	1	0	0	0	0	1	1	2	9
TR	0	0	0	0	0	0	0	0	0	0	0	0	0
Total	7	5	8	13	6	6	5	15	7	4	5	5	86

Table 72. Rain events for each two hour category by weather type expressed as percent of total. July, Abilene

	Hour											
	1-2	3-4	5-6	7-8	9-10	11-12	13-14	15-16	17-18	19-20	21-22	23-00	Total
TRW, A	29	20	50	15	33	50	60	40	57	50	40	0	36
RW	57	80	25	77	50	50	40	60	43	25	40	60	53
R, L	14	0	25	8	17	0	0	0	0	25	20	40	11
TR	0	0	0	0	0	0	0	0	0	0	0	0	0

Table 73. a) all convective category (TRW, A, RW) and b) convective category with Cu, Cb reported 1 hour prior to rain event, expressed as percent of total rain events. July, Abilene

	Hour											
	1-2	3-4	5-6	7-8	9-10	11-12	13-14	15-16	17-18	19-20	21-22	23-00	Total
a	86	100	75	92	83	100	100	100	100	75	80	60	89
b	29	60	50	23	33	67	60	93	86	75	40	20	55

Table 74. Two hourly rain event frequencies by weather type as reported on the WABAN 10 forms.

AUGUST ABILENE

	Hour											
	1-2	3-4	5-6	7-8	9-10	11-12	13-14	15-16	17-18	19-20	21-22	23-00	Total
TRW, A	1	2	1	1	0	1	2	7	5	5	2	2	29
RW	2	5	3	5	4	3	4	4	2	3	0	2	37
R, L	0	0	1	1	0	0	0	1	0	3	0	0	6
TR	0	0	0	0	0	0	0	0	0	0	0	0	0
Total	3	7	5	7	4	4	6	12	7	11	2	4	72

Table 75. Rain events for each two hour category of weather type expressed as percent of total. August, Abilene

	Hour											
	1-2	3-4	5-6	7-8	9-10	11-12	13-14	15-16	17-18	19-20	21-22	23-00	Total
TRW, A	33	29	20	14	0	25	33	58	71	45	100	50	40
RW	67	71	60	71	100	75	67	33	29	27	0	50	51
R, L	0	0	20	14	0	0	0	8	0	27	0	0	8
TR	0	0	0	0	0	0	0	0	0	0	0	0	0

Table 76. a) all convective category (TRW, A, RW) and b) convective category with Cu, Cb reported 1 hour prior to rain event, expressed as percent of total rain events. August, Abilene

	Hour											
	1-2	3-4	5-6	7-8	9-10	11-12	13-14	15-16	17-18	19-20	21-22	23-00	Total
a	100	100	80	85	100	100	100	91	100	72	100	100	91
b	67	29	20	29	25	75	67	92	86	64	100	50	60

Table 77. Two hourly rain event frequencies by weather type as reported on the WABAN 10 forms.

JUNE MIDLAND

	Hour												
	1-2	3-4	5-6	7-8	9-10	11-12	13-14	15-16	17-18	19-20	21-22	23-00	Total
TRW, A	1	0	1	0	0	1	2	5	8	6	6	4	34
RW	1	1	3	1	4	2	3	4	3	1	3	5	31
R, L	4	2	3	3	1	0	0	1	1	4	2	1	22
TR	0	0	0	0	0	0	0	0	0	0	0	0	0
Total	6	3	7	4	5	3	5	10	12	11	11	10	87

Table 78. Rain events for each two hour category by weather type expressed as percent of total. June, Midland

	Hour												
	1-2	3-4	5-6	7-8	9-10	11-12	13-14	15-16	17-18	19-20	21-22	23-00	Total
TRW, A	17	0	14	0	0	33	40	50	67	55	55	40	39
RW	17	33	43	25	80	67	60	40	25	9	27	50	36
R, L	67	67	43	75	20	0	0	10	8	36	18	10	25
TR	0	0	0	0	0	0	0	0	0	0	0	0	0

Table 79. a) all convective category (TRW, A, RW) and b) convective category with Cu, Cb reported 1 hour prior to rain event, expressed as percent of total rain events. June, Midland

	Hour												
	1-2	3-4	5-6	7-8	9-10	11-12	13-14	15-16	17-18	19-20	21-22	23-00	Total
a	34	33	57	25	80	100	100	90	92	64	82	90	75
b	33	33	14	25	20	67	80	70	67	55	73	50	53

Table 80. Two hourly rain event frequencies by weather type as reported on the WABAN 10 forms.

JULY MIDLAND

	Hour											
	1-2	3-4	5-6	7-8	9-10	11-12	13-14	15-16	17-18	19-20	21-22	23-00	Total
TRW, A	2	1	0	3	2	3	6	8	10	4	4	2	45
RW	2	1	5	5	2	5	4	7	4	4	3	4	46
R, L	3	3	2	3	0	1	0	0	1	1	1	1	16
TR	0	0	0	0	0	0	0	0	0	0	0	0	0
Total	7	5	7	11	4	9	10	15	15	9	8	7	107

Table 81. Rain events for each two hour category by weather type expressed as percent of total. July, Midland

	Hour											
	1-2	3-4	5-6	7-8	9-10	11-12	13-14	15-16	17-18	19-20	21-22	23-00	Total
TRW, A	29	20	0	27	50	33	60	53	67	44	50	29	42
RW	29	20	71	45	50	56	40	47	27	44	38	57	43
R, L	43	60	29	27	0	11	0	0	7	11	13	14	15
TR	0	0	0	0	0	0	0	0	0	0	0	0	0

Table 82. a) all convective category (TRW, A, RW) and b) convective category with Cu, Cb reported 1 hour prior to rain event, expressed as percent of total rain events. July, Midland

	Hour											
	1-2	3-4	5-6	7-8	9-10	11-12	13-14	15-16	17-18	19-20	21-22	23-00	Total
a	58	40	17	72	100	89	100	100	94	88	88	86	85
b	29	20	57	27	25	67	60	73	80	56	50	71	56

Table 83. Two hourly rain event frequencies by weather type as reported on the WABAN 10 forms.

AUGUST MIDLAND

	Hour											
	1-2	3-4	5-6	7-8	9-10	11-12	13-14	15-16	17-18	19-20	21-22	23-00	Total
TRW, A	1	1	1	1	0	1	5	5	6	3	0	4	28
RW	2	3	4	1	2	3	5	6	4	3	2	3	38
R, L	1	1	4	1	0	0	2	2	0	0	1	1	13
TR	0	0	0	1	0	0	0	0	0	0	0	0	1
Total	4	5	9	4	2	4	12	13	10	6	3	8	80

Table 84. Rain events for each two hour category by weather type expressed as percent of total, August, Midland

	Hour											
	1-2	3-4	5-6	7-8	9-10	11-12	13-14	15-16	17-18	19-20	21-22	23-00	Total
TRW, A	25	20	11	25	0	25	42	38	60	50	0	50	35
RW	50	60	44	25	100	75	42	46	40	50	67	38	48
R, L	25	20	44	25	0	0	17	15	0	0	33	13	16
TR	0	0	0	25	0	0	0	0	0	0	0	0	1

Table 85. a) all convective category (TRW, A, RW) and b) connective category with Cu, Cb reported 1 hour prior to rain event, expressed as percent of total rain events. August, Midland

	Hour											
	1-2	3-4	5-6	7-8	9-10	11-12	13-14	15-16	17-18	19-20	21-22	23-00	Total
a	78	80	55	50	100	100	84	84	100	100	67	88	83
b	50	40	22	0	50	75	75	69	80	83	33	75	60

Table 86. Total number of convective category (TEW, A, KW) rain events at Billings (BIL), Glasgow (GGW), Goodland (GLD), Abilene (ABI), and Midland (MAF).

Month	BIL	GGW*	GLD	ABI	MAF
June	214	161	158	94	65
July	133	138	135	77	91
August	142	101	147	66	66

Table 87. Total number of convective category rain events with Cu, Cb reported 1 hour prior to the rain event for the convective period (11-22 LST).

Month	BIL	GGW*	GLD	ABI	MAF
June	109	80	84	37	35
July	81	77	80	32	44
August	79	34	76	33	35

Table 88. Total number of shower (KW) rain events with Cu, Cb reported 1 hour prior to the rain event for the convective period (11-22 LST).

Month	BIL	GGW*	GLD	ABI	MAF
June	74	43	28	16	9
July	54	29	30	16	18
August	43	16	29	12	18

* Record incomplete for 21-22 LST.

Table 89. Total number of thundershower (TRW, A) rain events with Cu, Cb reported 1 hour prior to the rain event for the convective period (11-22 LST).

Month	BIL	GGW*	GLD	ABI	MAF
June	45	37	56	21	26
July	27	48	50	16	26
August	36	18	47	21	17

Table 90. Ratio: Thundershowers (TRW, A) / Showers (RW) for Tables 88 and 89.

Month	BIL	GGW*	GLD	ABI	MAF
June	0.6	0.9	2.0	1.3	2.9
July	0.5	1.7	1.7	1.0	1.4
August	0.8	1.1	1.6	1.8	0.9

Table 91, Time period of maximum convective activity.

Month	BIL	GGW*	GLD	ABI	MAF
June	13-16	15-18	17-20	19-20	15-22
July	15-16	15-16	17-18	15-16	15-18
August	13-16	19-22	19-22	15-16	13-16

* Record incomplete for 21-22 LST.

does not share the Midland regime. Thundershowers are most dominant in August. The disparity between the two Texas sites is also evident in the time period of maximum convective activity shown in Table 91. Convective rain events occur late (19-20 LST) at Abilene in June and early (13-16 LST) at Midland in August. The earlier times for convective activity usually occur when airmasses are fairly moist and unstable and require less surface heating to initiate moderately deep convection. This same condition contrasts the Billings and Goodland time periods. Convective activity maximizes early at Billings (showers) throughout the summer and it maximizes late at Goodland (thundershowers).

This study has revealed some differing meteorological characteristics for the five stations. The mountainous Billings area is shower-dominated - characteristic of moderately deep convection - and the Goodland area is characteristic of deep convection (thundershower-dominated). Midland experiences a transition from thundershower to shower-dominated regimes, Glasgow becomes thundershower-dominated in July and Abilene in August. The number of convective rain events for which cumulus or cumulonimbus are reported one hour prior to the event varies considerably from site to site and month to month among and between sites.

(3) Subjective Typing of Rain Events to Isolate Single Cloud Rains. This study was initiated upon the observation by HIPLEX Montana operations personnel that many cumulus clouds appeared to draw upon moisture supplies located in the middle troposphere. Cloud bases were reported as high and the lower troposphere was dry. This would suggest that the mid-tropospheric moisture possibly exceeds the low level moisture over Montana and is the real supply for convective development. It was apparent that a seeding practice that increased the airflow through the cloud base might actually result in a decrease in rainfall if drier air from below was drawn into the cloud. Thus it was necessary to determine whether the wet over dry airmass was a climatological feature of the Montana and Kansas High Plains.

In order to establish appropriate relationships for days on which "single cloud rains" were most probable, rain days for June 1965-1971 in Kansas and Montana were categorized by rain type using hourly rainfall data. The subjective criteria used in the typing are shown in the flow chart in figure 14. The specific criteria used are based partly on scientific judgment and partly on the frequency distributions of the various parameters. Days eliminated from the sample, in addition to those with no rain, were those on which the following rain types were most probable: (1) widespread stratiform rain, (2) convective elements embedded in stratiform rain, including organized squall lines often followed by a period of light continuous rain, and (3) system rains not included in the previous two types but suspected of being accompanied by widespread (perhaps middle level) cloudiness. The rains in

Figure 14. Single Cloud Experiment

Flow chart for eliminating widespread stratiform rains, stratiform rains with embedded conveotive elements for Kansas and Montana.

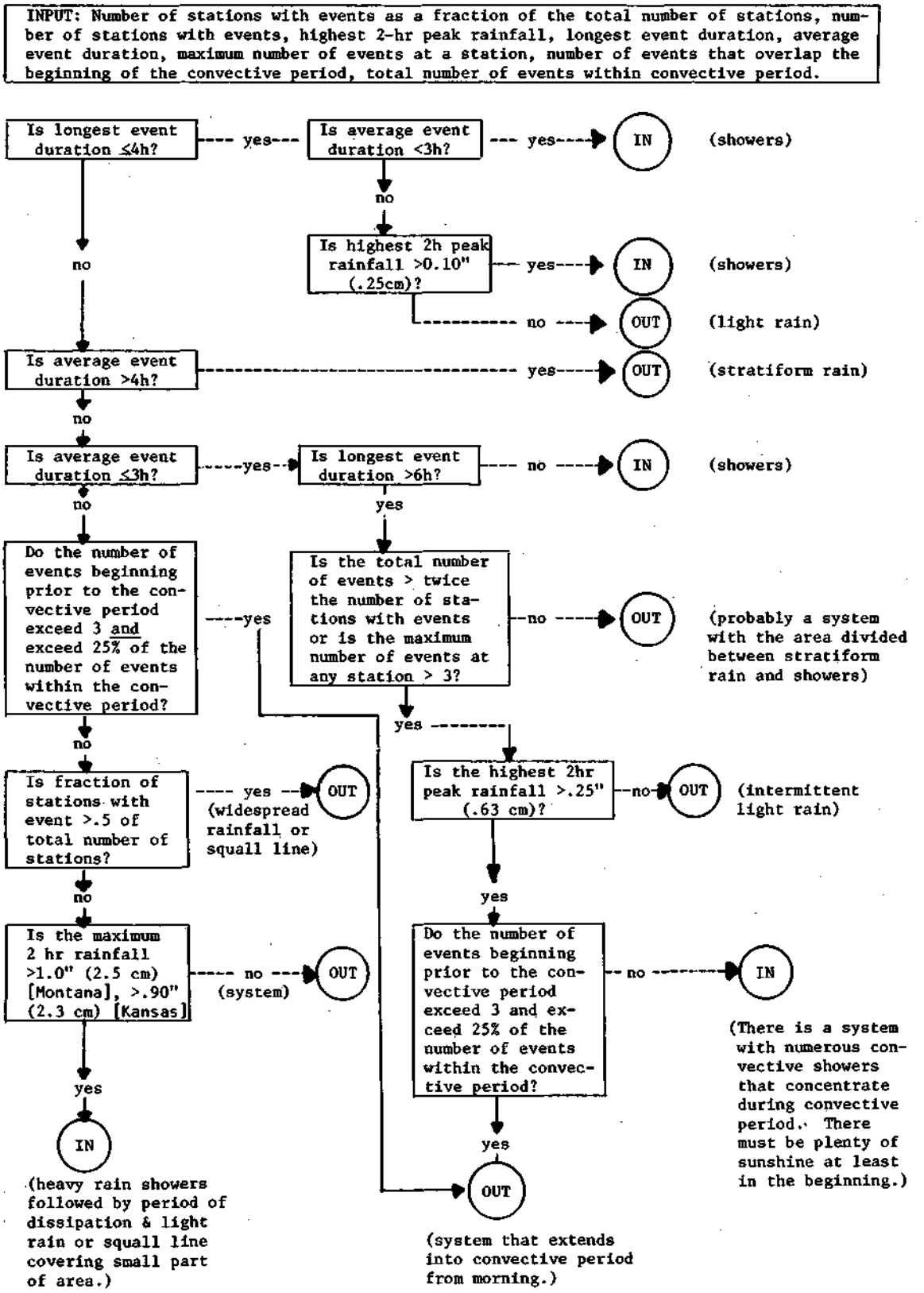

type 3 usually carry over from nighttime rains or develop in the hours just prior to the convective period. These systems are characterized by a large number of rain events that begin prior to and extend into the convective period. Twenty-four rain days were eliminated from the 7 Junes in Kansas and 32 from the 7 Junes in Montana (see Table 92) .

Table 92. Number of rain days, 1965-71 on which system rains were most probable, and those on which "single-cloud" rains were most probable.

	Montana		Kansas	
	System Rains	Single-Cloud Rains	System Rains	Single-Cloud Rains
June	32	115	24	100
July	13	108	19	127
August	16	65	14	102
Total	61	288	57	329

Those days with precipitation that remain should include squall lines that don't fall into type 2, organized complexes or groups of storms, lines of scattered storms, and randomly scattered airmass storms.

The 12 GMT morning rawinsbnde ascents for the single-cloud days were used to determine whether there is climatologically "more moisture in the middle levels than in the low levels" in the Montana experimental area. The precipitable water (a measure of the water actually present) and the relative humidity were calculated for six 100 mb layers beginning at 300 mb and ending at 900 mb. Frequency tables at 10% intervals for relative humidity and at 0.5 cm intervals for precipitable water were constructed for each level.

Table 93 presents the relative humidity, precipitable water and cumulative frequencies of relative humidity for the set of convective days extracted from the Montana site hourly rainfall data by the methods outlined above. Results for a subset of days that were characterized by numerous light showers are presented in Table 94. Only the August relative humidities are higher in mid-levels than at the lowest levels. The cumulative frequency of relative humidity for August shows a trend toward higher frequency

Table 93. Relative humidity and precipitable water summaries for the Montana site for 1965-1971 for convective days.

Average relative humidity and precipitable water

Layer in 100's mb	Relative Humidity (%)			Precipitable Water (cm)		
	June	July	August	June	July	August
3-4	32	28	32	0.3	0.3	0.4
4-5	36	33	39	0.7	0.8	0.9
5-6	43	40	46	1.5	1.8	2.0
6-7	53	47	49	2.9	3.2	3.4
7-8	56	48	48	4.4	4.9	4.8
8-9	53	46	44	5.7	6.6	6.2

Cumulative frequency of relative humidity (%)

Layer in 100's mb	50-100	60-100	70-100	80-100	90-100	Total No. of Soundings
June						
3-4	m	m	m	m	m	
4-5	40	25	16	5	0	456
5-6	78	52	24	8	8	
6-7	121	81	49	25	10	
7-8	127	88	60	32	8	
8-9	116	75	47	29	10	
July						
3-4	m	m	m	m	m	
4-5	39	21	10	4	0	210
5-6	60	37	19	8	3	
6-7	80	51	28	8	2	
7-8	87	51	21	7	2	
8-9	80	45	15	8	1	
August						
3-4	m	m	m	m	m	
4-5	36	22	8	3	0	260
5-6	57	36	21	6	2	
6-7	62	39	17	5	1	
7-8	58	27	8	4	1	
8-9	40	27	12	5	1	

Table 94. Relative humidity and precipitable water summaries for the Montana site for 1965-1971 for the subset of convective days.

Average relative humidity and precipitable water

Layer in 100's mb	Relative Humidity (%)			Precipitable Water (cm)		
	June	July	August	June	July	August
3-4	40	32	34	0.5	0.3	0.4
4-5	41	39	44	0.5	0.9	1.1
5-6	51	47	52	1.6	1.9	2.1
6-7	62	54	57	3.2	3.6	3.5
7-8	65	56	58	4.6	5.0	5.1
8-9	62	55	54	5.9	7.4	6.6

Cumulative frequency of relative humidity (%)

Layer in 100's mb	50-100	60-100	70-100	80-100	90-100	Total No. of Soundings
			June			
3-4	m	m	m	m	m	
4-5	16	7	4	0	0	120
5-6	31	20	8	2	2	
6-7	42	33	18	12	3	
7-8	44	39	26	14	3	
8-9	46	31	22	13	4	
			July			
3-4	m	m	m	m	m	
4-5	5	4	2	0	0	52
5-6	12	6	3	1	0	
6-7	15	9	4	0	0	
7-8	19	10	3	1	0	
8-9	17	10	3	2	0	
			August			
3-4	m	m	m	m	m	
4-5	7	6	2	1	0	44
5-6	13	9	6	0	0	
6-7	16	11	5	1	0	
7-8	16	12	5	2	0	
8-9	12	11	6	2	1	

for high relative humidities to occur in the 700-500 mb layers. Since system rains have been removed from the data set, the high mid-level humidities should not be attributed to rawinsonde ascents through stratiform cloudiness. Similar trends are not present in the subset days frequency of Table 94. It should be remembered that the actual water present (precipitable water) is always greatest in the lower levels. Thus there is no real indication that the wet-over-dry airmass structure is a climatological feature of the Montana high plains.

(4) Severe Weather Occurrences and Their Relationship with the Areal Rainfall at Dodge City, Kansas. The frequency at which severe weather (large hail, damaging winds, and tornadoes) occurs at or near an experimental seeding site can have important ramifications for the design and operational aspects of HIPLEX. What constitutes severe weather as well as some criteria that identify severe weather days must be determined if these days are to be eliminated from the experiment for aircraft safety and legal considerations. These criteria will, in turn, feed back to the design. The length of the experiment could increase as more potentially convective "candidate cloud" days are eliminated. If a large class of days was removed, 1) the predictor variables might have to be re-examined, 2) relationships with convective rainfall might have to be re-developed, and 3) in the extreme cases, choices for experimental sites might have to be re-evaluated.

All three proposed HIPLEX experimental sites are frequented by severe weather. Consequently, some criteria for advance warning must be available to HIPLEX operations personnel. The National Severe Storms Forecast Center (NSSFC) tornado and severe thunderstorm watches provide one possible set of criteria. Here, watch information is compared with daily precipitation for 10 Junes in Kansas from 1965-1974.

The data for this study have been extracted from the NSSFC tornado, severe thunderstorm and aviation severe thunderstorm watch areas for the entire United States from 1952-1975. The watch areas are defined by a specified distance in nautical miles either side of a line connecting two points given in latitude and longitude. A second magnetic tape contains the NSSFC tornado logs from 1950-1974. Included are cumulative sums of tornadoes by day and by state, detailed specifications of conditions under which the tornadoes occurred and information concerning their locations, path lengths, widths, etc. A third data set contains the daily rainfall records for Kansas.

The Kansas study area has been divided into six rainfall sampling areas (see Fig. 4). The latitude and longitude coordinates of the rainfall sampling areas and the coordinates and widths of the NSSFC watch areas were converted to a Lambert Conformal map image frame. Then, if any part of a watch box fell within any part of a

sampling area, that sampling area was designated to be under a severe weather watch. The day was divided into 3-hour periods; if the watch valid time included all or part of a 3-hour period, that period was designated to be under a watch.

The severe weather watch day was defined to include watches within the daily rainfall period, 7 AM - 7 AM. This was advantageous since the minimum watch frequency occurs during the morning hours. Watches issued during the late afternoon often overlap into the early morning hours of the next day. These are included in the same watch day.

We have developed 7 operations scenarios which draw upon 1) watch information within the DDC sampling area which is defined as the experimental area, and 2) watch information within the five surrounding precipitation sampling areas which are defined as extra-areas. There are two ways in which the extra-area watches can influence operational decisions. First, a watch may be issued for areas upwind from the DDC area. Operations may be terminated for fear that watches will soon be issued for the experimental area and/or severe weather will move in later in the day. Second, a watch may be issued for areas downwind from the DDG area. Operations may be terminated for fear that seeding material may drift downwind into the watch valid area and interact with storms there. These influences are treated as one 'extra-area influence'. Please note that we do not have sampling areas southwest, south, or southeast of the DDC area. Thus, results that include extra-area influences may be somewhat optimistic. The 7 operations scenarios are:

1. Total Kansas Watches - This is the conservative approach. In the event that a severe weather watch of any kind is issued either within the operations area or within the surrounding areas, operations are terminated. Thus, with reference to the climatological data set, any day with a valid severe weather watch in a Kansas sampling area is extracted from the sample.

2. DDC Area Watches - This conservative approach leads to the termination of operations for any severe weather watch falling within the DDC sampling area. Extra-area influences are not taken into consideration.

3. Kansas Tornado Watches - This operations scenario includes consideration of extra-area effects but operations are cancelled only upon issuance of tornado watches.

4. DDC Area Tornado Watches - Same as 3, but extra-area influences are neglected.

5. Kansas Tornado - Only those days during which tornadoes are reported in Kansas are dropped from the sample. In this approach, the tornado forecast technology has improved such that tornado days can be forecasted with 100% precision.

6. Kansas Tornado - DDC watch - Only those Kansas tornado days with a tornado watch valid in the DDC sampling area are days for which operations are terminated.

7. DDC Area Tornado - Only those days with a tornado reported in the DDC sampling area are designated as stand downs.

A set of tables has been prepared to illustrate the limitations placed upon a seeding experiment operating out of the Dodge City area when the aforementioned severe weather operations scenarios are used.

June tornado and severe weather watch information for Kansas for 1965-1974 is presented in Table 95. The number of June tornadoes varies from 1 in 1972 to 23 in 1967. This number is probably an underestimate as it does not include the unobserved, unreported, or unverified tornadoes. The June average is 10.3 tornadoes. The number of Kansas June tornado days ranges from 1 to 9, an average of 5.4 tornado days per June. This corresponds to scenario 5; approximately 20% of all June days would be severe weather-related stand-downs. When DDC area tornado days are considered, the annual June number drops to 1,3 tornado days.

The fourth line of Table 95 gives the number of days with a severe weather watch within the DDC sampling area (scenario 2). The number ranges from 4 in 1974 to 19 in 1965, On the average, about one third (9.9) of the June days would be stand-downs. Should extra-area influences be included (scenario 1), more than one half (15.2) of the June days would have operations terminated because of severe weather watches. In 1965, only two June days were free of severe weather watches.

The severe weather watch days were categorized by tornado watch days, severe thunderstorm watch days and aviation severe thunderstorm watch days. The latter two are the same with regard to expected weather but the last is issued to aviation interests only. The categories are mutually exclusive. Any day with a tornado watch was a tornado watch day regardless of the number of other watches for that day. Any day with both types of severe thunderstorm watches was a severe thunderstorm watch day and days with only aviation severe thunderstorm watches were aviation severe thunderstorm watch days.

Line 6 of Table 95 gives the Kansas tornado watch days (scenario 3). The average of 6,6 tornado watch days compares favorably with the average of 5.4 tornado days. Unfortunately,

Table 95. Summary of June 1965-74 tornado and severe weather watch information taken from NSSFC weather logs.

	Year										
	65	66	67	68	69	70	71	72	73	74	Ave
Total Kansas Tornadoes	14	15	23	7	5	13	11	1	5	11	10.3
Total Kansas Tornado Days	6	6	9	6	5	7	7	1	2	5	5.4
Total DDC Area Tornado Days	0	0	4	2	0	2	1	0	1	1	1.3
No. of DDC Area Watch Days	19	13	15	8	9	9	12	5	5	4	9.9
Total Kansas Watch Days	28	22	22	15	12	12	14	8	10	7	15.2
Total Kansas Tornado Watch Days	9	6	11	6	9	5	10	1	5	4	6.6
Total Kansas Svr Tstm Watch Days	15	11	7	5	2	7	4	7	5	3	6.6
Total Kansas Aviation Watch Days	4	5	4	4	1	-	-	-	-	-	3.6*

* Based on period 1965-69

Table 96. Percentages of June precipitation that falls on days specified as stand-downs by operational scenarios.

		Year							
		65	66	67	68	69	70	71	Ave
	Total June Precipitation	154.8	50.0	165.1	77.9	74.5	69.5	73.0	95.0
1.	All Kansas Watches	100	96	90	97	16	93	59	82
2.	DDC Area Watches	91	85	57	58	16	90	55	66
3.	All Kansas Tornado Watches	64	1	48	65	16	67	55	50
4.	DDC Area Tornado Watches	62	1	42	42	16	67	52	45
5.	All Kansas Tornado Days	39	25	30	20	10	69	35	33
6.	DDC Area Tornado Watches Kansas Tornado Days	32	1	28	10	7	67	33	28
7.	DDC Area Tornado Days	0	0	28	9	0	51	7	14

not all tornado days were tornado watch days. In fact, 33% of the tornado days were not forecasted. The average number of severe thunderstorm watch days was the same as the tornado watch days. These and the aviation severe thunderstorm watch days account for the apparent over-prediction when line 5 is compared with line 2. We do not have large hail and/or damaging wind reports independent of tornado reports to compare the accuracy of these forecasts.

Table 96 gives percentages of precipitation that fell on tornado or severe weather watch days. The first line gives the June rainfall for each year (1965-1971) and the average rainfall for that period. The wet years, 1965 and 1967, had twice the rainfall of any of the other five years. If the operations are planned according to scenario 1, about 82% of the DDC area rainfall would occur on stand-down days. In 1965, only two days in June were without severe weather watches. If extra-area influences are not taken into consideration (scenario 2), about two-thirds of the June rainfall occurs during severe weather conditions. The next two lines show the percentages of rainfall on tornado watch days (scenarios 3 and 4). Approximately one-half of the precipitation would have escaped possible treatment. The small decrease in the percentage of precipitation falling under stand-down conditions when extra-area influences are neglected can be explained by observing that large areas are included in tornado watches. If a tornado watch was valid within any of the surrounding sampling areas, there was a good chance that the watch was also valid in the DDC sampling area.

About one-third of the June rainfall would be eliminated if operations were terminated for all Kansas tornado days (scenario 5). That value decreases to 28% for scenario 6. If the DDC area tornado days could be accurately forecasted, scenario 7 shows that only 14% of the June rainfall would be eliminated.

It was suspected that the figures in Table 96 might be biased toward pessimism because tornado days might be days characterized by widespread and/or heavy squall line or system-type rainfall. These days would have already been judged unsuitable for candidate clouds by other criteria. However, it is instructive to view the percentages of rains that fall under these conditions.

Table 97 gives the percentages of rain days that would be eliminated from the experiment by severe weather scenario stand-downs. The percentages are presented in amount classes to give the opportunity to view the dependence of severe weather related stand-downs upon the average areal rainfall for the Dodge City sampling area. If scenario 1 was the operations stand-down criteria, 75% of the days for the 7 Junes would have been stand-down days. This value is weighted strongly by the very light (0,3-3.0 mm) rain days for which "only" 66% would have been stand-down days. Scenario 4 is the most optimistic currently obtainable stand-down

Table 97. Scenario eliminated rain days expressed as percent of total number of rain days by DDC area average precipitation amount category.

Amount	Scenario Number 1	2	3	4	5	6	7	Total Number of Rain Days
0.3-3.0	66	43	23	16	24	11	0	61
3- 6	95	84	58	53	58	32	21	19
6-12	81	63	44	38	38	31	13	16
12-25	86	64	64	57	29	29	21	14
>25 mm	75	50	25	25	25	25	0	4
Total	75	55	37	31	32	20	8	114

Table 98. Summary of watches valid on wet and dry days for Kansas Junes.

	Year 65	66	67	68	69	70	71	Average
Dry days with DDC area Tornado watch	1	2	2	0	3	1	0	1.3
Wet days without DDC area Tornado watch	14	14	11	9	11	9	11	11.3
Wet days without any DDC area watch	6	8	7	6	6	8	8	7.0
Wet days without any Kansas watch	1	3	3	1	1	5	6	2.9

criteria. Approximately 31% of the rain days would be eliminated. Only 16% of the very light rain days would be stand-downs as compared with approximately one half of the heavier 3-25 mm average area rains.

Only 8% of the rain days would have been eliminated if those days on which tornadoes were reported in the DDC area could have been perfectly predicted. Recall that scenario 4 produced 31% stand-downs for the same period. Clearly, the NSSFC tornado watch procedures carry a high false alarm rate (watches cover very large areas or are issued for non-tornado days).

Table 98 shows that few tornado watches were issued on days without precipitation. There is an average of 11.3 wet days without tornado watches in the DDC area. The number decreases to 7 days per month if all DDC area watches (scenario 2) are included. For scenario 1, there would be only 2.9 operational days per month.

Depending upon the severe weather-related operations scenario, the length of a seeding experiment in Kansas could be increased 42-400%. Obviously, scenario 1 is unrealistic. Scenario 4 is the most optimistic currently obtainable stand-down criteria. Yet this criteria could increase the length of the experiment by a factor of 1.4. It should be noted that scenario 7, if obtainable, has the smallest increase in the length of the experiment (10%) but it is developed only for tornadoes. Inclusion of large hail and damaging wind in stand-down criteria would necessarily lead to the results of the more pessimistic scenarios.

Throughout this study, it has been assumed that watch days were severe weather days and severe weather days were watch days. The failure rate - the number of tornado days that occur in the absence of tornado watches - is also critically important to the HIPLEX operations program. Operations scenarios which draw heavily upon tornado watches are jeopardized if the tornado watches fail to include those times during which tornadoes actually occurred. No forecast system is completely fail-safe. There were 11 June tornado days in the DDC square from 1965-1974, but on only six of these days were tornado watches valid in the same area. For this sample, there was a failure rate of 46% (5 of 11 tornado days were not forecast). Further, there were no tornado watches valid in any of the surrounding Kansas areas on those days; 3 days had severe thunderstorm watches, 1 day had an aviation severe thunderstorm watch, and 1 day had no watch of any kind. Inclusion of the other watches in stand-down criteria to eliminate failures would necessarily increase the number of false alarms and lead to an unrealistic number of days eliminated (scenarios 1 and 2).

Our severe storm study shows that June tornadoes are relatively infrequent in western Kansas and, if correctly forecasted, would lead to the elimination of 8% of the possible June rain data on the

average. The attainment of the correct tornado forecast is another matter. The tornado watch as an operations stand-down criteria appears to be limited by a high failure rate.

Summary and Conclusions. The sounding SPECs were found to be unimportant in explaining the daily and 6-hour rainfall variance. This was largely due to the low correlations of sounding variables to which the transience problem contributed.

The correlation of surface SPECs with rainfall were also low, but were higher than the correlations of soundings with rainfall. The upslope vertical velocity (observed wind) ranked high for both daily and 6-hour rainfall in June and August, but not in July. In general, the wind (pressure) related SPECs were best for the June and August daily rainfall. However, no SPEC ranked consistently high throughout the 3-month period. Also, no outstanding field pattern and no single physical process was identified to be productive to high plains rainfall.

The overall correlation of the surface variables with rainfall was somewhat greater for daily rainfall than for 6-hour rainfall. This may be due to the greater sparsity of hourly stations with respect to daily stations.

The factor analysis scheme was found to be useful for incorporating pattern information into the SPEC-rainfall relationships. Interpretation of the factors indicated that some factor-rainfall correlations were consistent with known physical processes that lead to convective rainfall. However, some factor patterns were physically inconsistent and others were not revealing.

SPECs from the cloud model were poorly correlated with the daily rainfall and were of similar magnitude as the sounding correlations. The correlations with 6-hour rainfall were extremely low. The low correlations are likely due to the cloud model initialization which was not representative of atmospheric conditions that accompany transient weather systems.

The radar SPEC of percent areal coverage for Dodge City during 1200-1800 (i.e., the percent of the Dodge City sampling area covered by the envelope containing radar echoes) explained 25% of the rainfall variance. When the Dodge City radar SPEC was used as a dependent variable and was correlated with the surface factors, the range of correlation was .14 to .47. This range was slightly higher than the correlation of the 6-hour rainfall with the factors (range of correlation was 0-.38). The increase may be due in part to the capability of the radar to observe precipitation echoes on days when no rain fell at the hourly raingage sites.

Prewetness and the rainfall from the surrounding areas were included in the 6-hour SPEC-rainfall relationships, and the rain from surrounding areas was included in the daily SPEC-rainfall relationships. These SPECs ranked consistently high throughout the 3-month period. Overall, the prewetness and the rain from the surrounding areas were found to be the most consistent of all SPECs investigated.

The incorporation of the SPECs into the SPEC equation indicated that the amount of variance explained by the SPEC equations varies from 44.9% to 57.8% for daily data, and from 26.2% to 46.2% for precipitation during the period 1200-1800. The independent data test for the daily data in June indicated that the variance explained for the daily data might be as low as 32.8% to 44.5%. However, it is noted that the independent data test was based only on SPEC equations from the period 1965-1970. In an actual experiment, the equations could be updated each year with the inclusion of previous years into the SPEC equation. That is, 1965-1971 would be used to predict 1972, 1965-1972 would be used to predict 1973, and so on.

Also, the non-seeded days from the experiment could be used to 1) adjust equations, if necessary, or 2) develop the SPEC equation, if necessary, or 3) develop the SPEC equations without historical data. Thus, it is believed that the 44.9% to 57.8% values for daily data and the 26.2% to 46.2% for 6-hour precipitation are possible and that the 32.8% to 44.5% figures represent a lower limit to the amount of variance it is possible to explain. Although there was insufficient time on this project to perform independent data tests for the daily rain in July and August, and the 6-hour rain in June, July, and August, such tests would be desirable to firm up the percentage estimates indicated above.

Estimates of sample size were obtained for an areal design of the mean areal rainfall for the Dodge City sampling area. These estimates were based on a log-normal model of the daily mean areal rainfall from the Dodge City sampling area. New estimates of the sample size were then obtained based on the inclusion of SPECs into the design.

It was found that for a 50% chance of detecting a 20% increase, a period of 6.3 years is required for a 40% increase, a period of 1.9 years is required; and for a 60% increase, a period <1 year is required. For a 70% chance of detecting a 20% increase, a period of 11.0 years is required; for a 40% increase, a period of 3,2 years is required; and for a 60% increase, a period of 1.7 years is required.

A comparison of these sample sizes to those obtained without SPECs indicated that the overall sample sizes were reduced on the order of 36% to 50% by the inclusion of the SPECs into the design. However, the estimates of sample size were only approximate since

the true amount of log variance reduction on rain days was unknown. To obtain the true amount of log variance on the rain days, the SPEC equations would need to be re-developed for rain days only. Thus, any future research on SPECs should include the development of SPEC equations for rain days only.

The diurnal rainfall studies indicated that rainfall is more frequent in eastern Kansas and has a tendency to occur anytime throughout the day, but tends to occur most often during the early morning hours (0300-0600). In western Kansas the rainfall is less frequent and occurs primarily during the late evening period (1800-midnight). Thus, the diurnal variability of rainfall is higher in western Kansas, although the rainfall is more frequent in eastern Kansas.

The maximum rainfall frequency in the Goodland-Colby area is from 1800-midnight. Seeding opportunities for the single cloud experiment should exist before this period because towering cumulus clouds which will develop into showers that intensify and merge should be present. After 2100 LST, the precipitation frequencies generally decline. However, Bark (1975) notes that 1) 35% of the echoes forming over western Kansas did so at night and 2) the percentage of treatable size clouds is the same for darkness and daylight. Thus, a seeding experiment should be prepared to extend beyond 2100 LST.

Studies of convective rain events indicate that a great variability exists in the frequency of rain events between the Montana, Kansas, and Texas sites. Furthermore, there is a great variability in the types of events between sites. For example, showers are most frequent at Billings, thunderstorms are most frequent at Goodland, and a transition from thunderstorms to showers throughout the summer period is observed at Midland.

The time period of maximum convective activity also varies between sites. Rainfall is more frequent from 1300-1600 LST at Billings, from 1700-2200 at Goodland, and shifts from 1500-2200 in June to 1300-1600 in August at Midland. The variability in timing, frequency, and types of rain events between the sites suggest that there may be a difference in the rainfall mechanisms at each locale. This would suggest that seeding technology developed at one site may need to be modified before transferability to another site is feasible.

A study was conducted to determine whether the moisture supply for Montana high plains clouds was located in the middle or lower troposphere. It was found from this climatological study that there was more moisture in the lower levels than in the middle levels. Thus, a seeding practice that increases the airflow through cloud base would not be expected to draw dry air into the cloud from below.

A study of severe weather indicates that the length of the seeding experiment can be increased by the elimination of potential convective days through severe weather-related operation stand-downs. Seven operational scenarios that draw upon Kansas tornado climatology, severe weather watches, and extra area "influences" were developed for the Dodge City sampling area. It was found that the first four scenarios, those currently possible, could lead to an increase in the length of a June Kansas seeding experiment from 40-400%. The optimistic scenarios did not take into account occurrences of severe hail and/or wind. Further, the tornado watches had a 46% failure rate (tornadoes occurred in the absence of tornado watches 46% of the time). These findings suggest that there is no presently accurate means of predicting tornadoes at Dodge City in June that would not lead to an unreasonable (in terms of experiment length) number of stand-downs.

Radar Studies For HIPLEX

Introduction. The three studies which make up this section investigate various applications of radar to the problems of HIPLEX.

The first study considers the application of radar to rainfall measurement, using the technique of Brandes (1975) to combine gage and radar rainfall measurements. This technique assumes that data from the two instruments, each with its own inaccuracies, can be combined to provide a final rainfall measurement which is superior to that of either instrument taken alone. In the case of HIPLEX data from Montana, this expected result is not found, and the combination of gage and radar data is found to be slightly less accurate than the gage data taken alone. It is suggested that this perplexing result is due to evaporation of rainfall, and that this may not be a general result. The study give some hope for moderately accurate short duration gage-radar rainfall analyses. Finally, the study suggests that the gage density can probably be reduced somewhat from that used in the HIPLEX Montana experiment. It is suggested that the necessary gage density can be based on storm size, a climatological feature of any area.

The second study considers the effects of attenuation on the HIPLEX 5-cm radars. Since 5-cm radars are known to be attenuated in some cases, this is an important question, particularly in a situation where the radars might be used to measure precipitation. The effects of attenuation on 5-cm radar are illustrated and an iterative attenuation correction scheme is presented. It is shown that 5-cm radar measurements are essentially unattenuated for storms with maximum reflectivities less than about 40 dbZ, and can be seriously attenuated for storms with reflectivity maxima above 50 dbZ. The attenuation correction scheme is shown to be promising for storms with reflectivity maxima of 45 to 60 dbZ if the radar is very accurately calibrated. It is suggested that for accurate rainfall measurements, gages are needed to calibrate the radar, and that for accurate rain measurements in attenuating situations, the gage density should be related to storm size.

The final study uses radar first echo observations to investigate precipitation initiation mechanisms across the high plains. This literature survey indicates that southern and midwestern regions are dominated by warm precipitation initiation processes, the mid-high plains (e.g. Kansas and Nebraska) have a much higher likelihood of ice initiation, and that northern regions (e.g. Montana) are dominated by

ice initiation. Several observations are presented which suggest that large storms are likely to have ice initiation processes even in southern regions where warm precipitation initiation would otherwise be the rule.

An Analysis of Radar and Gage Rainfall Measurements in the HIPLEX; Montana Experiment. *(]) General Background.* This report makes an assessment of. the precipitation-measuring capabilities of the HIPLEX 5-cm radar and raingage network located near Miles City, Montana. The problems of measuring rainfall using radar and gages are discussed and a method is presented for combining the information from the two instruments. This rainfall data processing technique is evaluated using data from the HIPLEX Montana experiment, and some recommendations are presented for the use and operation of gageradar precipitation measuring systems in weather modification experiments.

Use of a combined gageradar rainfall measurement technique is desirable, because both instruments have defects which prevent them from being satisfactory when used alone. Use of gages alone is frequently regarded as a costly, time-consuming method of measuring precipitation amounts, and gages are known to be poor measures of rainfall on small time and space scales. However, the accuracies and efforts involved in gage measurements are well-known (e.g., Huff, 1970) and gages •_ rovide accurate mean areal measurements for long periods. Radar measurement of rainfall is an attractive alterne. ive to gages, mostly because of the ease of data collection. Radar data analyses, however, are complicated by extensive problems including errors in the Z-R relation and radar calibration, plus the likely effects of attenuation, evaporation and advection. Consequently, many investigators (e.g. Woodley, et. al., 1975; Brandes, 1975; and Wilson, 1975) have turned to techniques of gage calibration of radar data to provide rainfall measurements. The hypothesis has been that gage calibration of radar rainfall measurements can give measurements with the point accuracy of the gages and the spatial resolution of the radars.

These investigations have used gage calibration of radar data in siutations where experimental considerations preclude having sufficient gages to measure the rainfall accurately enough to satisfy the experimental objectives. While these studies have shown gage calibrated radar rainfall measurements to be a promising technique, several questions remain unanswered. Most importantly, the relative accuracy of the gage-only and gage-radar rainfall analyses has not been considered for a variety of gage densities and analysis intervals.

(a) Gage rainfall measurement. The work of Huff (1970, 1971) suggests that gage networks can measure mean areal rainfall amounts quite accurately. Huff considered the accuracy of gage-only precipitation measurements using gage networks of 49 gages in 400 mi^2 and 49 gages in 550 mi^2 located in Illinois. He compared the results from various gage densities, time intervals, network areas and precipitation amounts and derived the regression equation

$$\log E = -1.5069 + 0.65 \log P + 0.82 \log G - 0.22 \log T - 0.45 \log A \quad (25)$$

where E is the average sampling error in inches, P is the mean areal precipitation in inches, G is area per gage in mi^2, T is the time in hours, and A is network area in mi^2. Some sample applications of this equation for a gage network of 600 mi^2 are listed in Table 99 for various values of P, G, and T. The HIPLEX gage network (109 gages in 600 mi^2) is similar to that used by Huff. The climatology of the two locations (Illinois versus Montana) is different, so strict adherence of the HIPLEX results to the Huff equation should not be expected.

Table 99 shows that the percent error in the gage precipitation estimate increases with decreasing gage density, precipitation amount and storm duration. This is not surprising, for decreases in gage density, precipitation amount or storm duration should decrease the accuracy with which the rainfall is sampled, hence decrease the accuracy of the precipitation measurement.

Table 99. Percent error of precipitation measurements based on Huff's equation for gage networks. Network area is 600 mi^2; percent error is shown for various storm durations, mean areal rainfall amounts and gage densities. See text for equation and for restrictions on its use.

Analysis Duration (min)	Mean Precip. Amount (mm)	Gage Density (gages/mi^2) 1/24	1/36	1/60	1/96	1/120
120	1	6	9	13	20	24
	4	4	5	8	12	15
	10	3	4	6	9	11
60	1	7	10	16	23	28

Table 99 (continued)

Duration (min)	Precip. Amount (mm)	Gage 1/24	1/36	Density 1/60	1/96	1/120
				(gages/mi^2)		
	4	5	6	10	14	17
	10	3	5	7	10	12
30	1	9	12	18	27	32
	4	5	7	11	16	20
	10	4	5	8	12	14

Huff's work suggests that for gage densities greater than 1 per 36 mi^2, and durations longer than approximately 1 hour, gage measurements of rainfall are likely to be within 10% of the true mean areal amount. The most likely single gage errors result from mis-measurement and from gage undercatch in windy situations (Larson and Peck, 1974). These errors are usually smaller than or equal to this 10% error; hence, the gage precipitation measurements provide a standard of accuracy which can be used to evaluate various methods of rainfall measurement. For example, gage-calibrated radar rainfall measurements for high gage densities and long analysis time intervals should be within 10% of the gage-only measurements. Consequently, one hour high density gage-only rainfall analyses were used to adjust various parameters in the analysis programs and to evaluate the accuracy of the analyses for various gage densities and analysis durations.

(b) Radar rainfall measurements. Use of radar to measure rainfall, while originally investigated as a method of replacing raingages, has proved to be a moderate failure. The primary reason for the radar's inadequacy is the lack of an accurate relation between the reflectivity factor and the rainfall rate. While average ZR relations are easily formulated on the basis of theory, observation of raindrop size distributions, or empirical correlations of observed values of Z and R, these ZR relations are mean values and as means do not reflect daily, storm to storm, or within storm variability of drop size distributions. In addition, the inevitable slight errors in the calibration of any radar, though small, are enough (together with the errors in the chosen Z-R relation) to make the radar rainfall estimate accurate only to within about 50%. Additional problems with radar rainfall measurement involve the effects of attenuation, evaporation, and advection of the rain.

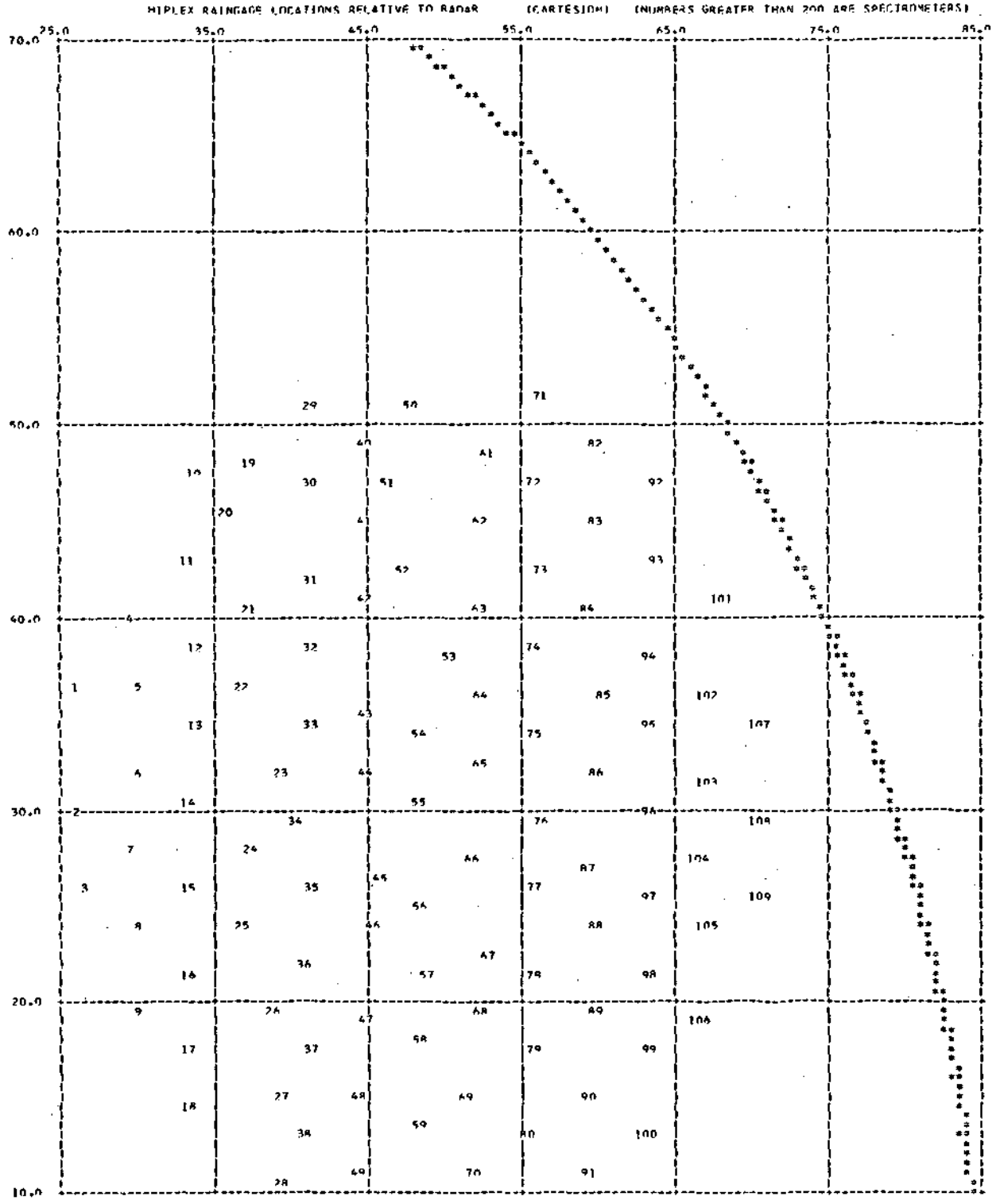

Figure 15. HIPLEX raingage locations relative to Miles City Radar. Distances are in km from radar. Gage numbers are SWS gage numbers.

SWS NUMBER	HIPLEX LABEL	LATITUDE DEG	MIN	SEC	LONGITUDE DEG	MIN	SEC	EAST KM	NORTH KM	RANGE KM	AZIMUTH DEG
1	SD	46	44	26	105	34	10	26.1	36.6	44.8	35.6
2	SE	46	40	58	105	34	1	24.7	30.0	39.0	41.1
3	SH	46	38	54	105	33	57	26.3	26.2	37.1	45.1
4	SB	46	46	26	105	31	27	29.6	40.1	49.8	36.4
5	TC	46	44	24	105	31	8	30.0	36.4	47.2	39.5
6	TE	46	42	2	105	31	11	29.9	32.0	43.8	43.1
7	TG	46	39	47	105	31	20	29.7	27.8	40.7	46.9
8	TI	46	37	45	105	31	7	30.0	24.1	38.5	51.2
9	TK	46	35	16	105	31	7	29.9	19.5	35.7	56.9
10	UX	46	50	29	105	27	57	34.7	47.4	58.4	35.7
11	UZ	46	47	53	105	28	19	33.7	42.8	54.5	38.2
12	UR	46	45	34	105	28	12	33.8	39.5	51.2	41.5
13	UO	46	43	22	105	28	12	33.8	34.5	48.3	44.4
14	UF	46	41	12	105	28	24	33.5	30.4	45.2	47.8
15	UH	46	38	41	105	28	15	33.7	25.8	42.4	52.6
16	UJ	46	36	28	105	28	13	33.7	21.7	40.1	57.2
17	UL	46	34	5	105	28	12	33.7	17.3	37.9	62.8
18	UN	46	31	42	105	28	17	33.6	14.7	36.7	66.4
19	VW	46	50	44	105	25	25	37.5	48.1	61.0	37.9
20	VY	46	49	14	105	26	29	36.1	46.3	59.9	38.6
21	VB	46	46	45	105	25	18	37.6	40.7	55.4	42.7
22	VC	46	44	20	105	25	49	36.9	36.3	51.8	45.5
23	VE	46	42	8	105	23	51	39.4	32.2	50.9	50.7
24	VG	46	39	53	105	25	43	37.4	28.0	46.7	53.2
25	VI	46	37	37	105	25	43	37.0	23.8	44.0	57.2
26	VK	46	35	15	105	24	11	38.9	19.4	43.5	63.5
27	VM	46	32	58	105	23	42	39.5	15.2	42.3	69.0
28	VO	46	30	30	105	23	51	39.3	10.8	40.7	74.9
29	WV	46	52	13	105	22	16	41.6	50.0	65.7	39.3
30	WX	46	50	15	105	22	27	41.4	47.2	62.8	41.3
31	WZ	46	47	32	105	22	29	41.3	42.9	59.0	44.4
32	WR	46	45	29	105	22	24	41.4	38.6	56.5	47.2
33	WO	46	43	16	105	22	22	41.4	34.3	53.8	50.4
34	WF	46	40	42	105	23	5	40.4	29.5	50.0	53.9
35	WH	46	38	43	105	22	20	41.4	25.8	48.8	58.1
36	WJ	46	36	49	105	22	37	41.0	22.1	46.6	61.7
37	WL	46	34	8	105	22	9	41.5	17.4	45.0	67.3
38	WN	46	31	51	105	22	28	41.1	13.1	43.1	72.3
39	XP	46	54	21	105	22	28	41.1	58.5	62.7	38.3
40	XW	46	51	12	105	19	31	45.7	49.0	66.7	42.7
41	XY	46	49	10	105	19	42	44.9	45.2	63.7	44.8
42	XA	46	46	49	105	19	26	45.2	40.9	61.0	47.9
43	XC	46	43	44	105	19	25	45.2	36.2	57.3	52.1
44	XE	46	42	4	105	19	24	45.2	33.1	55.6	54.6
45	XG	46	39	11	105	19	34	44.2	28.7	53.4	60.0
46	XI	46	37	40	105	19	4	45.5	23.9	51.4	62.3
47	XK	46	35	6	105	19	23	44.1	19.1	49.4	67.0
48	XM	46	32	55	105	19	40	44.7	15.1	47.7	71.3
49	XO	46	30	42	105	19	51	44.5	11.0	45.8	76.1
50	XV	46	52	24	105	17	13	48.2	51.2	70.3	43.3
51	XX	46	50	6	105	18	21	46.7	46.9	66.2	44.9
52	XZ	46	47	50	105	17	43	47.5	42.7	63.9	48.0
53	XR	46	45	23	105	15	33	50.3	38.2	63.2	52.8
54	XO	46	43	15	105	16	52	48.3	33.2	59.3	54.8
55	XF	46	41	12	105	16	55	48.4	30.4	57.2	57.9
56	XH	46	38	14	105	16	39	48.7	25.0	54.7	62.8
57	XJ	46	36	23	105	16	19	49.1	21.5	53.6	66.4
58	XL	46	34	29	105	16	47	48.5	18.0	51.7	69.4
59	XN	46	31	59	105	16	37	48.7	13.4	50.5	74.6
60	XP	46	29	35	105	16	28	48.8	8.9	49.4	79.7
61	YW	46	51	0	105	13	36	52.9	48.6	71.9	47.4
62	YY	46	48	59	105	13	47	52.6	44.9	69.2	49.5
63	YA	46	46	32	105	13	53	52.4	40.3	66.1	52.4
64	YC	46	44	18	105	13	44	52.4	36.2	63.7	55.4
65	YE	46	42	11	105	13	40	52.7	32.3	61.8	58.5
66	YG	46	39	43	105	14	5	52.1	27.7	59.0	62.0
67	YI	46	36	53	105	13	14	53.1	22.6	57.6	67.1
68	YK	46	35	13	105	13	48	52.4	19.4	55.9	69.7
69	YM	46	32	45	105	14	14	51.7	14.8	53.8	74.0
70	YO	46	30	35	105	14	1	52.0	10.8	53.1	78.3
71	SV	46	57	26	105	10	58	56.3	51.3	76.2	47.7
72	SX	46	56	6	105	11	2	56.2	48.9	73.9	50.2
73	SZ	46	47	48	105	10	58	56.3	47.7	70.7	52.8
74	SR	46	45	33	105	11	5	56.1	38.5	68.0	55.5
75	SO	46	43	13	105	10	55	56.2	36.2	65.8	58.7
76	SF	46	40	47	105	10	52	56.3	29.7	63.7	62.2
77	SH	46	38	42	105	10	56	56.1	25.8	61.7	65.3
78	SJ	46	36	25	105	10	53	56.1	21.8	60.2	69.0
79	SL	46	34	12	105	10	53	56.1	17.5	58.8	72.7
80	SN	46	31	49	105	11	20	55.5	13.0	57.0	76.8
81	SP	46	29	35	105	10	50	56.1	8.9	56.8	81.0
A2	6W	46	51	16	105	R	R	60.0	49.1	77.5	50.7
A3	6Y	46	49	0	105	R	3	60.1	44.9	75.0	53.2
A4	A&	46	46	44	105	R	24	59.6	40.7	72.2	55.7
A5	6C	46	46	12	105	7	49	60.3	36.0	70.2	59.2
A6	6E	46	43	8	105	R	5	59.9	32.2	68.0	61.7
A7	6G	46	39	27	105	R	15	59.6	27.2	65.5	65.5
A8	6I	46	37	45	105	7	56	60.0	24.1	64.7	68.1
A9	6K	46	35	13	105	R	5	59.8	19.4	62.9	72.0
90	6M	46	32	58	105	R	12	59.6	15.2	61.5	75.7
91	6O	46	30	39	105	R	4	59.7	10.9	60.7	79.7
92	7X	46	50	12	105	5	R	63.9	47.1	79.4	53.6
93	7Z	46	47	51	105	5	11	63.8	42.8	76.8	56.1
94	7R	46	45	20	105	5	10	63.7	38.1	74.2	59.1
95	7O	46	43	25	105	5	22	63.6	34.6	72.2	61.4
96	7F	46	40	50	105	5	31	63.4	29.8	70.1	64.8
97	7H	46	38	31	105	5	19	63.6	25.5	68.3	68.1
98	7J	46	36	16	105	5	11	63.5	21.3	67.0	71.5
99	7L	46	34	5	105	5	14	63.6	17.3	65.7	74.7
100	7N	46	31	49	105	5	19	63.6	13.1	64.6	78.3
101	AA	46	46	47	105	1	41	68.3	60.8	79.6	59.1
102	AC	46	44	17	105	2	15	67.5	56.9	76.6	61.8
103	AE	46	41	54	105	2	20	67.4	51.7	74.9	64.8
104	AG	46	39	39	105	2	23	67.2	47.6	72.8	67.7
105	AI	46	37	37	105	2	8	67.5	43.8	71.6	70.6
106	AK	46	35	7	105	2	25	67.1	39.2	69.8	74.0
107	AO	46	63	14	104	59	24	71.2	34.3	79.0	66.3
108	9F	46	40	45	104	59	34	70.9	29.8	76.8	67.3
109	9H	46	38	32	104	59	34	70.8	25.5	75.3	70.2

NUMBER OF RAINGAGES 109

SWS NUMBER	HIPLEX LABEL	LATITUDE DEG	MIN	SEC	LONGITUDE DEG	MIN	SEC	EAST KM	NORTH KM	RANGE KM	AZIMUTH DEG
201	DR	46	45	57	105	31	29	29.6	39.2	49.1	37.1
202	HM	46	47	23	105	20	25	44.0	41.9	60.8	46.4
203	RS	46	46	42	105	18	4	47.0	40.6	62.1	49.2
206	ST	46	45	14	105	18	6	47.0	37.9	60.4	51.1
205	FH	46	45	17	105	16	31	49.0	38.0	62.0	52.2
206	AO	46	47	19	105	15	54	49.8	41.8	65.1	50.0
207	DT	46	46	32	105	15	8	50.8	40.3	64.8	51.8
208	LT	46	46	33	105	14	23	51.8	36.1	63.5	54.7
209	JP	46	46	18	105	12	30	52.2	30.9	67.3	53.6
210	JG	46	49	12	105	7	21	41.0	45.3	76.0	53.4

Table 100. HIPLEX gage and disdrometer locations and SWS numbers. Latitude and longitude of gages as well as distance from Miles City Radar are given. Disdrometers are numbered 201 through 210.

In this study, these problems were underscored by the large apparent discrepancy between the radar and the gage rainfall values: the radar consistently measured considerably less rain than the gages. This fact, noted by this study and several others, seems certain, but is also curious since the radar and gage rainfall measurement systems have been checked and rechecked, and no apparent error was ever detected. While the cause of this discrepancy was not located during the course of the study, it appears that, at least for the purposes of the type of rainfall analysis proposed herein, the discrepancy is of little consequence: the analysis method corrects for the bias in the radar measurements.

(2) Sources of Data. In the HIPLEX Montana experiment, 109 recording raingages were located in a 600 mi^2 area in the vicinity of Terry, Montana. The network is shown in Figure 15 and the gage locations are tabulated in Table 100. Also listed in Table 100 are the HIPLEX and Illinois State Water Survey (ISWS) gage numbers. (Renumbering of the gages facilitated ISWS gage chart digitization and subsequent gage data processing.) Gage charts were digitized using the ISWS digitizing machine and software to produce 5 minute rainfall amounts. This digitization involved measurement of the end points of the 7 days of data from each chart; unfolding of the full 7 days computationally; and, finally, dividing the data up into 5-minute segments. Data from these 5-minute segments compare well with HIPLEX-measured 15-minute rainfall amounts, provided that some adjustments are made to account for differences in the measuring techniques.

The data from the HIPLEX Montana radar were recorded originally at a density of 1 sample per 0.5 km in range and 1 degree in azimuth and elevation. Mean equivalent radar reflectivity factor values are provided at this density in BSCAN format.

Additional data were obtained from rain disdrometers operated by the Illinois State Water Survey and located as shown in Figure 16, and from the MRI aircraft.

(3) Data Processing. *(a) Technique.* The method of combining the gage and radar data is that of Brandes (1975) and was used by Wilson (1975, 1977). A flow diagram of the data processing is included in Figure 17. For a chosen time period, radar data are loaded into the program and converted into rainfall amounts using a climatologically appropriate ZR relation. (See Appendix A for a discussion of Z-R relations: $Z=417\ R^{1.35}$ is used for this study.)

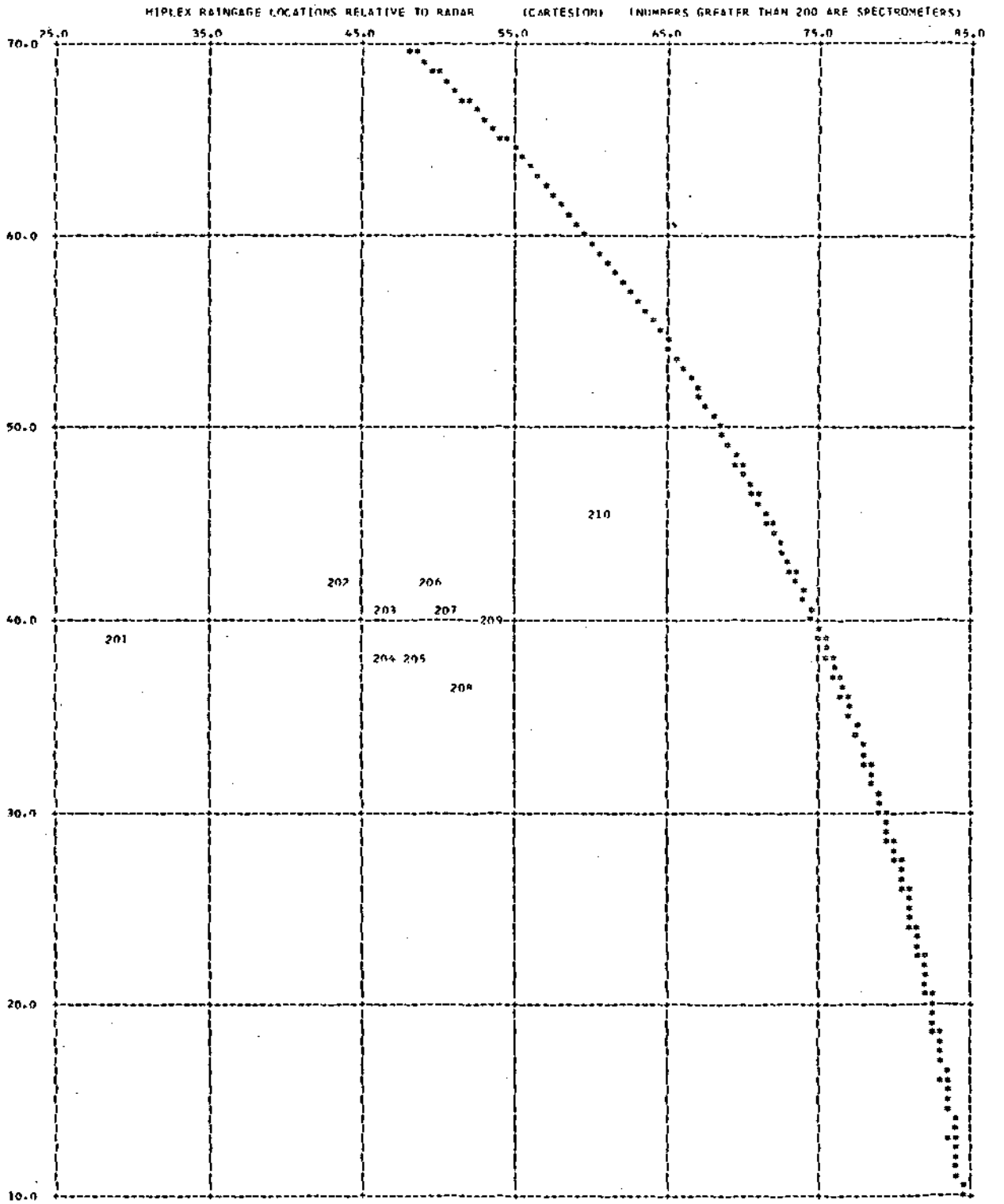

Figure 16. HIPLEX disdrometer locations relative to Miles City Radar.

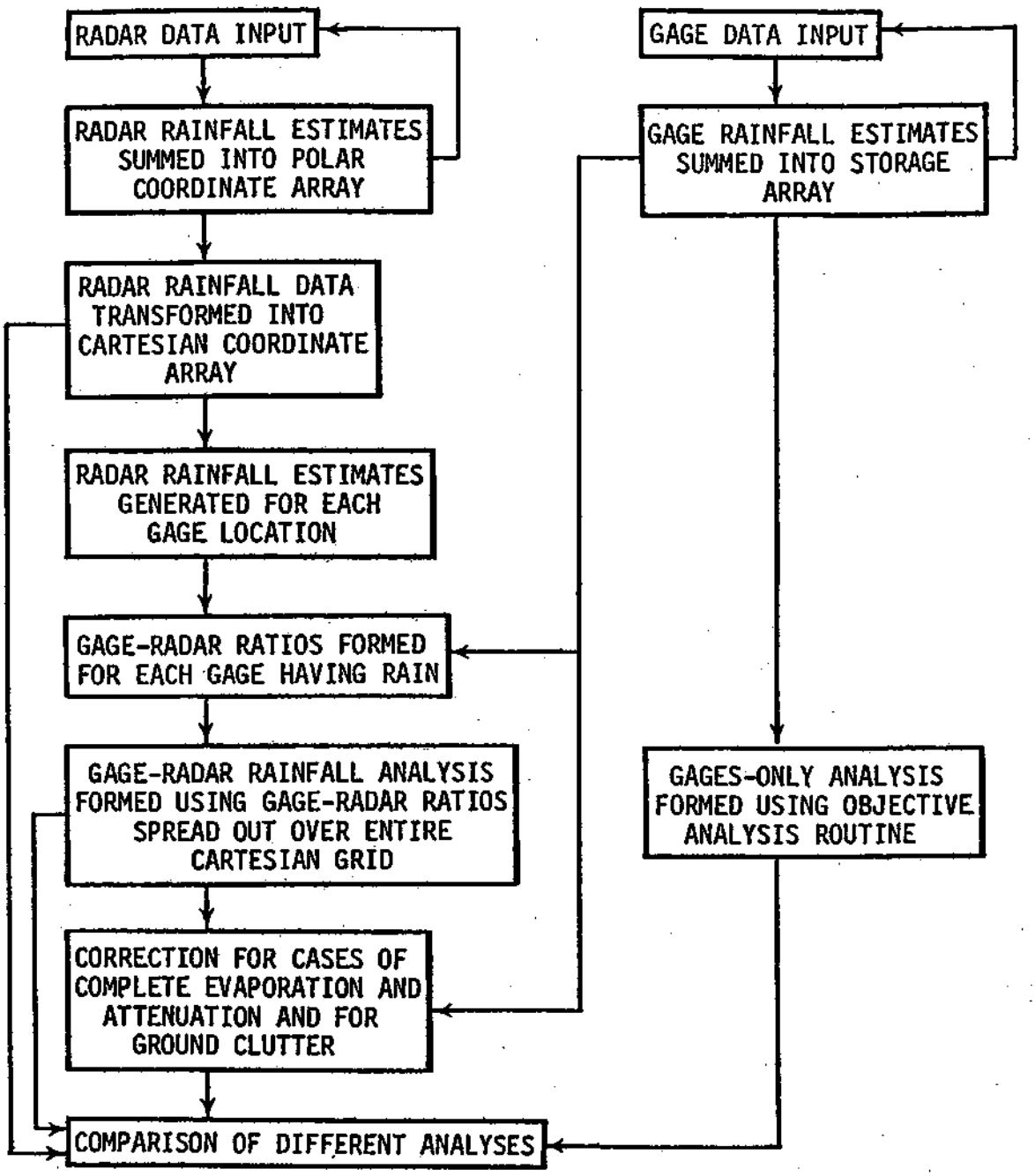

Figure 17. Flow diagram of gage-radar rainfall analysis program.

These rainfall amounts are summed into a polar radar rainfall array for the desired time interval. The time interval is adjusted for the time it takes the rain to fall from the radar observation level to the ground. In the case of this study, the radar data were obtained at 1° radar elevation angle and about 60 km range. If the median drop fallspeed is assumed to be 4 m/s, then the time adjustment should be about 4 mintues. Use of a 4 minute time adjustment was found to be slightly more accurate (in comparison with gage only rainfall amounts) than no time adjustment, and considerably better than other (presumably incorrect) adjustments.

When all radar data for the time interval are collected, the data are transformed onto a cartesian grid with 0.5 km spacing (Figure 18). This transformation is done using a weighted average of the four polar grid points surrounding each cartesian grid point. Selection of the weighting function is discussed below in section 3c.

The polar-to-cartesian conversion can be adjusted to account for advection of the rain between the time of radar observation and the time it hits the ground; however, tests of the effects of advecting the radar data showed that in convective situations, this was not advisable. In convective rain it is likely that the precipitation is moving as much as 90 degrees away from the ambient winds in the lowest levels. This likely difference explains the poor response to advection in our tests. Therefore, no correction for advection was made.

Once the cartesian radar analysis is completed and the gage data are loaded, gage-radar ratio values, $E_i = G_i/R_i$, are calculated for each gage. The radar estimates of rainfall at each gage location are calculated using an inverse linear distance-weighted average of the cartesian radar rainfall values within an adjustable radius of the gage location. The magnitude of the E_i values primarily takes into account the effects of radar calibration error, errors in the assumed Z-R relation, evaporation and attenuation. Calculational errors as well as advection and time offset errors should primarily increase the variability of the E_i values. Consequently, it is important to consider variations in both E and ΣE when adjusting the variables in this type of analysis.

The E_i values are then used as input data for an objective analysis scheme which uses a Gaussian weighting as suggested by Barnes (1964) and used by both Brandes and Wilson. (It should be noted that there is little or any physical basis for this Gaussian weighting.) The weighting at any grid point is taken to be

$$W_i = \exp(-X^2/RE) \qquad (26)$$

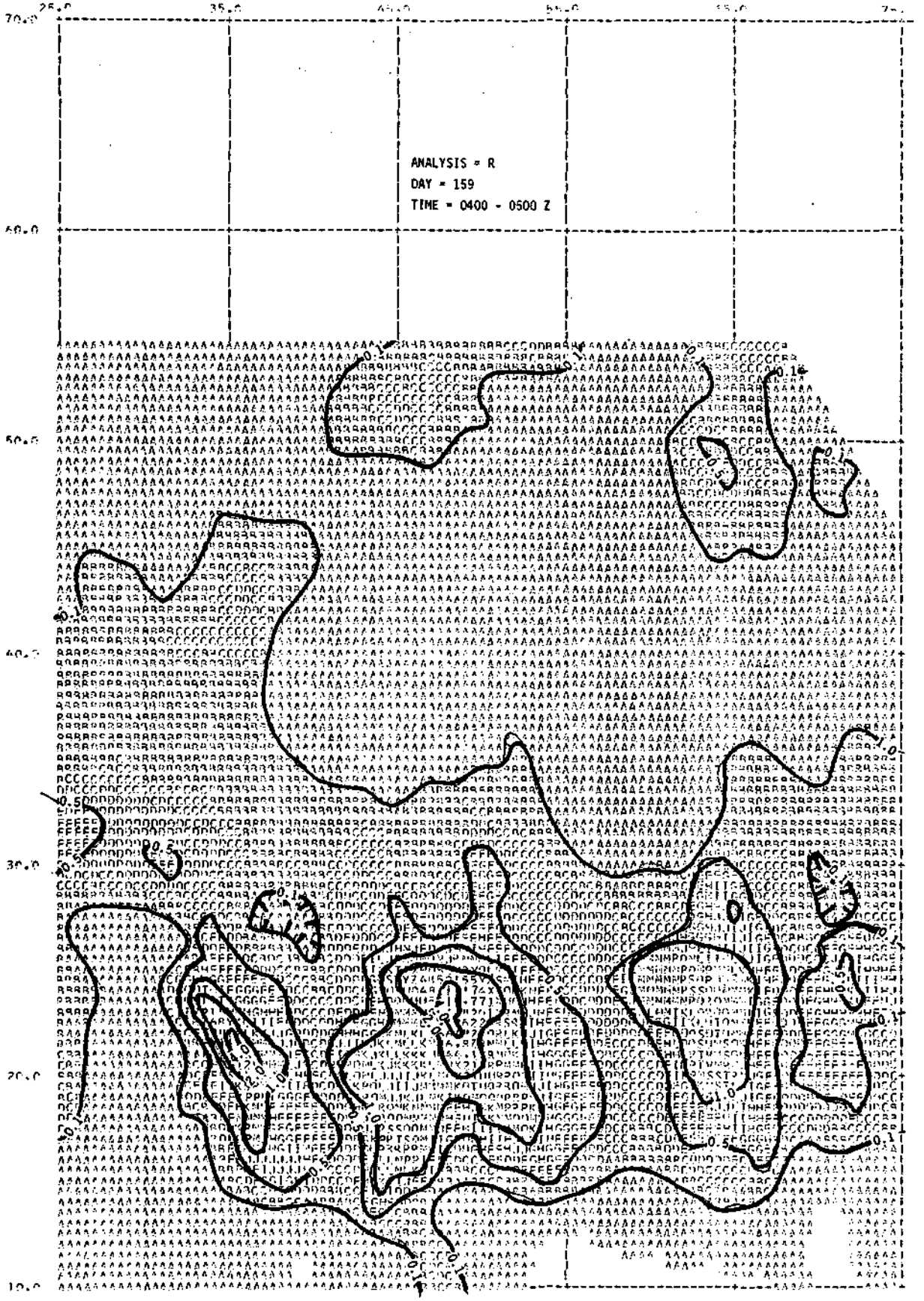

Figure 18. Radar rainfall analysis for day 159 and the one hour period 0400 through 0500 Z. Rainfall amounts in mm.

where X is the distance from a data point under consideration, and RE is a variable weighting factor. The values of X^2/RE were limited to being ≤ 12, thus insuring that $W_i > 10^{-5}$. In consideration of the large amount of data, this seemed to be a reasonable limit.

The value of RE was calculated on the basis of number of gages. (A maximum of 108 gages were in operation over the 1700 km^2 area network.) If the area around each gage is circular in form, then that area would have a radius of

$$R = (1700\ km^2/\pi\ NG)^{1/2} \qquad (27)$$

where NG is the number of gages. This, with the limit on the value of X^2/RE, gives $RE \geq X^2/12$. If the radius, R, is equal to X, then the minimum value of RE is

$$RE = 1700/12\ \pi\ NG. \qquad (28)$$

This proved to be a good radius for the second (fine scale) pass of the objective analysis routine. For the first pass, a value ten time larger was used. While this technique proved to be reliable in this study, we were able to fairly accurately assume that the gages were evenly distributed. Were that not true, larger values of RE would have to be used.

The results of this objective analysis consist of an array of E values (gage-radar ratios) for each grid point which, when multiplied by the radar rainfall amounts, will equal the gage rainfall amounts at the gage locations, and will provide some sort of calibration of the radar rainfall amounts between the gages. This analysis (illustrated in Figure 19 and hereafter referred to as GR') has the characteristic that it agrees with the gages at the gage locations, while preserving the shape of the radar precipitation analysis between the gage locations.

A final analysis (GR) is calculated from the GR' analysis by correcting for cases of total evaporation or attenuation, and cases in which ground clutter obscures a portion of the analysis grid. This is done by searching for gage locations at which either the gage or the radar report precipitation, but not both. At such locations, the gages are assumed to be correct and the final analysis is set to the gage value within a certain radius of the gage. As before, the radius was calculated using Eqn. 27. The gage value was spread out over this large distance in order to enable complete forcing of the final GR analysis (Figure 20) to zero when neighboring gages indicated no rain and the radar indicated rain.

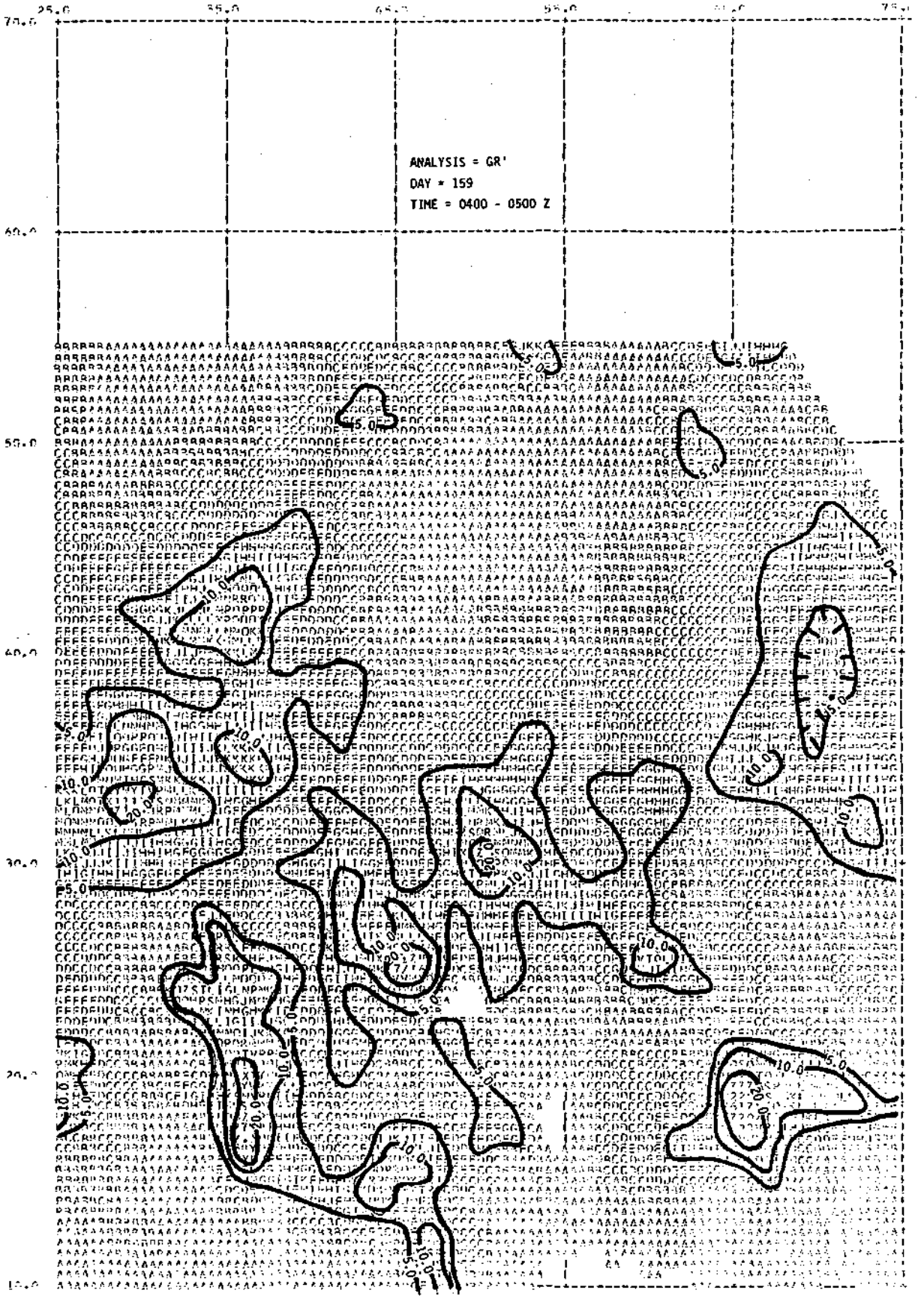

Figure 19. Gage adjusted radar rainfall analysis without evaporation correction for same period as in Figure 18.

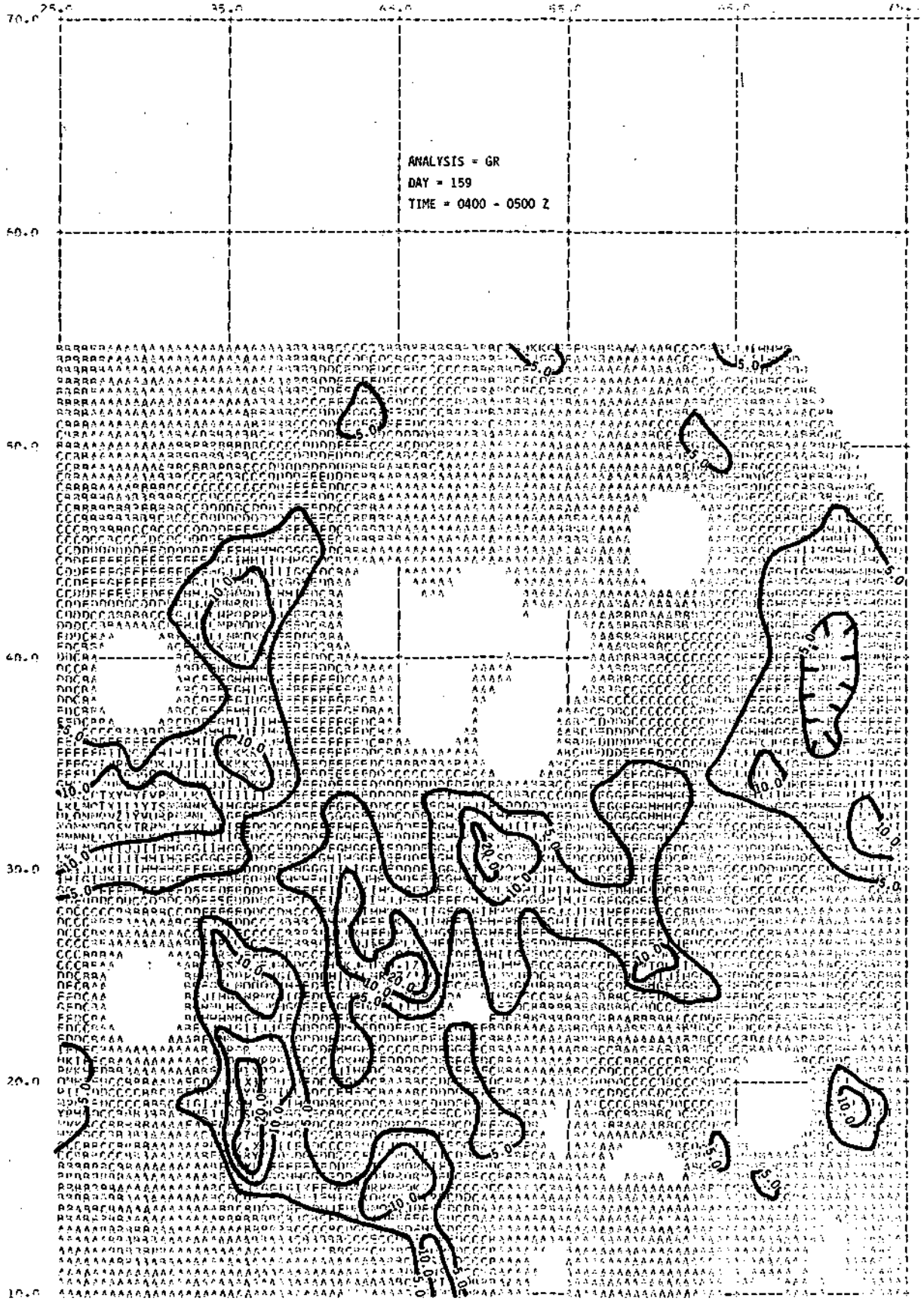

Figure 20. Gage adjusted radar rainfall analysis with evaporation correction for same period as in Figure 18.

The gages only (G) analysis (Figure 21) is produced using the same objective analysis routine and RE values as were used to spread the E_i values out over the entire grid. Summary information for each analysis includes values of $\bar{E}$, σE, and mean precipitation amounts for the radar (R), gage-radar ($\overline{GR}$) and gage-only ($\bar{G}$) analyses.

(b) Evaluation of rainfall estimates. The precipitation data processing program produces four estimates of the precipitation: R, GR', GR, and G. These analyses can be summarized by their mean values ($\bar{R}$, $\overline{GR'}$, $\overline{GR}$, and $\bar{G}$) and by their standard deviations. As pointed out in Section lb, the gage-produced mean areal rainfall amounts ($\bar{G}$ values) should be accurate for times as long as an hour or more. This suggests that the relative accuracy of the analyses can be determined through comparison of $\bar{R}$, $\overline{GR'}$, and $\overline{GR}$ with $\bar{G}$ for long time periods. Additional methods of comparing the analyses and of elucidating the qualities of GR versus G will be presented in section 4a.

(c) Adjustment of the data processing technique. The point that one hour values of G should be accurate provides the ability to adjust various parameters in the data processing program so as to minimize errors; that is, to make $\bar{R}$, $\overline{GR'}$, and $\overline{GR}$ as close as possible to $\bar{G}$ for long time periods. Accordingly, using a number of one hour data sets, the following analysis parameters were adjusted so as to minimize the difference between $\overline{GR}$ and $\bar{G}$:

1) advection
2) adjustment for fall time of precipitation
3) weighting function for polar to cartesian conversion
4) minimum acceptable rainfall amounts
5) radius used in calculation of gage-radar ratios

As mentioned in section 3a, these tests indicated that correction for advection was not advisable, and that adjustment for time of fall of the precipitation slightly improved the final $\overline{GR}$ accuracy. Tests of variables 3, 4, and 5 are summarized in Appendix C and are more concisely presented in Table 101.

i) Polar to cartesian conversion. The methods of weighting in the polar to cartesian conversion of the radar data included Gaussian, even and use of the maximum value. In all cases only the four radar bins closest to the cartesian grid point were used to determine the value at the grid point. Use of the maximum value was tested because of the suggestion that averaging in the presence of reflectivity gradients would produce underestimates of radar rainfall. As can be seen in the top section of Table 101, the even

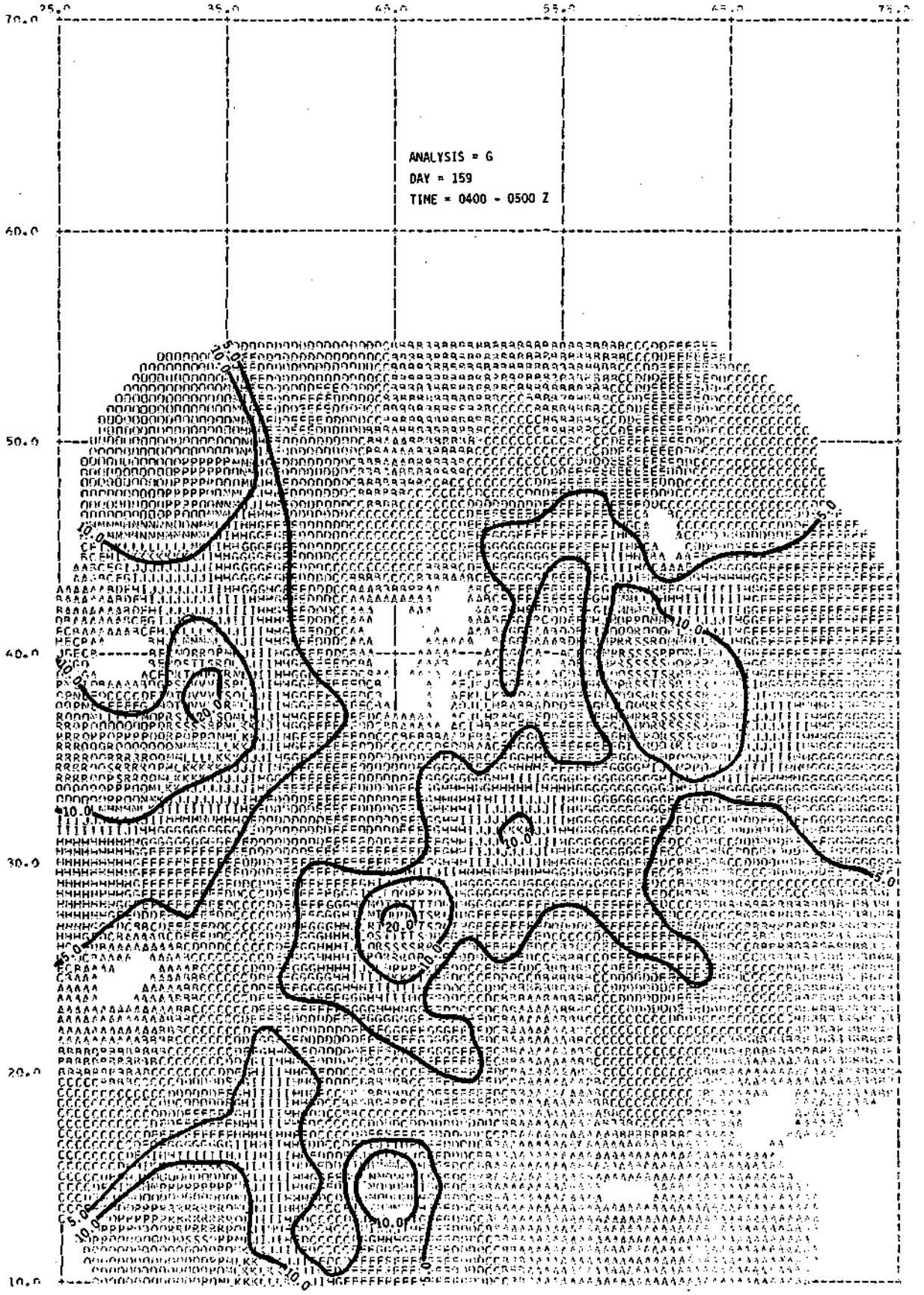

Figure 21. Gage rainfall analysis for same period as in Figure 18.

weighting was the best of the three tested, while the Gaussian was only slightly worse. It is not surprising to note that use of the maximum value in every case produces the smallest mean gage-radar ratio values (see Appendix B), but that it is also the worst method of converting from cartesian to polar coordinates.

Table 101. Percent error ([GRG]/$\bar{G}$)X 100 for analysis variable tests. Summarized from Appendix standard = Gaussian wt., radius = 1 km, R_{min} =0.1 mm.

		158 (0400)	158 (0500)	159 (0500)	mean value $\bar{x}$
weighting:	Gaussian	64	7	9	27
	even	18	5	5	9
	max	91	12	3	35
radius (km)	0.5	54	0	8	21
	1.0	64	7	9	27
	2.0	18	14	12	15
min. radar rainfall (mm)	0.10	64	7	9	27
		0.01	0	7	9
WT = even radius = 1.0 R_{min} = 0.1		9	2	7	6

ii) Minimum aeeeptable radar rainfall amount. The minimum acceptable radar rainfall amount was tested using values of 0.01 and 0.10 mm. (The minimum acceptable gage rainfall amount was fixed at 0.10 mm.) Use of the 0.01 mm value allows the program to accept radar data in more marginal situations than does the larger minimum; however, it has the drawback that some large Ei values can be generated in the process. This was a problem for this experiment, because of the persistent radar underestimates of rainfall...large spurious E_i values can have a large effect on $\bar{E}$, which is used at locations where gages received no rain. Tests of the effects of the minimum radar rainfall value are summarized in Table 101, and only a slight difference exists between the two values. The larger value (0.1) gave slightly smaller $\bar{E}$

values and a slightly better (a few percent) agreement between the GR and G analyses. However, the smaller value produced better results for short time periods (5 to 15 minutes) since it allowed the program to accept more radar data. A compromise value of 0.02 mm was therefore used as the standard in subsequent data processing. This value was chosen on the basis of visual comparisons between the raw radar and gage data and the desire that the general precipitation boundaries for the two data types should be similar. It is likely that a preferable minimum value determination would be related to the duration of the analysis.

iii) Radius used in calculation of gage-radar ratios. In order to calculate gage-radar ratios at gage locations (E_i values), an average radar rainfall amount must be determined for the gage location. An inverse linear distance weighting was used: radar rainfall values were given full weighting at the gage location, zero weighting at some radius away from the gage and a linear weight in between. This weighting was used because previous investigators used it and because the polartocartesian considerations suggested it would not be too far from being correct. It is important to note, however, that this weighting does not have any relation to the distribution of rainfall and hence cannot be considered optimal.

The maximum radius was tested for radii of 0.5, 1.0, 2.0 and 5.0 km, and for each test $\overline{GR}$ was compared with $\overline{G}$. The results of these tests indicated that radii of 1 and 2 km seemed best, that 0.5 was slightly worse, and that 5 km was considerably worse than the other three. (Values for 0.5, 1.0 and 2.0 km only are shown in Table 101.) This test suggests that a grid spacing of 1 km could probably have been used, because the precipitation generally appears to have maximum variability on scales larger than 0.5 km.

(4) Analysis of the gage-radar rainfall estimates. (a) The hypothesis. The basic hypothesis upon which the gage-radar rainfall technique has been developed is that the combination of the gages and the radar should provide a rainfall estimate with the point accuracy of the gages and the spacial resolution of the radar. The gages accurately measure rainfall at isolated points and the radar accurately (it is hoped) measures variations in rainfall. Thus, the gage + radar analysis should be comparable to a gage-only rainfall analysis of much higher density.

This hypothesis suggests three characteristics which can be tested:

1) For long times, the GR and G analyses should be equal (on the average) to within the accuracy of the gage-only analysis. If this is not true, then Huff's results and the veracity of the analysis must be questioned.

2) Decreased gage density should degrade the GR analysis less than the G analysis. This test is the central test of the gage radar rainfall analysis technique. If this test fails, then the technique clearly is not productive.

3) If the technique is successful, then rainfall analyses from short time intervals should be moderately accurate. This can be tested by summing consecutive short duration analyses and comparing the sums with longer duration analyses.

(b) Comparison of GR and G analyses. For each of the nine hours of data used in the study, the $\overline{R}$, $\overline{GR'}$, $\overline{GR}$, and G values are listed in Table 102 along with the percent differences between $\overline{G}$ and the other three means. A comparison of the $\overline{GR}$ and $\overline{G}$ values and the percent differences between $\overline{GR}$ and $\overline{G}$ indicates that the two analyses agree fairly well, considering the likely errors in G (gage sampling problems) and in GR (numerical errors). (It should be noted that three interpolations or objective analyses are performed in the course of operating the data analysis program.) Therefore, although the mean difference of 16% is a little larger than is desirable, it is acceptable on the basis of preconceptions.

The substantial increase in accuracy between the GR' and the GR analyses illustrates the large effect which evaporation plays on precipitation in the Montana climate. The only difference between the GR' and GR analyses is the correction for total evaporation, attenuation or ground clutter. As described in Section 3a, this evaporation correction routine was fairly crude and it is likely that further effort in this area could noticeably improve the accuracy of the final GR analysis. The importance of this correction for evaporation is made obvious for the Montana climate by the consistent overestimates of precipitation in the GR' analyses.

Table 102. Comparison of $\overline{R}$, $\overline{GR'}$, $\overline{GR}$, and $\overline{G}$ Values.

		Mean Areal Amount (mm)				% Differences		
Day	Time	$\overline{R}$	$\overline{GR'}$	$\overline{GR}$	$\overline{G}$	R	GR'	GR
158	0400	0.14	1.84	1.36	1.06	87	74	28
158	0500	1.05	6.15	4.41	4.27	75	44	3
159	0400	0.26	4.22	3.58	5.04	95	17	30
159	0500	0.53	14.47	12.55	13.28	96	9	5

Table 102 (continued)

Day	Time	$\bar{R}$	$\overline{GR'}$	$\overline{GR}$	$\bar{G}$	R	GR'	GR
184	1700	0.29	2.66	2.14	2.44	88	9	12
184	1800	0.54	5.86	3.99	3.75	86	56	6
184	1900	0.41	6.96	5.29	3.54	88	97	49
195	0200	0.18	0.74	0.59	0.65	72	14	9
201	0130	0.10	0.64	0.30	0.35	71	83	3
mean		-	-	-	-	84	45	16

The consistently large bias between R and G values shown in Table 102 convincingly illustrates the persistent difference between the radar and gage rainfall values. Although disconcerting and unexplained, considerations presented in the following paragraph suggest the discrepancy may be well-handled by the analysis routine.

The capabilities of the analysis routine to handle radar calibration errors and other errors were tested in two ways. First, an hour of radar data were selected and some test gage data which exactly agreed with the radar data at the test gage locations were generated. Parallel runs were made in which the radar data were multiplied by various constant factors. These runs resulted in full incorporation of the multiplier into the gage-radar ratio. In all cases, the final analyses remained completely unchanged. Second, naturally generated errors in the radar data were provided through making parallel runs using 1° and 2° radar elevation angles in the separate runs. Here, the radar data were altered by the processes of evaporation, advection and the natural sorting of the precipitation while falling; however, the final GR analyses agreed well. These tests indicate the capabilities of the analysis technique to incorporate various errors in the gage-radar ratios and to produce fairly accurate rainfall analyses.

(c) Relation of gage density to analysis accuracy. As a test of the effects of gage density on analysis accuracy, 15 and 60 minute rainfall analyses were run for gage densities including full density (1 gage per 15.5 km^2) and 1/2, 1/4, 1/8 and 1/16 of full density. For the 60 minute analyses, 1/30 density was also tested and parallel runs were made using 0.02 and 0.10 mm minimum radar rainfall amounts. The results of these tests are summarized in Table 103 and in Appendix C, where the mean areal rainfall amounts for the various gage densities are verified against amounts for the corresponding full density analyses. Thus, the reduced density G analyses were verified against full density

G analyses, and GR analyses were verified against GR analyses. This means of verification was used, since there is no way of knowing a priori whether the full density G or GR rainfall estimates are correct. Thus, there is no clear means of choosing whether to verify against the G or GR analyses. The 15 minute data are verified on a 15 minute basis; 60 minute data are verified on a 60 minute basis.

These data show the expected increase of analysis accuracy with increasing gage density; however, they also show the unexpected result that, *on the average, the G analysis appears to be better than the GR analysis*. This result is contrary to the expectation upon which the gage-radar analysis technique is based. The parallel 60 minute runs show the enhancement of GR analysis accuracy produced using a larger minimum radar rainfall.

Table 103. Percent error in G and GR rainfall analyses for different gage densities and analysis durations.

Gage Density Fraction Of Full Density	Gages km^2	15 min Analyses G	15 min Analyses GR	60 min analyses R_{min}=0.02 G	60 min analyses R_{min}=0.02 GR	60 min analyses R_{min}=0.10 G	60 min analyses R_{min}=0.10 GR
1	1/15.5	-	-	-	-	-	-
1/2	1/31	19	25	9	16	9	11
1/4	1/62	27	52	18	26	8	17
1/8	1/124	57	57	32	60	29	22
1/16	1/248	47	89	51	75	47	61
1/30	1/465	-	-	52	57	48	50

(d) Relation of analysis duration and accuracy. For each of the 9 hours of data used in this study, parallel runs were made using analysis durations of 5, 15, 30 and 60 minutes and full gage density. While for the gage-only data, the summation of short period analyses should clearly give the results of a longer period analysis plus some analysis error, this should not be the case for the GR analysis. Presumably, although they add up, the G analyses should be progressively less accurate for short durations. On the other hand, if the gage-radar technique works, the GR analyses should sample short durations better than the G analyses due to better sampling. To test this, the sum of

short duration GR analyses are compared with longer duration GR analyses. If these summations compare well with the longer term values, then we can have some confidence in assuming the GR analyses are improved over the G analyses for these short periods. Note that this is not a sufficient condition to prove any short duration superiority for the GR analyses.

The GR rainfall amounts (summed over the hour) are compared with the one hour GR amounts in Table 104 (and Appendix E), where percent error values for 5, 15 and 30 minute analyses are presented. These data indicate only slight degradation of the analyses in going from 60 to 30 minute periods, but that a larger degradation occurs for shorter durations.

Table 104. Effects of analysis duration for full gage density.

		Analysis Duration (minutes)				
Day	Time		5		15	30
158	0400	(15)	29		7	4
	0500	(16)	37	(30)	48	2
159	0400	(34)	45		39	33
	0500	(44)	49		27	13
184	1700		14		6	4
	1800	(8)	16		15	4
	1900	(21)	2		8	0
195	0200		2		3	2
201	0130		0		8	8
		(17)	22	(16)	18	8
		(15)				

The values in parentheses are derived using an adjustment for missing data. In the rainfall analysis program, cases with short period of missing radar or gage data were corrected for by multiplying the rainfall total for the analysis period by a factor which adjusted for the duration of missing rainfall assuming stationarity. For example, if 5 minutes of data were missing out of 60 then the rainfall totals for the 60 minute period were multiplied by 12/11, on the assumption

that this correction was preferable to no correction. The values in parentheses reflect a similar, rough correction which enhances the comparison of the results of different analysis durations. As can be seen from the mean values at the bottom of Table 104, this correction reduces the apparent errors in the 5 and 15 minute analyses, but does not produce a substantial change in the results. It is clear that while expedient, this sort of correction is not preferable, and that situations with missing data should be corrected either by elimination or through acquisition of the missing data.

In order to investigate whether this adjustment for missing data is introducing significant errors into the results, the data from 30 minute time periods with no missing data are tabulated in Table 105. There, the 5 and 15 minute analyses are compared with the GR and G analyses, with e_{GR} and e_G indicating percent difference between the 5 and 15 minute sums and the 30 minute $\overline{GR}$ and $\overline{G}$ values, respectively. The last column indicated the percent difference between the 30 minute analysis $\overline{GR}$ and $\overline{G}$ values.

These numbers indicate that, on the average, little error is introduced by shortening the analysis duration from 30 minutes to 15 or 5 minutes, and that the major uncertainty in the analyses lie in the basic differences between the GR and G analyses. This result is basically the same as that obtained from Table 104, and suggests that the method of handling missing data is not a significant source of error in the program. This was confirmed by recalculation of the percent error values for 15 minute data from the gage density study (Table 103). This recalculation, or inspection of Appendix D, indicates only slight changes in the percent error values for any of the tested gage densities and for either the G or the GR analysis.

Table 105. Effects of analysis duration. 5 and 15 minute GR analysis compared with 30 minute GR and G analyses, and 30 minute GR and G analyses compared.

Day	Time Interval	5			15			30		
		GR	e_{GR}	e_G	R	e_{GR}	e_G	GR	G	e
		(mm)	(%)	(%)	(mm)	(%)	(%)	(mm)	(mm)	(%)
158	0430-5000	0.92	30	6	1.34	2	37	1.32	0.98	35
158	0530-0600	1.46	15	30	1.20	6	7	1.27	1.12	13
159	0430-0500	1.47	12	60	1.16	11	69	1.31	3.69	64
159	0530-0600	2.17	32	45	2.83	11	28	3.19	3.95	19
184	1700-1730	1.03	14	27	1.06	12	25	1.20	1.41	15

Table 105 (continued)

Day	Time Interval	5 GR (mm)	5 e_{GR} (%)	5 e_G (%)	15 R (mm)	15 e_{GR} (%)	15 e_G (%)	30 GR (mm)	30 G (mm)	30 e (%)
184	1730-1800	0.81	6	21	0.95	10	8	0.86	1.03	17
184	1800-1830	2.07	10	15	1.70	26	6	2.29	1.80	27
184	1900-1930	3.80	4	61	3.90	7	65	3.65	2.36	55
195	0200-0230	0.31	0	6	0.30	3	9	0.31	0.33	6
195	0230-0300	0.29	4	9	0.28	0	13	0.28	0.32	13
201	0200-0230	0.22	12	8	0.25	0	4	0.25	0.24	4
	means	-	5	26	-	8	25	-	-	24

(5) Discussion of the results. **This investigation** of radar rainfall analyses has led to several conclusions:

1) For the conditions of this experiment, use of radar data does not appear to improve measurement of mean areal rainfall over what gages can provide alone. In general, the gage-radar (GR) analyses were slightly less accurate than the gage-only (G) analyses for the same gage density. This result is contrary to the hypotheses upon which the gage-radar rainfall estimation technique was developed. This result is also contrary to the findings of several other similar investigations which were performed in other climates. These investigations include those of Brandes (1975), Wilson (1975, 1977) and (Towery, 1977: Personal communcation concerning the results of an experiment in the Chicago area involving similar gage densities and analysis durations).

There are several possible explanations for the unexpected result of this research:

a) A primary source for the relatively low quality of the GR analyses is very likely the climatology of Montana, where low level dryness accentuates evaporation and makes the radar-only rainfall analyses moderately dissimilar to the gage-only patterns. (See Figures 18 and 21, and Appendix B.) This is not the case in more moist climates, where the radar rainfall patterns can be expected to be fairly accurate. In addition, the storms used in this study predominantly produced widespread precipitation, which the gages are likely to measure

fairly accurately. The widespread precipitation and extreme low-level evaporation both would be expected to degrade the ability of the radar to measure rainfall relative to the gage's ability.

b) An additional possible explanation for the unexpected result lies in analysis errors. There are a number of possibilities including the evaporation correction scheme, the distance weighting schemes used for the polar-to-cartesian conversion and calculation of the gage-radar ratios, and the selection of minimum rainfall amounts. The discussion at the end of Section 4d suggests that the handling of missing data is not a significant source of error. However, considering the magnitude of the correction for evaporation (that is, the improvement between the GR' and GR analyses), it is likely that additional efforts could be applied there quite profitably. Similarly, the substantial improvements in analysis quality produced by the tests of Section 3c suggests that these decisions are important. While these tests plus others considerably improved the final GR analysis quality, there is no reason to think perfection was achieved. It should be noted that three interpolations to analysis grids take place within the gage-radar analysis technique, and that variable, and possibly considerable, analysis errors occur with each interpolation. It therefore seems appropriate that future investigations in this subject should be carried out by persons specializing in objective analysis and not by radar meteorologists.

c) A final possible explanation for the poor quality of the GR analyses may lie in the unexplained persistent bias between the radar and the gage rainfall amounts. While the considerations presented at the end of Section 4b suggest that the gage-radar technique should handle various sorts of errors, this suggestion should continue to be considered until a more complete explanation is found.

2) Short duration analyses were found to be fairly accurate, and although the shorter duration analyses were less accurate than the long duration analyses, the inaccuracies did not appear to be large with respect to the effects of lowering gage density, or to the basic uncertainty in any rainfall analysis.

It is clear from the preceeding discussion that radar cannot be depended upon to produce substantial improvements in rainfall measurements; at least not by using the present

analysis for summertime rains in eastern Montana. It seems likely that the results could be different for climates with more isolated storms and less low level evaporation of the rain, but this will have to be tested in future projects.

There are several conclusions about use of radar in precipitation modification experiments which can be drawn from this research.

1) For measurements of hourly mean areal amounts, gage densities can be reduced to one gage per 30 to 60 km^2 without sacrificing too much measurement accuracy. The extent to which this reduction in gage density can be done is most likely related to a climatological storm size or rainfall footprint size. The basic requirement is that all areas of significantly different precipitation characteristics must be measured by a gage, whether or not a radar is used. These different "precipitation characteristics" include changes in dropsize distribution (hence Z-R relation), evaporation or attenuation.

2) For any gage density, the gage-radar rainfall analysis can be substituted for the gage-only analysis without markedly increasing areal mean rainfall measurement errors. Although not tested in this study, it can be expected that the rainfall pattern will be improved through use of the radar data. This is more likely to be true in moist climates than in Montana, but is probably valid there, also. This improvement in rainfall pattern description can be expected to help monitor changes in single cell precipitation rates.

3) There appears to be some promise for gage-radar measurement of short duration rainfall amounts. Sampling considerations suggest that gages alone do not accurately measure rainfall over periods as short as 5-15 min. However, the results of this investigation suggest only small decreases in mean areal rainfall measurement accuracy for these short periods. This capability can be expected to help in measurement of the effects of seeding single raincells.

(6) Appendices. (a) Appendix A: Z-R relations. The rain disdrometers were located as in Figure 2. Disdrometer data from three selected periods yield Z-R relations as indicated in Table 106, and Figure 22. These Z-R relations result from considerable averaging for data from all of the disdrometers (6 to 10 on any day), and many 5 minute samples were taken together to produce Figure 22. Some selected daily Z-R relations based on data from the MRI aircraft are

also shown in Table 106. These aircraft data indicate more scatter than the disdrometer data and, in general, lower values of the multiplier and higher values of the exponent of R. The increased scatter is expected, for the sampling time and volume of the aircraft particle probes is smaller than that of the disdrometers.

Differences between the aircraft and disdrometer Z-R relations should be due to differences in characteristics of the precipitation. The size distribution could have changed considerably through coalescence and evaporation between the aircraft and the ground. It is noteworthy that the variability between the Z-R relations is as large as the difference between the typical Z-R relation for the two instruments. This suggests that the day-to-day variations are large enough so that no Z-R relation can be expected to be exceptionally accurate for any given day. The MRI aircraft data from individual clouds show considerably more variability than do these daily values. These facts underscore the need for fine scale gage-calibration of the radar data, using a method such as the Brandes technique which will accommodate the inaccuracies of the Z-R relations.

For reasons summarized in a study of 5-cm radar attenuation (Hildebrand, 1977), use of Z-R relations derived from comparisons of gage and radar data is ill-advised; a thunderstorm relation appears the best for the HIPLEX Montana data. Consequently, the Selkan-Srivastava relation $Z=417\ R^{1.35}$ was used in this study.

Table 106. Z-R relations based on data from Water Survey ground-based dropsize disdrometers (D) and MRI aircraft (A) for selected dates and periods.

Date	Instrument	Z-R Relation
15-19 June	D	$500\ R^{1.41}$
19-22 June	D	$500\ R^{1.24}$
13 July	D	$600\ R^{1.34}$
13 July	A	$470\ R^{1.63}$
19 July	A	$500\ R^{1.40}$
20 July	A	$339\ R^{1.90}$
21 July	A	$562\ R^{1.38}$
22 July	A	$537\ R^{1.38}$

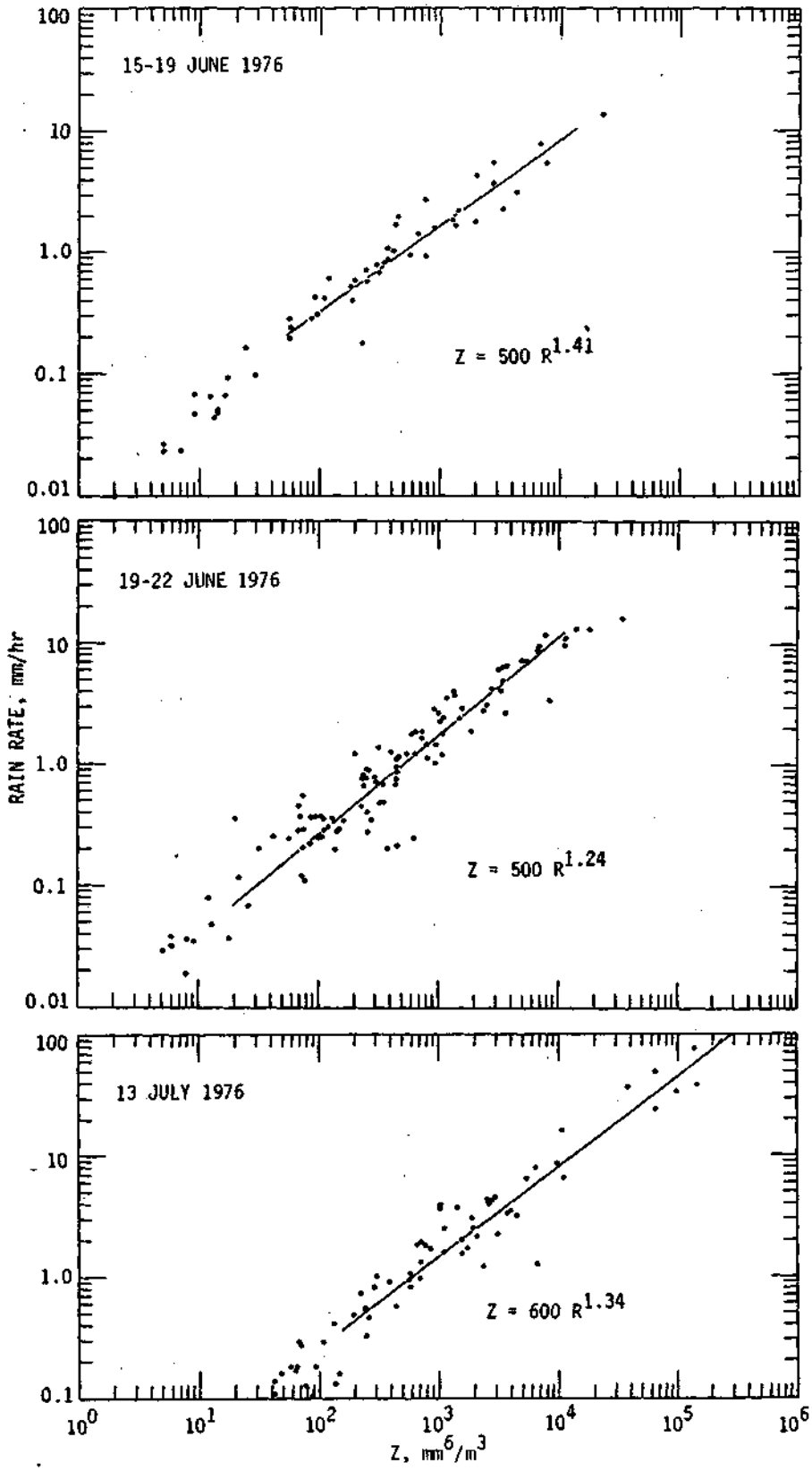

Figure 22. Z-R relations derived from SWS disdrometer network operated in the vicinity of Terry, Montana.

(b) Appendix B: Sample rainfall maps for three hourly analyses.

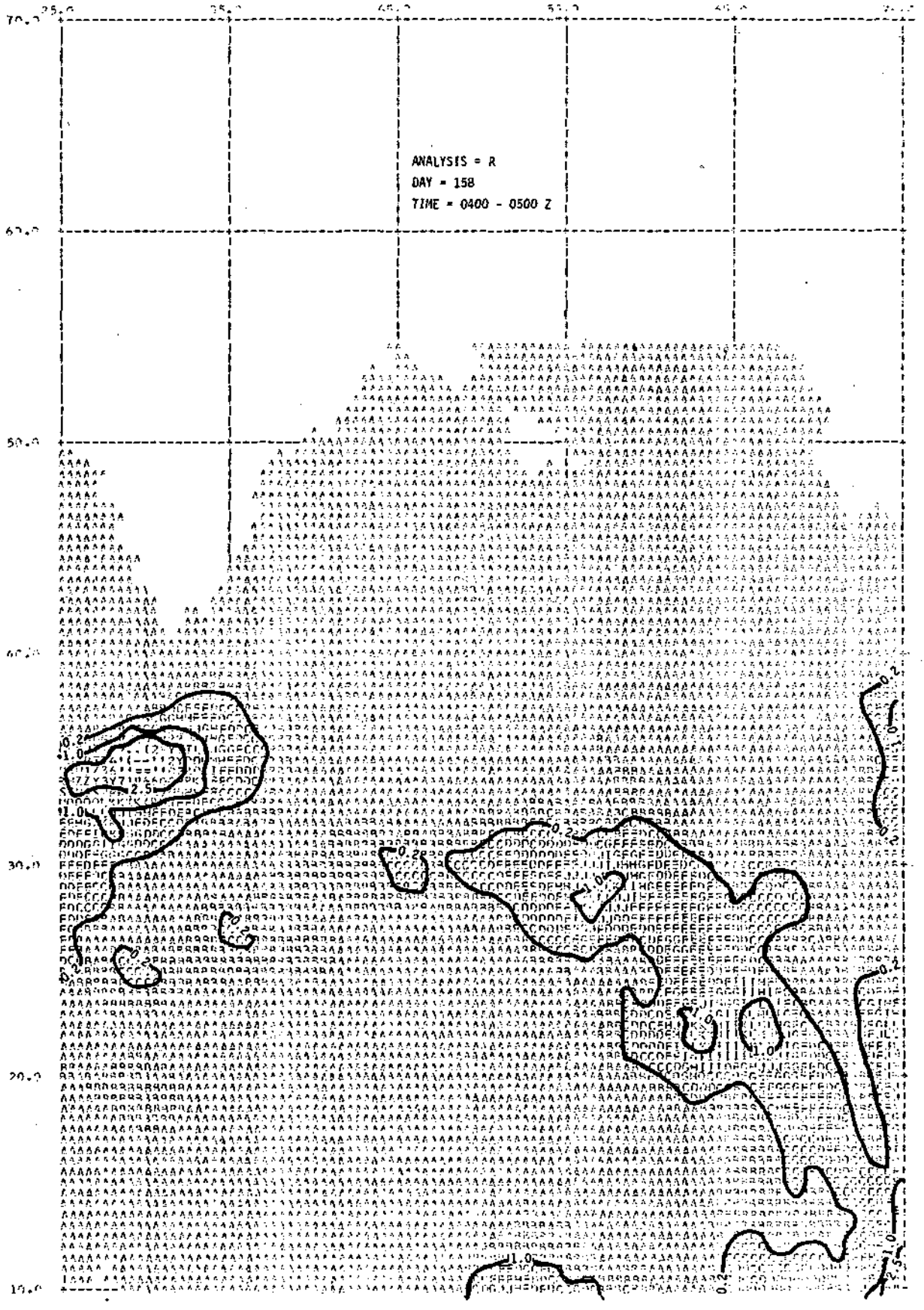

Figrure *23. Radar rainfall analysis, day 158, 0400-0500Z. Rainfall amounts in mm.*

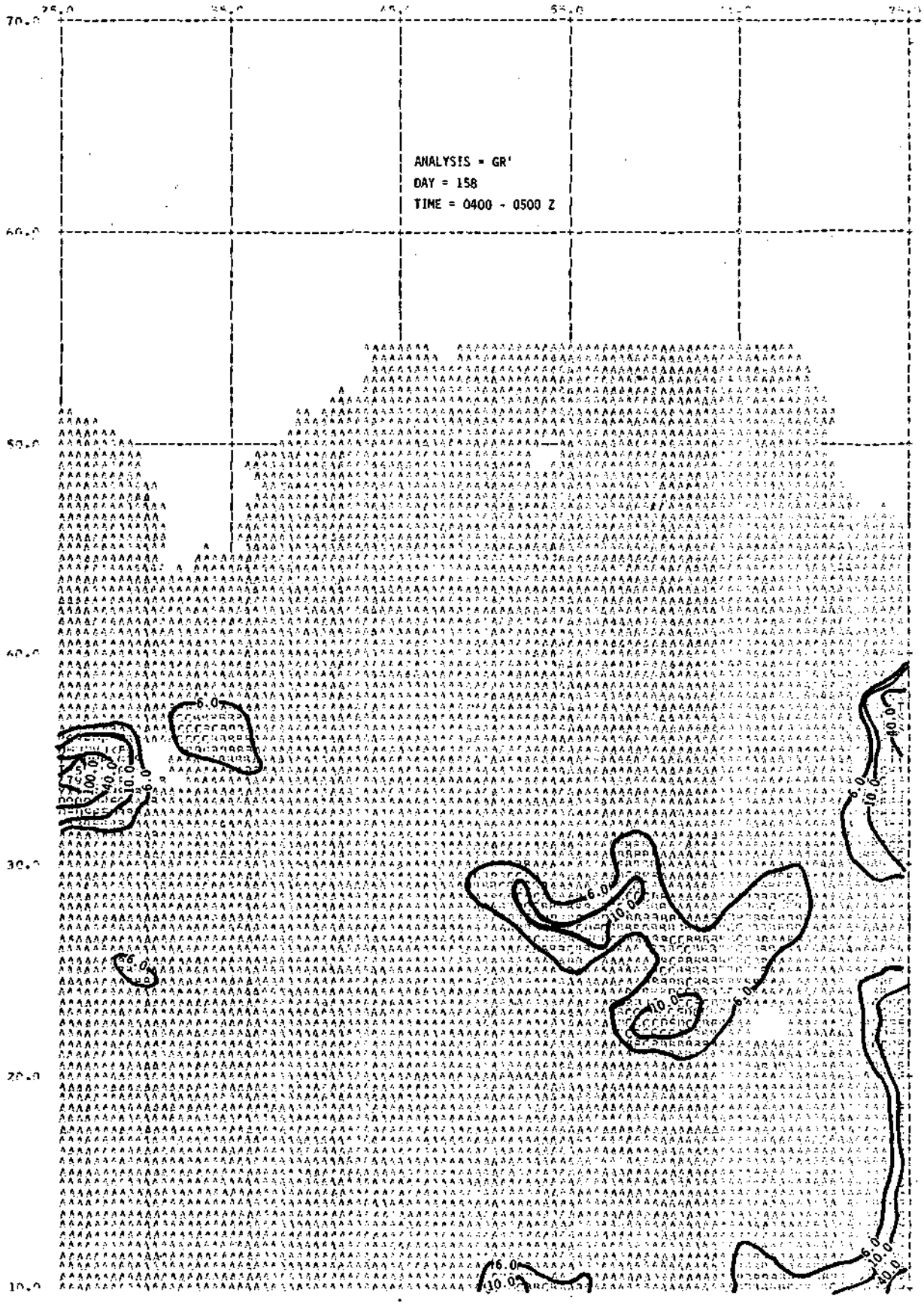

Figure 24. Gage adjusted radar rainfall analysis without evaporation correction for same periods as in Figure 23.

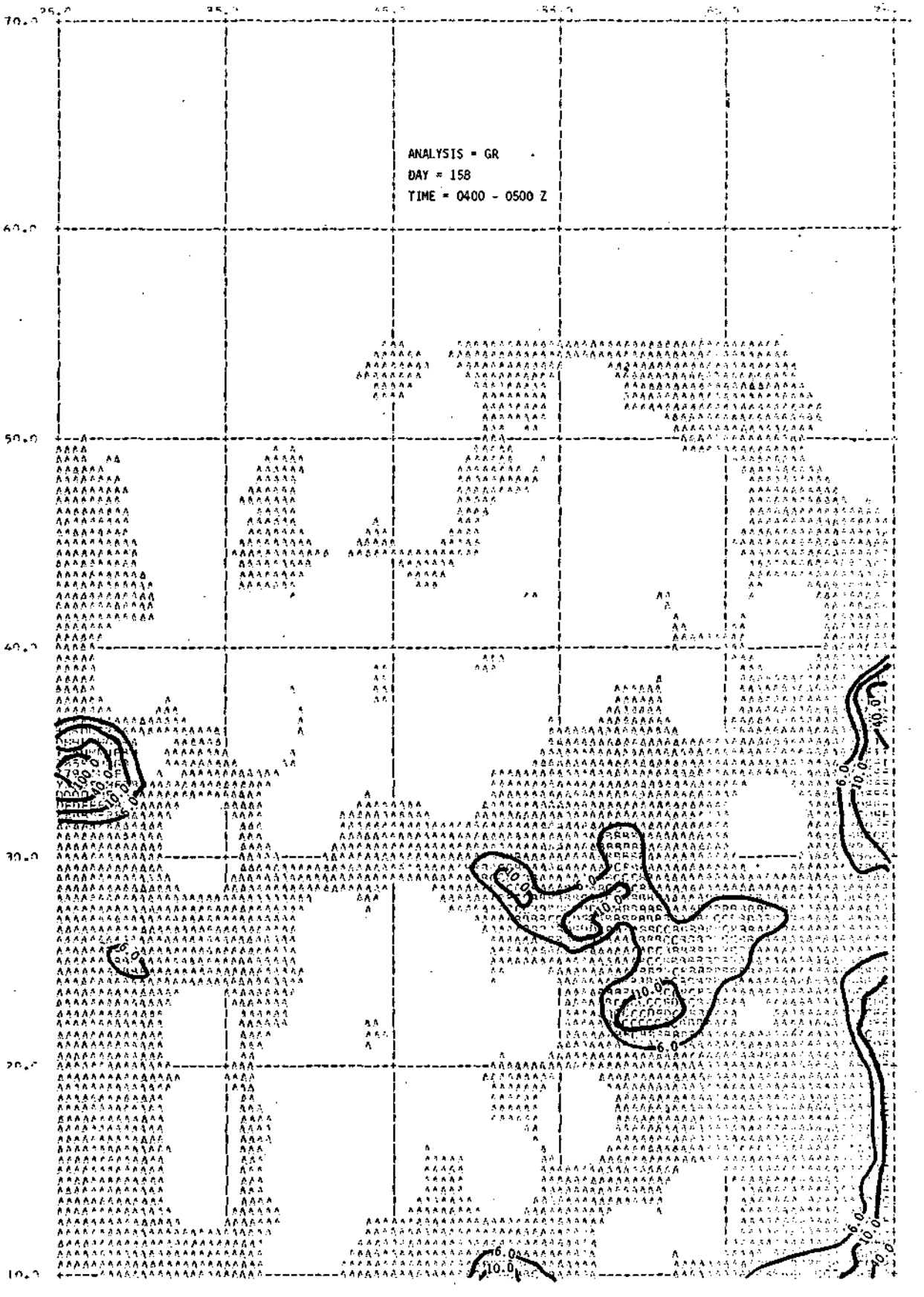

Figure 25. Gage adjusted radar rainfall analysis with evaporation correction for same period as in Figure 23.

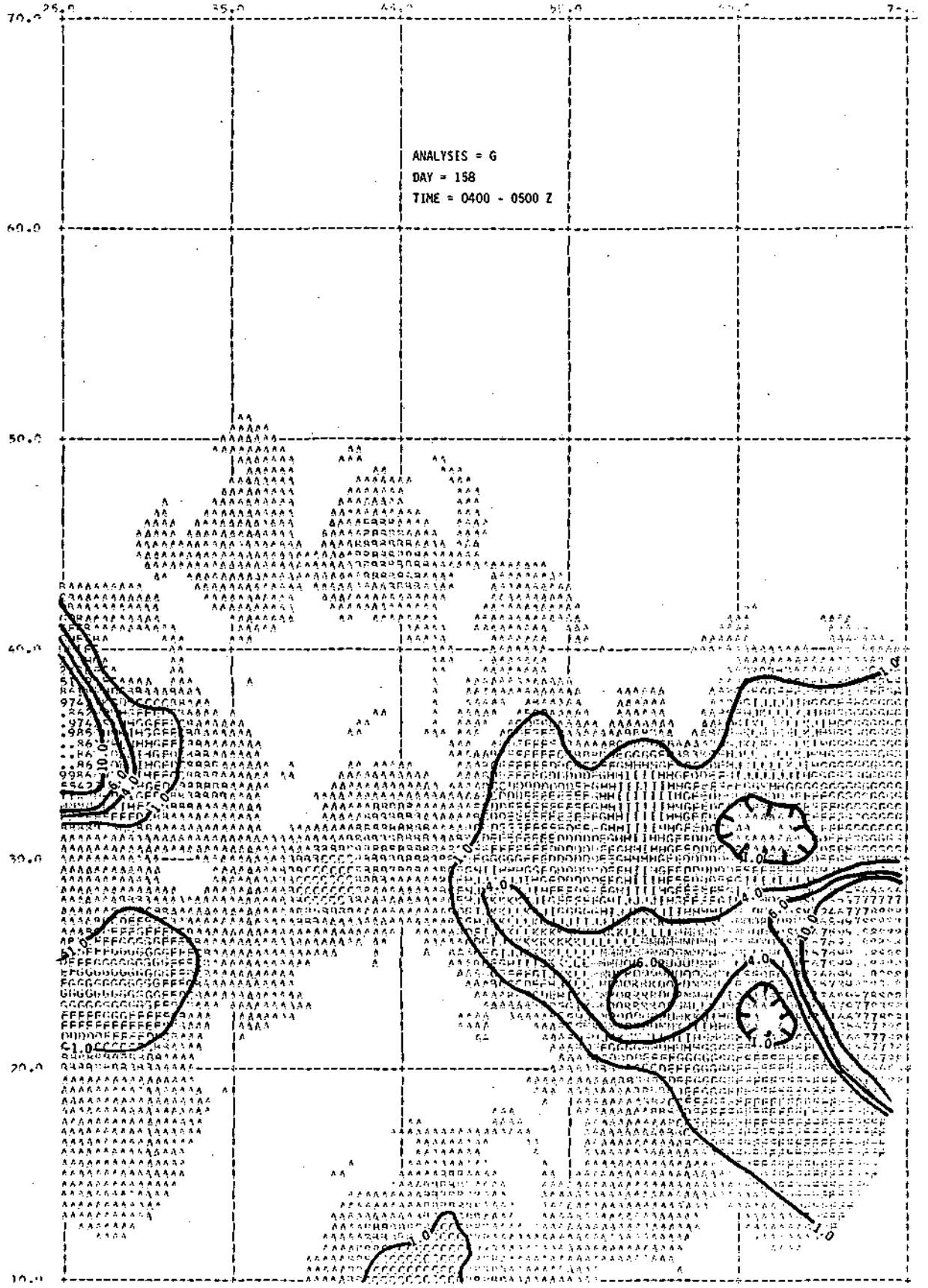

Figure 26. Gage rainfall analysis for same period as in Figure 23.

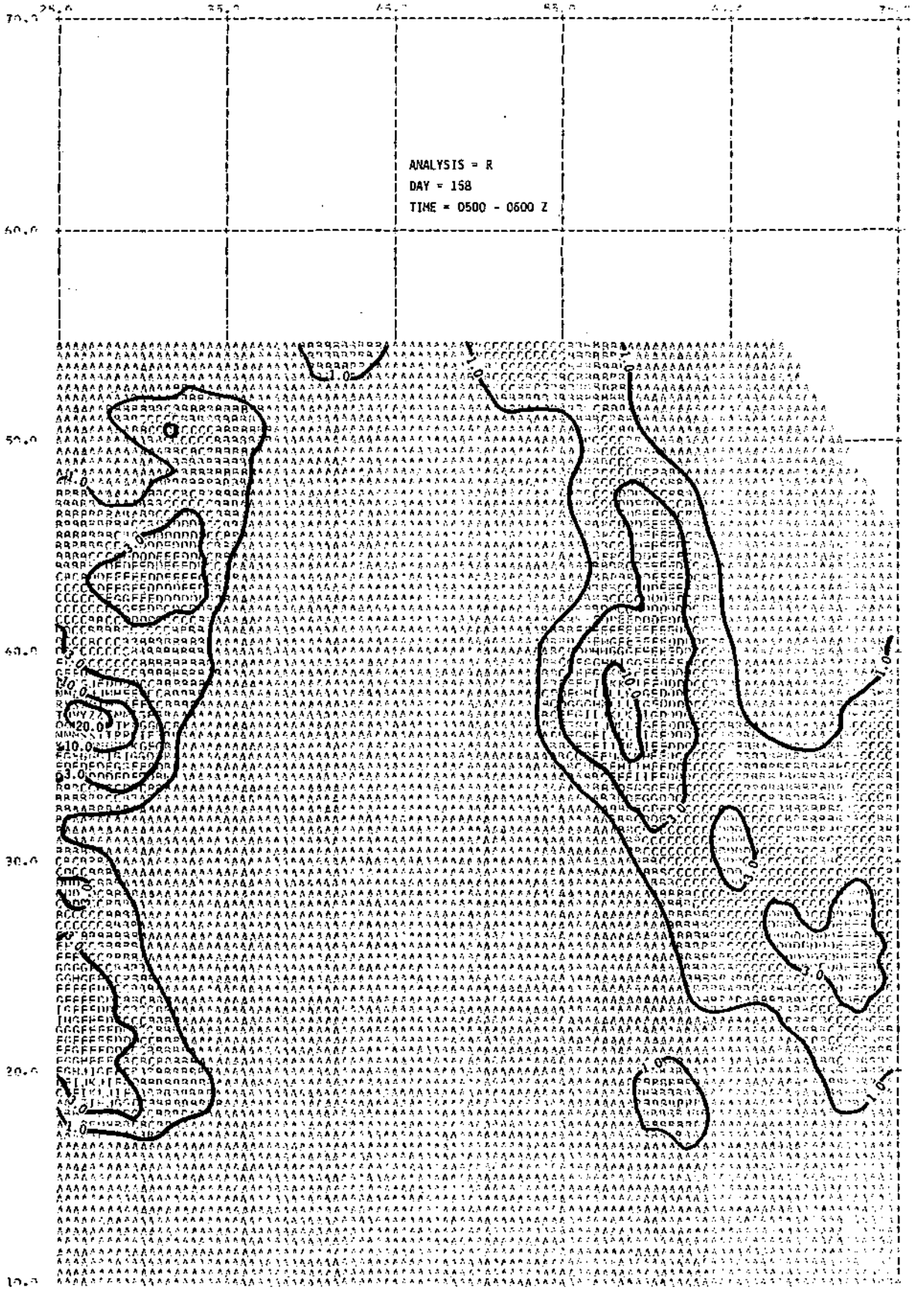

Figure 27. Radar rainfall analysis for day 158, 0500-06007,. Rainfall amounts in mm.

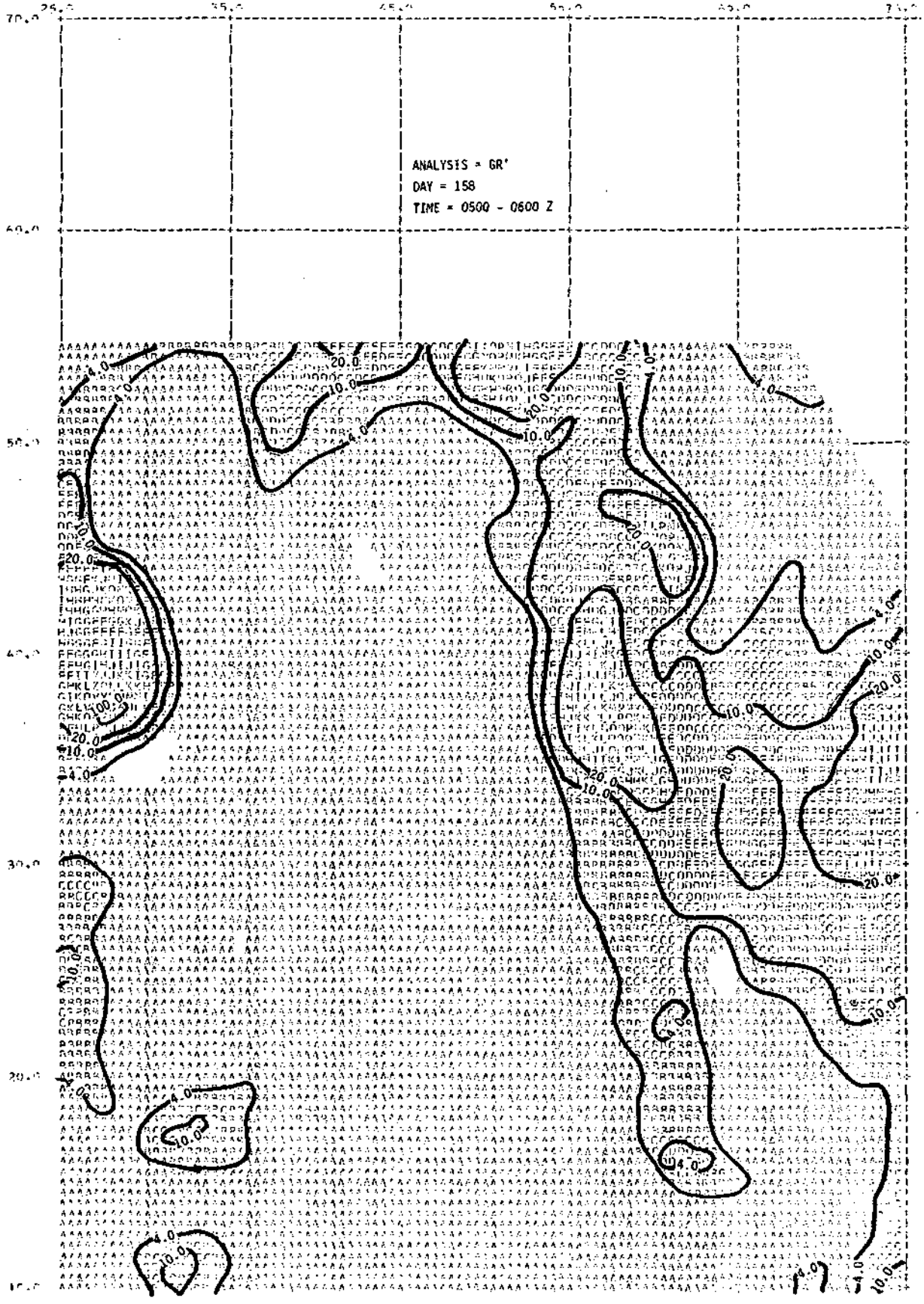

Figure 28. Gage adjusted radar rainfall analysis without evaporation correction for same period as in Figure 27.

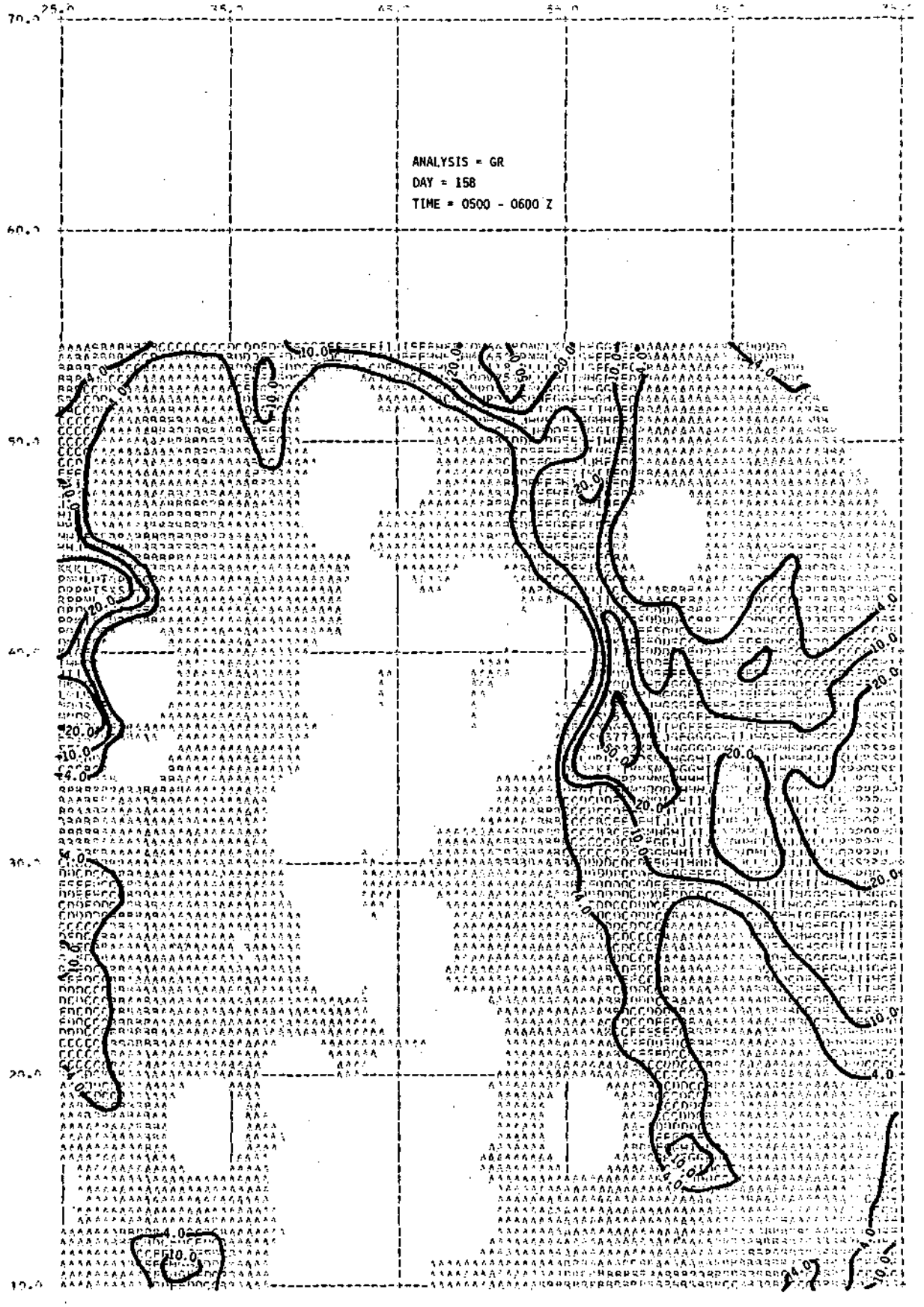

Figure 29. Gage adjusted radar rainfall analysis with evaporation correction for same period as in Figure 27.

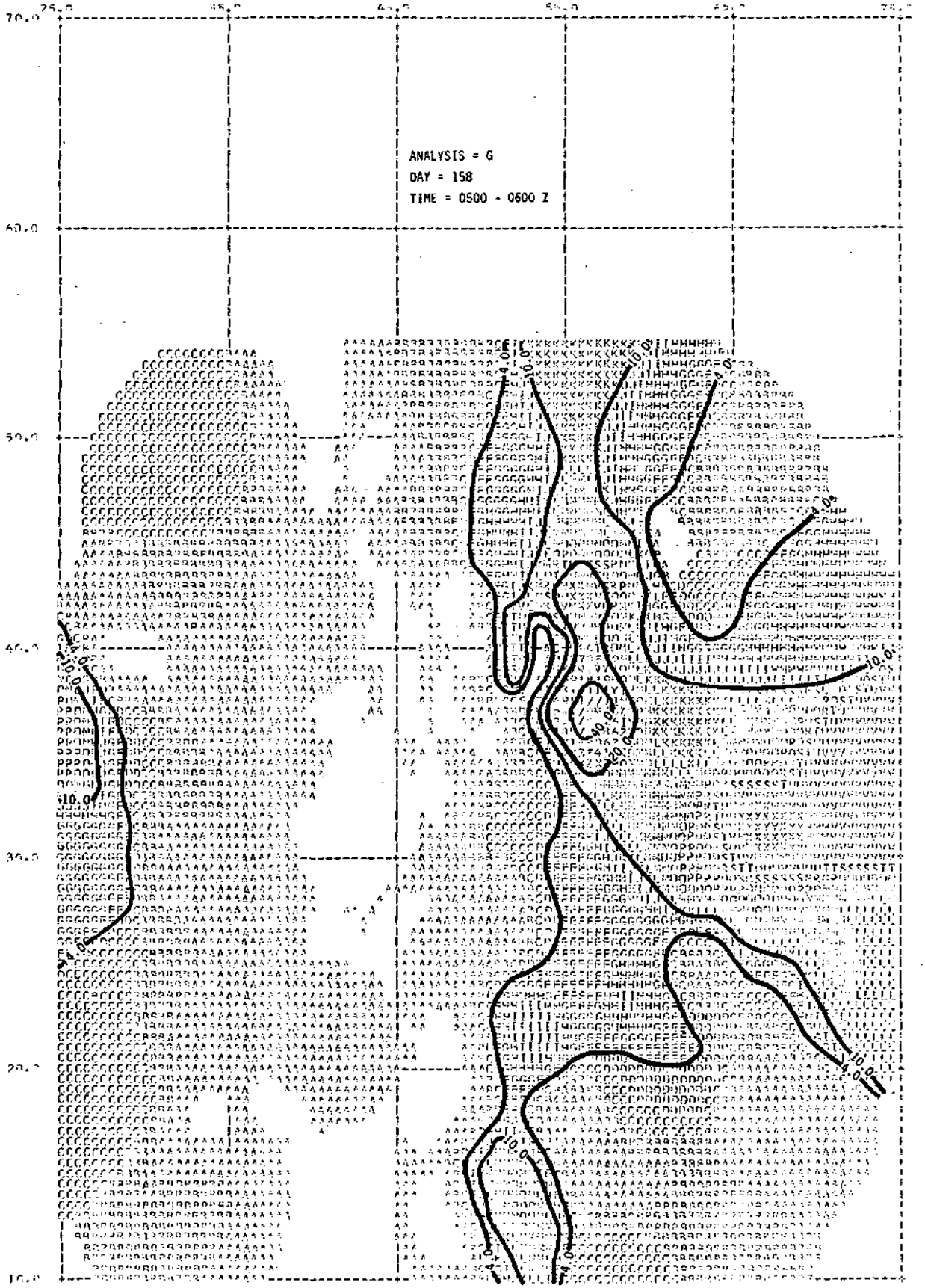

Figure 30. Gage rainfall analysis for same period as in Figure 27.

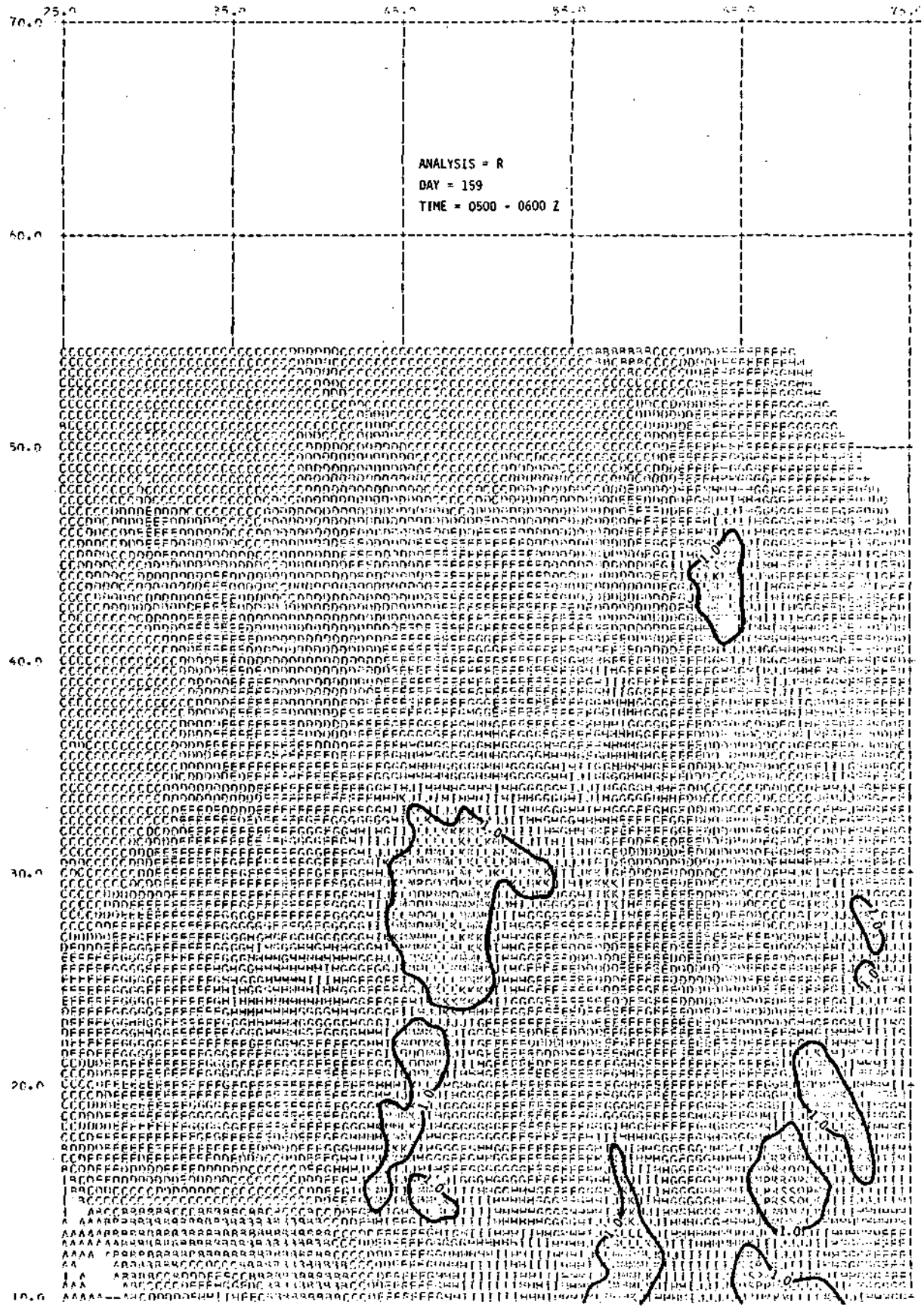

Figure 31. Radar rainfall analysis for day 159, 0500-0600Z. Rainfall amounts in mm.

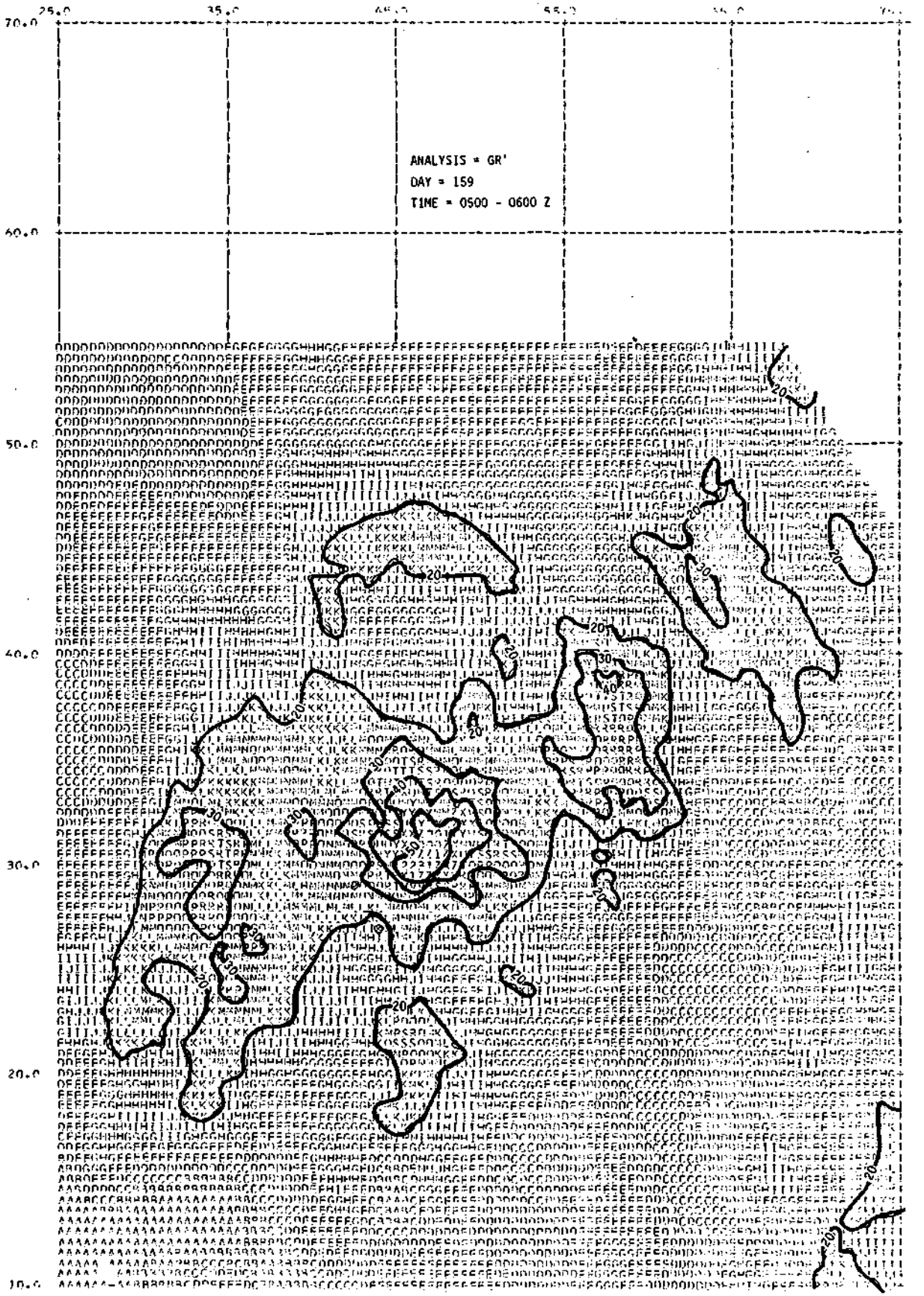

Figure 32. Gage adjusted radar rainfall analysis without evaporation correction for same period as in Figure 31.

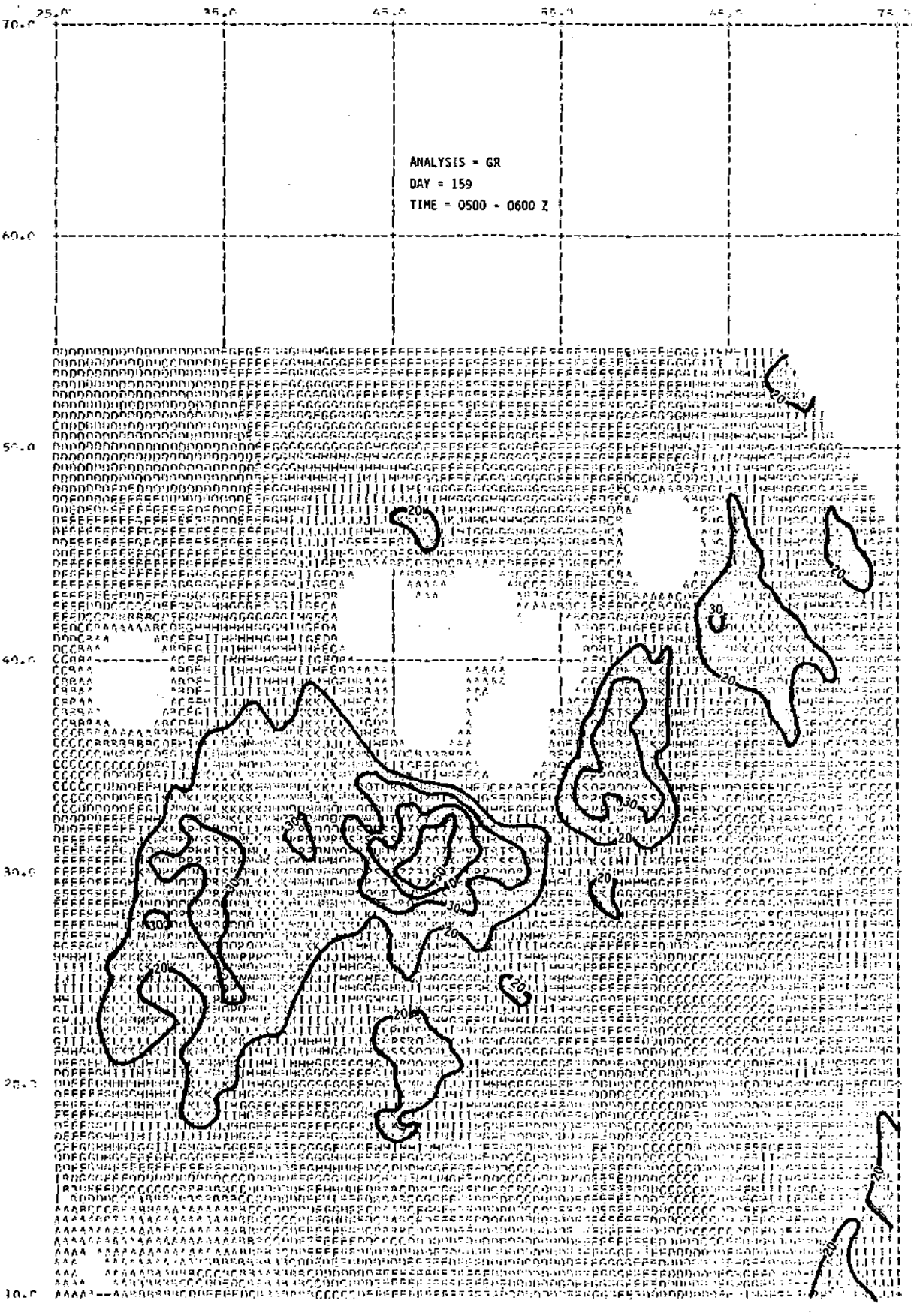

Figure 33. Gage adjusted radar rainfall analysis with evaporation correction for same period as in Figure 31.

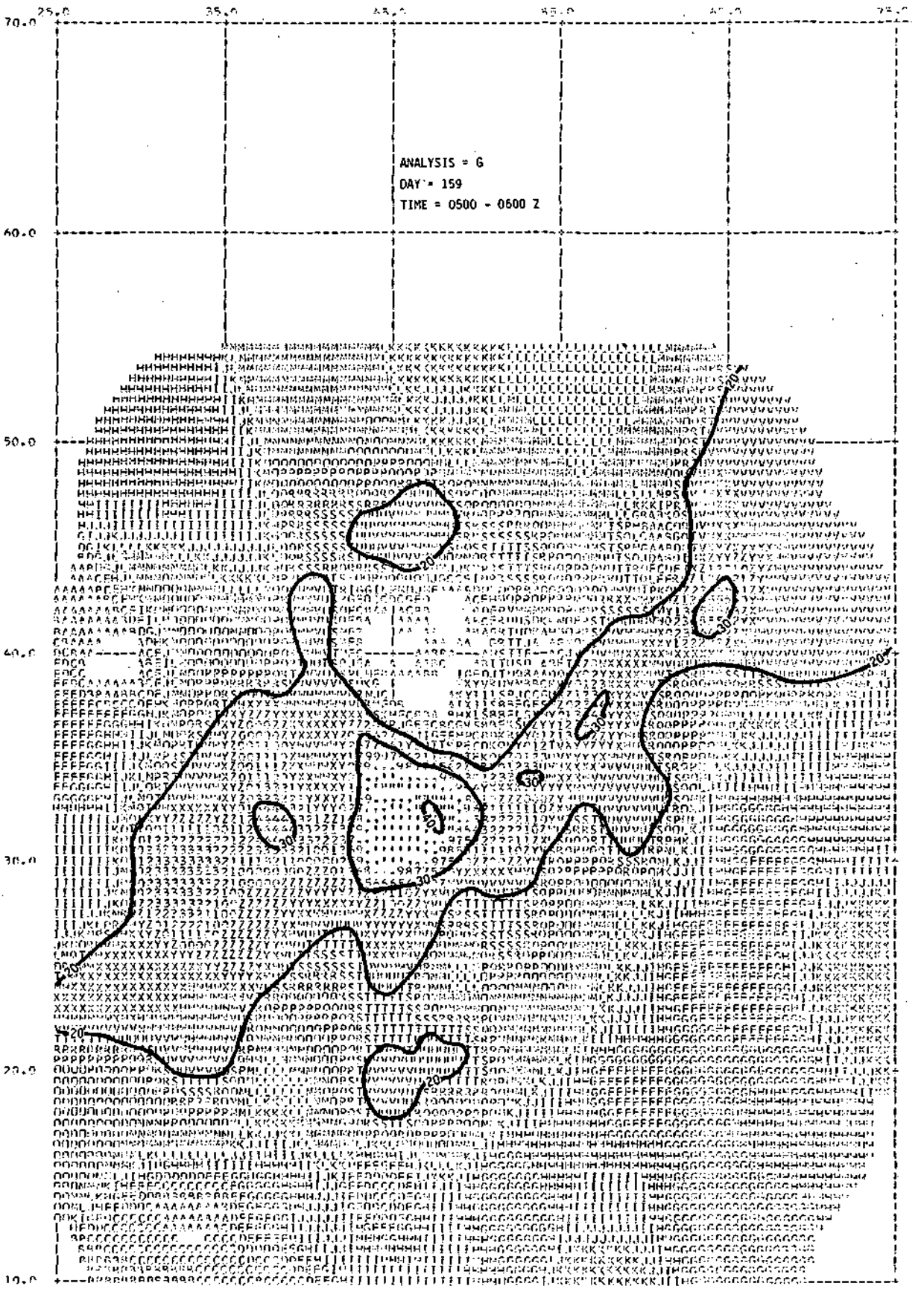

Figure 34. Gage rainfall analysis for same period as in Figure 31.

(c) Appendix C: Comparative test runs of gage-radar analyses routine. Factors in the last three columns were tested: WT is weighting factor for polar to cartesian conversion with 1 = Gaussian, 2 = even, 3 = use of maximum value. RMIN is minimum radar rainfall amount accepted for analysis in mm.

Table 107.

RADAR-GAGE RAINFALL ANALYSES FOR DAY 158 OF 1976 BEGINNING AT 60000. RUN DURATION = 120 MIN

GAGE DENSITY	NUMBER OF GAGES TOTAL	G/R	EVAP	RADAR MEAN	RADAR STDEV	RAINFALL AMOUNTS (MM) GAGE MEAN	GAGE STDEV	GAGE+RADAR MEAN	GAGE+RADAR STDEV	GAGE+RADAR (EVAP) MEAN	GAGE+RADAR (EVAP) STDEV	GAGE-RADAR RATIO MEAN	GAGE-RADAR RATIO STDEV	WT	RMIN (MM)	RADIUS (KM)
1/ 1	97	56	33	1.0	1.3	5.3	7.4	6.6	10.6	5.1	9.5	10.6	16.2	1	0.10	1.0
1/ 1	97	56	33	1.0	1.3	5.3	7.4	6.8	11.5	5.2	10.3	11.7	19.5	1	0.10	3.0
1/ 1	97	61	33	1.0	1.3	5.3	7.4	6.7	12.2	5.4	11.3	11.0	15.0	1	0.01	1.0
1/ 1	97	61	33	1.0	1.3	5.3	7.4	7.3	14.0	5.9	13.0	11.9	16.3	1	0.01	3.5
1/ 1	97	62	33	1.0	1.3	5.3	7.4	6.0	9.9	4.7	9.0	10.9	14.2	1	0.10	2.0
1/ 1	97	61	31	1.1	1.4	5.3	7.4	6.8	10.3	5.5	9.9	10.3	13.8	2	0.10	0.5
1/ 1	97	53	31	1.1	1.3	5.3	7.4	6.7	10.1	5.3	9.0	9.8	12.4	2	0.10	1.0
1/ 1	97	59	31	1.7	2.9	5.3	7.4	8.3	13.3	6.4	11.4	9.5	16.5	3	0.10	1.0

RADAR-GAGE RAINFALL ANALYSES FOR DAY 158 OF 1976 BEGINNING AT 40000. RUN DURATION = 60 MIN

GAGE DENSITY	NUMBER OF GAGES TOTAL	G/R	EVAP	RADAR MEAN	RADAR STDEV	RAINFALL AMOUNTS (MM) GAGE MEAN	GAGE STDEV	GAGE+RADAR MEAN	GAGE+RADAR STDEV	GAGE+RADAR (EVAP) MEAN	GAGE+RADAR (EVAP) STDEV	GAGE-RADAR RATIO MEAN	GAGE-RADAR RATIO STDEV	WT	RMIN (MM)	RADIUS (KM)
1/ 1	97	24	60	0.1	0.4	1.1	3.2	2.3	10.2	1.8	10.1	16.1	18.5	1	0.10	1.0
1/ 1	97	20	60	0.1	0.4	1.1	3.2	2.2	12.8	1.7	12.7	12.5	18.8	1	0.10	0.5
1/ 1	97	29	60	0.1	0.4	1.1	2.6	1.6	3.0	1.2	2.0	13.4	16.9	1	0.01	1.0
1/ 1	97	29	60	0.1	0.4	1.1	2.4	1.7	5.4	1.2	5.3	14.7	18.4	1	0.01	0.5
1/ 1	97	27	60	0.1	0.5	1.1	2.6	1.4	3.1	1.3	3.1	12.5	16.3	2	0.10	2.0
1/ 1	97	22	58	0.1	0.5	1.1	2.6	1.7	7.4	1.5	7.3	12.1	17.4	2	0.10	0.5
1/ 1	97	23	59	0.1	0.3	1.1	2.6	1.3	4.8	1.0	4.7	11.4	12.2	2	0.10	1.0
1/ 1	97	25	60	0.3	0.7	1.1	2.6	2.5	10.1	2.1	10.1	9.3	14.3	3	0.10	1.0

RADAR-GAGE RAINFALL ANALYSES FOR DAY 158 OF 1976 BEGINNING AT 50000. RUN DURATION = 60 MIN

GAGE DENSITY	NUMBER OF GAGES TOTAL	G/R	EVAP	RADAR MEAN	RADAR STDEV	RAINFALL AMOUNTS (MM) GAGE MEAN	GAGE STDEV	GAGE+RADAR MEAN	GAGE+RADAR STDEV	GAGE+RADAR (EVAP) MEAN	GAGE+RADAR (EVAP) STDEV	GAGE-RADAR RATIO MEAN	GAGE-RADAR RATIO STDEV	WT	RMIN (MM)	RADIUS (KM)
1/ 1	97	54	37	0.9	2.0	4.3	6.2	5.4	11.2	4.0	9.4	12.0	16.1	1	0.10	1.0
1/ 1	97	56	37	0.9	2.0	4.3	6.2	5.8	12.6	4.3	11.2	12.7	17.1	1	0.10	0.5
1/ 1	97	56	37	0.9	2.0	4.3	6.2	5.4	11.2	4.0	9.4	13.6	16.1	1	0.01	1.0
1/ 1	97	56	37	0.9	2.0	4.3	6.2	5.8	12.6	4.3	11.2	12.7	17.1	1	0.01	0.5
1/ 1	97	58	37	0.9	2.0	4.3	6.2	5.8	8.5	3.7	7.5	13.8	17.8	1	0.10	2.0
1/ 1	97	55	36	1.1	1.8	4.3	6.2	6.3	10.7	4.5	8.4	13.8	18.7	2	0.10	0.5
1/ 1	97	56	36	1.1	1.9	4.3	6.2	6.1	10.6	4.4	8.1	13.2	17.8	2	0.10	1.0
1/ 1	97	56	35	1.7	3.3	4.3	6.2	8.4	11.2	4.8	8.4	8.6	12.4	3	0.10	1.0

RADAR-GAGE RAINFALL ANALYSES FOR DAY 159 OF 1976 BEGINNING AT 50000. RUN DURATION = 60 MIN

GAGE DENSITY	NUMBER OF GAGES TOTAL	G/R	EVAP	RADAR MEAN	RADAR STDEV	RAINFALL AMOUNTS (MM) GAGE MEAN	GAGE STDEV	GAGE+RADAR MEAN	GAGE+RADAR STDEV	GAGE+RADAR (EVAP) MEAN	GAGE+RADAR (EVAP) STDEV	GAGE-RADAR RATIO MEAN	GAGE-RADAR RATIO STDEV	WT	RMIN (MM)	RADIUS (KM)
1/ 1	97	87	9	0.5	0.3	13.3	8.3	14.0	9.9	12.1	9.9	31.3	15.4	1	0.10	1.0
1/ 1	97	87	9	0.5	0.3	13.3	8.3	14.3	10.3	12.3	10.3	31.5	15.7	1	0.10	0.5
1/ 1	97	87	9	0.5	0.3	13.3	8.3	14.0	9.9	12.1	9.9	31.3	15.4	1	0.01	1.0
1/ 1	97	87	9	0.5	0.3	13.3	8.3	14.3	10.3	12.3	10.3	31.5	15.7	1	0.01	0.5
1/ 1	97	87	9	0.5	0.3	13.3	8.3	13.6	9.4	11.7	9.3	30.5	14.7	1	0.10	2.0
1/ 1	97	87	8	0.5	0.3	13.3	8.3	14.5	8.5	12.6	8.8	31.2	15.3	2	0.10	0.5
1/ 1	97	87	8	0.9	0.3	13.3	8.3	14.5	8.5	12.6	8.7	33.1	15.2	3	0.10	1.0
1/ 1	97	87	8	0.7	0.5	13.3	8.3	14.9	8.8	12.9	8.6	24.4	12.9	3	0.10	1.5

(d) Appendix D: Tabulation of gage density test results. Tables 108 and 109 include the 60 minute runs for RMIN = 0.10 and 0.02 mm rainfall. The additional pages (Table 110) contain data for the 15 minute analyses, using RMIN = 0.02 mm. The number of gage's columns indicate, respectively, the total number of gages input into a run, the number actually used for calculating gage-radar ratios, and the number (having zero rain) which were used in the correction for evaporation.

RADAR-GAGE RAINFALL ANALYSES FOR DAY 158 OF 1976 BEGINNING AT 40000. RUN DURATION = 60 MIN
COORD XFORM WT = 2 MIN RADAR RAIN = 0.02 MM RADIUS FOR G/R RATIOS = 1.0 KM

GAGE DENSITY	NUMBER OF GAGES TOTAL	G/R	EVAP	RADAR MEAN	RADAR STDEV	RAINFALL AMOUNTS (MM) GAGE MEAN	GAGE STDEV	(EVAP) GAGE+RADAR MEAN	(EVAP) GAGE+RADAR STDEV	PERCENT ERROR GAGE ONLY MEAN	PERCENT ERROR GAGE ONLY STDEV	PERCENT ERROR GAGE+RADAR MEAN	PERCENT ERROR GAGE+RADAR STDEV	GAGE-RADAR RATIO MEAN	GAGE-RADAR RATIO STDEV
1/ 1	97	31	58	0.14	0.33	1.06	2.45	1.84	4.77	1.34	6.71	0.0	0.0	0.0	0.0	15.3	19.0
1/ 2	48	14	27	0.14	0.33	1.15	3.73	2.04	7.38	1.35	4.72	2.8	13.7	0.0	29.7	16.8	30.2
1/ 4	27	12	14	0.14	0.33	1.55	3.29	1.47	6.96	0.95	2.97	44.6	34.1	30.1	54.4	13.1	14.4
1/ 8	11	2	8	0.14	0.33	0.33	0.74	0.35	1.02	2.96	9.45	89.1	69.0	115.6	40.7	42.2	29.6
1/16	6	1	4	0.14	0.33	0.84	2.16	3.73	9.02	1.29	4.01	18.5	11.8	4.2	40.5	27.5	0.0

RADAR-GAGE RAINFALL ANALYSES FOR DAY 158 OF 1976 BEGINNING AT 50000. RUN DURATION = 60 MIN
COORD XFORM WT = 2 MIN RADAR RAIN = 0.02 MM RADIUS FOR G/R RATIOS = 1.0 KM

GAGE DENSITY	NUMBER OF GAGES TOTAL	G/R	EVAP	RADAR MEAN	RADAR STDEV	RAINFALL AMOUNTS (MM) GAGE MEAN	GAGE STDEV	(EVAP) GAGE+RADAR MEAN	(EVAP) GAGE+RADAR STDEV	PERCENT ERROR GAGE ONLY MEAN	PERCENT ERROR GAGE ONLY STDEV	PERCENT ERROR GAGE+RADAR MEAN	PERCENT ERROR GAGE+RADAR STDEV	GAGE-RADAR RATIO MEAN	GAGE-RADAR RATIO STDEV
1/ 1	97	56	36	1.05	1.94	4.27	6.20	6.15	10.37	4.41	8.05	0.0	0.0	0.0	0.0	13.2	17.4
1/ 2	48	24	19	1.05	1.94	4.47	5.97	7.36	17.71	5.73	14.86	4.8	3.7	29.8	84.5	14.8	19.3
1/ 4	27	15	10	1.05	1.94	3.94	4.49	8.83	21.37	6.44	16.36	7.6	27.5	44.0	109.2	12.1	14.9
1/ 8	11	5	5	1.05	1.94	5.20	6.95	13.29	24.26	0.0	0.0	21.9	12.2	201.3	201.3	24.4	29.8
1/16	6	5	2	1.05	1.94	4.85	8.55	10.84	28.35	16.28	19.56	13.7	31.9	269.1	143.0	19.4	30.8

RADAR-GAGE RAINFALL ANALYSES FOR DAY 159 OF 1976 BEGINNING AT 40000. RUN DURATION = 60 MIN
COORD XFORM WT = 2 MIN RADAR RAIN = 0.02 MM RADIUS FOR G/R RATIOS = 1.0 KM

GAGE DENSITY	NUMBER OF GAGES TOTAL	G/R	EVAP	RADAR MEAN	RADAR STDEV	RAINFALL AMOUNTS (MM) GAGE MEAN	GAGE STDEV	(EVAP) GAGE+RADAR MEAN	(EVAP) GAGE+RADAR STDEV	% PERCENT ERROR GAGE ONLY MEAN	% PERCENT ERROR GAGE ONLY STDEV	% PERCENT ERROR GAGE+RADAR MEAN	% PERCENT ERROR GAGE+RADAR STDEV	GAGE-RADAR RATIO MEAN	GAGE-RADAR RATIO STDEV
1/ 1	97	63	12	0.26	0.46	5.09	4.46	4.22	4.42	3.58	4.16	0.0	0.0	0.0	0.0	33.3	30.1
1/ 2	48	31	6	0.26	0.46	4.95	3.95	5.56	10.10	5.19	10.18	2.6	15.2	46.2	144.5	34.5	30.3
1/ 4	27	18	3	0.26	0.46	5.56	4.17	5.65	10.45	5.93	10.49	9.3	10.4	48.0	151.9	35.9	33.6
1/ 8	11	7	2	0.26	0.46	4.95	3.14	7.68	11.42	5.69	8.95	2.6	32.5	53.3	115.1	39.5	24.3
1/16	6	3	0	0.26	0.46	7.60	8.14	9.23	21.72	0.0	0.0	46.4	74.8	154.0	427.9	44.5	29.5

RADAR-GAGE RAINFALL ANALYSES FOR DAY 159 OF 1976 BEGINNING AT 50000. RUN DURATION = 60 MIN
COORD XFORM WT = 2 MIN RADAR RAIN = 0.02 MM RADIUS FOR G/R RATIOS = 1.0 KM

GAGE DENSITY	NUMBER OF GAGES TOTAL	G/R	EVAP	RADAR MEAN	RADAR STDEV	RAINFALL AMOUNTS (MM) GAGE MEAN	GAGE STDEV	(EVAP) GAGE+RADAR MEAN	(EVAP) GAGE+RADAR STDEV	PERCENT ERROR GAGE ONLY MEAN	PERCENT ERROR GAGE ONLY STDEV	PERCENT ERROR GAGE+RADAR MEAN	PERCENT ERROR GAGE+RADAR STDEV	GAGE-RADAR RATIO MEAN	GAGE-RADAR RATIO STDEV
1/ 1	97	87	8	0.53	0.28	13.29	8.29	14.47	8.66	12.35	8.75	0.0	0.0	0.0	0.0	31.1	15.2
1/ 2	48	43	5	0.53	0.28	13.49	7.58	14.24	7.67	11.63	7.68	1.5	11.6	7.4	12.2	30.2	13.0
1/ 4	27	25	2	0.53	0.28	14.68	7.28	16.75	9.39	12.11	7.15	9.0	12.2	3.5	19.2	29.8	14.1
1/ 8	11	10	1	0.53	0.28	15.62	7.56	15.02	9.23	12.11	8.50	2.6	14.8	4.0	2.4	29.9	16.0
1/16	6	6	0	0.53	0.28	12.54	11.99	19.69	11.91	0.0	0.0	5.0	43.6	49.9	34.2	37.3	12.0

RADAR-GAGE RAINFALL ANALYSES FOR DAY 184 OF 1976 BEGINNING AT 170000. RUN DURATION = 60 MIN
COORD XFORM WT = 2 MIN RADAR RAIN = 0.02 MM RADIUS FOR G/R RATIOS = 1.0 KM

GAGE DENSITY	NUMBER OF GAGES TOTAL	G/R	EVAP	RADAR MEAN	RADAR STDEV	RAINFALL AMOUNTS (MM) GAGE MEAN	GAGE STDEV	(EVAP) GAGE+RADAR MEAN	(EVAP) GAGE+RADAR STDEV	PERCENT ERROR GAGE ONLY MEAN	PERCENT ERROR GAGE ONLY STDEV	PERCENT ERROR GAGE+RADAR MEAN	PERCENT ERROR GAGE+RADAR STDEV	GAGE-RADAR RATIO MEAN	GAGE-RADAR RATIO STDEV
1/ 1	111	71	32	0.29	0.33	2.44	3.73	2.66	3.28	2.14	3.37	0.0	0.0	0.0	0.0	12.9	12.6
1/ 2	57	35	19	0.29	0.33	2.40	3.97	2.81	3.72	2.11	3.75	0.4	3.6	1.3	11.4	12.7	13.5
1/ 4	29	19	6	0.29	0.33	3.29	5.26	2.74	4.42	2.35	4.48	34.6	40.8	9.8	32.9	11.6	14.1
1/ 8	15	8	7	0.29	0.33	2.07	2.72	3.83	4.25	2.65	3.65	12.2	46.5	6.3	17.8	16.3	15.2
1/14	7	7	0	0.29	0.33	1.52	1.54	3.44	4.65	0.0	0.0	25.7	58.1	61.0	38.0	14.9	13.8
1/30	3	3	0	0.29	0.33	1.29	1.20	2.66	3.27	0.0	0.0	47.8	67.9	24.4	3.0	9.8	6.4

RADAR-GAGE RAINFALL ANALYSES FOR DAY 184 OF 1976 BEGINNING AT 180000. RUN DURATION = 60 MIN
COORD XFORM WT = 2 MIN RADAR RAIN = 0.02 MM RADIUS FOR G/R RATIOS = 1.0 KM

GAGE DENSITY	NUMBER OF GAGES TOTAL	G/R	EVAP	RADAR MEAN	RADAR STDEV	RAINFALL AMOUNTS (MM) GAGE MEAN	GAGE STDEV	(EVAP) GAGE+RADAR MEAN	(EVAP) GAGE+RADAR STDEV	PERCENT ERROR GAGE ONLY MEAN	PERCENT ERROR GAGE ONLY STDEV	PERCENT ERROR GAGE+RADAR MEAN	PERCENT ERROR GAGE+RADAR STDEV	GAGE-RADAR RATIO MEAN	GAGE-RADAR RATIO STDEV
1/ 1	110	74	31	0.54	0.70	3.75	5.62	5.86	8.30	3.99	7.20	0.0	0.0	0.0	0.0	15.7	18.7
1/ 2	46	32	14	0.54	0.70	3.95	4.11	4.73	6.21	2.95	5.02	24.1	27.0	24.0	30.3	12.6	15.1
1/ 4	27	18	9	0.54	0.70	2.77	3.79	4.78	6.05	3.10	4.76	28.2	32.6	22.4	33.9	13.5	16.9
1/ 8	15	10	5	0.54	0.70	4.16	5.02	5.68	8.17	3.64	7.33	10.8	10.9	12.2	1.7	12.6	14.5
1/14	7	5	1	0.54	0.70	11.48	12.94	8.63	8.50	5.75	8.49	209.9	139.1	42.0	17.4	11.2	4.1
1/30	3	3	0	0.54	0.70	3.50	3.72	6.66	11.29	0.0	0.0	6.8	33.9	64.9	56.7	11.6	11.8

RADAR-GAGE RAINFALL ANALYSES FOR DAY 184 OF 1976 BEGINNING AT 190000. RUN DURATION = 60 MIN
COORD XFORM WT = 2 MIN RADAR RAIN = 0.02 MM RADIUS FOR G/R RATIOS = 1.0 KM

GAGE DENSITY	NUMBER OF GAGES TOTAL	G/R	EVAP	RADAR MEAN	RADAR STDEV	RAINFALL AMOUNTS (MM) GAGE MEAN	GAGE STDEV	(EVAP) GAGE+RADAR MEAN	(EVAP) GAGE+RADAR STDEV	PERCENT ERROR GAGE ONLY MEAN	PERCENT ERROR GAGE ONLY STDEV	PERCENT ERROR GAGE+RADAR MEAN	PERCENT ERROR GAGE+RADAR STDEV	GAGE-RADAR RATIO MEAN	GAGE-RADAR RATIO STDEV
1/ 1	110	55	45	0.41	0.74	3.54	4.92	6.96	12.39	5.29	10.70	0.0	0.0	0.0	0.0	21.4	20.5
1/ 2	56	27	24	0.41	0.74	3.71	7.07	7.26	12.87	6.78	9.88	4.8	2.2	9.8	7.7	26.1	24.2
1/ 4	27	12	14	0.41	0.74	3.44	4.72	7.44	14.44	5.22	12.21	3.0	5.9	1.3	14.1	23.7	23.0
1/ 8	15	6	7	0.41	0.74	4.26	7.48	8.67	16.97	2.69	6.53	19.8	8.1	53.9	48.4	10.6	6.0
1/14	7	5	2	0.41	0.74	2.40	3.44	5.77	11.27	6.41	9.46	24.4	50.5	12.9	11.5	21.9	16.4
1/30	3	1	2	0.41	0.74	1.05	1.99	5.39	9.41	3.04	8.35	70.3	71.3	42.6	22.0	13.0	0.0

RADAR-GAGE RAINFALL ANALYSES FOR DAY 201 OF 1976 BEGINNING AT 130000. RUN DURATION = 60 MIN
COORD XFORM WT = 2 MIN RADAR RAIN = 0.02 MM RADIUS FOR G/R RATIOS = 1.0 KM

GAGE DENSITY	NUMBER OF GAGES TOTAL	G/R	EVAP	RADAR MEAN	RADAR STDEV	RAINFALL AMOUNTS (MM) GAGE MEAN	GAGE STDEV	(EVAP) GAGE+RADAR MEAN	(EVAP) GAGE+RADAR STDEV	PERCENT ERROR GAGE ONLY MEAN	PERCENT ERROR GAGE ONLY STDEV	PERCENT ERROR GAGE+RADAR MEAN	PERCENT ERROR GAGE+RADAR STDEV	GAGE-RADAR RATIO MEAN	GAGE-RADAR RATIO STDEV
1/ 1	112	29	48	0.10	0.22	0.35	1.09	0.64	1.55	0.36	1.46	0.0	0.0	0.0	0.0	7.3	7.8
1/ 2	56	15	22	0.10	0.22	0.53	1.38	0.64	1.60	0.38	1.36	20.3	17.8	2.8	6.5	6.3	6.3
1/ 4	27	7	11	0.10	0.22	0.33	0.94	0.60	2.10	0.82	2.03	3.8	11.5	4.4	30.7	9.2	8.5
1/ 8	14	6	5	0.10	0.22	0.74	2.19	0.82	2.39	0.64	1.75	139.9	101.3	29.1	20.0	4.7	2.7
1/14	7	2	2	0.10	0.22	0.14	0.20	0.45	1.30	0.37	1.06	49.3	81.3	2.5	28.3	7.7	4.3
1/30	3	1	1	0.10	0.22	0.04	0.09	0.23	0.49	0.03	0.05	83.7	91.7	93.2	94.3	2.2	0.0

DENSITY	MEAN PERCENT ERROR GAGE ONLY MEAN	GAGE ONLY STDEV	GAGE+RADAR MEAN	GAGE+RADAR STDEV	GAGE-RADAR RATIO MEAN	GAGE-RADAR RATIO STDEV
1/ 1	0.0	0.0	0.0	0.0	18.8	17.4
1/ 2	9.2	11.8	14.3	45.9	19.0	19.0
1/ 4	17.4	21.9	26.7	54.2	12.4	17.3
1/ 8	11.5	24.1	60.2	56.9	12.4	17.3
1/16	50.7	41.0	75.3	92.1	73.5	13.8
1/30	42.1	44.3	54.5	44.4	8.1	2.6

Table 108. 60 minute rainfall analyses for several gage densities and with RMIN = 0.02 mm.

RADAR-GAGE RAINFALL ANALYSES FOR DAY 158 OF 197A BEGINNING AT 40000. RUN DURATION = 60 MIN
COORD XFORM WT = 2 MIN RADAR RAIN = 0.10 MM RADIUS FOR G/R RATIOS = 1.0 KM

GAGE DENSITY	NUMBER OF GAGES TOTAL	G/R	EVAP	RADAR MEAN	RADAR STDEV	RAINFALL AMOUNTS (MM) GAGE MEAN	GAGE STDEV	GAGE+RADAR MEAN	GAGE+RADAR STDEV	(EVAP) GAGE+RADAR MEAN	(EVAP) GAGE+RADAR STDEV	PERCENT ERROR GAGE ONLY MEAN	PERCENT ERROR GAGE ONLY STDEV	PERCENT ERROR GAGE+RADAR MEAN	PERCENT ERROR GAGE+RADAR STDEV	GAGE-RADAR RATIO MEAN	GAGE-RADAR RATIO STDEV
1/ 1	97	73	58	0.14	0.33	1.06	2.65	1.35	4.76	0.99	4.72	0.0	0.0	0.0	0.0	11.4	12.2
1/ 2	49	10	27	0.14	0.33	1.15	3.78	1.65	5.31	0.80	3.10	0.8	13.7	4.3	32.3	11.7	13.4
1/ 4	27	9	14	0.14	0.33	1.55	3.28	1.39	6.36	0.43	2.54	44.6	34.1	15.7	44.2	11.1	14.2
1/ 8	0	1	9	0.0	0.0	0.0	0.0	0.0	0.0	0.0	0.0	-99.0	-99.0	-99.0	-99.0	0.0	0.0
1/16	4	1	4	0.14	0.33	0.86	2.14	3.73	9.02	1.22	4.01	18.5	11.8	29.6	15.1	27.5	0.0
1/30	2	1	1	0.14	0.33	0.74	1.36	1.45	3.56	0.43	1.46	29.8	44.4	55.9	69.0	10.7	0.0

RADAR-GAGE RAINFALL ANALYSES FOR DAY 158 OF 197A BEGINNING AT 50000. RUN DURATION = 60 MIN
COORD XFORM WT = 2 MIN RADAR RAIN = 0.10 MM RADIUS FOR G/R RATIOS = 1.0 KM

GAGE DENSITY	NUMBER OF GAGES TOTAL	G/R	EVAP	RADAR MEAN	RADAR STDEV	RAINFALL AMOUNTS (MM) GAGE MEAN	GAGE STDEV	GAGE+RADAR MEAN	GAGE+RADAR STDEV	(EVAP) GAGE+RADAR MEAN	(EVAP) GAGE+RADAR STDEV	PERCENT ERROR GAGE ONLY MEAN	PERCENT ERROR GAGE ONLY STDEV	PERCENT ERROR GAGE+RADAR MEAN	PERCENT ERROR GAGE+RADAR STDEV	GAGE-RADAR RATIO MEAN	GAGE-RADAR RATIO STDEV
1/ 1	97	56	36	1.05	1.94	4.27	6.20	4.15	10.37	4.41	8.05	0.0	0.0	0.0	0.0	13.7	17.8
1/ 2	49	24	19	1.05	1.94	4.47	5.97	7.84	17.71	5.73	14.84	4.8	3.7	29.8	44.4	14.8	19.3
1/ 4	27	15	10	1.05	1.94	3.96	6.49	4.93	21.37	6.44	16.36	7.6	27.5	44.0	103.2	12.1	15.9
1/ 8	11	4	5	1.05	1.94	5.20	6.95	7.23	19.77	5.87	11.82	21.9	12.3	33.2	44.8	0.5	8.0
1/16	6	3	2	1.05	1.94	4.85	8.55	10.24	29.35	16.24	19.56	13.7	37.9	269.1	143.0	19.4	30.8
1/30	2	2	0	1.05	1.94	2.98	4.95	4.50	12.11	0.0	0.0	30.3	20.1	47.4	50.5	6.7	1.8

RADAR-GAGE RAINFALL ANALYSES FOR DAY 159 OF 197A BEGINNING AT 50000. RUN DURATION = 60 MIN
COORD XFORM WT = 2 MIN RADAR RAIN = 0.10 MM RADIUS FOR G/R RATIOS = 1.0 KM

GAGE DENSITY	NUMBER OF GAGES TOTAL	G/R	EVAP	RADAR MEAN	RADAR STDEV	RAINFALL AMOUNTS (MM) GAGE MEAN	GAGE STDEV	GAGE+RADAR MEAN	GAGE+RADAR STDEV	(EVAP) GAGE+RADAR MEAN	(EVAP) GAGE+RADAR STDEV	PERCENT ERROR GAGE ONLY MEAN	PERCENT ERROR GAGE ONLY STDEV	PERCENT ERROR GAGE+RADAR MEAN	PERCENT ERROR GAGE+RADAR STDEV	GAGE-RADAR RATIO MEAN	GAGE-RADAR RATIO STDEV
1/ 1	97	87	8	0.53	0.28	13.28	8.29	14.67	9.44	12.55	8.75	0.0	0.0	0.0	0.0	31.1	15.2
1/ 2	48	43	5	0.53	0.28	13.48	7.38	14.36	7.67	11.43	7.08	1.5	11.0	3.4	12.2	30.2	15.0
1/ 4	27	25	2	0.53	0.28	13.68	7.22	14.25	7.39	12.11	7.16	9.0	12.2	3.5	18.2	29.8	14.1
1/ 8	11	10	1	0.53	0.28	13.42	7.56	15.05	9.23	11.74	8.30	2.6	8.8	7.3	2.4	29.9	16.0
1/16	6	6	0	0.53	0.28	13.54	11.89	13.64	11.91	0.0	0.0	5.6	43.4	6.9	36.2	37.3	12.0
1/30	2	2	0	0.53	0.28	8.02	9.16	19.14	10.71	0.0	0.0	39.6	10.5	58.0	22.9	37.4	9.3

RADAR-GAGE RAINFALL ANALYSES FOR DAY 184 OF 197A BEGINNING AT 170000. RUN DURATION = 60 MIN
COORD XFORM WT = 2 MIN RADAR RAIN = 0.10 MM RADIUS FOR G/R RATIOS = 1.0 KM

GAGE DENSITY	NUMBER OF GAGES TOTAL	G/R	EVAP	RADAR MEAN	RADAR STDEV	RAINFALL AMOUNTS (MM) GAGE MEAN	GAGE STDEV	GAGE+RADAR MEAN	GAGE+RADAR STDEV	(EVAP) GAGE+RADAR MEAN	(EVAP) GAGE+RADAR STDEV	PERCENT ERROR GAGE ONLY MEAN	PERCENT ERROR GAGE ONLY STDEV	PERCENT ERROR GAGE+RADAR MEAN	PERCENT ERROR GAGE+RADAR STDEV	GAGE-RADAR RATIO MEAN	GAGE-RADAR RATIO STDEV
1/ 1	111	63	32	0.29	0.33	2.44	3.73	2.59	3.31	2.11	3.38	0.0	0.0	0.0	0.0	11.3	12.1
1/ 2	57	32	19	0.29	0.33	2.40	3.97	2.42	3.44	1.98	3.35	4.4	3.4	4.5	6.9	11.8	14.2
1/ 4	28	16	9	0.29	0.33	2.29	3.26	2.25	3.92	1.96	3.96	34.6	40.8	7.6	17.0	7.8	9.3
1/ 8	15	8	5	0.29	0.33	2.07	2.00	3.55	4.13	2.07	3.49	15.2	44.5	1.9	2.4	14.7	11.0
1/16	7	7	0	0.29	0.33	1.42	1.54	3.17	4.56	0.0	0.0	25.7	54.1	54.0	34.8	17.0	12.2
1/30	3	3	0	0.29	0.33	1.24	1.20	2.54	3.27	0.0	0.0	47.8	47.4	25.9	3.3	9.8	8.6

RADAR-GAGE RAINFALL ANALYSES FOR DAY 184 OF 197A BEGINNING AT 180000. RUN DURATION = 60 MIN
COORD XFORM WT = 2 MIN RADAR RAIN = 0.10 MM RADIUS FOR G/R RATIOS = 1.0 KM

GAGE DENSITY	NUMBER OF GAGES TOTAL	G/R	EVAP	RADAR MEAN	RADAR STDEV	RAINFALL AMOUNTS (MM) GAGE MEAN	GAGE STDEV	GAGE+RADAR MEAN	GAGE+RADAR STDEV	(EVAP) GAGE+RADAR MEAN	(EVAP) GAGE+RADAR STDEV	PERCENT ERROR GAGE ONLY MEAN	PERCENT ERROR GAGE ONLY STDEV	PERCENT ERROR GAGE+RADAR MEAN	PERCENT ERROR GAGE+RADAR STDEV	GAGE-RADAR RATIO MEAN	GAGE-RADAR RATIO STDEV
1/ 1	110	74	31	0.54	0.70	3.75	5.62	5.64	8.30	3.99	7.20	0.0	0.0	0.0	0.0	15.7	18.7
1/ 2	56	39	14	0.54	0.70	2.95	4.11	4.73	6.21	2.95	5.02	24.1	27.0	24.0	30.3	12.6	15.1
1/ 4	27	19	9	0.54	0.70	2.77	3.79	4.79	6.05	3.10	4.76	26.2	32.6	22.4	33.9	13.5	16.0
1/ 8	15	10	5	0.54	0.70	4.16	5.02	5.44	8.17	3.46	7.33	10.8	10.9	13.2	3.7	12.5	14.5
1/16	7	7	0	0.54	0.70	11.48	13.94	6.48	8.50	5.75	8.49	205.9	130.1	44.0	17.8	11.2	4.1
1/30	3	3	0	0.54	0.70	3.50	5.72	4.66	11.29	0.0	0.0	6.8	33.9	54.9	56.7	11.5	11.8

RADAR-GAGE RAINFALL ANALYSES FOR DAY 184 OF 1976 BEGINNING AT 190000. RUN DURATION = 60 MIN
COORD XFORM WT = 2 MIN RADAR RAIN = 0.10 MM RADIUS FOR G/R RATIOS = 1.0 KM

GAGE DENSITY	NUMBER OF GAGES TOTAL	G/R	EVAP	RADAR MEAN	RADAR STDEV	RAINFALL AMOUNTS (MM) GAGE MEAN	GAGE STDEV	GAGE+RADAR MEAN	GAGE+RADAR STDEV	(EVAP) GAGE+RADAR MEAN	(EVAP) GAGE+RADAR STDEV	PERCENT ERROR GAGE ONLY MEAN	PERCENT ERROR GAGE ONLY STDEV	PERCENT ERROR GAGE+RADAR MEAN	PERCENT ERROR GAGE+RADAR STDEV	GAGE-RADAR RATIO MEAN	GAGE-RADAR RATIO STDEV
1/ 1	110	55	45	0.41	0.74	3.56	6.93	4.94	12.39	5.29	10.70	0.0	0.0	0.0	0.0	21.4	20.5
1/ 2	56	27	24	0.41	0.74	3.71	7.07	7.25	12.87	4.78	9.83	4.8	2.2	9.8	7.7	24.1	24.2
1/ 4	27	12	14	0.41	0.74	3.44	6.72	7.44	14.44	5.22	12.21	3.0	2.9	1.3	14.1	23.7	23.0
1/ 8	15	6	7	0.41	0.74	4.24	7.49	5.41	6.57	2.26	5.53	19.8	8.1	51.9	48.4	10.6	6.0
1/16	7	5	2	0.41	0.74	2.60	3.44	8.77	11.27	4.61	9.64	26.4	50.2	12.9	11.4	21.9	16.4
1/30	3	1	2	0.41	0.74	1.05	1.99	5.39	9.61	3.04	8.35	70.3	71.3	42.4	22.0	13.0	0.0

RADAR-GAGE RAINFALL ANALYSES FOR DAY 195 OF 197A BEGINNING AT 20000. RUN DURATION = 60 MIN
COORD XFORM WT = 2 MIN RADAR RAIN = 0.10 MM RADIUS FOR G/R RATIOS = 1.0 KM

GAGE DENSITY	NUMBER OF GAGES TOTAL	G/R	EVAP	RADAR MEAN	RADAR STDEV	RAINFALL AMOUNTS (MM) GAGE MEAN	GAGE STDEV	GAGE+RADAR MEAN	GAGE+RADAR STDEV	(EVAP) GAGE+RADAR MEAN	(EVAP) GAGE+RADAR STDEV	PERCENT ERROR GAGE ONLY MEAN	PERCENT ERROR GAGE ONLY STDEV	PERCENT ERROR GAGE+RADAR MEAN	PERCENT ERROR GAGE+RADAR STDEV	GAGE-RADAR RATIO MEAN	GAGE-RADAR RATIO STDEV
1/ 1	105	64	26	0.18	0.12	0.45	0.58	0.72	0.54	0.58	0.58	0.0	0.0	0.0	0.0	4.2	1.5
1/ 2	55	33	14	0.18	0.12	0.64	0.58	0.75	0.54	0.58	0.58	1.7	0.5	1.4	0.5	4.5	1.7
1/ 4	27	15	7	0.18	0.12	0.49	0.59	0.75	0.57	0.57	0.42	6.9	1.4	2.1	2.4	4.3	3.4
1/ 8	14	10	3	0.18	0.12	0.77	0.63	0.91	0.59	0.84	0.63	19.4	9.3	10.1	9.2	4.9	2.3
1/16	5	3	1	0.18	0.12	0.51	0.45	0.74	0.57	0.43	0.38	20.8	22.5	6.8	0.5	4.2	1.8
1/30	1	1	0	0.18	0.12	0.15	0.22	0.91	0.35	0.0	0.0	76.4	59.5	13.5	40.0	2.8	0.5

RADAR-GAGE RAINFALL ANALYSES FOR DAY 201 OF 197A BEGINNING AT 13000. RUN DURATION = 60 MIN
COORD XFORM WT = 2 MIN RADAR RAIN = 0.10 MM RADIUS FOR G/R RATIOS = 1.0 KM

GAGE DENSITY	NUMBER OF GAGES TOTAL	G/R	EVAP	RADAR MEAN	RADAR STDEV	RAINFALL AMOUNTS (MM) GAGE MEAN	GAGE STDEV	GAGE+RADAR MEAN	GAGE+RADAR STDEV	(EVAP) GAGE+RADAR MEAN	(EVAP) GAGE+RADAR STDEV	PERCENT ERROR GAGE ONLY MEAN	PERCENT ERROR GAGE ONLY STDEV	PERCENT ERROR GAGE+RADAR MEAN	PERCENT ERROR GAGE+RADAR STDEV	GAGE-RADAR RATIO MEAN	GAGE-RADAR RATIO STDEV
1/ 1	112	25	48	0.10	0.22	0.35	1.09	0.55	1.47	0.33	1.41	0.0	0.0	0.0	0.0	5.3	5.4
1/ 2	55	13	22	0.10	0.22	0.23	1.28	0.53	1.52	0.33	1.36	20.9	17.8	1.8	3.9	5.1	6.5
1/ 4	27	5	11	0.10	0.22	0.33	0.96	0.47	1.92	0.65	1.82	5.9	1.5	34.3	29.1	6.0	6.4
1/ 8	14	4	5	0.10	0.22	0.74	2.19	0.83	1.79	0.46	1.35	109.9	101.3	39.3	24.0	6.6	2.9
1/16	7	2	2	0.10	0.22	0.14	0.20	0.38	0.81	0.24	0.73	40.3	41.5	27.1	60.2	4.0	0.4
1/30	3	1	1	0.10	0.22	0.06	0.09	0.22	0.47	0.03	0.05	83.7	91.7	91.9	95.3	2.1	0.0

DENSITY	MEAN PERCENT ERROR GAGE ONLY MEAN	GAGE ONLY STDEV	GAGE+RADAR MEAN	GAGE+RADAR STDEV	GAGE-RADAR RATIO MEAN	GAGE-RADAR RATIO STDEV
1/ 1	0.0	0.0	0.0	0.0	14.2	12.9
1/ 2	9.1	9.9	11.9	21.5	14.3	13.6
1/ 4	17.3	20.4	14.7	31.0	13.5	12.7
1/ 8	28.3	28.0	22.9	19.5	12.4	8.8
1/16	47.1	56.4	41.8	34.4	12.8	9.8
1/30	48.1	49.0	50.3	45.0	11.8	3.7

Table 109. 60 minute rainfall analyses for several gage densities and with RMIN = 0.10 mm.

RADAR-GAGE RAINFALL ANALYSES FOR DAY 158 OF 1976 BEGINNING AT 40000. RUN DURATION = 15 MIN
COORD XFORM WT = 2 MIN RADAR RAIN = 0.02 MM RADIUS FOR G/R RATIOS = 1.0 KM

GAGE DENSITY	NUMBER OF GAGES TOTAL	G/R	EVAP	RADAR MEAN	RADAR STDEV	RAINFALL AMOUNTS (MM) GAGE MEAN	GAGE STDEV	GAGE+RADAR MEAN	GAGE+RADAR STDEV	(EVAP) GAGE+RADAR MEAN	(EVAP) GAGE+RADAR STDEV	PERCENT ERROR GAGE ONLY MEAN	GAGE ONLY STDEV	GAGE+RADAR MEAN	GAGE+RADAR STDEV	GAGE-RADAR RATIO MEAN	GAGE-RADAR RATIO STDEV
1/ 1	97	2	40	0.00	0.01	0.03	0.12	0.04	0.07	0.01	0.04	0.0	0.0	0.0	0.0	13.2	8.6
1/ 2	0	1	0	0.0	0.0	0.0	0.0	0.0	0.0	0.0	0.0	-99.0	-99.0	-99.0	-99.0	0.0	0.0
1/ 4	0	1	0	0.0	0.0	0.0	0.0	0.0	0.0	0.0	0.0	-99.0	-99.0	-99.0	-99.0	0.0	0.0
1/ 8	0	1	0	0.0	0.0	0.0	0.0	0.0	0.0	0.0	0.0	-99.0	-99.0	-99.0	-99.0	0.0	0.0
1/16	0	1	0	0.0	0.0	0.0	0.0	0.0	0.0	0.0	0.0	-99.0	-99.0	-99.0	-99.0	0.0	0.0

RADAR-GAGE RAINFALL ANALYSES FOR DAY 158 OF 1976 BEGINNING AT 41500. RUN DURATION = 15 MIN
COORD XFORM WT = 2 MIN RADAR RAIN = 0.02 MM RADIUS FOR G/R RATIOS = 1.0 KM

GAGE DENSITY	NUMBER OF GAGES TOTAL	G/R	EVAP	RADAR MEAN	RADAR STDEV	RAINFALL AMOUNTS (MM) GAGE MEAN	GAGE STDEV	GAGE+RADAR MEAN	GAGE+RADAR STDEV	(EVAP) GAGE+RADAR MEAN	(EVAP) GAGE+RADAR STDEV	PERCENT ERROR GAGE ONLY MEAN	GAGE ONLY STDEV	GAGE+RADAR MEAN	GAGE+RADAR STDEV	GAGE-RADAR RATIO MEAN	GAGE-RADAR RATIO STDEV
1/ 1	97	8	64	0.01	0.02	0.05	0.18	0.22	0.68	0.10	0.63	0.0	0.0	0.0	0.0	17.1	15.2
1/ 2	48	3	28	0.01	0.02	0.04	0.16	0.13	0.27	0.04	0.16	20.0	8.0	63.3	75.4	12.5	8.5
1/ 4	27	3	18	0.01	0.02	0.08	0.24	0.13	0.27	0.03	0.12	40.0	34.7	84.3	20.7	12.5	8.5
1/ 8	0	1	0	0.0	0.0	0.0	0.0	0.0	0.0	0.0	0.0	-99.0	-99.0	-99.0	-99.0	0.0	0.0
1/16	0	1	0	0.0	0.0	0.0	0.0	0.0	0.0	0.0	0.0	-99.0	-99.0	-99.0	-99.0	0.0	0.0

RADAR-GAGE RAINFALL ANALYSES FOR DAY 158 OF 1976 BEGINNING AT 43000. RUN DURATION = 15 MIN
COORD XFORM WT = 2 MIN RADAR RAIN = 0.02 MM RADIUS FOR G/R RATIOS = 1.0 KM

GAGE DENSITY	NUMBER OF GAGES TOTAL	G/R	EVAP	RADAR MEAN	RADAR STDEV	RAINFALL AMOUNTS (MM) GAGE MEAN	GAGE STDEV	GAGE+RADAR MEAN	GAGE+RADAR STDEV	(EVAP) GAGE+RADAR MEAN	(EVAP) GAGE+RADAR STDEV	PERCENT ERROR GAGE ONLY MEAN	GAGE ONLY STDEV	GAGE+RADAR MEAN	GAGE+RADAR STDEV	GAGE-RADAR RATIO MEAN	GAGE-RADAR RATIO STDEV
1/ 1	97	17	69	0.03	0.08	0.16	0.47	0.56	1.93	0.26	1.46	0.0	0.0	0.0	0.0	17.7	23.1
1/ 2	48	9	31	0.03	0.08	0.22	0.64	0.51	1.98	0.21	1.06	51.4	43.4	14.9	27.1	16.7	23.4
1/ 4	27	7	17	0.03	0.08	0.32	0.82	0.56	2.96	0.18	0.65	119.6	73.5	32.1	24.6	19.6	20.0
1/ 8	11	1	7	0.03	0.08	0.02	0.10	0.57	1.32	0.26	1.12	84.7	17.9	1.6	23.6	17.2	0.0
1/16	0	1	0	0.0	0.0	0.0	0.0	0.0	0.0	0.0	0.0	-99.0	-99.0	-99.0	-99.0	0.0	0.0

RADAR-GAGE RAINFALL ANALYSES FOR DAY 158 OF 1976 BEGINNING AT 44500. RUN DURATION = 15 MIN
COORD XFORM WT = 2 MIN RADAR RAIN = 0.02 MM RADIUS FOR G/R RATIOS = 1.0 KM

GAGE DENSITY	NUMBER OF GAGES TOTAL	G/R	EVAP	RADAR MEAN	RADAR STDEV	RAINFALL AMOUNTS (MM) GAGE MEAN	GAGE STDEV	GAGE+RADAR MEAN	GAGE+RADAR STDEV	(EVAP) GAGE+RADAR MEAN	(EVAP) GAGE+RADAR STDEV	PERCENT ERROR GAGE ONLY MEAN	GAGE ONLY STDEV	GAGE+RADAR MEAN	GAGE+RADAR STDEV	GAGE-RADAR RATIO MEAN	GAGE-RADAR RATIO STDEV
1/ 1	97	21	57	0.09	0.26	0.83	2.24	1.37	5.49	1.08	5.45	0.0	0.0	0.0	0.0	19.5	23.3
1/ 2	48	11	26	0.09	0.26	0.89	2.44	1.70	6.07	1.15	4.87	6.6	8.9	4.4	10.4	25.2	27.1
1/ 4	27	8	13	0.09	0.26	1.16	2.88	1.15	4.65	0.71	2.56	39.6	28.8	33.9	53.1	15.8	16.5
1/ 8	11	1	8	0.09	0.26	0.31	0.76	8.53	25.66	3.96	14.20	63.6	66.2	256.9	160.6	98.8	0.0
1/16	6	1	4	0.09	0.26	0.85	2.12	2.52	7.59	0.77	3.15	1.9	9.3	29.0	42.2	28.6	0.0

RADAR-GAGE RAINFALL ANALYSES FOR DAY 158 OF 1976 BEGINNING AT 50000. RUN DURATION = 15 MIN
COORD XFORM WT = 2 MIN RADAR RAIN = 0.02 MM RADIUS FOR G/R RATIOS = 1.0 KM

GAGE DENSITY	NUMBER OF GAGES TOTAL	G/R	EVAP	RADAR MEAN	RADAR STDEV	RAINFALL AMOUNTS (MM) GAGE MEAN	GAGE STDEV	GAGE+RADAR MEAN	GAGE+RADAR STDEV	(EVAP) GAGE+RADAR MEAN	(EVAP) GAGE+RADAR STDEV	PERCENT ERROR GAGE ONLY MEAN	GAGE ONLY STDEV	GAGE+RADAR MEAN	GAGE+RADAR STDEV	GAGE-RADAR RATIO MEAN	GAGE-RADAR RATIO STDEV
1/ 1	0	0	0	0.0	0.0	0.0	0.0	0.0	0.0	0.0	0.0	-99.0	-99.0	-99.0	-99.0	0.0	0.0
1/ 2	0	0	0	0.0	0.0	0.0	0.0	0.0	0.0	0.0	0.0	-99.0	-99.0	-99.0	-99.0	0.0	0.0
1/ 4	0	0	0	0.0	0.0	0.0	0.0	0.0	0.0	0.0	0.0	-99.0	-99.0	-99.0	-99.0	0.0	0.0
1/ 8	0	0	0	0.0	0.0	0.0	0.0	0.0	0.0	0.0	0.0	-99.0	-99.0	-99.0	-99.0	0.0	0.0
1/16	0	0	0	0.0	0.0	0.0	0.0	0.0	0.0	0.0	0.0	-99.0	-99.0	-99.0	-99.0	0.0	0.0

RADAR-GAGE RAINFALL ANALYSES FOR DAY 158 OF 1976 BEGINNING AT 51500. RUN DURATION = 15 MIN
COORD XFORM WT = 2 MIN RADAR RAIN = 0.02 MM RADIUS FOR G/R RATIOS = 1.0 KM

GAGE DENSITY	NUMBER OF GAGES TOTAL	G/R	EVAP	RADAR MEAN	RADAR STDEV	RAINFALL AMOUNTS (MM) GAGE MEAN	GAGE STDEV	GAGE+RADAR MEAN	GAGE+RADAR STDEV	(EVAP) GAGE+RADAR MEAN	(EVAP) GAGE+RADAR STDEV	PERCENT ERROR GAGE ONLY MEAN	GAGE ONLY STDEV	GAGE+RADAR MEAN	GAGE+RADAR STDEV	GAGE-RADAR RATIO MEAN	GAGE-RADAR RATIO STDEV
1/ 1	97	35	47	0.31	0.83	1.45	2.48	1.53	3.43	1.10	2.77	0.0	0.0	0.0	0.0	9.3	10.2
1/ 2	48	15	24	0.31	0.83	1.48	2.44	2.27	7.22	1.99	8.30	2.3	1.7	81.2	127.6	10.6	13.7
1/ 4	27	10	12	0.31	0.83	1.54	2.60	2.69	8.49	1.80	5.93	6.6	4.8	64.0	114.3	10.4	15.6
1/ 8	11	3	6	0.31	0.83	1.60	3.16	3.00	9.25	1.90	4.81	10.3	13.6	73.8	73.8	13.0	10.5
1/16	6	3	3	0.31	0.83	1.72	3.12	1.40	4.84	4.41	5.38	18.6	25.5	302.3	94.3	3.5	2.9

RADAR-GAGE RAINFALL ANALYSES FOR DAY 158 OF 1976 BEGINNING AT 53000. RUN DURATION = 15 MIN
COORD XFORM WT = 2 MIN RADAR RAIN = 0.02 MM RADIUS FOR G/R RATIOS = 1.0 KM

GAGE DENSITY	NUMBER OF GAGES TOTAL	G/R	EVAP	RADAR MEAN	RADAR STDEV	RAINFALL AMOUNTS (MM) GAGE MEAN	GAGE STDEV	GAGE+RADAR MEAN	GAGE+RADAR STDEV	(EVAP) GAGE+RADAR MEAN	(EVAP) GAGE+RADAR STDEV	PERCENT ERROR GAGE ONLY MEAN	GAGE ONLY STDEV	GAGE+RADAR MEAN	GAGE+RADAR STDEV	GAGE-RADAR RATIO MEAN	GAGE-RADAR RATIO STDEV
1/ 1	97	40	50	0.29	0.66	0.84	1.37	1.31	2.71	0.78	1.69	0.0	0.0	0.0	0.0	12.4	10.1
1/ 2	48	18	27	0.29	0.66	0.98	1.56	1.91	5.65	1.06	3.58	16.7	13.7	35.3	112.0	15.3	20.9
1/ 4	27	10	16	0.29	0.66	0.79	1.31	2.27	6.04	1.44	4.30	5.4	4.2	85.2	164.9	12.0	22.0
1/ 8	11	5	5	0.29	0.66	0.94	1.58	2.61	6.43	1.81	7.09	14.2	15.6	137.3	329.2	21.2	25.8
1/16	6	5	2	0.29	0.66	0.74	1.04	2.38	7.85	2.52	5.95	12.3	23.6	223.3	252.8	13.6	25.0

RADAR-GAGE RAINFALL ANALYSES FOR DAY 158 OF 1976 BEGINNING AT 54500. RUN DURATION = 15 MIN
COORD XFORM WT = 2 MIN RADAR RAIN = 0.02 MM RADIUS FOR G/R RATIOS = 1.0 KM

GAGE DENSITY	NUMBER OF GAGES TOTAL	G/R	EVAP	RADAR MEAN	RADAR STDEV	RAINFALL AMOUNTS (MM) GAGE MEAN	GAGE STDEV	GAGE+RADAR MEAN	GAGE+RADAR STDEV	(EVAP) GAGE+RADAR MEAN	(EVAP) GAGE+RADAR STDEV	PERCENT ERROR GAGE ONLY MEAN	GAGE ONLY STDEV	GAGE+RADAR MEAN	GAGE+RADAR STDEV	GAGE-RADAR RATIO MEAN	GAGE-RADAR RATIO STDEV
1/ 1	97	25	46	0.19	0.37	0.24	0.69	0.84	2.22	0.42	1.55	0.0	0.0	0.0	0.0	6.2	11.1
1/ 2	48	11	29	0.19	0.37	0.35	0.86	1.44	5.72	0.78	2.98	26.0	25.6	33.8	91.6	8.6	14.8
1/ 4	27	8	15	0.19	0.37	0.27	0.83	2.04	8.00	1.68	7.91	2.5	7.9	294.0	404.9	8.1	16.8
1/ 8	11	1	8	0.19	0.37	0.40	0.91	0.68	1.31	0.24	0.55	41.6	32.7	43.3	44.3	3.6	0.0
1/16	6	1	4	0.19	0.37	0.11	0.22	1.99	5.18	0.65	2.40	61.6	67.8	53.6	54.4	8.1	10.9

Table 110. 15 minute rainfall analyses for several gage densities using RMIN = 0.02 mm.

RADAR-GAGE RAINFALL ANALYSES FOR DAY 159 OF 1976 BEGINNING AT 40000. RUN DURATION = 15 MIN
COORD XFORM WT = 2 MIN RADAR RAIN = 0.02 MM RADIUS FOR G/R RATIOS = 1.0 KM

GAGE DENSITY	NUMBER OF GAGES TOTAL	G/R	EVAP	RADAR MEAN	RADAR STDEV	RAINFALL AMOUNTS (MM) GAGE MEAN	GAGE STDEV	GAGE+RADAR MEAN	GAGE+RADAR STDEV	(EVAP) GAGE+RADAR MEAN	(EVAP) GAGE+RADAR STDEV	PERCENT ERROR GAGE ONLY MEAN	PERCENT ERROR GAGE ONLY STDEV	PERCENT ERROR GAGE+RADAR MEAN	PERCENT ERROR GAGE+RADAR STDEV	GAGE-RADAR RATIO MEAN	GAGE-RADAR RATIO STDEV
1/ 1	97	25	45	0.11	0.25	0.36	0.58	0.92	2.01	0.32	0.81	0.0	0.0	0.0	0.0	13.5	16.0
1/ 2	48	11	22	0.11	0.25	0.30	0.62	0.75	2.05	0.27	0.77	17.8	8.2	15.0	5.4	9.5	15.1
1/ 4	27	7	15	0.11	0.25	0.20	0.35	0.70	1.73	0.13	0.39	44.6	39.4	54.7	52.8	6.8	5.1
1/ 8	11	1	5	0.11	0.26	0.42	0.93	0.13	0.30	0.07	0.13	15.7	41.6	74.4	82.5	1.2	0.0
1/16	6	2	2	0.11	0.25	0.34	0.59	1.92	4.37	1.57	3.89	5.0	2.8	391.9	378.4	16.2	8.4

RADAR-GAGE RAINFALL ANALYSES FOR DAY 159 OF 1976 BEGINNING AT 41500. RUN DURATION = 15 MIN
COORD XFORM WT = 2 MIN RADAR RAIN = 0.02 MM RADIUS FOR G/R RATIOS = 1.0 KM

GAGE DENSITY	NUMBER OF GAGES TOTAL	G/R	EVAP	RADAR MEAN	RADAR STDEV	RAINFALL AMOUNTS (MM) GAGE MEAN	GAGE STDEV	GAGE+RADAR MEAN	GAGE+RADAR STDEV	(EVAP) GAGE+RADAR MEAN	(EVAP) GAGE+RADAR STDEV	PERCENT ERROR GAGE ONLY MEAN	PERCENT ERROR GAGE ONLY STDEV	PERCENT ERROR GAGE+RADAR MEAN	PERCENT ERROR GAGE+RADAR STDEV	GAGE-RADAR RATIO MEAN	GAGE-RADAR RATIO STDEV
1/ 1	97	44	33	0.15	0.54	1.03	1.95	1.78	6.56	0.71	1.97	0.0	0.0	0.0	0.0	19.2	22.4
1/ 2	48	22	19	0.15	0.54	0.98	2.21	3.04	12.27	0.87	2.32	4.3	13.1	23.0	22.2	21.6	25.5
1/ 4	27	12	10	0.15	0.54	1.24	2.17	4.03	15.29	0.97	2.99	21.6	41.7	37.3	44.8	26.8	24.2
1/ 8	11	6	5	0.15	0.54	0.36	0.56	0.53	1.27	0.45	1.24	84.9	71.2	86.0	33.9	5.1	2.6
1/16	6	2	4	0.15	0.54	0.93	2.12	2.39	8.96	0.64	2.33	9.5	8.0	9.5	21.1	16.3	4.1

RADAR-GAGE RAINFALL ANALYSES FOR DAY 159 OF 1976 BEGINNING AT 43000. RUN DURATION = 15 MIN
COORD XFORM WT = 2 MIN RADAR RAIN = 0.02 MM RADIUS FOR G/R RATIOS = 1.0 KM

GAGE DENSITY	NUMBER OF GAGES TOTAL	G/R	EVAP	RADAR MEAN	RADAR STDEV	RAINFALL AMOUNTS (MM) GAGE MEAN	GAGE STDEV	GAGE+RADAR MEAN	GAGE+RADAR STDEV	(EVAP) GAGE+RADAR MEAN	(EVAP) GAGE+RADAR STDEV	PERCENT ERROR GAGE ONLY MEAN	PERCENT ERROR GAGE ONLY STDEV	PERCENT ERROR GAGE+RADAR MEAN	PERCENT ERROR GAGE+RADAR STDEV	GAGE-RADAR RATIO MEAN	GAGE-RADAR RATIO STDEV
1/ 1	97	23	30	0.05	0.15	1.32	2.17	0.95	2.52	0.39	0.96	0.0	0.0	0.0	0.0	24.9	24.3
1/ 2	48	14	14	0.05	0.15	1.13	1.76	1.23	3.59	0.56	1.44	14.1	18.9	41.9	49.4	30.6	27.0
1/ 4	27	7	7	0.02	0.13	1.32	1.84	1.53	4.45	0.50	1.21	0.4	14.4	27.7	26.1	33.9	28.5
1/ 8	11	3	2	0.05	0.15	1.17	1.75	1.93	5.52	0.83	2.07	11.4	19.7	111.7	115.5	42.1	28.3
1/16	0	1	0	0.0	0.0	0.0	0.0	0.0	0.0	0.0	0.0	-99.0	-99.0	-99.0	-99.0	0.0	0.0

RADAR-GAGE RAINFALL ANALYSES FOR DAY 159 OF 1976 BEGINNING AT 44500. RUN DURATION = 15 MIN
COORD XFORM WT = 2 MIN RADAR RAIN = 0.02 MM RADIUS FOR G/R RATIOS = 1.0 KM

GAGE DENSITY	NUMBER OF GAGES TOTAL	G/R	EVAP	RADAR MEAN	RADAR STDEV	RAINFALL AMOUNTS (MM) GAGE MEAN	GAGE STDEV	GAGE+RADAR MEAN	GAGE+RADAR STDEV	(EVAP) GAGE+RADAR MEAN	(EVAP) GAGE+RADAR STDEV	PERCENT ERROR GAGE ONLY MEAN	PERCENT ERROR GAGE ONLY STDEV	PERCENT ERROR GAGE+RADAR MEAN	PERCENT ERROR GAGE+RADAR STDEV	GAGE-RADAR RATIO MEAN	GAGE-RADAR RATIO STDEV
1/ 1	97	13	27	0.01	0.02	2.38	3.07	0.60	1.17	0.77	1.34	0.0	0.0	0.0	0.0	56.9	25.6
1/ 2	48	6	15	0.01	0.02	2.53	2.37	0.85	1.55	1.13	1.73	6.6	23.7	48.2	29.3	80.0	13.4
1/ 4	27	3	7	0.01	0.02	2.79	1.92	0.82	1.54	1.16	1.54	17.3	37.4	52.1	14.8	75.1	14.1
1/ 8	11	1	5	0.01	0.02	3.01	3.05	0.74	1.33	0.78	1.36	26.5	0.7	2.2	1.5	70.6	0.0
1/16	6	2	0	0.01	0.02	2.95	3.73	0.41	0.72	0.0	0.0	23.9	21.5	46.1	46.2	37.4	18.5

RADAR-GAGE RAINFALL ANALYSES FOR DAY 159 OF 1976 BEGINNING AT 50000. RUN DURATION = 15 MIN
COORD XFORM WT = 2 MIN RADAR RAIN = 0.02 MM RADIUS FOR G/R RATIOS = 1.0 KM

GAGE DENSITY	NUMBER OF GAGES TOTAL	G/R	EVAP	RADAR MEAN	RADAR STDEV	RAINFALL AMOUNTS (MM) GAGE MEAN	GAGE STDEV	GAGE+RADAR MEAN	GAGE+RADAR STDEV	(EVAP) GAGE+RADAR MEAN	(EVAP) GAGE+RADAR STDEV	PERCENT ERROR GAGE ONLY MEAN	PERCENT ERROR GAGE ONLY STDEV	PERCENT ERROR GAGE+RADAR MEAN	PERCENT ERROR GAGE+RADAR STDEV	GAGE-RADAR RATIO MEAN	GAGE-RADAR RATIO STDEV
1/ 1	97	33	14	0.08	0.16	4.34	4.40	2.56	4.66	2.59	4.84	0.0	0.0	0.0	0.0	41.6	26.3
1/ 2	48	18	8	0.08	0.16	4.56	4.27	2.43	4.25	2.57	4.25	5.1	2.8	0.9	12.2	39.2	23.8
1/ 4	27	11	3	0.08	0.16	4.07	3.84	2.32	4.16	2.35	4.14	6.2	13.6	9.5	14.3	37.5	25.6
1/ 8	11	4	2	0.08	0.16	3.44	4.06	2.45	3.95	2.39	3.97	26.6	7.6	7.7	17.8	31.4	21.3
1/16	6	1	1	0.08	0.16	1.92	2.51	5.83	11.34	5.75	11.10	55.7	42.8	122.2	129.5	72.6	0.0

RADAR-GAGE RAINFALL ANALYSES FOR DAY 159 OF 1976 BEGINNING AT 51500. RUN DURATION = 15 MIN
COORD XFORM WT = 2 MIN RADAR RAIN = 0.02 MM RADIUS FOR G/R RATIOS = 1.0 KM

GAGE DENSITY	NUMBER OF GAGES TOTAL	G/R	EVAP	RADAR MEAN	RADAR STDEV	RAINFALL AMOUNTS (MM) GAGE MEAN	GAGE STDEV	GAGE+RADAR MEAN	GAGE+RADAR STDEV	(EVAP) GAGE+RADAR MEAN	(EVAP) GAGE+RADAR STDEV	PERCENT ERROR GAGE ONLY MEAN	PERCENT ERROR GAGE ONLY STDEV	PERCENT ERROR GAGE+RADAR MEAN	PERCENT ERROR GAGE+RADAR STDEV	GAGE-RADAR RATIO MEAN	GAGE-RADAR RATIO STDEV
1/ 1	97	62	9	0.20	0.23	5.00	5.92	3.78	6.08	3.79	6.09	0.0	0.0	0.0	0.0	24.7	24.1
1/ 2	48	30	5	0.20	0.23	4.41	4.72	3.86	6.55	3.93	6.25	11.7	20.3	3.7	2.7	23.0	24.5
1/ 4	27	19	3	0.20	0.23	4.84	4.72	4.69	8.11	4.62	7.89	3.1	20.2	21.8	16.5	27.7	28.2
1/ 8	11	7	1	0.20	0.23	3.34	3.43	2.55	2.63	2.39	2.62	33.2	42.0	37.0	57.0	17.1	12.4
1/16	6	2	0	0.20	0.23	5.05	6.56	5.68	6.84	0.0	0.0	1.1	10.8	49.7	12.3	30.9	19.1

RADAR-GAGE RAINFALL ANALYSES FOR DAY 159 OF 1976 BEGINNING AT 53000. RUN DURATION = 15 MIN
COORD XFORM WT = 2 MIN RADAR RAIN = 0.02 MM RADIUS FOR G/R RATIOS = 1.0 KM

GAGE DENSITY	NUMBER OF GAGES TOTAL	G/R	EVAP	RADAR MEAN	RADAR STDEV	RAINFALL AMOUNTS (MM) GAGE MEAN	GAGE STDEV	GAGE+RADAR MEAN	GAGE+RADAR STDEV	(EVAP) GAGE+RADAR MEAN	(EVAP) GAGE+RADAR STDEV	PERCENT ERROR GAGE ONLY MEAN	PERCENT ERROR GAGE ONLY STDEV	PERCENT ERROR GAGE+RADAR MEAN	PERCENT ERROR GAGE+RADAR STDEV	GAGE-RADAR RATIO MEAN	GAGE-RADAR RATIO STDEV
1/ 1	97	83	11	0.15	0.15	3.36	4.52	3.13	4.28	2.30	3.73	0.0	0.0	0.0	0.0	21.4	16.7
1/ 2	48	40	5	0.15	0.15	3.98	4.91	3.50	4.32	2.78	3.70	15.5	3.5	0.2	12.2	21.2	16.8
1/ 4	27	23	3	0.15	0.15	4.82	5.98	3.56	4.10	2.54	3.47	61.5	33.5	10.6	1.7	19.6	16.4
1/ 8	11	9	2	0.15	0.15	4.34	6.28	3.68	4.42	1.68	2.55	30.1	16.9	27.1	27.7	22.5	19.3
1/16	6	6	0	0.15	0.15	5.24	6.21	3.74	4.53	0.0	0.0	56.0	37.5	62.7	28.5	22.2	10.4

RADAR-GAGE RAINFALL ANALYSES FOR DAY 159 OF 1976 BEGINNING AT 54500. RUN DURATION = 15 MIN
COORD XFORM WT = 2 MIN RADAR RAIN = 0.02 MM RADIUS FOR G/R RATIOS = 1.0 KM

GAGE DENSITY	NUMBER OF GAGES TOTAL	G/R	EVAP	RADAR MEAN	RADAR STDEV	RAINFALL AMOUNTS (MM) GAGE MEAN	GAGE STDEV	GAGE+RADAR MEAN	GAGE+RADAR STDEV	(EVAP) GAGE+RADAR MEAN	(EVAP) GAGE+RADAR STDEV	PERCENT ERROR GAGE ONLY MEAN	PERCENT ERROR GAGE ONLY STDEV	PERCENT ERROR GAGE+RADAR MEAN	PERCENT ERROR GAGE+RADAR STDEV	GAGE-RADAR RATIO MEAN	GAGE-RADAR RATIO STDEV
1/ 1	97	65	28	0.09	0.11	0.59	0.79	0.68	0.86	0.53	0.83	0.0	0.0	0.0	0.0	9.0	9.0
1/ 2	48	31	16	0.09	0.11	0.64	0.87	0.77	1.28	0.53	0.93	9.0	9.2	0.8	18.1	7.9	5.3
1/ 4	27	17	9	0.09	0.11	0.75	1.10	0.76	1.49	0.65	1.50	26.7	38.9	22.6	80.9	6.9	3.8
1/ 8	11	6	3	0.09	0.11	0.52	0.50	1.29	2.62	0.97	2.46	29.9	37.3	62.1	196.4	10.0	7.4
1/16	6	6	0	0.09	0.11	0.32	0.29	0.61	0.68	0.0	0.0	45.8	64.0	14.3	18.2	6.8	1.1

Table 110. (continued) Page 2 of 5.

RADAR-GAGE RAINFALL ANALYSES FOR DAY 184 OF 1976 BEGINNING AT 170000. RUN DURATION = 15 MIN
COORD XFORM WT = 2 MIN RADAR RAIN = 0.02 MM RADIUS FOR G/R RATIOS = 1.0 KM

GAGE DENSITY	NUMBER OF GAGES TOTAL	G/R	EVAP	RADAR MEAN	RADAR STDEV	RAINFALL AMOUNTS (MM) GAGE MEAN	GAGE STDEV	GAGE+RADAR MEAN	GAGE+RADAR STDEV	(EVAP) GAGE+RADAR MEAN	(EVAP) GAGE+RADAR STDEV	PERCENT ERROR GAGE ONLY MEAN	GAGE ONLY STDEV	PERCENT ERROR GAGE+RADAR MEAN	GAGE+RADAR STDEV	GAGE-RADAR RATIO MEAN	GAGE-RADAR RATIO STDEV
1/ 1	111	45	44	0.09	0.15	0.69	1.51	0.93	1.55	0.52	1.38	0.0	0.0	0.0	0.0	12.1	11.1
1/ 2	57	21	25	0.09	0.15	0.57	0.79	0.65	1.06	0.33	0.57	17.7	47.9	37.3	58.4	10.2	11.1
1/ 4	28	12	9	0.07	0.15	0.68	0.78	0.61	1.03	0.30	0.50	1.0	48.1	41.3	63.8	9.4	7.3
1/ 8	15	5	6	0.09	0.15	0.61	1.04	0.43	0.70	0.19	0.40	11.8	31.0	63.1	71.0	5.5	3.0
1/16	7	6	2	0.09	0.15	0.73	1.04	1.22	2.05	0.85	1.54	6.5	31.0	63.5	11.6	17.3	14.2

RADAR-GAGE RAINFALL ANALYSES FOR DAY 184 OF 1976 BEGINNING AT 171500. RUN DURATION = 15 MIN
COORD XFORM WT = 2 MIN RADAR RAIN = 0.02 MM RADIUS FOR G/R RATIOS = 1.0 KM

GAGE DENSITY	NUMBER OF GAGES TOTAL	G/R	EVAP	RADAR MEAN	RADAR STDEV	RAINFALL AMOUNTS (MM) GAGE MEAN	GAGE STDEV	GAGE+RADAR MEAN	GAGE+RADAR STDEV	(EVAP) GAGE+RADAR MEAN	(EVAP) GAGE+RADAR STDEV	PERCENT ERROR GAGE ONLY MEAN	GAGE ONLY STDEV	PERCENT ERROR GAGE+RADAR MEAN	GAGE+RADAR STDEV	GAGE-RADAR RATIO MEAN	GAGE-RADAR RATIO STDEV
1/ 1	111	34	40	0.06	0.13	0.72	1.71	1.10	1.87	0.54	1.34	0.0	0.0	0.0	0.0	25.1	26.6
1/ 2	57	18	28	0.06	0.13	0.79	2.04	0.92	1.72	0.34	0.80	9.7	19.8	37.4	40.9	20.3	18.5
1/ 4	28	7	13	0.06	0.13	1.30	3.05	1.20	2.31	0.43	1.15	79.4	78.9	21.1	14.4	24.1	23.0
1/ 8	15	5	7	0.06	0.13	0.74	1.51	1.04	1.80	0.41	1.04	1.9	11.3	24.6	22.5	19.5	11.2
1/16	7	3	3	0.06	0.13	0.41	0.44	2.23	5.59	1.04	3.56	43.6	94.0	90.8	165.0	39.5	41.1

RADAR-GAGE RAINFALL ANALYSES FOR DAY 184 OF 1976 BEGINNING AT 173000. RUN DURATION = 15 MIN
COORD XFORM WT = 2 MIN RADAR RAIN = 0.02 MM RADIUS FOR G/R RATIOS = 1.0 KM

GAGE DENSITY	NUMBER OF GAGES TOTAL	G/R	EVAP	RADAR MEAN	RADAR STDEV	RAINFALL AMOUNTS (MM) GAGE MEAN	GAGE STDEV	GAGE+RADAR MEAN	GAGE+RADAR STDEV	(EVAP) GAGE+RADAR MEAN	(EVAP) GAGE+RADAR STDEV	PERCENT ERROR GAGE ONLY MEAN	GAGE ONLY STDEV	PERCENT ERROR GAGE+RADAR MEAN	GAGE+RADAR STDEV	GAGE-RADAR RATIO MEAN	GAGE-RADAR RATIO STDEV
1/ 1	111	42	41	0.06	0.11	0.50	1.23	0.94	1.96	0.37	1.01	0.0	0.0	0.0	0.0	26.2	29.0
1/ 2	57	22	25	0.06	0.11	0.63	1.61	0.83	1.81	0.28	0.74	25.0	30.8	24.2	26.7	23.0	30.4
1/ 4	28	11	12	0.06	0.11	0.72	1.27	1.47	2.99	0.47	1.65	44.1	3.5	81.3	63.0	38.1	34.3
1/ 8	15	4	7	0.06	0.11	0.09	0.15	0.38	0.91	0.08	0.24	82.8	88.1	79.3	76.1	10.2	15.3
1/16	7	4	4	0.06	0.11	0.29	0.66	0.98	1.90	0.60	0.95	41.9	44.5	61.8	6.2	32.0	26.7

RADAR-GAGE RAINFALL ANALYSES FOR DAY 184 OF 1976 BEGINNING AT 174500. RUN DURATION = 15 MIN
COORD XFORM WT = 2 MIN RADAR RAIN = 0.02 MM RADIUS FOR G/R RATIOS = 1.0 KM

GAGE DENSITY	NUMBER OF GAGES TOTAL	G/R	EVAP	RADAR MEAN	RADAR STDEV	RAINFALL AMOUNTS (MM) GAGE MEAN	GAGE STDEV	GAGE+RADAR MEAN	GAGE+RADAR STDEV	(EVAP) GAGE+RADAR MEAN	(EVAP) GAGE+RADAR STDEV	PERCENT ERROR GAGE ONLY MEAN	GAGE ONLY STDEV	PERCENT ERROR GAGE+RADAR MEAN	GAGE+RADAR STDEV	GAGE-RADAR RATIO MEAN	GAGE-RADAR RATIO STDEV
1/ 1	111	48	51	0.07	0.13	0.53	0.92	1.16	1.98	0.58	1.27	0.0	0.0	0.0	0.0	23.6	22.5
1/ 2	57	23	31	0.07	0.13	0.61	1.15	1.21	2.50	0.52	1.39	15.8	24.9	10.8	9.7	21.3	20.2
1/ 4	28	11	14	0.07	0.13	0.58	0.94	1.77	3.62	0.77	1.90	10.2	2.3	33.2	49.6	25.8	17.5
1/ 8	15	4	8	0.07	0.13	0.64	1.14	1.61	3.33	0.74	2.16	20.6	23.8	26.7	70.7	23.9	32.3
1/16	7	4	4	0.07	0.13	0.38	0.67	1.21	2.26	0.18	0.34	28.3	26.9	68.7	73.2	16.8	8.5

RADAR-GAGE RAINFALL ANALYSES FOR DAY 184 OF 1976 BEGINNING AT 180000. RUN DURATION = 15 MIN
COORD XFORM WT = 2 MIN RADAR RAIN = 0.02 MM RADIUS FOR G/R RATIOS = 1.0 KM

GAGE DENSITY	NUMBER OF GAGES TOTAL	G/R	EVAP	RADAR MEAN	RADAR STDEV	RAINFALL AMOUNTS (MM) GAGE MEAN	GAGE STDEV	GAGE+RADAR MEAN	GAGE+RADAR STDEV	(EVAP) GAGE+RADAR MEAN	(EVAP) GAGE+RADAR STDEV	PERCENT ERROR GAGE ONLY MEAN	GAGE ONLY STDEV	PERCENT ERROR GAGE+RADAR MEAN	GAGE+RADAR STDEV	GAGE-RADAR RATIO MEAN	GAGE-RADAR RATIO STDEV
1/ 1	111	38	38	0.11	0.23	0.94	2.87	1.50	3.18	0.66	2.25	0.0	0.0	0.0	0.0	18.1	17.7
1/ 2	57	21	32	0.11	0.23	0.58	1.15	1.42	3.00	0.62	2.42	39.9	60.2	6.8	7.3	16.9	15.3
1/ 4	28	11	13	0.11	0.23	0.67	1.11	1.75	4.01	0.66	2.62	28.8	61.6	0.6	1.6	18.4	16.6
1/ 8	15	5	8	0.11	0.23	0.67	1.00	1.34	2.58	0.55	1.85	32.0	65.4	17.1	13.5	15.4	16.5
1/16	7	3	3	0.11	0.23	6.17	12.64	0.74	1.46	0.54	1.42	553.5	337.1	18.5	36.9	7.4	3.1

RADAR-GAGE RAINFALL ANALYSES FOR DAY 184 OF 1976 BEGINNING AT 181500. RUN DURATION = 15 MIN
COORD XFORM WT = 2 MIN RADAR RAIN = 0.02 MM RADIUS FOR G/R RATIOS = 1.0 KM

GAGE DENSITY	NUMBER OF GAGES TOTAL	G/R	EVAP	RADAR MEAN	RADAR STDEV	RAINFALL AMOUNTS (MM) GAGE MEAN	GAGE STDEV	GAGE+RADAR MEAN	GAGE+RADAR STDEV	(EVAP) GAGE+RADAR MEAN	(EVAP) GAGE+RADAR STDEV	PERCENT ERROR GAGE ONLY MEAN	GAGE ONLY STDEV	PERCENT ERROR GAGE+RADAR MEAN	GAGE+RADAR STDEV	GAGE-RADAR RATIO MEAN	GAGE-RADAR RATIO STDEV
1/ 1	110	46	49	0.16	0.34	0.88	1.62	2.07	4.53	1.04	2.92	0.0	0.0	0.0	0.0	16.1	15.0
1/ 2	56	22	29	0.16	0.34	0.74	1.46	2.31	5.20	1.05	3.37	15.9	9.7	0.8	15.6	15.2	14.3
1/ 4	27	10	13	0.16	0.34	0.79	1.24	2.51	5.27	1.34	3.78	9.5	23.5	28.2	29.5	16.6	15.5
1/ 8	15	7	7	0.16	0.34	1.34	2.58	2.70	5.66	1.05	3.38	63.6	40.3	0.4	12.6	12.3	11.8
1/16	7	4	1	0.16	0.34	2.14	2.14	1.98	3.99	1.67	3.70	144.8	32.2	60.2	26.7	14.2	9.4

RADAR-GAGE RAINFALL ANALYSES FOR DAY 184 OF 1976 BEGINNING AT 183000. RUN DURATION = 15 MIN
COORD XFORM WT = 2 MIN RADAR RAIN = 0.02 MM RADIUS FOR G/R RATIOS = 1.0 KM

GAGE DENSITY	NUMBER OF GAGES TOTAL	G/R	EVAP	RADAR MEAN	RADAR STDEV	RAINFALL AMOUNTS (MM) GAGE MEAN	GAGE STDEV	GAGE+RADAR MEAN	GAGE+RADAR STDEV	(EVAP) GAGE+RADAR MEAN	(EVAP) GAGE+RADAR STDEV	PERCENT ERROR GAGE ONLY MEAN	GAGE ONLY STDEV	PERCENT ERROR GAGE+RADAR MEAN	GAGE+RADAR STDEV	GAGE-RADAR RATIO MEAN	GAGE-RADAR RATIO STDEV
1/ 1	110	40	56	0.14	0.29	1.01	2.07	1.93	4.14	0.76	1.66	0.0	0.0	0.0	0.0	17.4	17.7
1/ 2	56	19	32	0.14	0.29	0.89	1.67	2.01	4.43	0.59	1.61	16.0	19.5	21.8	2.9	17.7	17.4
1/ 4	27	8	17	0.14	0.29	0.94	2.03	2.08	4.61	0.89	2.80	7.5	2.2	16.7	68.7	18.3	23.2
1/ 8	15	5	8	0.14	0.29	1.21	1.71	2.65	5.90	1.18	3.97	19.8	17.6	55.7	139.3	17.2	11.6
1/16	7	4	2	0.14	0.29	2.35	3.91	0.77	1.64	0.53	1.14	132.3	88.8	29.6	31.4	5.5	4.0

RADAR-GAGE RAINFALL ANALYSES FOR DAY 184 OF 1976 BEGINNING AT 184500. RUN DURATION = 15 MIN
COORD XFORM WT = 2 MIN RADAR RAIN = 0.02 MM RADIUS FOR G/R RATIOS = 1.0 KM

GAGE DENSITY	NUMBER OF GAGES TOTAL	G/R	EVAP	RADAR MEAN	RADAR STDEV	RAINFALL AMOUNTS (MM) GAGE MEAN	GAGE STDEV	GAGE+RADAR MEAN	GAGE+RADAR STDEV	(EVAP) GAGE+RADAR MEAN	(EVAP) GAGE+RADAR STDEV	PERCENT ERROR GAGE ONLY MEAN	GAGE ONLY STDEV	PERCENT ERROR GAGE+RADAR MEAN	GAGE+RADAR STDEV	GAGE-RADAR RATIO MEAN	GAGE-RADAR RATIO STDEV
1/ 1	110	32	53	0.12	0.28	0.94	1.90	1.98	4.97	0.92	2.66	0.0	0.0	0.0	0.0	22.2	23.1
1/ 2	56	15	29	0.12	0.28	0.72	1.40	2.21	5.39	0.94	2.77	22.8	26.1	1.7	3.9	23.3	27.4
1/ 4	27	8	14	0.12	0.28	0.58	1.13	2.17	4.62	0.80	2.78	38.4	40.3	13.0	4.4	24.4	26.3
1/ 8	15	3	7	0.12	0.28	0.96	1.38	0.41	0.97	0.27	0.74	2.1	27.7	70.7	72.3	2.8	3.4
1/16	7	3	4	0.12	0.28	0.84	1.60	4.52	11.04	1.68	5.98	10.5	15.7	82.9	124.6	34.4	22.4

RADAR-GAGE RAINFALL ANALYSES FOR DAY 184 OF 1976 BEGINNING AT 190000. RUN DURATION = 15 MIN
COORD XFORM WT = 2 MIN RADAR RAIN = 0.02 MM RADIUS FOR G/R RATIOS = 1.0 KM

GAGE DENSITY	NUMBER OF GAGES TOTAL	G/R	EVAP	RADAR MEAN	RADAR STDEV	RAINFALL AMOUNTS (MM) GAGE MEAN	GAGE STDEV	GAGE+RADAR MEAN	GAGE+RADAR STDEV	(EVAP) GAGE+RADAR MEAN	(EVAP) GAGE+RADAR STDEV	PERCENT ERROR GAGE ONLY MEAN	PERCENT ERROR GAGE ONLY STDEV	PERCENT ERROR GAGE+RADAR MEAN	PERCENT ERROR GAGE+RADAR STDEV	GAGE-RADAR RATIO MEAN	GAGE-RADAR RATIO STDEV
1/ 1	110	33	47	0.11	0.20	1.23	2.51	2.59	5.44	1.93	5.38	0.0	0.0	0.0	0.0	27.2	26.9
1/ 2	56	16	27	0.11	0.20	1.08	2.22	2.19	4.50	1.32	3.54	12.1	11.5	32.0	34.2	26.4	30.4
1/ 4	27	8	13	0.11	0.20	1.26	2.50	2.05	3.85	1.19	3.06	2.6	0.4	34.7	43.0	23.3	27.8
1/ 8	15	3	8	0.11	0.28	1.15	2.16	1.55	3.45	0.88	2.45	6.2	14.2	54.2	54.5	19.1	24.4
1/16	7	5	1	0.11	0.20	0.93	1.73	2.26	5.02	2.14	4.93	24.3	31.4	10.6	8.4	26.4	17.8

RADAR-GAGE RAINFALL ANALYSES FOR DAY 184 OF 1976 BEGINNING AT 191500. RUN DURATION = 15 MIN
COORD XFORM WT = 2 MIN RADAR RAIN = 0.02 MM RADIUS FOR G/R RATIOS = 1.0 KM

GAGE DENSITY	NUMBER OF GAGES TOTAL	G/R	EVAP	RADAR MEAN	RADAR STDEV	RAINFALL AMOUNTS (MM) GAGE MEAN	GAGE STDEV	GAGE+RADAR MEAN	GAGE+RADAR STDEV	(EVAP) GAGE+RADAR MEAN	(EVAP) GAGE+RADAR STDEV	PERCENT ERROR GAGE ONLY MEAN	PERCENT ERROR GAGE ONLY STDEV	PERCENT ERROR GAGE+RADAR MEAN	PERCENT ERROR GAGE+RADAR STDEV	GAGE-RADAR RATIO MEAN	GAGE-RADAR RATIO STDEV
1/ 1	110	27	53	0.11	0.26	1.14	3.05	2.28	6.22	1.97	6.12	0.0	0.0	0.0	0.0	26.2	24.5
1/ 2	56	13	27	0.11	0.26	1.26	3.08	2.22	6.23	1.88	5.10	11.3	0.0	4.6	0.4	24.4	17.7
1/ 4	27	7	15	0.11	0.26	1.19	2.90	2.31	7.41	2.08	7.37	4.9	9.1	5.4	20.5	20.1	13.4
1/ 8	15	3	7	0.11	0.26	1.15	2.31	1.50	3.10	0.81	2.02	1.1	24.2	59.0	67.0	24.3	24.7
1/16	7	4	1	0.11	0.26	0.99	1.53	0.99	2.41	0.80	2.09	13.1	49.9	59.6	65.8	17.3	19.6

RADAR-GAGE RAINFALL ANALYSES FOR DAY 184 OF 1976 BEGINNING AT 193000. RUN DURATION = 15 MIN
COORD XFORM WT = 2 MIN RADAR RAIN = 0.02 MM RADIUS FOR G/R RATIOS = 1.0 KM

GAGE DENSITY	NUMBER OF GAGES TOTAL	G/R	EVAP	RADAR MEAN	RADAR STDEV	RAINFALL AMOUNTS (MM) GAGE MEAN	GAGE STDEV	GAGE+RADAR MEAN	GAGE+RADAR STDEV	(EVAP) GAGE+RADAR MEAN	(EVAP) GAGE+RADAR STDEV	PERCENT ERROR GAGE ONLY MEAN	PERCENT ERROR GAGE ONLY STDEV	PERCENT ERROR GAGE+RADAR MEAN	PERCENT ERROR GAGE+RADAR STDEV	GAGE-RADAR RATIO MEAN	GAGE-RADAR RATIO STDEV
1/ 1	110	19	51	0.10	0.30	0.81	2.46	1.72	5.44	1.17	3.77	0.0	0.0	0.0	0.0	22.6	22.5
1/ 2	56	10	28	0.10	0.30	1.02	2.70	1.98	5.92	1.34	3.89	26.4	9.6	14.7	3.2	24.6	26.5
1/ 4	27	5	13	0.10	0.30	0.81	1.91	2.04	6.63	1.91	4.67	4.0	22.1	21.1	24.0	26.6	27.0
1/ 8	15	3	8	0.10	0.30	1.56	4.04	2.37	6.90	1.19	3.65	93.5	64.3	1.9	3.1	30.7	29.9
1/16	7	3	2	0.10	0.30	0.52	0.87	1.77	5.41	1.34	4.11	36.0	64.8	15.2	9.0	25.6	16.8

RADAR-GAGE RAINFALL ANALYSES FOR DAY 184 OF 1976 BEGINNING AT 194500. RUN DURATION = 15 MIN
COORD XFORM WT = 2 MIN RADAR RAIN = 0.02 MM RADIUS FOR G/R RATIOS = 1.0 KM

GAGE DENSITY	NUMBER OF GAGES TOTAL	G/R	EVAP	RADAR MEAN	RADAR STDEV	RAINFALL AMOUNTS (MM) GAGE MEAN	GAGE STDEV	GAGE+RADAR MEAN	GAGE+RADAR STDEV	(EVAP) GAGE+RADAR MEAN	(EVAP) GAGE+RADAR STDEV	PERCENT ERROR GAGE ONLY MEAN	PERCENT ERROR GAGE ONLY STDEV	PERCENT ERROR GAGE+RADAR MEAN	PERCENT ERROR GAGE+RADAR STDEV	GAGE-RADAR RATIO MEAN	GAGE-RADAR RATIO STDEV
1/ 1	110	14	51	0.08	0.36	0.37	0.94	1.25	6.27	0.63	3.27	0.0	0.0	0.0	0.0	16.4	10.8
1/ 2	56	7	28	0.08	0.36	0.34	0.77	1.45	7.22	0.61	2.49	6.5	18.6	3.6	23.7	20.1	7.1
1/ 4	27	3	15	0.08	0.36	0.38	0.82	1.35	8.58	1.04	4.96	2.7	13.3	63.9	51.9	23.1	6.1
1/ 8	15	4	7	0.08	0.36	0.38	0.74	1.13	6.14	0.29	0.95	3.3	21.1	54.7	70.9	17.9	7.0
1/16	7	2	1	0.08	0.36	0.17	0.18	1.35	6.33	1.34	5.71	53.1	80.9	111.2	74.6	16.8	6.7

RADAR-GAGE RAINFALL ANALYSES FOR DAY 195 OF 1976 BEGINNING AT 20000. RUN DURATION = 15 MIN
COORD XFORM WT = 2 MIN RADAR RAIN = 0.02 MM RADIUS FOR G/R RATIOS = 1.0 KM

GAGE DENSITY	NUMBER OF GAGES TOTAL	G/R	EVAP	RADAR MEAN	RADAR STDEV	RAINFALL AMOUNTS (MM) GAGE MEAN	GAGE STDEV	GAGE+RADAR MEAN	GAGE+RADAR STDEV	(EVAP) GAGE+RADAR MEAN	(EVAP) GAGE+RADAR STDEV	PERCENT ERROR GAGE ONLY MEAN	PERCENT ERROR GAGE ONLY STDEV	PERCENT ERROR GAGE+RADAR MEAN	PERCENT ERROR GAGE+RADAR STDEV	GAGE-RADAR RATIO MEAN	GAGE-RADAR RATIO STDEV
1/ 1	105	53	47	0.04	0.04	0.18	0.21	0.27	0.18	0.16	0.21	0.0	0.0	0.0	0.0	5.1	2.4
1/ 2	55	28	27	0.04	0.04	0.17	0.19	0.24	0.18	0.15	0.19	7.3	9.4	7.5	9.1	4.7	2.1
1/ 4	27	14	13	0.04	0.04	0.18	0.20	0.26	0.17	0.16	0.21	2.8	7.5	10.6	15.9	5.0	2.5
1/ 8	14	7	7	0.04	0.04	0.17	0.18	0.24	0.19	0.15	0.21	5.6	10.9	9.5	0.5	4.2	1.6
1/16	5	3	2	0.04	0.04	0.13	0.15	0.53	0.31	0.20	0.34	24.6	27.2	25.0	63.5	5.5	3.1

RADAR-GAGE RAINFALL ANALYSES FOR DAY 195 OF 1976 BEGINNING AT 21500. RUN DURATION = 15 MIN
COORD XFORM WT = 2 MIN RADAR RAIN = 0.02 MM RADIUS FOR G/R RATIOS = 1.0 KM

GAGE DENSITY	NUMBER OF GAGES TOTAL	G/R	EVAP	RADAR MEAN	RADAR STDEV	RAINFALL AMOUNTS (MM) GAGE MEAN	GAGE STDEV	GAGE+RADAR MEAN	GAGE+RADAR STDEV	(EVAP) GAGE+RADAR MEAN	(EVAP) GAGE+RADAR STDEV	PERCENT ERROR GAGE ONLY MEAN	PERCENT ERROR GAGE ONLY STDEV	PERCENT ERROR GAGE+RADAR MEAN	PERCENT ERROR GAGE+RADAR STDEV	GAGE-RADAR RATIO MEAN	GAGE-RADAR RATIO STDEV
1/ 1	105	48	50	0.04	0.04	0.15	0.19	0.25	0.19	0.14	0.19	0.0	0.0	0.0	0.0	6.4	3.4
1/ 2	55	24	27	0.04	0.04	0.15	0.20	0.26	0.20	0.14	0.21	1.3	3.1	2.9	10.6	6.4	3.0
1/ 4	27	12	13	0.04	0.04	0.18	0.21	0.28	0.21	0.15	0.21	17.6	10.8	8.7	13.8	6.4	2.8
1/ 8	14	7	7	0.04	0.04	0.14	0.15	0.23	0.21	0.16	0.24	10.5	23.7	11.6	13.2	6.0	3.2
1/16	5	3	2	0.04	0.04	0.13	0.13	0.29	0.25	0.17	0.28	16.3	30.4	25.2	47.9	6.9	3.4

RADAR-GAGE RAINFALL ANALYSES FOR DAY 195 OF 1976 BEGINNING AT 23000. RUN DURATION = 15 MIN
COORD XFORM WT = 2 MIN RADAR RAIN = 0.02 MM RADIUS FOR G/R RATIOS = 1.0 KM

GAGE DENSITY	NUMBER OF GAGES TOTAL	G/R	EVAP	RADAR MEAN	RADAR STDEV	RAINFALL AMOUNTS (MM) GAGE MEAN	GAGE STDEV	GAGE+RADAR MEAN	GAGE+RADAR STDEV	(EVAP) GAGE+RADAR MEAN	(EVAP) GAGE+RADAR STDEV	PERCENT ERROR GAGE ONLY MEAN	PERCENT ERROR GAGE ONLY STDEV	PERCENT ERROR GAGE+RADAR MEAN	PERCENT ERROR GAGE+RADAR STDEV	GAGE-RADAR RATIO MEAN	GAGE-RADAR RATIO STDEV
1/ 1	105	52	36	0.04	0.04	0.19	0.25	0.26	0.25	0.18	0.25	0.0	0.0	0.0	0.0	6.9	3.7
1/ 2	55	28	18	0.04	0.04	0.20	0.24	0.27	0.26	0.17	0.25	4.1	2.0	2.3	3.3	6.9	2.9
1/ 4	27	12	10	0.04	0.04	0.19	0.21	0.24	0.22	0.13	0.21	3.1	13.3	24.4	14.6	6.6	3.1
1/ 8	14	8	4	0.04	0.04	0.25	0.23	0.31	0.29	0.19	0.22	27.8	8.1	7.6	11.0	7.2	1.3
1/16	5	3	1	0.04	0.04	0.17	0.22	0.33	0.34	0.25	0.28	10.8	12.1	40.9	13.0	8.0	3.5

RADAR-GAGE RAINFALL ANALYSES FOR DAY 195 OF 1976 BEGINNING AT 24500. RUN DURATION = 15 MIN
COORD XFORM WT = 2 MIN RADAR RAIN = 0.02 MM RADIUS FOR G/R RATIOS = 1.0 KM

GAGE DENSITY	NUMBER OF GAGES TOTAL	G/R	EVAP	RADAR MEAN	RADAR STDEV	RAINFALL AMOUNTS (MM) GAGE MEAN	GAGE STDEV	GAGE+RADAR MEAN	GAGE+RADAR STDEV	(EVAP) GAGE+RADAR MEAN	(EVAP) GAGE+RADAR STDEV	PERCENT ERROR GAGE ONLY MEAN	PERCENT ERROR GAGE ONLY STDEV	PERCENT ERROR GAGE+RADAR MEAN	PERCENT ERROR GAGE+RADAR STDEV	GAGE-RADAR RATIO MEAN	GAGE-RADAR RATIO STDEV
1/ 1	105	34	44	0.03	0.04	0.12	0.16	0.16	0.17	0.10	0.14	0.0	0.0	0.0	0.0	5.5	3.5
1/ 2	55	18	25	0.03	0.04	0.14	0.16	0.18	0.19	0.11	0.15	10.6	0.0	11.1	6.6	6.1	3.6
1/ 4	27	9	12	0.03	0.04	0.14	0.14	0.17	0.19	0.13	0.16	15.4	3.0	36.4	28.6	5.3	1.7
1/ 8	14	5	6	0.03	0.04	0.22	0.22	0.23	0.26	0.16	0.21	79.7	35.3	59.6	48.3	8.2	1.8
1/16	5	1	3	0.03	0.04	0.08	0.16	0.19	0.21	0.07	0.10	36.6	3.0	31.3	24.2	5.6	0.0

RADAR-GAGE RAINFALL ANALYSES FOR DAY 201 OF 1976 BEGINNING AT 13000. RUN DURATION = 15 MIN
COORD XFORM MT = 2 MIN RADAR RAIN = 0.02 MM RADIUS FOR G/R RATIOS = 1.0 KM

GAGE DENSITY	NUMBER OF GAGES TOTAL	G/R	EVAP	RADAR MEAN	RADAR STDEV	RAINFALL AMOUNTS (MM) GAGE MEAN	GAGE STDEV	GAGE+RADAR MEAN	GAGE+RADAR STDEV	(EVAP) GAGE+RADAR MEAN	(EVAP) GAGE+RADAR STDEV	PERCENT ERROR GAGE ONLY MEAN	PERCENT ERROR GAGE ONLY STDEV	PERCENT ERROR GAGE+RADAR MEAN	PERCENT ERROR GAGE+RADAR STDEV	GAGE-RADAR RATIO MEAN	GAGE-RADAR RATIO STDEV
1/ 1	112	2	17	0.01	0.04	0.01	0.04	0.02	0.08	0.01	0.07	0.0	0.0	0.0	0.0	3.6	2.4
1/ 2	55	2	7	0.01	0.04	0.02	0.06	0.02	0.08	0.01	0.07	88.9	39.0	30.0	1.4	3.6	2.4
1/ 4	27	2	3	0.01	0.04	0.02	0.06	0.02	0.06	0.01	0.05	122.2	46.3	10.0	35.3	3.6	2.6
1/ 8	0	1	0	0.0	0.0	0.0	0.0	0.0	0.0	0.0	0.0	-99.0	-99.0	-99.0	-99.0	0.0	0.0
1/16	0	1	0	0.0	0.0	0.0	0.0	0.0	0.0	0.0	0.0	-99.0	-99.0	-99.0	-99.0	0.0	0.0

RADAR-GAGE RAINFALL ANALYSES FOR DAY 201 OF 1976 BEGINNING AT 14500. RUN DURATION = 15 MIN
COORD XFORM MT = 2 MIN RADAR RAIN = 0.02 MM RADIUS FOR G/R RATIOS = 1.0 KM

GAGE DENSITY	NUMBER OF GAGES TOTAL	G/R	EVAP	RADAR MEAN	RADAR STDEV	RAINFALL AMOUNTS (MM) GAGE MEAN	GAGE STDEV	GAGE+RADAR MEAN	GAGE+RADAR STDEV	(EVAP) GAGE+RADAR MEAN	(EVAP) GAGE+RADAR STDEV	PERCENT ERROR GAGE ONLY MEAN	PERCENT ERROR GAGE ONLY STDEV	PERCENT ERROR GAGE+RADAR MEAN	PERCENT ERROR GAGE+RADAR STDEV	GAGE-RADAR RATIO MEAN	GAGE-RADAR RATIO STDEV
1/ 1	112	9	39	0.03	0.14	0.11	0.72	0.25	1.24	0.08	0.70	0.0	0.0	0.0	0.0	9.1	7.3
1/ 2	55	7	15	0.03	0.14	0.19	0.97	0.25	1.19	0.13	0.96	80.6	34.8	60.3	37.3	10.3	7.8
1/ 4	27	2	8	0.03	0.14	0.03	0.09	0.14	0.62	0.09	0.59	75.0	89.1	15.4	15.5	6.3	3.9
1/ 8	14	3	3	0.03	0.14	0.66	2.09	0.26	1.32	0.23	1.32	515.7	189.9	191.0	89.3	7.9	1.4
1/16	7	1	0	0.03	0.14	0.05	0.11	0.29	1.38	0.0	0.0	49.1	84.5	267.9	97.1	9.7	0.0

RADAR-GAGE RAINFALL ANALYSES FOR DAY 201 OF 1976 BEGINNING AT 20000. RUN DURATION = 15 MIN
COORD XFORM MT = 2 MIN RADAR RAIN = 0.02 MM RADIUS FOR G/R RATIOS = 1.0 KM

GAGE DENSITY	NUMBER OF GAGES TOTAL	G/R	EVAP	RADAR MEAN	RADAR STDEV	RAINFALL AMOUNTS (MM) GAGE MEAN	GAGE STDEV	GAGE+RADAR MEAN	GAGE+RADAR STDEV	(EVAP) GAGE+RADAR MEAN	(EVAP) GAGE+RADAR STDEV	PERCENT ERROR GAGE ONLY MEAN	PERCENT ERROR GAGE ONLY STDEV	PERCENT ERROR GAGE+RADAR MEAN	PERCENT ERROR GAGE+RADAR STDEV	GAGE-RADAR RATIO MEAN	GAGE-RADAR RATIO STDEV
1/ 1	112	17	45	0.04	0.10	0.12	0.46	0.25	0.67	0.12	0.58	0.0	0.0	0.0	0.0	7.9	11.4
1/ 2	55	7	23	0.04	0.10	0.13	0.48	0.43	1.38	0.13	0.75	8.1	5.0	13.7	29.6	12.2	16.4
1/ 4	27	2	14	0.04	0.10	0.18	0.62	1.24	3.85	0.52	2.13	47.6	35.7	348.7	348.6	31.6	19.9
1/ 8	14	5	5	0.04	0.10	0.05	0.10	0.18	0.46	0.10	0.40	56.5	78.0	15.4	31.8	5.3	2.1
1/16	0	1	0	0.0	0.0	0.0	0.0	0.0	0.0	0.0	0.0	-99.0	-99.0	-99.0	-99.0	0.0	0.0

RADAR-GAGE RAINFALL ANALYSES FOR DAY 201 OF 1976 BEGINNING AT 21500. RUN DURATION = 15 MIN
COORD XFORM MT = 2 MIN RADAR RAIN = 0.02 MM RADIUS FOR G/R RATIOS = 1.0 KM

GAGE DENSITY	NUMBER OF GAGES TOTAL	G/R	EVAP	RADAR MEAN	RADAR STDEV	RAINFALL AMOUNTS (MM) GAGE MEAN	GAGE STDEV	GAGE+RADAR MEAN	GAGE+RADAR STDEV	(EVAP) GAGE+RADAR MEAN	(EVAP) GAGE+RADAR STDEV	PERCENT ERROR GAGE ONLY MEAN	PERCENT ERROR GAGE ONLY STDEV	PERCENT ERROR GAGE+RADAR MEAN	PERCENT ERROR GAGE+RADAR STDEV	GAGE-RADAR RATIO MEAN	GAGE-RADAR RATIO STDEV
1/ 1	112	18	59	0.03	0.08	0.11	0.41	0.27	0.89	0.13	0.85	0.0	0.0	0.0	0.0	10.5	12.1
1/ 2	55	6	27	0.03	0.08	0.08	0.30	0.14	0.38	0.05	0.30	29.6	27.5	64.6	64.7	4.6	3.1
1/ 4	27	3	11	0.03	0.08	0.10	0.36	0.16	0.49	0.05	0.31	9.6	13.3	63.1	63.2	5.1	2.7
1/ 8	14	1	5	0.03	0.08	0.01	0.03	0.05	0.14	0.01	0.03	92.2	93.3	91.5	96.3	1.7	0.0
1/16	7	1	3	0.03	0.08	0.07	0.17	0.42	1.15	0.03	0.08	34.8	59.3	78.2	90.4	13.9	0.0

DENSITY	MEAN PERCENT ERROR GAGE ONLY MEAN	GAGE ONLY STDEV	GAGE+RADAR MEAN	GAGE+RADAR STDEV	GAGE-RADAR RATIO MEAN	GAGE-RADAR RATIO STDEV
1/ 1	0.0	0.0	0.0	0.0	17.6	16.2
1/ 2	19.2	17.7	23.6	29.0	18.3	15.8
1/ 4	26.4	26.8	49.9	62.0	19.1	15.6
1/ 8	49.0	41.8	55.9	67.0	18.5	10.3
1/16	93.9	48.5	84.2	70.7	19.3	10.3

Table 110. (continued) Page 5 of 5.

(e) Appendix E: Tabulation of analysis duration test results. This table summarizes analysis duration tests using a format similar to Appendix D. Data from individual hours are listed together with hourly sums for short duration analyses to facilitate comparison with longer duration runs.

In several cases, gage data were missing for five minute periods. In cases where no gage or radar data were available for an analysis, the analysis was not run. In some cases (usually 5 or 15 minute analyses), the missing data produced discrepancies in hourly mean areal rainfall amounts for different duration analyses taken from the same period. In cases where only part of the necessary data were missing for an analysis period, the remaining gage or radar rainfall amounts were multiplied by an appropriate factor to account for the missing data. These corrected rainfall amounts are indicated within parentheses.

For days 195 and 201, parallel analyses were made using a radar rainfall minimum of 0.10 mm for the sake of comparing the radar rainfall minimum decision for different analysis durations.

RADAR-GAGE RAINFALL ANALYSES FOR DAY 158 OF 1974 BEGINNING AT 40000. RUN DURATION = 5 MIN
COORD XFORM WT = 2 MIN RADAR RAIN = 0.02 MM RADIUS FOR G/R RATIOS = 1.0 KM

GAGE DENSITY	TIME (Z)	NUMBER OF GAGES TOTAL	G/R	EVAP	RAINFALL AMOUNTS (MM) RADAR MEAN	RADAR STDEV	GAGE MEAN	GAGE STDEV	GAGE+RADAR MEAN	GAGE+RADAR STDEV	GAGE+RADAR (EVAP) MEAN	GAGE+RADAR (EVAP) STDEV	GAGE-RADAR RATIO MEAN	GAGE-RADAR RATIO STDEV
1/ 1	40000	0	1	0	0.0	0.0	0.0	0.0	0.0	0.0	0.0	0.0	0.0	0.0
1/ 1	40500	0	1	0	0.0	0.0	0.0	0.0	0.0	0.0	0.0	0.0	0.0	0.0
1/ 1	41000	97	1	22	0.00	0.00	0.01	0.04	0.01	0.01	0.00	0.01	4.7	0.0
1/ 1	41500	97	1	49	0.00	0.00	0.01	0.04	0.03	0.07	0.01	0.05	16.7	0.0
1/ 1	42000	97	2	61	0.00	0.01	0.02	0.07	0.05	0.11	0.02	0.09	14.5	1.8
1/ 1	42500	97	3	64	0.01	0.01	0.02	0.07	0.04	0.12	0.02	0.06	10.4	3.9
1/ 1	43000	97	3	63	0.01	0.01	0.02	0.07	0.04	0.13	0.02	0.07	8.4	5.0
1/ 1	43500	97	8	67	0.01	0.02	0.05	0.20	0.17	0.44	0.04	0.31	17.7	14.8
1/ 1	44000	97	9	67	0.02	0.04	0.07	0.24	0.20	0.54	0.09	0.71	12.4	14.3
1/ 1	44500	97	10	63	0.02	0.04	0.11	0.37	0.17	0.54	0.07	0.38	11.4	12.4
1/ 1	45000	97	13	66	0.03	0.09	0.21	0.74	0.30	1.00	0.14	0.77	16.5	22.2
1/ 1	45500	97	18	59	0.04	0.11	0.31	1.27	0.76	2.58	0.34	2.47	23.8	27.1
SUMS					0.13		1.04 (1.24)		1.81		0.96 (1.15)		MEAN G/R = 11.4	8.4

RADAR-GAGE RAINFALL ANALYSES FOR DAY 158 OF 1974 BEGINNING AT 40000. RUN DURATION = 15 MIN
COORD XFORM WT = 2 MIN RADAR RAIN = 0.02 MM RADIUS FOR G/R RATIOS = 1.0 KM

GAGE DENSITY	TIME (Z)	NUMBER OF GAGES TOTAL	G/R	EVAP	RAINFALL AMOUNTS (MM) RADAR MEAN	RADAR STDEV	GAGE MEAN	GAGE STDEV	GAGE+RADAR MEAN	GAGE+RADAR STDEV	GAGE+RADAR (EVAP) MEAN	GAGE+RADAR (EVAP) STDEV	GAGE-RADAR RATIO MEAN	GAGE-RADAR RATIO STDEV
1/ 1	40000	97	2	40	0.00	0.01	0.03	0.12	0.04	0.07	0.01	0.04	13.2	8.6
1/ 1	41500	97	8	66	0.01	0.02	0.09	0.33	0.22	0.68	0.13	0.63	17.1	15.2
1/ 1	43000	97	17	69	0.03	0.08	0.16	0.47	0.56	1.93	0.25	1.48	17.1	23.1
1/ 1	44500	97	21	57	0.09	0.26	0.93	2.24	1.37	5.49	1.04	5.45	19.5	23.3
SUMS					0.14		1.06		2.20		1.45		MEAN G/R = 16.9	17.6

RADAR-GAGE RAINFALL ANALYSES FOR DAY 158 OF 1976 BEGINNING AT 40000. RUN DURATION = 30 MIN
COORD XFORM WT = 2 MIN RADAR RAIN = 0.02 MM RADIUS FOR G/R RATIOS = 1.0 KM

GAGE DENSITY	TIME (Z)	NUMBER OF GAGES TOTAL	G/R	EVAP	RAINFALL AMOUNTS (MM) RADAR MEAN	RADAR STDEV	GAGE MEAN	GAGE STDEV	GAGE+RADAR MEAN	GAGE+RADAR STDEV	GAGE+RADAR (EVAP) MEAN	GAGE+RADAR (EVAP) STDEV	GAGE-RADAR RATIO MEAN	GAGE-RADAR RATIO STDEV
1/ 1	40000	97	9	67	0.01	0.02	0.08	0.24	0.24	0.43	0.09	0.36	16.6	12.4
1/ 1	43000	97	29	59	0.13	0.32	0.98	2.41	1.76	6.86	1.32	6.81	17.4	20.6
SUMS					0.14		1.06		2.00		1.41		MEAN G/R = 16.9	16.5

RADAR-GAGE RAINFALL ANALYSES FOR DAY 158 OF 1976 BEGINNING AT 40000. RUN DURATION = 60 MIN
COORD XFORM WT = 2 MIN RADAR RAIN = 0.02 MM RADIUS FOR G/R RATIOS = 1.0 KM

GAGE DENSITY	TIME (Z)	NUMBER OF GAGES TOTAL	G/R	EVAP	RAINFALL AMOUNTS (MM) RADAR MEAN	RADAR STDEV	GAGE MEAN	GAGE STDEV	GAGE+RADAR MEAN	GAGE+RADAR STDEV	GAGE+RADAR (EVAP) MEAN	GAGE+RADAR (EVAP) STDEV	GAGE-RADAR RATIO MEAN	GAGE-RADAR RATIO STDEV
1/ 1	40000	97	31	58	0.14	0.33	1.06	2.45	1.84	6.77	1.36	6.71	15.3	18.0
SUMS					0.14		1.06		1.84		1.36		MEAN G/R = 15.3	18.0

RADAR-GAGE RAINFALL ANALYSES FOR DAY 158 OF 1976 BEGINNING AT 50000. RUN DURATION = 5 MIN
COORD XFORM WT = 2 MIN RADAR RAIN = 0.02 MM RADIUS FOR G/R RATIOS = 1.0 KM

GAGE DENSITY	TIME (Z)	NUMBER OF GAGES TOTAL	G/R	EVAP	RAINFALL AMOUNTS (MM) RADAR MEAN	RADAR STDEV	GAGE MEAN	GAGE STDEV	GAGE+RADAR MEAN	GAGE+RADAR STDEV	GAGE+RADAR (EVAP) MEAN	GAGE+RADAR (EVAP) STDEV	GAGE-RADAR RATIO MEAN	GAGE-RADAR RATIO STDEV
1/ 1	50000	0	0	0	0.0	0.0	0.0	0.0	0.0	0.0	0.0	0.0	0.0	0.0
1/ 1	50500	0	0	0	0.0	0.0	0.0	0.0	0.0	0.0	0.0	0.0	0.0	0.0
1/ 1	51000	0	0	0	0.0	0.0	0.0	0.0	0.0	0.0	0.0	0.0	0.0	0.0
1/ 1	51500	97	23	53	0.10	0.31	0.50	1.02	0.72	2.19	0.54	1.92	12.6	15.1
1/ 1	52000	97	25	57	0.10	0.29	0.50	0.89	0.65	2.06	0.47	1.67	11.2	14.0
1/ 1	52500	97	28	55	0.10	0.30	0.45	0.85	0.60	1.63	0.32	0.97	12.2	19.6
1/ 1	53000	97	32	51	0.11	0.31	0.33	0.53	0.58	1.54	0.30	0.84	13.7	23.0
1/ 1	53500	97	30	51	0.10	0.24	0.31	0.53	0.42	0.93	0.28	0.72	9.3	14.0
1/ 1	54000	97	33	46	0.08	0.22	0.20	0.38	0.34	0.74	0.18	0.50	8.0	13.0
1/ 1	54500	97	17	60	0.07	0.14	0.13	0.31	0.49	0.93	0.19	0.63	9.3	11.0
1/ 1	55000	97	4	77	0.06	0.16	0.05	0.20	0.83	2.24	0.29	1.32	14.2	25.1
1/ 1	55500	97	18	69	0.05	0.13	0.10	0.22	0.52	1.47	0.22	0.86	10.8	14.6
SUMS					0.79		2.57 (3.43)		5.17		2.79 (3.71)		MEAN G/R = 8.4	12.4

RADAR-GAGE RAINFALL ANALYSES FOR DAY 158 OF 1976 BEGINNING AT 50000. RUN DURATION = 15 MIN
COORD XFORM WT = 2 MIN RADAR RAIN = 0.02 MM RADIUS FOR G/R RATIOS = 1.0 KM

GAGE DENSITY	TIME (Z)	NUMBER OF GAGES TOTAL	G/R	EVAP	RAINFALL AMOUNTS (MM) RADAR MEAN	RADAR STDEV	GAGE MEAN	GAGE STDEV	GAGE+RADAR MEAN	GAGE+RADAR STDEV	GAGE+RADAR (EVAP) MEAN	GAGE+RADAR (EVAP) STDEV	GAGE-RADAR RATIO MEAN	GAGE-RADAR RATIO STDEV
1/ 1	50000	0	0	0	0.0	0.0	0.0	0.0	0.0	0.0	0.0	0.0	0.0	0.0
1/ 1	51500	97	35	47	0.31	0.83	1.45	2.48	1.53	3.43	1.19	2.77	9.3	10.2
1/ 1	53000	97	40	50	0.29	0.64	0.84	1.37	1.31	2.71	0.78	1.69	12.4	18.1
1/ 1	54500	97	25	66	0.19	0.37	0.28	0.69	0.84	2.22	0.42	1.55	4.2	11.1
SUMS					0.79		2.57 (3.43)		3.68		2.30 (3.07)		MEAN G/R = 7.0	9.9

RADAR-GAGE RAINFALL ANALYSES FOR DAY 158 OF 1976 BEGINNING AT 50000. RUN DURATION = 30 MIN
COORD XFORM WT = 2 MIN RADAR RAIN = 0.02 MM RADIUS FOR G/R RATIOS = 1.0 KM

GAGE DENSITY	TIME (Z)	NUMBER OF GAGES TOTAL	G/R	EVAP	RAINFALL AMOUNTS (MM) RADAR MEAN	RADAR STDEV	GAGE MEAN	GAGE STDEV	GAGE+RADAR MEAN	GAGE+RADAR STDEV	GAGE+RADAR (EVAP) MEAN	GAGE+RADAR (EVAP) STDEV	GAGE-RADAR RATIO MEAN	GAGE-RADAR RATIO STDEV
1/ 1	50000	97	43	45	0.62	1.67	3.15	5.41	4.14	8.94	3.03	7.24	16.2	17.4
1/ 1	53000	97	44	48	0.48	0.85	1.12	1.94	1.95	3.92	1.27	3.12	9.1	14.1
SUMS					1.10		4.27		6.09		4.30		MEAN G/R = 12.7	15.7

RADAR-GAGE RAINFALL ANALYSES FOR DAY 158 OF 1976 BEGINNING AT 50000. RUN DURATION = 60 MIN
COORD XFORM WT = 2 MIN RADAR RAIN = 0.02 MM RADIUS FOR G/R RATIOS = 1.0 KM

GAGE DENSITY	TIME (Z)	NUMBER OF GAGES TOTAL	G/R	EVAP	RAINFALL AMOUNTS (MM) RADAR MEAN	RADAR STDEV	GAGE MEAN	GAGE STDEV	GAGE+RADAR MEAN	GAGE+RADAR STDEV	GAGE+RADAR (EVAP) MEAN	GAGE+RADAR (EVAP) STDEV	GAGE-RADAR RATIO MEAN	GAGE-RADAR RATIO STDEV
1/ 1	50000	97	56	36	1.05	1.94	4.27	6.20	6.15	10.37	4.41	8.05	13.2	17.8
SUMS					1.05		4.27		6.15		4.41		MEAN G/R = 13.2	17.8

Table 111. Page 1 of 6.

RADAR-GAGE RAINFALL ANALYSES FOR DAY 159 OF 1976 BEGINNING AT 40000. RUN DURATION = 5 MIN
COORD XFORM WT = 2 MIN RADAR RAIN = 0.02 MM RADIUS FOR G/R RATIOS = 1.0 KM

GAGE DENSITY	TIME (Z)	NUMBER OF GAGES TOTAL	G/R	EVAP	RADAR MEAN	RADAR STDEV	RAINFALL AMOUNTS (MM) GAGE MEAN	GAGE STDEV	GAGE+RADAR MEAN	GAGE+RADAR STDEV	GAGE+RADAR (EVAP) MEAN	GAGE+RADAR (EVAP) STDEV	GAGE-RADAR RATIO MEAN	GAGE-RADAR RATIO STDEV
1/ 1	40000	97	5	52	0.03	0.11	0.11	0.24	0.89	2.97	0.14	0.63	29.6	24.7
1/ 1	40500	97	11	44	0.03	0.14	0.12	0.24	0.24	0.83	0.09	0.37	10.5	11.5
1/ 1	41000	97	18	48	0.04	0.12	0.14	0.24	0.47	1.34	0.11	0.36	13.4	10.4
1/ 1	41500	0	0	0	0.0	0.0	0.0	0.0	0.0	0.0	0.0	0.0	0.0	0.0
1/ 1	42000	0	0	0	0.0	0.0	0.0	0.0	0.0	0.0	0.0	0.0	0.0	0.0
1/ 1	42500	97	20	49	0.05	0.18	0.35	0.92	0.64	2.25	0.16	0.58	15.2	20.4
1/ 1	43000	97	21	44	0.06	0.14	0.37	0.79	1.28	4.41	0.21	0.75	34.9	29.3
1/ 1	43500	97	12	43	0.01	0.03	0.28	1.06	0.43	1.16	0.14	0.45	45.9	35.6
1/ 1	44000	97	3	28	0.00	0.01	0.66	1.06	0.02	0.04	0.10	0.53	2.9	2.3
1/ 1	44500	97	10	31	0.00	0.01	0.49	0.82	0.10	0.25	0.12	0.36	37.9	25.5
1/ 1	45000	97	13	36	0.00	0.01	0.65	1.04	0.17	0.41	0.19	0.42	41.0	21.1
1/ 1	45500	97	5	35	0.00	0.01	1.24	1.99	0.19	0.51	0.69	1.64	43.6	15.5
SUMS					0.22		4.40 (5.28)		4.61		1.98 (2.38)		MEAN G/R = 23.5	14.3

RADAR-GAGE RAINFALL ANALYSES FOR DAY 159 OF 1976 BEGINNING AT 40000. RUN DURATION = 15 MIN
COORD XFORM WT = 2 MIN RADAR RAIN = 0.02 MM RADIUS FOR G/R RATIOS = 1.0 KM

GAGE DENSITY	TIME (Z)	NUMBER OF GAGES TOTAL	G/R	EVAP	RADAR MEAN	RADAR STDEV	RAINFALL AMOUNTS (MM) GAGE MEAN	GAGE STDEV	GAGE+RADAR MEAN	GAGE+RADAR STDEV	GAGE+RADAR (EVAP) MEAN	GAGE+RADAR (EVAP) STDEV	GAGE-RADAR RATIO MEAN	GAGE-RADAR RATIO STDEV
1/ 1	40000	97	25	45	0.11	0.25	0.36	0.58	0.92	2.01	0.32	0.81	13.6	16.9
1/ 1	41500	97	24	33	0.15	0.34	1.03	1.95	1.78	6.56	0.71	1.98	16.5	22.4
1/ 1	43000	97	23	30	0.05	0.15	1.22	2.17	0.95	2.52	0.39	0.96	24.9	24.3
1/ 1	44500	97	13	27	0.01	0.02	2.38	3.07	0.60	1.17	0.77	1.34	56.9	25.6
SUMS					0.32		5.08		4.25		2.19		MEAN G/R = 28.6	22.1

RADAR-GAGE RAINFALL ANALYSES FOR DAY 159 OF 1976 BEGINNING AT 40000. RUN DURATION = 30 MIN
COORD XFORM WT = 2 MIN RADAR RAIN = 0.02 MM RADIUS FOR G/R RATIOS = 1.0 KM

GAGE DENSITY	TIME (Z)	NUMBER OF GAGES TOTAL	G/R	EVAP	RADAR MEAN	RADAR STDEV	RAINFALL AMOUNTS (MM) GAGE MEAN	GAGE STDEV	GAGE+RADAR MEAN	GAGE+RADAR STDEV	GAGE+RADAR (EVAP) MEAN	GAGE+RADAR (EVAP) STDEV	GAGE-RADAR RATIO MEAN	GAGE-RADAR RATIO STDEV
1/ 1	40000	97	50	32	0.26	0.49	1.39	2.19	2.54	5.29	1.08	2.09	18.4	21.4
1/ 1	43000	97	28	25	0.04	0.15	3.69	4.04	1.79	3.13	1.31	1.90	41.5	32.4
SUMS					0.30		5.08		4.33		2.39		MEAN G/R = 29.9	26.9

RADAR-GAGE RAINFALL ANALYSES FOR DAY 159 OF 1976 BEGINNING AT 40000. RUN DURATION = 60 MIN
COORD XFORM WT = 2 MIN RADAR RAIN = 0.02 MM RADIUS FOR G/R RATIOS = 1.0 KM

GAGE DENSITY	TIME (Z)	NUMBER OF GAGES TOTAL	G/R	EVAP	RADAR MEAN	RADAR STDEV	RAINFALL AMOUNTS (MM) GAGE MEAN	GAGE STDEV	GAGE+RADAR MEAN	GAGE+RADAR STDEV	GAGE+RADAR (EVAP) MEAN	GAGE+RADAR (EVAP) STDEV	GAGE-RADAR RATIO MEAN	GAGE-RADAR RATIO STDEV
1/ 1	40000	97	63	12	0.26	0.46	5.09	4.66	4.22	4.42	3.58	4.16	33.3	30.1
SUMS					0.26		5.09		4.22		3.58		MEAN G/R = 33.3	30.1

RADAR-GAGE RAINFALL ANALYSES FOR DAY 159 OF 1976 BEGINNING AT 50000. RUN DURATION = 5 MIN
COORD XFORM WT = 2 MIN RADAR RAIN = 0.02 MM RADIUS FOR G/R RATIOS = 1.0 KM

GAGE DENSITY	TIME (Z)	NUMBER OF GAGES TOTAL	G/R	EVAP	RADAR MEAN	RADAR STDEV	RAINFALL AMOUNTS (MM) GAGE MEAN	GAGE STDEV	GAGE+RADAR MEAN	GAGE+RADAR STDEV	GAGE+RADAR (EVAP) MEAN	GAGE+RADAR (EVAP) STDEV	GAGE-RADAR RATIO MEAN	GAGE-RADAR RATIO STDEV
1/ 1	50000	97	10	29	0.01	0.03	1.35	1.49	0.43	1.39	0.61	1.56	51.5	27.0
1/ 1	50500	0	0	0	0.0	0.0	0.0	0.0	0.0	0.0	0.0	0.0	0.0	0.0
1/ 1	51000	97	35	21	0.04	0.10	1.58	1.77	0.71	1.39	0.76	1.42	29.5	24.5
1/ 1	51500	97	43	18	0.03	0.10	1.78	2.39	0.77	2.01	0.97	2.17	23.4	24.6
1/ 1	52000	97	44	19	0.06	0.11	1.74	2.59	0.88	1.49	0.88	1.51	18.6	21.6
1/ 1	52500	97	58	12	0.08	0.14	1.45	2.30	1.07	2.11	1.06	2.16	19.0	19.9
1/ 1	53000	97	60	15	0.05	0.08	1.51	2.41	0.74	1.55	0.60	1.35	18.9	15.9
1/ 1	53500	97	69	17	0.05	0.07	1.12	1.41	0.86	1.24	0.58	0.90	19.0	15.5
1/ 1	54000	97	59	21	0.05	0.08	0.73	1.47	0.59	1.15	0.40	0.80	13.3	9.6
1/ 1	54500	97	42	44	0.06	0.06	0.39	0.49	0.51	0.35	0.31	0.73	15.5	8.9
1/ 1	55000	97	19	79	0.02	0.04	0.04	0.08	0.24	0.45	0.11	0.39	11.8	6.9
1/ 1	55500	97	47	43	0.03	0.03	0.17	0.18	0.24	0.25	0.17	0.26	9.8	9.3
SUMS					0.49		11.88 (12.96)		7.00		6.46 (7.03)		MEAN G/R = 19.2	15.1

RADAR-GAGE RAINFALL ANALYSES FOR DAY 159 OF 1976 BEGINNING AT 50000. RUN DURATION = 15 MIN
COORD XFORM WT = 2 MIN RADAR RAIN = 0.02 MM RADIUS FOR G/R RATIOS = 1.0 KM

GAGE DENSITY	TIME (Z)	NUMBER OF GAGES TOTAL	G/R	EVAP	RADAR MEAN	RADAR STDEV	RAINFALL AMOUNTS (MM) GAGE MEAN	GAGE STDEV	GAGE+RADAR MEAN	GAGE+RADAR STDEV	GAGE+RADAR (EVAP) MEAN	GAGE+RADAR (EVAP) STDEV	GAGE-RADAR RATIO MEAN	GAGE-RADAR RATIO STDEV
1/ 1	50000	97	33	16	0.08	0.14	4.34	4.60	2.56	4.84	2.59	4.84	41.6	26.3
1/ 1	51500	97	62	9	0.20	0.23	5.00	5.92	3.78	4.08	3.79	4.09	24.7	24.1
1/ 1	53000	97	83	11	0.15	0.15	3.36	4.52	3.13	4.28	2.30	3.53	21.6	16.7
1/ 1	54500	97	65	28	0.09	0.11	0.59	0.79	0.68	0.89	0.53	0.83	9.0	9.0
SUMS					0.51		13.29		10.14		9.21		MEAN G/R = 24.2	19.0

RADAR-GAGE RAINFALL ANALYSES FOR DAY 159 OF 1976 BEGINNING AT 50000. RUN DURATION = 30 MIN
COORD XFORM WT = 2 MIN RADAR RAIN = 0.02 MM RADIUS FOR G/R RATIOS = 1.0 KM

GAGE DENSITY	TIME (Z)	NUMBER OF GAGES TOTAL	G/R	EVAP	RADAR MEAN	RADAR STDEV	RAINFALL AMOUNTS (MM) GAGE MEAN	GAGE STDEV	GAGE+RADAR MEAN	GAGE+RADAR STDEV	GAGE+RADAR (EVAP) MEAN	GAGE+RADAR (EVAP) STDEV	GAGE-RADAR RATIO MEAN	GAGE-RADAR RATIO STDEV
1/ 1	50000	97	60	9	0.30	0.30	9.33	7.28	7.88	8.49	7.78	8.56	31.8	21.1
1/ 1	53000	97	83	11	0.24	0.19	3.95	4.99	4.05	4.72	3.19	4.15	16.1	11.6
SUMS					0.54		13.28		11.94		10.97		MEAN G/R = 23.9	16.4

RADAR-GAGE RAINFALL ANALYSES FOR DAY 159 OF 1976 BEGINNING AT 50000. RUN DURATION = 60 MIN
COORD XFORM WT = 2 MIN RADAR RAIN = 0.02 MM RADIUS FOR G/R RATIOS = 1.0 KM

GAGE DENSITY	TIME (Z)	NUMBER OF GAGES TOTAL	G/R	EVAP	RADAR MEAN	RADAR STDEV	RAINFALL AMOUNTS (MM) GAGE MEAN	GAGE STDEV	GAGE+RADAR MEAN	GAGE+RADAR STDEV	GAGE+RADAR (EVAP) MEAN	GAGE+RADAR (EVAP) STDEV	GAGE-RADAR RATIO MEAN	GAGE-RADAR RATIO STDEV
1/ 1	50000	97	87	8	0.53	0.28	13.23	8.29	14.47	8.46	12.55	8.75	31.1	15.2
SUMS					0.53		13.28		14.47		12.55		MEAN G/R = 31.1	15.2

RADAR-GAGE RAINFALL ANALYSES FOR DAY 184 OF 1974 BEGINNING AT 170000. RUN DURATION = 5 MIN
COORD XFORM WT = 2 MIN RADAR RAIN = 0.02 MM RADIUS FOR G/R RATIOS = 1.0 KM

GAGE DENSITY	TIME (Z)	NUMBER OF GAGES TOTAL	G/R	EVAP	RADAR MEAN	RADAR STDEV	RAINFALL AMOUNTS (MM) GAGE MEAN	GAGE STDEV	GAGE÷RADAR MEAN	GAGE÷RADAR STDEV	GAGE÷RADAR (EVAP) MEAN	GAGE÷RADAR (EVAP) STDEV	GAGE-RADAR RATIO MEAN	GAGE-RADAR RATIO STDEV
1/ 1	170000	112	21	44	0.03	0.06	0.28	0.67	0.21	0.40	0.15	0.53	8.9	7.8
1/ 1	170500	112	32	54	0.03	0.07	0.22	0.58	0.43	1.02	0.19	0.57	14.2	14.0
1/ 1	171000	111	20	52	0.03	0.07	0.18	0.44	0.46	1.19	0.21	0.72	14.5	20.9
1/ 1	171500	111	17	46	0.03	0.07	0.21	0.79	0.55	1.38	0.23	0.78	22.0	21.5
1/ 1	172000	111	19	46	0.03	0.06	0.22	0.68	0.22	0.53	0.13	0.39	10.9	6.9
1/ 1	172500	111	16	53	0.03	0.06	0.28	0.64	0.28	0.79	0.12	0.41	17.6	16.5
1/ 1	173000	111	46	52	0.03	0.08	0.28	0.80	0.29	1.05	0.18	0.88	19.7	21.8
1/ 1	173500	111	11	53	0.03	0.06	0.21	0.51	0.41	1.19	0.07	0.32	26.5	26.8
1/ 1	174000	111	13	50	0.03	0.05	0.11	0.30	0.15	0.41	0.05	0.15	9.1	7.9
1/ 1	174500	111	15	46	0.03	0.06	0.14	0.35	0.15	1.02	0.15	0.56	19.5	21.5
1/ 1	175000	111	20	56	0.03	0.05	0.18	0.30	0.43	0.94	0.17	0.56	23.5	19.3
1/ 1	175500	111	14	61	0.03	0.04	0.19	0.39	0.44	1.06	0.19	0.60	23.3	18.1
SUMS					0.29		2.45		4.39		1.84	MEAN G/R =	17.8	17.9

RADAR-GAGE RAINFALL ANALYSES FOR DAY 184 OF 1974 BEGINNING AT 170000. RUN DURATION = 15 MIN
COORD XFORM WT = 2 MIN RADAR RAIN = 0.02 MM RADIUS FOR G/R RATIOS = 1.0 KM

GAGE DENSITY	TIME (Z)	NUMBER OF GAGES TOTAL	G/R	EVAP	RADAR MEAN	RADAR STDEV	RAINFALL AMOUNTS (MM) GAGE MEAN	GAGE STDEV	GAGE÷RADAR MEAN	GAGE÷RADAR STDEV	GAGE÷RADAR (EVAP) MEAN	GAGE÷RADAR (EVAP) STDEV	GAGE-RADAR RATIO MEAN	GAGE-RADAR RATIO STDEV
1/ 1	170000	111	45	44	0.06	0.15	0.69	1.51	0.83	1.55	0.52	1.38	12.1	11.1
1/ 1	171500	111	34	44	0.06	0.13	0.72	1.71	1.10	1.87	0.34	1.34	25.1	24.6
1/ 1	173000	111	42	41	0.04	0.11	0.50	1.23	0.94	1.96	0.37	1.01	26.2	29.0
1/ 1	174500	111	48	51	0.07	0.13	0.93	0.99	1.16	1.98	0.58	1.27	23.5	22.5
SUMS					0.25		2.44		4.04		2.02	MEAN G/R =	21.7	22.3

RADAR-GAGE RAINFALL ANALYSES FOR DAY 184 OF 1974 BEGINNING AT 170000. RUN DURATION = 30 MIN
COORD XFORM WT = 2 MIN RADAR RAIN = 0.02 MM RADIUS FOR G/R RATIOS = 1.0 KM

GAGE DENSITY	TIME (Z)	NUMBER OF GAGES TOTAL	G/R	EVAP	RADAR MEAN	RADAR STDEV	RAINFALL AMOUNTS (MM) GAGE MEAN	GAGE STDEV	GAGE÷RADAR MEAN	GAGE÷RADAR STDEV	GAGE÷RADAR (EVAP) MEAN	GAGE÷RADAR (EVAP) STDEV	GAGE-RADAR RATIO MEAN	GAGE-RADAR RATIO STDEV
1/ 1	170000	111	58	37	0.14	0.23	1.41	2.78	1.74	2.65	1.20	2.51	15.5	15.7
1/ 1	173000	111	59	41	0.13	0.18	1.03	1.62	1.33	1.61	0.86	1.47	17.7	19.0
SUMS					0.39		2.44		3.07		2.06	MEAN G/R =	17.1	17.3

RADAR-GAGE RAINFALL ANALYSES FOR DAY 184 OF 1974 BEGINNING AT 170000. RUN DURATION = 60 MIN
COORD XFORM WT = 2 MIN RADAR RAIN = 0.02 MM RADIUS FOR G/R RATIOS = 1.0 KM

GAGE DENSITY	TIME (Z)	NUMBER OF GAGES TOTAL	G/R	EVAP	RADAR MEAN	RADAR STDEV	RAINFALL AMOUNTS (MM) GAGE MEAN	GAGE STDEV	GAGE÷RADAR MEAN	GAGE÷RADAR STDEV	GAGE÷RADAR (EVAP) MEAN	GAGE÷RADAR (EVAP) STDEV	GAGE-RADAR RATIO MEAN	GAGE-RADAR RATIO STDEV
1/ 1	170000	111	71	39	0.39	0.33	2.44	3.73	2.66	3.28	2.14	3.37	12.9	12.6
SUMS					0.79		2.44		2.66		2.14	MEAN G/R =	12.9	12.6

RADAR-GAGE RAINFALL ANALYSES FOR DAY 184 OF 1974 BEGINNING AT 180000. RUN DURATION = 5 MIN
COORD XFORM WT = 2 MIN RADAR RAIN = 0.02 MM RADIUS FOR G/R RATIOS = 1.0 KM

GAGE DENSITY	TIME (Z)	NUMBER OF GAGES TOTAL	G/R	EVAP	RADAR MEAN	RADAR STDEV	RAINFALL AMOUNTS (MM) GAGE MEAN	GAGE STDEV	GAGE÷RADAR MEAN	GAGE÷RADAR STDEV	GAGE÷RADAR (EVAP) MEAN	GAGE÷RADAR (EVAP) STDEV	GAGE-RADAR RATIO MEAN	GAGE-RADAR RATIO STDEV
1/ 1	180000	111	14	68	0.03	0.08	0.26	0.83	0.34	0.77	0.14	0.46	14.3	23.1
1/ 1	180500	111	20	67	0.04	0.12	0.35	1.12	0.73	2.59	0.30	2.09	24.3	22.0
1/ 1	181000	111	24	64	0.04	0.12	0.33	1.00	0.64	2.30	0.29	1.20	22.1	24.4
1/ 1	181500	111	33	69	0.05	0.16	0.37	0.50	1.00	3.02	0.54	2.46	24.6	25.9
1/ 1	182000	111	54	51	0.04	0.18	0.30	0.44	0.96	3.08	0.49	2.41	17.5	17.4
1/ 1	182500	110	29	62	0.05	0.15	0.31	0.70	0.77	2.27	0.31	1.44	15.9	13.6
1/ 1	183000	110	27	56	0.05	0.13	0.35	0.70	0.80	2.51	0.25	0.92	17.4	14.6
1/ 1	183500	110	21	66	0.05	0.12	0.37	0.86	1.04	2.67	0.25	0.69	23.2	22.5
1/ 1	184000	110	21	61	0.04	0.12	0.28	0.70	0.76	2.16	0.21	0.58	16.7	19.2
1/ 1	184500	110	33	64	0.04	0.12	0.29	0.67	0.63	1.80	0.26	0.86	17.5	20.3
1/ 1	185000	110	24	60	0.04	0.10	0.31	0.67	0.71	1.94	0.31	1.13	22.9	24.1
1/ 1	185500	0	0	0	0.0	0.0	0.0	0.0	0.0	0.0	0.0	0.0	0.0	0.0
SUMS					0.59		3.43 (3.74)		8.58		3.37 (3.68)	MEAN G/R =	18.5	18.4

RADAR-GAGE RAINFALL ANALYSES FOR DAY 184 OF 1974 BEGINNING AT 180000. RUN DURATION = 15 MIN
COORD XFORM WT = 2 MIN RADAR RAIN = 0.02 MM RADIUS FOR G/R RATIOS = 1.0 KM

GAGE DENSITY	TIME (Z)	NUMBER OF GAGES TOTAL	G/R	EVAP	RADAR MEAN	RADAR STDEV	RAINFALL AMOUNTS (MM) GAGE MEAN	GAGE STDEV	GAGE÷RADAR MEAN	GAGE÷RADAR STDEV	GAGE÷RADAR (EVAP) MEAN	GAGE÷RADAR (EVAP) STDEV	GAGE-RADAR RATIO MEAN	GAGE-RADAR RATIO STDEV
1/ 1	180000	111	38	58	0.11	0.29	0.94	2.89	1.50	3.18	0.66	2.25	18.1	17.7
1/ 1	181500	110	46	49	0.14	0.36	0.88	1.67	2.07	4.53	1.04	2.92	14.1	15.0
1/ 1	183000	110	40	54	0.14	0.29	1.01	2.07	1.93	4.14	0.76	1.66	17.4	17.7
1/ 1	184500	110	32	53	0.12	0.28	0.94	1.90	1.98	4.97	0.92	2.66	22.2	23.1
SUMS					0.54		3.77		7.49		3.38	MEAN G/R =	18.5	18.4

RADAR-GAGE RAINFALL ANALYSES FOR DAY 184 OF 1974 BEGINNING AT 180000. RUN DURATION = 30 MIN
COORD XFORM WT = 2 MIN RADAR RAIN = 0.02 MM RADIUS FOR G/R RATIOS = 1.0 KM

GAGE DENSITY	TIME (Z)	NUMBER OF GAGES TOTAL	G/R	EVAP	RADAR MEAN	RADAR STDEV	RAINFALL AMOUNTS (MM) GAGE MEAN	GAGE STDEV	GAGE÷RADAR MEAN	GAGE÷RADAR STDEV	GAGE÷RADAR (EVAP) MEAN	GAGE÷RADAR (EVAP) STDEV	GAGE-RADAR RATIO MEAN	GAGE-RADAR RATIO STDEV
1/ 1	180000	110	63	41	0.27	0.43	1.80	3.43	3.61	7.09	2.29	6.30	16.3	17.3
1/ 1	183000	110	53	44	0.27	0.48	1.95	3.60	3.50	6.73	1.55	3.13	18.9	20.3
SUMS					0.54		3.75		7.10		3.84	MEAN G/R =	17.6	18.8

RADAR-GAGE RAINFALL ANALYSES FOR DAY 184 OF 1974 BEGINNING AT 180000. RUN DURATION = 60 MIN
COORD XFORM WT = 2 MIN RADAR RAIN = 0.02 MM RADIUS FOR G/R RATIOS = 1.0 KM

GAGE DENSITY	TIME (Z)	NUMBER OF GAGES TOTAL	G/R	EVAP	RADAR MEAN	RADAR STDEV	RAINFALL AMOUNTS (MM) GAGE MEAN	GAGE STDEV	GAGE÷RADAR MEAN	GAGE÷RADAR STDEV	GAGE÷RADAR (EVAP) MEAN	GAGE÷RADAR (EVAP) STDEV	GAGE-RADAR RATIO MEAN	GAGE-RADAR RATIO STDEV
1/ 1	180000	110	76	31	0.54	0.70	3.75	5.62	5.86	8.30	3.99	7.20	15.7	18.7
SUMS					0.54		3.75		5.86		3.99	MEAN G/R =	15.7	18.7

Table 111. (continued) Page 3 of 6.

RADAR-GAGE RAINFALL ANALYSES FOR DAY 184 OF 1974 BEGINNING AT 190000. RUN DURATION = 5 MIN
COORD XFORM WT = 2 MIN RADAR RAIN = 0.02 MM RADIUS FOR G/R RATIOS = 1.0 KM

GAGE DENSITY	TIME (Z)	NUMBER OF GAGES TOTAL	G/R	EVAP	RADAR MEAN	RADAR STDEV	RAINFALL AMOUNTS (MM) GAGE MEAN	GAGE STDEV	GAGE+RADAR MEAN	GAGE+RADAR STDEV	GAGE+RADAR (EVAP) MEAN	GAGE+RADAR (EVAP) STDEV	GAGE-RADAR RATIO MEAN	GAGE-RADAR RATIO STDEV
1/ 1	190000	110	24	53	0.04	0.10	0.21	0.77	0.80	3.20	0.84	3.09	22.4	24.1
1/ 1	190500	110	27	65	0.04	0.09	0.14	0.73	1.00	3.73	0.48	2.63	29.6	27.1
1/ 1	191000	110	27	56	0.03	0.08	0.24	1.42	0.91	3.87	0.55	1.92	32.9	28.1
1/ 1	191500	110	27	55	0.02	0.07	0.15	1.04	0.94	3.34	0.74	2.35	24.8	26.0
1/ 1	192000	110	24	56	0.03	0.10	0.19	1.24	0.73	3.23	0.68	2.23	18.3	20.5
1/ 1	192500	110	27	60	0.04	0.15	0.30	1.16	0.74	3.22	0.59	1.98	19.9	16.8
1/ 1	193000	110	27	62	0.05	0.14	0.17	0.75	0.84	3.00	0.41	2.43	18.7	15.9
1/ 1	193500	110	26	62	0.03	0.11	0.24	0.95	0.56	1.49	0.30	1.52	21.9	14.2
1/ 1	194000	110	5	43	0.02	0.06	0.16	0.43	0.33	1.34	0.21	0.75	18.0	20.1
1/ 1	194500	110	5	44	0.09	0.19	0.19	0.44	0.49	4.39	1.38	1.95	35.1	25.6
1/ 1	195000	0	0	0	0.0	0.0	0.0	0.0	0.0	0.0	0.0	0.0	0.0	0.0
1/ 1	195500	0	0	0	0.0	0.0	0.0	0.0	0.0	0.0	0.0	0.0	0.0	0.0
SUMS					0.34		3.36 (4.03)		7.73		5.37 (6.44)		MEAN G/R = 20.5	18.5

RADAR-GAGE RAINFALL ANALYSES FOR DAY 184 OF 1974 BEGINNING AT 190000. RUN DURATION = 15 MIN
COORD XFORM WT = 2 MIN RADAR RAIN = 0.02 MM RADIUS FOR G/R RATIOS = 1.0 KM

GAGE DENSITY	TIME (Z)	NUMBER OF GAGES TOTAL	G/R	EVAP	RADAR MEAN	RADAR STDEV	RAINFALL AMOUNTS (MM) GAGE MEAN	GAGE STDEV	GAGE+RADAR MEAN	GAGE+RADAR STDEV	GAGE+RADAR (EVAP) MEAN	GAGE+RADAR (EVAP) STDEV	GAGE-RADAR RATIO MEAN	GAGE-RADAR RATIO STDEV
1/ 1	190000	110	33	47	0.11	0.20	1.23	2.51	2.59	5.64	1.93	5.38	27.2	24.9
1/ 1	191500	110	27	53	0.11	0.24	1.14	3.06	2.59	6.22	1.97	6.12	26.2	24.5
1/ 1	193000	110	19	51	0.13	0.30	0.51	2.40	1.72	5.44	1.17	3.77	22.6	22.5
1/ 1	194500	110	14	51	0.08	0.34	0.37	0.94	1.29	6.27	0.43	3.27	15.4	10.8
SUMS					0.40		3.54		7.85		5.71		MEAN G/R = 23.1	21.2

RADAR-GAGE RAINFALL ANALYSES FOR DAY 184 OF 1974 BEGINNING AT 190000. RUN DURATION = 30 MIN
COORD XFORM WT = 2 MIN RADAR RAIN = 0.02 MM RADIUS FOR G/R RATIOS = 1.0 KM

GAGE DENSITY	TIME (Z)	NUMBER OF GAGES TOTAL	G/R	EVAP	RADAR MEAN	RADAR STDEV	RAINFALL AMOUNTS (MM) GAGE MEAN	GAGE STDEV	GAGE+RADAR MEAN	GAGE+RADAR STDEV	GAGE+RADAR (EVAP) MEAN	GAGE+RADAR (EVAP) STDEV	GAGE-RADAR RATIO MEAN	GAGE-RADAR RATIO STDEV
1/ 1	190000	110	44	44	0.22	0.37	2.36	4.92	4.63	8.31	3.45	8.23	23.6	20.3
1/ 1	193000	110	23	55	0.16	0.55	1.17	3.08	2.56	7.82	1.63	4.84	17.1	14.8
SUMS					0.41		3.54		7.07		5.28		MEAN G/R = 20.3	18.7

RADAR-GAGE RAINFALL ANALYSES FOR DAY 184 OF 1974 BEGINNING AT 190000. RUN DURATION = 60 MIN
COORD XFORM WT = 2 MIN RADAR RAIN = 0.02 MM RADIUS FOR G/R RATIOS = 1.0 KM

GAGE DENSITY	TIME (Z)	NUMBER OF GAGES TOTAL	G/R	EVAP	RADAR MEAN	RADAR STDEV	RAINFALL AMOUNTS (MM) GAGE MEAN	GAGE STDEV	GAGE+RADAR MEAN	GAGE+RADAR STDEV	GAGE+RADAR (EVAP) MEAN	GAGE+RADAR (EVAP) STDEV	GAGE-RADAR RATIO MEAN	GAGE-RADAR RATIO STDEV
1/ 1	190000	110	55	45	0.41	0.74	3.54	4.92	4.95	12.39	5.29	10.70	21.4	20.5
SUMS					0.41		3.54		6.94		5.29		MEAN G/R = 21.4	20.5

Table 111. (continued) Page 4 of 6.

RADAR-GAGE RAINFALL ANALYSES FOR DAY 195 OF 1976 BEGINNING AT 20000. RUN DURATION = 5 MIN
COORD XFORM WT = 2 MIN RADAR RAIN = 0.10 MM RADIUS FOR G/R RATIOS = 1.0 KM

GAGE DENSITY	TIME (Z)	NUMBER OF GAGES TOTAL	G/R	EVAP	RAINFALL AMOUNTS (MM) RADAR MEAN	STDEV	GAGE MEAN	STDEV	GAGE+RADAR MEAN	STDEV	GAGE+RADAR (EVAP) MEAN	STDEV	GAGE-RADAR RATIO MEAN	STDEV
1/ 1	20000	0	1	0	0.0	0.0	0.0	0.0	0.0	0.0	0.0	0.0	0.0	0.0
1/ 1	20500	0	1	2	0.0	0.0	0.0	0.0	0.0	0.0	0.0	0.0	0.0	0.0
1/ 1	21000	105	1	63	0.02	0.02	0.04	0.07	0.04	0.05	0.03	0.04	2.0	0.0
1/ 1	21500	105	31	64	0.02	0.01	0.05	0.07	0.12	0.09	0.05	0.07	7.5	3.7
1/ 1	22000	0	1	0	0.0	0.0	0.0	0.0	0.0	0.0	0.0	0.0	0.0	0.0
1/ 1	22500	0	1	0	0.0	0.0	0.0	0.0	0.0	0.0	0.0	0.0	0.0	0.0
1/ 1	23000	0	1	0	0.0	0.0	0.0	0.0	0.0	0.0	0.0	0.0	0.0	0.0
1/ 1	23500	0	1	0	0.0	0.0	0.0	0.0	0.0	0.0	0.0	0.0	0.0	0.0
1/ 1	24000	0	0	0	0.0	0.0	0.0	0.0	0.0	0.0	0.0	0.0	0.0	0.0
1/ 1	24500	0	0	0	0.0	0.0	0.0	0.0	0.0	0.0	0.0	0.0	0.0	0.0
1/ 1	25000	0	0	0	0.0	0.0	0.0	0.0	0.0	0.0	0.0	0.0	0.0	0.0
1/ 1	25500	0	0	0	0.0	0.0	0.0	0.0	0.0	0.0	0.0	0.0	0.0	0.0
SUMS					0.06		0.11		0.18		0.08	MEAN G/R =	0.9	0.3

RADAR-GAGE RAINFALL ANALYSES FOR DAY 195 OF 1976 BEGINNING AT 20000. RUN DURATION = 15 MIN
COORD XFORM WT = 2 MIN RADAR RAIN = 0.10 MM RADIUS FOR G/R RATIOS = 1.0 KM

GAGE DENSITY	TIME (Z)	NUMBER OF GAGES TOTAL	G/R	EVAP	RAINFALL AMOUNTS (MM) RADAR MEAN	STDEV	GAGE MEAN	STDEV	GAGE+RADAR MEAN	STDEV	GAGE+RADAR (EVAP) MEAN	STDEV	GAGE-RADAR RATIO MEAN	STDEV
1/ 0	20000	105	23	47	0.06	0.04	0.18	0.21	0.23	0.18	0.14	0.20	4.1	1.2
1/ 0	21500	105	48	50	0.04	0.04	0.15	0.18	0.25	0.19	0.14	0.19	6.4	3.4
1/ 1	23000	105	52	36	0.04	0.04	0.19	0.25	0.24	0.25	0.18	0.25	6.9	3.7
1/ 1	24500	105	34	44	0.03	0.04	0.12	0.16	0.16	0.17	0.10	0.14	5.5	3.5
SUMS					0.18		0.65		0.91		0.56	MEAN G/R =	5.7	3.0

RADAR-GAGE RAINFALL ANALYSES FOR DAY 195 OF 1976 BEGINNING AT 20000. RUN DURATION = 30 MIN
COORD XFORM WT = 2 MIN RADAR RAIN = 0.10 MM RADIUS FOR G/R RATIOS = 1.0 KM

GAGE DENSITY	TIME (Z)	NUMBER OF GAGES TOTAL	G/R	EVAP	RAINFALL AMOUNTS (MM) RADAR MEAN	STDEV	GAGE MEAN	STDEV	GAGE+RADAR MEAN	STDEV	GAGE+RADAR (EVAP) MEAN	STDEV	GAGE-RADAR RATIO MEAN	STDEV
1/ 1	20000	105	44	36	0.10	0.07	0.33	0.37	0.41	0.32	0.29	0.36	4.1	1.7
1/ 1	23000	105	59	29	0.08	0.06	0.32	0.32	0.36	0.32	0.28	0.32	5.5	2.9
SUMS					0.18		0.65		0.77		0.58	MEAN G/R =	4.9	2.3

RADAR-GAGE RAINFALL ANALYSES FOR DAY 195 OF 1976 BEGINNING AT 20000. RUN DURATION = 60 MIN
COORD XFORM WT = 2 MIN RADAR RAIN = 0.10 MM RADIUS FOR G/R RATIOS = 1.0 KM

GAGE DENSITY	TIME (Z)	NUMBER OF GAGES TOTAL	G/R	EVAP	RAINFALL AMOUNTS (MM) RADAR MEAN	STDEV	GAGE MEAN	STDEV	GAGE+RADAR MEAN	STDEV	GAGE+RADAR (EVAP) MEAN	STDEV	GAGE-RADAR RATIO MEAN	STDEV
1/ 1	20000	105	64	26	0.18	0.12	0.65	0.58	0.73	0.54	0.58	0.58	4.3	1.5
SUMS					0.18		0.65		0.73		0.58	MEAN G/R =	4.3	1.5

RADAR-GAGE RAINFALL ANALYSES FOR DAY 195 OF 1976 BEGINNING AT 20000. RUN DURATION = 5 MIN
COORD XFORM WT = 2 MIN RADAR RAIN = 0.02 MM RADIUS FOR G/R RATIOS = 1.0 KM

GAGE DENSITY	TIME (Z)	NUMBER OF GAGES TOTAL	G/R	EVAP	RAINFALL AMOUNTS (MM) RADAR MEAN	STDEV	GAGE MEAN	STDEV	GAGE+RADAR MEAN	STDEV	GAGE+RADAR (EVAP) MEAN	STDEV	GAGE-RADAR RATIO MEAN	STDEV
1/ 1	20000	105	23	73	0.02	0.01	0.06	0.09	0.11	0.09	0.05	0.09	6.5	3.6
1/ 1	20500	105	31	70	0.02	0.01	0.06	0.08	0.12	0.08	0.04	0.08	6.4	2.7
1/ 1	21000	105	31	65	0.02	0.02	0.06	0.07	0.12	0.09	0.05	0.07	6.5	3.4
1/ 1	21500	105	31	64	0.02	0.01	0.05	0.07	0.12	0.09	0.05	0.07	7.5	3.7
1/ 1	22000	105	16	44	0.01	0.01	0.05	0.07	0.10	0.08	0.05	0.07	6.8	3.0
1/ 1	22500	105	21	45	0.01	0.01	0.05	0.07	0.11	0.09	0.05	0.08	8.3	3.3
1/ 1	23000	105	39	54	0.01	0.01	0.06	0.08	0.11	0.10	0.06	0.10	8.2	4.8
1/ 1	23500	105	34	50	0.01	0.01	0.07	0.11	0.12	0.13	0.07	0.09	9.6	5.3
1/ 1	24000	105	30	46	0.01	0.02	0.06	0.09	0.09	0.09	0.05	0.07	6.0	2.5
1/ 1	24500	105	22	58	0.01	0.02	0.05	0.07	0.10	0.11	0.05	0.07	7.4	4.0
1/ 1	25000	105	13	55	0.01	0.01	0.04	0.07	0.09	0.12	0.04	0.08	8.5	4.6
1/ 1	25500	105	6	34	0.01	0.01	0.03	0.06	0.06	0.09	0.02	0.05	7.1	2.7
SUMS					0.18		0.65		1.25		0.60	MEAN G/R =	7.5	3.6

RADAR-GAGE RAINFALL ANALYSES FOR DAY 195 OF 1976 BEGINNING AT 20000. RUN DURATION = 15 MIN
COORD XFORM WT = 2 MIN RADAR RAIN = 0.02 MM RADIUS FOR G/R RATIOS = 1.0 KM

GAGE DENSITY	TIME (Z)	NUMBER OF GAGES TOTAL	G/R	EVAP	RAINFALL AMOUNTS (MM) RADAR MEAN	STDEV	GAGE MEAN	STDEV	GAGE+RADAR MEAN	STDEV	GAGE+RADAR (EVAP) MEAN	STDEV	GAGE-RADAR RATIO MEAN	STDEV
1/ 1	20000	105	53	47	0.06	0.04	0.18	0.21	0.27	0.18	0.16	0.21	5.1	2.6
1/ 1	21500	105	48	50	0.04	0.04	0.15	0.18	0.25	0.19	0.14	0.19	6.4	3.4
1/ 1	23000	105	52	36	0.04	0.04	0.19	0.25	0.24	0.25	0.18	0.25	6.9	3.7
1/ 1	24500	105	34	44	0.03	0.04	0.12	0.16	0.16	0.17	0.10	0.14	5.5	3.5
SUMS					0.18		0.65		0.95		0.57	MEAN G/R =	5.9	3.3

RADAR-GAGE RAINFALL ANALYSES FOR DAY 195 OF 1976 BEGINNING AT 20000. RUN DURATION = 30 MIN
COORD XFORM WT = 2 MIN RADAR RAIN = 0.02 MM RADIUS FOR G/R RATIOS = 1.0 KM

GAGE DENSITY	TIME (Z)	NUMBER OF GAGES TOTAL	G/R	EVAP	RAINFALL AMOUNTS (MM) RADAR MEAN	STDEV	GAGE MEAN	STDEV	GAGE+RADAR MEAN	STDEV	GAGE+RADAR (EVAP) MEAN	STDEV	GAGE-RADAR RATIO MEAN	STDEV
1/ 1	20000	105	65	34	0.10	0.07	0.33	0.37	0.44	0.32	0.31	0.36	4.4	2.5
1/ 1	23000	105	59	29	0.08	0.06	0.32	0.32	0.36	0.32	0.28	0.32	5.5	2.9
SUMS					0.18		0.65		0.80		0.60	MEAN G/R =	5.0	2.7

RADAR-GAGE RAINFALL ANALYSES FOR DAY 195 OF 1976 BEGINNING AT 20000. RUN DURATION = 60 MIN
COORD XFORM WT = 2 MIN RADAR RAIN = 0.02 MM RADIUS FOR G/R RATIOS = 1.0 KM

GAGE DENSITY	TIME (Z)	NUMBER OF GAGES TOTAL	G/R	EVAP	RAINFALL AMOUNTS (MM) RADAR MEAN	STDEV	GAGE MEAN	STDEV	GAGE+RADAR MEAN	STDEV	GAGE+RADAR (EVAP) MEAN	STDEV	GAGE-RADAR RATIO MEAN	STDEV
1/ 1	20000	105	76	26	0.18	0.12	0.65	0.58	0.74	0.54	0.59	0.59	4.5	1.9
SUMS					0.18		0.65		0.74		0.59	MEAN G/R =	4.5	1.9

Table 111. (continued) Page 5 of 6.

RADAR-GAGE RAINFALL ANALYSES FOR DAY 201 OF 1976 BEGINNING AT 13000. RUN DURATION = 5 MIN
COORD XFORM WT = 2 MIN RADAR RAIN = 0.10 MM RADIUS FOR G/R RATIOS = 1.0 KM

GAGE DENSITY	TIME (Z)	NUMBER OF GAGES TOTAL	G/R	EVAP	RADAR MEAN	RADAR STDEV	RAINFALL AMOUNTS (MM) GAGE MEAN	GAGE STDEV	GAGE+RADAR MEAN	GAGE+RADAR STDEV	GAGE+RADAR (EVAP) MEAN	GAGE+RADAR (EVAP) STDEV	GAGE-RADAR RATIO MEAN	GAGE-RADAR RATIO STDEV
1/ 1	13000	0	1	9	0.0	0.0	0.0	0.0	0.0	0.0	0.0	0.0	0.0	0.0
1/ 1	13500	0	1	9	0.0	0.0	0.0	0.0	0.0	0.0	0.0	0.0	0.0	0.0
1/ 1	14000	0	1	9	0.0	0.0	0.0	0.0	0.0	0.0	0.0	0.0	0.0	0.0
1/ 1	14500	112	2	17	0.01	0.06	0.03	0.31	0.03	0.34	0.02	0.30	3.5	2.4
1/ 1	15000	112	3	29	0.01	0.07	0.04	0.36	0.14	0.84	0.04	0.39	12.0	9.9
1/ 1	15500	112	7	39	0.01	0.05	0.03	0.14	0.09	0.41	0.02	0.15	7.5	3.7
1/ 1	20000	112	8	37	0.01	0.04	0.03	0.19	0.07	0.26	0.02	0.19	4.8	5.5
1/ 1	20500	112	10	38	0.01	0.04	0.04	0.14	0.07	0.17	0.03	0.16	6.3	3.2
1/ 1	21000	112	6	54	0.01	0.04	0.04	0.32	0.17	0.45	0.05	0.33	15.8	17.6
1/ 1	21500	112	7	51	0.01	0.04	0.04	0.14	0.14	0.55	0.05	0.51	13.6	13.7
1/ 1	22000	112	8	44	0.01	0.03	0.03	0.12	0.09	0.24	0.03	0.20	9.9	4.2
1/ 1	22500	112	10	47	0.01	0.03	0.05	0.20	0.11	0.43	0.03	0.28	12.2	12.5
SUMS					0.10		0.35		0.89		0.30	MEAN G/R =	7.4	6.2

RADAR-GAGE RAINFALL ANALYSES FOR DAY 201 OF 1976 BEGINNING AT 13000. RUN DURATION = 15 MIN
COORD XFORM WT = 2 MIN RADAR RAIN = 0.10 MM RADIUS FOR G/R RATIOS = 1.0 KM

GAGE DENSITY	TIME (Z)	NUMBER OF GAGES TOTAL	G/R	EVAP	RADAR MEAN	RADAR STDEV	RAINFALL AMOUNTS (MM) GAGE MEAN	GAGE STDEV	GAGE+RADAR MEAN	GAGE+RADAR STDEV	GAGE+RADAR (EVAP) MEAN	GAGE+RADAR (EVAP) STDEV	GAGE-RADAR RATIO MEAN	GAGE-RADAR RATIO STDEV
1/ 1	13000	112	1	11	0.01	0.04	0.01	0.04	0.01	0.04	0.01	0.04	1.0	0.0
1/ 1	14500	112	9	39	0.03	0.14	0.11	0.72	0.25	1.24	0.08	0.70	9.1	7.3
1/ 1	20000	112	17	45	0.04	0.10	0.12	0.46	0.25	0.67	0.12	0.58	7.9	11.4
1/ 1	21500	112	18	50	0.03	0.08	0.11	0.41	0.27	0.89	0.13	0.85	10.5	12.1
SUMS					0.10		0.36		0.77		0.33	MEAN G/R =	7.1	7.7

RADAR-GAGE RAINFALL ANALYSES FOR DAY 201 OF 1976 BEGINNING AT 13000. RUN DURATION = 30 MIN
COORD XFORM WT = 2 MIN RADAR RAIN = 0.10 MM RADIUS FOR G/R RATIOS = 1.0 KM

GAGE DENSITY	TIME (Z)	NUMBER OF GAGES TOTAL	G/R	EVAP	RADAR MEAN	RADAR STDEV	RAINFALL AMOUNTS (MM) GAGE MEAN	GAGE STDEV	GAGE+RADAR MEAN	GAGE+RADAR STDEV	GAGE+RADAR (EVAP) MEAN	GAGE+RADAR (EVAP) STDEV	GAGE-RADAR RATIO MEAN	GAGE-RADAR RATIO STDEV
1/ 1	13000	112	5	35	0.04	0.16	0.12	0.74	0.20	1.08	0.04	0.74	4.7	3.1
1/ 1	20000	112	26	48	0.07	0.14	0.24	0.74	0.48	1.23	0.25	1.16	8.4	9.9
SUMS					0.11		0.36		0.68		0.33	MEAN G/R =	6.6	6.5

RADAR-GAGE RAINFALL ANALYSES FOR DAY 201 OF 1976 BEGINNING AT 13000. RUN DURATION = 60 MIN
COORD XFORM WT = 2 MIN RADAR RAIN = 0.10 MM RADIUS FOR G/R RATIOS = 1.0 KM

GAGE DENSITY	TIME (Z)	NUMBER OF GAGES TOTAL	G/R	EVAP	RADAR MEAN	RADAR STDEV	RAINFALL AMOUNTS (MM) GAGE MEAN	GAGE STDEV	GAGE+RADAR MEAN	GAGE+RADAR STDEV	GAGE+RADAR (EVAP) MEAN	GAGE+RADAR (EVAP) STDEV	GAGE-RADAR RATIO MEAN	GAGE-RADAR RATIO STDEV
1/ 1	13000	112	25	48	0.10	0.22	0.35	1.09	0.55	1.47	0.33	1.41	5.3	5.4
SUMS					0.10		0.35		0.55		0.33	MEAN G/R =	5.3	5.4

RADAR-GAGE RAINFALL ANALYSES FOR DAY 201 OF 1976 BEGINNING AT 13000. RUN DURATION = 5 MIN
COORD XFORM WT = 2 MIN RADAR RAIN = 0.02 MM RADIUS FOR G/R RATIOS = 1.0 KM

GAGE DENSITY	TIME (Z)	NUMBER OF GAGES TOTAL	G/R	EVAP	RADAR MEAN	RADAR STDEV	RAINFALL AMOUNTS (MM) GAGE MEAN	GAGE STDEV	GAGE+RADAR MEAN	GAGE+RADAR STDEV	GAGE+RADAR (EVAP) MEAN	GAGE+RADAR (EVAP) STDEV	GAGE-RADAR RATIO MEAN	GAGE-RADAR RATIO STDEV
1/ 1	13000	112	1	6	0.00	0.01	0.00	0.02	0.00	0.04	0.00	0.04	5.0	0.0
1/ 1	13500	0	1	6	0.0	0.0	0.0	0.0	0.0	0.0	0.0	0.0	0.0	0.0
1/ 1	14000	112	1	25	0.00	0.02	0.00	0.02	0.11	0.58	0.05	0.47	26.9	0.0
1/ 1	14500	112	4	23	0.01	0.04	0.03	0.31	0.05	0.37	0.03	0.32	7.2	4.6
1/ 1	15000	112	3	29	0.01	0.07	0.04	0.36	0.14	1.07	0.04	0.48	12.1	11.3
1/ 1	15500	112	7	39	0.01	0.05	0.03	0.14	0.08	0.41	0.02	0.15	7.5	3.7
1/ 1	20000	112	8	37	0.01	0.04	0.03	0.19	0.07	0.24	0.02	0.19	4.8	5.5
1/ 1	20500	112	10	38	0.01	0.04	0.04	0.14	0.07	0.17	0.03	0.16	6.3	3.2
1/ 1	21000	112	6	54	0.01	0.04	0.04	0.32	0.17	0.59	0.06	0.48	15.0	23.3
1/ 1	21500	112	7	51	0.01	0.04	0.04	0.14	0.14	0.55	0.05	0.51	13.6	13.7
1/ 1	22000	112	8	44	0.01	0.03	0.03	0.12	0.09	0.24	0.03	0.20	9.9	4.2
1/ 1	22500	112	10	47	0.01	0.03	0.05	0.20	0.11	0.43	0.03	0.28	12.2	12.5
SUMS					0.10		0.35 (0.38)		1.02		0.36 (0.39)	MEAN G/R =	10.0	7.0

RADAR-GAGE RAINFALL ANALYSES FOR DAY 201 OF 1976 BEGINNING AT 13000. RUN DURATION = 15 MIN
COORD XFORM WT = 2 MIN RADAR RAIN = 0.02 MM RADIUS FOR G/R RATIOS = 1.0 KM

GAGE DENSITY	TIME (Z)	NUMBER OF GAGES TOTAL	G/R	EVAP	RADAR MEAN	RADAR STDEV	RAINFALL AMOUNTS (MM) GAGE MEAN	GAGE STDEV	GAGE+RADAR MEAN	GAGE+RADAR STDEV	GAGE+RADAR (EVAP) MEAN	GAGE+RADAR (EVAP) STDEV	GAGE-RADAR RATIO MEAN	GAGE-RADAR RATIO STDEV
1/ 1	13000	112	2	17	0.01	0.04	0.01	0.04	0.02	0.08	0.01	0.07	3.6	2.4
1/ 1	14500	112	9	39	0.03	0.14	0.11	0.72	0.25	1.24	0.08	0.70	9.1	7.3
1/ 1	20000	112	17	45	0.04	0.10	0.12	0.46	0.25	0.67	0.12	0.58	7.9	11.4
1/ 1	21500	112	18	50	0.03	0.08	0.11	0.41	0.27	0.89	0.13	0.85	10.5	12.1
SUMS					0.10		0.36		0.78		0.33	MEAN G/R =	7.8	8.3

RADAR-GAGE RAINFALL ANALYSES FOR DAY 201 OF 1976 BEGINNING AT 13000. RUN DURATION = 30 MIN
COORD XFORM WT = 2 MIN RADAR RAIN = 0.02 MM RADIUS FOR G/R RATIOS = 1.0 KM

GAGE DENSITY	TIME (Z)	NUMBER OF GAGES TOTAL	G/R	EVAP	RADAR MEAN	RADAR STDEV	RAINFALL AMOUNTS (MM) GAGE MEAN	GAGE STDEV	GAGE+RADAR MEAN	GAGE+RADAR STDEV	GAGE+RADAR (EVAP) MEAN	GAGE+RADAR (EVAP) STDEV	GAGE-RADAR RATIO MEAN	GAGE-RADAR RATIO STDEV
1/ 1	13000	112	9	37	0.04	0.16	0.12	0.74	0.22	1.14	0.09	0.76	5.9	2.6
1/ 1	20000	112	26	48	0.07	0.14	0.24	0.74	0.48	1.23	0.25	1.16	8.4	9.9
SUMS					0.10		0.35		0.71		0.33	MEAN G/R =	7.2	6.3

RADAR-GAGE RAINFALL ANALYSES FOR DAY 201 OF 1976 BEGINNING AT 13000. RUN DURATION = 60 MIN
COORD XFORM WT = 2 MIN RADAR RAIN = 0.02 MM RADIUS FOR G/R RATIOS = 1.0 KM

GAGE DENSITY	TIME (Z)	NUMBER OF GAGES TOTAL	G/R	EVAP	RADAR MEAN	RADAR STDEV	RAINFALL AMOUNTS (MM) GAGE MEAN	GAGE STDEV	GAGE+RADAR MEAN	GAGE+RADAR STDEV	GAGE+RADAR (EVAP) MEAN	GAGE+RADAR (EVAP) STDEV	GAGE-RADAR RATIO MEAN	GAGE-RADAR RATIO STDEV
1/ 1	13000	112	29	48	0.10	0.22	0.35	1.09	0.64	1.55	0.36	1.46	7.3	7.8
SUMS					0.10		0.35		0.64		0.36	MEAN G/R =	7.3	7.8

Table 111. (continued) Page 6 of 6.

Iterative Correction for Attenuation of 5-cm Radar in Rain.

(1) General Background. Current use of 5-cm weather radars for meteorological research raises the question of attenuation of the 5-cm radar signal by hydrometeors. Here, the subject is reviewed, and a method is presented which gives an estimate of the original unattenuated signal. The results are interpreted in terms of the ability of 5-cm radar to estimate rainfall amounts.

(2) Attenuation of Radar Signals. For wavelengths longer than 3 cm the major attenuation of a radar signal is due to hydrometeors, with only minor effects from atmospheric gases (Hitschfeld and Bordon, 1954). If the hydrometeors are cloud or precipitation particles, then the attenuation is (Atlas, 1964, equation 33):

$$K = 0.4343 \sum_{1} Q_t \quad [db/km] \tag{29}$$

where $\sum_{1} Q_t$ is the total attenuation cross-section per unit volume, and Qt is in cm^2. Values of Q_t for water can be obtained from Herman et al. (1961)and for ice spheres from Herman and Battan (1961). In this study, we shall assume the hydrometeors are water drops. Since the measured values of Q_t for water are functions of temperature, both the temperature and particle size distribution must be known to calculate the attenuation of the radar signal.

Perhaps the most commonly used raindrop size distribution is that of Marshall and Palmer (1948), who for stratiform rain situations approximated the raindrop size distribution by:

$$N_D = N_o \, e^{-\Lambda D} \quad (cm^{-4}) \tag{30}$$

where

$$\begin{aligned} N_o &= 0.08 \quad (cm^{-4}), \\ \Lambda &= 41 \, R^{-0.21} \quad (cm^{-1}), \end{aligned} \tag{31}$$

and R is the rainfall rate in mm/hr. This drop spectrum is frequently accurate for stratiform precipitation drops larger than 1mm.

For thunderstorm rain, Sekhon and Srivastava (1971) used vertically pointing Doppler radar data to derive a similar exponential dropsize distribution with

$$N_o = 0.07\ R^{0.37}\ (cm^{-4})$$

and

$$\Lambda = 38\ R^{-0.14}\ (cm^{-1}). \qquad (32)$$

These dropsize distributions are based on data in the range $1 \leq R \leq 60$ mm/hr; hence, their use should be limited to roughly those rainfall rates. Jones (1956), Mueller and Jones (1960) and others have reported thunderstorm dropsize distributions which differ from the above in that they show a strong decrease in drop concentration for diameters less than 1 mm.

When the attenuation of a radar signal is calculated using Equation 29 and the tables of Herman et al. (1961), curves such as those shown in Figure 35 can be derived for the Marshall-Palmer (MP) dropsize distribution (right-hand set) and the Sekhon-Srivastava (SS) distribution (left-hand set). (These curves are off-set from each other for clarity in plotting.) These curves assume dropsizes ranging up from 0.35 mm, and include variations in temperature from -10 to +20 C. To test the effects of the observed lowering in drop concentration below 1 mm, additional curves (short dashed lines) are plotted for the MP and SS distributions for a temperature of 20 C, with dropsizes limited to larger than 1 mm. The long dashed line plotted within the MP curves is the attenuation relation $K = 0.0031\ R$ proposed by Wexler and Atlas (1963) for a Marshall-Palmer distribution at a temperature of 0 C. The Wexler-Atlas curve is fairly accurate for low rainfall rates, but produces large underestimates of attenuation for high rainfall rates. This can lead to sizeable errors if attenuation estimates are needed for precipitation measurement.

These curves show that for a 5-cm radar, attenuation is small for rainfall rates below about 10 mm/hr (about 40 dbZ). It can be seen that errors in assumptions about the temperature of the attenuating drops may possibly be important in attempts to correct for attenuation. Errors in the assumed dropsize distribution are likely to produce errors in attenuation estimate of about the same magnitude as a 10 degree error in temperature. (This conclusion is not in agreement with Waldteufel's (1973) conclusion that temperature effects are small in comparison with differences between the MP and SS dropsize distributions.) Finally, for rainfall rates above 5 to 10 mm/hr, the uncertainty of the dropsize distribution at sizes less than 1 mm is not important in comparison with likely errors in assumed dropsize distribution and temperature.

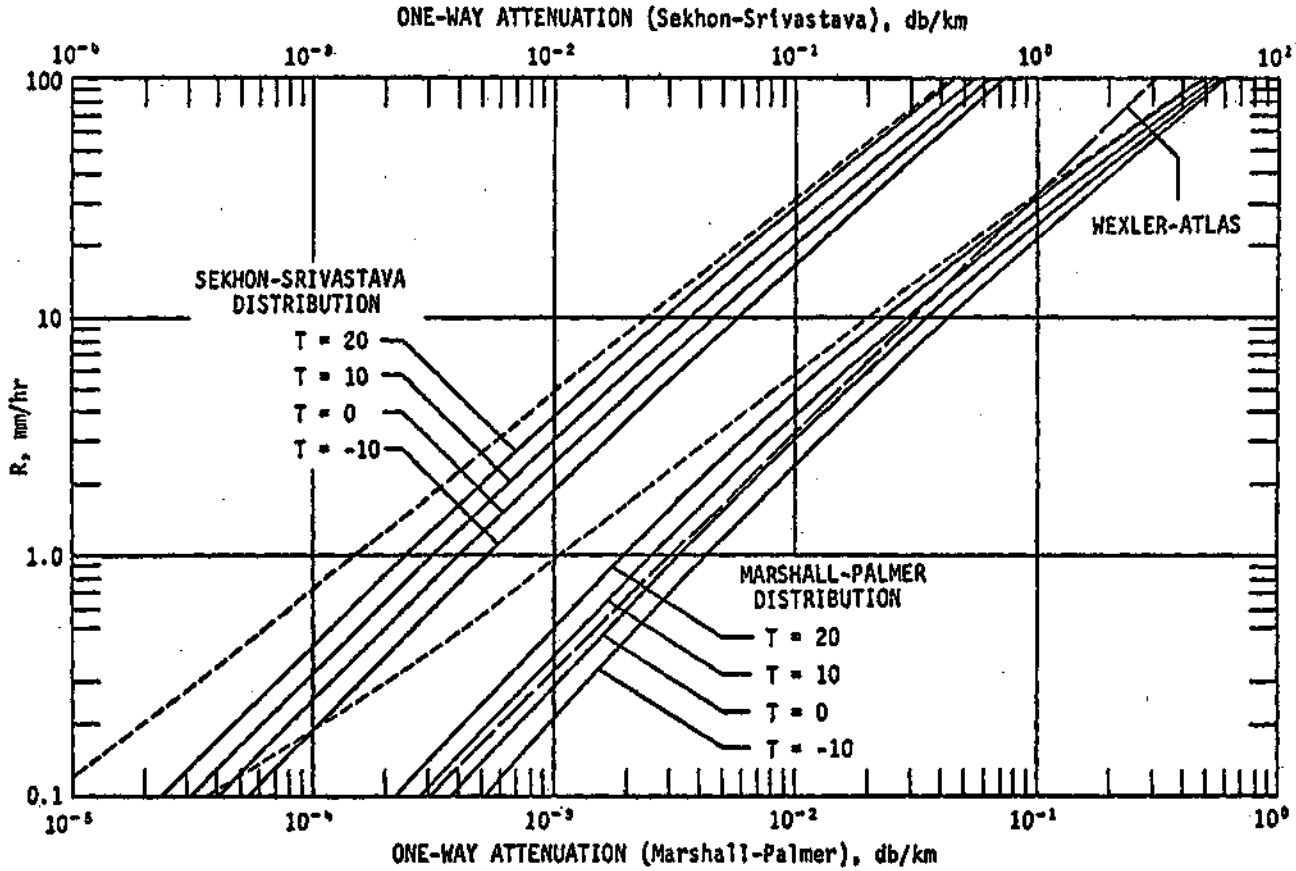

Figure 35. One way 5-cm radar attenuation curves for MP and SS dropsize distributions, for temperatures between -10 and 20 C. The MP and SS curves are displaced 10 db horizontally from each other for clarity in plotting. The short dashed lines represent the MP and SS curves at 20 C with dropsize distributions limited to sizes larger than 1 mm. The long dashed line is the Wexler-Atlas (1963) attenuation relation for 5-cm radar at 0 C.

The curvature of the K-R lines of Figure 35 and their variation with temperature suggests that a simple power law K-R relation (e.g., Wexler and Atlas, 1963) is not likely to produce accurate results for a range of rainfall rates. Therefore, empirical K-R relations were derived (Table 112) which account for temperature variations in the range -10 to +20 C. Due to the limitations on the dropsize distributions, use of these relations should be limited to reflectivities less than 60 dbZ.

Table 112. Empirical relations between one-way attenuation and rainfall rate using Marshall-Palmer (stratiform) and Sekhon-Srivastava (thunderstorm) raindrop size distributions, for temperatures between -10 and 20 C. One-way attenuation is in db/km and rainfall rate is in mm/hr.

Rainfall Rate	Marshall-Palmer	Sekhon-Srivastava
<10	$K=(.0045 - .00085T') R^{(.98 + .02T')}$	$K=(.0054 - .0010T') R^{(1.02 + .02T')}$
>10	$K=(.0030 - .0007T') R^{(1.155 + .065T')}$	$K=(.0043 - .0008T') R^{(1.115 + .025T')}$

$T' = (T/10.) + 1.0$

(3) Correction for Attenuation.

(a). Past work. Figure 35 shows that for 5-cm radar, attenuation can become substantial for high precipitation rates, particularly for widespread storms. This has been demonstrated by Geotis (1976) and Weible and Sirmans (1976) in their comparisons of 10-cm radar data with real or calculated 5-cm data. The continuing interest in deriving accurate precipitation estimates from radar has prompted attempts to correct the received radar signal for attenuation.

Hitschfeld and Bordon (1954) developed the radar equation in terms of the familiar Z-R and K-R relations, then derived a solution for rainfall rate. They showed that, for most reasonable cases, direct use of their rainfall equation (that is, correction for attenuation) is ill-advised for it produces errors which will dominate the determined rainfall amounts, particularly in the case of erroneous overestimates of received power (that is, in the case of radar calibration errors). They therefore recommend against attempting to correct for attenuation, noting the absurd possiblity of an infinite value of radar rainfall in cases of large overestimation of the received power.

Sims et al. (1964), in an investigation of precipitation estimation using 3-cm radar, suggest a scheme of attenuation underestimation as an alternative to previous schemes. In this technique, Z-R and K-R (or Z-K) equations are used. In order to correctly solve for attenuation, the correct (unattenuated) radar reflectivity must be used in the Z-K equation. Sims et al. use the attenuated measured value of radar reflectivity in the Z-K equation, thus resulting in an underestimate of the attenuation. They show several examples which demonstrate this technique to be an improvement over not making any correction for attenuation.

Geotis (1975) used 5- and 10-cm radar measurements and a disdrometer-derived Z-K relation, and applied this Z-K relation to the 5-cm radar values. He noticed an improvement in the corrected 5-cm values as compared with the 10-cm measurements; however, a considerable residual remained. He therefore concluded that an acceptable correction for attenuation had not been reached and expressed the need for improved Z-K relations.

(b) Iterative attenuation estimation. The attenuation estimation scheme presented here is an extension of the method of Sims et al. (1964). As in that method, the attenuated radar reflectivity factor measurements, Z (r) at ranges r, are converted to attenuated rainfall rates and to attenuation estimates, $K_a(r)$. Appropriate assumptions concerning dropsize distribution and temperature are made, and the radar is assumed to be correctly calibrated. With these data, a new estimate of reflectivity factor can be produced with the relation:

$$\log Z'(r) = \log Z_a(r) + 2 \sum_{x=1}^{r-1} K_a(x) \qquad (33)$$

If these new reflectivity factor estimates, Z'(r) are used to derive revised attenuation estimates, K'(r), another set of reflectivity factor estimates can be obtained from

$$\log Z''(r) = \log Z_a(r) + 2 \sum_{x=1}^{r-1} K'(x) \qquad (34)$$

In cases where the temperature and dropsize distribution are known and the radar is correctly calibrated, this iterative procedure can be continued until successive iterations do not produce a significant change in the estimated total attenuation along the radar beam. For the purposes of these calculations, iterations were terminated when

$$2 \sum_{x=1}^{rmax} K'(x)$$

changed by less than 1 db from the previous iteration.

In cases when the attenuation correction produces an overestimate of attenuation, the attenuation estimation calculation will diverge after several iterations. This can result from radar calibration errors, an overestimate of temperature, or the assumption of a MP dropsize distribution when the SS would have been more appropriate. In these cases the calculations were reinitiated, then stopped after a few iterations. The number of iterations on this second pass was empirically related to the number of iterations on the first pass.

(4) sample Calculations. The attenuation correction scheme was tested for various hypothetical storm sizes, errors in radar calibration, random errors, and errors in assumed temperature and dropsize distribution. Figure 36 illustrates the effects of the attenuation correction scheme for four storm sizes, assuming no sources of error, a MP dropsize distribution and a temperature of 0 C. The actual reflectivity profiles are indicated by the solid lines, the attenuated (measured) profiles by the short dashed lines, and the corrected profiles by the long dashed lines. For the curves in each test, the total range-integrated rainfall

$$R = \sum_{x=1}^{rmax} R(x)$$

was calculated for the true rainfall (R_t), the attenuated rainfall (R_a) and the corrected rainfall estimate (R_e). The values of the ratios $r_a = R_a/R_t$ and $r_e = R_e/R_t$ are presented in Figure 36 and Table 113 as a convenient means of evaluating the capabilities of the attenuation correction scheme in the context of rainfall estimation. This figure shows that for 5-cm radar, attenuation is not a significant problem for storms with radar reflectivity maxima below about 40 dbZ. In addition, it appears that the iterative attenuation estimation scheme works well, even for storms with 60 dbZ-maximum reflectivities. For the extended 60 dbZ-maximum storm the iterative solution diverged and had to be terminated prematurely. This is due to inaccuracies in the K-R relation (Table 113;) for reflectivities ≥60 dbZ. A similar run with an extended 57 dbZ maximum storm was handled correctly. As noted in Section 2, the dropsize distributions are not necessarily applicable for reflectivities higher than 60 dbZ and, in addition, for many climates hail is likely for high Z. Cases of divergence of the solution are indicated in Table 113 by asterisks located next to the r_e values. The attenuation estimation scheme was terminated in range at the point where the attenuated reflectivity dropped below 10 dbZ.

(a) Effect of radar calibration error. Hitschfeld and Bordon (1954) and Fedi (1974) point out that errors in radar calibration can inhibit attempts to correct received radar reflectivities for attenuation. The second section of Table 113 illustrates the effects of radar calibration errors ranging from -4 to +4 db in 2 db steps. The test storm used here is the 60 dbZ storm illustrated in the lower-left corner of Figure 36 and in line 3 of Table 113.

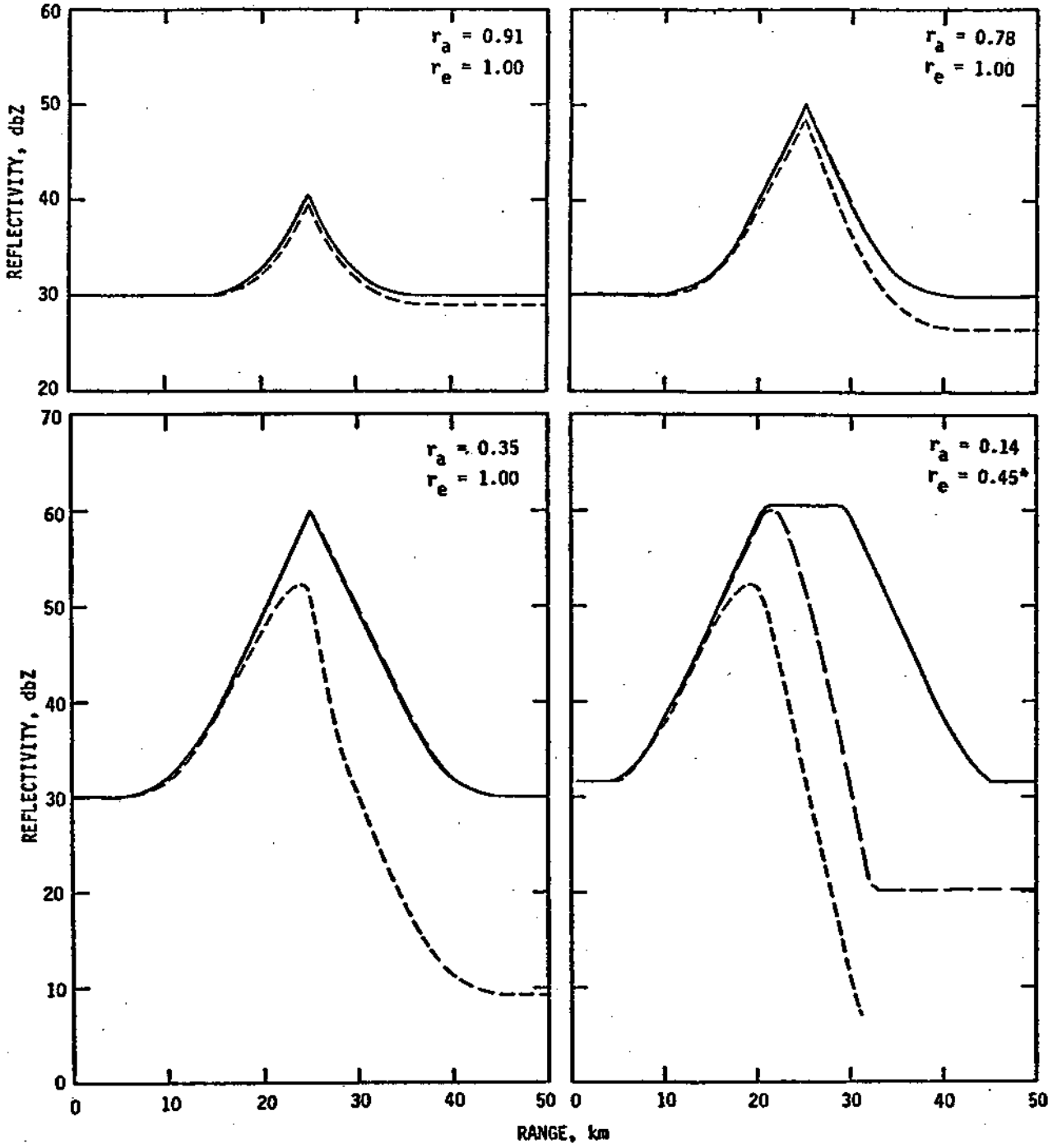

Fiqure 36. Effects of storm size on 5-cm radar estimates of rainfall and attenuation. The solid curve represents the actual radar reflectivity factor values, the short dashed curve indicates the attenuated reflectivities measured by the radar and the long dashed curve indicates the results of the attenuation estimator.

Table 113. Ratios of attenuated rainfall amount to true amount (r_a) and attenuation corrected rainfall amount to true amount (r_e) for various conditions of dropsize distribution, temperature, radar calibration error, and maximum storm reflectivity. The asterisk next to some r_e values indicates the iterative attenuation estimation calculation diverged and had to be stopped prematurely. In the dropsize distribution and temperature column, (1) indicates values used for attenuation calculations and (2) indicates values used for correction calculations.

Dropsize Distribution		Temperature (°C)		Radar Calibration Error	Z max		
1	2	1	2	(db)	(dbZ)	r_a	r_e
MP	MP	0	0	0	40	0.91	1.00
MP	MP	0	0	0	50	0.78	1.00
MP	MP	0	0	0	60	o.35	1.00
MP	MP	0	0	0	60(8km)	0.14	1.45*
MP	MP	10	10	-4	60	0.19	0.24
MP	MP	10	10	-2	60	0.27	0.39
MP	MP	10	10	2	60	0.51	0.98
MP	MP	10	10	4	60	0.69	1.97*
MP	MP	10	0	0	60	0.37	0.60*
MP	MP	0	10	0	60	0.35	0.74
MP	SS	10	10	0	60	0.37	0.59*
SS	MP	10	10	0	60	0.32	0.71
MP	SS	10	0	-2	60	0.27	0.51
MP	SS	10	0	0	60	0.37	0.65*
MP	SS	10	0	+2	60	0.51	1.22*
SS	MP	0	10	-2	60	0.20	0.28
SS	MP	0	10	0	60	0.28	0.51
SS	MP	0	10	+2	60	0.40	0.71

Here we see that the effects of radar miscalibration are serious, producing errors in the range integrated radar rainfall as large as r_a = 0.69 and 0.19, and r_e = 1.97 and 0.24 for +4 and -4 db calibration errors, respectively. The value of r_e = 1.97 for the +4 db calibration error illustrates that when the calibration error is larger than the maximum attenuation (db/km), attempts to correct for attenuation degrade the rainfall estimate in comparison with the attenuated rainfall estimate. Thus, for 5-cm radar calibrated within ±2 db, no attempts to correct for attenuation should be made for storms with reflectivity maxima of about 45 dbZ or less.

In the illustrated case of the 60 dbZ maximum storm with a ±2 db calibration error, the attenuation estimation scheme improves the values of r_a = 0.51 and 0.27 to values of r_e = 0.98 and 0.39, respectively. Although these r_e values are closer to 1.0 than the r_a values, the f_e =0.98 is a fortuitous result of early termination of the calculation, and r_e = 0.39 still does not represent an accurate precipitation estimate.

(b) Effect of random errors. For the small sample sizes used in many experiments, the measured radar reflectivity factor may have a sampling error on the order of 1 to 2 dbZ. To simulate the effects of such errors on the attenuation estimation scheme, a set of random errors ranging from -2 to +2 dbZ was added to the attenuated power measurements. For all cases tried, the effects of these random errors were observed to be small in comparison to the other likely sources of error.

(c) Effect of temperature. As mentioned in Section 2, the attenuation of the radar signal in precipitation is temperature dependent. The effects of an error in the assumed temperature are illustrated in the third section of Table 113, using the 60 dbZ test storm of Section 4a, no radar calibration error and a MP dropsize distribution. In all cases, the attenuation correction scheme improves rainfall estimates; however, it can be seen that assuming top high a temperature produces an underestimate of attenuation and assuming too low a temperature produces an overestimate of attenuation and consequent divergence of the iterative scheme. Since, in many cases, the temperature is known within better than 10 C (the temperature error illustrated here), temperature errors are not a serious source of error in rainfall estimation. This conclusion is in partial agreement with the findings of Waldteufel (1973) who suggested that temperature had a negligible effect on attenuation. Although the temperature effect is small, incorrect temperature assumptions will degrade attempts to correct for attentuation.

(d) Effect of dropsize distribution. The effects of the assumed dropsize distribution are illustrated in the fourth section of Table 113, for a temperature of 10 C, no radar calibration error, and using the 60 dbZ tests storm of Section 4a. Here, likely errors due to an incorrectly assumed dropsize distribution are seen to be equivalent to likely temperature-induced errors and are small in comparison with the effects of attenuation.

As before, the attenuation estimation scheme improves the quality of the rainfall estimate.

(e) Effects of multiple errors. In the preceding paragraphs, it was shown that the effects of typical temperature and dropsize distribution errors are small in comparison to the effects of attenuation. Radar calibration errors, however, present a serious problem, with the expected 1 to 2 db calibration errors frequently producing significantly degraded attenuation estimates.

The effects of combinations of temperature, dropsize distribution, and calibration errors are shown in the last section of Table 113 for 60 dbZ test storm used in the preceding sections. The combination of temperature and dropsize distribution errors were chosen so that they both produced underestimates or overestimates of attenuation; e.g., an underestimate of temperature was coupled with assumption of the SS distribution instead of MP, since both errors produced overestimates of attenuation in the attenuation estimation scheme. The values of r_a and r_e for 0 dbZ calibration error show that combined temperature and dropsize distribution errors are equivalent to either error taken alone.

If a radar calibration error is added to the other errors, the attenuated rainfall estimates are significantly modified, and the attenuation estimation scheme results are degraded. Additional test calculations for other reflectivity distributions and assumed temperature and dropsize distribution errors confirm these results.

(5) Results and Conclusions. This study indicates that 5-cm radar measurements of storms with reflectivity maxima greater than about 50 dbZ will be seriously attenuated. These results agree with the findings of Geotis (1976) and Weible and Sirmans (1976), and suggest that some sort of attenuation estimation scheme must be implemented if 5-cm radars are used to measure rainfall from large storms.

An iterative attenuation estimation scheme is presented which removes a large portion of the effects of attenuation, thereby producing a significant improvement in rainfall estimates. The effects of radar calibration error and errors in assumed dropsize distribution and temperature are considered, and it is shown that dropsize distribution and temperature errors can significantly degrade the attenuation estimates, but that these degradations are small in comparison with the effects of. radar calibration errors. It is shown that use of the iterative attenuation estimation scheme must be limited to cases in which the radar calibration error is smaller than the maximum attenuation (db/km). For a 5-cm radar calibrated to within 2 db, this limits use of the scheme to storms with reflectivity maxima of 45 dbZ or greater. Due to limitations mentioned in Section 4, the scheme does not work well for storms with reflectivity maxima greater than 60 dbZ. For many

climates this does not represent a problem, because high reflectivity radar rainfall estimates are frequently inaccurate due to the presence of hail.

The condition that the iterative attenuation estimation scheme cannot be applied in cases - when the maximum attenuation is less than the radar calibration error is similar to the infinite rainfall rate of Hitschfeld and Bordon (1954), and suggests that inaccuracies in radar calibration are likely to set the basic limit on any corrections for attenuation using single wavelength radar.

This study of 5-cm radar attenuation thus suggests that the most viable method of obtaining precipitation estimates is with a fairly dense raingage network, used in conjunction with the radar in a manner similar to that suggested by Brandes (1975). The gages can "calibrate" the radar precipitation estimates, correcting for radar calibration error, errors in assumed dropsize distribution (Z-R relation) and the effects of attenuation and evaporation. The strong time-space variability of precipitation (Joss et al., 1974) underscores the need for the gages and suggests the possibility that raingage spacing, for use in conjunction with radar, should be derived on the basis of the typical storm size - a measurable feature of the climate and storm type. Such a criterion would usually insure a gage within areas of significantly differing precipitation characteristics. As Hitschfeld and Bordon (1954) noted, accurate radar precipitation measurement requires a sufficiently high gage density to assure that gages are located in areas of significant attenuation. Due to the large time and space variability of precipitation, no sort of daily Z-R or Z-K relation or average value of gage-radar ratio will suffice. This conclusion suggests that an empirical Z-K approach is not likely to be promising. It should be noted, however, that in the case of large area, long term precipitation measurement (a case not considered here), many of the radar rainfall estimation problems may disappear in the average if carefully selected Z-R and Z-K relations are used. However, for most applications, the errors noted here and in other works underscore the ultimate reliance of accurate precipitation measurements on raingage data.

(6) Acknowledgments. This research was performed under the general supervision of Mr. Stanley A. Changnon, Jr., Head of the Atmospheric Sciences Section of the Illinois State Water Survey. Enjoyably spirited discussions with many members of the Illinois State Water Survey staff considerably aided this research. In particular, Mr. Griffith Morgan, Jr. suggested the possibility of the iterative attenuation estimation scheme. Dr. Arthur Jameson of the University of Chicago provided helpful criticism and the attenuation cross-section data on computer cards.

Precipitation Initiation and First Echo Climatology for HIPLEX.

(1) General Background. The location of radar first echoes with respect to height and temperature has often been used to infer precipitation initiation mechanisms within convective clouds. The location of the radar first echo (FE) has been taken to indicate the location of the first large (precipitation sized) particles within a cloud. The microphysical interpretation of the FE is not always clear because in many instances the FE could be due either to liquid or solid water particles. In the discussion which follows, observations of radar FE's will be presented along with comments concerning their interpretation. Emphasis will be placed on looking for regional differences in precipitation initiation mechanisms, particularly within the HIPLEX research area.

(2) First Echo Studies. Early work on precipitation initiation using radar information centerd on thunderstorm research (Workman and Reynolds, 1949; Reynolds and Braham, 1952; Battan, 1953) indicated that New Mexico thunderstorms usually had a FE temperature of about -10 C and Ohio thunderstorms usually had a FE temperature of -2 to +5 C. The interpretation of the New Mexico data was not clear at this point in time; however, the Ohio observations clearly indicated droplet coalescence as the predominent precipitation initiation mechanism.

More recent investigations of precipitation initiation in the southwest clearly indicate that warm rain processes are dominant in that region. Braham (1958) investigated 357 FE's in Arizona and found that all had tops colder than 0 C and nearly all had bases warmer than 0 C. He concluded that the variations within the sample were primarily due to large scale atmospheric effects and that the precipitation initiation mechanism a) was unchanged from day to day, and b) was not closely tied to temperature fluctuations (at least within the range of his experiment). Ackerman (1960), using data collected in the same region (294 FE's), found nearly the same results as did Braham, except that 40% of the FE's in her sample were totally colder than 0 C. This led to her conclusion that warm precipitation initiation was most common and that, in some cases, both warm and cold processes were active. She concluded that variations in the initiation mechanism were related to large-scale atmospheric structures. Clark (1960) observed 247 FE's in Texas and found an average FE top to be at -1.1 C and concluded that coalescence processes produced the precipitation.

Battan (1963) reanalyzed Braham's data using only data for which the FE was measured within 3 minutes of a previous radar scan of the same location. He found a correlation between the FE height and the height of the 0 C isotherm. Battan suggested that if the Bergeron process was active, lower cloud bases would

increase the cloud water content at any level, thereby increasing the height at which growing ice particles would become detectable by radar. (He assumed that the source of the ice crystals would be the region of coldest temperatures at the top of the cloud.) Conversely, if coalescence processes were active, lower cloud bases would lower FE levels. Hence he concluded that, in Braham's data, warm precipitation initiation was the rule, even though many FE's contained temperatures colder than 0 C.

This conclusion has been further verified by other experiments in many other regions of the world. In an extensive study of precipitation modification in southern Missouri, Braham (1962, 1963) found that 66% of FE's were wholly colder than 0 C. The average FE temperature, measured at the center of the FE, was about +5 C.

Sulakvelidze, et al. (1967) agree with the hypothesis of warm precipitation initiation, citing radar echo histories with FE temperatures warmer than -10 C for storms observed in the Soviet Union.

Dennis and Koscielski (1972) and Dennis et al. (1974) discussed the results of radar observations in South Dakota. They found a mean FE temperature of -13 C for 122 unseeded cases and warmer temperatures for the AgI and salt seeded cases. Dennis and Koscielski calculated correlations between FE temperature and height and various other parameters which included cloud base height, cloud base temperature, updraft speed and other measurements. Their unseeded data indicated that the FE temperature was strongly correlated with the updraft speed (inverse relation) and was positively related to cloud base temperature. They interpreted these and other findings to imply that coalescense was the primary precipitation initiation mechanism.

While these investigations suggest that in many instances coalescence is the primary precipitation initiation mechanism, there are indications that this is not necessarily true for all cases. Browning and Atlas (1965) observed some severe storms in Oklahoma for which the FE midpoint temperature was at or colder than -30 C. They suggested that, for severe storms, very cold FE's could be due to the extremely strong updrafts. The extremely cold temperatures of these FE's strongly suggests that an ice growth mechanism is responsible for these first echoes. These observations are consistent with the work of Changnon and Stout (1964) who found a FE midpoihfat about -40 C in a severe Illinois storm.

These observations of cold precipitation initiation are consistent with research being done as a part of the National Hail Research Experiment (NHRE) as summarized by Knight et al. (1974), Cannon et al. (1974), and Dye et al. (1974). This work indicates that in the northeastern Colorado hailstorms, the distribution of FE

temperatures is bimodal, with peaks at -15 and 0 C. These temperatures are the temperatures of maximum sublimation growth rate for ice crystals at the expense of water droplets and the melting temperature. This observation along with the extensive cloud physical observations of NHRE have led to the conclusion that northeastern Colorado hailstorms are dominated by ice precipitation initiation. Some of their supporting information includes a sharp cut-off in cloud droplets at a radius of 50 microns (implying collection of larger drops), the persistent appearance of graupel as hail embryos, and the fact that the observed ice alone could account for the observed radar reflectivity. They suggested that a low concentration of giant nuclei in the NHRE research area could account for the lack of an effective coalescence process.

These observations are in conflict with the aforementioned South Dakota work and are confusing since the NHRE research was carried out in a more southern location than the South Dakota research. The reason for this apparent conflict could be that the NHRE research area is drier than the South Dakota area because of the drying effect the Rocky Mountains have on the NHRE area (see Changnon et al., 1975). An additional reason for the difference between the NHRE and South Dakota results could be their differing experimental designs and goals.

Unfortunately, there is little additional FE data, particularly to the north of the areas already discussed. While the FE climatology for southwestern and midwestern locations is clear, there is not an adequate data base from which firm conclusions can be drawn concerning the central and northern high plains regions. Even the South Dakota work is based on a small sample, and although the work appears accurate, a larger sample would more fully assure adequate representation of all meteorological situations.

(3) Precipitation initiation - discussion. The above FE studies (summarized in Table 114 clearly indicate that for the southern Great Plains and the midwestern United States, coalescence is the dominant precipitation initiation process. This is confirmed by various cloud physical studies including the 1975 HIPLEX observations (Carbone, 1976) for both Texas and (to a limited extent) Kansas. In addition, Braham (1964) observed that coalescence was dominant at the -5 C level in the Missouri cumuli data. However, in many cases he observed rapid glaciation immediately following the warm initiation of precipitation-sized water drops. The frequent observation of frozen drop, hail embryos in hail collected away from the NHRE area (e.g. in Kansas, Missouri, Oklahoma; Knight, 1976) also supports the suggestion of predominant warm precipitation initiation.

The extension of the coalescence mechanism to temperatures below 0 C is further supported by Battan's correlation of Arizona FE

height with cloud base height, and by the South Dakota observations which relate FE temperature to updraft speed and cloud base temperature.

These results suggest that the Texas and Kansas sites are dominated by coalescence precipitation initiation, but that the probability of ice initiation is higher in Kansas. On the basis of the present information one can only speculate about the characteristics of the Montana site. Two observations are pertinent: a) Knight (1976) reports that most of the embryos from hail collected in South Dakota are graupel, b) Montana is colder and drier than South Dakota (Changnon et al., 1975). These observations, together with the Browning - Atlas (1965) suggestion of a different mechanism for severe storms suggests that South Dakota may be on the borderline for warm precipitation initiation and that Montana may be typified by an ice initiation mechanism. It is unfortunate that there is no radar evidence with which this suggestion can be tested.

Table 114. Temperatures At Center Height of Radar First Echo

Source	First Echo Height (^{o}C)	Location
Workman - Reynolds (1948)	-10	New Mexico
Reynolds - Braham (1952)	- 2	Ohio
Battan (1953)	+ 5*	Ohio
Braham (1958)	- 1*	Arizona
Ackerman (1960)	- 4*	Arizona
Clark (1960)	> 0	Texas
Carbone (1975)	+ 1	Texas
Braham (1962, 1963)	+ 5	Missouri
Sulakvelidze et al. (1967)	-10	Soviet Union
Dennis and Koscielski (1972)		
Dennis et al. (1974)	-13	South Dakota
Browning and Atlas (1965)	-30	Oklahoma (severe)
Changnon and Stout (1964)	-40	Illinois (severe)
Dye et al. (1974)	-15, 0	Colorado (NHRE)

There are several questions which can be raised in connection with this limited study:

First, the precipitation initiation climatology of the Kansas and Montana sites is inadequate. Although coalescence appears to predominate in Kansas, the relative importance of ice is unknown. The situation in Montana is much less clear and desperately needs to be improved upon if intelligent research decisions are to be made.

Second, the role of ice immediately after precipitation-sized water drops have developed needs to be clarified. Many workers have observed the initial development of a population of water drops, followed quickly by glaciation. Braham (1964) notes that the observed precipitation from Missouri clouds was substantially greater than could be explained by the Bergeron ice or the coalescence mechanisms alone. He suggested droplet splintering upon freezing to account for this. It is important to consider ice as a part of precipitation development and not only as a possible cause of precipitation initiation. In the context of precipitation development, the ice phase is more common and important than it is if considered only in the context of initiation.

Third, the suggestion of Browning and Atlas (1964) that severe storms have different (i.e. cold) initiation mechanism needs additional consideration. This may be particularly important in Kansas, where the chance of an important ice process is higher than in Texas.

It therefore appears that the future operation and decisions of the HIPLEX experiment could substantially benefit from a coordinated examination of first echo data collected at the three research sites. Although this need not be a time-consuming operation, it could be of substantial benefit. It should be remembered that much of the first echo data which have been presented here were obtained from radars which were neither calibrated nor range-normalized. Thus, what appeared as a first echo in one experiment might not be seen in another, and what was a first echo at one range might not be seen at another range. A calibrated, range normalized precipitation initiation study performed with a modern, digitally recording radar and an instrumented aircraft would greatly aid in further;, redesign and evaluation of experimental operations. A part of such a comprehensive first echo study should be an examination of the correlations of FE temperatures and heights with updraft strength, cloud base temperature and other parameters. Such an analysis should provide useful information about the initiation of precipitation.

REFERENCES

Abramowitz and Slegun, 1964: Handbook of Mathematical Functions with Formulas, Graphs, and Mathematical Tables. Nat'1. Bur. Standards. Washington, DC 1046 pp.

Achtemeier, G. L., 1975: On the initialization problem: A variational adjustment method. Mon. Wea. Rev. 103, 1089-1103.

Achtemeier, G. L., and G. M. Morgan, Jr., 1975: A short-term thunderstorm forecast system: Step 1, exploitation of the surface data. Preprints, 9th Conf. Severe Local Storms, Norman, Amer. Meteor. Soc, Boston, 18-24.

Achtemeier, G. L., and G. M. Morgan, Jr., 1976: A short-term thunderstorm forecast system utilizing the 4-dimensional evolution of mesoscale stability. Preprints, 6th Conf. on Weather Forecasting and Analysis Albany, Amer. Meteor. Soc, Boston, 238-241.

Ackerman, B., 1960: Orographic-convective precipitation as revealed by radar. H. Weickman, Ed., Physics of Precipitation, Geophysical Monograph No. 5, American Geophysical Union, Washington, DC, 79-85.

Ackerman, B., G. Achtemeier, H. Appleman, S. Changnon, Jr., F. Huff, G. Morgan, P. Schickedanz, and R. Semonin, 1976: Design of the High Plains Experiment with Specific Focus on Phase 2, Single Cloud Experimentation. Atmos. Sci. Sect., 111. State Water Survey, Report to Bureau of Reclamation, Contract 14-06-D-7197, 231 pp.

Ackermann, W. C., S. A. Changnon, Jr., and R. J. Davis, 1974: The New Weather Modification Law for Illinois. Bulletin Amer. Meteor. Soc, 55, 745-750.

Anderson, C. E., and L. W. Uccellini, 1974: Studies of meteorological factors involved in the formation of severe local storms in the northeast Colorado region. Preprints, 8th Conf. Severe Local Storms, Denver, CO, American Meteor. Society, 84-89.

Atlas, D., 1964: Advances in Radar Meteorology. Ed. H. E. Landsberg and J. VanMieghem, Advances in Geophysics, 10, New York, Academic Press, 318-478.

Bark, L. D., 1975: A Survey of the Radar Echo Population Over the Western Kansas High Plains, Vol. 1, Apr.-Sept. 1972-1974, Project 5-369, Dept. Physics, Kansas Agri. Exp. Station, Kansas State Univ., 68 pp.

Bergthorsson, P., and B. R. Doos, 1955: Numerical weather map analysis. Tellus 7, 329-340.

Barnes, S. L., 1964: A technique for maximizing details in numerical weather map analysis, J. Appl. Meteor., 3, 396-409.

_____, S. L., 1973: Mesoscale objective map analysis using weighted time-series observations. NOAA Tech. Memo 62, NSSL, 60 pp.

_____, S. L., (Editor), 1974: Papers on Oklahoma thunderstorms, April 29-30, 1970. NOAA Tech. Memo. ERL-NSSL-69, 233 pp.

Battan, L. J., 1953: Observations of the formation and spread of precipitation in convective clouds, J. Met., 10, 311-324.

_____, L. J. 1963: Relationship between cloud base and initial radar echo, J. Appl. Meteor., 2, 333-336.

Berkofsky, L., and E. Bertoni, 1960: Topographic Charts at One-Degree Intersections for the Entire Earth. GRD-42, Geophysical Res. Dir., Cambridge Res. Lab., Bedford, MA, 43 pp.

Bermowitz, R. J., 1971: Objectively Computed Surface Diagnostic Fields. NOAA Tech. Memo NWS TDL-38, 23 pp.

Berry, F. A., Jr., E. Bollay, and N. R. Beers, 1945: Handbook of Meteorology. McGraw-Hill, New York, 1056 pp.

Biondini, R., 1976: Cloud motion and rainfall statistics, J. Appl. Meteor., 15, 205-224.

_____, R., J. Simpson, and W. L. Woodley, 1977: Empirical Predictors for Natural and Seeded Rainfall in the Florida Area Cumulus Experiment (FACE) 1970-1975, submitted to J. Appl. Meteor.

Bonner, W. D., R. M. Reap, and J. E, Kemper, 1971: Preliminary results on severe storm prediction by screening regression using forecast predictors. Preprints, 7th Conf. Severe Local Storms, Kansas City, Amer. Meteor. Soc, Boston, 36-41.

Boyden, C. J., 1963: A simple instability index for use as a synoptic parameter. Meteor. Mag., 92, 198-210.

Braham, R. R., Jr., 1958: Cumulus cloud precipitation as revealed by radar -Arizona 1955, J. Met., 15, 75-83.

_____, R. R., Jr., 1962: Final Report to the National Science Foundation on work performed under Grant NSF-98214, Project Whitetop April 4, 1959 to April 3, 1962. Univ. of Chicago, Cloud Physics Laboratory.

, R. R. Jr., 1963: Report to the National Science Foundation on work performed under Grant NSF-G-22419. Project Whitetop April 4, 1962 to April 3, 1963. Univ. of Chicago, Cloud Physics Laboratory.

Braham, R. R., Jr., 1964: What is the role of ice in summer rain showers?, J. Atmos. Sci., 21, 640-645.

Brandes, E. A., 1975: Optimizing rainfall estimates with the aid of radar. J. Appl. Meteor., 14, 1339-1345.

Brier, G. W., 1974: Design and evaluation of weather modification experiment, Climate and Weather Modification, W. N. Hess (Ed.) Wiley, NY, 330 pp.

Brown, R. A., (Editor), 1976: The Union City, Oklahoma tornado of May 1973, NOAA Tech. Memo. ERL NSSL-80, 235 pp.

Browning, K. A., and D. Atlas, 1965: Initiation of Precipitation in vigorous covective clouds, J. Atmos. Sci., 22, 678-683.

Cahir, J. J., 1971: Implications of Circulations in the Vicinity of Jet Streaks at Subsynoptic Scales. Ph.D. Thesis, Penn. State University.

Cannon, T. W., J. E. Dye, and V. Toutenhoofd, 1974: The mechanism of precipitation formation in northeast Colorado cumulus II, Soilplane measurements, J. Atmos, Sci., 31, 2148-2151.

Carbone, R. E., 1976: personal communication.

Changnon, S. A., Jr., F. A. Huff, and P. T. Schickedanz, 1975: A high plains climatography, Special Report under Contract 14-06-D-7197, Illinois State Water Survey, Urbana, IL 119 pp.

_____, S. A., Jr. G. Morgan, 1976: Design of an Experiment to Suppress Hail in Illinois. ISWS Bull. 61, ISWS, 194 pp.

_____, S. A., Jr. and G. R. Stout, 1964: A detailed investigation of an Illinois hailstorm on August 8, 1963. Res. Report 18, prepared for the Crop-Hail Insurance Actuarial Association, Chicago, IL.

Charba, J., 1975: Operational scheme for short-range forecasts of severe local weather. Preprints, 9th Conf. Severe Local Storms, Norman, Amer. Meteor. Soc, Boston, 51-57.

Clark, R. A., 1960: A study of convective precipitation as revealed by radar observation, Texas 1958-59, J. Meteor., 17, 415-425.

Clark, R. E., 1973: Objective planning forecasts. Aerospace Sciences Review, AWS RF 105-2, 73-3, 7-14.

Cohen, S. H., 1977: Verification and refinement of forecast sounding techniques for the HIPLEX Kansas program. Preprints, 6th Conf. Planned and Inadv. Wea. Mod. 10-13 Oct. 1977, Champaign-Urbana, IL, Amer. Meteor. Soc, 252-253.

Cressman, G. P., 1959: An operational objective analysis system. Mon. Wea. Rev., 87, 367-374.

Darkow, G. L., 1968: The total energy environment of severe storms. J. Appl. Meteor., *1*, 199-205.

Darrt, D. G., 1972: Automated streamline analysis utilizing "optimum interpolation." J. Appl. Meteor., 11, 901-908.

David, C. L., 1974: Objective Probabilities of Severe Thunderstorms Using Predictors form FPUS and Observed Surface Data. NOAA Tech. Memo NWS CR-54.

_____, C. L., and J. Smith, 1971: An evaluation of seven stability indices as predictors of severe thunderstorms and tornadoes. Preprints, 7th Conf. Severe Local Storms, Kansas City, Amer. Meteor. Soc, Boston, 105-109.

Davis, R. A., 1969: A computer method to generate and plot stream-lines. USWB Pacific Region, ESSA, Tech. Memo. WBTM PR-5, 12 pp.

Dennis, A. S., M. R. Schock, A. Koscielski, and P. M. Mielke, 1967: Evaluation of Cloud Seeding Experiments in South Dakota During 1965 and 1966. Rept. 67-1, Inst. Atmos. Sci., S. Dakota School of Mines and Tech., 71 pp.

_____, A. S., and A. Koscielski, 1969: Results of a randomized cloud seeding experiment in South Dakota. J. Appl. Meteor., 8, 556-565.

_____, A. S., and A. Koscielski, 1972: Height and temperatures of first echoes in unseeded and seeded convective clouds in South Dakota, J. Appl. Meteor., 11, 994-1000.

_____, A. S., A. Koscielski, J. H. Hirsch, D. E. Cain, and P. L. Smith, 1974: Cloud catcher Report for 1972. Report 74-4, Institute of Atmospheric Sciences, South Dakota School of Mines and Technology, Rapid City, 121 pp.

_____, A. S., J. H. Hirsch, D. E. Cain, J. R. Miller, Jr., and A. Koscielske, 1975: The potential for rainfall increases from convective clouds in the Northern Plains. Rept. 75-12, Inst. of Atmos. Sci., S. Dak, School of Mines & Tech., Rapid City, 60 pp.

Dirks, R. A., 1969: A Climatology of Central Great Plains Mesoscale Convective Systems. Tech. Rept. E-10-686, Colo. State Univ., 60 pp.

Dye, J. E., C. A. Knight, V. Toutenhoofd, and T. W. Cannon, 1974: The mechanism of precipitation formation in northeastern Colorado cumulus III. Coordinated microphysical and radar observations and summary, J. Atmos. Sci., 31, 2152-2159.

Endlich, R. M. , and R. L. Mancusso, 1967: Environmental Conditions Associated with Severe Thunderstorms and Tornadoes. Stanford Res. Inst., Menlo Park, Calif., Cwb-11293, 106 pp.

Estoque, M. A., and J. J. Fernandez-Partagas, 1974: Precipitation dependence on synoptic-scale conditions and cloud seeding. Geofisica International, 14, 181-206.

Fedi, F., 1974: Attenuation: theory and measurements. J. Rech. Atmos., 8, 464-472.

Foster, D. S., 1964: Relationship among tornadoes, vorticity acceleration and air mass stability. Mon. Wea. Rev., 92, 339-343.

Fujita, T., and D. L. Bradbury, 1966: Stability and differential advection associated with tornado development. SMRP Research Paper 52, 17 pp.

Galway, J. G., 1956: The Lifted Index as a predictor of latent instability. Bull. Amer. Meteor. Soc, 37, 528-529.

George, J. J., et al, 1960: Weather Forecasting for Aeronautics. Academic Press, New York, 673 pp.

Geotis, S. G., 1975: Some measurements of the attenuation of 5-cm radiation in rain. Preprints, 16th Conf. on Radar Meteor., AMS, Boston, 63-66.

Girdzus, J., 1976: The 1975 CRMWD Weather Modification Program and Rainfall Record Evaluation. Rept. 76-1, Colorado River Municipal Water Dist., Big Spring, Texas, 39 pp.

Glahn, H. R., D. A. Lpwry, and G. W. Hollenbaugh, 1969: An Operational Subsynoptic Advection Model. ESSA Tech. Memo WBTM TDL-23, 26 pp.

Goff, R. C, 1976: Vertical structure of thunderstorm outflows. Mon. Wea. Rev. 104, 1429-1440.

____, R. C, and H. R. Hudson, 1972: The thermal structure of the lowest half kilometer in Central Oklahoma: December 9, 1966 - May 21, 1967, NOAA TM ERL NSSL 58, 53 pp.

Hammond, G., and R. Clark, 1975: Trajectory bulletin severe weather signature. Aerospace Sciences Review, 75-1, 36-42.

Harley, W. S., 1971: Convective storm diagnosis and prediction using two layer combined indices of potential and latent instability in combination with other special and standard significators. Preprints, 7th Conf. Severe Local Storms, Kansas City, Amer. Meteor. Soc, Boston, 23-30.

Hartzell, C. L., 1975: Summary of WSSI Support Services for HIPLEX 1975, Miles City, Montana. Second HIPLEX Tech. Conf., 16-18 Dec. 1975, Denver, 10 pp.

Havera, S. P., 1973: The Relationship of Illinois Weather and Agriculture to the Eastern Cottontail Rabbit. Technical Report No. 4, Contract D-7197, Illinois State Water Survey, Urbana,92 pp.

Herman, B. M., and L. J. Battan, 1961: Calculation of Mie backscattering of microwaves from ice spheres. Quart. J. Roy. Meteor. Soc, 87, 223-230.

_____, and S. R. Browning, and L. J. Battan, 1961: Tables of the radar cross sections of water spheres. Arizona Univ. Inst. Atmos. Phys., Techn. Rept. No. 9, (obtained for 5.45-cm radar from Lab. for Atmos. Probing, Dept. of Geophysics, U. of Chicago).

Hess, S. L., 1959: Introduction to Theoretical Meteorology. Holt and Co., New York, p. 49.

Heymsfield, G. M., 1976: Statistical objective analysis of dual-doppler radar data from a tornadic storm. J. Appl. Meteor. l5, 59-68.

Hildebrand, P., 1977: Attenuation of 5-cm radar in rain (submitted to J. Appl. Meteor.)

Hitschfeld, W., and J. Bordon, 1954: Errors inherent in the radar measurement of rainfall at attenuating wavelengths, J. Meteor., 11, 58-67.

Hohn, R. E., 1960: Elementary Matrix Algebra, The Macmillan Company, New York, 305 pp.

Holloway, L. J., 1958: Smoothing and Filtering of time series and space fields. Advances in Geophysics, Vol. 4, Academic Press, New York, 351-389.

Huff, F. A., 1970: Sampling Errors in Measurement of Mean Precipitation, J. Appl. Meteor., 9, 35-44.

_____, F. A., 1971: Evaluation of precipitation records in weather modification experiments, Advances in Geophysics, Vol. 15, H. E. Landsberg, Ed., Academic Press, 59-135.

_____, F. A. and S. A. Changnort, Jr., 1972: Evaluation of potential effects of weather modification on agriculture in Illinois. J. Appl. Meteor., 11, 376-384.

Huff, F. A., 1973a: Evaluation of Potential Benefits} of Weather Modification on Water Supply. Technical Report No. 1, Contract D-7197, Illinois State Water Survey, Urbana, 59 pp.

_____, F. A., 1973b: Potential of Precipitation Modification in Moderate to Severe Droughts. Technical Report No. 2, Contract D-7197, Illinois State Water Survey, Urbana, 26 pp.

Jefferson , G. J., 1963: A modified instability index. Meteor. Mag., 92, 92-96.

Jones, D. M. A., 1956: Rainfall dropsize distribution and radar reflectivity. Illinois State Water Survey, Meteor. Lab. Res. Rept. No. 6., (N.T.I.S. # AD101799.)

Joss, J., R. Cavalli, and R. K. Crane, 1974: Good agreement between theory and experiment for attenuation data, J. Rech. Atmos., 8, 299-318.

Kim, J., 1975: Factor Analysis, Statistical Package for the Social Sciences by N. N. Nie, C. H. Hull, J. G. Jenkins, K. Steninbrenner, and D. H. Bent, Second Editor, McGraw-Hill Book Co., New York, 469-515.

Knight, C. A., N. C. Knight, J. E. Dye, and V. Toutenhoofd, 1974: The mechanism (etc.) I, Observations of the precipitation itself, J. Atmos. Sci., 31, 2142-47.

Knight, N. C, 1976: personal communication.

Kreitzberg, C, and D. Perkey, 1976: Release of potential instability: Part 1. A sequential plume model within a hydrostatic primitive equation model. J. Atmos. Sci., 33, 456-475.

Kyle, T. G., 1976: Reply. J. Appl. Meteor., 15, 191-192.

Larson, L. W., and E. L. Peck, 1974: Accuracy of precipitation measurements for hydrologic modeling. Water Resources Res., 10, 857-863.

Leichter, I., 1974: Moisture Flux and Precipitation Studies of Convective Storms in Western South Dakota. Rept. 74-11, Inst. Atmos. Sci., S. Dakota School of Mines and Tech., Rapid City, 63 pp.

Long, M. J., 1963: Serial soundings near squall lines. Preprints, 3rd Conf. Severe Local Storms, Urbana, Amer. Meteor. Soc, Boston, 1-5.

Maddox, R. A., 1973: A severe thunderstorm surface potential index (SPOT) Preprints, 8th Conf. Severe Local Storms, Denver, Amer. Meteor. Soc.

Madigan, E. F., 1959: An Objective Technique for Forecasting Summertine Air Mass Thunderstorms at Fort Riley, Kansas. Detahcment 15, 25th Wea. Squad. (AWS-MATS) USAF, Fort Riley, Kansas, 13 pp.

Marshall, J. S., and W. McK. Palmer, 1948: The distribution of raindrops with size- J. Meteor., 5, 165-166.

Matthews, D. A., and J. Henz, 1975: Verification of numerical model simulation of cumulus-environmental interaction in the High Plains. J. Pure and Appl. Geophys., 113, 803-823.

Merritt, L. P., K. E. Wilk, and M. L. Weible, 1974: Severe rainstorm at Enid, Oklahoma - October 10, 1973, NOAA Tech. Memo. ERL NSSL-73, 50 pp.

Mielke, P. W., 1972: Asymptotic behaviour of two-sample tests based on powers of ranks for detecting scale and location alternatives. J. Amer. Statist. Assoc., 67, 850-854.

Miller, R. C, 1967: Notes on Analysis and Severe Storm Forecasting Procedures of the Military Weather Warning Center. Tech. Rept. 200, AWS-USAF, 89 pp.

_____, R. C, A. Bidner, and R. A. Maddox, 1971: The use of computer productes in severe weather forecasting (the SWEAT Index). Preprints 7th Conf. Severe Local Storms, Kansas City, Amer. Meteor. Soc, Boston, 1-6.

Miller, J. R., A. S. Dennis, E. I. Boyd, P. L. Smith, Jr., and D. E. Cain, 1974: The North Dakota Pilot Project Annual Report for 1973. Rept. 74-5, Inst. Atmos. Sci., S. Dakota School of Mines and Tech., 46 pp.

Morgan, G. M., Jr., D. G. Brunkow, and R. C. Beebe, 1975: Climatology of surface fronts. ISWS-75-CIR 122, Urbana, 46 pp.

Moses, H., and M. A. Bogner, 1967: Fifteen year climatological summary, AEC Resaerch and Development Report, Argonne National Laboratory, 226-246.

Mueller, E. Q., and D. M. A. Jones, 1960: Dropsize distributions in Florida. Proc. 8th Wea. Radar Conf., AMS, Boston, 299-305.

Neyman, J., and E. L. Scott, 1967: Note on techniques of evaluation of single rain simulation experiments. Proceedings of the Fifth Berkeley Symposium on Mathematical Statistics and Probability, 371-384.

Neyman, J., and E. Scott, 1967: Planning an experiment with cloud seeding. Proc. 5th Berkeley Symp. on Math., Stat., and Prob., 5, Wea. Mod. Exper., Berkeley, U of Calif. Press, 327-350.

Olsen, A. R., 1974: Development and comparison of Bayesian and classical statistical methods as applied to randomized weather modification experiment, 4th Conf. on Wea. Mod., Fort Lauderdale, FL, AMS.

Politte, F. E., M. D. Hale, and D. A. Matthews, 1977: The Bureau of Reclamation's Enviornmental Data Network, Preprints, 6th Conf. Planned and Inadv. Wea. Mod. 10-13 Oct. 1977, Champaign-Urbana, IL Amer. Meteor. Soc, 362-363.

Rackliff, P. G., 1962: Application of an instability index to regional forecasting. Meteor. Mag., 91, 113-120.

Rasmusson, E. M., 1971: Diurnal variation of summertime thunderstorm activity over the United States. USAFETAC TN 71-4, Bldg. 159, Navy Yard Annex, Washington, DC, 12 pp.

Ray, P. S., 1976: Vorticity and divergence fields within tornadic storms from dual-doppler observations. J. Appl. Meteor., 15, 879-890.

Reap, R. M., 1975: Thunderstorm and Severe Weather Probabilities Based on Model Output Statistics, No. 3. NOAA-NWS Tech. Proc. Bull. No. 138, 4 pp.

_____, 1976: Thunderstorm and Severe Weather Probabilities Based on Model Output Statistics, No. 4. NOAA-NWS Tech. Proc. Bull. No. 138, 4 pp.

_____,. M. A. Alaka, 1969: An objective quasi-Lagrangian index for predicting convective weather outbreaks. Preprints, 6th Conf. Severe Local Storms, Chicago, Amer. Meteor. Soc, Boston, 119-124.

_____, D. S. Foster, 1975: New operational thunderstorm and severe storm probability forecasts based on model output statistics. Preprints, 9th Conf. Severe Local Storms, Norman, Amer. Meteor, Soc, Boston, 58-63.

Renne, D. S., and P. C. Sinclair, 1969: Stability and synoptic features of High Plains hailstorm formation. Preprints, 6th Conf. Severe Local Storms, Chicago, Amer. Meteor. Soc, Boston, 125-130.

Reynolds, S. E., and R. R. Braham, 1952: Significance of the initial radar echo, Bulletin, American Meteor. Soc, 33, 123.

Saucier, W. J., 1955: Principles of Meteorological Analysis. The Univ. of Chicago Press. 438 pp.

Schaefer, J. T., 1973: On the computation of the surface divergence field. J. Appl. Meteor., 12, 546-547.

_____, 1975: Non-linear bi-constituent diffusion: A possible trigger of convection. J. Atmos. Sci., 32, 2278-2284.

Schickedanz, P. T., and G. F. Krause, 1970: A test for the scale parameters of two gamma distributions using the generalized likelihood ratio, J. Appl. Meteor., 9, 13-16.

Schickedanz, P. T., and S. A. Changnon, 1970: A Study of Crop-Hail Insurance Records for Northeastern Colorado with respect to the design of the National Hail Experiment. Appendix C, 88 pp.

_____, S. A. Changnon, 1970: A Study of Crop-Hail Insurance Records for Northeastern Colorado with Respect to the Design of the Nat'l Hail Experiment. Final Rept. to NCAR, ISWS, 86 pp.

_____, 1976: The effect of irrigation on precipitation in the Great Plains. Final Rept. NSF(RANN) GI-43871, 105 pp.

_____, and R. Sun, 1977: Statistical techniques for the incorporation of covariates into the design and evaluation of HIPLEX, Preprints, 6th Conf. on Inadv. & Plnd. Wea. Mod., Urbana, AMS.

Schleusener, R., and A. Auer, Jr., 1964: Hailstorms in the High Plains. Final Rept. NSF G-23706, Colo. State Univ. CER64RAS36, 100 pp.

Sekhon, R. S., and R. C. Srivastava, 1971: Doppler radar observation of dropsize distribution in a thunderstorm, J. Atmos. Sci., 28, 983-994.

Showalter, A. K., 1953: A stability index for thunderstorm forecasting. Bull. Amer. Meteor. Soc, 34, 250-252.

Simpson, J., W. L. Woodley, A. Olsen, and J. C. Eden, 1973: Bayesian statistics applied to dynamic modification experiments on Florida cumulus clouds, J. Atmos. Sci. , 30, 1178-1190.

_____, W. L. Woodley, 1974: Florida Area Cumulus Experiments 1970-1973 Rainfall Results, 4th Conf. on Wea. Mod. Fort Lauderdale, FL, AMS

_____, V. Wiggert, 1971: 1968 Florida cumulus seeding Experiment: Numerical model results. Mon. Wea. Rev., 99, 87-118.

Sims, A. L., E. A. Mueller, G. E. Stout, and T. E. Larson, 1964: Investigation of the quantitative determination of point and areal precipitation by radar echo measurements. Ninth Tech. Report, U. S. Army Electronics Research and Development Lab., Ft. Monmouth, N. J., Contract DA-36-039 SC-87280; DA task #3A99-07-001-01 (available from the author).

Sly, W. K., 1966: A convective index as an indicator of cumulonimbus development. J. Appl. Meteor., 5, 839-846.

Smith, P. L., 1976: Comments on "The measurement of water content by an evaporator." J. Appl. Meteor., 15, 189-191.

Smith, T. B., D. M. Takenchi, and C. W. Chien, 1974: San Angelo Cumulus Project, Final Report. Rept. MRI 74-FR 1244, Meteorology Res. Inc., Altadena, Calif., 100 pp.

Spar, J., 1957: Project SCUD, Meteor. Mono., 2, 5-23.

Stephens, J. J., 1967: Filtering responses of selected distance-dependent weight functions. Mon. Wea. Rev., 95, 45-46.

_____, J. M. Stitt, 1970: Optimum influence radii for interpolation with the method of successive corrections. Mon. Wea. Rev., 98, 680-687.

_____, A. L. Polan, 1971: Spectral modification by objective analysis. Mon. Wea. Rev., 99, 374-378.

Sulakvelidze, G. K., N. Sh. Bibilashvili, and V. F. Lapcheva, 1967: Formation of precipitation and modification of hail processes. Israel Program for Scientific Translations, Jerusalem, 208 pp.

Waldteufel, P., 1973: Atténuation des ondes hypérfrequences par la pluie: une mise an point. Ann. Té1écommunic., 28, 255-272.

Wallace, J. M., 1975: Diurnal variations in precipitation and thunderstorm frequency over the conterminous United States. Mon. Wea. Rev., 103, 406-419.

Weible, M. L., and D. Sirmans, 1976: Simulation of attenuation by rainfall at a wavelength of 5 cm. Preprints, 17th Conf. on Radar Meteor., AMS, Boston, 75-78.

Wexler, R., and D. Atlas, 1963: Radar reflectivity and attenuation in rain J. Appl. Meteor., 2, 276-280.

Whitehead, D. R., 1971: A Comparison of Objective Convective Activity Indices. Univ. Oklahoma, OURI-1828-71-1, 66 pp.

Whittaker, T. M., 1977: Automated streamline analysis. Mon. Wea. Rev. 105., 786-788.

Williams, P., Jr., 1968: Small Scale Analysis and Prediction. Tech. Memo WBTM WR-29, 94 pp.

Wilson, J. W., 1975: Radar-gage precipitation measurements during the IFYGL. Rep. No. 4177-540, The Center for the Environment and Man, Inc., Hartford, Conn., 131 pp.

_____, 1977: Effect of Lake Ontario on precipitation, J. Appl. Meteor., 105, 207-214.

Woodley, W. L., A. R. Olsen, A. Herndon, and V. Wiggert, 1975: Comparison of Gage and Radar Methods of Convective Rain Measurement, J. Appl. Meteor., 14, 909-928.

Woodley, W. L., J. Simpson, R. Biondini, and J. Berkely, 1977: Rainfall results, 1970-1975: Florida Area Cumulus Experiment. Science, 195, 735-742.

Workman, E. J., and S. E. Reynolds, 1949: Electrical activity as related to thunderstorm cell growth, Bull. Airier. Meteor. Soc., 3(), 142-144.

LIST OF PROJECT REPORTS AND PUBLICATIONS

1. "Precipitation Enhancement Program for Illinois." By S. A. Changnon. Journal of the Irrigation and Drainage Division of ASCE, Sept. 1973.

2. Can Weather Modification Usefully Augment the Water Resources of the Humid Midwestern United States? By S. A. Changnon. Proceedings of Symposium on Water Resources Planning, Mexico City, Dec. 1972.

3. "Feasibility Studies of Precipitation Enhancement in Illinois." By S. A. Changnon. Proceedings Southern Plains Region Cloudtap Conference, Dallas, October 1972, 101-109.

4. "The Determination of Soluble Cadmium, Lead, Silver and Indium in Rainwater and Streamwater with the Use of Flameless Atomic Absorption." By A. Rattonetti. Analytical Chemistry, 46, 739-742, 1974.

5. Evaluation of Potential Benefits of Weather Modification on Water Supply. By F. A. Huff. Technical Report No. 1 on Illinois PEP, Illinois State Water Survey, Urbana, 59 pp.

6. Potential of Precipitation Modification in Moderate to Severe Droughts. By F. A. Huff-. Technical Report No. 2 on Illinois PEP, Illinois State Water Survey, Urbana, 26 pp.

7. The Relationship of Illinois Weather and Agriculture to the Eastern Cottontail Rabbit. By S. P. Havera. Technical Report No. 4 on Illinois PEP, Illinois State Water Survey, Urbana, 92 pp.

8. Trace Element Chemistry Studies. By D. F. Gatz. Technical Report No. 7 on Illinois PEP, Illinois State Water Survey, Urbana, 9 pp.

9. Legislative Activities Relating to Weather Modification in Illinois. By S. A. Changnon. Technical Report No. 3 on Illinois PEP. Illinois State Water Survey, Urbana, 12 pp.

10. Modeling Studies for Evaluation and Planning of Precipitation Enhancement in Illinois. By H. T. Ochs, III, and B. F. Ceselski. Technical Report No. 6 on Illinois PEP. Illinois State Water Survey, Urbana, 75 pp.

11. Climatic Studies of Extra-Area Effects from Seeding. By P. T. Schickedanz. Technical Report No. 5 on Illinois PEP, Illinois State Water Survey, Urbana, 53 pp.

12. "Numerical Prediction of Organized Convection over the Central United States." By B. F. Ceselski. Preprints 8th Conference on Severe Local Storms, AMS, 315-319.

13. "The New Weather Modification Law for Illinois." By W. C. Ackermann, S. A. Changnon, and R. J. Davis. Bulletin Amer. Meteor. Soc, 55, 745-750.

14. "A Review of Methods to Evaluate Precipitation Modification in North America." By Stanley A. Changnon. Proceedings International Conference on Weather Modification, WMO, Geneva, 397-422, 1973.

15. "Cumulus Convection in Weak and Strong Tropical Disturbances." By B. F. Ceselski. J. Atmos. Sciences, 31, 1241-1255, 1974.

16. "Potential of Precipitation Modification in Moderate to Severe Drought." By F. A. Huff and R. G. Semonin. Preprints 4th Conference on Weather Modification, AMS, Boston, 490-495, 1974.

17. A High Plains Climatography. By S. A. Changnon, F. Huff and P. Schickedanz. Special Report Contract D-7197. Illinois State Water Survey, Urbana, 121 pp.

18. Cloud Seeding - A Decision for Illinois. By s. A. Changnon, J. W. Brother, L. J. Ivens, R. G. Semonin. Illinois State Water Survey, Urbana, 12 pp. 1972.

19. "The Partition of Liquid Water Near the Freezing Level." By B. Ackerman, Preprints Conference on Cloud Physics, AMS, Boston, 300-304, 1974.

20. "Climatic Studies of Extra-Area Effects in Midwest Rainfall." By P. T. Schickedanz. Preprints 4th Conference on Weather Modification, AMS, Boston, 504-509, 1974.

21. "Background Silver Concentrations in Illinois Precipitation and River Water." By D. F. Gatz. Journal of Applied Meteorology, 14, 217-221, 1975.

22. Design of the High Plains Experiment with Specific Focus on Phase 2, Single Cloud Experimentation. By B. Ackerman, G. Achtemeier, H. Appleman, S. A. Changnon, F. Huff, G. Morgan, P. Schickedanz, and R. Semonin. Report on Contract D-7197, Illinois State Water Survey, Urbana, 231 pp.

23. "Present and Future of Weather Modification: Regional Issues." By S. A. Changnon. Journal of Weather Modification, 7, 154-176, 1975.

24. "Priorities for Research in Inadvertent and Intentional Weather Modification." By S. A. Changnon. Proc. Conf. on Wea. Mod, in the United States: Potential and Problems for Interstate Action, S. Dakota, 152-160, 1974.

25. "Potential of Precipitation Modification in Moderate to Severe Droughts." By F. A. Huff and R. G. Semonin; J. Appl. Meteor., 14, 974-979, 1975.

HIPLEX related publications

"A Short-Term Thunderstorm Forecast System Utilizing the 4-Dimensional Evolution of Mesoscale Stability." By G. L. Achtemeier and G. M. Morgan, Jr. Preprints 6th Conference on Weather Forecasting and Analysis, AMS, 3 238-241.

"Meteorological and Physical Selection of Candidate Covariates for HIPLEX." By G. L. Achtemeier and R. Y. Sun. Preprints, 6th Conference on Inadvertent and Planned Weather Modification, AMS, 234-237.

APPENDICES

LIST OF FIGURES FOR APPENDICES

APPENDICES: MISCELLANEOUS ANALYSES IN SUPPORT OF THE HIPLEX DESIGN EFFORT

This section summarizes the analysis schemes that were developed in support of the HIPLEX design effort. These techniques include the equations for the Lambert conformal conic map projection used in the surface analyses. The BOBARY objective interpolation scheme was developed for the economical analysis of the approximately 36000 fields of surface data.

An objective streamline analysis technique that displays streamlines constructed from gridded fields of surface and upper air winds was initially developed and placed into an operational mode at the National Severe Storms Laboratory. This method was subsequently revised and reprogrammed; the modifications realized an order of magnitude savings in computer resources.

A diagnostic-prognostic (4-D) scheme that modifies spatially and temporally extrapolated soundings according to the surface layer temperature and moisture and the vertical displacements implied from the surface wind field has been developed. The scheme can yield SPECs directly from the modified soundings or from a one dimensional cloud model interfaced with it. It can also be easily adapted for an operational setting. The 4-D scheme was upgraded using Illinois data. It did not reach the stage of development to be useful for the SPEC analysis.

1. Appendix A: Map Projection for the Kansas Site Surface Field Analyses

For purposes of weather analysis and viewing data, it is often desirable to depict the meteorological parameters observed in the Earth's atmosphere on charts. This requires the representation of the Earth's surface on a plane surface. Map projections which preserve distance are termed isometric, and those which preserve the angle between two intersecting curves are conformal. We use the Lambert conformal conic projection true at 30 and 60 degrees latitude.

Map projections enter into calculations that involve distance related variables such as the wind velocity. Since the conformal projection does not conserve distance, there will exist length distortions when transformations from the earth to the map are carried out. Divergence calculations which are proportioned to elemental areas, are sensitive to these distortions. If the working grid covers a mesoscale area the distortions are relatively small and may be neglected in the velocity related calculations. If the working grid covers a sub-synoptic scale area, the distortions can become important. The map distortions should always be included when calculations are carried out using larger grids.

Consider the Lambert conformal conic map projection where the points on the spherical earth surface are projected to a cone. The projection,

shown schematically in figure 11, is taken from the center of the Earth. The cone surface intersects the surface of the globe at two latitudes of intersection which are called standard latitudes.

The quantities listed below are used in the derivation of the map projection.

Ψ^* The colatitude at which a line from the center of the Earth intersects the surface of the cone at a right angle.

Ψ_o The standard colatitude.

Ψ The colatitude of an arbitrary point to be projected from the earth to the map.

r The distance measured from the cone origin to the projected point on the map.

a The radius of the earth.

Other quantities used in the derivation shown in fig 1 will be explained within the following discussion.

The distance O'A in fig 1 is related to Ψ^* by

$$\tan \Psi^* = \frac{O'A}{d} \quad . \tag{1}$$

Thus, $$O'A = d \tan \Psi^* . \tag{2}$$

Since d is unknown directly, it may be found as a function of colatitude and Earth radius. The angle between OB and OA is $\Psi^* - \Psi_o$
From fig 1,

$$d = a \cos (\Psi^* - \Psi_o). \tag{3}$$

Thus,

$$O'A = a \tan \Psi^* \cos (\Psi^* - \Psi_o). \tag{4}$$

Returning to the map image, the distance r can be found by taking the difference between 0'A and X'A. The angle between the lines OX' and OA is $\Psi^* - \Psi$. Thus,

$$X'A = d \tan (\Psi^* - \Psi), \tag{5}$$

and r becomes

$$r = d[\tan \Psi^* - \tan (\Psi^* - \Psi)]. \tag{6}$$

Utilizing trigonometric identities (6) becomes

$$r = d[\tan\Psi^* - \frac{\tan \Psi^* - \tan \Psi}{1 + \tan \Psi^* \tan\Psi}]. \tag{7}$$

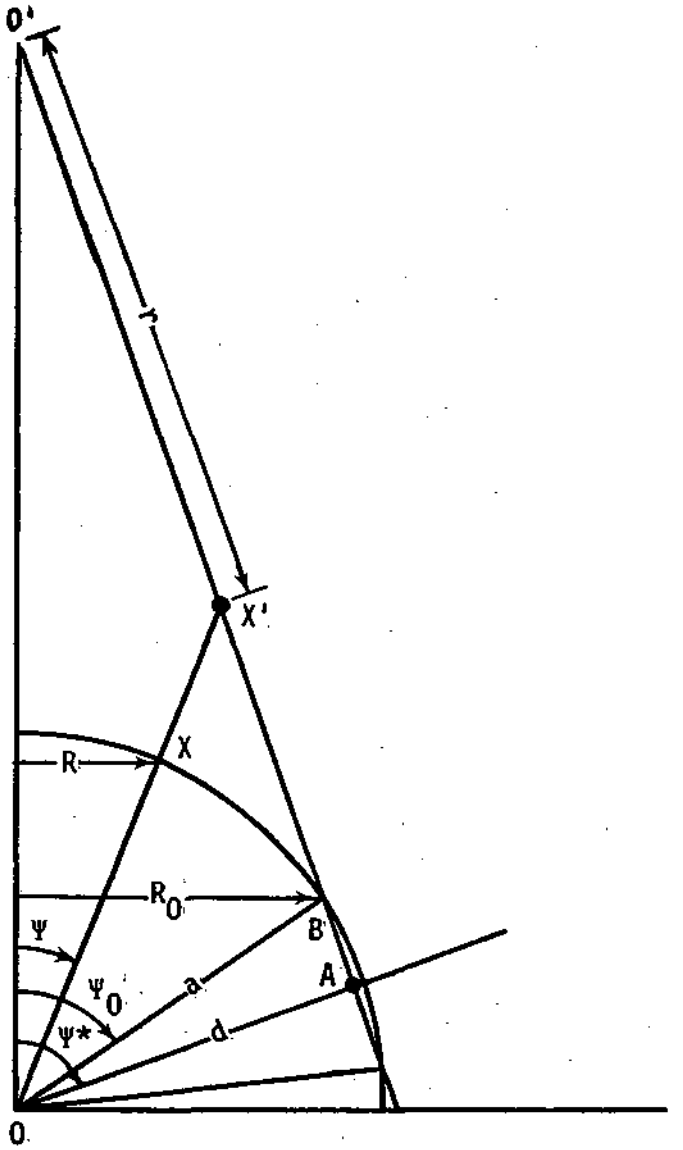

Figure 1. A schematic representation of the projection of points from the surface of a sphere to the surface of a cone.

Further conversions give

$$r = d \frac{\sin\Psi}{\cos\Psi^*} \quad \frac{1}{\cos\ (\Psi^* - \Psi)}. \tag{8}$$

Then substitution for d from (3) gives r as a function of Earth radius and known colatitudes;

$$r = a \frac{\sin\Psi}{\cos\Psi^*} \quad \frac{\cos\ (\Psi^* - \Psi_o)}{\cos\ (\Psi^* - \Psi)} \ . \tag{9}$$

At the standard colatitudes, $\Psi=\Psi_o$, $R_o = a \sin\Psi_o$, and

$$r = R_o/\cos\Psi^*. \tag{10}$$

Saucier (1955) defines $n = \cos\psi^*$ a cone constant that is determined by the choice of standard colatitudes. Further, the map distortion m is defined by

$$m = \frac{\cos\ (\Psi^* - \Psi_o)}{\cos\ (\Psi^* - \Psi)}. \tag{11}$$

Thus the Lambert conformal conic map projection is

$$r = \frac{am \sin\Psi}{n}. \tag{12}$$

Define an orthogonal coordinate system with the origin at the north pole and the abscissa along some reference longitude X where X is positive eastward (over the U. S. X is positive westward).

The distance around a latitude circle on Earth and the equivalent distance on the map are, respectively,

$$\ell_E = 2\pi\ a \sin\ \Psi,$$

$$\ell_M = 2\pi\ n\ r. \tag{13}$$

The angular distance on Earth is $\lambda=2\pi$. The equivalent angular distance on the map is $\lambda m = 2\pi n$. Thus, $\lambda m = n\lambda$.

The projected positions x,y on the map image coordinate system are

$$X = \frac{am}{n} \sin\ \Psi \cos\ n\lambda,$$
$$Y = \frac{am}{n} \sin\ \Psi \sin\ n\lambda. \tag{14}$$

Our analysis procedure requires that the working grid be defined on the map. Therefore, the colatitude and longitude of each grid point must be known so the map distortions which make the wind velocities compatible with the map frame can be calculated. In the following derivation the grid point X,Y is treated with respect to the polar origin, not the local grid origin. To find the grid point colatitude and longitude, define

$$C = \frac{a}{n} \cos (\Psi^* - \Psi_0). \tag{15}$$

Then it follows that

$$X = \frac{C \sin \Psi \cos n\lambda}{\cos (\Psi^* - \Psi)},$$

$$Y = \frac{C \sin \Psi \sin n\lambda.}{\cos (\Psi^* - \Psi)} \tag{16}$$

First find the longitude A by dividing (Y) by (X) to get

$$Y/X = \frac{\sin n\lambda}{\cos n\lambda} \tag{17}$$

Then

$$\lambda = \frac{1}{n} \text{Arctan } Y/X \tag{18}$$

The colatitude ψ is much harder to find. To eliminate X square (16) and add to get

$$X^2 + Y^2 = C^2 (\cos^2 n\lambda + \sin^2 n\lambda) \frac{\sin^2 \Psi}{\cos^2 (\Psi^* - \Psi)}. \tag{19}$$

If $R = (X^2 + Y^2)/C^2$, (19) becomes

$$R = \frac{\sin^2 \Psi}{\cos^2 (\Psi^* - \Psi)}. \tag{20}$$

To solve (20) for ψ, it is necessary to remove the angle difference in the denominator. From trigonometric identities, we note that

$$\cos^2 (\Psi^* - \Psi) = 1/2 [\cos 2 (\Psi^* - \Psi) + 1]. \tag{21}$$

We will always use the standard Lambert conformal conic projection which has standard latitudes true at 30° and 60° north. Then,

$$\Psi^* = 1/2 (\Psi_{o_1} + \Psi_{o_2}) = 45^o, \tag{22}$$

and (21) becomes

$$\cos^2 (\Psi^* - \Psi) = 1/2 \ (\sin 2\Psi + 1). \tag{23}$$

Thus the expression for R can be simplified to

$$R = \frac{2 \sin^2 \Psi}{\sin 2\Psi + 1}. \tag{24}$$

Further, from trigonometry,

$$\sin^2 \Psi = 1/2 \ (1 - \cos^2 \Psi), \tag{25}$$

and (24) becomes

$$R = \frac{(1-\cos 2\Psi)}{(1+ \sin 2\Psi)} = \frac{1-\cos\alpha}{1+\sin\alpha}, \tag{26}$$

where a = 24ψ. Expanding (26) and squaring leads to

$$\sin^2\alpha(R^2 + 1) + \sin\alpha \ [2(R^2 - R)] + (R^2 - 2R) = 0, \tag{27}$$

a quadratic expression in sina. Its physically meaningful positive root solution is of the form

$$\sin\alpha = \frac{-(R^2 - R) + [(R^2 - R)^2 - (R^2 + 1)(R^2 - 2R)]^{1/2}}{R^2 + 1}, \tag{28}$$

$$= S.$$

Thus the colatitude of the grid point is given by

$$\Psi = 1/2 \ \text{Arcsin}(S). \tag{29}$$

We found that the solution of (29) is symmetric about ψ*, hence the map distortion field is also symmetric about ψ*. This comes about through the cosine of equal positive and negative angles. The inverse function of Z also includes the inverse of the cosine and will give only the positive angle solution. Thus if ψ*-ψ < o, (29) will give the symmetric counterpart for ψ.

2. Appendix B: The Objective Analysis Scheme for the Surface Analysis

Surface observations of pressure, temperature, dew point temperature, wind speed and wind direction were interpolated to an 8 X 6 regular mesh to allow the computation of the many derivative quantities that composed the surface PROGSPECs. The necessary interpolation of the five basic

variables eight times a day for the three summer months for the historical period of 10 years (1965-74) requires in excess of 3600 objectively analyzed fields. Part of our effort to develop the surface PROGSPECs was directed to finding a fast and economical objective interpolation method to produce these initial fields.

This objective map analysis technique is a modification of a successive corrections scheme developed by Barnes (1964) and further elaborated by Barnes (1973). It is similar in many respects to the Cressman (1959) method by which observational discrepancies from a guess field at station locations are successively interpolated to find estimates at points on a regular mesh. The interpolation is accomplished by a linear combination of the point discrepancies within some influence radius about the mesh point. The weight accorded to each observation varies inversely with its distance from the mesh point according to a prescribed function and is normalized by its sum with the weights of all other stations within the influence radius. The method is applied with two scans with the influence radius the same for each scan, however the influence radius is allowed to vary spatially according to the average distance of the stations within the influence radius from the mesh point.

The Barnes (1974) method allows the selection of the weight factor to maximize details supportable by the observation density and representativeness. All data are used to determine the grid point value although the outlying stations receive small weights. This procedure takes advantage of the response characteristics of the normal probability curve (Holloway, 1958) and, though computationally time consuming, is thought to avoid undesirable amplification of certain wavelengths found in other methods that use finite influence radii (Stephens, 1967; Stephens and Polan, 1971). However, weights for outlying stations become so small as to be essentially zero. Since there stations do not contribute to the interpolated value at the grid point, it can be argued that their deletion will not substantially alter the response characteristics. The validity of this argument is the subject of the following treatise.

Following Barnes (1973), the response function for the exponential weight function is given by

$$D(\lambda, K, R) = \frac{1}{2K} \int_0^R J_0\left(\frac{2\pi r}{\lambda}\right) \exp^{(-r^2/4K)} \, r\,dr \qquad (1)$$

where J is a zero-order Bessel function and and 4K are, respectively, the wavelength and a shape factor. Integration of (1) over infinite limits gives the response for the normal probability curve. The response of an exponential weight function with finite influence radius can be found by expanding the Bessel function into its infinite series (Abramowitz and Stegun, 1964) and integrating (1) by parts. The variables R, X, and 4K have been nondimensionalized by the average station separation d. The nondimensional variables are

$$\delta = R/d \; ; \gamma = \frac{\lambda}{2d} \quad \beta = \sqrt{\frac{4K}{d}} \, . \qquad (2)$$

In this scheme, γ-1.0 is the Nyquist wave.

The response function for finite influence radii is

$$D(\beta,\gamma,\delta) = \exp^{-\left(\frac{\pi\beta}{2\gamma}\right)^2} - \exp^{-(\delta/\beta)^2} \left\{1 + \sum_{n=1}^{N} \frac{(-1)^n}{n!} \left(\frac{\pi\beta}{2\gamma}\right)^{2n} \left[1 + \sum_{j=1}^{n} \frac{1}{j!} \left(\frac{\delta}{\gamma}\right)^{2j}\right]\right\} \qquad N \to \infty . \qquad (3)$$

The response for the infinite influence radius is given by the first term of (3). Its wavelength dependent modification by the second term is determined by the ratio of the influence radius to the shape factor. The spatial distribution of weights approaches the running mean when the weight curve, broadened by a large shape factor, is truncated by a small influence radius.

Stephens and Stitt (1970),, for the Cressman weight, show that the optimum influence radius was approximately 1.5 times the average station separation for an ensemble of randomly distributed station arrays. The number of stations contained within the influence area defined by the area of the circle with the optimum influence radius is found by dividing the influence area by the area of square cells of length equal to the average station separation. An average of seven stations occur within the specified optimum influence radius.

Figure 2 shows the response curves at normalized wavelengths $1.0 \leq \gamma \leq 10.0$ for selected shape factors β. The curves are given for fixed influence radii of δ=1.5 (7 observations) and δ=2.0 (12 observations) . These curves show the extent to which wavelengths are filtered as a consequence of the choice of the shape factor. As the shape factors increase (the outlying stations are accorded greater relative weights), the percentage of the shorter waves retained, given by the response times 100, is decreased. For most analyses, it is desired to retain most of the variance of the $\gamma>1$ waves. This can be accomplished by using shape factors $\beta \leq 0.8$ for δ=1.5 and $\beta \leq 1.0$ for δ=2.0. However, it is also necessary to filter out the waves shorter than γ=l-0 for these will be aliased into the longer wavelenghts. Both sets of curves show that the shape factors should not be less than β=0.6.

The behavior of the response curves in the range $0 \leq \gamma \leq 1.0$ for δ=1.5 and δ=2.0 is illustrated in figure 3. Amplification lobes do not appear for shape factors less than β=0.9. Small negative lobes appear for β=1.0 for the influence radius of δ=2.0. The dashed lines extrapolate the response curves back to γ=0.0. Other negative lobes may be present but their amplitudes must approach zero as the curves approach the origin.

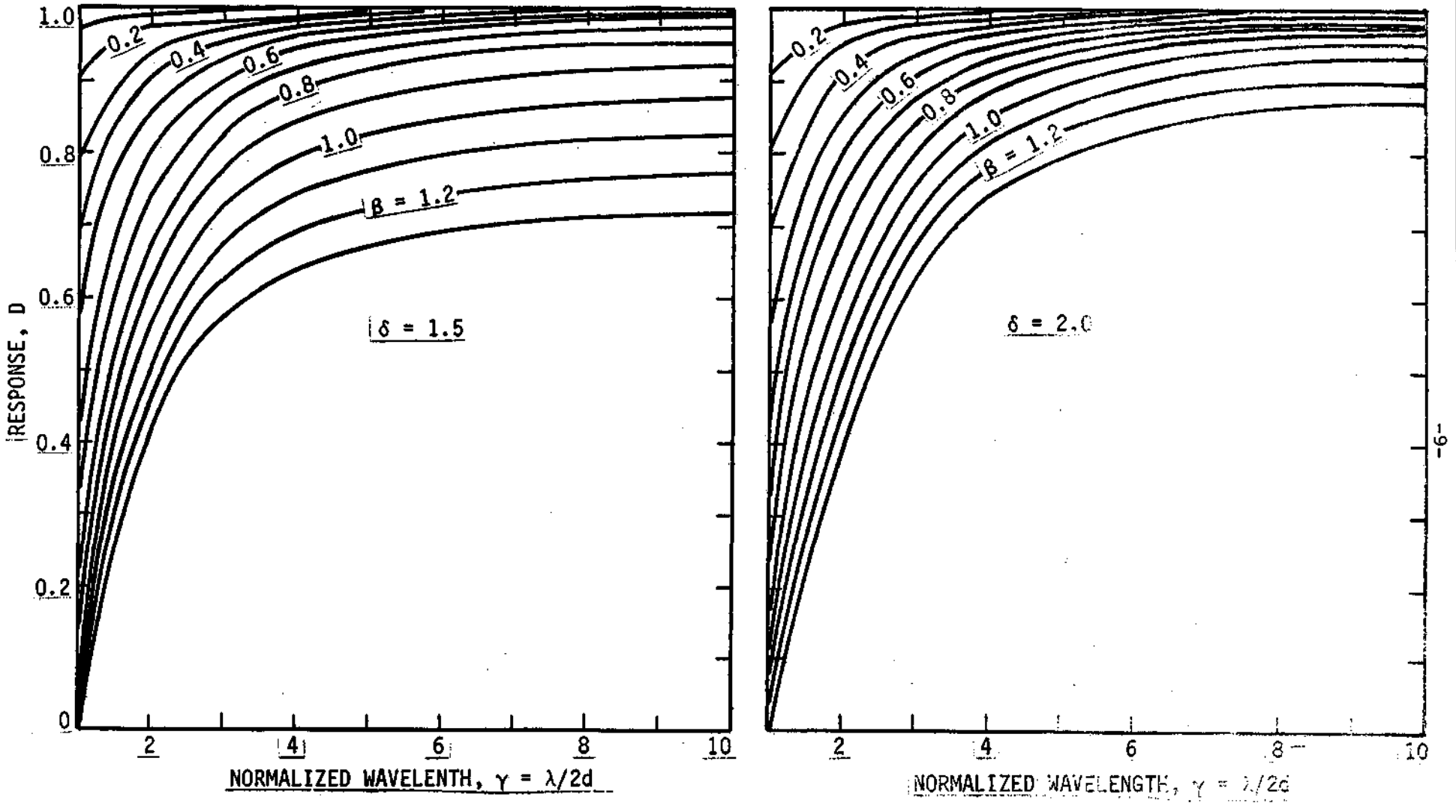

Figure 2. Relationship of the response function to the normalized wavelength γ *for selected shape factors* β *for influence radii of* $\delta = 1.5$ *and* $\delta = 2.0$.

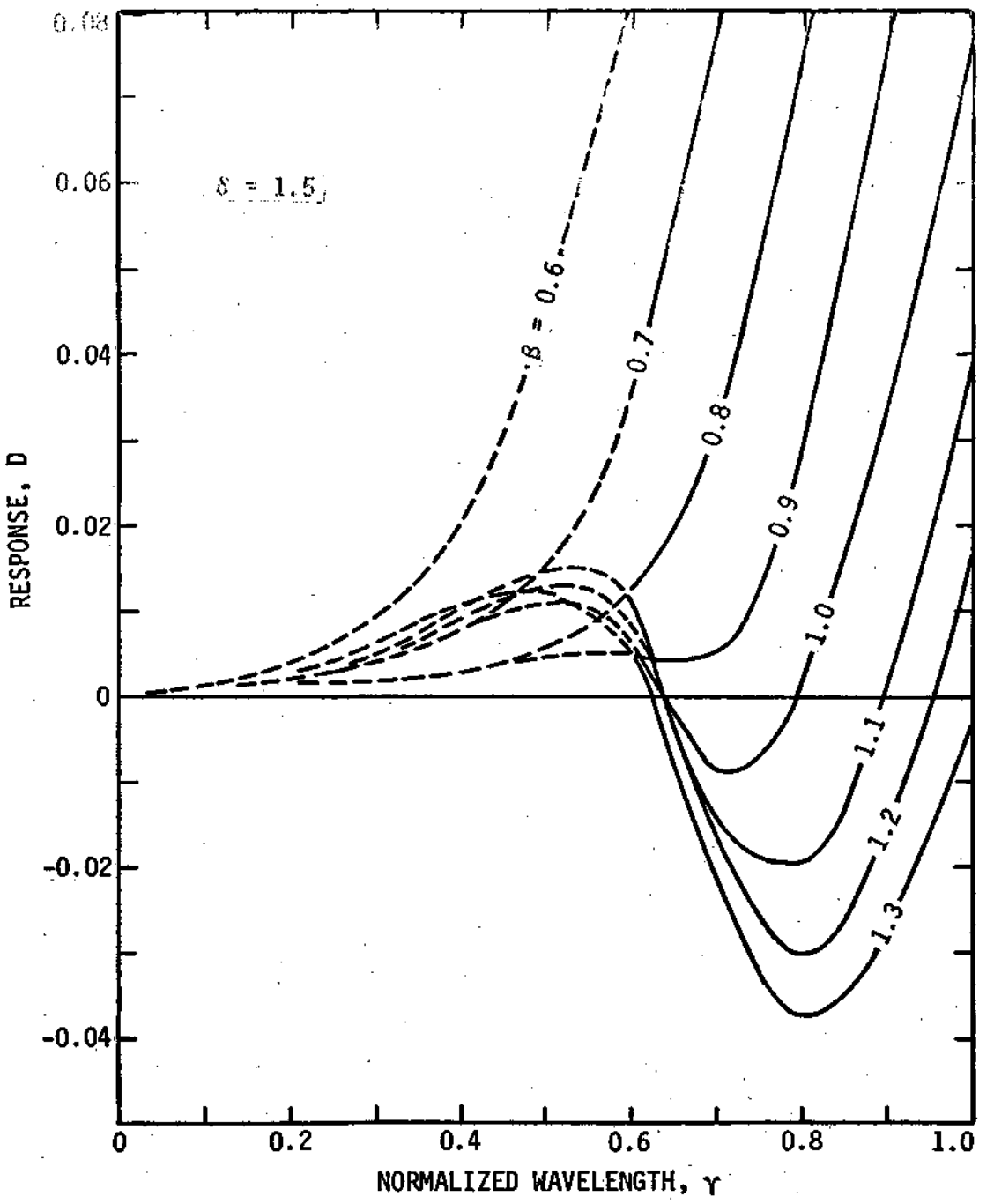

Figure 3. Relationship of response function less than 0.1 to normalized wavelength less than 1.0 for selected shape factors for the influence radius equal to 1.5.

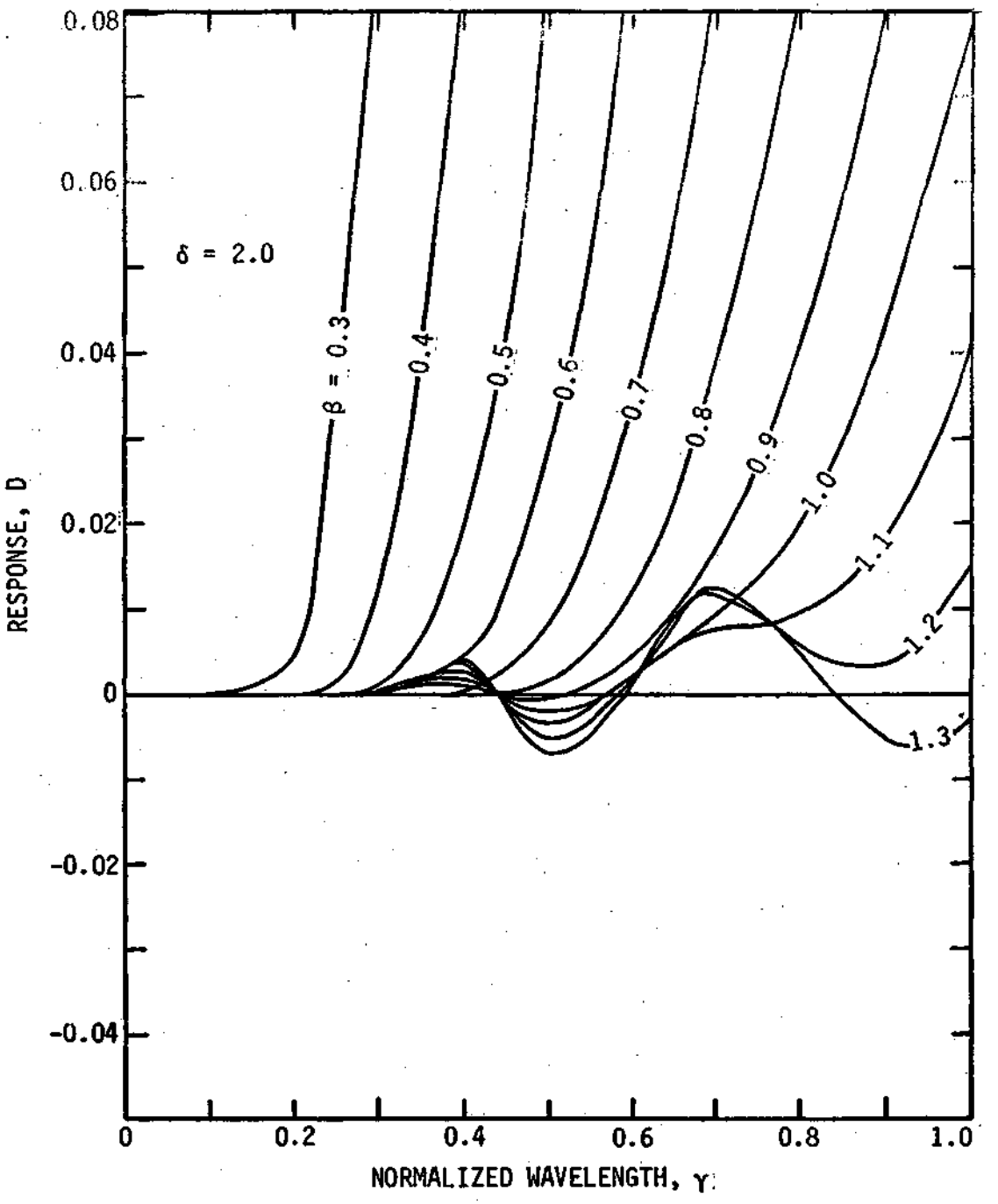

Figure 3. (Continued)

Thus there would appear to be a narrow range of shape factors ($0.6 \leq \beta \leq 0.8$ for $\delta=1.5$ and $0.6 \leq \beta \leq 1.0$ for $\gamma=2.0$) for which the exponential weight function will allow retention of most of the variance of the longer waves but filter out most of the short waves without a substantial change in the response characteristics. Please note that this derivation has been made by assuming a data continuum and the negative responses may be reintroduced with discretes sampling (Stephens and Polan, 1971).

The Barnes method is modified so that observations beyond the influence radius are not included in the interpolation. Substantial computer time is saved because the weights for the stations surrounding a grid point can be computed once and stored for subsequent scans and analyses if the observations remain fixed in space and if there are not many missing observations.

The weight for the ith station is an exponential function of its distance from the grid point expressed as a fraction of normalized influence radius, and the normalized shape factor:

$$W_i = \exp -\left(a_i \, \delta / \beta\right)^2 \tag{4}$$

where

$$\beta = \sqrt{\frac{C}{2.3}} \; \frac{\delta}{N} \sum_{i=1}^{N} a_i \tag{5}$$

The shape parameter C is chosen so that the weights decrease to 0.1C at a distance equal to the average distance of the stations from the grid point. Since the weights are computed with a fixed number of stations, the influence radius automatically increases as the station density decreases. Thus the maximum information content permissible by the local data field can be retained.

Stephens and Stitt (1970) show that the average distance to the ith order station is given by

$$r_i = \left(\frac{i}{\pi}\right)^{1/2} d. \tag{6}$$

Normalizing by the station density gives

$$a_i = \left(\frac{i}{\pi}\right)^{1/2} \frac{1}{\delta} \, . \tag{7}$$

Thus, from (5),

$$\beta = \sqrt{\frac{C}{2.3}} \; \frac{1}{N} \sum_{i=1}^{N} \left(\frac{i}{\pi}\right)^{1/2} . \tag{8}$$

The relationship between 3 and C is illustrated in Figure 4 for N=7 observations (δ=1.5) and N=12 observations (δ=2.0). For δ=1.5, C ranges between 0.7 and 1.25 for the shape factor range 0.6-0.8. For δ=2.0, C ranges between 0.4 and 1.2 for $0.6 \leq \beta \leq 1.0$. weight curves for selected values of C are shown as a function of the normalized fractional distance along the influence radius 6 in fig 5. Truncation at a=1.0 is clearly evident for C>1.0.

The value C shown in Figure 5 is equivalent to the CHNG parameter in the objective analysis computer program. The response characteristics and the number of observations per grid point are preselected for the analysis needs. These choices uniquely determine the shape factor constant C. Examples of the objective analysis are given in Figure 3 (text).

3. Appendix C: An Operational Objective Streamline Analysis for the Environmental Data Network (EDN).

The Bureau of Reclamation's research programs in meteorology require some unique analyses and forecasts that are not available through the National Weather Service's facsimile and teletype circuits. With this requirement in mind, the Bureau has developed an Environmental Data Network (EDN), (Politte, et.al., 1977). The EDN products are available to users many of whom have interests within an operational setting.

Accurate, legible, real-time analyses of meteorological data are essential to the forecast effort for HIPLEX operations. Wind field streamlines at levels both surface and aloft can reveal circulation centers, confluence and difluence zones, and other wind field perturbations that might identify potential precipitation producing weather systems. An automated streamline analysis technique releases valuable time to skilled meteorologists that formerly was consumed in manually producing streamlines (Saucier, 1955). However, the objective method should accurately describe the instantaneous wind field so as not to lead the forecast personnel to errors in pattern interpretations..

The objective streamline analysis (SLX) was developed at the National Severe Storms Laboratory[1] and was placed into operation there in Spring 1973. The SLX was reprogrammed at the ISWS as part of the HIPLEX design effort and was adapted to the EDN in 1976.

Objective streamline analysis schemes described in the literature fall into one of two categories. These are the predictor-only (PO) method in which a line segment is extrapolated forward at an angle tangent to the unit wind vector at the beginning point, and the predictor-corrector (PC) method in which the wind direction at the beginning and at the end of the PO line segment are averaged and the line segment is extrapolated forward at the

---

[1] This phase of the work was done while Dr. Achtemeier was an NRC Post-Doctoral Research Associate at the National Severe Storms Laboratory.

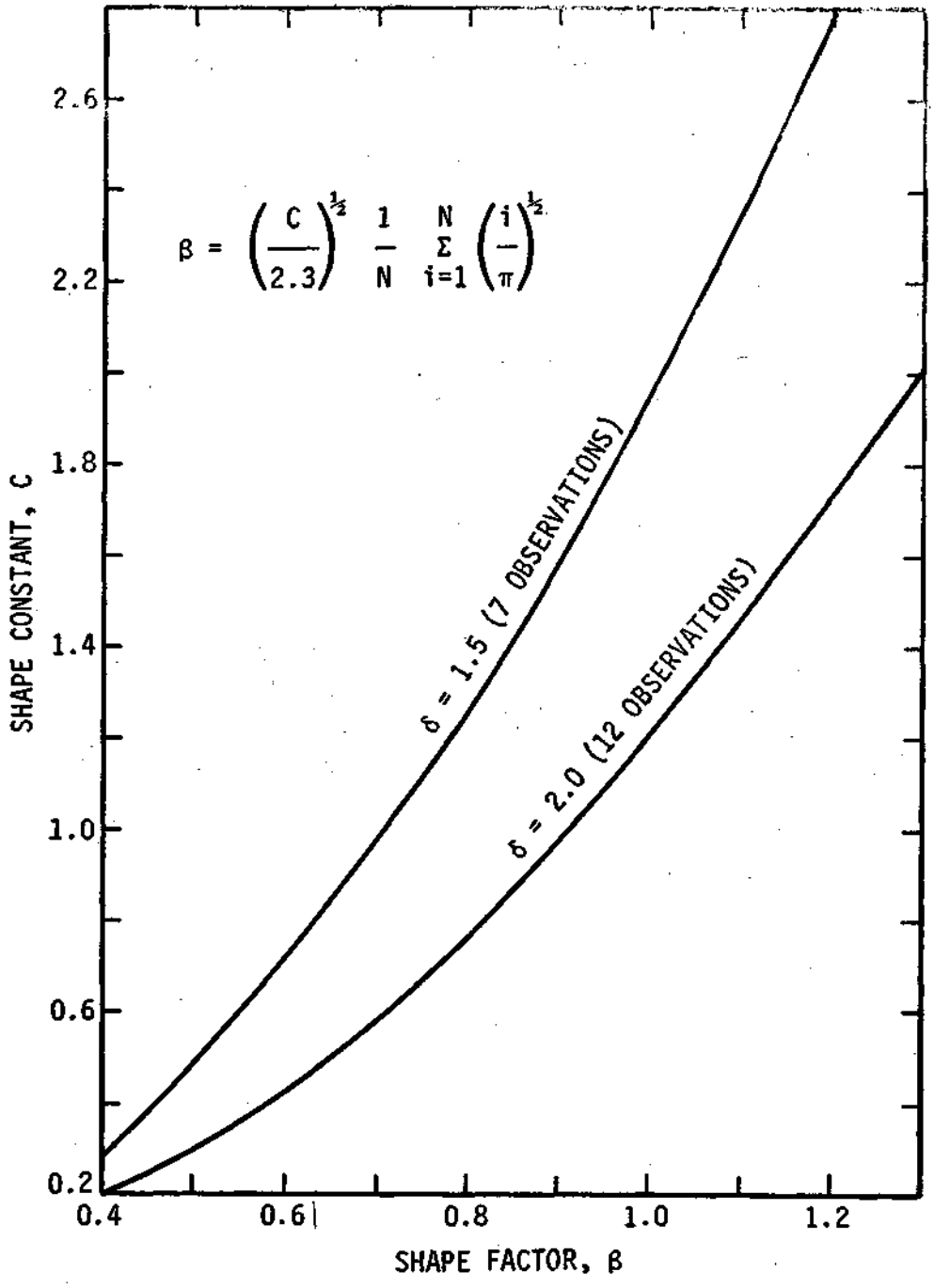

Figure 4. Relationship between the shape factor 3 *and the shape constant C for selected influence radii S.*

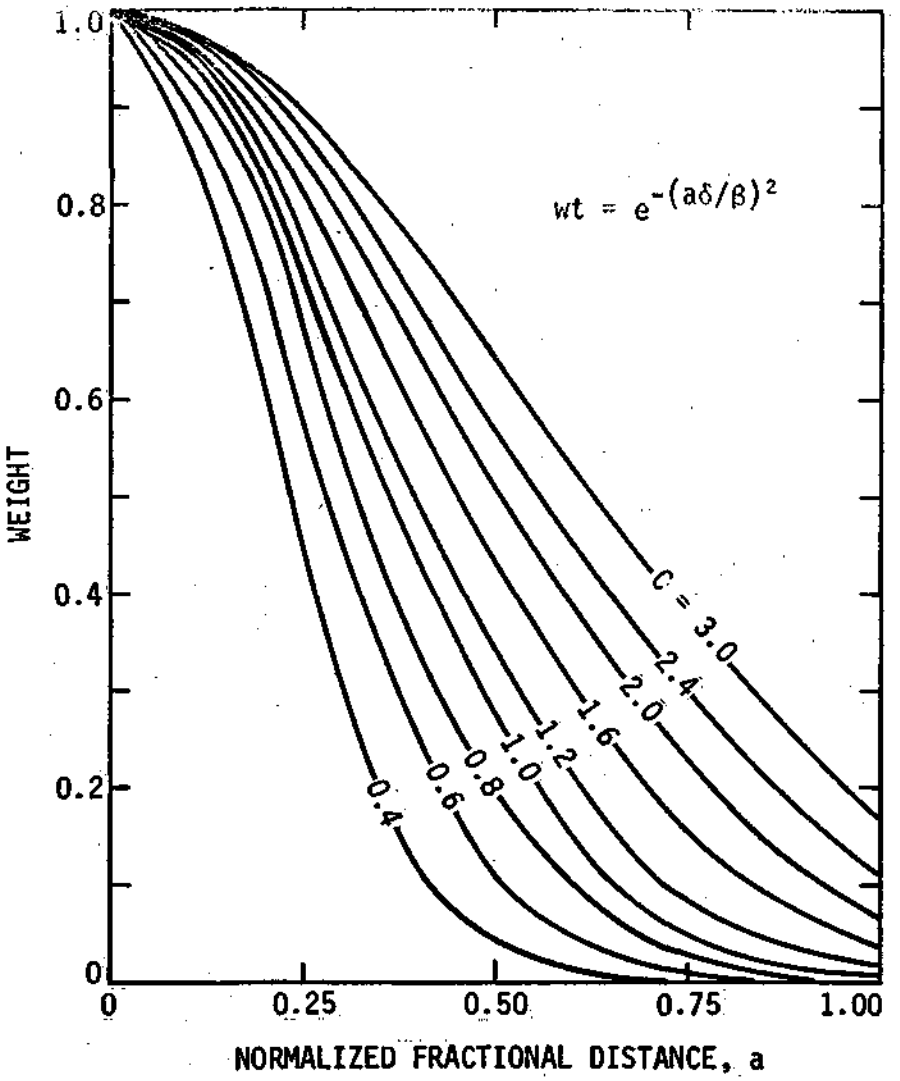

Figure 5. Weight curves for the exponential weight function for selected shape constants C.

average angle. Predictor-only methods are described by Davis (1969), Darrt (1972), and Whittaker (1977). The NCAR streamline model[2] and the SLX method described here are predictor-corrector methods.

The SLX method requires two master arrays containing u and v wind components presented at mesh points of a regular grid. The wind components are interpolated bi-lineraly to the points of a sub-grid mesh and there converted to directions. The number of sub-grid intervals per master grid interval is an integer which can be specified according to the discretion of the analyist. Two sub-grids, one containing the wind directions and the other containing streamline identifier symbols, are required for the analysis. Figure 6 illustrates a 9-element sub-grid within 1-element of the master grid. Wind directions are provided at the sub-grid points. If a streamline passes through the square designated by the dashed lines centered about a sub-grid point, its identifier is recorded on the same grid point in the identifier array. If that point contains the identifier for another streamline, the streamline is terminated. The SLX streamlines can be displayed by either some automated line drawing device or by listing the array of unique identifier symbols on a line printer.

Streamlines can be started at any sub-grid point provided it is not within some specified distance from another streamline. The density of the streamlines is controlled by the analyist.

Once a starting point for a new streamline has been determined, the streamline is drawn in two directions: first forward using the PC method described earlier, then backward by reversing the unit direction vector 180 degrees. The streamline is given by the succession of straight line segments of length determined by entry and exit points through the sub-grid squares. The construction method is illustrated schematically in figure 7. A streamline enters the sub-grid square at point A at an angle αb determined from linear interpolation between the corner angles 6, on the side of entry. A line segment tangent to the entry angle is extrapolated forward. This line intersects the opposite side of the sub-grid square at C where the end-of-segment angle α_e is determined by linear interpolation between the corner angles on the side of exit. The segment begin and end angles are averaged and the PC segment is extrapolated forward at this angle, a_a. Perhaps the actual streamline entered the box at A and exited through B. Then, the distance BD would be a measure of the error by the PC method.

The streamline is terminated when:

1) The streamline intersects the boundary of the master grid.

---

[2] Lackman personal communication.

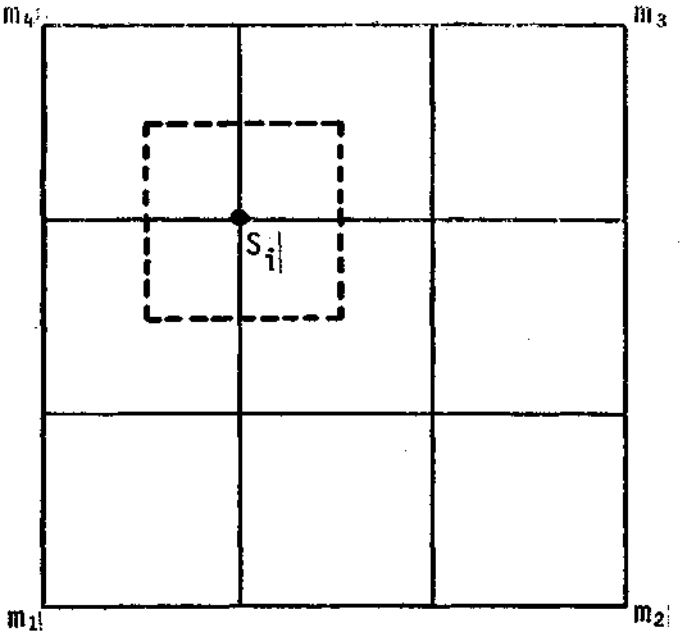

Figure 6. Illustration of a 9-point subgrid within one grid square of a master grid.

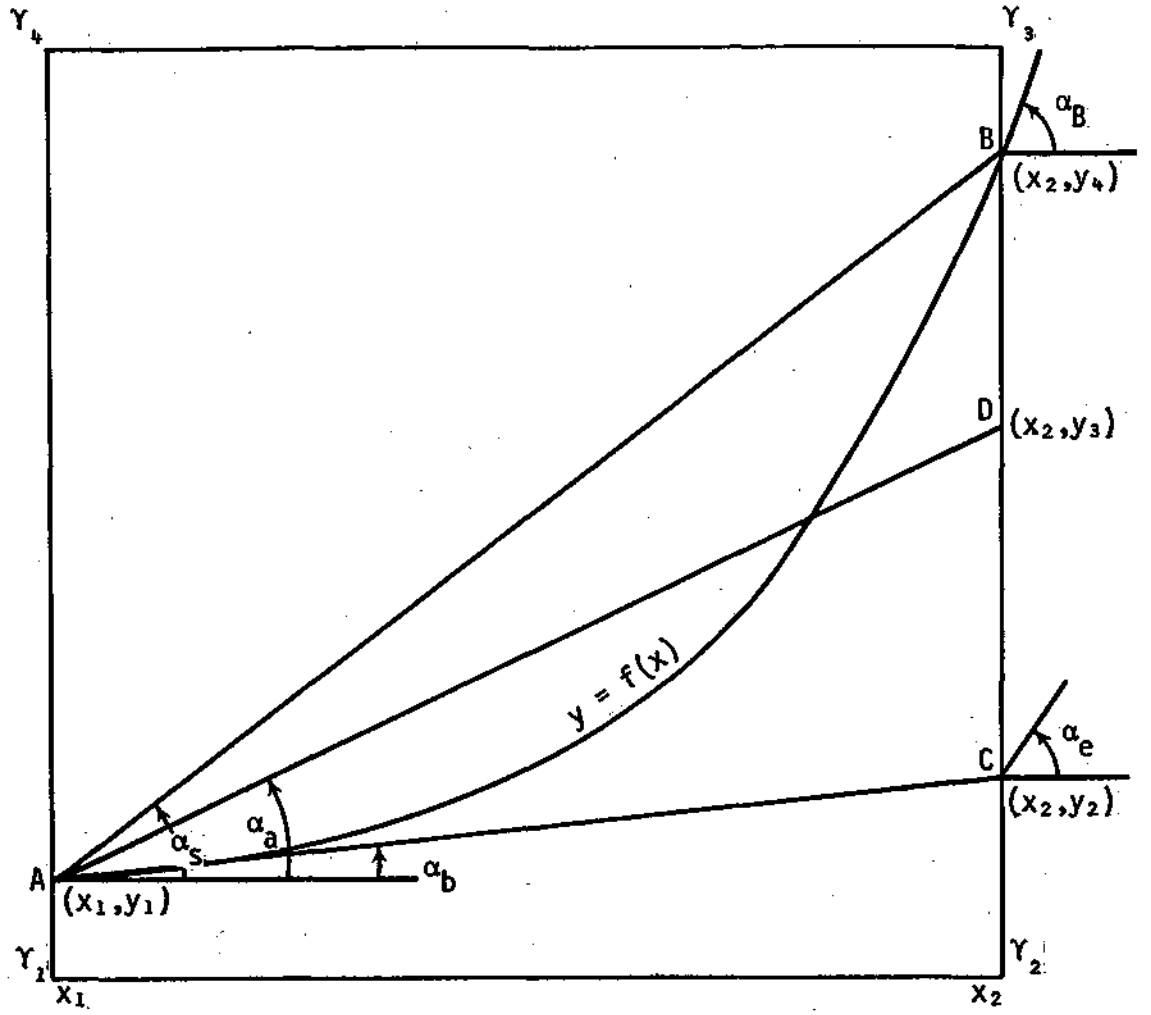

Figure 7. An illustration of the PO and PC streamline construction methods for an arbitrary streamline passing through a subgrid square.

2) The streamline comes within one-half of the sub-grid interval of a grid point containing the identifier of another streamline.

3) The streamline comes within one-half of the sub-grid interval of a grid point containing its identifier (the streamline intersects itself).

4) The angle between two successive line segments exceeds 90 degrees. Here streamlines are terminated to prevent "sawtooth" curves from being constructed at the interface between airmasses with opposing flow.

Examples of the SLX may be found in Achtemeier (1975), Heymsfield (1976), Ray (1976), Goff (1975), Brown (1976), Barnes (1974), and Merritt, etal. (1974).

An automated streamline analysis technique should accurately describe the instantaneous flow field. Since the sequence of extrapolated line segments is an approximation to the true streamlines, some analysis error should be expected. A foreknowledge of the magnitude and character of this error is essential to determine the level of confidence that should be placed on an analysis. The analysis errors for known streamline equations have been obtained for the PO and PC methods. The character of these errors gives some insight into the methods' limitations and reveals those areas of streamline fields which should be interpreted with caution.

Again, consider the sub-grid square illustrated in figure 7. The corner angles γi, i=1, 4, have been found by bi-linear interpolation from u and v components of the wind at points on the larger master grid. The schematic streamline enters the box at A and exits the box at B. The precise objective method must approximate the streamline by the chord AB. However, only the entry location A and the begin-of-segment angle, a_b, are initially known. Thus some method must be found that determines B directly or the chord angle a_s along which the line segment AB can be constructed.

Estimate the chord angle, a_s, from some linear combination of the begin-of-segment angle, a_b, and the end-of-segment angle, a_e, which is found by linear interpolation between the corner angles once point C has been found by the PO method. Then the error between the estimated and true values of a_s is given by

$$R \quad \alpha_s - \frac{1}{I+W} (\alpha_b + w\alpha_e) \tag{1}$$

Let $R^* = \tan (2R)$

so that $$R^* = \tan \left[2\alpha_s - \frac{2}{I+w} (\alpha_b + w\alpha_e)\right] \tag{2}$$

These angle sums and differences can be removed by the successive application of trigonometric identities. Then, R* is expressed by

$$R^* = [2 \tan \alpha_s (1 - \tan \frac{2\alpha_b}{1+w} \tan \frac{2w\alpha_e}{1+w} - (1 - \tan^2\alpha_s)(\tan \frac{2\alpha_b}{1+w} + \tan \frac{2w\alpha_e}{1+w}) (1 + \tan^2\alpha) (1 - \tan \frac{2\alpha}{1+w} \tan \frac{2 \alpha}{1+w} + 2 \tan \alpha_s (\tan \frac{2\alpha}{1+w} + \tan \frac{2 \alpha}{1+w} \quad . \tag{3}$$

For the predictor-corrector method, w=l, and (3) reduces to

$$R^*= [2 \tan \alpha_s (1 - \tan\alpha_b \tan\alpha_e) - (1 - \tan^2\alpha_s) (\tan\alpha_b + \tan\alpha_e)] / [(1+\tan^2\alpha_s)(1-\tan\alpha \tan\alpha_e)+ 2 \tan\alpha_s (\tan\alpha_b+\tan+\alpha_e)] \tag{4}$$

To find the error for the predictor-only method (W = 0), define $R^+=\tan R$ so that (1) becomes

$$R^+ = \tan (\alpha_s - \alpha_b) \tag{5}$$

Application of trigonometric identities gives

$$R^+= \frac{\tan\alpha_s-\tan\alpha_b}{1 + \tan\alpha_s \tan\alpha_b} \tag{6}$$

for the PO method.

If the streamline passing through points A and B in figure 7 is given by y=f(x) and the streamline passing through point C is given by y=g(x), the following are true:

$$\alpha_b = \text{Arctan } f'(x_1),$$
$$\alpha_e = \text{Arctan } g'(x_2), \tag{7}$$
$$\alpha_s = \text{Arctan } [\frac{f(x_2) - f(x_1)}{x_2-x_1}] = \text{Arctan } \bar{f}' (x).$$

It follows that (6) reduces to

$$R^+ = \frac{\bar{f}' (x) - f' (x_1)}{1 + \bar{f}' (x) f'(x_1)} , \tag{8}$$

and (4) becomes

$$R^* = \frac{2 \bar{f}' (x) [1 - f' (x_1) g' (x_2)] - [1 - \bar{f}' (x)^2] f' (x_1) + g' (x_2)]}{[1 - \bar{f}' (x)^2 [1 - f' (x_1) g' (x_2)] + 2\bar{f}' (x) [f' (x_1) + g' (x_2)]} \tag{9}$$

Equations (8) and (9) can be solved algebraically for R^+ and R^* and the results played back through the relationships between R^+ and R and between R^* and R to find the angular errors for each PO and PC streamline segment, $\Delta X = X_2 - X_1$. For small angle errors, the error, $\mathcal{E}$, in the position of the streamline can be approximated by

$$\mathcal{E} = R(X_2 - X_1) \tag{10}$$

The total error between the true and extrapolated streamlines is given by the sum of the individual errors as the streamline passes through a succession of sub-grid boxes. It is difficult to compute the total error from box to box because the streamline may enter or exit from the bottom or the top of the grid box. The ΔX would have to be determined for both the true and extrapolated streamline for each box. Instead, equations (8) and (9) have been solved by stepping forward along the analytical curve in increments equal in leng to ΔX. This appears to be a reasonable assumption because the longest possible streamline segment is $\sqrt{2\Delta X}$ along the sub-grid box diagonal and many segments can be much shorter than AX.

Another simplification of the computations has been made by the assumption that $g(x)=f(x)$. The additional error caused by making this assumption will be the subject of actual streamline calculations presented in this section.

High and low pressure centers frequently perturb the troposphere at all levels. When the circulations associated with these pressure centers are non-divergent, the wind field streamlines should form closed curves. These curves are often nearly elliptical in shape. The individual and cumulative errors for a circuit around ellipses of varying eccentricity were calculated using (8) and (9). Let the ellipse be d fined by

$$f(x) = -\frac{1}{\epsilon}\,(a^2 - x^2)^{1/2} \tag{11}$$

where e is the minor/major axis ratio, and a is the minor axis radius. Equations (7) become

$$f'(x_1) = \frac{x_1}{\epsilon\beta_1},$$

$$f'(x_2) = \frac{x_2}{\epsilon\beta_2}, \tag{12}$$

$$\bar{f}'(x) = -\frac{(\beta_2 - \beta_1)}{\epsilon(x_2 - x_1)},$$

where

$$\beta_1 = (a^2 - x_1^2)^{1/2}$$

$$\beta_2 = (a^2 - x_2^2)^{1/2} \tag{13}$$

For the predictor-only method

$$R^{+} = -\varepsilon \frac{[\beta_1(\beta_2-\beta_1) + x_1(x_2- x_1)]}{\varepsilon^2\beta_1(x_2- x_1) - x_1(\beta_2-\beta_1)} \tag{14}$$

After some manipulation, the predictor-corrector method yields

$$R^{*}= \{\varepsilon(1-\varepsilon^2)\ (x_2- x_1)\ [2a^2(\beta_1-\beta_2) + (x_2+ x_1)(x_1\beta_2- x_2\beta_1)]\}/$$
$$\{(1-\varepsilon^2)\ [(x_2- x_1)^2\ (-\varepsilon^2\beta_1\beta_2- x_1x_2) + 2x_1x_2(x_1x_2-$$
$$\beta_1\beta_2+ a^2)]\ + 2\varepsilon^2a^2(-\beta_1\beta_2+ a^2- x_1x_2)\} \tag{15}$$

Equations (14 and 15 show that for both PO and PC methods, the extrapolation error will be zero for the straight line (ε =0.0). However, the extrapolation error for the circle (ε =1.0) also vanishes for the PC method. This means that, if g(x)=f(x), the average of the begin-of-segment angle with the end-of-segment angle will always yield the circle chord angle a_s.

Figure 8 is included to show the shades of the ellipses used in this study. They range from the circle (ε =1.0) to the highly skewed (ε =0.05) ellipse for which most of the curvature is concentrated in the first few points near the ordinate. Figure 9 gives the PC method cumulative error out to 10 step increments for the same set of ellipses. The AX increment was chosen so that the ratio of the minor axis radius to AX, a/AX, was only 3.5. The figure shows that most of the extrapolation error was contained within the part of the curve with the most curvature, the first step increment, for ellipses with ε<0.25. Beyond the first few step increments, the additional error was essentially zero. The cumulated error also approaches zero as the ellipse becomes circular.

Figure 10 shows the total error for the PO and PC methods for selected ε for one circuit around an ellipse. The length of the circuit is longer for low ε ellipses, however, it was found that most of the error was concentrated within a few step increments near the ordinate. The errors for most of the length of the circuit was negligible. The total error was greater than zero for all ellipses; the constructed streamlines tend to spiral outward to greater radii. This tendency is most pronounced for the small ellipses. The PC errors were much smaller than the PO errors for the same circuits. The PC total errors tend to zero as the ellipses become circular. Both sets of curves approach zero as the step increment decreases ($a/\Delta X \to \infty$). Thus the greatest gain in accuracy achieved by decreasing AX is found for the smaller ε ellipses which are most sensitive to the step increment size.

The total errors presented in figure 10 were normalized by dividing by AX and are shown in figure 11.

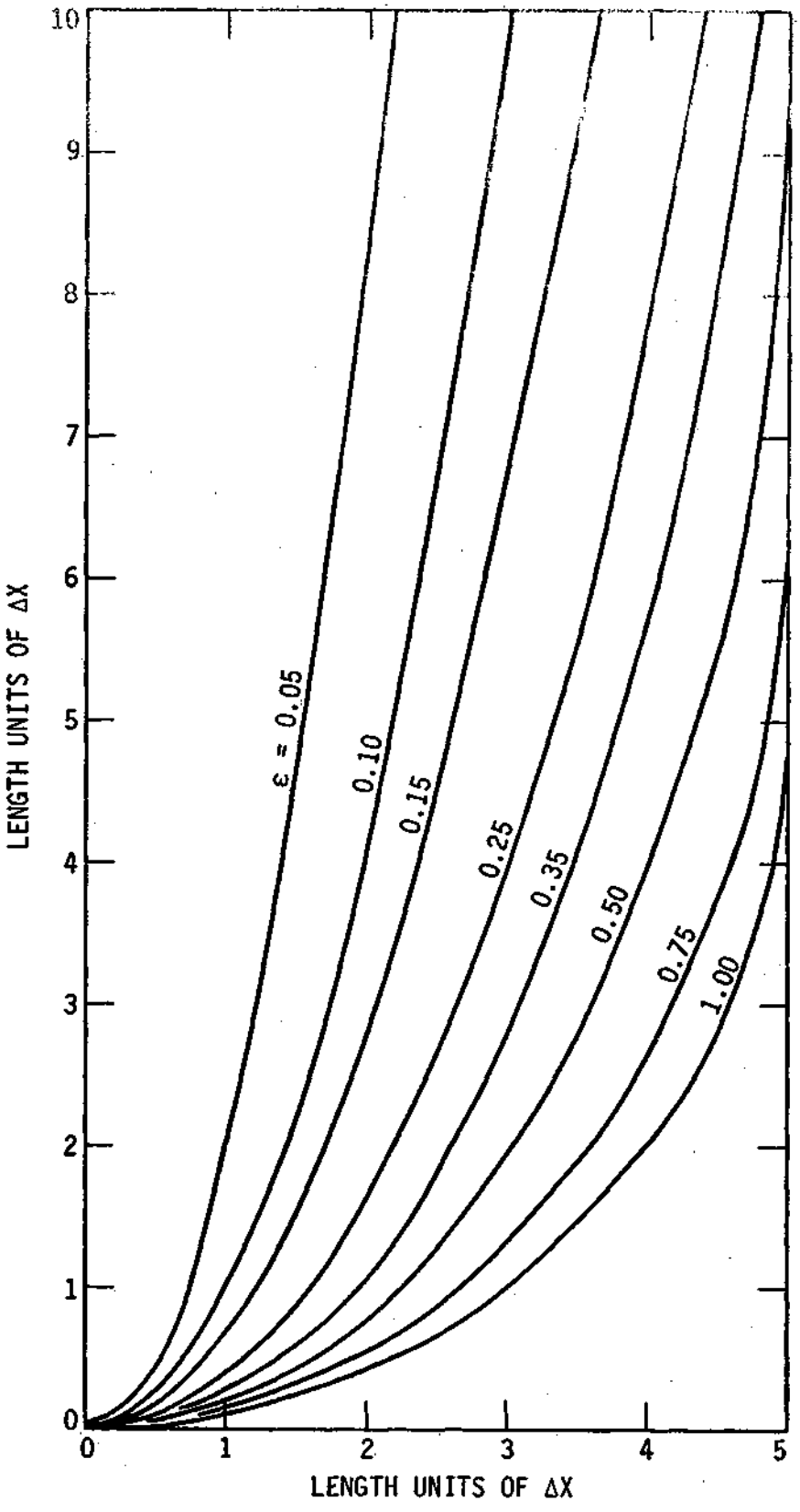

Figure 8. Shapes of elliptical curves used for the streamline error analysis.

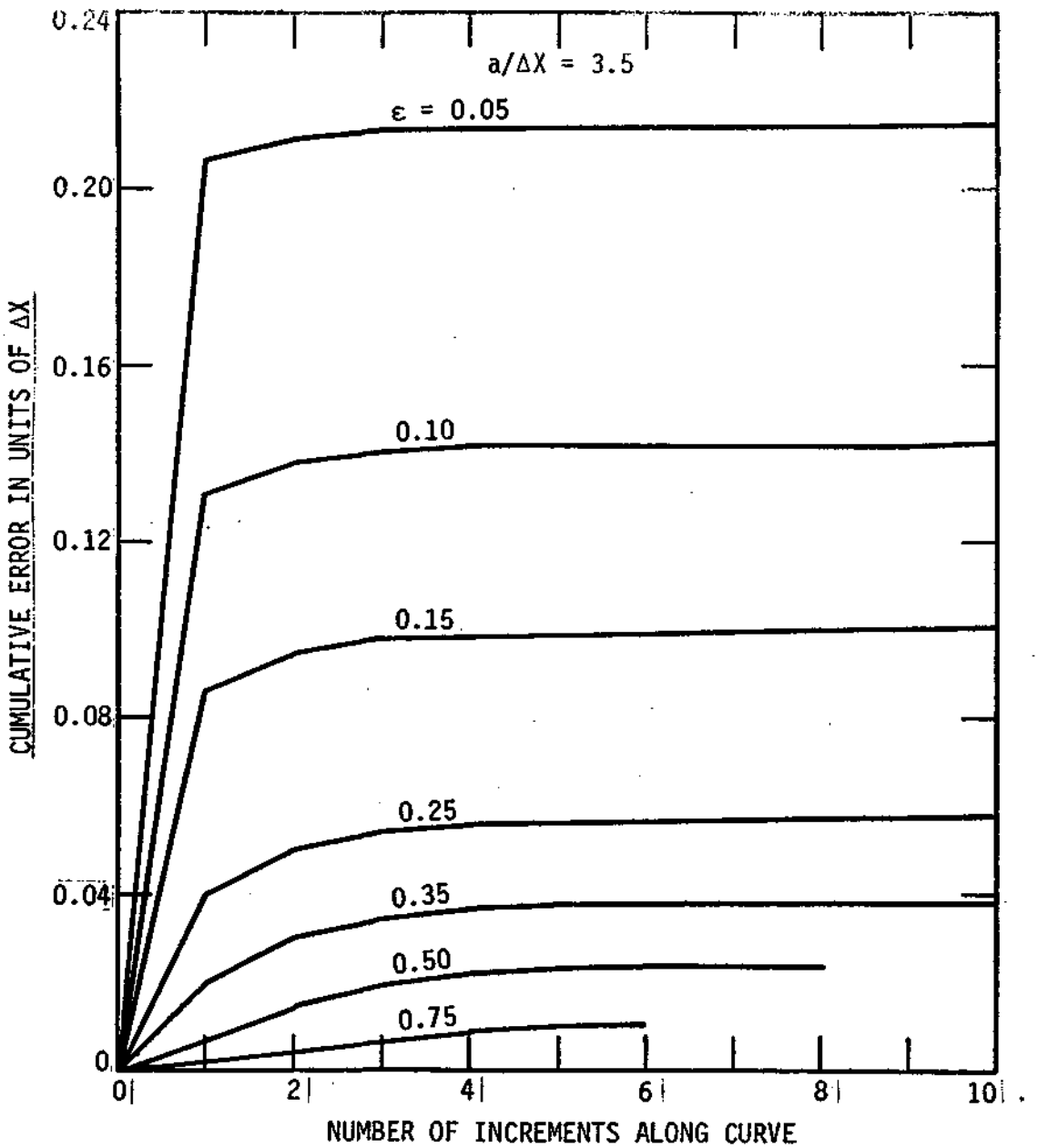

Figure 9. Cumulative error for the PC method out to 10 increments for the curves shown in figure 8.

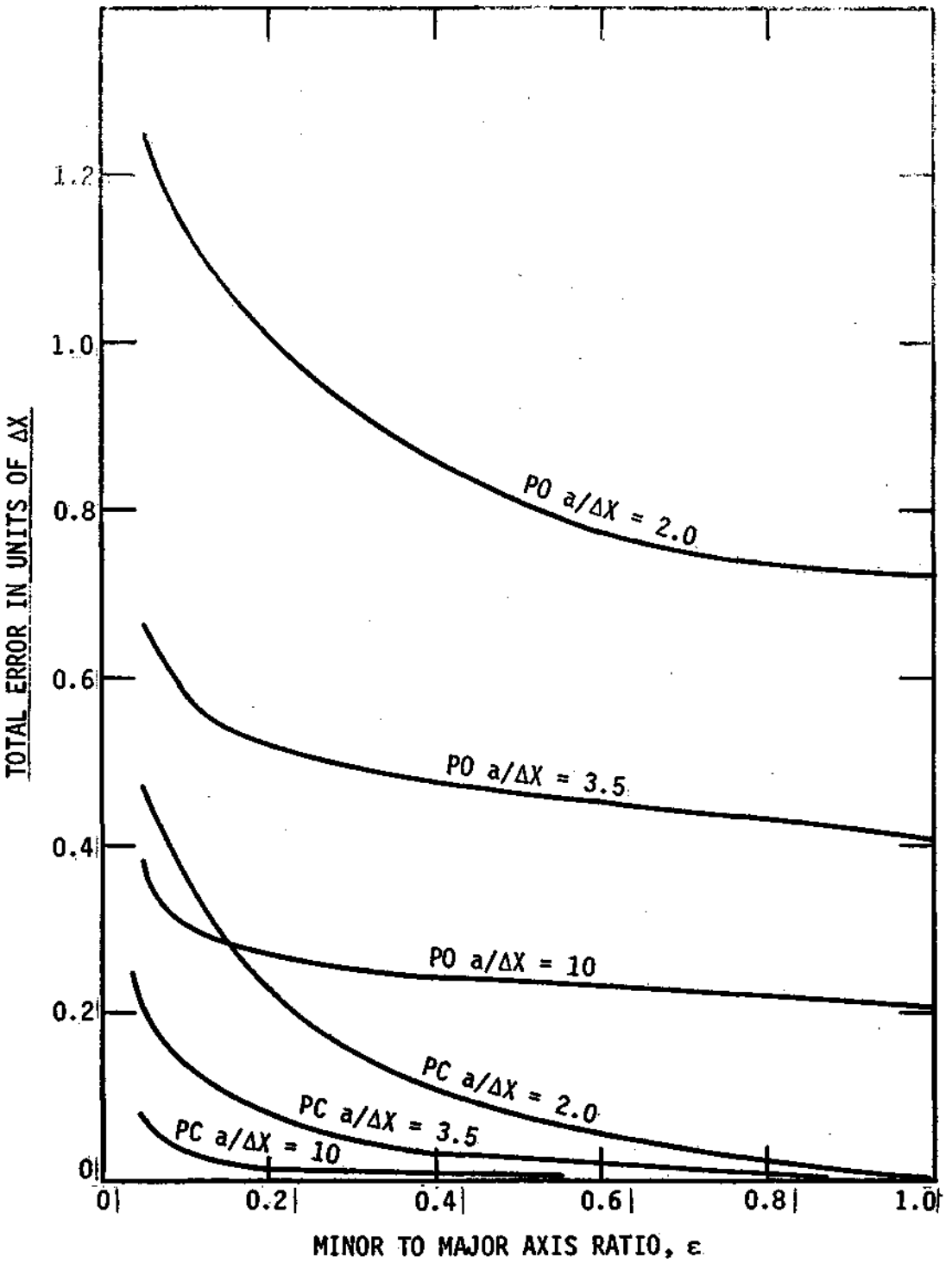

Figrure *10. Total error for one circuit around ellipses of varying shape for selected ratios of minor axis radius to step increment.*

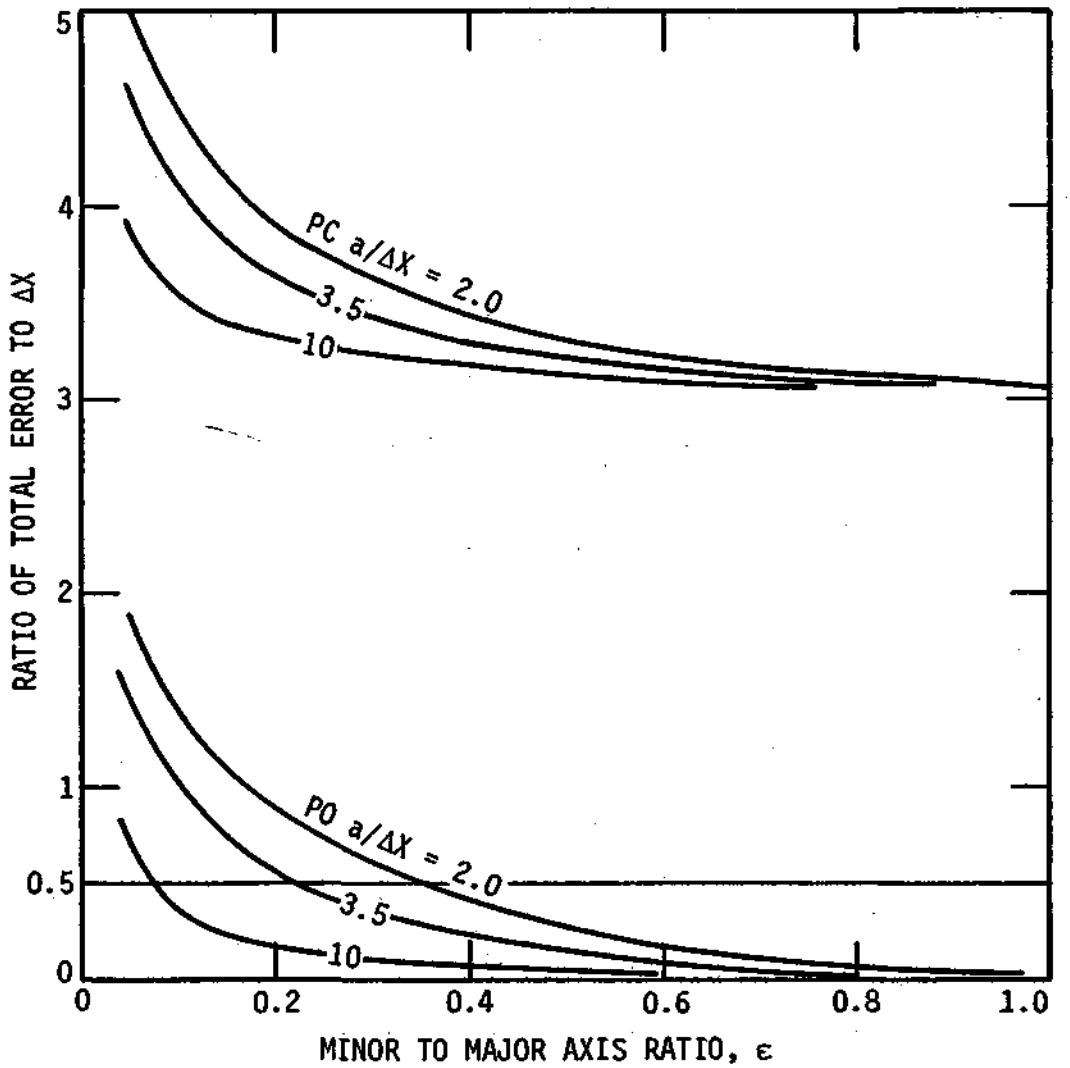

Figure 11. Same as figure 10 except the total error has been normalized by the step increment.

As the minor axis to step increment ratio increases, the error approaches zero for the PC method and approaches about 3AX for the PO method. Note that the absolute error approaches zero for both methods as the step increment is decreased (fig 10). As the streamline completes its circuit, it must pass within 0.5 AX (shown by the horizontal line at 0.5) for it to close upon itself and be terminated according to the method described by figure 6. All other elliptical streamlines with error greater than 0.5 ΔX will spiral outward unless some other method for termination is devised. All PO streamlines will spiral outward and, if the step increments are large, the spiral will be clearly evident since the outward spiral will be greater than 3AX at the end of one circuit. The PC streamlines will spiral outward for low e ellipses and small a/AX ratios but, as the spiral radius increases to larger a/ΔX ratios, the streamline will terminate on itself.

With the assumption g(x)=f(x), the predictor-corrector method has been shown to be more accurate than the predictor-only method. However, this assumption is seldom true because slight differences in the angles at grid corners exist even for families of curves and there must be some discrepancy between the calculated end-of-segment and true streamline exit angles unless the end of the segment, point C in figure 7, falls upon the streamline exit point B. Then there would be no need for a predictor-corrector method.

The predictor-corrector SLX method was used to objectively produce streamlines for circles of varying radii. The coordinates of each line increment were listed and checked for any departure from the initial radius of the circle. Since the step increment error was always zero for g(x) f(x), discrepancies found here occurred because g(x)≠f(x).

Figure 12 shows the cumulated discrepancies between the true and calculated streamlines for three circles. The abscissa gives the angular distance in the mathematical framework around the circuit, that is, moving counterclockwise beginning with the first (upper right hand) quadrant. The three solid lines give the cumulated discrepancies for circles constructed counterclockwise around the circuit. Then the directions were reversed and the discrepancies calculated for streamlines constructed clockwise around the circuit (dashed lines).

Figure 12 reveals that the cumulative error oscillates with a frequency of π/2. The streamlines are observed to spiral outward from O-π/4 and to spiral inward from π/4-π/2 and so on. The total error for one circuit approaches zero for most of the streamlines. The variations between the curves arise because there are differences in the placement of the streamlines within successive sub-grid boxes. However the variations are small as are the cumulated discrepancies. The maximum error is only a few hundredths of the step increment and appears to be independent of the minor axis radius to step increment ratio. Thus, it is concluded that g(x)=f(x) is a very good assumption which will not significantly weaken the results presented above.

The theoretical error analysis presented herein shows that the predictor-corrector SLX objective streamline analysis constructs highly accurate streamlines when the streamlines are either straight lines or form elliptical patterns. An error analysis for other analytical curves has yet to be completed, however, preliminary results suggest that the cumulative errors for these

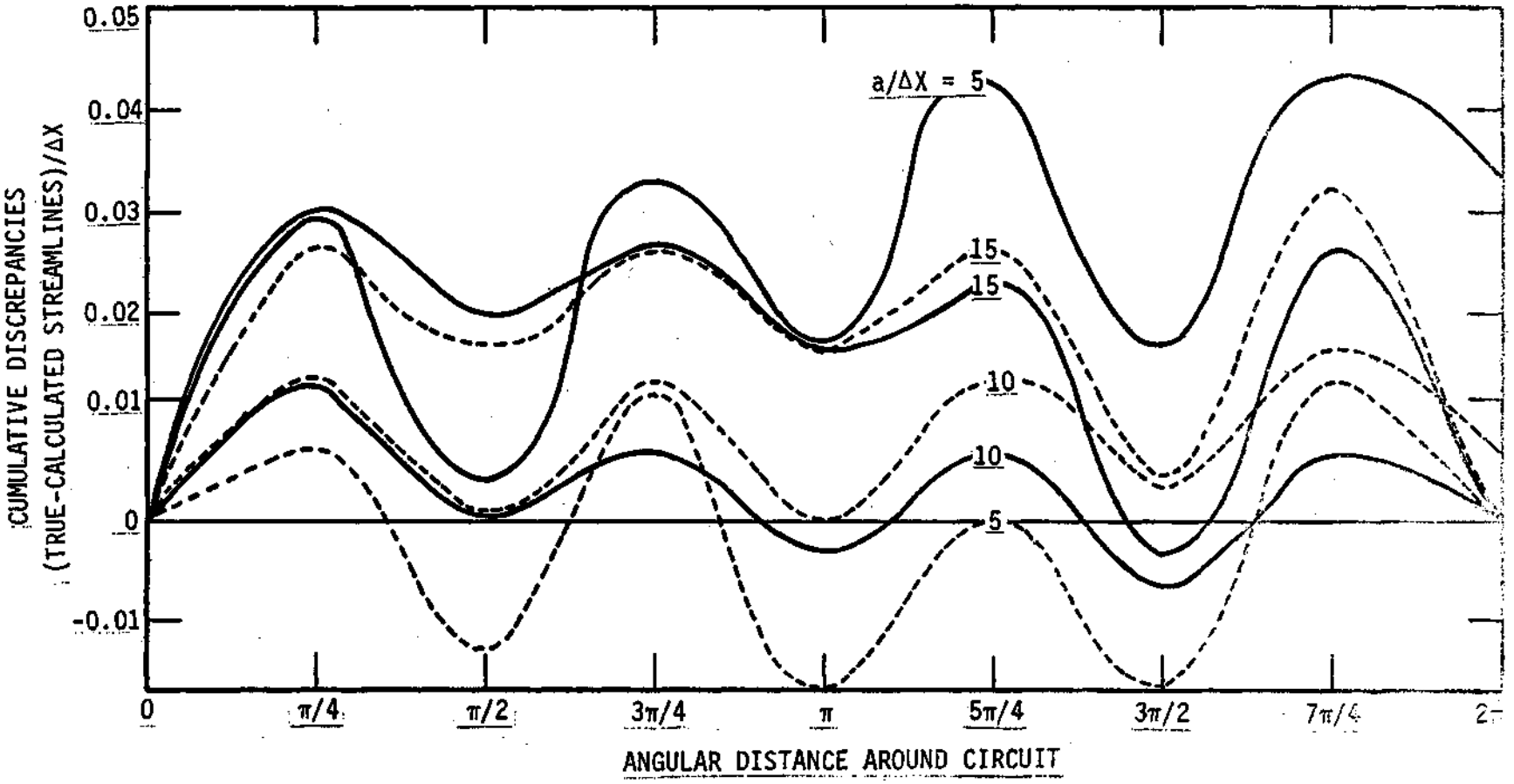

Figure 12. Cumulative discrepancies, true minus calculated streamlines normalized by the step increment for 3 circles calculated directly from the PC streamline program SLX.

curves will not differ greatly from the errors reported here. Since any curve segment can be represented by a normalized weighted sum of known curve equations, the error for any curve can not exceed the weighted sum of the errors for the known curves. Thus it is concluded that, with the exception of a few curves of very sharp curvature (and therefore of limited spatial coverage), the SLX method is precise and will not lead to errors in the interpretation of the instantaneous flow field. It is also concluded that the predictor-corrector method is superior to the predictor-only method for automated streamline construction.

4. Appendix D: A Four-Dimensional Analysis of Surface and Upper-Air Data

In the section on the problem of transience it was suggested that PROGSPECs derived from the early morning soundings are likely to have little or no correlation with events that occur later in the days when precipitation is initiated by a dynamic trigger. Stability indices are particularly sensitive to local variations in moisture and temperature stratifications. Moisture variables are subject to changes as dry air masses advance or retreat locally. PROGSPECs derived from wind observations cannot carry those events where circulations associated with dynamic triggers are small in scale.

Correlations between the sounding SPECs and the 3 hourly areal mean rainfall for Dodge City, Kansas, (see fig.4 in text) were found to decline rapidly with time (fig.5 in text). It was concluded that the decline was caused by temporal changes within the troposphere such that environmental conditions at one time were not representative of environmental conditions at a later time. Therefore, PROGSPECs calculated from morning soundings were poorly correlated with convective period precipitation.

The correlations did not improve when the soundings, modified for the surface heating and moisture conditions at the time of maximum temperature, were processed with a one dimensional cloud model (Kreitzberg and Perkey, 1976). The cloud model is extremely sensitive to the initial conditions, particularly the low level stability and moisture. The High Plains atmosphere is frequently convectively unstable but the moisture and heat needed for convection is often trapped below an inversion at low to mid levels. Often this inversion can be penetrated only after having undergone meso-synoptic scale lifting.

Correlations with the convective period rainfall improved when spatial fields of meteorological variables were used as candidate PROGSPECs. Transient triggering mechanisms could be detected within these fields at locations remote from the rainfall sampling area 6-12 hours prior to the rainfall period. Preferred locations of transient systems that would produce precipitation later at Dodge City were found.

Although the surface data provide the most highly correlated PROGSPECs, it was recognized that the relationship with rainfall could be increased if the PROGSPEC s were calculated from a four-dimensional matrix of atmosphere structure brought about by coupling the surface data with the upper air observations. Conceptually, a meso-scale primitive equation prediction model could provide simulations of the four-dimensional atmospheric structure.

However, 1) the development has not progressed to the point to where these models are readily available for general use; 2) the models currently being investigated have computer requirements that make them unfit for real time operations; and 3) the performance of these models when initialized with real observations has not been thoroughly documented.

A simple four-dimensional analysis model would be attractive for the HIPLEX for several reasons. It can produce a set of nonlinear PROGSPECs that follow through several scales of nonlinear processes that culminate in convective rainfall. Processes at the cloud scale can be simulated by the cloud model. These are coupled with environmental conditions adjusted nonlinearly according to low level temperature and moisture changes and vertical mass displacements. Nonlinear PROGSPECs that simulate rainfall processes would be expected to correlate better with rainfall than linear parameters that carry only a small fraction of these processes.

A 4-D analysis increases the spatial resolution of the stability and vertical moisture distributions to a scale equal to the resolution of the surface observations. PROGSPECs computed from these fields could increase the sensitivity of the statistical tests if the storm is to be used as the sampling unit. The 4-D analysis as an update model is also useful for operations. Surface triggering mechanisms reveal areas of potentially increased instability. The cloud model can determine the general cloud character for these areas. Then aircraft could be directed to these instability areas perhaps before convective clouds begin to develop.

Finally, a simple 4-D analysis model can be useful for determining the quantities, both observed and derived, which are most vital to convective processes. The model will be updated hourly with the surface observations; the analyses will be a succession of initial states. The spatial and temporal variability and the sensitivity to observational noise of these quantities as determined from the 4-D model may aid the assessment of the types and accuracies of observations required to initialize the more complicated numerical meso-scale models.

The 4-D analysis is illustrated conceptually in figure 13. A surface network that includes measurements of temperature, dew point temperature, wind speed and wind direction is complimented by a single sounding taken near the left side of the grid. The schematic sounding shows a mixed dry adiabatic boundary layer capped by the deep inversion given by the thick solid lines. The inversion cannot be penetrated by convective thermals, and a cloud model would predict cloudless conditions.

The sounding environment is representative of the undisturbed environment everywhere. However, the surface data reveal a disturbance in the form of a convergence line located a short distance from the sounding site. Here, convergence has displaced the air column upward and has weakened the inversion. The dashed lines give the vertical displacement in meters. The inversion has been destroyed along a narrow zone of maximum vertical displacement. Convective clouds form within this favorable local environment.

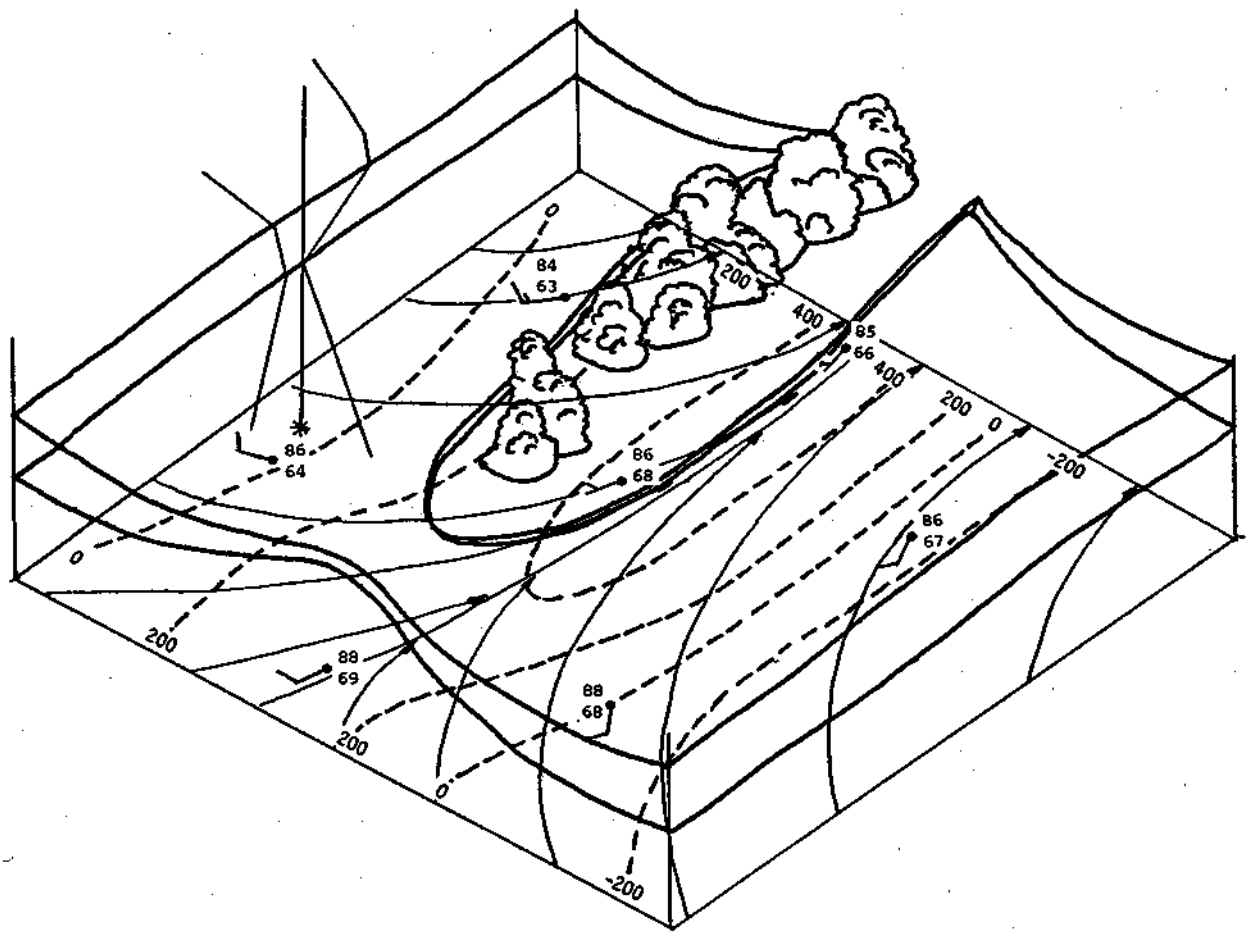

Figure 13. An illustration of the multidimensional simulation of atmospheric structure through the combination of data obtained from surface observations and a single sounding.

Although relatively simple physical processes determine the spatial and temporal distribution of stability, a number of assumptions are necessary so that those processes can be estimated from hourly surface observations and the twice daily synoptic radiosonde network or special ascents. Some of these assumptions are:

1) The vertically integrated effects of sub-synoptic and mesoscale systems are detectable in the surface observations, both in space and time,

2) The systems that perturb the surface fields extend vertically throughout much of the troposphere,

3) The wind observations are free of systematic direction or speed contamination by poor instrument exposure near man made structures and trees or channeling by local topography,

4) The convergence throughout a 1 km deep layer surface layer is constant and equal to the surface convergence,

5) The magnitude of the convergence of a weather system is equal to the calculated convergence cumulated over the residence time of a typical mesosystem between stations, and

6) The vertical motion within any column of air from the surface to 200 mb follows a prescribed profile, the amplitude of which is determined by the surface convergence.

If the surface data are complimented by a single sounding, then

7) The sounding is representative of the undisturbed (vertical displacement equal to zero) environment over the entire grid at all times before adjustments for surface conditions are made,

8) The horizontal temperature gradient over the grid is negligible, and

9) The horizontal temperature advection over the grid is negligible.

If the surface data are complimented by synchronous multiple soundings, then,

10) The horizontal temperature gradient is caused by systems of scale equal to or larger than the separation between sites, and

11) The temperature advection is constant or varies according to a prescribed relationship (Cohen, 1977).

Further,

12) All non-cloud model calculated subsidence is dry adiabatic (moist subsidence is permitted within the cloud model.),

13) There is no feedback between the cloud model modified environment and the initial environment,

14) The modification of the mixing layer using surface temperature and moisture is confined to below a specified level (800 mb in Illinois).

15) Surface temperature varies with cloudiness according to a function of time and amount of cloudiness, and

16) If the surface temperature is cooler than the temperature at sounding time, the sounding temperature decreases linearly from a specified level (900 mb in Illinois) to the surface.

The 4-D analysis has been developed with the view that advection of thermodynamic properties, diabatic heating, and dynamical lifting may act in any combination to change the tropospheric temperature profiles. The local temperature tendency, derived from the First Law of Thermodynamics, is

$$\frac{\partial T}{\partial t} = \frac{1}{c_p}\frac{dH}{dt} - \vec{V}.\nabla T - w(\gamma_d - \gamma) \quad . \qquad (1)$$

The local temperature, T, removed from an initial temperature, T_i, by some time At, can be approximated by the integration of (1) with respect to time. The result is

$$T = T_i + \frac{1}{c_p}\overline{\Delta H} - \overline{\vec{V}.\nabla T}\,\Delta t - \overline{(\gamma_d - \gamma)}\,\Delta z. \qquad (2)$$

The second term to the right of the equal sign represents the effect of diabatic heating. This term contributes to the local temperature through 1) surface heating which increases the net energy in the surface layer, 2) cooling due to nocturnal long wave radiation to space, and 3) latent heat released when moist air is lifted beyond its condensation level and/or cooled below its condensation temperature. The third and fourth terms, respectively, contribute to the local temperature through the time integrated average horizontal temperature advection and the net vertical displacement of the airmass. It is also necessary to assume that the horizontal and vertical gradients of temperature remain constant through the interval Δt. The stability can be easily obtained once the temperature has been found for all significant and standard levels from a given sounding. The terms of (2) are described with emphasis on the assumptions necessary for their calculation.

a) Term 1: The Initial Temperature.

When the vertical temperature profile is available from a single sounding, the sounding is assumed to be valid everywhere on the grid at all times before any adjustment for surface layer conditions is made. Achtemeier and Morgan (1976) inverted the thermal wind equation to solve for the horizontal temperature

gradient as a function of the vertical wind shear. The temperatures at any point on the mesh were found by multiplying the components of the temperature gradients by the respective components of the distances between the grid points and the observation site.

The temperature profiles constructed in this manner were found to contain unrealistic superadiabatic temperature gradients and large amplitude small scale perturbations. We abandoned the thermal wind inversion approach in favor of assumption 8. The summertime north-south temperature gradient was estimated by taking the temperature differences between Peoria and Salem, Illinois for 50 mb levels between 800-300 mb for 11-31 August 1972. Peoria is located approximately 250 km north northwest of Salem. These results, given by the bar graphs in figure 14, show that the horizontal temperature gradients between the two stations were generally small for this 20 day period. About 73% of the temperature differences ere within the standard temperature measurement error of 1.0 C. About 93* of the temperature differences were within ±2.0 C. The mean of the differences was 0.27 C; temperatures at Salem tended to be warmer than the temperatures at Peoria.

The larger differences of either sign generally revealed local meteorological conditions at one station such as cold front passages, soundings taken through clouds, extensions of thunderstorm mesohighs above 800 mb, or inversions that peak near 50 mb levels at one station but are found between 50 mb levels at the other station.

There results suggest that the temperature differences at two upper air stations at different locations within the area of the analysis were small, meaning that the temperature gradients were also small. Thus our adoption of assumption 8 seemed justified.

b) Term 2: Diabatic Heating.

Daytime heating and nocturnal cooling at the surface can be easily monitored with the hourly surface temperature observations. We have assumed that the temperature decreases linerly from 900 mb to the surface for those -instances where nocturnal cooling has decreased the surface temperature taken at the time and location of the sounding.

Studies by Moses and Bogner (1967) and Goff and Hudson (1972) show that daytime lapse rates in the lowest 50 m often deviate considerably from diurnal and hourly means and that much of the deviation can be explained by meteorological factors that control the surface heat budget such as airmass (haze, dust, windiness, origin) and cloudiness.

Moses and Bogner (1967) show that summer lapse rates in the layer from 204 m at Argonne, Illinois, often exceeded 35 T_d during the daylight heating period. During the summer month of June the 2-42 m lapse rate often approached or exceeded 4 T_d. On half the June days the lapse rates exceeded 3 T_d and on another 25% of the days the lapse rate during the hottest hours was found to be less than 2 T_d. Goff and Hudson (1972) showed that lapse rates for the 45-90 m layer varied from 1.11 T_d for cloudy days to 1.35 T_d

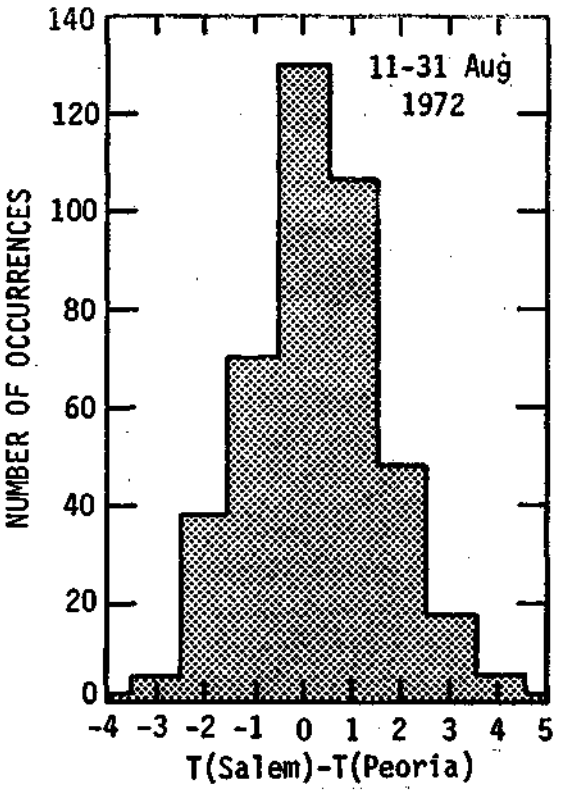

Figure 14. The distribution of summer time tropospheric temperature differences between Salem and Peoria, Illinois, for 11-13 August 1972.

for clear days within continental polar air masses. Similar variations were found (when data was available) for maritime tropical air masses.

It is assumed that cloudiness is the dominant factor that determines the extent of the departures of the low level lapse rates from the hourly means. We separated the observed hourly cloudiness into three categories: clear skies and scattered clouds (0 to 5/10 coverage), broken clouds (6/10 to 9/10 coverage), and overcast (10/10 coverage). Using the Argonne measurements, we constructed a table that contained cumulative frequencies of lapse rates in the 2-42 m layer by hours. Then we designated lapse rates at the 75% cumulative frequency level to occur with clear skies and scattered clouds, lapse rates at the 50% cumulative frequency level to occur with broken clouds and lapse rates at the 25% cumulative frequency level to °ccur with the overcast category. These lapse rates are tabulated as functions of loud category and daylight hour in Table 1.

To integrate the results from Goff and Hudson (1972) with the results of Moses and Bogner (1967) we assumed that in the 50-100 m layer, the lapse rate was equal to T_d if the 0-50 m lapse rate was less than 1.3 T_d and that the lapse rate was equal to 1.25 T_d when the 0-50 m lapse rate exceeded 1.3T_d. For a given 2 m surface temperature, the 2-42 m 3.7 T_d lapse rate and the 500-100 m 1.25 T_d lapse rate combine to give a 100 m temperature that is 1.5°C cooler than the 100 m temperature found when the dry adiabatic lapse rate is used.

Table 1. Lapse rates in the 2-42 m layer as multiples of T_d for three cloud categories for selected daylight hours

Hour LST	Cloud Coverage 0-5/10	6/10-9/10	10/10
0600	1.0	1.0	1.0
0700	2.5	1.3	1.0
0800	3.1	2.1	1.0
0900	3.4	2.5	1.5
1000	3.6	2.8	1.7
1100	3.7	2.9	1.9
1200	3.7	2.9	1.9
1300	3.6	2.8	1.7
1400	3.4	2.3	1.2
1500	2.8	1.9	1.0
1600	2.3	1.2	1.0
1700	1.2	1.0	1.0
1800	1.0	1.0	1.0

Above 100 m, the lapse rate is assumed to be dry adiabatic to 800 mb or to the pressure level where the dry adiabat intersects the temperature sounding curve, whichever comes first.

Another source of diabatic heating is latent heat released when moist air is lifted beyond its condensation level and/or cooled below its condensation temperature. The lifted condensation level (LCL) temperatures and pressures are computed for each significant and standard level between the surface and 500 mb. The LCLtemperature is obtained from the reported temperature and relative humidity which are incorporated into an equation derived from the Clausius-Clapeyron equation and the relationship between mixing ratio, pressure and vapor pressure. By definition the relative humidity R is related to mixing ratio by $R = w/w_s$. Also $w_s = \varepsilon e_s/p$ and $w = w_{sc} = \varepsilon e/p = \varepsilon e_{sc}/P_c$ where e_s is the saturation vapor pressure at pressure p and e is the saturation vapor pressure found when moist air with mixing ratio w is lifted to its condensation pressure level P_c. The ratio between e_{sc} and e_s is

$$\frac{e_{sc}}{e_s} = \frac{w P_c}{w_s p} = \frac{R p_c}{p} \qquad (3)$$

and, from the Clausius-Clapeyron equation, the ratio is

$$\frac{e_{sc}}{e_s} = \exp\left[- c_1 \left(\frac{1}{T_c} - \frac{1}{T}\right) \right] \qquad (4)$$

where T_c is the temperature at the LCL and c_1 is equal to $M_v L/R^*$ (see Hess, 1959, p. 49). Equations (3) and (4) are combined and the reference to pressure eliminated through the Poisson equation. Further manipulation gives

$$\frac{T}{c_1} \ln R - \frac{T}{c_1 K} \ln \frac{T}{T_c} = - \left(\frac{T}{T_c} - 1\right) \qquad (5)$$

where K = 2/7. The $\ln T/T_c$ expanded into logarithmic series is

$$\ln \frac{T}{T_c} = \left(\frac{T}{T_c} - 1\right) - \frac{1}{2}\left(\frac{T}{T_c} - 1\right)^2 + \frac{1}{3}\left(\frac{T}{T_c} - 1\right)^3 \ldots \qquad (6)$$

for $0 < T/T_c < 2$ which is always true for the ranges of initial and cloud base temperatures considered for the model. We truncate (6) after the first term and solve (7) to get a first guess T_{cf} for T_c. This is

$$T_{cf} = T \left[1 + \frac{T}{c_1} \ln / \frac{T}{c_1 K} - 1) \right]^{-1} \qquad (7)$$

We recover part of the truncation error by a quadratic correction to T_{cf}. The final estimate for T_c is

$$T_c = T_{cf} - 8.0 \times 10^{-4} (T - T_{cf}) (T - 125\ R^2 + 160\ R \quad (8)$$

Equation (8) yields LCL temperature correct to within ±0.15°C of LCL temperature given in the Smithsonian Meteorological Tables for temperatures that range from -10.0 to 40.0°C and relative humidities that range from 10% to 100%. The pressure at the LCL is obtained from Poisson's equation.

Moist air lifted beyond its LCL rises moist adiabatically. The moist adiabatic lapse rate is determined by linear interpolation from a set of pressure, temperature and wet bulb potential temperature tables.

c) Term 3: Temperature Advection.

When the vertical temperature profile is available from single serial soundings, the horizontal temperature gradient is assumed to be zero during the time interval between ascents (assumption 9). This assumption was adopted after tests with the thermal wind inversion failed to produce realistic temperature profiles. In that method, the temperature advection at each pressure level was determined by multiplying the thermal wind deduced temperature gradient by the wind velocity at that level. The total temperature change was obtained by assuming the advection to be constant and multiplying by the time interval between to the surface observation time and the sounding ascent time.

The temperature gradients and advections deduced from unsmoothed wind profiles led to unrealistic lapse rates. The wind profiles were smoothed to eliminate small scale variations which violated the geostrophic assumption used to derive the thermal wind equations. From the smoothed wind vectors, the horizontal temperatures were computed, converted to temperature advections, and extrapolated for 11 hours. The .11 hour temperature changes were then verified against the 12 hour temperature changes between successive soundings for seven cases where the effects of vertical displacements, precipitation, and clouds were minimal. In four cases, the 1700 CST temperature profiles extrapolated from the 0600 CST (1200 GMT) soundings were compared with the following 1800 CST (0000 GMT) soundings. In the remaining three cases, the 0500 CST temperatures were extrapolated from the 1800 CST soundings and compared with the following 0600 CST soundings. The results from comparisons at low and mid tropospheric levels not near small scale temperature fluctuations are summarized in figure 15.

The computed 11 hour temperature changes ranged from -5.0C to 9.0C with most values clustered between 4.0C. Most of the observed 12 hour temperature changes were found between -1.0C and 2.0C. The figure shows no apparent trends between the computed and observed changes either in magnitude or in sign.

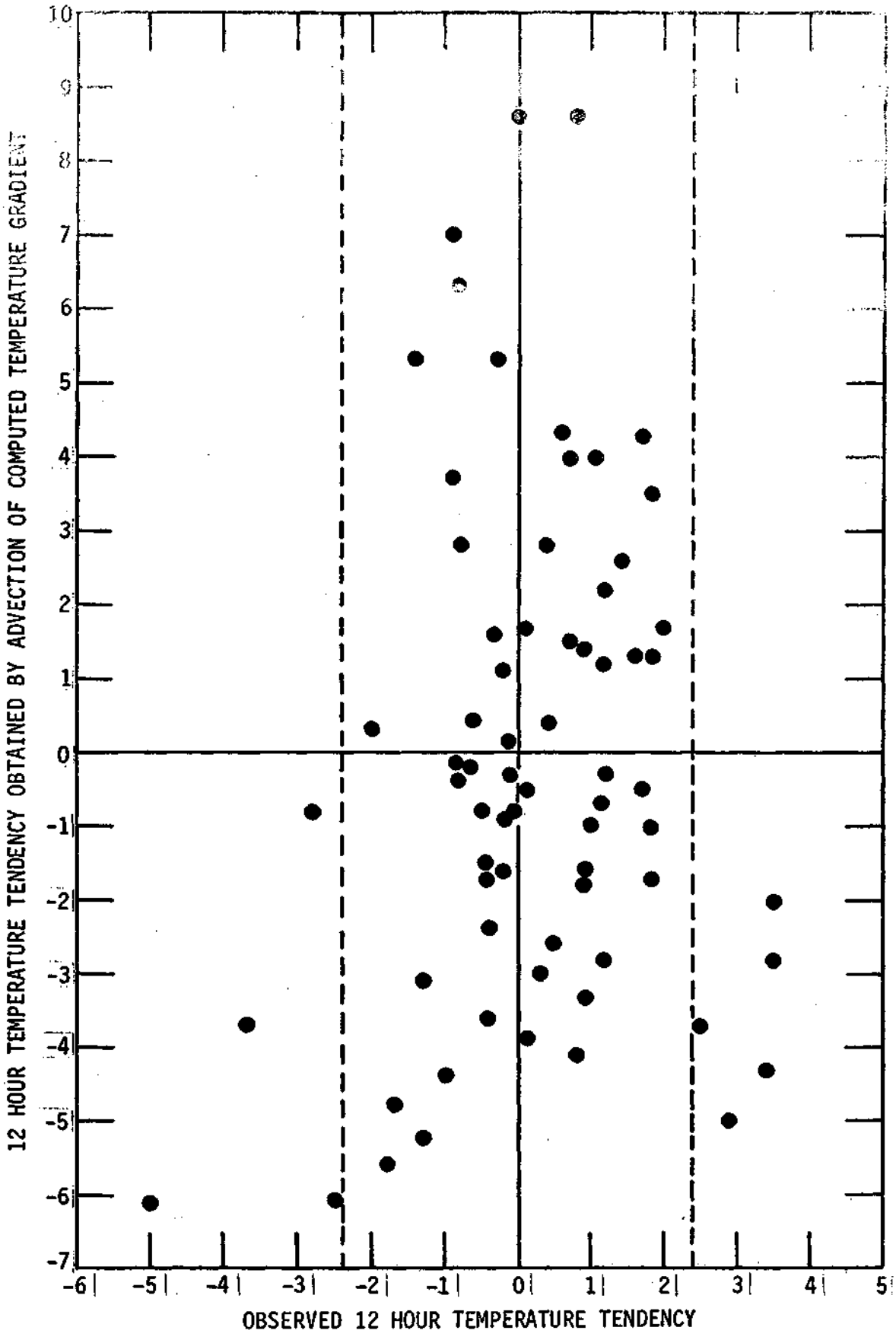

Figure 15. A comparison between calculated and observed mid-tropospheric temperature difference over periods of 11 hours (calculated) and 12 hours (observed) for selected cases from the summer of 1972.

As a further check on the sensitivity of the calculated temperature changes, an initial wind shear error of ±1.0 m sec^{-1} in 50 mb for a 10 m sec^{-1} wind was found to yield a 12 hour temperature change of ±2.4C. Most of the observed 12 hour changes are contained within the limits of this error (dashed lines in figure 25). Thus the thermal wind inversion method was found to be too sensitive to small errors in the winds and to other noise to be useful for estimating temperature tendencies.

A method that develops predicted raobs from temperatures predicted at 12 hour intervals from the National Weather Service LFM forecast model has been made operational at the Bureau of Reclamation's Environmental Data network (Politte, et at. 1977). Cohen (1977) compared the accuracy of errors between the observed and forecasted temperatures and between the observed and persistence (no temperature advection) temperatures for levels up to 700 mb for 30 soundings taken at Goodland, Kansas. The predicted temperatures were found to be no more accurate than the persistence temperatures.

d) Term 4: Vertical Displacement.

Following a method presented by Achtemeier and Morgan (1975) , the convergence computed from observations of the surface wind field is converted to vertical displacements upon the assumptions that the convergence is constant through a 1 km deep layer and is constant through a time span of 1 hour. The vertical displacements are then summed over 5-hour sliding periods to compute a quantity called cumulative lift. The 5-hour period was chosen as representative of the residence time of a typical mesosystem between observation sites with average separation similar to that of the current United States surface network.

The basic supposition is that vertically integrated effects of sub-synoptic and mesoscale phenomena are detectable in the surface observations, both in space and time. This is not to say that these systems can be accurately described by the surface observations, but just that their presence can be detected in them. Further, it is inferred that the systems that produce the patterns of cumulative lift extend vertically through much of the depth of the troposphere. Circulations with deep convective systems that are not coupled with the surface layer will not be detected by the cumulative lift method.

It was originally intended to compute the vertical displacement by taking the difference between the cumulative lift at the observation site and time and the cumulative lift at each point on the grid. However, it was found that many soundings were not characteristic of airmasses that had undergone large vertical displacements even though they were located in areas with large vertical displacements calculated from the surface observations. The cumulated convergence spreads over an area essentially determined by the average station spacing whereas convergence zones associated with meso-scale triggering mechanisms are concentrated along narrow bands much smaller in scale. Further, soundings taken near convective systems could be subject to cloud scale subsidence. Thus all soundings were designated as characteristic of undisturbed airmasses and the grid point vertical displacements were calculated from zero.

With the assumptions stated above, (2) is expressed by

$$T = T_i + \frac{1}{cp} \Delta H - \overline{(\gamma_d - \gamma)} \Delta s \qquad (9)$$

The method for calculating temperatures from (9) is as follows: For each spatial and temporal gridpoint, the initial sounding temperature and humidity is adjusted by vertically displacing the sounding according to the 5-hour cumulative lift. All low level convergence occurs below 1 km Agl. All compensatory divergence occurs above 300 mb. Positive vertical velocities between these levels increases upward by vertical stretching. The opposite to the above discussion follows when there is surface level divergence.

After the sounding has been adjusted for vertical displacements, the mixing layer up to 800 mb is adjusted according to the low level temperature and moisture. The layer is given a constant mixing ratio (well mixed) and the temperature is dry adiabatic from the surface to the level where the dry adiabat passing through the modified surface temperature intersects the sounding temperature curve or the 800 mb surface, whichever comes first, unless the lifted condensation level is reached first. Then, within the layer cloud above the LCL, the dry adiabatic lapse rate is replaced by the moist adiabatic lapse rate. All subsidence is dry adiabatic.

If the surface temperature was colder than the sounding surface temperature, the lapse rate was assumed to be linear from 900 mb to the surface temperature. The moisture lapse rate was assumed to be linear from 900 mb to the surface moisture value.

The twice daily rawinsondes from Peoria and from Salem, Illinois, were modified at 3 hourly intervals according to the temperature, moisture, and the 5-hour cumulated convergence from the hourly surface observations interpolated to points on a 49 point grid located over much of Illinois and parts of Iowa, Missouri, and Indiana (figure 16). A grid spacing of 62 km was used. Fifty-eight days, including 06-30 June and 28 July-30 August, 1972, were processed for wind components, temperature, dewpoint temperature, and cloudiness. Surface data modified soundings provided initial data for the Kreitzberg and Perkey (1976) one dimensional quasi-time dependent cloud model(MESOCU). No feedback from the model to later soundings was allowed. The model could generate a succession of up to 5 clouds. Cloud information such as duration, base height, top height, depth, cloud base mass flux, precipitation, areal coverage, areal precipitation, maximum updraft, height of the maximum updraft, and cloud efficiency for each cloud was stored on magnetic tape for further analysis. A total of 22,736 modified soundings were processed by MESOCU.

The 4-D sounding analysis was verified against radar echo tops and precipitation patterns presented from the National Weather Service hourly radar summary RADU charts summarized to 3 hour periods centered about the modified sounding times. Figure 17 compares the maximum RADU echo tops with the maximum calculated cloud tops anywhere in the grid for the 9 day period 06-15 June 1972. RADU echo top (calculated cloud top) trends are given by the solid (dashed) lines. An M was entered when one or more hours of surface data within the 5-hour period ending at the modified sounding time was missing. A U was entered when radar echoes were reported within the grid but no echo top information was given.

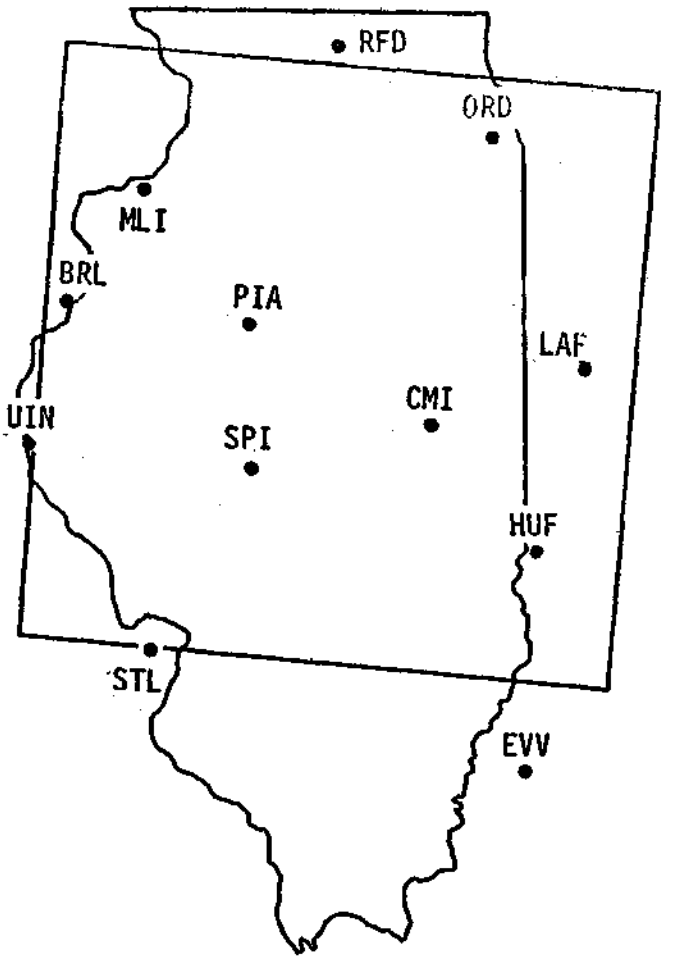

Figure 16. Map of Illinois showing the surface grid and the 12 surface stations used for calculation of surface fields.

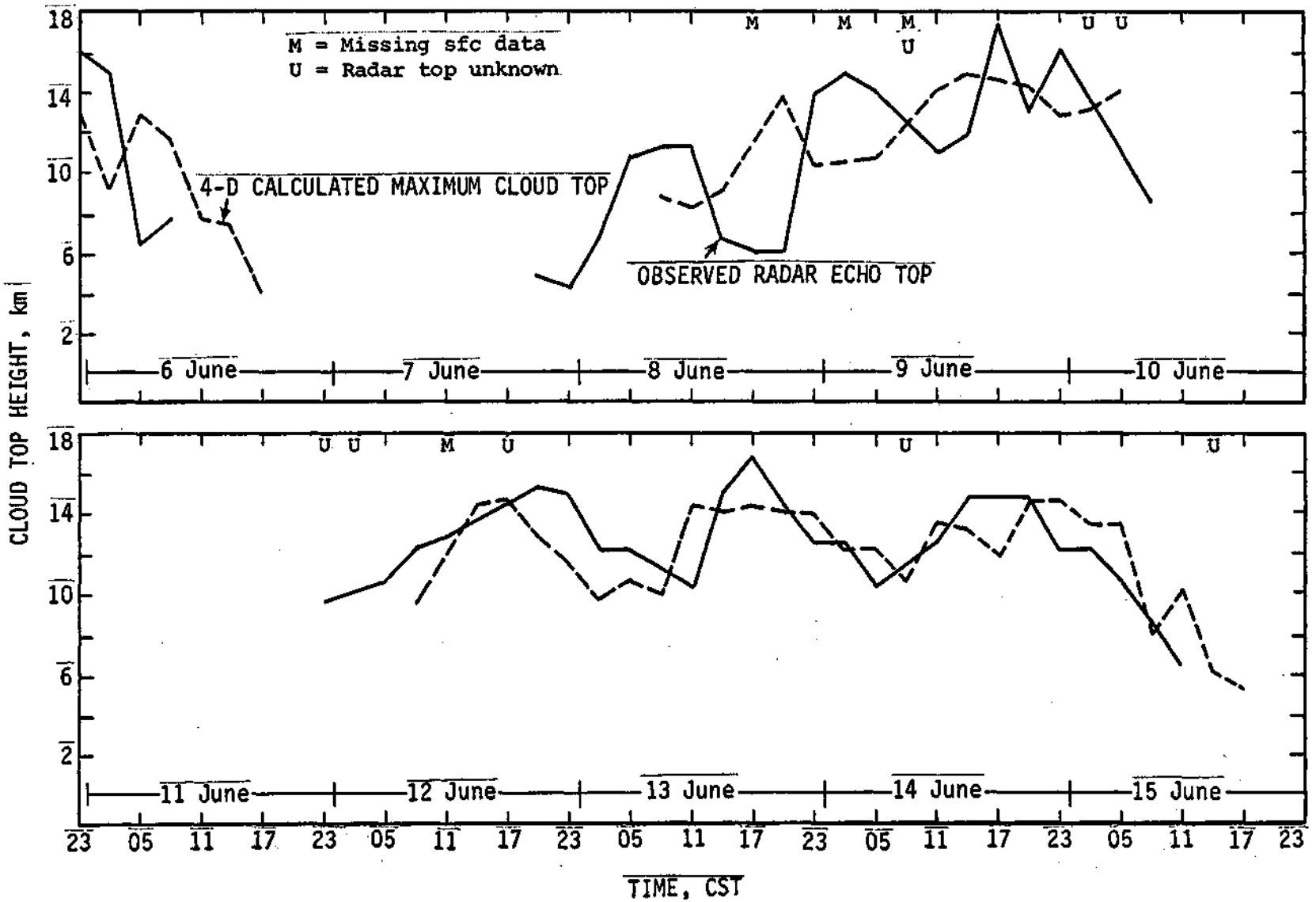

Figure 17. Three-hourly heights of RADU echo tops (solid lines) and 4-D model calculated maximum cloud tops anywhere on grid for 06-15 June 1972.

Both sets of curves reveal oscillations in the cloud top trends with the higher tops found generally around 1800 CST and lower tops found generally in the early to mid morning hours. The differences between the model calculated

and the weather systems. Small differences ranged from 0.0-1.0 km but some differences as large as 6 km were found when the calculated tops peaked before or after the observed RADU tops or when the RADU tops exceeded 14 km. The cloud model seldom produced tops above 14 km.

On some occasions, radar echoes were present on the grid for several hours before the cloud model calculated deep clouds. One such lapse occurred from 07 June to 0800 CST 08 June when the Peoria sounding was taken through a stable dry airmass ahead of a warm front. There were other times (0800-1400 CST, 06 June) when the model calculated deep clouds for several hours after the weather system had dissipated or had moved off the grid. The delay in the model response could have been caused by 1) convergence was included for times aged up to 5 hours from the current time, 2) the vertical motion fields within stable post precipitationconvergent flows were confined to a shallow layer not well represented by the 4-D model assumptions, or 3) the cloud model was not allowed to feed back subsided precipitation processed temperature lapse rates to the 4-D analysis.

There was also found a tendency for a 3-6 hour phase shift between the RADU and 4-D calculated cloud tops. Whether this shift is predictive of future events or is a lag caused by inclusion of data aged up to 5 hours is the subject of investigation.

An example of the spatial correspondence between the RADU precipitation patterns, RADU echo tops and the model calculated echo tops for 1700 CST 19 June 1972 is presented in figure 18. This case is an 11 hour extrapolation of the morning sounding and was characterized by explosive thunderstorm development over a large area where no radar echoes were reported 3 hours earlier. The 4-D model calculated cloud tops to exceed 11 km over Illinois east of Peoria (PIA). High cloud tops generally above 7 km were calculated for a narrow zone from Rockford (RFD) southward, then southwestward between Peoria and Springfield (SPI) and westward to Quincy (UIN). Cloud tops from 5-7 km covered much of the grid east and south of this line.

The model calculated no clouds for a large area in the northwest (upper left) part of the grid. Sharp transitions to highest cloud tops occurred within the distance of one grid space (62 km) along the interface between the no cloud area and the deep cloud line.

The second panel in figure 18 shows the RADU distribution of cloud tops and precipitation patterns for 1600-1800 CST. Radar echoes were confined to an area northwest of a line from east of Chicago (ORD) to east of St. Louis (STL). There was also a small echo free area between RFD and Moline (MLI). The maximum reported cloud tops were found in three areas; tops from 9.1-10.7 km southeast 6f RFD, tops from 12.2-12.8 km along a line from PIA to STL, and tops from 9.1-13.4 km along the Mississippi River area in western Illinois.

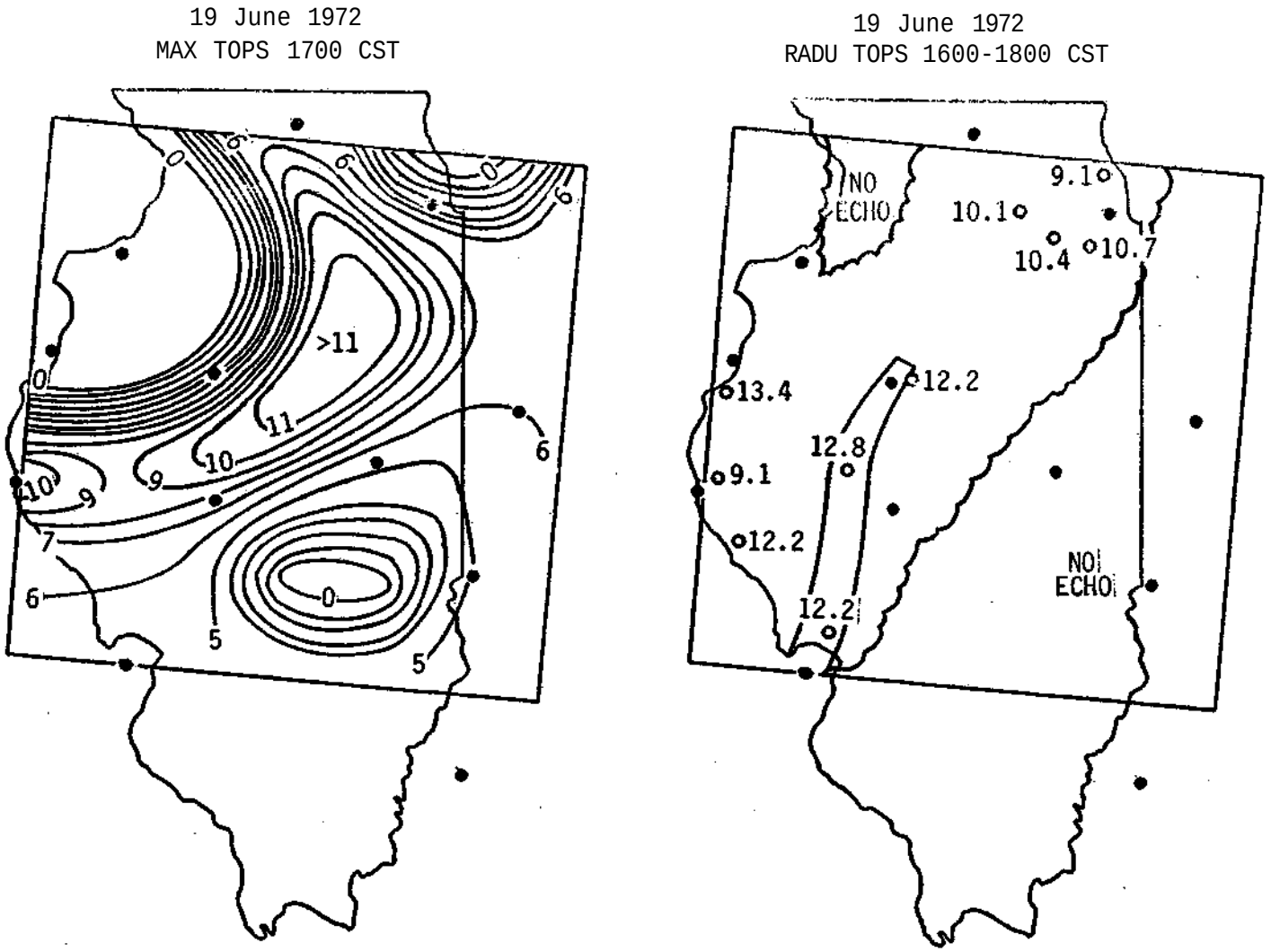

Figure 18. Spatial distribution of 4-D model calculated cloud tops for 1700 CST 19 June 1972 (panel 1) and 1600-1800 CST RADU summary precipitation patterns and echo tops (panel 2).

A comparison of these with the model calculated cloud tops shows that, generally, the high radar tops were found within or near the zone of maximum calculated cloud tops. The 4-D model did not produce high tops in the area covered by the line of echoes from SPI southward to STL. A comparison of the RADU and calculated tops for all the 58 day analyses revealed that many calculated cloud top patterns did not correspond exactly with the observed echo patterns. Some reasons for this are:

1) The sounding was unrepresentative of the undisturbed environment. The sounding was taken through clouds, taken within subsidence or lift areas near convective systems, or taken behind cold fronts that straddled the grid.

2) The 5-hour cumulative convergence spreads the net vertical displacements over large areas.

3) Showers were displaced from the surface positions of warmfronts and stagnant precipatation caused mesohighs.

4) The shower triggering mechanisms were not coupled with the surface layer.

5) The shower systems were too small in areal coverage to be detected by the current surface network.

6) The station distributions and variations in station spacing were such to cause the objective interpolation method to consistently place maximum convergence areas within data voids between stations. Figure 18 shows the area of maximum calculated cloud tops east of PIA and an area of no clouds located between HUF and STL - one, a zone of maximized convergence the other, a zone of maximum divergence - were located in large data void areas.

7) The surface observations were contaminated by errors caused by poor instrument exposure, poor instrument calibration, errors in observation or transmission, channeling by local topography, or the effects of sub-scale phenomena.

The 4-D analysis shows promise as a method for post analysis and now casting (short term forecasts). The calculated cloud tops and spatial patterns generally compare well with the observed echo patterns and tops. Locally, however, the cloud patterns and tops do not compare well. Some doubt remains whether the 4-D can produce analyses of the accuracy required for the HIPLEX predictor variable studies. In particular, more accurate objective analyses of surface data await a new objective method suitable for interpolation with small data sets. This method is currently being developed on another project.